STUDY OF DOWNLINK MULTI-USER MIMO-NOMA USING VARIED PRECODING, CLUSTERING, DIVERSITY AND POWER ALLOCATION SCHEMES WITH EXPERIMENTAL VALIDATION

A thesis submitted towards partial fulfilment of the requirements for the degree of

MASTER OF ENGINEERING
IN
ELECTRONICS AND TELECOMMUNICATION ENGINEERING

Submitted by

SAYANTI JANA
ROLL NO.: 002110702007
REGISTRATION NO.: 160206 of **2021-2022**

Under the guidance of

PROF. ITI SAHA MISRA
DEPARTMENT OF ELECTRONICS AND TELECOMMUNICATION ENGINEERING
JADAVPUR UNIVERSITY
KOLKATA-700032

FACULTY OF ENGINEERING AND TECHNOLOGY
JADAVPUR UNIVERSITY
KOLKATA-700032
JUNE 2023

M.E. (**Electronics and Telecommunication Engineering**) course affiliated to

Faculty of Engineering and Technology,

Jadavpur University, Kolkata, India

CERTIFICATE OF RECOMMENDATION

This is to certify that the dissertation entitled **"STUDY OF DOWNLINK MULTI-USER MIMO-NOMA USING VARIED PRECODING, CLUSTERING, DIVERSITY AND POWER ALLOCATION SCHEMES WITH EXPERIMENTAL VALIDATION"** has been carried out by **SAYANTI JANA** (**University Registration No.**: **160206** of **2021-2022**, **University Roll No.**: **002110702007)** under the guidance and supervision of **PROF. ITI SAHA MISRA** and be accepted in partial fulfilment of the requirements for the degree of **Master of Engineering** in **Electronics and Telecommunication Engineering**. The research results presented in the thesis have not been included in any other places submitted for any degree to any other University or Institute.

Prof. Iti Saha Misra (SUPERVISOR)

Department of Electronics and Telecommunication Engineering,

Jadavpur University, Kolkata - 700032

Prof. Manotosh Biswas (HOD)

Department of Electronics and Telecommunication Engineering,

Jadavpur University, Kolkata - 700032

Prof. Ardhendu Ghoshal (DEAN)

Department of Electronics and Telecommunication Engineering,

Jadavpur University, Kolkata - 700032

M.E. (**Electronics and Telecommunication Engineering**) course affiliated to

Faculty of Engineering and Technology,

Jadavpur University, Kolkata, India

CERTIFICATE OF APPROVAL

This foregoing thesis is hereby approved as a credible study of an engineering subject carried out and presented in a manner satisfactorily to warranty its acceptance as a prerequisite to the degree for which it has been submitted. It is understood that by this approval the undersigned do not endorse or approve any statement made or opinion expressed or conclusion drawn therein but approve the thesis only for purpose for which it has been submitted.

External Examiner

Internal Examiner

** Only in case the thesis is approved.

DECLARATION OF ORIGINALITY AND COMPLIANCE OF ACADEMIC ETHICS

I, hereby, declare that this thesis contains literature survey and original research work by the undersigned candidate, as part of her **Master of Engineering in Electronics and Telecommunication Engineering** curriculum during academic session 2022- 2023.

All information in this document has been obtained and presented in accordance with academic rules and ethical conduct.

I also declare that, as required by the rules and conduct, I have fully cited and referred all material and results that are not original to this work.

NAME: **SAYANTI JANA**

EXAMINATION ROLL NUMBER: **M4ETC23014**

UNIVERSITY ROLL NUMBER: **002110702007**

THESIS TITLE: **STUDY OF DOWNLINK MULTI-USER MIMO-NOMA USING VARIED PRECODING, CLUSTERING, DIVERSITY AND POWER ALLOCATION SCHEMES WITH EXPERIMENTAL VALIDATION**

_____ _____

SIGNATURE DATE

ACKNOWLEDGEMENT

I would like to express my heartfelt gratitude to my supervisor Prof. Iti Saha Misra for her constant guidance, support, active supervision, innovative ideas and patience throughout the entire process of writing this thesis paper. I was privileged to witness her enthusiastic and dedicated interest towards advanced research that motivates me and enriches my growth as a student and a researcher. Her insight, editing, and encouragement were instrumental in helping me produce a significant quality piece of work.

I would like to thank the entire department of "Electronics and Telecommunication Engineering" for imparting invaluable knowledge in their respective fields and helping me achieve one of the major goals of my life.

Finally, I am forever grateful to my parents for their unwavering support and encouragement during all my years in academia.

Place: Kolkata
Date:

(Ms. Sayanti Jana)

Electronics and Telecommunication Engineering,
Jadavpur University, Kolkata - 700032

ABSTRACT

Multiple-Input-Multiple-Output (MIMO) technology has gained significant attention in recent years to upgrade the performance of wireless communication systems. It allows the use of multiple antennas at both transmitting and receiving ends, thereby enabling more robust reception and increased system capacity. Non-Orthogonal Multiple Access (NOMA) is another promising radio access technology that outperforms the conventional multiple access techniques in order to maximize the spectral efficiency and minimize latency, thereby allowing users to share the same frequency, time, and code resources. A combination of MIMO and NOMA techniques, known as MIMO-NOMA, is said to be a propitious technology in further improving the system performance in various use cases, such as in beyond 5G broadband and machine-to-machine communication. In this thesis, a detailed performance analysis, based on MATLAB simulation, is presented for a multi-user MIMO power-domain NOMA (MU-MIMO-PD-NOMA) paradigm for varied combination of antenna diversity techniques, different types of precoding techniques and clustering methodologies using various modulation schemes and power allocation strategies. Also, a new precoding technique based on Singular Value Decomposition (SVD) precoding is proposed along with a novel clustering methodology and their performance is thereafter examined and compared with the existing precoding and clustering methods respectively. The modulation schemes used are namely, BPSK, QPSK and a combination of BPSK-QPSK, i.e., an Adaptive modulation technique. The power allocation strategies employed involve both fixed and dynamic power allocation. Under dynamic power allocation, Constrained Optimization and Convex Optimization algorithms are applied to the system respectively. Apart from simulation, a real-time test-bed implementation of (2x2) MIMO, without precoding and with different types of precoding, was performed on a Software Defined Radio (SDR) kit named WARP v3, in the 2.4GHz band. Physical implementation of two-user MIMO-PD-NOMA using fixed power allocation was also conducted on the WARP v3 board for the proposed and existing precoding schemes, at an experimentally determined optimum user position. The simulation and experimental performance parameters taken into consideration are Bit Error Rate, Sum Capacity, Spectral Efficiency and Constellation Diagram. The results were studied and a comparative analysis on grounds of the performance parameters, for different modulation schemes, is also presented in this thesis paper.

TABLE OF CONTENTS

ABBREVIATIONS

ADC:	Analog-to-Digital Converter
AGC:	Automatic Gain Control
AWGN:	Additive White Gaussian Noise
BER:	Bit Error Rate
BPSK:	Binary Phase Shift Keying
BWB:	Best-With-Best
BWW:	Best-With-Worst
BS:	Base Station
CFO:	Carrier Frequency Offset
COPA:	Constrained Optimization Power Allocation
CON-OPA:	Convex Optimization Power Allocation
CSI:	Channel State Information
DAC:	Digital-to-Analog Converter
DIST A:	Distance Combination A
DIST B:	Distance Combination B
DIST C:	Distance Combination C
DL:	Downlink
FF:	Fairness Factor
FMC:	FPGA Mezzanine Card
FPA:	Fixed Power Allocation
FPGA:	Field Programmable Gate Array
IoT:	Internet of Things
LCC:	Least Channel Correlation

LTS:	Long Training Sequence
MA:	Multiple Access
MF:	Matched Filter
MIMO:	Multiple-Input-Multiple-Output
MIMO-PD-NOMA/	
MIMO-NOMA:	MIMO Power-Domain NOMA
MRC:	Maximal Ratio Combining
MRT:	Maximal Ratio Transmission
MU:	Multi-User
NOMA:	Non-Orthogonal Multiple Access
OFDM:	Orthogonal Frequency Division Multiplexing
OMA:	Orthogonal Multiple Access
PA:	Power Allocation
PD-NOMA:	Power-Domain NOMA
QoS:	Quality of Service
QPSK:	Quadrature Phase Shift Keying
RAS:	Receiver Antenna Selection
RAN:	Random
RF:	Radio Frequency
RX:	Receiver
RZF:	Regularized Zero-Forcing
SC:	Superposition Coding
SDR:	Software Defined Radio
SE:	Spectral Efficiency
SFO:	Sampling Frequency Offset

SIC:	Successive Interference Cancellation
SINR:	Signal-to-Interference-Noise Ratio
SNR:	Signal-to-Noise Ratio
STS:	Short Training Sequence
SVD:	Singular Value Decomposition
TAS:	Transmit Antenna Selection
TX:	Transmitter
UE:	User Equipment
WARP:	Wireless Open-Access Research Platform
ZF:	Zero-Forcing

LIST OF FIGURES

LIST OF TABLES

Chapter 1 INTRODUCTION

1.1. OVERVIEW

Wireless communication, ever since its inception, has witnessed a wide range of technological developments in different domains and has become a vital part of everyday life. With the boost in global population, the number of devices has also increased significantly, whereby the same radio spectrum is required to be reused several times by varied applications and/or users. Furthermore, the future is heading towards a realm of Internet of Things (IoT) which demands every person, machine and object to be connected to and through the internet. The phenomenal growth of IoT devices in 6G scenarios, like smart city, connected health, industrial internet, vehicle network and such like, have led to a broad deployment of a large number of wireless-enabled sensors. Hence, a great amount of sensing data is collected sporadically and is thereafter forwarded to the cloud via connected IoT devices, cellular networks and the internet [1,2]. A report by Ericsson predicted that the number of short-range and cellular IoT devices will reach 17.8 billion and 4.1 billion by 2024, respectively [3]. Therefore, the proliferation of IoT devices will pose the necessity of massive wireless connections to confront the future paradigm of 6G and beyond. Since, the current communication systems have stringent limitations to meet the above demands; therefore, researchers have been exploring suitable techniques and technologies that may be integrated with the next-generation wireless communication systems in order to fundamentally fulfill the emerging requirements; such as very high spectral efficiency, very low latency, massive device connectivity, very high achievable data rate, ultra-high reliability, optimum user fairness, diverse Quality of Service (QoS), energy efficiency and a substantial reduction in the cost [4]. In order to satisfy the aforementioned targets and to address the challenges of future generations, both academia and industry have come up with varied potential technologies, out of which the concept of Multiple-Input-Multiple-Output (MIMO) seems to be the most promising one.

In recent years, MIMO technology has gained significant attention owing to its skill of improving capacity and overall performance in wireless communication systems. It allows the use of multiple antennas at both transmitting and receiving ends, enabling spatial diversity gain and enhanced system capacity. Apart from MIMO, in fields of Multiple Access (MA), a new radio access technology, named Non-Orthogonal Multiple Access (NOMA) has been developed by researches to be used in next-generation communication networks due to its capability of increasing the system capacity and user fairness. The previous generations of cellular network have employed Orthogonal Multiple Access (OMA) schemes, such as Frequency Division Multiple Access (FDMA) of first generation (1G), Time Division Multiple Access (TDMA) of 2G, Code Division Multiple Access (CDMA) of 3G, and Orthogonal Frequency Division Multiple Access (OFDMA) of 4G. In OMA, each user could exploit orthogonal communication resources within either a specific time slot, frequency band, or code, in order to avoid multiple access interference. On the contrary, NOMA allows multiple users to utilize non-orthogonal resources concurrently, by yielding a high spectral efficiency and simultaneously enabling some degree of multiple access interference at the receivers. Therefore, NOMA technique allows multiple users to share the same frequency, time, and code resources, resulting in high spectral efficiency. Among the various variants of NOMA, the most popular one is Power-Domain NOMA (PD-NOMA), wherein different users are allocated different power coefficients according to their channel conditions, in order to achieve a high system performance. In particular, multiple users' information signals are superimposed at the transmitter side and at the receiver side successive interference cancellation (SIC) is applied for decoding the signals one by one until the desired user's signal is obtained, thereby providing a good trade-off between the throughput of the system and the user fairness.

As both MIMO and NOMA techniques have a lot of capabilities, hence, researchers have combined the two and named the amalgamation as MIMO-NOMA, which is said to provide additional degrees of freedom for further system performance improvement and also holds significant application in various use cases, such as in 6G and beyond wireless systems. In MIMO-NOMA, multiple antennas are allocated to each user while the non-

orthogonal resources are shared among them. Each user is assigned a different power level based on their channel quality information (CQI) and user priority. The users with good channel conditions and high priority are allocated higher power, while the users with poor channel conditions and lower priority are allocated lower power. The combination of MIMO and NOMA techniques enable these signal streams to be transmitted simultaneously, allowing for high robustness, spectral efficiency, and increased capacity.

One of the key advantages of MIMO-NOMA over other multiple access schemes is its ability to eliminate interference and improve system reliability. The use of diversity and precoding techniques in MIMO-NOMA enables signals to be steered to specific users while reducing interference, enhancing robust reception, thereby leading to better quality of service (QoS) and overall system performance. MIMO-NOMA also offers significant benefits in power and spectral efficiency and enables users to transmit larger data volumes with fewer resources.

Thus, MIMO-NOMA is a promising technique that combines the benefits of MIMO and NOMA to enable improved system performance in wireless communication. It offers high spectral efficiency, improved reliability, and increased capacity while reducing interference and resource usage.

1.2. OBJECTIVE OF THE THESIS

In this thesis, the concept and potential of Multiple-Input-Multiple-Output Power-Domain NOMA (MIMO-PD-NOMA) is explored for different diversity, precoding and clustering techniques on a simulation platform for Rayleigh fading channel. Thereafter, the performance of the system is analyzed, for different modulation schemes, on basis of Bit Error Rate (BER), Sum Capacity and Spectral Efficiency (SE). The impact of fixed and dynamic power allocation strategies in compliance with MIMO-PD-NOMA is also studied. The major part of the thesis is based on MATLAB simulation followed by experimental validation, in the 2.4 GHz band, on a Software

Defined Radio (SDR) kit, named WARP v3. The performance of a proposed and existing precoding techniques and the effect of diversity is closely observed for a MIMO-WITHOUT-NOMA setup. Additionally, it is experimentally proved that MIMO-NOMA has higher spectral efficiency than MIMO-WITHOUT-NOMA. Also, an optimum user-position, in terms of BER and SE, is determined for the indoor environment wherein the experiment had been conducted. Finally, at the optimum user-position, MIMO-PD-NOMA for different precoding techniques and modulation schemes was experimentally performed and their performance was extensively analyzed.

1.3. LITERATURE SURVEY

Multiple-Input Multiple-Output (MIMO) technology is a communication technique that leverages multiple antennas to transmit and receive signals simultaneously in wireless communication systems. Non-orthogonal multiple access (NOMA) enables multiple users to share the same resource thereby differentiating on grounds of power allocation; thus, enhancing the spectral efficiency of wireless communication systems. When these two technologies are combined, it results in MIMO-NOMA, which is a propitious technology that has gained significant attention from researchers in recent years. By combining the advantages of MIMO and NOMA technologies, MIMO-NOMA is expected to provide an excellent solution to overcome the challenges of 6G and beyond networks, such as limited frequency spectrum, high throughput, and reliability [5].

In [6], the authors have scrutinized the performance of MIMO-NOMA and MIMO-OMA schemes and have concluded through simulation that the former offers better capacity than the latter. The authors of [7] proposed a transmission framework, using signal alignment, for the downlink and uplink MIMO-NOMA system and also explored fixed and cognitive power allocation to evaluate NOMA system performance. In [8] and [9], a study was carried out on the performance and security of a MIMO-NOMA system using a transmit antenna selection (TAS) scheme for a Rayleigh fading channel. In [10], the authors calculated the Outage Probability for a MIMO-

NOMA system using Monte-Carlo simulations and employing TAS technique, maximal ratio combining (MRC) receivers and Rayleigh fading. The authors of [11] proposed a MIMO-NOMA system, wherein users were grouped into small-sized clusters and thereafter NOMA principle was applied to each cluster. However, joint power allocation and beamforming designs were not considered in [11]. The optimization designs of MIMO-NOMA, with respect to power allocation and user scheduling, in millimetre-wave technology have been investigated in [12] and [13]. In [14], a zero-forcing based beamforming and user pairing scheme was proposed for the downlink multiuser NOMA system, assuming that perfect channel state information was available at the transmitter (CSIT). [15-16] deals with a scenario wherein each user has a single antenna and hence, various algorithmic frameworks have been proposed for optimizing the design of beamforming in NOMA transmission system. The application of MIMO-NOMA to the downlink mobile communication networks is addressed in [17]. The authors in [17] employed MIMO-NOMA to both cellular and cognitive inspired wireless networks. Additionally, through simulation, they explored the outage probability for MIMO-NOMA systems and studied the sum-rate difference between NOMA-based networks and their orthogonal multiple access (OMA) counterparts.

In [18], the authors examined the use of generalized singular value decomposition (GSVD) for coordinated beamforming in MIMO systems and thereby concluded through simulation results that the proposed technique performed better, in terms of bit error rate (BER), than the conventional SVD technique based on block diagonalization (BD). In [19], two novel coordinated beamforming techniques were developed to enhance the performance of MIMO-NOMA systems in presence of inter-cell interference. Although, the proposed schemes showed to increase the cell-edge users' throughput but nothing was mentioned about the improvement in the bit/symbol error rate at the user's end. [20] presented a survey on the performance of downlink MIMO-NOMA systems with and without CSIT. It has been stated by [20] that when it is difficult to acquire CSIT, open-loop operation could be considered as an option. However, when users are clustered, it is always advisable to exploit closed-loop operation for such a scenario. [20] compares these two methods analytically and through simulation and designs the closed-loop system based on Karhunen-Loeve

channel decomposition. The authors of [21] came up with a power allocation scheme for each user in a downlink (DL) MIMO-NOMA system and analysed its performance based on a trade-off between spectral efficiency and energy efficiency. In [22], the authors have proposed a joint interference alignment and power allocation approach for multi-user MIMO-NOMA systems and the aforementioned framework aims to maximize the sum-rate of the entire system. It is shown that the proposed method does indeed enhance the sum-rate compared to the conventional schemes but nothing has been stated about its impact on the outage probability (OP) or bit error rate (BER) of the system.

Apart from beamforming, user clustering also plays a crucial role in MIMO-NOMA systems and have a significant impact on system performance. In [23], the authors propose a user clustering and power allocation scheme for MIMO-NOMA systems with limited feedback, aiming to maximize the sum-rate. They utilize a hierarchical clustering algorithm and jointly optimized power allocation and user clustering to enhance system performance. Zhang et al. in [24] proposed a user clustering and power allocation scheme for MIMO-NOMA systems based on partial channel state information (CSI). They developed an optimization framework to maximize the system sum rate by jointly optimizing user clustering and power allocation, considering imperfect CSI at the base station. The proposed scheme improved system performance by mitigating inter-cluster interference and exploiting partial CSI knowledge. The authors of [25] developed an iterative algorithm that jointly optimizes user clustering and precoding matrices to maximize the system sum-rate, considering both inter-cluster and intra-cluster interference. The proposed scheme improves the performance of multi-antenna NOMA systems by effectively managing interference and enhancing spectral efficiency.

Thus, MIMO-NOMA has opened up new avenues for research in wireless communication systems and the literature so far suggests that MIMO-NOMA can provide significant performance gains in terms of spectral efficiency, reliability, and energy efficiency for future wireless networks. The different aspects of antenna diversity, precoding and clustering techniques on basis of varied performance parameters and power allocation strategies have not yet been simultaneously and thoroughly explored along with experimental validation of MIMO-NOMA systems for a real-time environment. This thesis looks forward to fulfil this agenda through its work.

1.4. OUTLINE OF THE THESIS

- Chapter 2 provides a background study of the fundamental concepts of MIMO and Power-Domain NOMA, along with different modulation schemes and performance analysis parameters used in simulation as well as in physical implementation.

- Chapter 3 is a contributory chapter that deals with analyzing the performance of downlink (2x2)-MIMO-PD-NOMA for different combination of antenna diversity techniques using different modulation schemes and power allocation strategies on a simulation platform for Rayleigh fading channel.

- Chapter 4 is a contributory chapter that examines the performance of downlink (2x2) and (4x4) MIMO-PD-NOMA for a proposed and existing precoding techniques using different modulation schemes and power allocation strategies on a simulation platform for Rayleigh fading channel.

- Chapter 5 is a contributory chapter that studies the performance of downlink (2x2) and (4x4) MIMO-PD-NOMA for a novel and conventional clustering methodologies using different precoding techniques, modulation schemes and power allocation strategies on a simulation platform for Rayleigh fading channel.

- Chapter 6 is a contributory chapter that presents an extensive analysis on real-time physical implementation, in the 2.4 GHz band on WARP v3 board, of MIMO-WITHOUT-NOMA and MIMO-PD-NOMA for a proposed and existing precoding techniques, along with determining an optimum user-position for the respective indoor environment.

- Chapter 7 gives a brief highlight of the conclusions obtained throughout the contributory chapters and also provides different directions for future works in research.

Chapter 2 BACKGROUND STUDY

2.1. INTRODUCTION

This chapter provides a brief description on the basic concepts of Multiple-Input-Multiple-Output (MIMO) and Power-Domain Non-Orthogonal Multiple Access (PD-NOMA) technologies, like diversity techniques, precoding schemes, superposition coding, successive interference cancellation and power allocation strategies respectively. It also presents an explanation of the general system model of a downlink multi-user MIMO-PD-NOMA (DL MU-MIMO-PD-NOMA) scenario and gives a mathematical scrutiny of the model. The concept of clustering and a few of its popular methods are also discussed along with a theoretical exposition of the digital modulation schemes used in simulation and real-time test-bed implementation work of this thesis. Finally, the respective performance parameters that are used for analysis throughout the thesis are described in a nutshell.

2.2. FUNDAMENTAL CONCEPTS OF MIMO-PD-NOMA

2.2.1. SYSTEM MODEL DESCRIPTION

In this thesis, two cases of multi-user MIMO-PD-NOMA (MU-MIMO-PD-NOMA) system in a downlink scenario are explored. In the first case, no clustering is employed and hence, all the users in the system take part in the same NOMA principle. In the second case, all the users are grouped into different clusters and herein each cluster separately applies NOMA only on the respective users of the cluster. The general system models for the two cases are presented and discussed as follows:

CASE I:

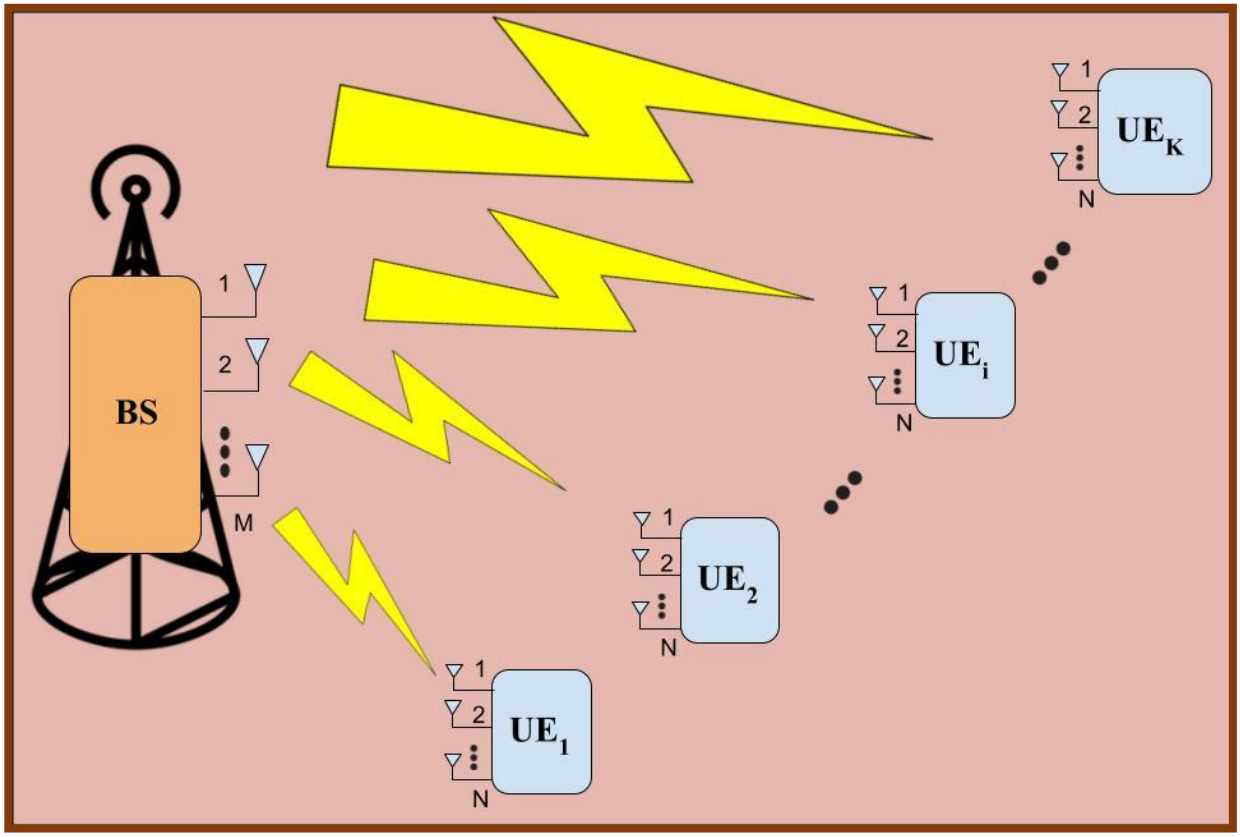

Fig.2.1: Generic Downlink Multi-User MIMO-PD-NOMA System Model

Fig.2.1 represents a typical multi-user MIMO-PD-NOMA system in a single-cell downlink communication scenario, wherein a single base station (BS), equipped with M antennas, communicates with K user equipments (UE_i), equipped with N antennas each, where $i \in \{1,2,\dots,K\}$. The UE_1 is situated at the smallest distance from the BS, whereas UE_K is located at the farthest distance from the BS. Each UE has (NxM) communication channel paths between the BS and itself. It is assumed that the total transmitter power is P_t and the wireless links experience independent and identically distributed (i.i.d.) Rayleigh fading with Additive White Gaussian Noise (AWGN). The effective channel gains of the UEs are sorted as: $|z_1 H_1 p_1|^2 \geq |z_2 H_2 p_2|^2 \geq \cdots \geq |z_i H_i p_i|^2 \geq \cdots \geq |z_K H_K p_K|^2$, wherein H_i indicates the (NxM) Rayleigh fading channel matrix from the BS to the i^{th} UE; and p_i and z_i are the precoding and post-coding vectors respectively, for the i^{th} UE, if and only if the concept of precoding is employed in the system. Therefore, UE_1 has the highest channel gain and is hence referred to as the strong user while other users are labelled

as weak users successively. At the BS, as per the NOMA principle, the signals for the different users are allocated different fraction of the total power and thereafter superposed to be transmitted over the same channel. The strong user is given the least fraction of power compared to other weak users. Hence, the power allocation order of the UEs is as follows: $P_1 < P_2 < \cdots < P_i < \cdots < P_K$. The superposed signal may thereafter be precoded and then applying transmit diversity, the resultant signal is transmitted through all the M antennas of the BS. At the receiving end, each UE receives the transmitted signal, through its N antennas, corresponding to the employed receiver diversity scheme followed by post-coding, if any precoding scheme is applied at the transmitter. After that, all the UEs except UE_K perform SIC while UE_K applies direct decoding to its received signal. UE_i $(i \neq K)$ employs SIC to decode and subtract the signals of $UE_{i+1}\ to\ UE_K$ from the received signal and thereby, treats the other signals from $UE_{i-1}\ to\ UE_1$ as interference.

CASE II:

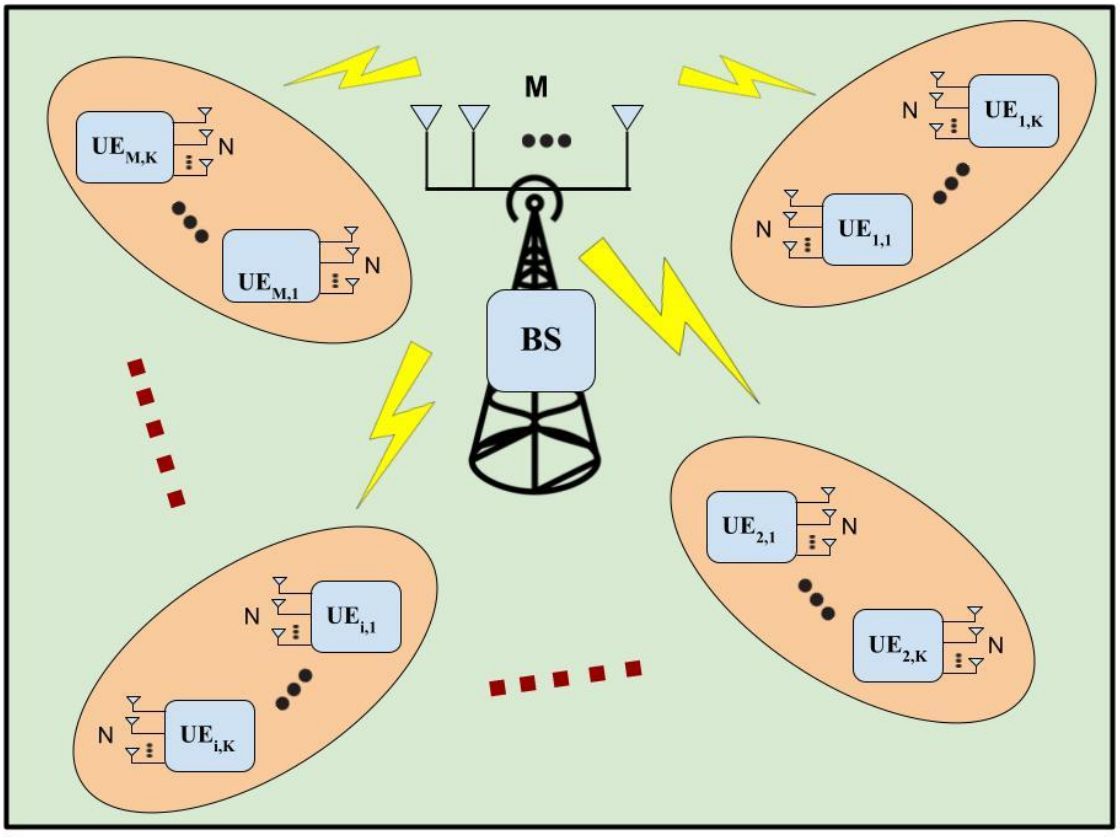

Fig.2.2: Generic Downlink Multi-User MIMO-PD-NOMA System Model with Clustering

Fig.2.2 represents a multi-user MIMO-PD-NOMA system in a single-cell downlink scenario, wherein a single base station (BS), equipped with M antennas, communicates with M number of clusters, each having B user equipments ($UE_{i,j}$), equipped with N antennas each, where $i \in \{1,2,\dots,M\}$ and $j \in \{1,2,\dots,B\}$. The UEs are clustered based on a suitable clustering algorithm. Each cluster employs NOMA principle individually, i.e. only among the users in the respective cluster. The $UE_{i,1}$ is situated closest to the BS, whereas $UE_{i,B}$ is located at the farthest distance from the BS. Each UE has (NxM) communication channel paths between the BS and itself. It is assumed that the total transmitter power is P_t and the wireless links experience independent and identically distributed (i.i.d.) Rayleigh fading with Additive White Gaussian Noise (AWGN). The effective channel gains of the UEs in a cluster are sorted as: $|z_{i,1}H_{i,1}p_{i,1}|^2 \geq \left|z_{i,2}H_{i,2}p_{i,2}\right|^2 \geq \cdots \geq \left|z_{i,j}H_{i,j}p_{i,j}\right|^2 \geq \cdots \geq \left|z_{i,B}H_{i,B}p_{i,B}\right|^2$, wherein $H_{i,B}$ indicates the (NxM) Rayleigh fading channel matrix, from the BS to the j^{th} UE in the i^{th} cluster; and $p_{i,B}$ and $z_{i,B}$ are the precoding and post-coding vectors respectively, for the j^{th} UE in the i^{th} cluster. Therefore, $UE_{i,1}$ has the highest channel gain and is hence referred to as the strong user while other users, in the respective cluster, are labelled as weak users successively. At the BS, as per the NOMA principle, the signals for the different users of a cluster, are allocated different fraction of the total power and thereafter superposed to be transmitted over the same channel. The strong user of a cluster is given the least fraction of power compared to other weak users in the respective cluster. Hence, the power allocation order of the UEs in a cluster is as follows: $P_{i,1} < P_{i,2} < \cdots < P_{i,j} < \cdots < P_{i,B}$. Whenever clustering is implemented in a MU-MIMO-NOMA system, there are primarily two kinds of interference that need to be handled. The first is intra-cluster interference that is looked after through SIC; and the other is inter-cluster interference that is dealt by using an appropriate precoding scheme. Therefore, the superposed signals are precoded and the resultant signals are transmitted through the M antennas of the BS. At the receiving end, the chosen receiver diversity scheme is employed followed by post-coding, depending on the precoding scheme applied at the transmitter. After that, all the UEs except $UE_{i,B}$ perform SIC while $UE_{i,B}$ applies direct decoding to its received signal. $UE_{i,j}$ ($j \neq B$) employs SIC to decode and subtract the signals of $UE_{i,(j+1)}$ to $UE_{i,B}$ from the received signal and thereby, treats the other signals from $UE_{i,(j-1)}$ to $UE_{i,1}$ as

interference.

2.2.2. DIVERSITY TECHNIQUES

In context of wireless communication, diversity refers to the use of multiple antennas or communication paths to improve the performance and reliability of a wireless transmission. It is based on the fact that individual channels experience fades and interference at different levels, i.e., they are independent or at least highly uncorrelated[26]. Therefore, diversity is a technique that exploits multipath propagation and hence, is employed to combat the challenges posed by fading and other channel impairments encountered in radio propagation. The use of diversity techniques in wireless communication system enhances the reliability, capacity, and quality of wireless links, thereby reducing the impact of fading and interference, and enabling better coverage, increased data rates, and improved overall performance[27].

There are several types of diversity that are commonly used in wireless communication, like time diversity, polarization diversity and such like. Out of them, the most popular one is Spatial/Space Diversity, also known as Antenna Diversity. In this diversity scheme, there are multiple transmitter antennas (Transmit Diversity) and/or multiple receiver antennas (Receiver Diversity), in order to combat fading[28,29]. At the transmitter, the same information can be transmitted over multiple antennas, whereby the signals take different paths and experience different fading conditions. At the receiver, the signals from multiple antennas can be combined or the best received signal can be selected, thereby enhancing the signal quality and reducing the impact of fading.

The following sub-sections throw light on the different kinds of Antenna Diversity techniques used in this thesis:

2.2.2.1. TRANSMIT ANTENNA SELECTION

Transmit Antenna Selection (TAS) is a type of Transmit Diversity technique wherein among the multiple antennas at the transmitter, the best antenna is selected for transmission. The selection process to determine the best antenna for signal transmission typically involves evaluating the channel conditions, such as

Signal-to-Noise Ratio (SNR), signal quality, channel fading or channel gain. The antenna with the highest quality or highest channel gain or strongest signal is thereafter chosen to transmit the data[30].

2.2.2.2. MAXIMAL RATIO TRANSMISSION

Maximal Ratio Transmission (MRT) is a type of Transmit Diversity technique wherein signals are transmitted from multiple antennas after being optimally weighted and combined in such a way that they reinforce each other at the receiver, thereby maximizing the received signal power. The combining process takes into account the channel conditions and weights the contribution of each antenna based on its signal quality and the channel's characteristics like channel gain[31].

2.2.2.3. RECEIVER ANTENNA SELECTION

Receiver Antenna Selection (RAS) is a type of Receiver Diversity technique wherein the receiver, having multiple antennas, selects the optimal antenna to improve signal quality and reliability. The selection process of the best antenna is based on criteria such as received signal strength, Signal-to-Noise Ratio (SNR) or other metrics that indicate the quality of the received signal and thereby provides the best reception for a given transmission[32].

2.2.2.4. MAXIMAL RATIO COMBINING

Maximal Ratio Combining (MRC) is a type of Receiver Diversity technique wherein the signals from the multiple receiving antennas are optimally weighted and combined in such a way that maximizes the received signal power and improves the overall signal quality. The combining process depends upon the channel conditions and the weights for each antenna is based on its respective received signal quality and channel characteristics like channel gain[33].

2.2.3. PRECODING TECHNIQUES

Precoding is a technique used in wireless communication systems, particularly in MIMO systems, to orient and optimize the signals at the transmitter side before they are transmitted through the wireless channel. It involves manipulating the signals to improve received signal quality, increase capacity, enhance overall system performance and mitigate the effects of fading, interference and other channel impairments. Therefore, the primary goal of precoding is to optimize the transmitted signals based on the channel conditions, characteristics and system requirements[34].

Precoding can be broadly classified into linear and non-linear precoding types. However, since non-linear precoding mechanism is not practically feasible due to its high complexity; hence linear precoding schemes are preferred as they provide reasonable performance with lower complexity.

The following sub-sections briefly discuss about some of the most prominent linear precoding techniques that have been explored in this thesis.

2.2.3.1. MATCHED FILTER

Matched Filter (MF) is a precoding technique wherein the transmit signals are weighted based on the channel gains, thereby taking into account the channel conditions. The weights are proportional to the complex conjugate of the channel coefficients, which effectively aligns the transmit signals in a way that they constructively interfere at the receiver, thereby maximizing the received signal power.

The expression for MF precoding matrix is as follows [35]:

$$P_{MF} = (conj(H))^T = H^H \tag{2.1}$$

where, H is the channel matrix,

$(.)^T$ is the transpose operator,

$(.)^H$ is the Hermitian operator.

The mathematical analysis of MF precoding scheme is as follows:

Proof:

Considering N and M to be the number of receiver and transmitter antennas respectively, and H to be a $(N\text{x}M)$ channel matrix, then

$$r = HP_{MF}s + w \tag{2.2}$$

where, r is a $(N\text{x}1)$ received signal vector;

s is a $(N\text{x}1)$ transmitted signal vector;

P_{MF} is a $(M\text{x}N)$ precoding matrix;

w is a $(N\text{x}1)$ Additive White Gaussian Noise (AWGN) vector.

Therefore, using equation (2.1), P_{MF} is replaced with its respective form, whereby equation (2.2) becomes:

$$r = HH^{H}s + w \tag{2.3}$$

Therefore, it can be seen from equation (2.3) that the transmitted signal will be received with a multiplexed gain matrix that is produced by the multiplication of H with its conjugate transpose. This matrix holds certain channel characteristics that has its impact on each of the corresponding transmitted symbol, whereby it is not able to effectively align the phase of the transmitted signal with that of the channel. However, it shows near optimal performance when the number of transmitter antennas are more than the receiver antennas.

2.2.3.2. ZERO-FORCING

Zero-Forcing (ZF) is a precoding technique that aims to nullify the interference caused by other users or signals, thereby transmitting the signal towards the intended user only. It eliminates interference from other user signals at the receiver side by aligning the transmit signals with the null space of the channel

matrix. However, it is said to amplify the noise along with the desired signal, particularly when the channel matrix is ill-conditioned. This can result in degraded performance and increased noise power at the receiver. Also, ZF precoding relies on accurate channel estimation and hence, any errors or inaccuracies in the estimated channel information can affect the effectiveness of interference cancellation.

The expression for ZF precoding matrix is as follows [36]:

$$P_{ZF} = H^H(HH^H)^{-1} \tag{2.4}$$

where, $(.)^{-1}$ is the inverse operator.

Equation (2.4) is known as the right Moore-Penrose pseudo inverse of H [37].

The mathematical analysis of ZF precoding scheme is as follows:

Proof:

Considering N and M to be the number of receiver and transmitter antennas respectively, and H to be a $(N\text{x}M)$ channel matrix, then

$$r = HP_{ZF}s + w \tag{2.5}$$

where, r is a $(N\text{x}1)$ received signal vector;

s is a $(N\text{x}1)$ transmitted signal vector;

P_{ZF} is a $(M\text{x}N)$ precoding matrix;

w is a $(N\text{x}1)$ Additive White Gaussian Noise (AWGN) vector.

Therefore, using equation (2.4), P_{ZF} is replaced with its respective form, whereby equation (2.5) becomes:

$$r = HH^H(HH^H)^{-1}s + w \tag{2.6}$$

Therefore, it can be seen from equation (2.6) that the channel effects are nullified and hence, the transmitted signal is received along with AWGN noise. Thus, in

absence of noise, ZF is an optimal precoding scheme but when noise is present, it can amplify the noise effects.

2.2.3.3. REGULARIZED ZERO-FORCING

Regularized Zero-Forcing (RZF) is a precoding technique, which is an enhanced version of ZF precoding, effectively nullifies the interference caused by the other signals at the intended user, along with taking into account the noise enhancement issue associated with ZF precoding. Therefore, it addresses the limitations of the latter by incorporating a positive regularization parameter that helps balance the trade-off between interference cancellation and noise enhancement, thereby resulting in an improved overall SNR at the respective receiver. The regularizing factor depends on the system dimensions, the noise variance, and uncertainty of channel at the transmitter[38].

The expression for RZF precoding matrix is as follows [39]:

$$P_{RZF} = H^H((HH^H) + G + \beta I_N)^{-1} \tag{2.7}$$

where, G is a Hermitian non-negative matrix ,

β is the regularization factor.

The mathematical analysis of RZF precoding scheme is as follows:

Proof:

Considering N and M to be the number of receiver and transmitter antennas respectively, and H to be a (NxM) channel matrix, then

$$r = HP_{RZF}s + w \tag{2.8}$$

where, r is a (Nx1) received signal vector;

s is a (Nx1) transmitted signal vector;

P_{RZF} is a (MxN) precoding matrix;

w is a (Nx1) Additive White Gaussian Noise (AWGN) vector.

Therefore, using equation (2.7), P_{RZF} is replaced with its respective form, whereby equation (2.8) becomes:

$$r = HH^H((HH^H) + G + \beta I_N)^{-1}s + w \quad (2.9)$$

Therefore, if $G = 0$, then equation (2.9) becomes a MF precoder for $\beta \rightarrow \infty$, and a ZF precoder for $\beta \rightarrow 0$. Thus, RZF's performance lies in between that of these two precoders.

2.2.3.4. SINGULAR VALUE DECOMPOSITON

Singular Value Decomposition (SVD) is a precoding technique that leverages the concept of SVD to optimize the transmit signals based on the channel conditions, thereby maximizing the system's capacity and improving the signal quality at the receiver. The channel matrix is decomposed into its singular values and singular vectors using SVD. The singular values represent the magnitude of the channel gains, while the singular vectors represent the spatial directions of the dominant components of the channel. The transmitter selects a subset of the singular vectors corresponding to the strongest singular values to form the precoding matrix while the singular vectors represent the spatial beams or eigen beams that will be used to transmit the signals. The transmit signals are multiplied by the precoding matrix to align the transmit signals with the chosen eigen beams. This optimizes the transmit signals based on the channel condition and spatial characteristics, thereby enhancing the signal quality at the receiver. SVD precoding helps reduce interference by transmitting the signals on different eigen beams. Also, by carefully selecting the eigen beams based on the channel conditions, the interference from other users or signals can be minimized, which in turn improves the signal-to-interference-plus-noise ratio (SINR) at the receiver. Thus, SVD precoding is flexible and adaptable to different channel conditions and system configurations, thereby allowing for efficient utilization of the available resources[40].

The expression for SVD precoding matrix is obtained as follows [41]:

$$H = UDV^H \quad (2.10)$$

where, D is a diagonal matrix containing the singular values;

U and V are unitary matrices whose columns represent the left and right singular vectors respectively.

Therefore, V is the precoding matrix that is employed at the transmitter while U^H is the post-coding matrix that is used at the receiver.

The mathematical analysis of SVD precoding scheme is as follows[41]:

Proof:

Considering N and M to be the number of receiver and transmitter antennas respectively, and H to be a (NxM) channel matrix, then

$$r = HPs + w \tag{2.11}$$

where, r is a (Nx1) received signal vector;

s is a (Mx1) transmitted signal vector;

P is a (MxM) precoding matrix;

w is a (Nx1) Additive White Gaussian Noise (AWGN) vector.

The SVD of the channel matrix be given as from equation (2.10):

$$H = UDV^H$$

where, U and V are (NxN) and (MxM) unitary matrices respectively; and,

$$D = diag\{\sqrt{g_1}, \sqrt{g_2}, \dots, \sqrt{g_N}\}$$

where, D a (NxM) diagonal matrix; and

$\sqrt{g_i}$ is the singular value of $H^H H$.

Therefore, replacing P with the precoding vector V and H with its SVD form respectively, equation (2.11) becomes:

$$r = UDV^H Vs + w \tag{2.12}$$

At the receiver, the received signal is multiplied by the post-coding vector U^H as:

$$U^H r = U^H(UDV^H Vs + w) \tag{2.13}$$

$$\Rightarrow \hat{r} = U^H UDV^H Vs + U^H w$$

$$\Rightarrow \hat{r} = (U^H U)D(V^H V)s + U^H w \tag{2.14}$$

Since, both U and V are unitary matrices, therefore by the property of unitary matrices,

$$U^H U = I_N = UU^H \tag{2.15}$$

$$V^H V = I_M = VV^H \tag{2.16}$$

Thus, the received signal after post-coding process is as follows:

$$\hat{r} = Ds + \widehat{w} \tag{2.17}$$

where, $\widehat{w} = U^H w$

Therefore, it can be seen from equation (2.17) that the transmitted signal will be received with a gain matrix *D* that employs a gain of $\sqrt{g_i}$ on each of the transmitted symbol.

2.2.4. SUPERPOSITION CODING

Superposition Coding (SC) was first proposed in [42] and from thereon has been stated as a technique of simultaneously communicating information to several receivers by a single source. It, therefore, allows the transmitter to transmit multiple users' information at the same time. For instance, in a two-user scenario, the transmitter will have to contain two point-to-point encoders that map their respective inputs to complex-valued sequences of the two-user signal. It can be stated that SC is a recognized non-orthogonal scheme that attains the capacity on a scalar Gaussian broadcast channel. In the superposition encoding phase, two point-to-point encoders, $x_1: \{0,1\}^{\lfloor 2^{LR_1} \rfloor} \rightarrow C^L$ and $x_2: \{0,1\}^{\lfloor 2^{LR_2} \rfloor} \rightarrow C^L$ first map the respective input bits to

two output bit sequences $s_1(n)$ and $s_2(n)$, respectively, each of block length L. Here R_1 and R_2 denote the transmission rates of user 1 and user 2, respectively, and $\lfloor\ \rfloor$ represents the floor operator. C is nothing but a code library. Thereafter, a summation device provides an output sequence as follows:

$$s(n) = \sqrt{P\alpha_1}s_1(n) + \sqrt{P\alpha_2}s_2(n) \tag{2.18}$$

where, α_i represents a fraction of the total power P assigned to the user i, subject to the constraint on $\alpha_1 + \alpha_2 = 1$.

2.2.5. SUCCESSIVE INTERFERENCE CANCELLATION

In order to decode the superposed information at each receiver, Cover first proposed the Successive Interference Cancellation (SIC) technique [42]. SIC is conceivable by exploiting specifications on the differences in signal strength among the signals of interest. The basic idea of SIC is that user signals are successively decoded. After one user's signal is decoded, it is subtracted from the combined signal before the next user's signal is decoded. When SIC is applied, one of the user signals is decoded, treating the other user signal as an interferer, but the latter is then decoded with the benefit of the signal of the former having already been removed. However, prior to SIC, users are ordered according to their signal strengths, so that the receiver can decode the stronger signal first, subtract it from the combined signal, and isolate the weaker one from the residue. Each user is decoded treating the other interfering users as noise in signal reception. In brief, the particular process involved in decoding the superposed messages can be mathematically expressed as follows [43]:

1) At user 2, a single-user decoder f_2: $C^L \rightarrow \{0,1\}^{\lfloor 2^{LR_2} \rfloor}$ decodes the message $s_2(n)$ by treating $s_1(n)$ as noise.
2) User 1 performs the following steps to successively recover its message from its received signal $y_1(n)$:
    a) Decode user 2's message $s_2(n)$ by using the single-user decoder f_2: $C^L \rightarrow \{0,1\}^{\lfloor 2^{LR_2} \rfloor}$.
    b) Subtract $\sqrt{P\alpha_2}h_1s_2(n)$ from the received signal $y_1(n)$ as follows:

$$y'_1(n) = y_1(n) - \sqrt{P\alpha_2}h_1 s_2(n),$$

where, h_1 is the complex channel gain at user 1.

c) Decode user 1's message $s_1(n)$ by applying another single-user decoder f_1: $C^L \rightarrow \{0,1\}^{\lfloor 2^{LR_1} \rfloor}$ on $y'_1(n)$.

2.2.6. POWER ALLOCATION STRATEGIES

Power allocation in Power-Domain Non-Orthogonal Multiple Access (PD-NOMA) is a critical aspect that determines how the available power resources are allocated among multiple users sharing the same time and frequency resources. The goal of power allocation in NOMA is to optimize system performance, enhance spectral efficiency, and ensure fairness among users. The choice of power allocation strategy depends on the specific system requirements, network conditions, and optimization objectives. Thus, power allocation in NOMA is a complex task that often involves solving optimization problems to find the optimal power levels for different users. The objective function can vary depending on the specific requirements, and the algorithms used can be influenced by the system constraints and the available channel state information (CSI). Thus, power allocation in NOMA is crucial for achieving efficient resource utilization, maximizing system capacity, and promising user fairness. It plays a significant role in enhancing the performance of wireless communication systems. Additionally, power allocation in MIMO-NOMA can be performed jointly with other techniques like user clustering, beamforming, or precoding to achieve improved system performance. There are different power allocation strategies and algorithms that can be employed in NOMA, depending on the specific objectives and system constraints[44].

The following sub-sections discuss about the power allocation strategies employed in this thesis.

2.2.6.1. FIXED POWER ALLOCATION

Fixed Power Allocation (FPA) in NOMA refers to a power allocation scheme wherein the power levels allocated to different users in the NOMA system remain fixed and do not change over time or adapt to varying channel conditions or individual user needs. In FPA, the power distribution is predetermined and remains

constant throughout the transmission. The power levels are typically allocated based on a predefined criterion or rule. Thus, FPA is relatively simple to implement and requires less computational complexity compared to dynamic power allocation schemes. However, it may not fully exploit the potential gains of NOMA, especially in scenarios with varying channel conditions or different user requirements. FPA assumes a uniform power allocation strategy and does not adapt to changing network conditions or individual user needs[45]. Therefore, it is a suitable choice in scenarios with limited complexity requirements or stable channel conditions, where dynamic power adaptation is not necessary, as it offers simplicity and ease of implementation while providing a baseline power allocation strategy for NOMA systems.

The commonly used FPA techniques in NOMA are as follows:

1) **Equal Power Allocation**: In this scheme, the total available power is divided equally among the users. Each user receives the same power level, regardless of their channel conditions or quality. Equal power allocation ensures fairness among users but may not optimize system performance[46].
2) **Fractional Power Allocation**: Fractional power allocation assigns different fractions of the total power to different users based on their channel conditions. Users with better channel conditions receive smaller fraction of the total power while the users with weaker channel conditions receive larger power fractions. The power fractions can be determined based on the channel gains between the users and the base station[47].

In this thesis, wherever Fixed Power Allocation is employed, it refers to Fractional Power Allocation.

2.2.6.2. DYNAMIC POWER ALLOCATION

Dynamic power allocation schemes in NOMA, adaptively allocate power to users based on varying channel conditions, user requirements, or optimization objectives. These dynamic schemes aim to maximize system performance, enhance spectral efficiency and provide better fairness among users. Therefore, dynamic power allocation schemes offer advantages in terms of adaptability to changing network conditions, user needs like target throughput, and optimization objectives[48]. By adjusting power levels based on real-time information, these schemes can optimize resource allocation, improve system capacity, and enhance overall performance in wireless communication systems. However, dynamic power

allocation schemes typically require accurate real-time channel state information (CSI), which may be obtained through channel estimation or feedback mechanisms. They also involve more complex algorithms and computational overhead compared to fixed power allocation schemes. The choice of a specific dynamic power allocation scheme depends on the specific system requirements, network conditions, available CSI, and optimization objectives[49].

2.2.6.2.1. CONSTRAINED OPTIMIZATION POWER ALLOCATION

Constrained Optimization Power Allocation (COPA) is a dynamic power allocation mechanism whose goal is to maximize the sum capacity of the system under a fairness constraint for the PD-NOMA system[50]. The fairness factor indicates how fairly the system capacity has been shared among the users. The Fairness Factor (FF) is given by:

$$FF = \frac{(\sum R_i)^2}{K\sum {R_i}^2} \tag{2.19}$$

where, K is the total number of users in the system; and,

R_i is the throughput of the i^{th} user.

The constrained optimization problem statement is defined as:

maximize $R_S = \sum_{i=1}^{K} R_i$, (2.20)

subject to the following constraints:

$$\sum_{i=1}^{K} P_i \leq P_t \tag{2.21}$$

$$P_i \geq 0, \forall i \tag{2.22}$$

$$FF \geq F_T \tag{2.23}$$

where, P_t is the total transmission power;

P_i is the power allocated to the i^{th} user; and

F_T is the target Fairness Factor of the system.

The optimum power allocation coefficients α_i for each user is obtained through an exhaustive and iterative search. The algorithm which describes the technique for optimizing the power allocation coefficients is given in Table 2.1:

Table 2.1: Algorithm for Constrained Optimization Power Allocation (COPA)

```
Initialization
Initialize power_coefficient_matrix including all possible values
Set maximum_capacity to zero
for i in power_coefficient_matrix do
    calculate sum_capacity
    calculate   fairness_factor
    if   fairness_factor > target_fairness_factor
       if sum_capacity(i) >= maximum_capacity
            maximum_capacity = sum_capacity (i)
            set required_set to power_coefficient_matrix
         end if
    end if
end for
```

2.2.6.2.2. CONVEX OPTIMIZATION POWER ALLOCATION

Convex Optimization Power Allocation (CON-OPA) is a dynamic power allocation mechanism whose goal is to determine the optimal power allocation coefficients for all the users in the system while maximizing the sum capacity of the PD-NOMA system. The power allocation problem can be formulated as follows[51]:

$$\text{maximize} \quad \sum_{i=1}^{K} R_i = \sum_{i=1}^{K} \log_2(1 + SINR_i) \tag{2.24}$$

such that,

$$S_1 : P_i \geq 0, \ \forall i \tag{2.25}$$

$$S_2 : \sum_{i=1}^{K} P_i \leq P_t \tag{2.26}$$

$$S_3 : R_i \geq R_{i_{min}}, \forall i \tag{2.27}$$

where, K is the total number of users in the system;

R_i is the throughput of the i^{th} user;

P_t is the total transmission power;

P_i is the power allocated to the i^{th} user; and

$R_{i_{min}}$ is the minimum throughput for the i^{th} user.

The constraints S_1, S_2 and S_3 indicate that non-negative power is allocated to each user; the transmitted power cannot exceed the maximum total transmission power; and that each user should get a minimum data rate of $R_{i_{min}}$, respectively.

Since, the constraint S_3 is non-linear, hence it can be converted into a linear case as follows:

$$S_3 : |H_i^H|^2 P_i - \rho \left|H_i^H\right|^2 \sum_{l=1}^{i-1} P_l \geq \varphi, \ \forall i \tag{2.28}$$

where, $\varphi = \rho\sigma^2$

$\rho = 2^{R_{i_{min}}} - 1$ and,

σ^2 is the variance of zero mean complex Additive White Gaussian Noise (AWGN).

Also, the objective function is non-convex, which makes it difficult to acquire the closed-form expression. Therefore, using Sherman-Morrison-Woodbury formula, the objective function can be expressed as a convex function as follows:

$$\text{maximize} \quad \sum_{i=1}^{K} \left(-\log_2 \left(\frac{\tau_i}{\tau_i + |H_i{}^H|^2 P_i} \right) \right) \tag{2.29}$$

$$\text{where,} \quad \tau_i = |H_i{}^H|^2 \sum_{l=1}^{i-1} P_l + \sigma^2$$

subject to the constraints S_1, S_2 and S_3.

As the objective function is convex, hence every local minimum will be a global minimum and if it is strictly convex, then the problem has atmost one optimal solution. Thus, the obtained P_i , using Lagrange multiplier method and Karush-Kuhn-Tucher (KKT) conditions[52], will be an optimal solution.

The algorithm describing the technique for determining the optimal power allocation coefficients is given in the following Table 2.2:

Table 2.2: Algorithm for Convex Optimization Power Allocation (CON-OPA)

Initialization

Set K to total number of users in the system;

Set P_t *to total transmission power of the system;*

Set $R_{i_{min}}$ *to the desired minimum throughput value for all the users respectively;*

Set i to one;

Set maximum_iteration to a suitable value;

Initialize power_coefficient_set to zero;

Determine H_i *for all the users respectively;*

for i *<=* ***K***

Set v to zero;

for ***v*** *<* ***maximum iteration***

calculate $\rho = 2^{R_{i_{min}}} - 1$

calculate λ *from* $\lambda(\sum_{i=1}^{K} P_i - P_t) = 0$

calculate Ω_i *from* $\Omega_i \epsilon_i = 0 \,, \forall i$

where, $\epsilon_i = \rho \left|H_i^{\,H}\right|^2 \sum_{l=1}^{i-1} P_l - \left|H_i^{\,H}\right|^2 P_i + \varphi$

calculate $P_i = \frac{|H_i^{\,H}|^2 - \tau_i \mu}{|H_i^{\,H}|^2 \mu}$

where,

$\tau_i = |H_i^{\,H}|^2 \sum_{l=1}^{i-1} P_l + \sigma^2$ *and,*

$$\mu = \lambda - \Omega_i \left|H_i^{\,H}\right|^2 + \sum_{l=i+1}^{K} \Omega_l \rho \left|H_i^{\,H}\right|^2 , \lambda \geq 0, \Omega_i \geq 0$$

end inner for loop

$power\_coefficient\_set(i) = P_i / P_t$

end outer for loop

2.2.7. MATHEMATICAL MODEL

In accordance to the system models defined in Section 2.2.1, the mathematical model is also segregated into two cases. The first case pertains to a generic downlink MU-MIMO-PD-NOMA system, without any kind of clustering, wherein all the users in the system take part in the same NOMA scheme. The second case is concerned with user clustering in a downlink MU-MIMO-PD-NOMA environment, in which each cluster employs NOMA separately, i.e., only among the users of the respective cluster.

CASE I:

The general expression for the signals transmitted by the BS, in a downlink MU-MIMO-PD-NOMA system, is given as follows:

$$x = \begin{cases} \widetilde{w}\,, & when\ no\ precoding\ is\ employed \\ P\tilde{s}\,, & when\ precoding\ is\ employed \end{cases} \tag{2.30}$$

where, $\widetilde{w}$ and $\tilde{s}$ are (Mx1) vectors, each containing M copies of the superposed signal s; and,

P is a (MxM) precoding matrix that depends on the applied precoding scheme.

The superposed signal is given as follows:

$$s = \sum_{i=1}^{K} \sqrt{P_t \alpha_i} m_i \tag{2.31}$$

where, m_i is the information signal for the i^{th} UE with unit energy;

P_t is the overall transmission power at the BS; and,

α_i is the power coefficient allocated to the i^{th} UE, subjected to the following condition:

$$\sum_{i=1}^{K} \alpha_i = 1 \tag{2.32}$$

and $\alpha_1 \leq \alpha_2 \leq \cdots \leq \alpha_K$, since without loss of generality, as per NOMA principle, the effective channel gains have been assumed to be in the following order:

$$|z_1 H_1 p_1|^2 \geq |z_2 H_2 p_2|^2 \geq \cdots \geq |z_K H_K p_K|^2 \tag{2.33}$$

where, p_i and z_i are precoding and post-coding vectors respectively, that depend on the employed precoding scheme and $|z_i p_i| = 1$, when no precoding is employed; and,

H_i is a $(N\text{x}M)$ Rayleigh fading channel coefficient matrix from the BS to the i^{th} UE .

The general expression for the received signal at the i^{th} UE, is as follows:

$$r_i = H_i x + g_i \tag{2.34}$$

where, g_i is a $(N\text{x}1)$ zero mean AWGN vector with a variance of ${\sigma_n}^2$.

After applying the post-coding vector, if required as per the applied precoding scheme, the modified received signal can be written as follows:

$$y_i = z_i H_i x + z_i g_i \tag{2.35}$$

The Signal to Interference-Noise Ratio (SINR) at the i^{th} UE, except the 1^{st} UE, can be expressed as follows[53]:

$$SINR_i = \frac{\alpha_i \gamma |z_i H_i p_i|^2}{\gamma |z_i H_i p_i|^2 \sum_{q=1}^{i-1} \alpha_q + 1}, \forall i \neq 1 \tag{2.36}$$

The Signal to Interference-Noise Ratio (SINR) at the 1^{st} UE is as follows[53]:

$$SINR_1 = \alpha_1 \gamma |z_1 H_1 p_1|^2 \tag{2.37}$$

where, $\gamma = P_t/{\sigma_n}^2$, represents the transmit Signal to Noise Ratio (SNR).

The Throughput of the i^{th} UE in Downlink MU-MIMO-PD-NOMA system is given as follows:

$$R_i = B \log_2(1 + SINR_i) \tag{2.38}$$

where, B is the available transmission bandwidth.

Thus, the Sum Capacity of Downlink MU-MIMO-PD-NOMA system can be expressed as follows:

$$R_S = \sum_{i=1}^{K} R_i \tag{2.39}$$

CASE II:

The general expression for the signals transmitted by the BS to the M clusters, in a downlink MU-MIMO-PD-NOMA system, is given as follows [54]:

$$x = P\tilde{s} \tag{2.40}$$

where, P is a $(M\text{x}M)$ precoding matrix that depends on the applied precoding scheme; and,

$\tilde{s}$ is a $(M\text{x}1)$ vector containing M superposed signals as follows:

$$\tilde{s} = \begin{bmatrix} \sqrt{P_t \alpha_{1,1}} s_{1,1} + \cdots + \sqrt{P_t \alpha_{1,B}} s_{1,B} \\ \vdots \\ \sqrt{P_t \alpha_{M,1}} s_{M,1} + \cdots + \sqrt{P_t \alpha_{M,B}} s_{M,B} \end{bmatrix} \triangleq \begin{bmatrix} \widetilde{s_1} \\ \vdots \\ \widetilde{s_M} \end{bmatrix} \tag{2.41}$$

where, $s_{i,j}$ denotes the information signal to be transmitted to the j^{th} UE in the i^{th} cluster, with normalized signal power, i.e., $E\{|s_{i,j}|^2\} = 1$;

P_t is the overall transmission power at the BS; and,

$\alpha_{i,j}$ is the NOMA power coefficient allocated to the j^{th} UE in the i^{th} cluster, subjected to the following condition:

$$\sum_{j=1}^{B} \alpha_{i,j} = 1 \tag{2.42}$$

and $\alpha_{i,1} \leq \alpha_{i,2} \leq \cdots \leq \alpha_{i,B}$, since without loss of generality, as per NOMA principle, the effective channel gains have been assumed to be in the following order:

$$|z_{i,1} H_{i,1} p_{i,1}|^2 \geq \left|z_{i,2} H_{i,2} p_{i,2}\right|^2 \geq \cdots \geq \left|z_{i,B} H_{i,B} p_{i,B}\right|^2 \tag{2.43}$$

where, $p_{i,j}$ and $z_{i,j}$ are precoding and post-coding vectors respectively, that depend on the employed precoding scheme; and,

$H_{i,j}$ is a $(N\text{x}M)$ Rayleigh fading channel coefficient matrix from the BS to the

j^{th} UE in the i^{th} cluster.

The general expression for the received signal at the j^{th} UE, in the i^{th} cluster, is as follows:

$$r_{i,j} = H_{i,j}x + g_{i,j} \tag{2.44}$$

where, $g_{i,j}$ is a $(N\text{x}1)$ zero mean AWGN vector with a variance of ${\sigma_n}^2$.

After applying the post-coding vector, if required as per the applied precoding scheme, the modified received signal can be written as follows:

$$y_{i,j} = z_{i,j}H_{i,j}x + z_{i,j}g_{i,j} \tag{2.45}$$

The Signal to Interference-Noise Ratio (SINR) at the j^{th} UE, except the 1^{st} UE, in the i^{th} cluster, can be expressed as follows:

$$SINR_{i,j} = \frac{\alpha_{i,j}\gamma|z_{i,j}H_{i,j}p_{i,j}|^2}{\gamma|z_{i,j}H_{i,j}p_{i,j}|^2 \sum_{q=1}^{j-1}\alpha_{i,q}+1}, \forall j \neq 1 \tag{2.46}$$

The Signal to Interference-Noise Ratio (SINR) at the 1^{st} UE, in the i^{th} cluster, is as follows:

$$SINR_{i,1} = \alpha_{i,1}\gamma|z_{i,1}H_{i,1}p_{i,1}|^2 \tag{2.47}$$

where, $\gamma = P_t/{\sigma_n}^2$, represents the transmit Signal to Noise Ratio (SNR).

The Throughput of the j^{th} UE, in the i^{th} cluster, in Downlink MU-MIMO-PD-NOMA system is given as follows:

$$R_{i,j} = B\log_2(1 + SINR_{i,j}) \tag{2.48}$$

where, B is the available transmission bandwidth.

Therefore, the Sum Capacity of the i^{th} cluster in the Downlink MU-MIMO-PD-NOMA system can be expressed as follows:

$$R_{S_i} = \sum_{j=1}^{B} R_{i,j} \quad (2.49)$$

Thus, the Spectral Efficiency of the i^{th} cluster in the Downlink MU-MIMO-PD-NOMA system is given as follows:

$$SE_i = \frac{R_{S_i}}{B} \quad (2.50)$$

2.3. CLUSTERING METHODOLOGIES

Clustering in wireless communication refers to the grouping or partitioning of wireless devices or users into clusters or subgroups based on certain criteria. The purpose of clustering is to improve the efficiency, performance, and management of wireless communication systems by optimizing resource allocation, mitigating interference, enhancing spectral and energy efficiency, and supporting scalability and mobility. Clustering can be applied in various wireless communication scenarios, including ad hoc networks, sensor networks, cellular networks, and cognitive radio networks. The clustering algorithm to be employed depends on the specific wireless communication scenario and system requirements[55].

The following sub-sections gives a brief outline of the clustering methodologies employed in the MU-MIMO-PD-NOMA system of this thesis.

2.3.1. RANDOM CLUSTERING

Random (RAN) clustering is a clustering technique used in wireless communication systems where the grouping of devices or users into clusters is done randomly without considering specific criteria or parameters. In random clustering, there is no predetermined rule or optimization objective guiding the cluster formation process[56]. Instead, devices are assigned to clusters based on a random selection or assignment mechanism. Random clustering can be employed in scenarios where there are no strict requirements for performance optimization or when the network dynamics and user distributions are highly unpredictable. It can serve as a simple approach for initial cluster formation, which can be followed by more sophisticated algorithms or protocols to refine the clustering or optimize the network performance further.

2.3.2. BEST-WITH-WORST CLUSTERING

Best-With-Worst (BWW) clustering technique is based on Channel State Sorting (CSS) algorithm [57] wherein all the users are arranged in descending order of their channel gains and divided into *K* groups, where *K* is the number of users required to be in a cluster. Thereafter users from each of the *K* groups are selected to form a cluster. Thus, this clustering methodology clusters/pairs a good channel-condition user with a poor channel-condition user. The algorithm for best-with-worst clustering mechanism is depicted in the following flowchart:

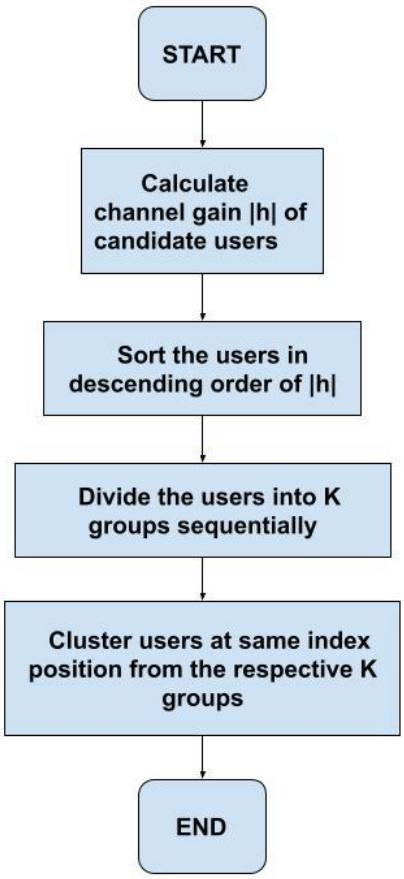

Fig.2.3: FLOWCHART FOR BEST-WITH-WORST CLUSTERING

2.3.3. BEST-WITH-BEST CLUSTERING

Best-With-Best (BWB) clustering technique is a user-grouping mechanism wherein all the users are arranged in descending order of their channel gains and

thereafter each user is clustered/paired with its *K* adjacent users, where *K* is the number of users required to be in a cluster[58]. Therefore, this clustering methodology clusters/pairs users having adjacent channel-conditions. The algorithm for best-with-best clustering mechanism is portrayed in the following flowchart:

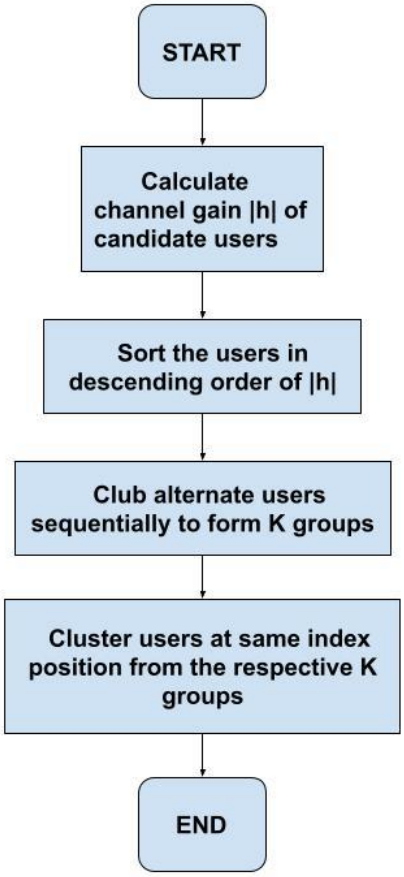

Fig.2.4: FLOWCHART FOR BEST-WITH-BEST CLUSTERING

2.4. DIGITAL MODULATION SCHEMES

Modern mobile communication systems use digital modulation techniques as advancements in Very Large-Scale Integration (VLSI) and Digital Signal Processing (DSP) technology have made digital modulation more cost effective than analog transmission systems. Digital modulation offers many advantages over its analog counterpart, such as greater noise immunity, robustness to channel impairments,

easier multiplexing of various forms of information (like voice, data and video) and greater security. Also, digital transmissions accommodate digital error-control codes which detect and/or correct transmission errors and support complex signal conditioning and processing techniques like source coding, encryption and equalization to improve the performance of the overall communication link. In digital wireless communication systems, the modulating signal (i.e., the message) may be represented as a time sequence of symbols or pulses, where each symbol has *m* finite states and represents *n* bits of information, where $n = \log_2 m$ bits/symbol. The choice of a digital modulation scheme is influenced by several factors. A desirable modulation scheme provides low bit error rates at low received signal-to-noise ratios, performs well in multipath and fading conditions, occupies a minimum of bandwidth and is easy and cost-effective to implement [59].

The following sub-sections give a brief description of the linear modulation schemes that are used in this thesis.

2.4.1. BINARY PHASE SHIFT KEYING (BPSK)

In binary phase shift keying (BPSK), the phase of a constant amplitude carrier signal is switched between two values according to the two possible signals m_1 and m_2 corresponding to binary 1 and 0, respectively. In general, the two phases are separated by 180°. If the sinusoidal carrier has an amplitude A_c, energy per bit $E_b = \frac{1}{2}{A_c}^2 T_b$ and m_1 and m_2 are generalized as a binary data signal $m(t)$, which takes one of two possible pulse shapes, then the transmitted BPSK signal may be represented as follows [26]:

$$S_{BPSK}(t) = m(t)\sqrt{\frac{2E_b}{T_b}}\cos(2\pi f_c t + \theta_c), \quad 0 \le t \le T_b \qquad (2.51)$$

where, $m(t) = \begin{cases} 1, & for\ binary\ 1 \\ -1, & for\ binary\ 0 \end{cases}$

and T_b is the bit duration.

The BPSK signal is equivalent to a double sideband suppressed carrier amplitude

modulated waveform, where $\cos(2\pi f_c t)$ is applied as the carrier and the data signal $m(t)$ is applied as the modulating waveform. The probability of bit error in BPSK, for an Additive White Gaussian Noise (AWGN) channel, with a noise spectral density N_0, is given as follows:

$$P_{e,\ BPSK} = Q\left(\sqrt{\frac{2E_b}{N_0}}\right) \tag{2.52}$$

2.4.2. QUADRATURE PHASE SHIFT KEYING (QPSK)

In quadrature phase shift keying (QPSK), two bits are transmitted in a single modulation symbol and hence, it has twice the bandwidth efficiency of BPSK. The phase of the carrier takes on one of four equally space values, such as $0, \pi/2, \pi, 3\pi/2$, where each value of phase corresponds to a unique pair of message bits. The QPSK signal for this set of symbol states may be defined as follows [26]:

$$S_{QPSK}(t) = \sqrt{\frac{2E_s}{T_s}}\cos\left[2\pi f_c t + (i-1)\frac{\pi}{2}\right],\ \ 0 \le t \le T_s\ ,\ i = 1,2,3,4. \tag{2.53}$$

where, T_s is the symbol duration and is equal to twice the bit period.

The probability of bit error in QPSK, for an AWGN channel is given as follows:

$$P_{e,\ QPSK} = Q\left(\sqrt{\frac{2E_b}{N_0}}\right) \tag{2.54}$$

2.5. PERFORMANCE ANALYSIS PARAMETERS

Performance analysis parameters in wireless communication systems are used to assess and evaluate the quality, efficiency, and reliability of the communication link. These parameters provide insights into the system's performance and help in optimizing network design, resource allocation, and overall system performance. They are typically measured, monitored, and analysed during network planning, deployment, and operation to assess the performance of wireless communication systems. They help in identifying bottlenecks, optimizing system parameters, and ensuring efficient and reliable communication[60].

The following sub-sections give an insight into the performance analysis parameters that have been explored in this thesis.

2.5.1. BIT ERROR RATE

Bit Error Rate (BER) measures the percentage of bits received incorrectly or corrupted during transmission. It is unitless and is an essential parameter for evaluating the reliability of the communication link. A lower BER indicates better transmission quality and error performance. The BER is defined as the following ratio[61]:

$$BER = \frac{Number\ of\ erroneous\ bits\ received}{Total\ number\ of\ bits\ transmitted} \tag{2.55}$$

2.5.2. SUM CAPACITY

Sum Capacity is the sum of the throughputs delivered to all the users in the system. Throughput refers to the amount of data successfully transmitted over a wireless link within a given time period. Both Sum Capacity and Throughput are crucial parameters in assessing the system's spectral efficiency. Throughput is usually measured in bits per second (bits/s or bps) and hence, even Sum Capacity holds the same unit. The general expression for Sum Capacity is as follows[62,63]:

$$Sum\ Capacity = \sum_{j=1}^{Q} R_j \tag{2.56}$$

where, Q is the total number of users in the system,

R_j is the throughput of the j^{th} user in the system.

2.5.3. SPECTRAL EFFICIENCY

Spectral Efficiency (SE) or Bandwidth Efficiency describes the ability of a modulation scheme to accommodate data within a limited bandwidth. It measures the amount of information or data that can be transmitted over a given bandwidth. It, therefore, indicates how efficiently the allocated bandwidth is utilized. The unit of SE is bps/Hz. SE is numerically defined as follows[64]:

$$SE = \frac{R}{B} \tag{2.57}$$

where, R is the throughput in bps,

B is the bandwidth in Hz.

2.5.4. CONSTELLATION DIAGRAM

A constellation diagram is a graphical representation of a digital modulation scheme that shows the complex symbols used to transmit digital data. It provides a visual depiction of the constellation points in the signal space, where each point represents a unique symbol or signal state. In a constellation diagram, the x-axis typically represents the real component (in-phase) of the signal, while the y-axis represents the imaginary component (quadrature) of the signal. Each point in the diagram represents a specific symbol or data value encoded in the modulation scheme. The arrangement and distribution of these points in the diagram reflect the modulation scheme being used. Different modulation schemes have distinct constellation patterns. By examining the constellation diagram, one can gain insights into the properties of the modulation scheme, such as the number of distinguishable symbols, the distance between adjacent symbols, and the susceptibility to noise and interference. The distance between constellation points determines the robustness of the modulation scheme; with larger distances providing better noise immunity. Thus, the constellation diagram is a useful tool for analysing and troubleshooting wireless communication systems. It helps in evaluating the quality of received signals, identifying transmission errors, and optimizing system performance. Additionally, it aids in the design and implementation of demodulation algorithms for signal recovery at the receiver end[65].

2.6. CONCLUSION

This chapter provides a brief insight into the fundamental topics related to MIMO, NOMA, algorithms of conventional clustering methodologies, different kinds of digital modulation schemes as well as the performance analysis parameters that are analysed throughout this thesis. It also showcases the system models and their respective mathematical descriptions that have been used in the following chapters for the performance analysis of the MIMO-NOMA system.

Chapter 3 EXPLORATION OF MU-MIMO-PD-NOMA FOR VARIED COMBINATION OF ANTENNA DIVERSITY TECHNIQUES

3.1. ABSTRACT

Diversity techniques are a fundamental asset of MIMO technology and hence, have become integral to wireless communication systems as they mitigate the effects of fading, enhance signal quality, and improve overall system performance. Therefore, diversity techniques are applied to MIMO-NOMA systems so that the benefits offered by these techniques can be experienced by the users sharing the resources through NOMA principle. This chapter provides a detailed performance analysis, with respect to system Bit Error Rate (BER) and Sum Capacity, of a downlink MIMO-PD-NOMA system for a two-user model, considering varied combination of antenna diversity techniques like TAS-RAS, TAS-MRC, MRT-RAS and MRT-MRC respectively. In order to employ the NOMA principle, the total transmission power needs to be judiciously distributed among the users and hence, different kinds of power allocation strategies are explored to determine the optimum power allocation technique for such a scenario. The power allocation strategies used are fixed power allocation (FPA) and dynamic power allocation using constrained optimization (COPA) and convex optimization (CON-OPA) algorithms respectively. The entire analysis is carried out under different modulation schemes to showcase the effect on system BER of the MU-MIMO-PD-NOMA system.

3.2. SYSTEM MODEL

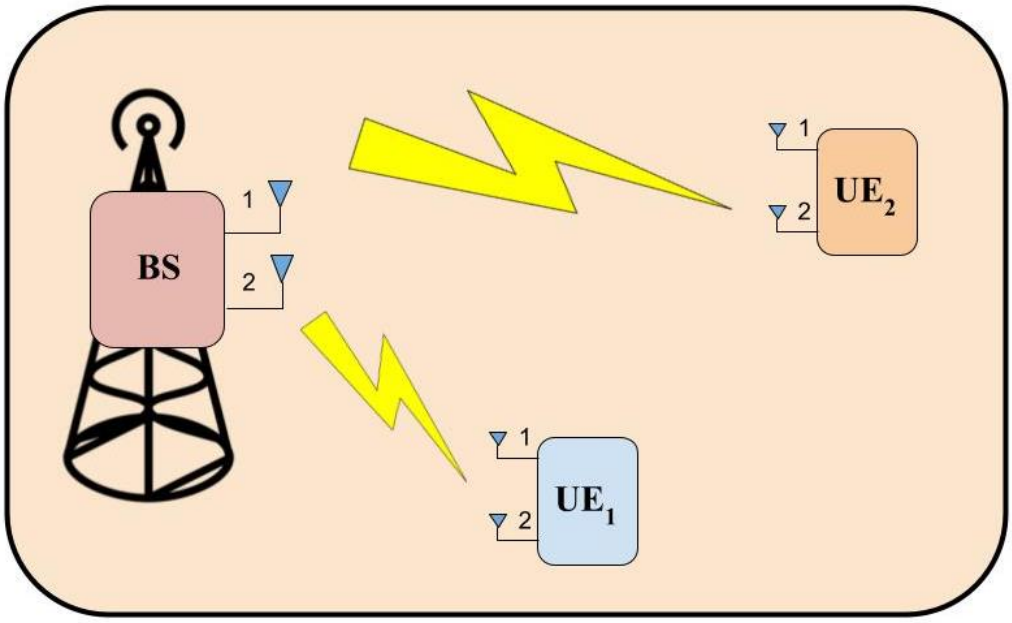

Fig.3.1: DOWNLINK TWO-USER (2x2)-MIMO-PD-NOMA MODEL

Fig.3.1 represents a two-user MIMO-PD-NOMA system in a single-cell downlink communication scenario, wherein a single base station (BS), equipped with *M=2* antennas, communicates with *K=2* user equipments (UE_i), equipped with *N=2* antennas each, where $i \in \{1,2\}$. The UE_1 is situated at the smallest distance from the BS, whereas UE_2 is located at the farthest distance from the BS. Each UE has a maximum of (2x2) communication channel paths between the BS and itself. It is assumed that the total transmitter power is P_t and the wireless links experience independent and identically distributed (i.i.d.) Rayleigh fading with Additive White Gaussian Noise (AWGN). The effective channel gains of the UEs are sorted as: $|H_1|^2 \geq |H_2|^2$, wherein H_i indicates the Rayleigh fading channel matrix from the BS to the i^{th} UE. Therefore, UE_1 has the highest channel gain and is hence referred to as the strong user while the other user is labelled as weak user. At the BS, as per the NOMA principle, the signals for the different users are allocated different fraction of the total power and thereafter superposed to be transmitted over the same channel. The strong user is given the least fraction of power compared to the weak user. Hence, the power allocation order of the UEs is as follows: $P_1 < P_2$. The superposed signal is thereafter transmitted through the M antennas of the BS, as per the respective employed transmit diversity technique. At the receiving end, each UE

receives the transmitted signal, through its N antennas, corresponding to the applied receiver diversity scheme. After that, UE_1 performs SIC to decode and subtract out the information signal intended for UE_2 ; while UE_2 applies direct decoding to its respective resultant received signal.

3.3. PERFORMANCE ANALYSIS OF SIMULATION MODEL

In the following sub-sections, an extensive analysis of simulation results, with respect to system BER and Sum Capacity, of downlink two-user MIMO-PD-NOMA model have been presented for different combination of antenna diversity techniques and varied power allocation strategies. The power allocation strategies employed are fixed power allocation (FPA), constrained optimization power allocation (COPA) and convex optimization power allocation (CON-OPA) mechanisms respectively. The simulation is conducted using MATLAB software. Each simulation is performed multiple times, and their ensemble average is considered to account for the various characteristics of the fading environment. The different combination of transmit and receiver antenna diversity techniques that have been analyzed in the aforementioned system are as follows:

1. Transmit Antenna Selection (TAS) – Receiver Antenna Selection (RAS)
2. Transmit Antenna Selection (TAS) – Maximal Ratio Combining (MRC)
3. Maximal Ratio Transmission (MRT)–Receiver Antenna Selection (RAS)
4. Maximal Ratio Transmission (MRT)–Maximal Ratio Combining (MRC)

All the analysis regarding system BER and Sum Capacity have been made considering three types of modulation schemes, under Rayleigh fading channel, as follows:

a) BPSK modulation scheme for both near and far user
b) QPSK modulation scheme for both near and far user
c) QPSK modulation for near user and BPSK for far user, i.e., an Adaptive Modulation scheme

The parameters used for simulation in MATLAB, considering downlink two-user (2x2)-MIMO-PD-NOMA model are enlisted in the following Table 3.1:

Table 3.1: Simulation Parameters for Downlink (2x2)-MIMO-PD-NOMA Model

PARAMETERS	VALUES
Transmitter Power	5 Watt
Number of Transmitter Antenna at the Base Station	2
Number of Receiver Antenna per User Equipment (UE_i)	2
Power Allocation Coefficient for near user (UE_1), when employing FPA	0.2
Power Allocation Coefficient for far user (UE_2), when employing FPA	0.8
Target Fairness Factor, when employing COPA	0.7
Bandwidth	80 MHz

3.3.1. Simulation Result Analysis of two-user MIMO-PD-NOMA model for different combination of antenna diversity techniques using varied modulation schemes and FPA mechanism:

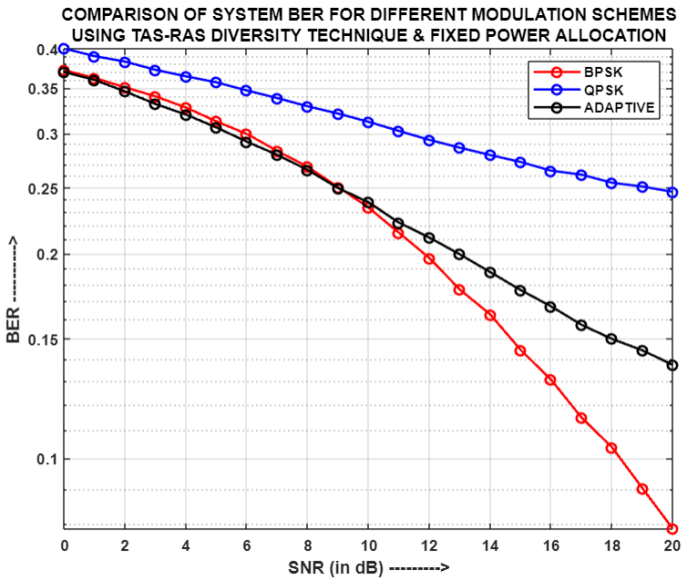

Fig.3.2: Comparison of System BER for different modulation schemes using TAS-RAS and FPA

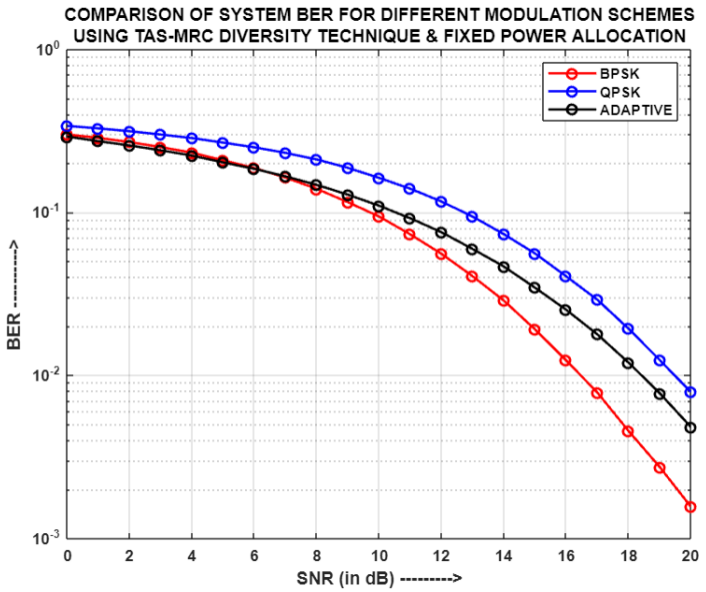

Fig.3.3: Comparison of System BER for different modulation schemes using TAS-MRC and FPA

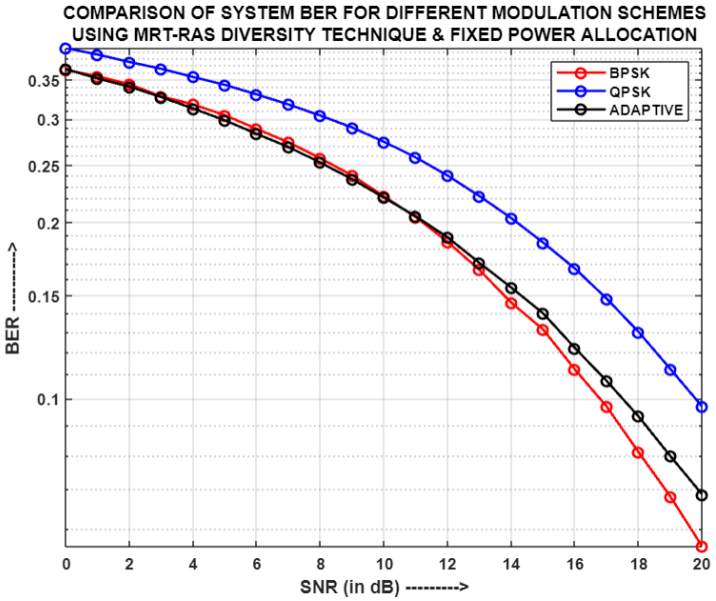

Fig.3.4: Comparison of System BER for different modulation schemes using MRT-RAS and FPA

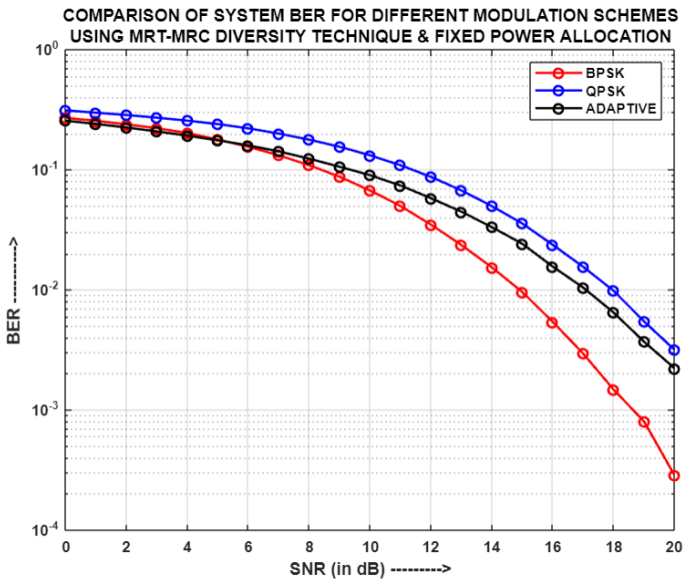

Fig.3.5: Comparison of System BER for different modulation schemes using MRT-MRC and FPA

Fig.3.2, Fig.3.3, Fig.3.4 and Fig.3.5 depicts the comparison of system BER for different modulation schemes using TAS-RAS, TAS-MRC, MRT-RAS and MRT-MRC diversity mechanisms respectively, and fixed power allocation (FPA). It is observed that for all the four pairs of transmit-receive diversity combinations, Adaptive modulation scheme produces a BER that lies in between that of BPSK and QPSK, while the least and highest BER are produced by BPSK and QPSK respectively. This is so because in case of BPSK each transmitted symbol contains a single bit, whereby at the receiver only one bit can be erroneous at a time which reduces the chance of higher bit error probability compared to that of QPSK, wherein two bits are transmitted at a time, thereby indicating a higher chance of bit error probability at the receiver. As Adaptive modulation is a mixture of BPSK and QPSK, therefore its performance lies in the middle of the two, implying that for the aforementioned scenario and FPA, although its BER is good enough but it neither surpasses the BER of BPSK nor is above the BER of QPSK.

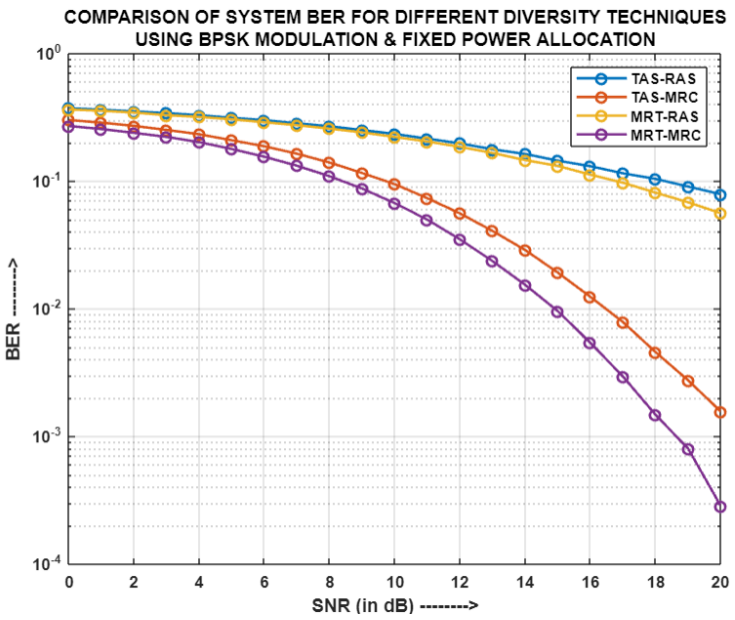

Fig.3.6: Comparison of System BER for different diversity techniques using BPSK and FPA

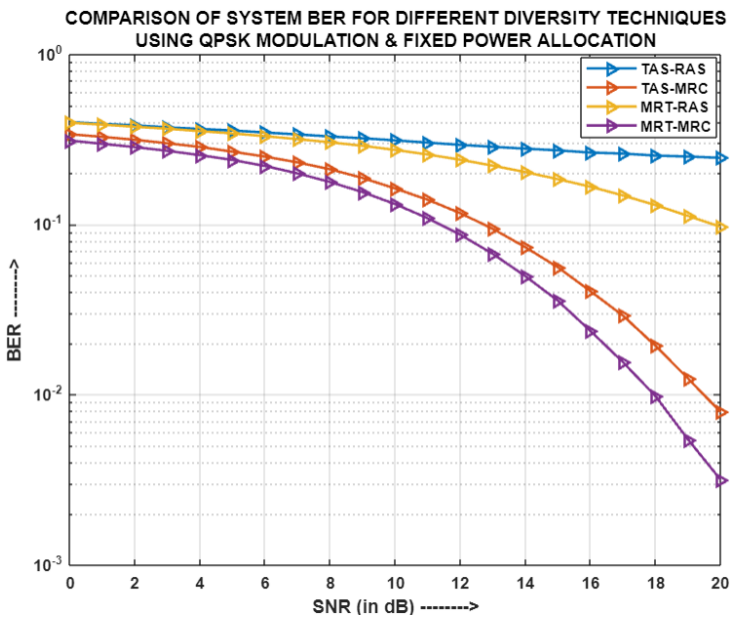

Fig.3.7: Comparison of System BER for different diversity techniques using QPSK and FPA

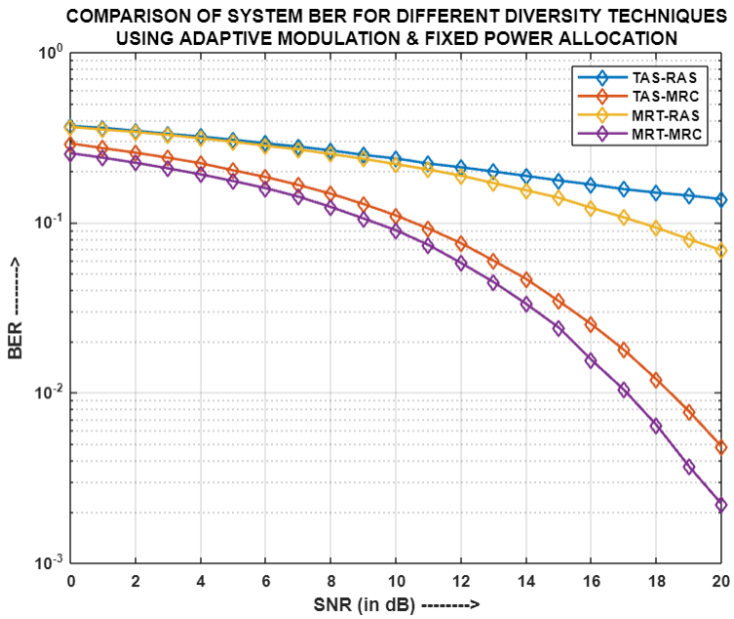

Fig.3.8: Comparison of System BER for different diversity techniques using Adaptive Modulation and FPA

Fig.3.6, Fig.3.7 and Fig.3.8 portrays the comparison of system BER for the four pairs of diversity combinations using BPSK, QPSK and Adaptive modulations respectively, and FPA. It can be seen that for all the three kinds of modulation schemes, MRT-MRC produces the least system BER followed by TAS-MRC, MRT-RAS and TAS-RAS, respectively. This is so because both MRT-MRC and TAS-MRC employ MRC diversity at the receiver, which weights the received signals with certain parameters that are influenced from the channel characteristics and then combines all of them to generate a resultant signal which is used for the next stages of processing. MRT-MRC performs better than TAS-MRC because in the former multiple antennas transmit the same information signal whereas in the latter, only the selected antenna, out of the multiple antennas, is responsible for transmission. Thus, more the number of transmitting antennas involved in transmission, higher the chance of better signal reception at the receiver. On the contrary, MRT-RAS and TAS-RAS don't perform as good as the other two pairs of diversity combinations, because the former two pairs employ RAS receiver diversity scheme, wherein only one out of the many received signals is selected for further processing in the next stages. Also, the selected received signal is not weighted as per the channel characteristics, whereby its performance gets flawed. MRT-RAS still performs slightly better than TAS-RAS as in the former multiple antennas transmit a resultant

signal, obtained by weighting the information signal with the different channel path characteristics and combining them, whereby better form of the signal is received. However, in TAS-RAS, only the selected antenna transmits the information signal, without any kind of processing related to the channel characteristics, leading to unpredictable signal reception. Therefore, MRT-RAS gives better system BER results than TAS-RAS.

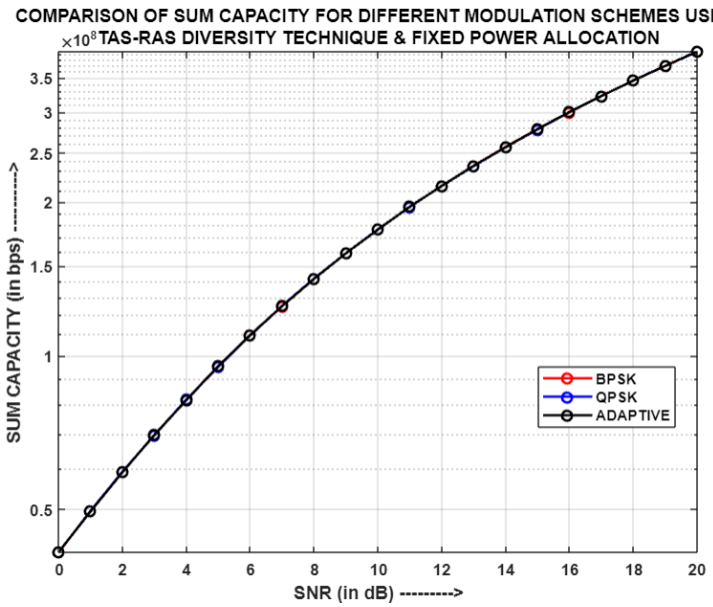

Fig.3.9: Comparison of Sum Capacity for different modulation schemes using TAS-RAS and FPA

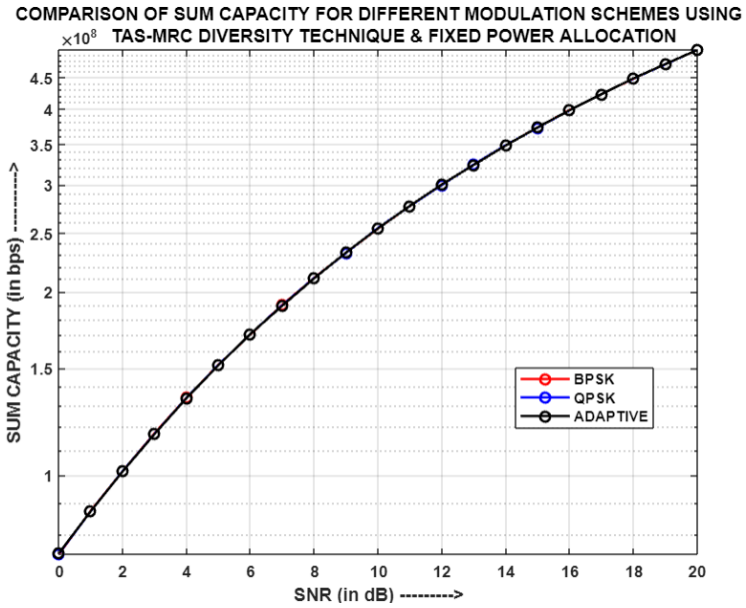

Fig.3.10: Comparison of Sum Capacity for different modulation schemes using TAS-MRC and FPA

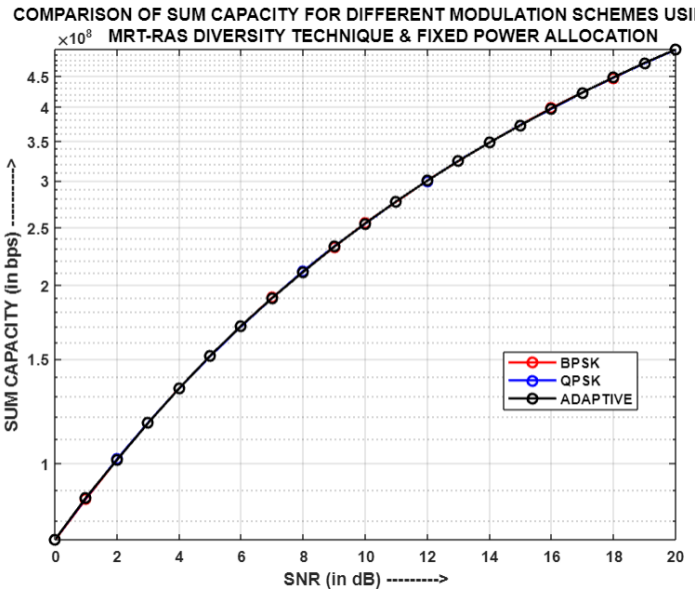

Fig.3.11: Comparison of Sum Capacity for different modulation schemes using MRT-RAS and FPA

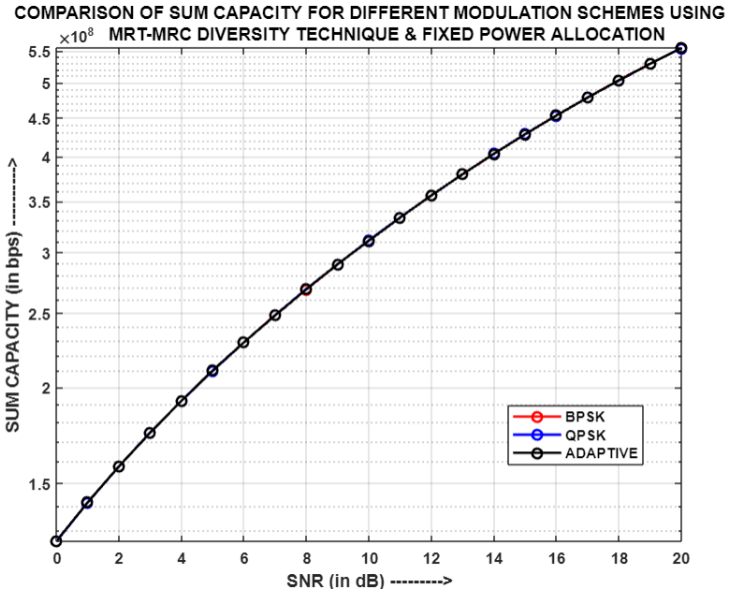

Fig.3.12: Comparison of Sum Capacity for different modulation schemes using MRT-MRC and FPA

Fig.3.9, Fig.3.10, Fig.3.11 and Fig.3.12 represent the comparison of Sum Capacity for different modulation schemes using TAS-RAS, TAS-MRC, MRT-RAS and MRT-MRC diversity mechanisms respectively, and fixed power allocation (FPA). It has been noticed that the sum capacities for BPSK, QPSK and Adaptive modulation schemes have merged for all the four pairs of diversity combinations because the sum capacity depends on the throughput of the two users in the system, which in turn mainly rely on the channel gain, noise power and power allocation coefficients respectively. Since, these above-mentioned parameters are mostly same for all the three modulation schemes, hence similar nature of sum capacities have been produced by the three modulation techniques.

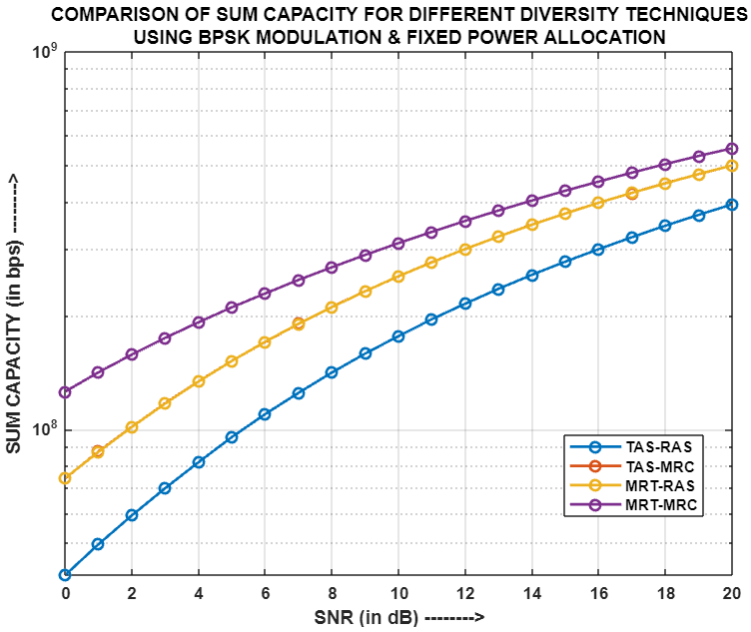

Fig.3.13: Comparison of Sum Capacity for different diversity techniques using BPSK and FPA

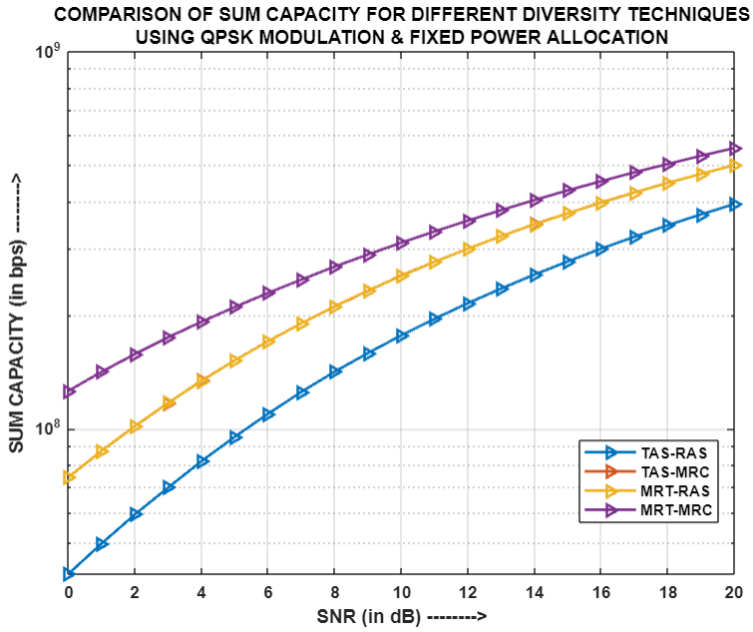

Fig.3.14: Comparison of Sum Capacity for different diversity techniques using QPSK and FPA

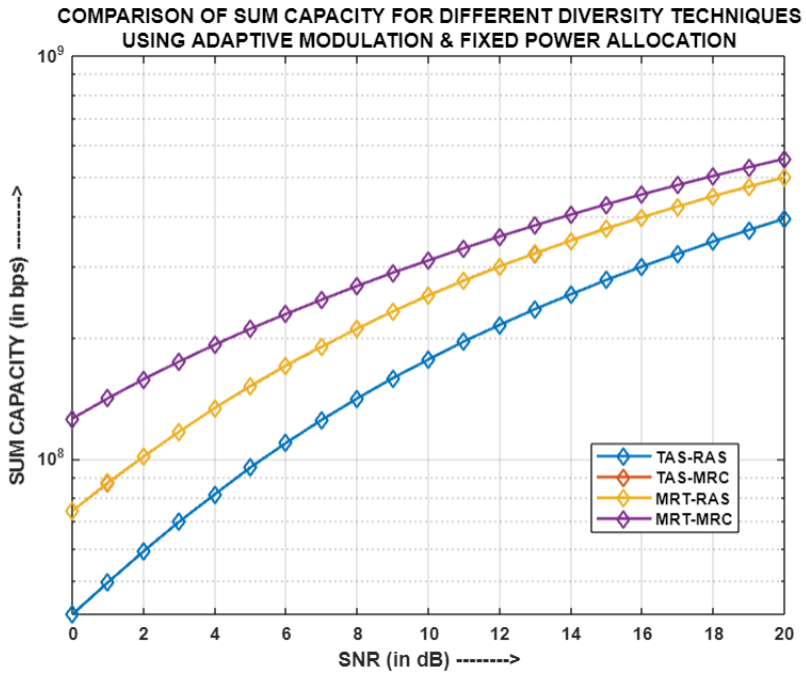

Fig.3.15: Comparison of Sum Capacity for different diversity techniques using Adaptive Modulation and FPA

Fig.3.13, Fig.3.14 and Fig.3.15 shows the comparison of Sum Capacity for the four pairs of diversity combinations using BPSK, QPSK and Adaptive modulations respectively, and FPA. It has been seen that MRT-MRC and TAS-RAS pairs offer the highest and the least sum capacity respectively. The sum capacities of TAS-MRC and MRT-RAS have merged and lie in the middle of the above two pairs. MRT-MRC produces the highest sum capacity because, in this system, it entails (2x2) number of channel paths for each user. The more the number of channel paths for transmission and reception, the higher will be the throughput per user, since the user receives data from multiple paths, and hence the sum capacity of the system will be enhanced. On the contrary, TAS-RAS provides (1x1) channel path for each user in this system, whereby it produces the least sum capacity, since each user receives data through a single path only. The sum capacities of TAS-MRC and MRT-RAS are same because both the diversity pairs transmit and receive information, to each user, through the same number of channel paths, i.e. (1x2) and (2x1) respectively. Therefore, due to the total number of channel paths involved in transmission and reception, TAS-MRC and MRT-RAS pairs have a higher sum capacity than TAS-RAS but a lower sum capacity than MRT-MRC.

3.3.2. Simulation Result Analysis of two-user MIMO-PD-NOMA model for different combination of antenna diversity techniques using varied modulation schemes and COPA mechanism:

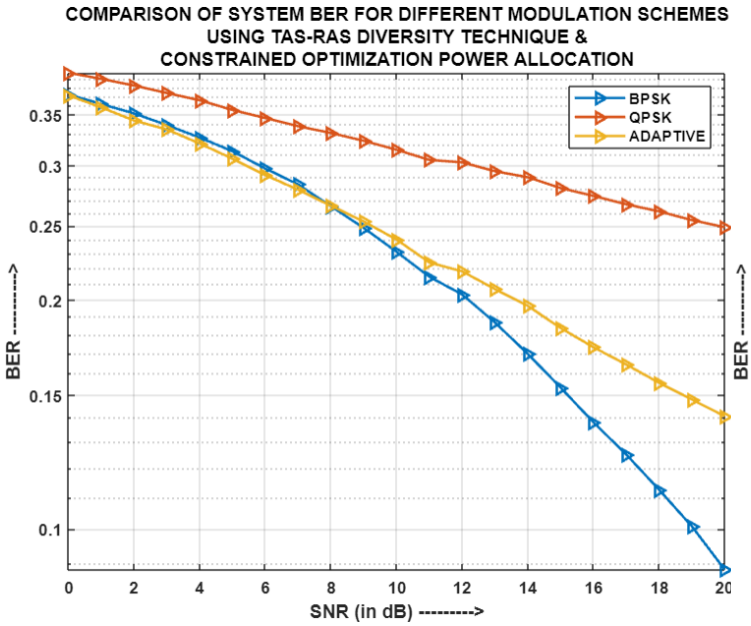

Fig.3.16: Comparison of System BER for different modulation schemes using TAS-RAS and COPA

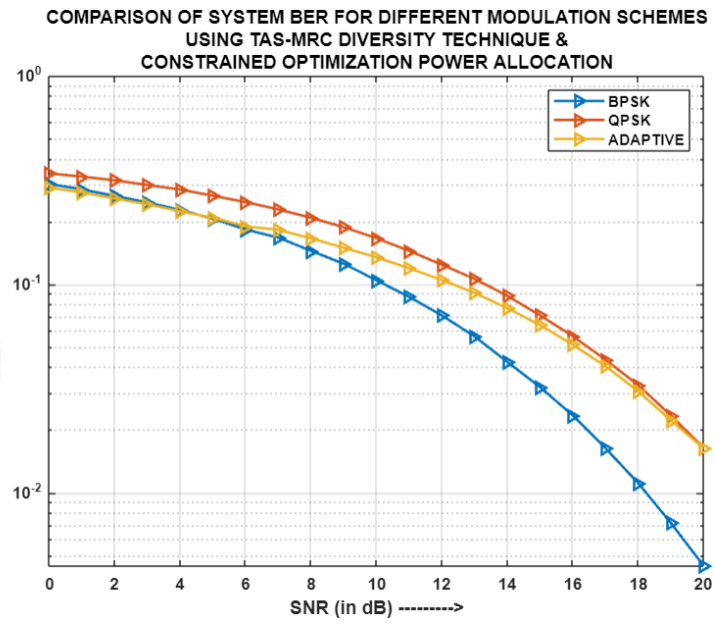

Fig.3.17: Comparison of System BER for different modulation schemes using TAS-MRC and COPA

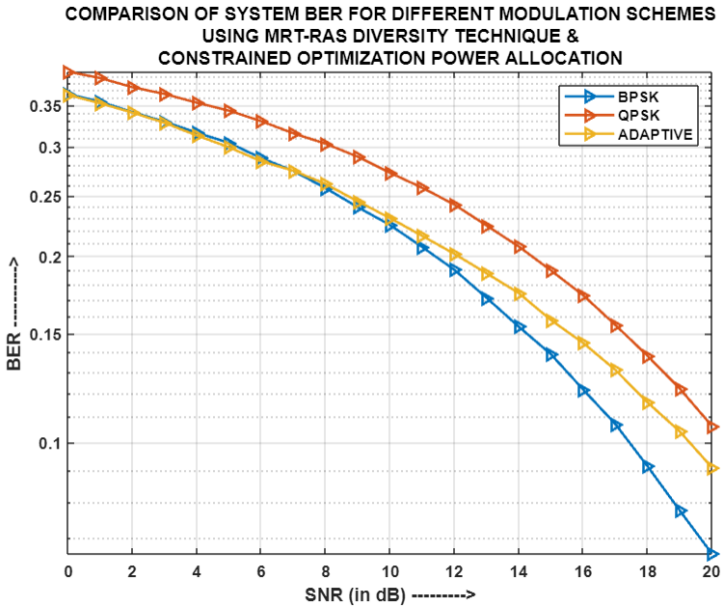

Fig.3.18: Comparison of System BER for different modulation schemes using MRT-TAS and COPA

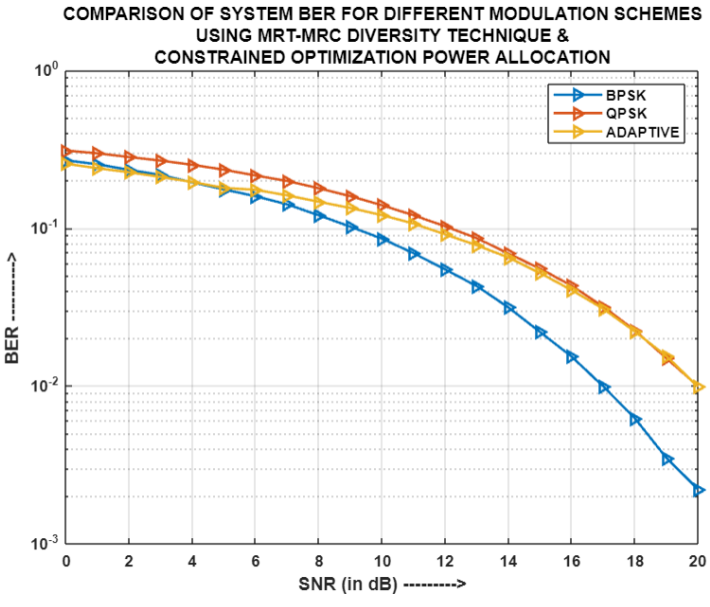

Fig.3.19: Comparison of System BER for different modulation schemes using MRT-MRC and COPA

Fig.3.16, Fig.3.17, Fig.3.18 and Fig.3.19 depicts the comparison of system BER for different modulation schemes using TAS-RAS, TAS-MRC, MRT-RAS and MRT-MRC diversity mechanisms respectively, and constrained optimization power allocation (COPA). It has been observed that for all the four pairs of transmit-receive diversity combinations, BPSK produces the least system BER while QPSK provides the highest system BER. This is so because in case of BPSK each transmitted symbol contains a single bit, whereby at the receiver only one bit can be erroneous at a time which reduces the chance of higher bit error probability compared to that of QPSK, wherein two bits are transmitted at a time, thereby indicating a higher chance of bit error probability at the receiver. The Adaptive modulation scheme is a mixture of BPSK and QPSK, and hence, its BER should lie in the middle of the two. Although for TAS-RAS and MRT-RAS duos, the Adaptive modulation scheme does satisfy the above theory but for TAS-MRC and MRT-MRC pairs, the aforementioned modulation technique generates a system BER that is similar to that of BPSK in the low SNR range and traces the QPSK system BER trajectory in the high SNR range. The reason behind such a behaviour is that the COPA mechanism, aiming to maximize the sum capacity, selects different sets of power allocation coefficients for differing SNR ranges. Therefore, the performance of Adaptive modulation scheme in terms of system BER varies depending on the chosen power allocation coefficient set.

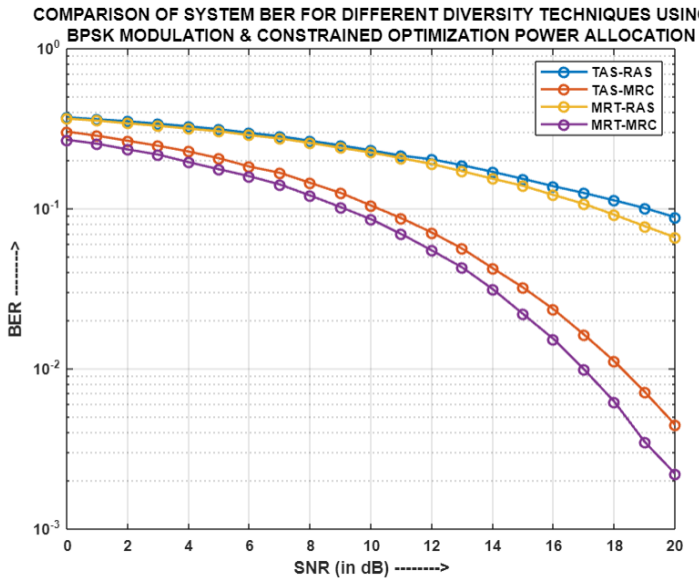

Fig.3.20: Comparison of System BER for different diversity techniques using BPSK and COPA

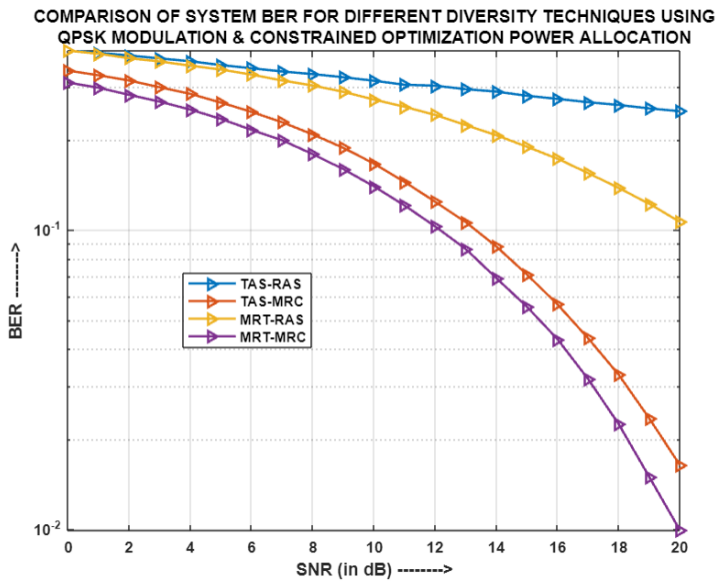

Fig.3.21: Comparison of System BER for different diversity techniques using QPSK and COPA

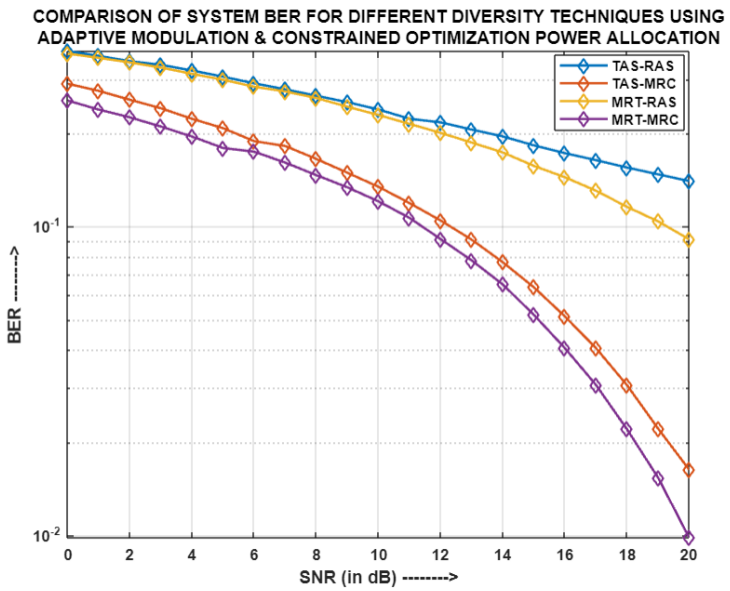

Fig.3.22: Comparison of System BER for different diversity techniques using Adaptive Modulation and COPA

Fig.3.20, Fig.3.21 and Fig.3.22 portrays the comparison of system BER for the four pairs of diversity combinations using BPSK, QPSK and Adaptive modulations respectively, and COPA. It can be spotted that for all the respective modulation schemes, MRT-MRC produces the least system BER followed by TAS-MRC, MRT-RAS and TAS-RAS, respectively. This is because both MRT-MRC and TAS-MRC employ MRC diversity at the receiver, which weights the received signals with certain parameters that are influenced from the channel characteristics and then combines all of them to generate a resultant signal, which is thereafter used. MRT-MRC performs better than TAS-MRC because in the former, multiple antennas transmit the same information signal whereas in the latter, only the selected antenna, out of the multiple antennas, is responsible for transmission. Thus, more the number of transmitting antennas taking part in transmission, higher is the chance of better signal reception at the receiver. On the contrary, MRT-RAS and TAS-RAS don't achieve as good a performance as the other two pairs of diversity combinations, because the former two pairs apply RAS receiver diversity scheme, wherein only one out of the many received signals is selected for further usage in the next stages. Also, the selected received signal is not weighted as per the channel characteristics, whereby its performance gets imprecise. MRT-RAS still performs slightly better than TAS-RAS as in the former multiple antennas transmit a resultant

signal, obtained by weighting the information signal with the different channel path characteristics and combining them, whereby better form of the signal is received. However, in TAS-RAS, only the selected antenna transmits the information signal, without any kind of processing related to the channel characteristics, leading to unpredictable signal reception. Therefore, MRT-RAS gives better system BER results than TAS-RAS.

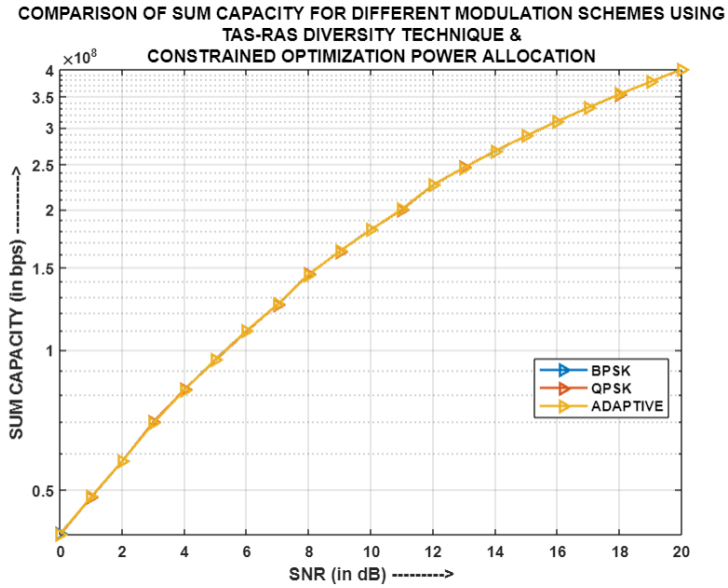

Fig.3.23: Comparison of Sum Capacity for different modulation schemes using TAS-RAS and COPA

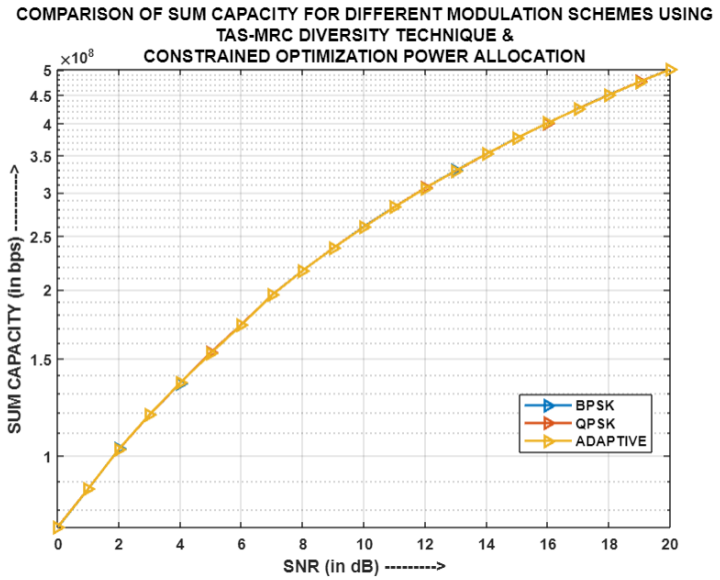

Fig.3.24: Comparison of Sum Capacity for different modulation schemes using TAS-MRC and COPA

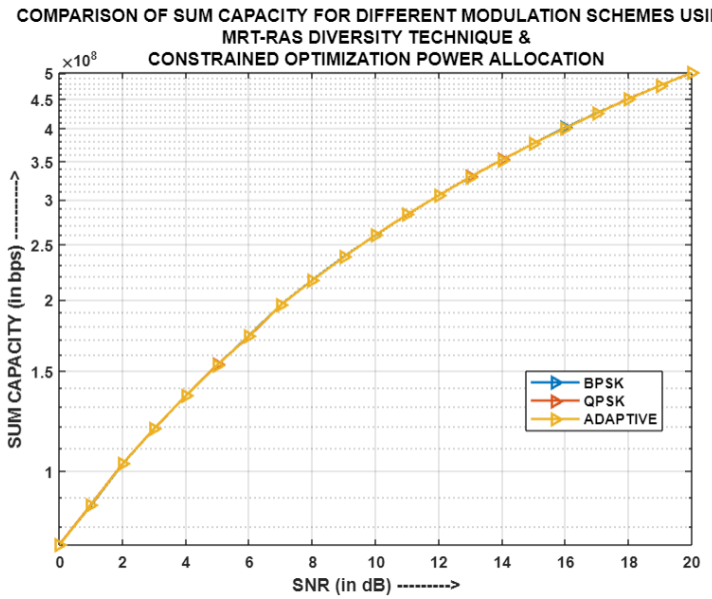

Fig.3.25: Comparison of Sum Capacity for different modulation schemes using MRT-RAS and COPA

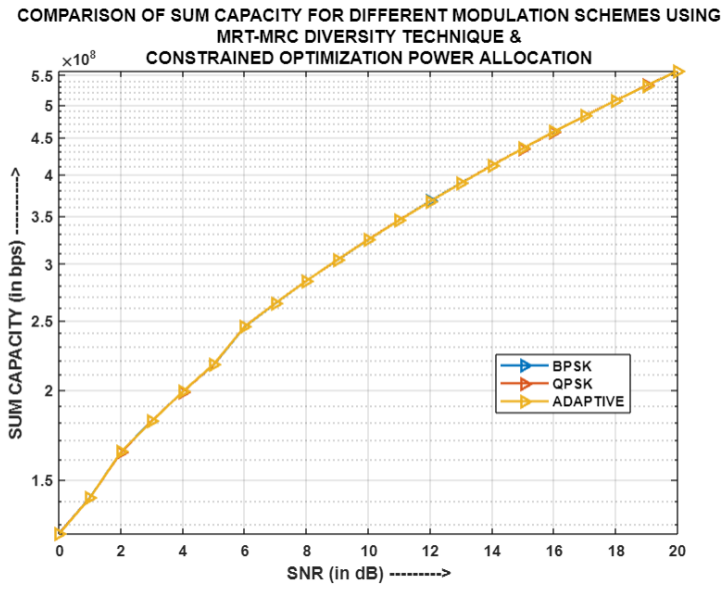

Fig.3.26: Comparison of Sum Capacity for different modulation schemes using MRT-MRC and COPA

The comparison of Sum Capacity for various modulation schemes using different diversity mechanisms is shown in Fig.3.23, Fig.3.24, Fig.3.25, and Fig.3.26. These diversity combinations include TAS-RAS, TAS-MRC, MRT-RAS, and MRT-MRC, along with COPA mechanism. It is observed that the sum capacities of BPSK, QPSK, and Adaptive modulation schemes have converged for all four combinations of diversity mechanisms. This convergence occurs because the sum capacity relies on the throughput of the two users in the system, which is primarily influenced by the channel gain, noise power, and power allocation coefficients. Although owing to COPA mechanism, different sets of power allocation coefficients are chosen for the three modulation schemes; but the rest two parameters remain the same for the three and because of higher influence of channel gain on the throughputs, the sum capacities exhibit a comparable behaviour across all the three modulation techniques.

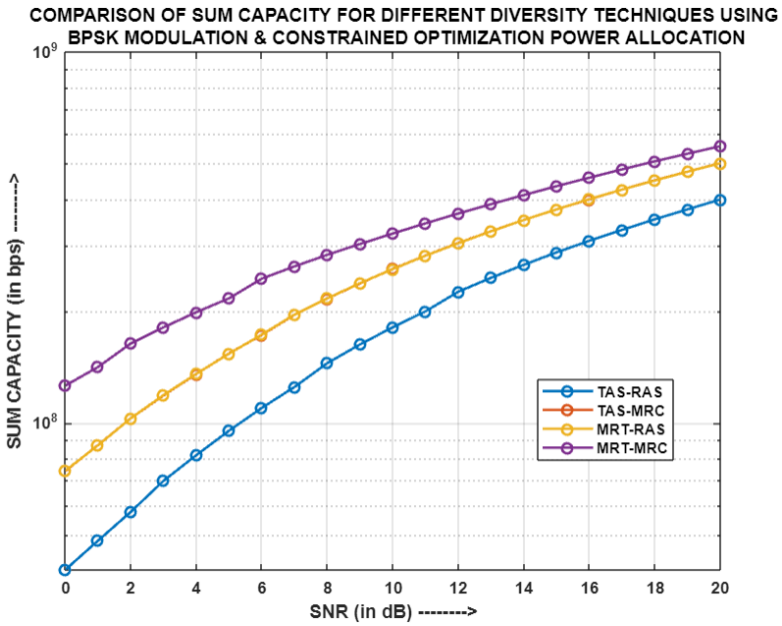

Fig.3.27: Comparison of Sum Capacity for different diversity techniques using BPSK and COPA

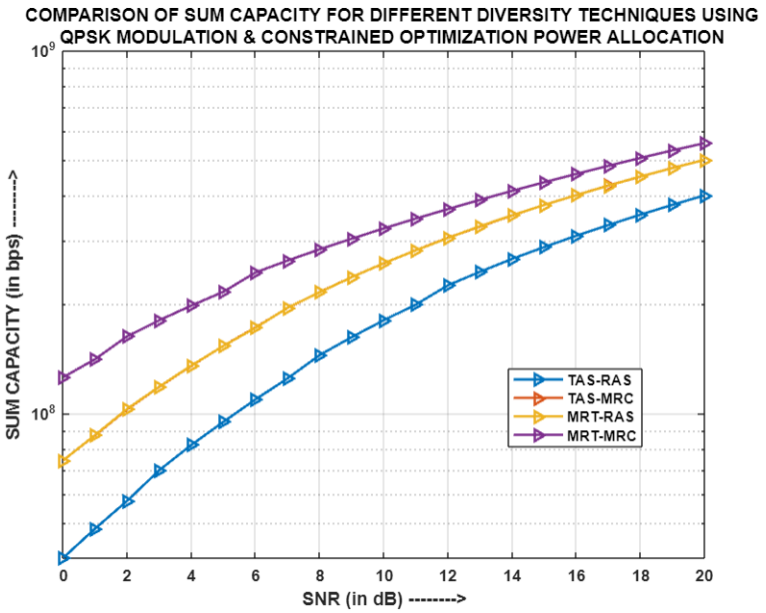

Fig.3.28: Comparison of Sum Capacity for different diversity techniques using QPSK and COPA

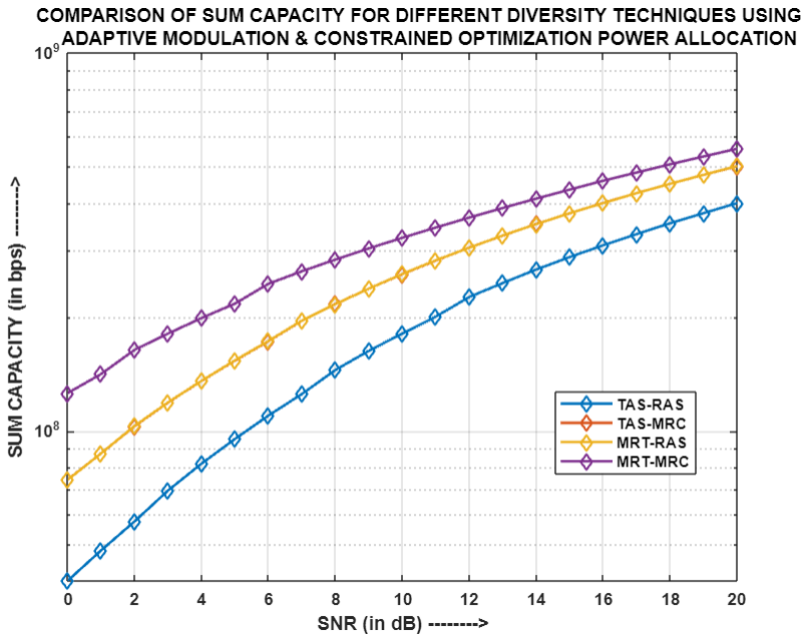

Fig.3.29: Comparison of Sum Capacity for different diversity techniques using Adaptive Modulation and COPA

Fig.3.27, Fig.3.28 and Fig.3.29 provide a comparison of Sum Capacity for the four diversity combinations using BPSK, QPSK, and Adaptive modulations, respectively, along with COPA mechanism. Notably, the highest and lowest sum capacities are offered by the MRT-MRC and TAS-RAS pairs, respectively. The sum capacities of TAS-MRC and MRT-RAS fall in between these two pairs. MRT-MRC achieves the highest sum capacity due to its utilization of (2x2) channel paths for each user. The increased number of channel paths for transmission and reception leads to higher user throughput, as data is received through multiple paths, thereby enhancing the system's overall sum capacity. Conversely, TAS-RAS provides (1x1) channel paths for each user, resulting in the lowest sum capacity, as each user receives data through a single path only. TAS-MRC and MRT-RAS exhibit the same sum capacities because both diversity pairs transmit and receive information through an equal number of channel paths, namely (1x2) and (2x1), respectively and also the COPA mechanism selects the same power allocation coefficient sets for both the pairs. Thus, due to the total number of channel paths involved in transmission and reception, TAS-MRC and MRT-RAS pairs possess higher sum capacities than TAS-RAS but lower sum capacities than MRT-MRC.

3.3.3. Simulation Result Analysis of two-user MIMO-PD-NOMA model for different combination of antenna diversity techniques using varied modulation schemes and CON-OPA mechanism:

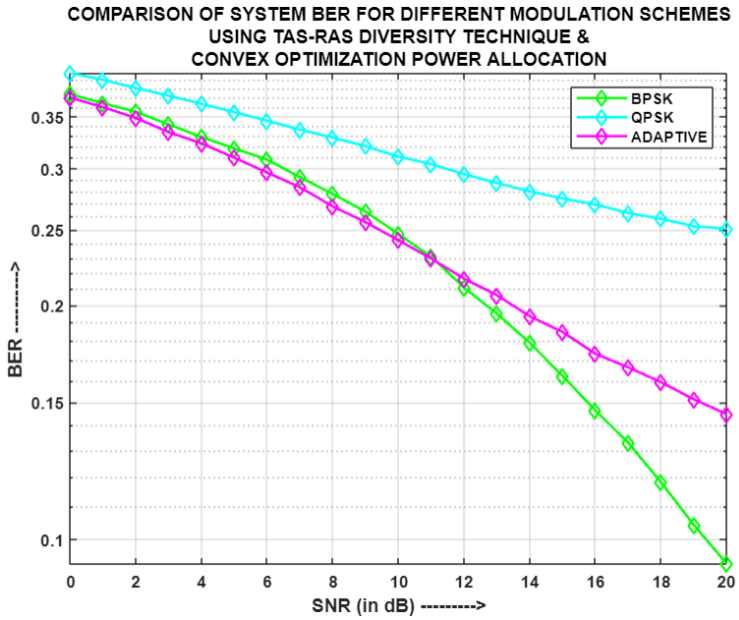

Fig.3.30: Comparison of System BER for different modulation schemes using TAS-RAS and CON-OPA

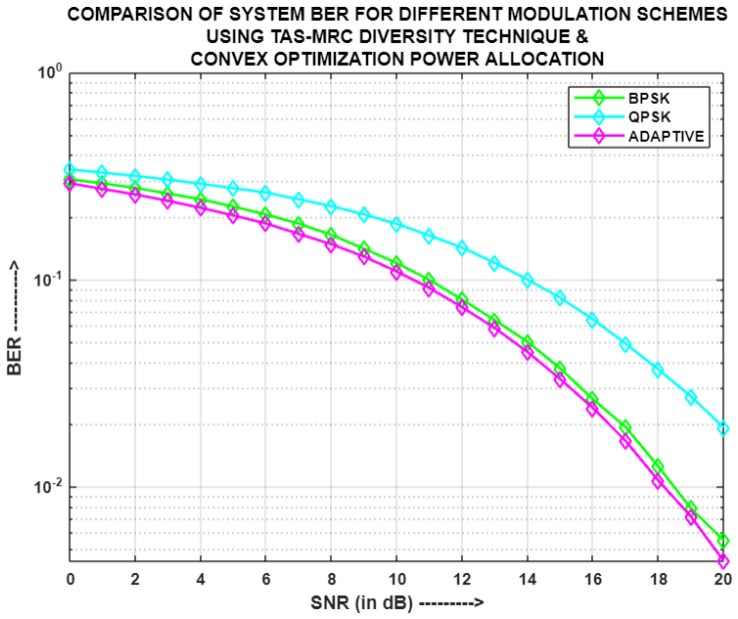

Fig.3.31: Comparison of System BER for different modulation schemes using TAS-MRC and CON-OPA

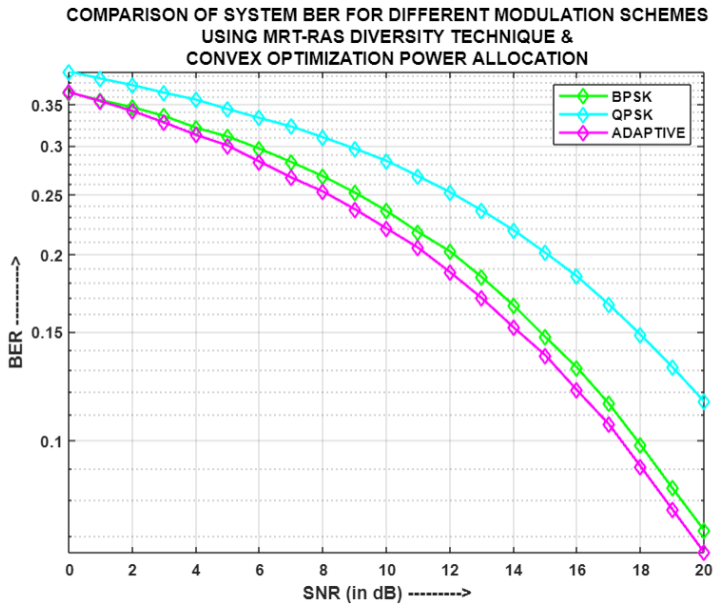

Fig.3.32: Comparison of System BER for different modulation schemes using MRT-RAS and CON-OPA

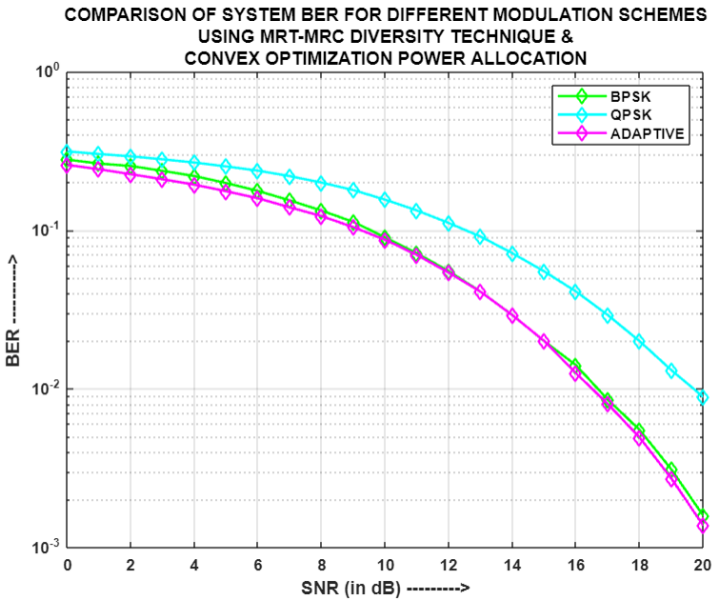

Fig.3.33: Comparison of System BER for different modulation schemes using MRT-MRC and CON-OPA

Fig.3.30, Fig.3.31, Fig.3.32 and Fig.3.33 illustrates the comparison of system BER among various modulation schemes employing TAS-RAS, TAS-MRC, MRT-RAS, and MRT-MRC diversity mechanisms respectively, along with convex optimization power allocation (CON-OPA). It has been observed that only for TAS-RAS pair, the least and highest system BERs are produced by BPSK and QPSK respectively, while the system BER of Adaptive modulation scheme lies in the middle of the two. The reason for this is that in the case of BPSK, each transmitted symbol corresponds to a single bit. As a result, at the receiver, only one bit can be in error at a time, reducing the likelihood of a higher bit error probability compared to QPSK, wherein two bits are transmitted simultaneously, which increases the probability of bit errors occurring at the receiver. The Adaptive modulation scheme is a mixture of BPSK and QPSK, and hence, its BER lies in between the two. However, for TAS-MRC, MRT-RAS and MRT-MRC pairs, it has been witnessed that the Adaptive modulation technique yields the lowest system BER followed by BPSK and QPSK. This is because of the CON-OPA mechanism that selects different sets of power allocation coefficients for the different modulation schemes, as well as varying SNR values, thereby aiming to maximize the overall sum capacity. The chosen sets of power allocation coefficients, for different SNR values, seemed to have enhanced the performance of Adaptive modulation scheme in terms of system BER, whereby it even surpasses BPSK's system BER.

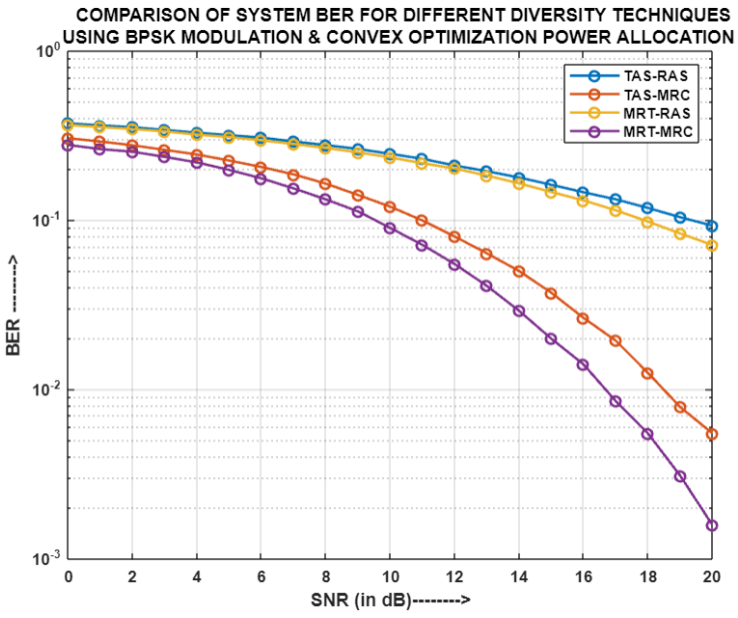

Fig.3.34: Comparison of System BER for different diversity techniques using BPSK and CON-OPA

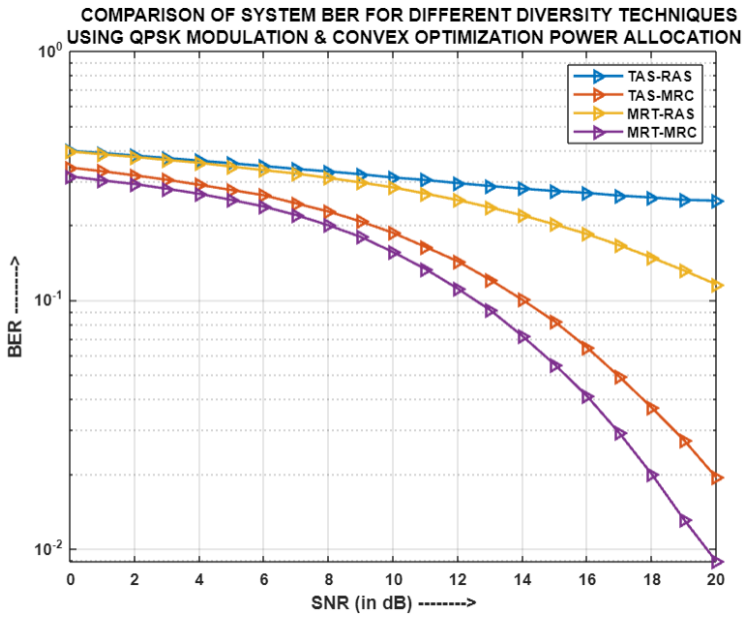

Fig.3.35: Comparison of System BER for different diversity techniques using QPSK and CON-OPA

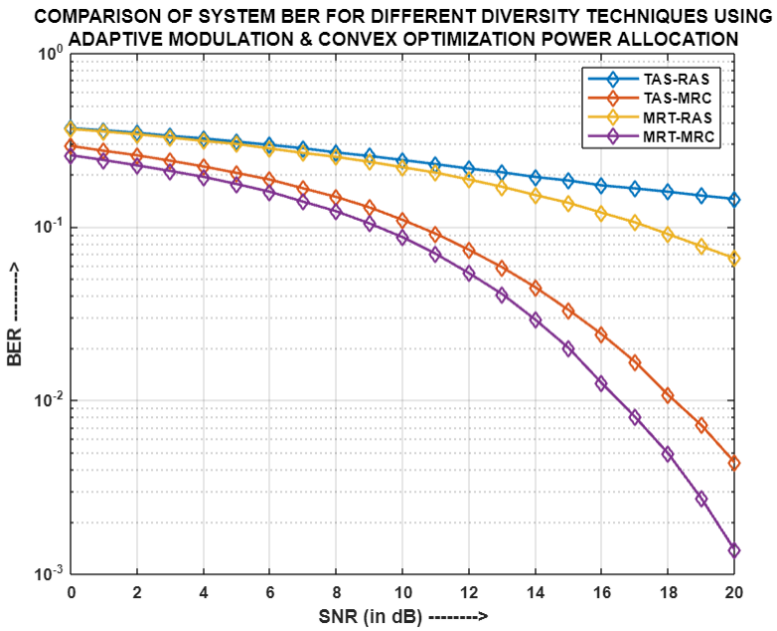

Fig.3.36: Comparison of System BER for different diversity techniques using Adaptive Modulation and CON-OPA

Fig.3.34, Fig.3.35 and Fig.3.36 displays the comparison of system BER for the four diversity combinations using BPSK, QPSK, and Adaptive modulations respectively, along with CON-OPA mechanism. It is evident that across all the stated modulation schemes, MRT-MRC exhibits the lowest system BER, followed by TAS-MRC, MRT-RAS, and TAS-RAS, respectively. This distinction arises from the utilization of MRC diversity at the receiver in both MRT-MRC and TAS-MRC pairs. MRC weights the received signals based on channel characteristics and combines them to generate a composite signal for further processing. MRT-MRC outperforms TAS-MRC because it involves multiple antennas transmitting the same information signal, whereas TAS-MRC relies on a single selected antenna for transmission. Consequently, the involvement of multiple transmitting antennas enhances the likelihood of improved signal reception at the receiver. In contrast, MRT-RAS and TAS-RAS demonstrate inferior performance compared to the other two diversity combinations. These pairs employ RAS diversity, wherein only one received signal is selected for the subsequent stages without considering channel characteristics. The selected signal's performance is thus compromised due to the lack of weighting based on channel characteristics. MRT-RAS performs slightly better than TAS-RAS as it transmits a composite signal obtained by weighting the information signal with different channel path characteristics, resulting in improved

signal quality upon reception. Conversely, TAS-RAS transmits the information signal solely through the selected antenna, without any processing related to channel characteristics, leading to unpredictable signal reception. Therefore, MRT-RAS yields better system BER outcome than TAS-RAS.

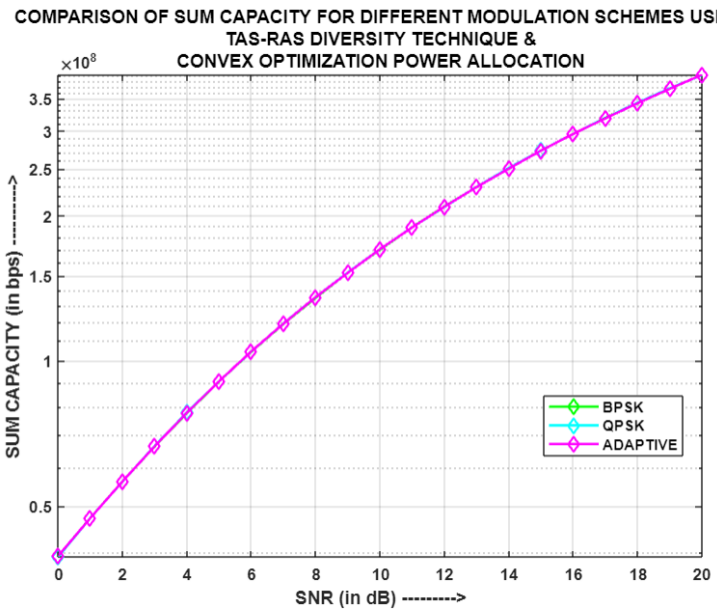

Fig.3.37: Comparison of Sum Capacity for different modulation schemes using TAS-RAS and CON-OPA

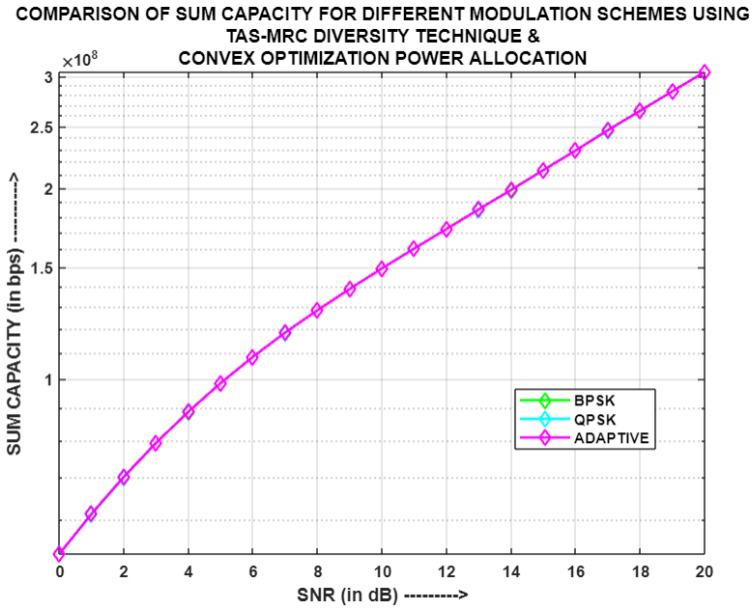

Fig.3.38: Comparison of Sum Capacity for different modulation schemes using TAS-MRC and CON-OPA

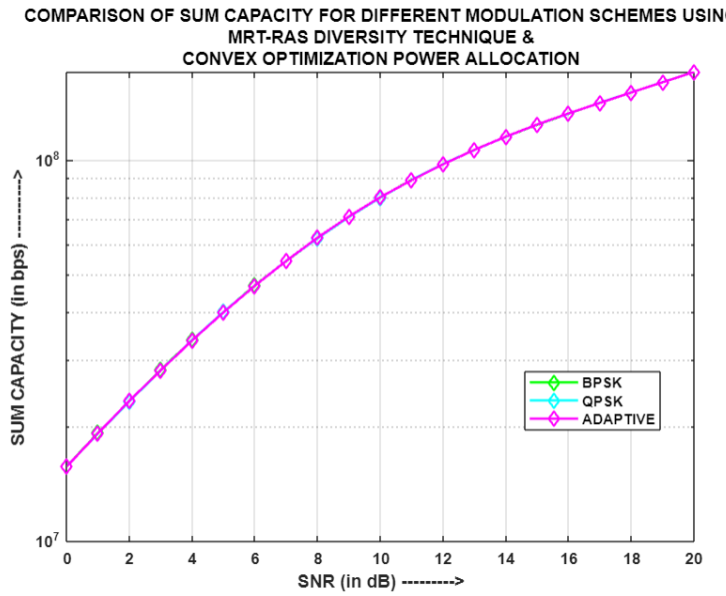

Fig.3.39: Comparison of Sum Capacity for different modulation schemes using MRT-RAS and CON-OPA

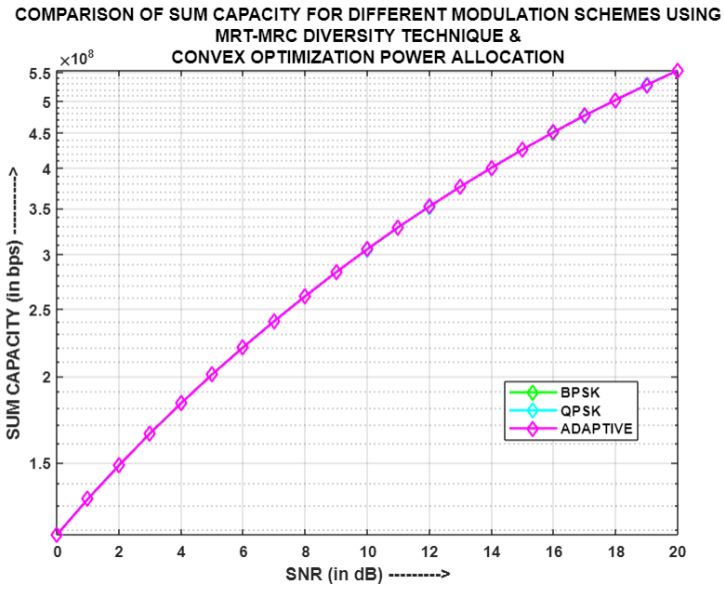

Fig.3.40: Comparison of Sum Capacity for different modulation schemes using MRT-MRC and CON-OPA

The comparison of Sum Capacity for different modulation schemes, using various diversity mechanisms respectively, is depicted in Figures 3.37, 3.38, 3.39 and 3.40. These diversity combinations include TAS-RAS, TAS-MRC, MRT-RAS, and MRT-MRC, in conjunction with the CON-OPA mechanism. It is noteworthy that the sum capacities of BPSK, QPSK, and Adaptive modulation schemes have converged for all four diversity combinations. This convergence arises from the fact that the sum capacity is dependent on the throughput of the two users in the system, which is primarily influenced by channel gain, noise power, and power allocation coefficients. Although the CON-OPA mechanism introduces different sets of power allocation coefficients for the three modulation schemes, the remaining two parameters remain consistent across all three schemes. Due to the higher impact of channel gain on the throughputs, the sum capacities exhibit a comparable behavior among the three modulation techniques.

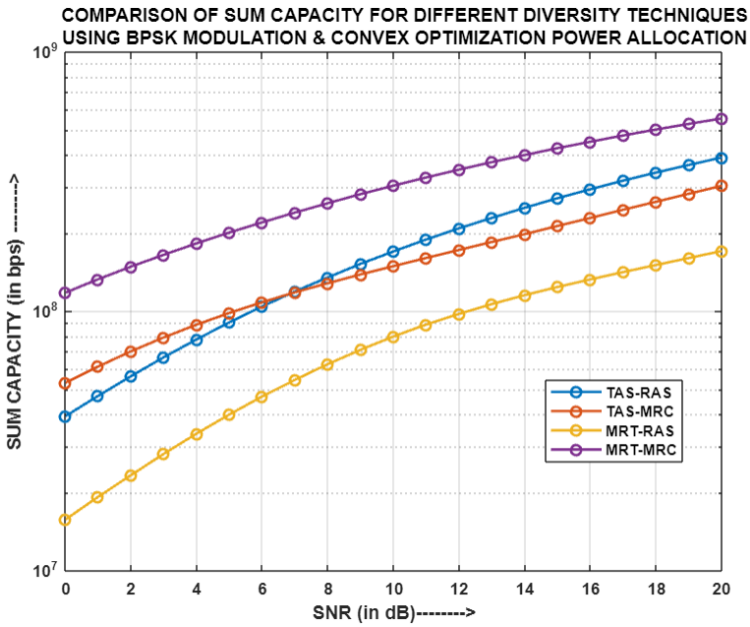

Fig.3.41: Comparison of Sum Capacity for different diversity techniques using BPSK and CON-OPA

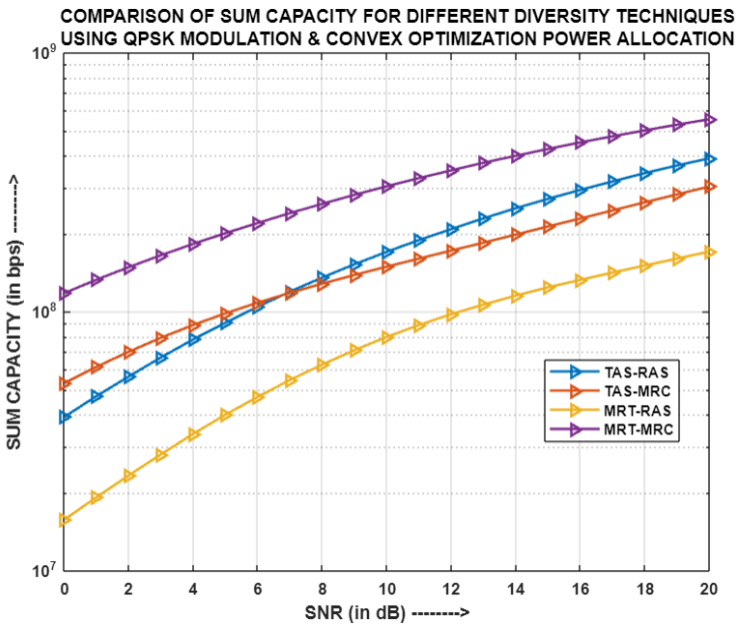

Fig.3.42: Comparison of Sum Capacity for different diversity techniques using QPSK and CON-OPA

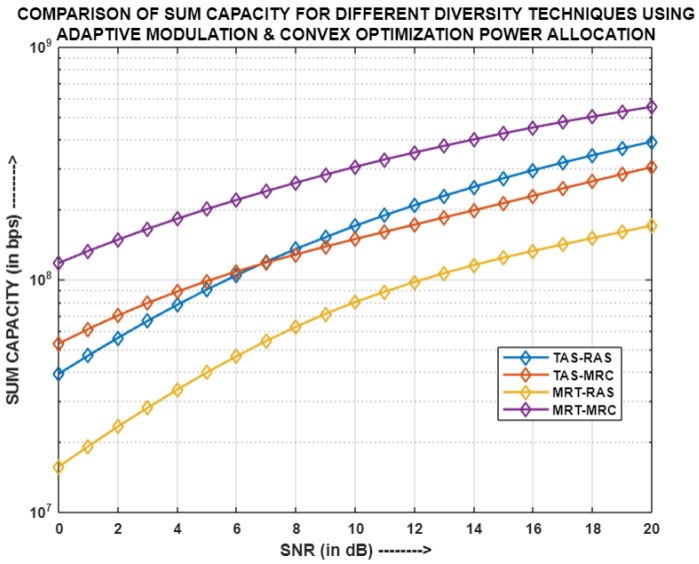

Fig.3.43: Comparison of Sum Capacity for different diversity techniques using Adaptive Modulation and CON-OPA

Figures 3.41, 3.42 and 3.43 present a comparative analysis of Sum Capacity for the four diversity combinations using BPSK, QPSK, and Adaptive modulations respectively, along with the CON-OPA mechanism. Remarkably, the MRT-MRC pair demonstrates the highest sum capacity, while the MRT-RAS pair exhibits the lowest sum capacity. The sum capacities of TAS-RAS and TAS-MRC lie in between these two pairs. The superior performance of MRT-MRC can be attributed to its utilization of (2x2) channel paths for each user, in this system. With multiple paths for transmission and reception, the user throughput increases, as data is received through multiple paths, leading to enhanced overall system sum capacity. Unlike in case of FPA and COPA, TAS-MRC and MRT-RAS have differing sum capacities, even though both the pairs transmit and receive information through an equal number of channel paths, namely (1x2) and (2x1), respectively. This is because the CON-OPA mechanism selects different power allocation coefficient sets for both TAS-MRC and MRT-RAS pairs, whereby the effect of the chosen power allocation coefficients on the user throughputs is such that MRT-RAS pair yields the lowest sum capacity. In contrast, although TAS-RAS employs (1x1) channel paths for each user, but still due to optimum selection of power allocation coefficients, TAS-RAS pair yields a sum capacity comparable to TAS-MRC. Since, the sum capacity is directly influenced by the change in power allocation coefficient sets, hence up to SNR value of 7dB, TAS-MRC produces higher sum capacity than TAS-RAS and

beyond 7dB, the reverse happens. Therefore, considering the total number of channel paths, involved in transmission and reception, and with the significant contribution of power allocation coefficients, TAS-MRC and TAS-RAS pairs demonstrate higher sum capacities than MRT-RAS but lower sum capacities than MRT-MRC.

3.3.4. Comparative Analysis of simulation results of two-user MIMO-PD-NOMA model for different power allocation strategies, diversity techniques and modulation schemes:

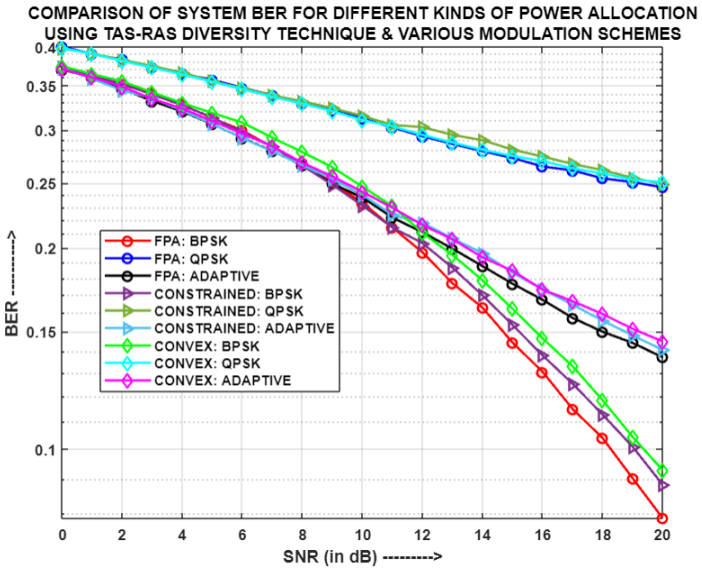

Fig.3.44: Comparison of System BER for different power allocation strategies using TAS-RAS

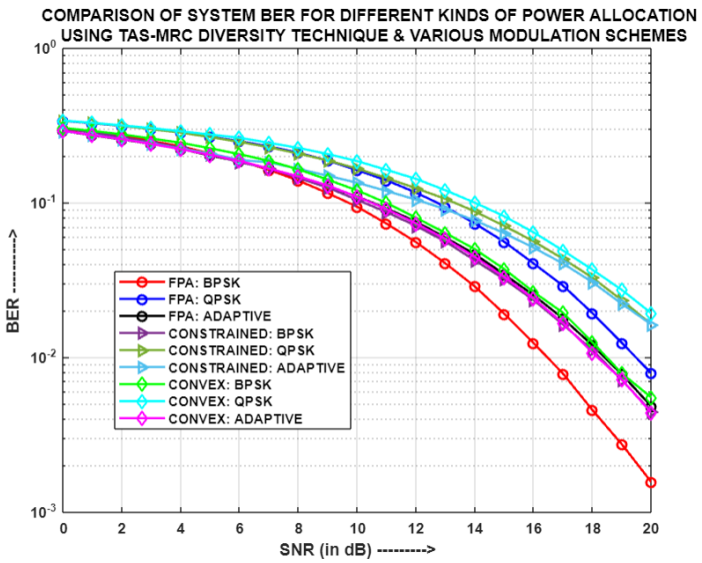

Fig.3.45: Comparison of System BER for different power allocation strategies using TAS-MRC

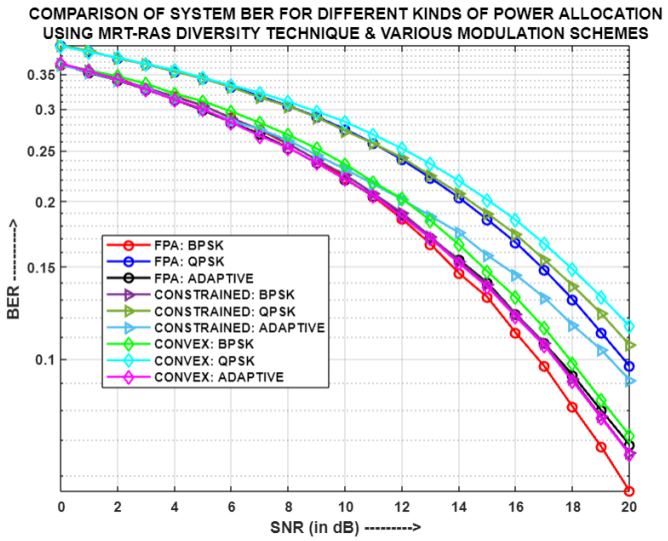

Fig.3.46: Comparison of System BER for different power allocation strategies using MRT-RAS

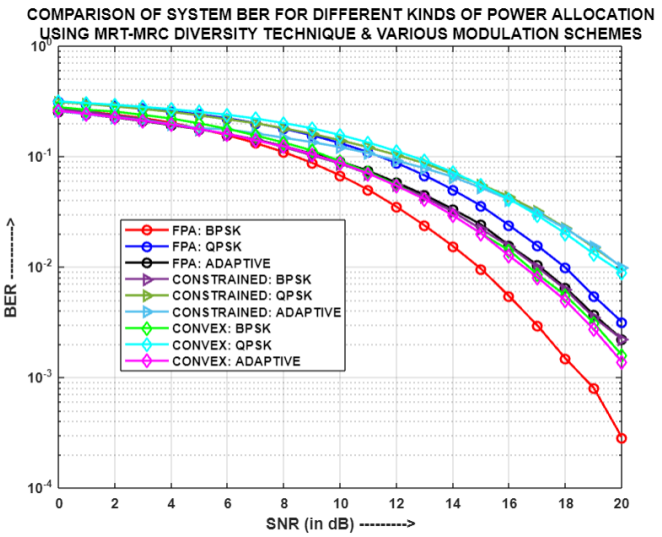

Fig.3.47: Comparison of System BER for different power allocation strategies using MRT-MRC

Fig.3.44, Fig.3.45, Fig.3.46 and Fig.3.47 depicts the comparison of system BER for different power allocation (PA) strategies, namely fixed power allocation (FPA), constrained optimization power allocation (COPA) and convex optimization power allocation (CON-OPA), using varied diversity combinations and modulation schemes.

It has been observed from Fig.3.44, that for TAS-RAS pair, in case of all three power allocation mechanisms, BPSK modulation scheme produces the least system BER followed by Adaptive and QPSK modulations. In reference to TAS-RAS, for BPSK and Adaptive modulations, FPA mechanism yields the lowest system BER, succeeded by COPA and CON-OPA. This is because of the different selection of power allocation coefficient sets for the three strategies. In FPA, the same power allocation set was utilized for the entire SNR range; while in COPA and CON-OPA, varying sets of power allocation were chosen for the entire SNR span. However, in case of QPSK modulation, in regard to TAS-RAS pair, all the PA strategies happened to have selected the same power allocation coefficient set and hence, their system BERs have merged.

In Fig.3.45, for TAS-MRC pair, FPA produces the lowest system BER followed by the other two PA mechanisms, for both BPSK and QPSK modulations. Again, for both BPSK and QPSK, the system BERs yielded by COPA and CON-OPA have almost merged due to the selection of similar power allocation coefficient sets, for the varying SNR range. However, in case of Adaptive modulation scheme, the highest system BER is generated by COPA while the lowest system BER is produced by both FPA and CON-OPA, as they follow the same trajectory, implying that CON-OPA mechanism happened to generate the same power coefficient set as used in FPA, thereby indicating it to be the optimum choice of power allocation for the two users.

In case of MRT-RAS pair, as shown in Fig.3.46, for both BPSK and QPSK modulations, the least system BER is produced by FPA followed by COPA and CON-OPA mechanisms, as different power allocation sets are used for the three PA strategies. However, in the context of Adaptive modulation scheme, it is observed that the COPA mechanism yields the highest system BER, whereas both FPA and CON-OPA produce the lowest system BER, as they exhibit a similar trend. This suggests that the CON-OPA mechanism coincidentally generates the same power

coefficient set as employed in FPA, indicating that it is an optimal choice for power allocation between the two users.

In regard to Fig.3.47, for MRT-MRC pair, in case of both BPSK and QPSK, the least system BER is produced by FPA mechanism while both COPA and CON-OPA yield similar system BERs for the above mentioned modulations respectively, due to the selection of comparable power coefficients for the latter two PA strategies. However, in case of Adaptive modulation, the lowest system BER is yielded by CON-OPA, succeeded by FPA and COPA mechanisms, indicating that a better power coefficient set is generated by the CON-OPA algorithm in comparison to the other two PA mechanisms.

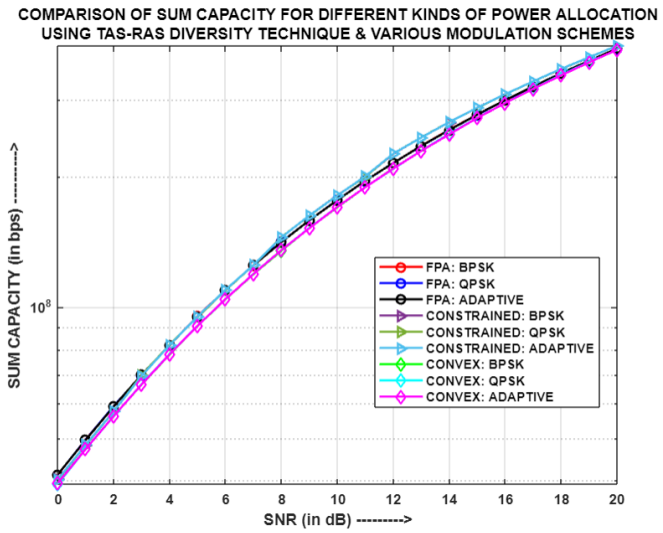

Fig.3.48: Comparison of Sum Capacity for different power allocation strategies using TAS-RAS

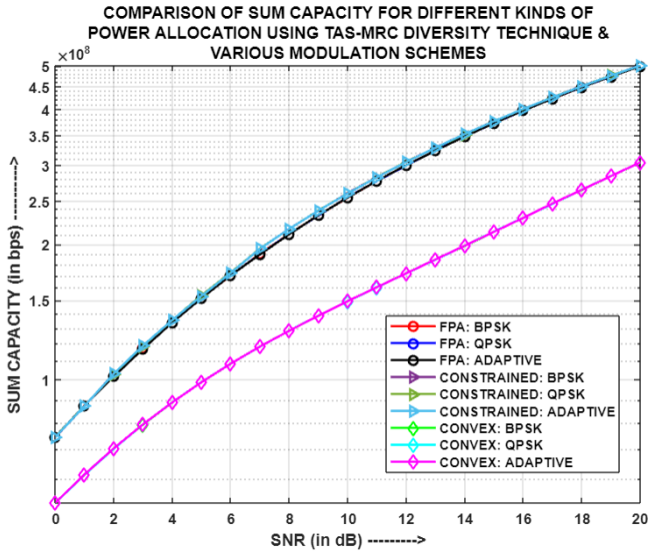

Fig.3.49: Comparison of Sum Capacity for different power allocation strategies using TAS-MRC

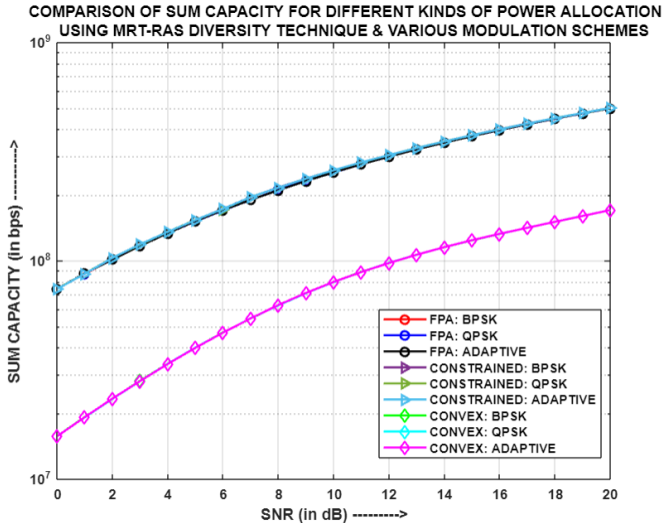

Fig.3.50: Comparison of Sum Capacity for different power allocation strategies using MRT-RAS

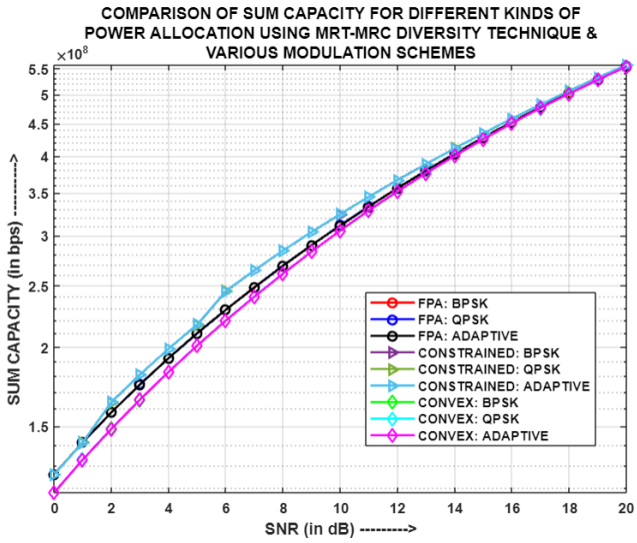

Fig.3.51: Comparison of Sum Capacity for different power allocation strategies using MRT-MRC

Fig.3.48, Fig.3.49, Fig.3.50 and Fig.3.51 portrays the comparison of Sum Capacity for different power allocation (PA) strategies, namely fixed power allocation (FPA), constrained optimization power allocation (COPA) and convex optimization power allocation (CON-OPA), using varied diversity combinations and modulation schemes. In context of TAS-RAS and MRT-MRC pairs, the sum capacities yielded by different PA strategies, using the three modulation schemes, seem to almost merge with another, even though different power coefficient sets might have been used for some of the cases. This is so because the channel gains for the aforementioned scenarios are same and also the power allocation coefficients utilized for the different cases don't differ much from one another, whereby the contribution of channel gains take a higher weightage. However, in case of TAS-MRC and MRT-RAS pairs, the sum capacities generated by FPA and COPA mechanisms merge and are higher than those generated by CON-OPA, for all the three modulation schemes. The reason behind such a behaviour is that, even though the channel gains are same and have a significant contribution in the users' throughput and hence, sum capacity, but the power coefficient sets determined by the CON-OPA algorithm vary vastly from those used in the other two PA strategies. Therefore, FPA and COPA yield similar sum capacities, across all modulations, due to same channel gains and comparable power allocation coefficients, while CON-OPA produces lower sum capacities, owing to its significantly different selection of power coefficient sets.

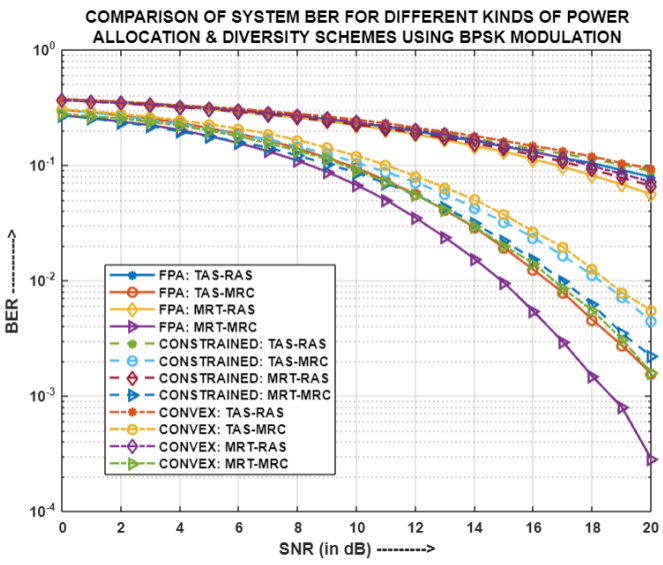

Fig.3.52: Comparison of System BER for different power allocation strategies and diversity schemes using BPSK

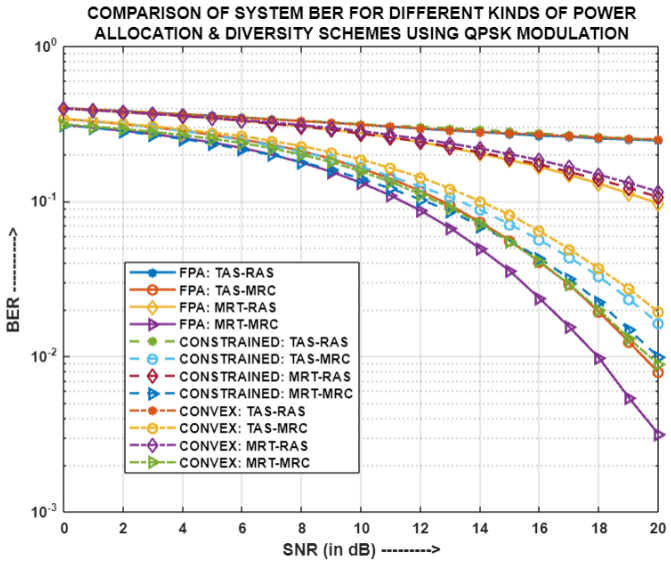

Fig.3.53: Comparison of System BER for different power allocation strategies and diversity schemes using QPSK

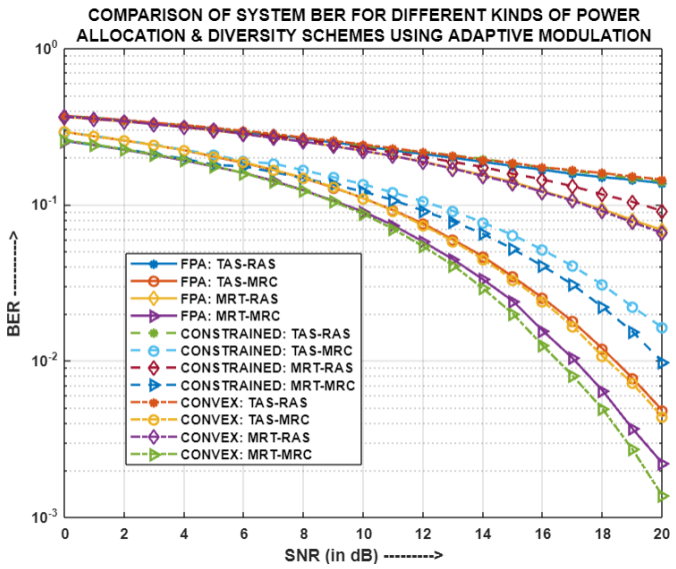

Fig.3.54: Comparison of System BER for different power allocation strategies and diversity schemes using Adaptive modulation

Fig.3.52, Fig.3.53 and Fig.3.54 illustrates a comparison of system BER for BPSK, QPSK and Adaptive modulations respectively, using all four pairs of diversity combinations and different power allocation (PA) strategies. It is evident that for both BPSK and QPSK, MRT-MRC and TAS-MRC pairs with FPA yields a better system BER compared to the same pairs with COPA and CON-OPA. However, in case of Adaptive modulation, MRT-MRC and TAS-MRC pairs with CON-OPA produce a lower system BER in comparison to the same pairs with FPA and COPA. This is because of the selection and usage of different power allocation coefficient sets for the three PA strategies. In case of BPSK, TAS-RAS and MRT-RAS pairs yield similar system BER performance across all PA strategies as comparable power coefficients sets were chosen for the system. On the contrary, for QPSK and Adaptive modulation schemes, MRT-RAS pair performs better than TAS-RAS pair, for all PA strategies, since the power allocation coefficients chosen for the former pair tends to slightly improve its performance compared to the latter pair.

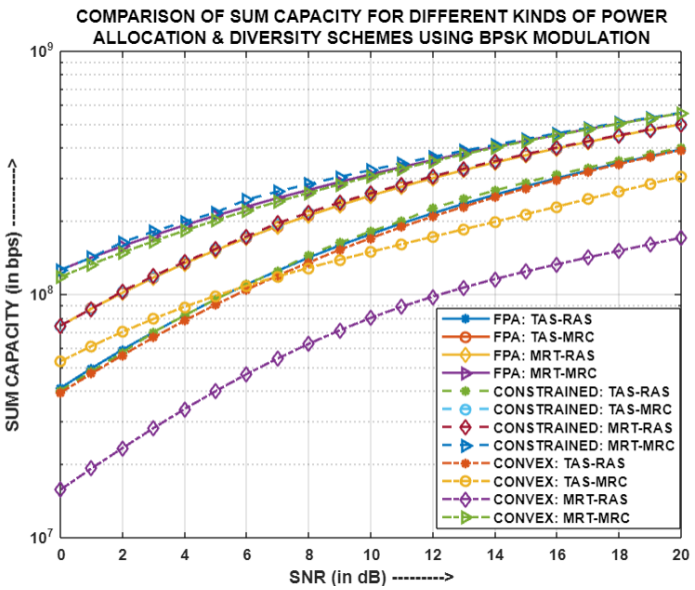

Fig.3.55: Comparison of Sum Capacity for different power allocation strategies and diversity schemes using BPSK

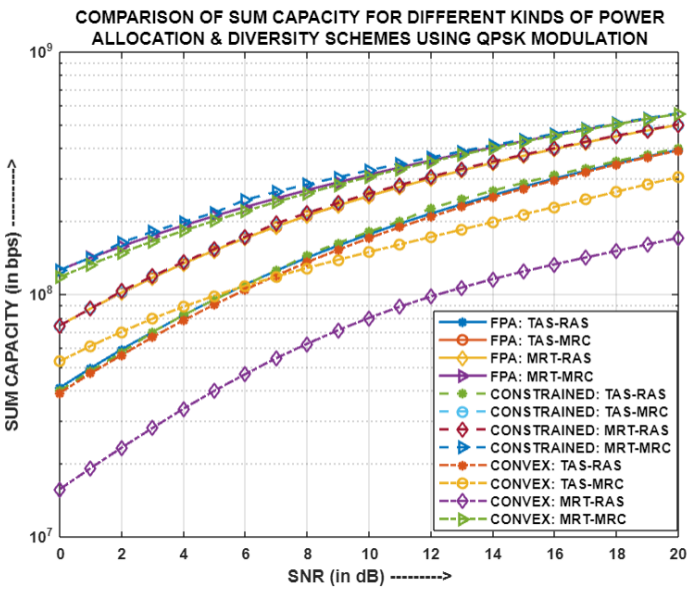

Fig.3.56: Comparison of Sum Capacity for different power allocation strategies and diversity schemes using QPSK

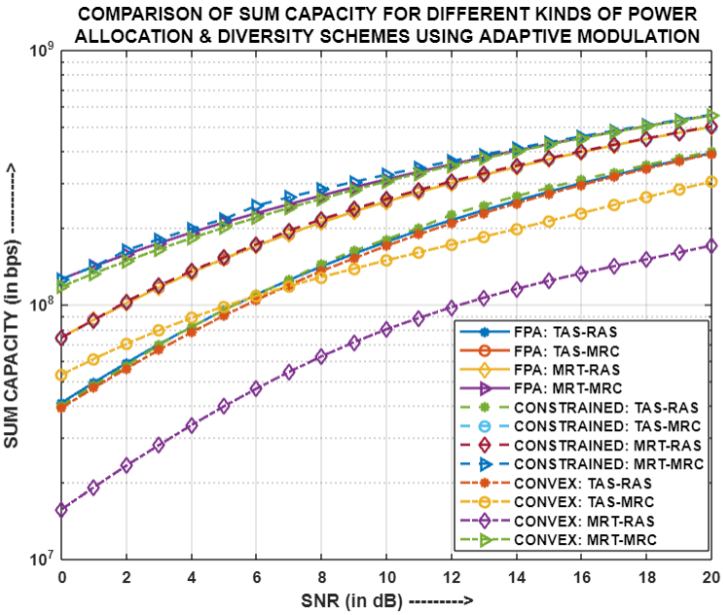

Fig.3.57: Comparison of Sum Capacity for different power allocation strategies and diversity schemes using Adaptive modulation

Fig.3.55, Fig.3.56 and Fig.3.57 illustrates a comparison of Sum Capacity for BPSK, QPSK and Adaptive modulations respectively, using all four pairs of diversity combinations and different power allocation (PA) strategies. It has been

observed that MRT-MRC pair yields the highest and merged sum capacities for all the PA strategies, since although different power allocation coefficients are chosen across the varied PA mechanisms but the channel gains being the same hold significant contribution in producing comparable sum capacities. It is for this reason that even TAS-RAS pair produces similar sum capacities across all PA strategies. TAS-MRC and MRT-RAS pairs with FPA and COPA generate merged and higher sum capacities than TAS-RAS pair due to additional number of channel paths involved in transmission-reception, that enhance the channel gain, throughput and thereby, sum capacity of the system. The merged nature is due to selection of similar power allocation coefficients. However, both TAS-MRC and MRT-RAS pairs with CON-OPA yield lower sum capacities than the other two PA strategies because the computed power coefficients in CON-OPA vary vastly from the ones applied in the latter two. As considerable difference in power coefficients can immensely affect the sum capacity of the system, hence such variation in sum capacities is noticed.

Table 3.2: Compilation of Result Analysis for (2x2)-MIMO-PD-NOMA for different combination of Antenna Diversity techniques

TX-RX Diversity Techniques	Modulation Scheme	Power Allocation Strategy	System BER	Sum Capacity	Remarks
TAS -RAS	BPSK	FPA	Least	High	• BPSK, using all power allocation mechanisms, yields optimum performance, for both System BER and Sum Capacity.
		COPA	Least	High	
		CON-OPA	Least	High	
	QPSK	FPA	Highest	High	
		COPA	Highest	High	
		CON-OPA	Highest	High	
	Adaptive Modulation	FPA	Moderate	High	
		COPA	Moderate	High	
		CON-OPA	Moderate	High	
TAS-MRT	BPSK	FPA	Least	High	• BPSK performs well using both FPA and COPA. • Adaptive modulation excels in case of CON-OPA.
		COPA	Least	High	
		CON-OPA	Moderate	High	
	QPSK	FPA	Highest	High	
		COPA	Highest	High	
		CON-OPA	Highest	High	
	Adaptive Modulation	FPA	Moderate	High	
		COPA	Moderate	High	
		CON-OPA	Least	High	
MRT-RAS	BPSK	FPA	Least	High	• BPSK performs the best for both FPA and COPA. • Adaptive modulation surpasses BPSK and QPSK, for CON-OPA.
		COPA	Least	High	
		CON-OPA	Moderate	High	
	QPSK	FPA	Highest	High	
		COPA	Highest	High	
		CON-OPA	Highest	High	
	Adaptive Modulation	FPA	Moderate	High	
		COPA	Moderate	High	
		CON-OPA	Least	High	
MRT-MRC	BPSK	FPA	Least	High	• Again, BPSK is the most suitable choice only when used with FPA and COPA, respectively. • Adaptive modulation outperforms BPSK and QPSK, for CON-OPA.
		COPA	Least	High	
		CON-OPA	Moderate	High	
	QPSK	FPA	Highest	High	
		COPA	Highest	High	
		CON-OPA	Highest	High	
	Adaptive Modulation	FPA	Moderate	High	
		COPA	Moderate	High	
		CON-OPA	Least	High	

3.4. DISCUSSION

It is clearly evident from Table that BPSK showcases optimum overall system performance, with respect to both System BER and Sum Capacity, using fixed and constrained optimization power allocation mechanisms respectively, for all four pairs of antenna diversity techniques. However, it is the Adaptive modulation scheme that performs surprisingly well, except for TAS-RAS, when it is applied along with convex optimization power allocation strategy. Therefore, the choice of power allocation coefficients, in order to employ the NOMA principle, play a significant role in controlling the BER of respective users and subsequently, the system BER; along with influencing the user's throughput that impact the sum capacity of the system. The channel gain also has a vital role in influencing the throughput of the corresponding users, as for a higher channel gain, the throughput increases, thereby improving the sum capacity; whereas for comparable channel gains, similar sum capacities are obtained, even when the modulation schemes differ. Additionally, the selection of the appropriate transmit-receive diversity techniques are essential for better quality signal reception, as they mitigate the effects of fading.

3.5. CONCLUSION

This chapter vastly explored MIMO-NOMA in conjunction with four pairs of transmit-receive diversity pairs, i.e. TAS-RAS, TAS-MRT, MRT-RAS and MRT-MRC, on grounds of System BER and Sum Capacity, for different power allocation strategies and modulation schemes. The MRT-MRC diversity pair emerged as the winner in all of the cases studied. The performance of the diversity pair is indeed influenced by the chosen power allocation mechanism and the modulation scheme used, along with its own capability of combating the fading environment. Therefore, the appropriate choice of transmit-receive diversity technique needs to be made depending upon the application area. Diversity techniques have been employed in 4G LTE and 5G cellular networks, wireless LANs, satellite communications, broadcast systems, like television and radio, and such like. With the combination of NOMA, these MIMO diversity techniques can serve more number of user equipments, atleast double, thereby using the same bandwidth; and hence, enhancing the spectral efficiency of the system, without compromising on the power efficiency. Thus, MIMO-NOMA employing diversity techniques ensures robust and efficient communication among all kinds of user equipments.

Chapter 4 STUDY OF A PROPOSED PRECODING SCHEME OVER EXISTING TECHNIQUES FOR MULTI-USER MIMO-PD-NOMA

4.1. ABSTRACT

Precoding is one of the major aspects of MIMO technology and a pivotal technique in wireless communication systems that aims to enhance the performance and reliability of data transmission. It involves the manipulation of transmit signals at the transmitter side to exploit the spatial characteristics of the communication channel. By precoding the signals, various objectives such as improving signal quality, mitigating interference, maximizing capacity, and ensuring reliable communication can be achieved. Therefore, precoding is chosen to be employed in MIMO-NOMA systems to explore its effect on the system. This chapter gives a comprehensive insight into the performance analysis, with respect to system Bit Error Rate and Sum Capacity, of a downlink two-user MIMO-PD-NOMA system, considering different precoding schemes. A new precoding scheme is proposed, which is a modified version of SVD, and hence, its performance is compared with the existing precoding techniques like MF, ZF, RZF and SVD itself. The two-user MIMO-PD-NOMA system model is explored for two scenarios of MIMO, in which the first scenario provides each entity in the system with two antennas, while the second scenario equips all the entities in the system with four antennas each. A comparative analysis of the results for both the MIMO scenarios is also presented in this chapter. As NOMA principle requires the total transmission power to be judiciously allocated among the users, therefore different kinds of power allocation strategies are inspected to determine the optimum power allocation mechanism for the aforementioned system models. The power allocation strategies used are fixed power allocation (FPA) and dynamic power allocation using constrained optimization (COPA) and convex optimization (CON-OPA) algorithms respectively. The whole analysis is carried out under different modulation schemes to study the effect on system BER of the two-user MIMO-PD-NOMA system.

4.2. SYSTEM MODEL

The following two cases depict two different kinds of system models that have been explored in this chapter.

CASE I:

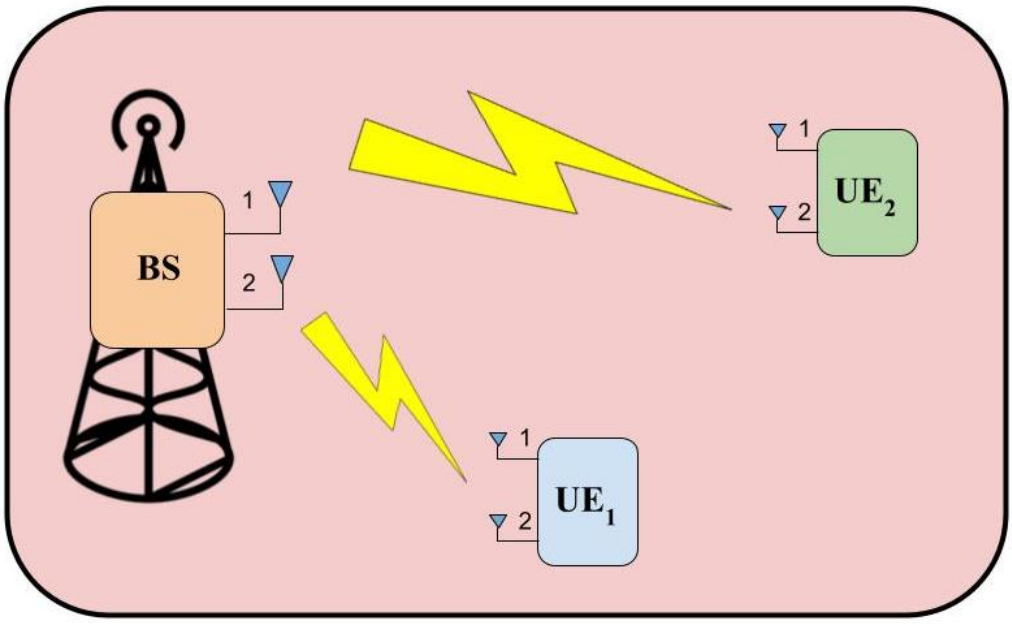

Fig.4.1: Downlink Two-User (2x2)-MIMO-PD-NOMA Model

Fig.4.1 represents a two-user (2x2)-MIMO-PD-NOMA system in a single-cell downlink communication scenario, wherein a single base station (BS), equipped with *M=2* antennas, communicates with *K=2* user equipments (UE_i), equipped with *N=2* antennas each, where $i \in \{1,2\}$. The UE_1 is situated at the smallest distance from the BS, whereas UE_2 is located at the farthest distance from the BS. Each UE has (2x2) communication channel paths between the BS and itself. It is assumed that the total transmitter power is P_t and the wireless links experience independent and identically distributed (i.i.d.) Rayleigh fading with Additive White Gaussian Noise (AWGN). The effective channel gains of the UEs are sorted as: $|z_1 H_1 p_1|^2 \geq |z_2 H_2 p_2|^2$, wherein H_i indicates the (2x2) Rayleigh fading channel matrix from the BS to the i^{th} UE; and p_i and z_i are the precoding and post-coding vectors respectively, for the i^{th} UE.

CASE II:

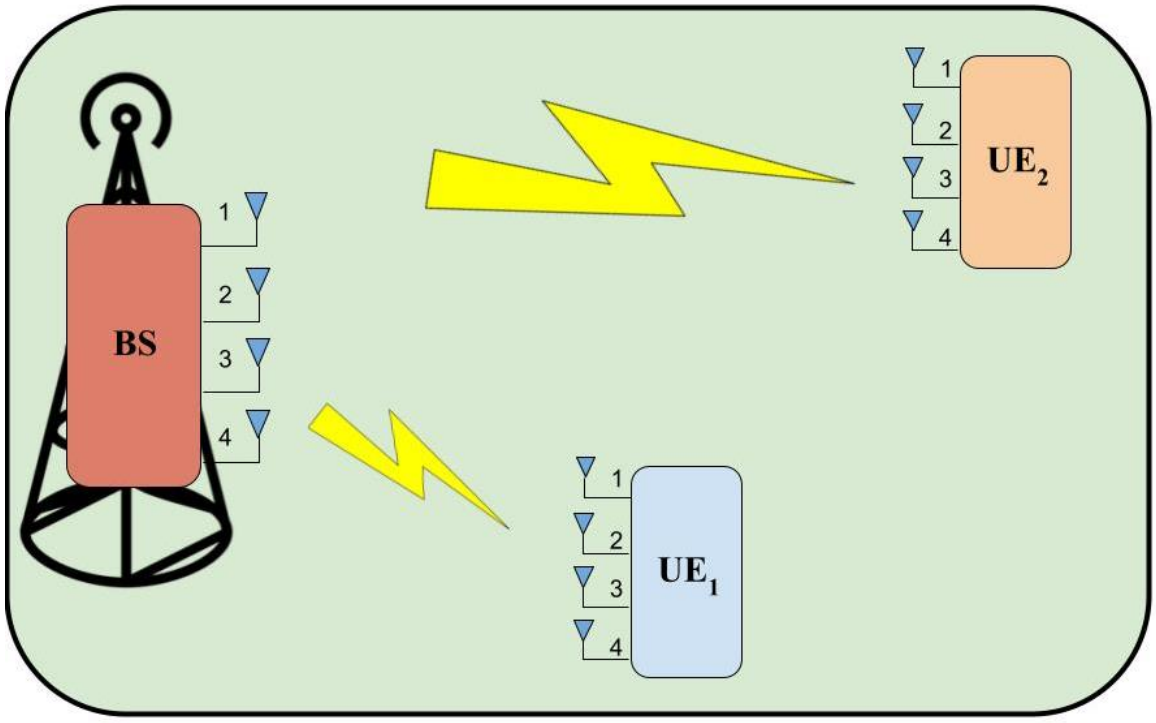

Fig.4.2: Downlink Two-User (4x4)-MIMO-PD-NOMA Model

Fig.4.2 represents a two-user (4x4)-MIMO-PD-NOMA system in a single-cell downlink communication scenario, wherein a single base station (BS), equipped with *M=4* antennas, communicates with *K=2* user equipments (UE_i), equipped with *N=4* antennas each, where $i \in \{1,2\}$. The UE_1 is situated at the smallest distance from the BS, whereas UE_2 is located at the farthest distance from the BS. Each UE has (4x4) communication channel paths between the BS and itself. It is assumed that the total transmitter power is P_t and the wireless links experience independent and identically distributed (i.i.d.) Rayleigh fading with Additive White Gaussian Noise (AWGN). The effective channel gains of the UEs are sorted as: $|z_1 H_1 p_1|^2 \geq |z_2 H_2 p_2|^2$, wherein H_i indicates the (4x4) Rayleigh fading channel matrix from the BS to the i^{th} UE; and p_i and z_i are the precoding and post-coding vectors respectively, for the i^{th} UE.

Therefore, UE_1 has the highest channel gain and is hence referred to as the

strong user while the other user is labelled as weak user. At the BS, as per the NOMA principle, the signals for the different users are allocated different fraction of the total power and thereafter superposed to be transmitted over the same channel. The strong user is given the least fraction of power compared to the weak user. Hence, the power allocation order of the UEs is as follows: $P_1 < P_2$. The superposed signal is thereafter precoded, as per the respective precoding scheme, and the resultant signal is transmitted through M antennas of the BS. At the receiving end, each UE receives the transmitted signal, through its N antennas, corresponding to MRC receiver diversity scheme, followed by post-coding, if required as per the precoding scheme applied at the transmitter. After that, UE_1 performs SIC to decode and subtract out the information signal intended for UE_2 ; while UE_2 applies direct decoding to its respective resultant received signal.

The mathematical model for the above cases is given in Section 2.2.7 of Chapter 2.

4.3. PROPOSED PRECODING SCHEME

The proposed precoding scheme is based on Singular Value Decomposition (SVD) and since it is a modification of the aforementioned scheme; hence, it has been named MODIFIED SVD. On performing SVD of a channel coefficient matrix, H, it is noted that three matrices, i.e. U, D and V respectively, are obtained. It is shown as follows:

$$svd(H) = [U \;\; D \;\; V^H] \tag{4.1}$$

where, H is a $(N\text{x}M)$ channel coefficient matrix;

V is a $(M\text{x}M)$ unitary matrix;

U is a $(N\text{x}N)$ unitary matrix; and,

D is a $(N\text{x}M)$ diagonal matrix.

V and U are two unitary matrices that are employed at the transmitter and receiver, for corresponding precoding and post-coding purposes. However, the D matrix, which is a diagonal matrix containing singular values, is not utilized anywhere. Therefore, in MODIFIED SVD, this D matrix is squared and employed as an amplification matrix, along with the precoding and post-coding matrices. The squared D matrix happens to contain diagonal values that are comparable to the

respective channel gains, and subsequently, the usage of the gain matrix strengthens the transmitted and received signal. Thus, the resultant precoding (P_{TX}) and post-coding (P_{RX}) matrices that are applied at the transmitter and receiver respectively, are as follows:

$$P_{TX} = V(D^T D) \tag{4.2}$$

$$P_{RX} = (DD^T)U^H \tag{4.3}$$

where, $(.)^T$ is a Transpose operator; and,

$(.)^H$ is a Hermitian operator.

The mathematical analysis of MODIFIED SVD precoding scheme is as follows:

Proof:

Considering N and M to be the number of receiver and transmitter antennas respectively, and H to be a (NxM) channel matrix, then

$$r = HP_{TX}s + w \tag{4.4}$$

where, r is a (Nx1) received signal vector;

s is a (Mx1) transmitted signal vector;

P_{TX} is a (MxM) precoding matrix;

w is a (Nx1) Additive White Gaussian Noise (AWGN) vector.

The SVD of the channel matrix can be stated from equation (4.1):

$$H = UDV^H \tag{4.5}$$

where, U and V are (NxN) and (MxM) unitary matrices respectively; and,

$$D = diag\{\sqrt{g_1}, \sqrt{g_2}, \ldots, \sqrt{g_N}\}$$

where, D a (NxM) diagonal matrix; and

$\sqrt{g_i}$ is the singular value of $H^H H$.

Therefore, using equations (4.2) and (4.5), P_{TX} and H are replaced with the respective forms, whereby equation (4.4) becomes:

$$r = UDV^H V(D^T D)s + w \tag{4.6}$$

At the receiver, the received signal is multiplied by the post-coding vector P_{RX} as:

$$P_{RX}r = P_{RX}(UDV^H Vs + w) \tag{4.7}$$

Using equation (4.3), P_{RX} is replaced with its respective form, whereby equation (4.7) becomes:

$$\hat{r} = (DD^T)U^H(UDV^H V(D^T D)s + w) \tag{4.8}$$

$$\Rightarrow \hat{r} = (DD^T)U^H UDV^H V(D^T D)s + (DD^T)U^H w$$

$$\Rightarrow \hat{r} = (DD^T)(U^H U)D(V^H V)(D^T D)s + (DD^T)Uz^H w \tag{4.9}$$

Since, both U and V are unitary matrices, therefore by the property of unitary matrices,

$$U^H U = I_N = UU^H \tag{4.10}$$

$$V^H V = I_M = VV^H \tag{4.11}$$

Thus, the received signal after post-coding process is as follows:

$$\hat{r} = (DD^T)D(D^T D)s + (DD^T)U^H w \tag{4.12}$$

By the property of diagonal matrix,

$$D^T = D \tag{4.13}$$

Therefore, equation (4.12) becomes

$$\hat{r} = D^2 DD^2 s + \widehat{w} \tag{4.14}$$

$$\Rightarrow \hat{r} = D^5 s + \widehat{w} \tag{4.15}$$

where, $\widehat{w} = (DD^T)U^H w$

Therefore, it can be seen from equation (4.15) that the transmitted signal s will be received with a gain matrix D^5, that employs a gain of $g_i{}^{5/2}$ on each of the

transmitted symbol. This is five times the gain that is applied to the transmitted signal in case of SVD, as shown in Chapter 2.

4.4. PERFORMANCE ANALYSIS OF SIMULATION MODEL

In the following sub-sections, a vast analysis of simulation results, with respect to system BER and Sum Capacity, of downlink two-user (2x2) and (4x4) MIMO-PD-NOMA models have been presented for different types of precoding schemes and varied power allocation strategies. The power allocation strategies employed are fixed power allocation (FPA), constrained optimization power allocation (COPA) and convex optimization power allocation (CON-OPA) mechanisms respectively. The simulation is conducted using MATLAB software. To account for the various aspects of fading environment, each simulation is performed multiple times, and the ensemble average of the results is considered. This approach ensures that different realizations of the fading phenomenon are taken into account and provides a comprehensive understanding of its effects. The various precoding schemes that have been analyzed in the aforementioned system are as follows:

1. Matched Filter (MF)
2. Zero-Forcing (ZF)
3. Regularized Zero-Forcing (RZF)
4. Singular Value Decomposition (SVD)
5. Modified Singular Value Decomposition, i.e., MODIFIED SVD

All the analysis regarding system BER and Sum Capacity have been made considering three types of modulation schemes, under Rayleigh fading channel, as follows:

a) BPSK modulation scheme for both near and far user
b) QPSK modulation scheme for both near and far user
c) QPSK modulation for near user and BPSK for far user, i.e., an Adaptive Modulation scheme

The parameters used for simulation in MATLAB, considering downlink two-user (2x2) and (4x4) MIMO-PD-NOMA models are enlisted in the following tables, i.e., Table 4.1 and Table 4.2 respectively:

Table 4.1: Simulation Parameters for Downlink Two-User (2x2)-MIMO-PD-NOMA Model

PARAMETERS	VALUES
Transmitter Power	5 Watt
Number of Transmitter Antenna at the Base Station	2
Number of Receiver Antenna per User Equipment (UE_i)	2
Power Allocation Coefficient for near user (UE_1), when employing FPA	0.2
Power Allocation Coefficient for far user (UE_2), when employing FPA	0.8
Target Fairness Factor, when employing COPA	0.7
Bandwidth	80 MHz

Table 4.2: Simulation Parameters for Downlink Two-User (4x4)-MIMO-PD-NOMA Model

PARAMETERS	VALUES
Transmitter Power	5 Watt
Number of Transmitter Antenna at the Base Station	4
Number of Receiver Antenna per User Equipment (UE_i)	4
Power Allocation Coefficient for near user (UE_1), when employing FPA	0.2
Power Allocation Coefficient for far user (UE_2), when employing FPA	0.8
Target Fairness Factor, when employing COPA	0.7
Bandwidth	80 MHz

4.4.1. Simulation Result Analysis of two-user (2x2)-MIMO-PD-NOMA model for different precoding techniques using FPA:

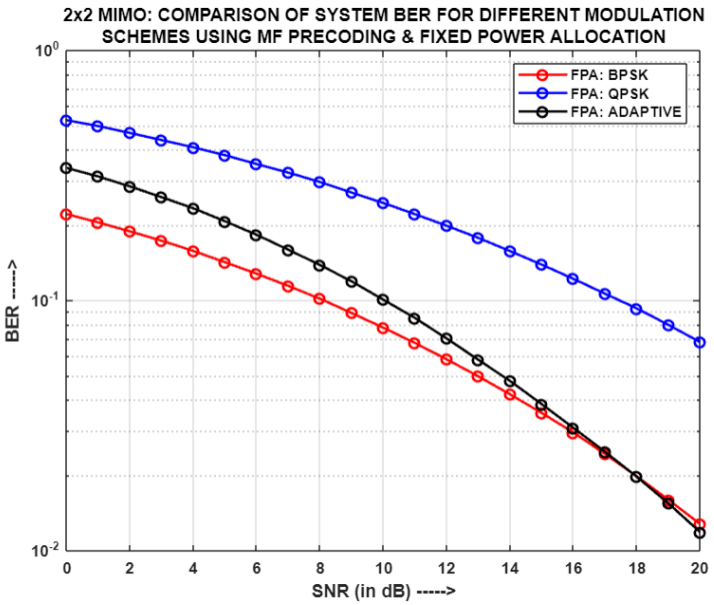

Fig.4.3: For (2x2)-MIMO-NOMA: Comparison of System BER for different modulation schemes using MF and FPA

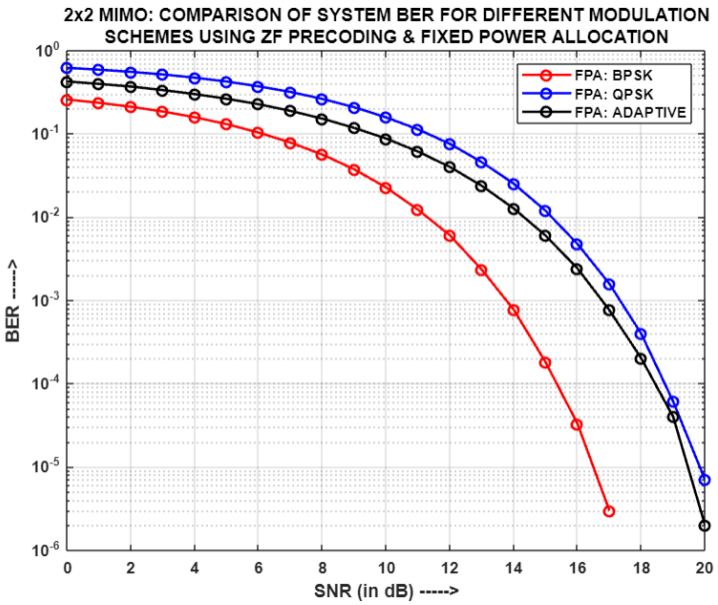

Fig.4.4: For (2x2)-MIMO-NOMA: Comparison of System BER for different modulation schemes using ZF and FPA

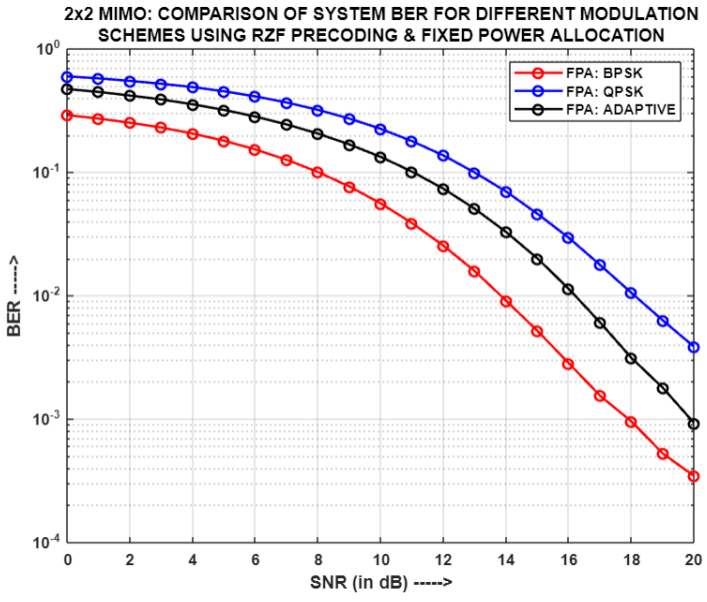

Fig.4.5: For (2x2)-MIMO-NOMA: Comparison of System BER for different modulation schemes using RZF and FPA

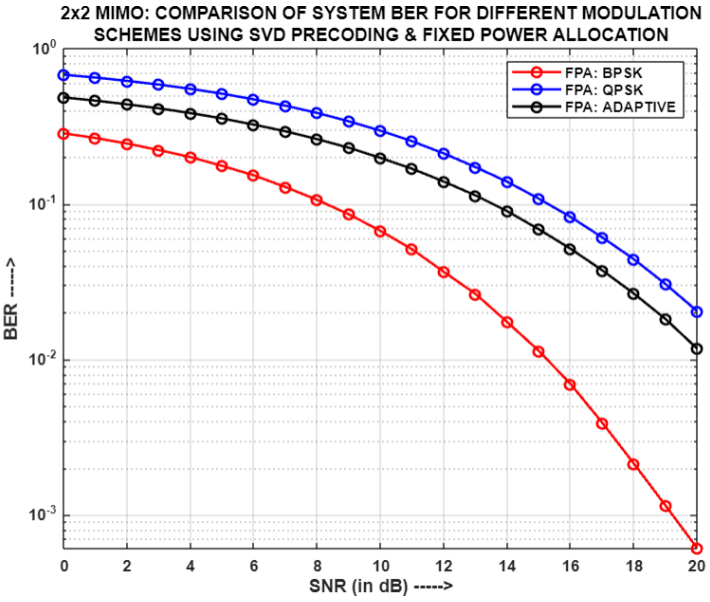

Fig.4.6: For (2x2)-MIMO-NOMA: Comparison of System BER for different modulation schemes using SVD and FPA

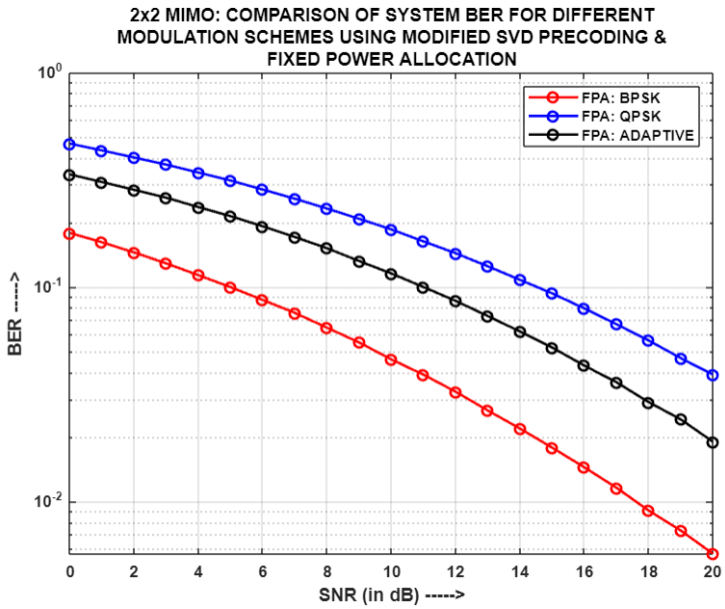

Fig.4.7: For (2x2)-MIMO-NOMA: Comparison of System BER for different modulation schemes using MODIFIED SVD and FPA

Fig.4.3, Fig.4.4, Fig.4.5, Fig.4.6 and Fig.4.7 depicts the comparison of system BER for different modulation schemes using MF, ZF, RZF, SVD and MODIFIED SVD precoding techniques respectively, with two antennas per entity in the system, and fixed power allocation (FPA). It has been observed that for all the five precoding mechanisms, BPSK and QPSK yield the lowest and the highest system BER respectively. This is because in case of BPSK, each transmitted symbol contains only one bit, thereby reducing the likelihood of multiple bit errors at the receiver. On the other hand, QPSK transmits two bits simultaneously, increasing the probability of bit errors at the receiver. However, since Adaptive modulation is a combination of BPSK and QPSK, therefore it demonstrates a system BER that lies in between the two mentioned modulation schemes. Thus, for the aforementioned scenario, the system BER of Adaptive modulation is satisfactory, but it neither does surpass that of BPSK nor exceeds that of QPSK.

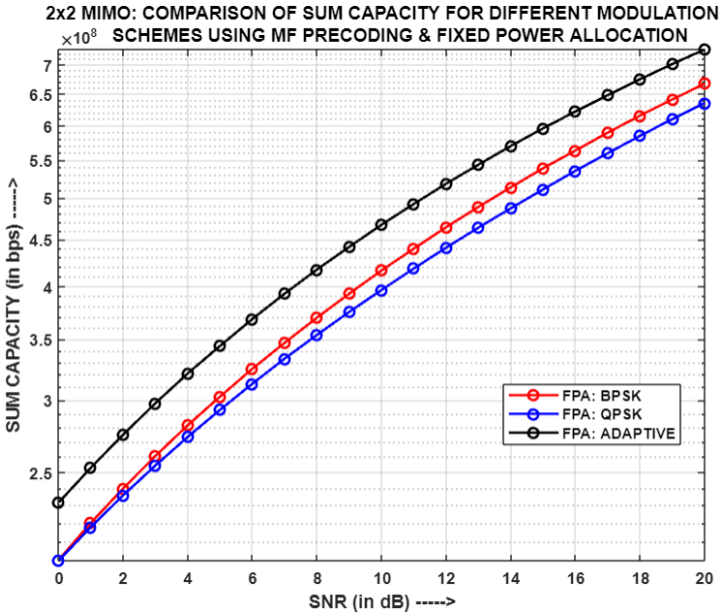

Fig.4.8: For (2x2)-MIMO-NOMA: Comparison of Sum Capacity for different modulation schemes using MF and FPA

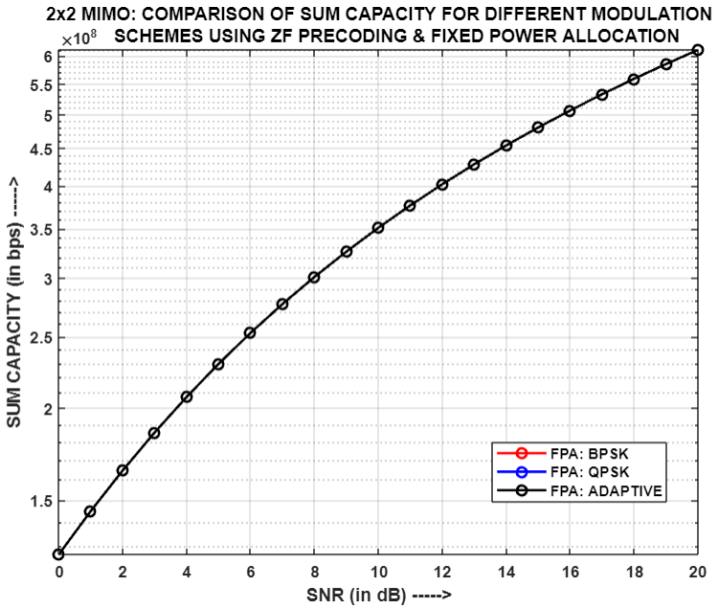

Fig.4.9: For (2x2)-MIMO-NOMA: Comparison of Sum Capacity for different modulation schemes using ZF and FPA

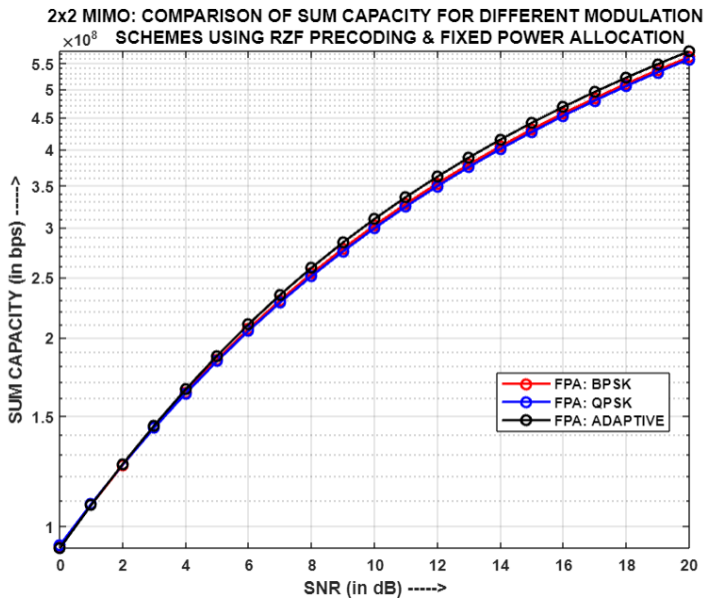

Fig.4.10: For (2x2)-MIMO-NOMA: Comparison of Sum Capacity for different modulation schemes using RZF and FPA

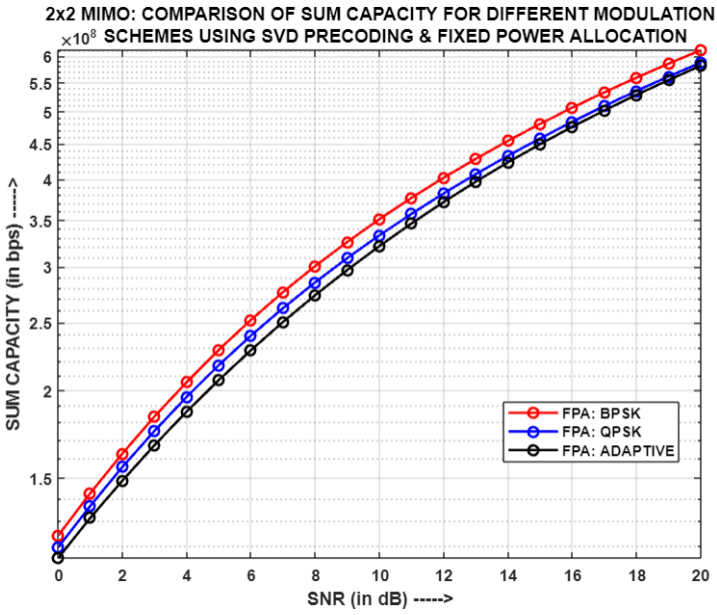

Fig.4.11: For (2x2)-MIMO-NOMA: Comparison of Sum Capacity for different modulation schemes using SVD and FPA

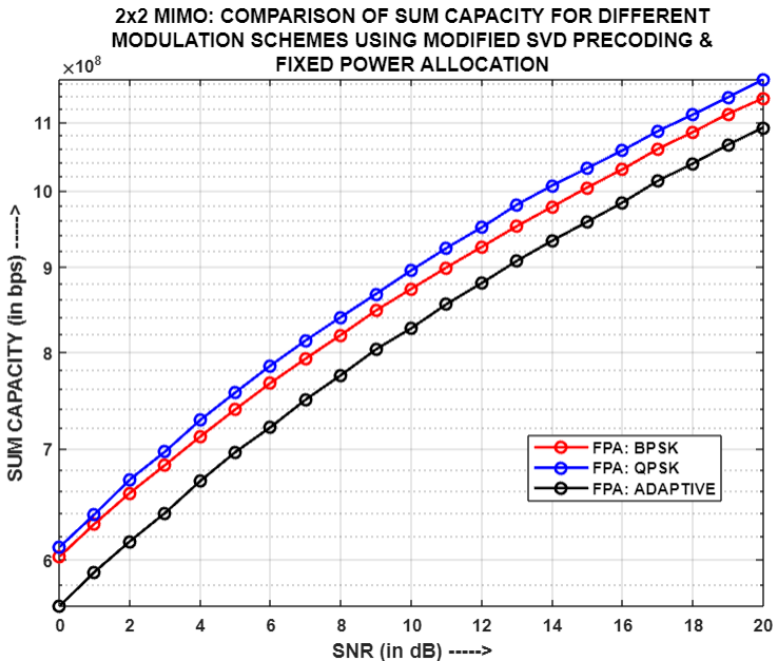

Fig.4.12: For (2x2)-MIMO-NOMA: Comparison of Sum Capacity for different modulation schemes using MODIFIED SVD and FPA

Fig.4.8, Fig.4.9, Fig.4.10, Fig.4.11 and Fig.4.12 portrays the comparison of Sum Capacity for different modulation schemes using MF, ZF, RZF, SVD and MODIFIED SVD precoding techniques respectively, with two antennas per entity in the system, and FPA. It has been noticed that for ZF and RZF precoding mechanisms, the sum capacities for BPSK, QPSK and Adaptive modulations have merged because of similar channel gains and usage of same power allocation coefficient set, for the respective users in the system. However, in case of MF, SVD and MODIFIED SVD, although the same set of power coefficients have been used but still it can be seen that the sum capacities for the different modulations vary slightly from one another. One of the vital reasons behind such a behaviour can be the differing channel gains for the three modulation schemes. As channel gain of a user directly affects its throughput and hence, sum capacity; therefore, such variations in sum capacities is witnessed for different precoding and modulation schemes.

4.4.2. Simulation Result Analysis of two-user (4x4)-MIMO-PD-NOMA model for different precoding techniques using FPA:

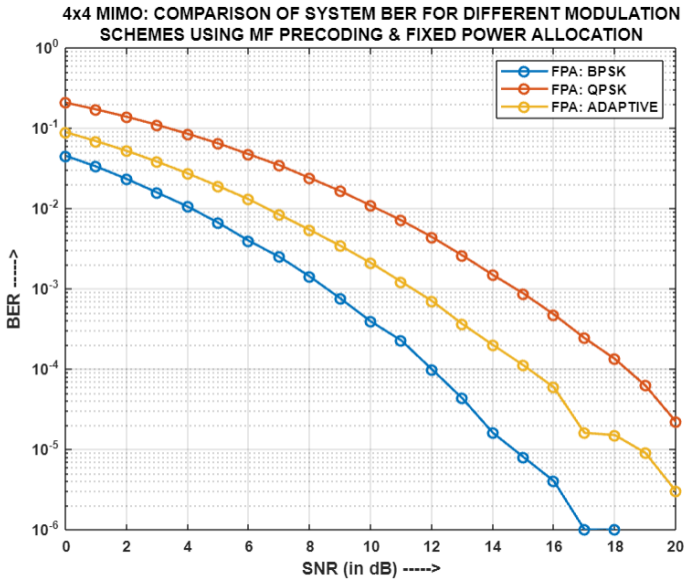

Fig.4.13: For (4x4)-MIMO-NOMA: Comparison of System BER for different modulation schemes using MF and FPA

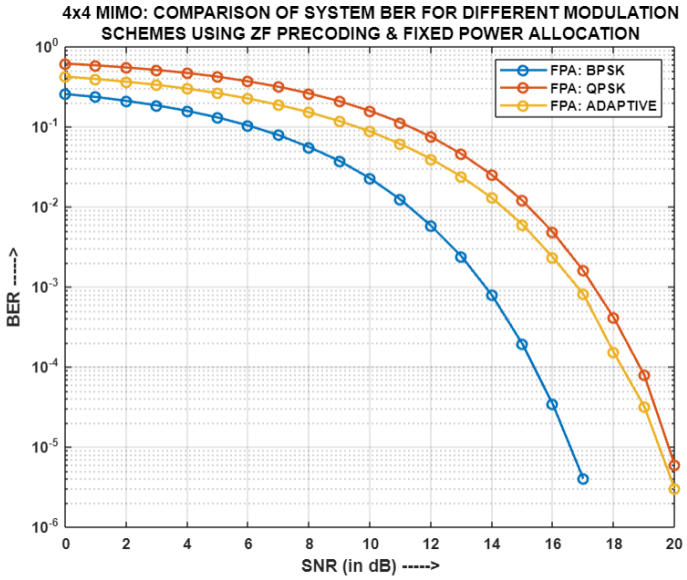

Fig.4.14: For (4x4)-MIMO-NOMA: Comparison of System BER for different modulation schemes using ZF and FPA

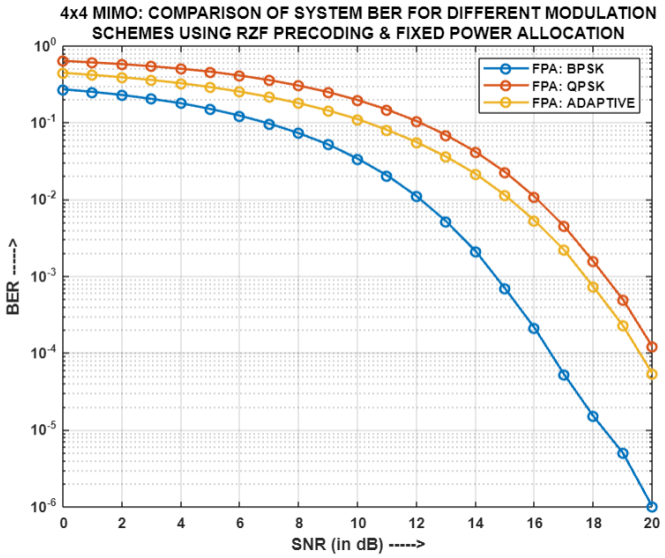

Fig.4.15: For (4x4)-MIMO-NOMA: Comparison of System BER for different modulation schemes using RZF and FPA

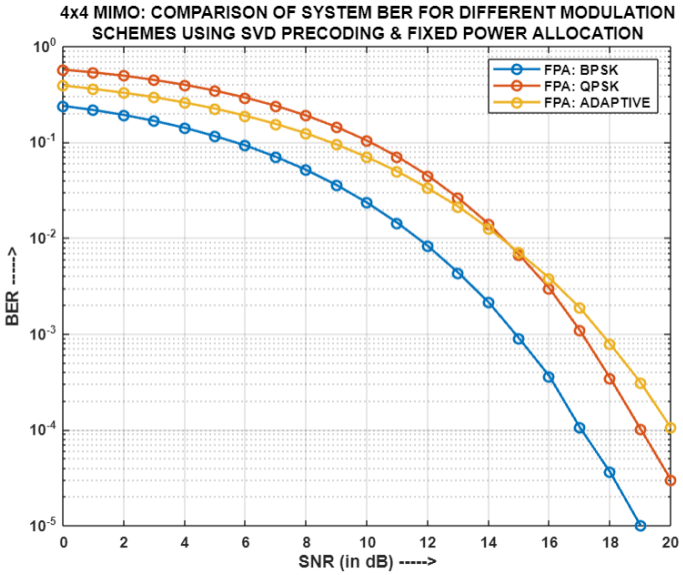

Fig.4.16: For (4x4)-MIMO-NOMA: Comparison of System BER for different modulation schemes using SVD and FPA

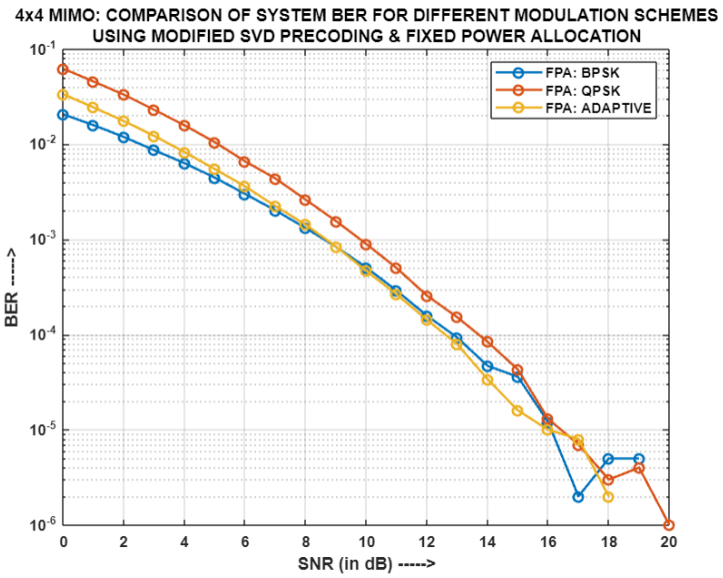

Fig.4.17: For (4x4)-MIMO-NOMA: Comparison of System BER for different modulation schemes using MODIFIED SVD and FPA

Fig.4.13, Fig.4.14, Fig.4.15, Fig.4.16 and Fig.4.17 presents the comparison of system BER for different modulation schemes using MF, ZF, RZF, SVD and MODIFIED SVD precoding techniques respectively, with four antennas per entity in the system, and fixed power allocation (FPA). It has been noted that among MF, ZF and RZF precoding mechanisms, BPSK exhibits the lowest system BER, while QPSK shows the highest. This distinction arises from the fact that BPSK transmits one bit per symbol, minimizing the chances of multiple bit errors at the receiver. Conversely, QPSK transmits two bits concurrently, leading to a higher probability of bit errors at the receiver. However, Adaptive modulation, being a fusion of BPSK and QPSK, falls in between these two modulation schemes in terms of its system BER, for MF, ZF and RZF precoding schemes respectively. In case of SVD, although BPSK yields the least system BER but the performance of QPSK and Adaptive modulations vary slightly from the conventional way. This is because of the usage of more number of antennas at the receiver, which considerably enhances the signal reception for QPSK in the high SNR range, whereby it even crosses the system BER of Adaptive modulation scheme. Again, owing to the utilization of more number of receiver antennas, for better signal reception, as well as because of the supremacy of the MODIFIED SVD precoding scheme, the systems BERs for all three modulations, for the respective precoding, are comparable to each other for almost the entire SNR range.

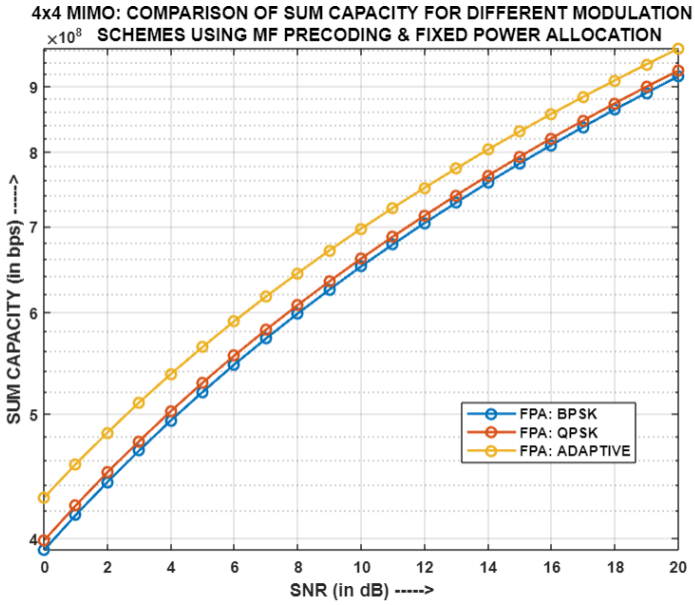

Fig.4.18: For (4x4)-MIMO-NOMA: Comparison of Sum Capacity for different modulation schemes using MF and FPA

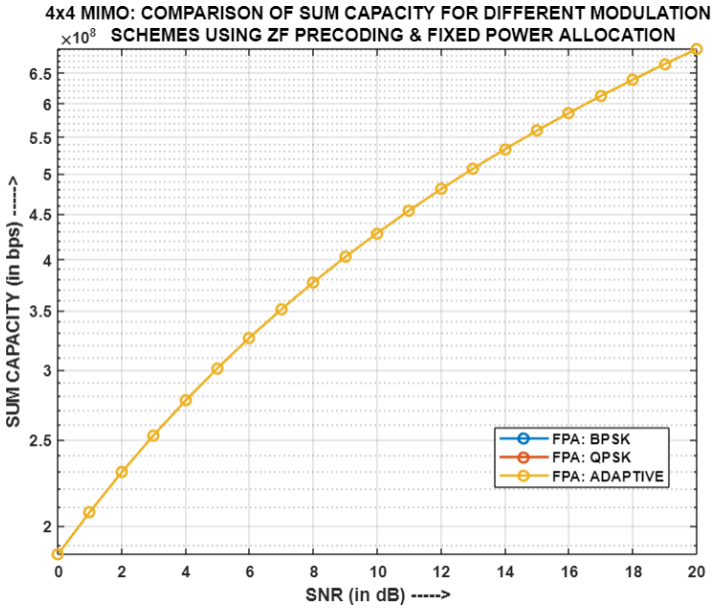

Fig.4.19: For (4x4)-MIMO-NOMA: Comparison of Sum Capacity for different modulation schemes using ZF and FPA

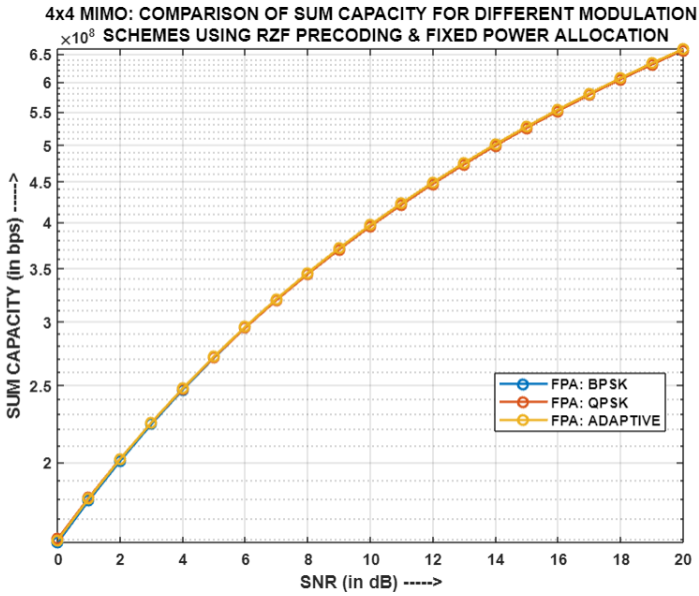

Fig.4.20: For (4x4)-MIMO-NOMA: Comparison of Sum Capacity for different modulation schemes using RZF and FPA

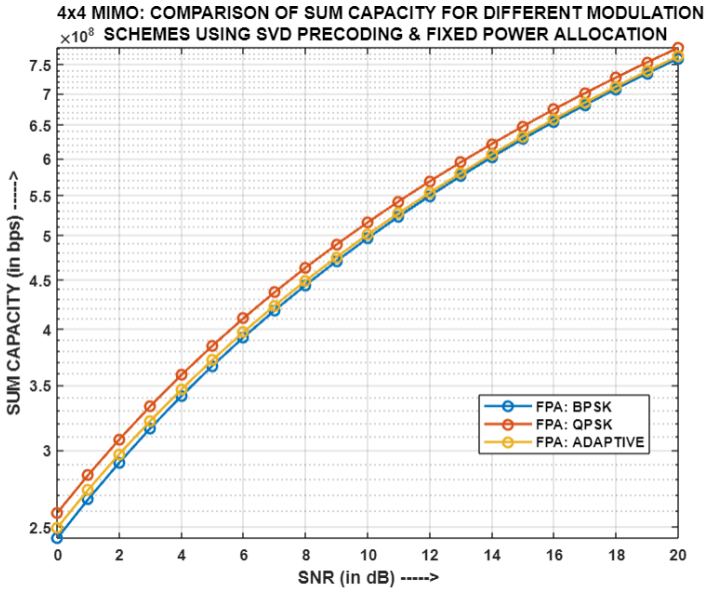

Fig.4.21: For (4x4)-MIMO-NOMA: Comparison of Sum Capacity for different modulation schemes using SVD and FPA

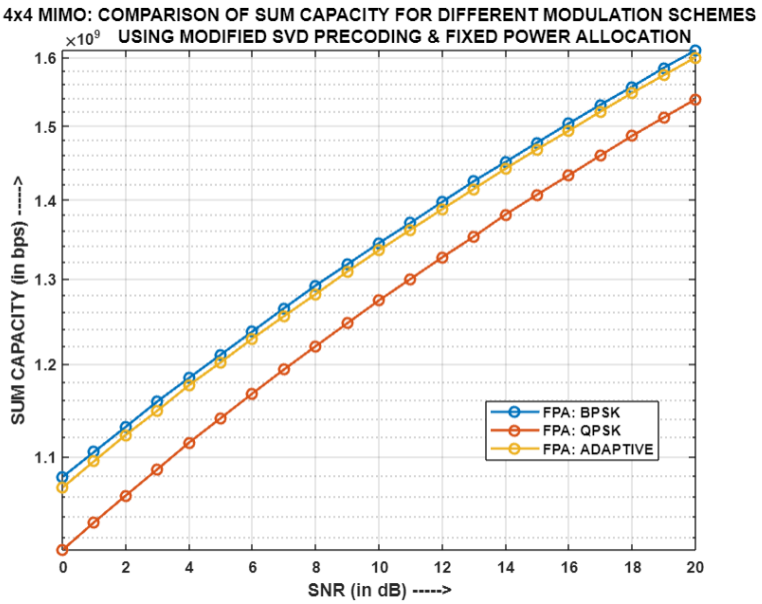

Fig.4.22: For (4x4)-MIMO-NOMA: Comparison of Sum Capacity for different modulation schemes using MODIFIED SVD and FPA

Figures 4.18, 4.19, 4.20, 4.21 and 4.22 represent a comparison of the Sum Capacity for different modulation schemes using various precoding techniques: MF, ZF, RZF, SVD, and MODIFIED SVD. The system configuration includes four antennas per entity and utilizes FPA. Notably, the sum capacities for BPSK, QPSK, and Adaptive modulations appear to merge in the case of ZF and RZF precoding due to similar channel gains and the use of identical power allocation coefficient set for corresponding users. However, with MF, SVD, and MODIFIED SVD, even though the same set of power coefficients is employed, slight variations in sum capacities can be observed among the different modulations. This discrepancy can be attributed to differing channel gains associated with each modulation scheme. Since the channel gain directly impacts user throughput and subsequently the sum capacity, hence such variations in sum capacities are witnessed across different precoding and modulation schemes.

4.4.3. Comparative Analysis of simulation results of two-user (2x2) and (4x4) MIMO-PD-NOMA models for different precoding techniques using FPA:

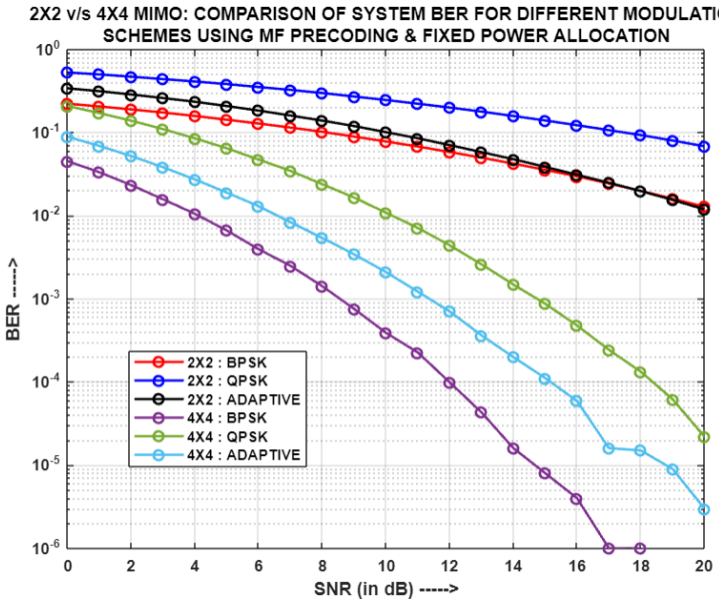

Fig.4.23: (2x2) v/s (4X4) MIMO-NOMA: Comparison of System BER for different modulation schemes using MF and FPA

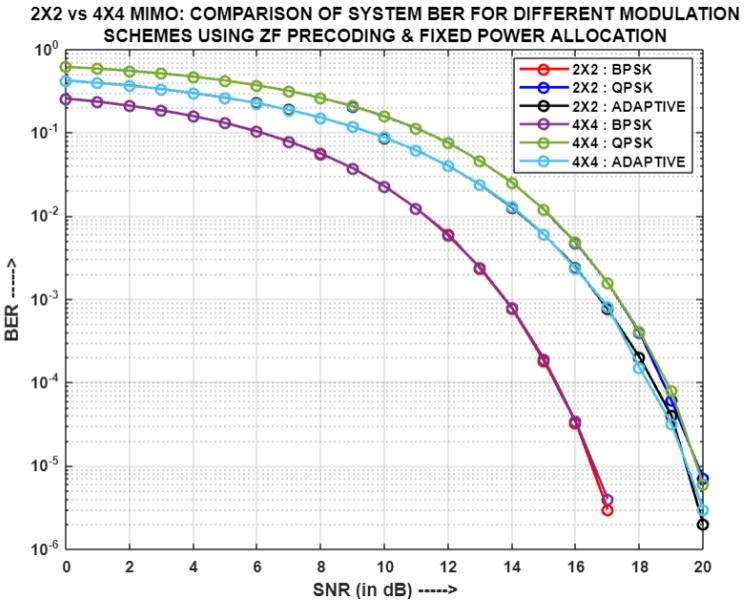

Fig.4.24: (2x2) v/s (4X4) MIMO-NOMA: Comparison of System BER for different modulation schemes using ZF and FPA

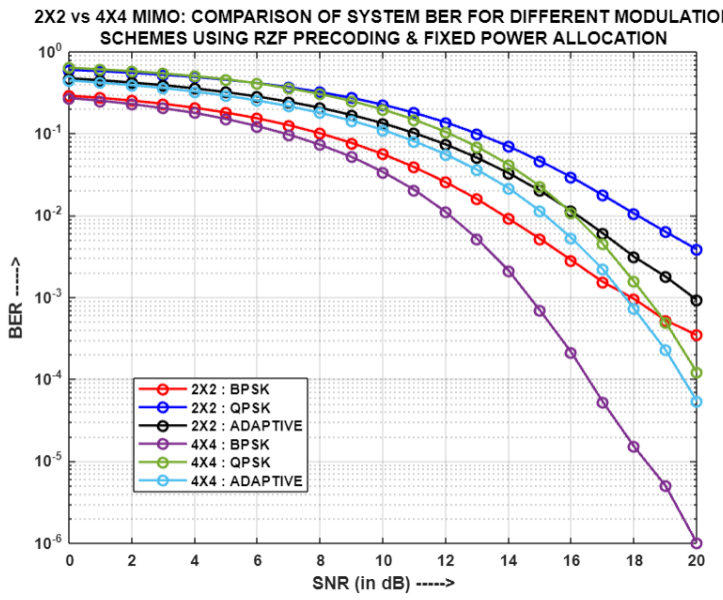

Fig.4.25: (2x2) v/s (4X4) MIMO-NOMA: Comparison of System BER for different modulation schemes using RZF and FPA

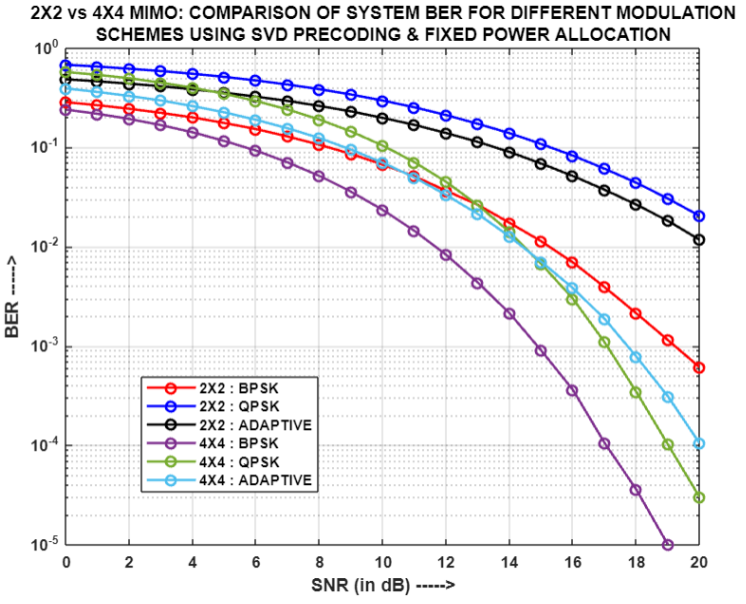

Fig.4.26: (2x2) v/s (4X4) MIMO-NOMA: Comparison of System BER for different modulation schemes using SVD and FPA

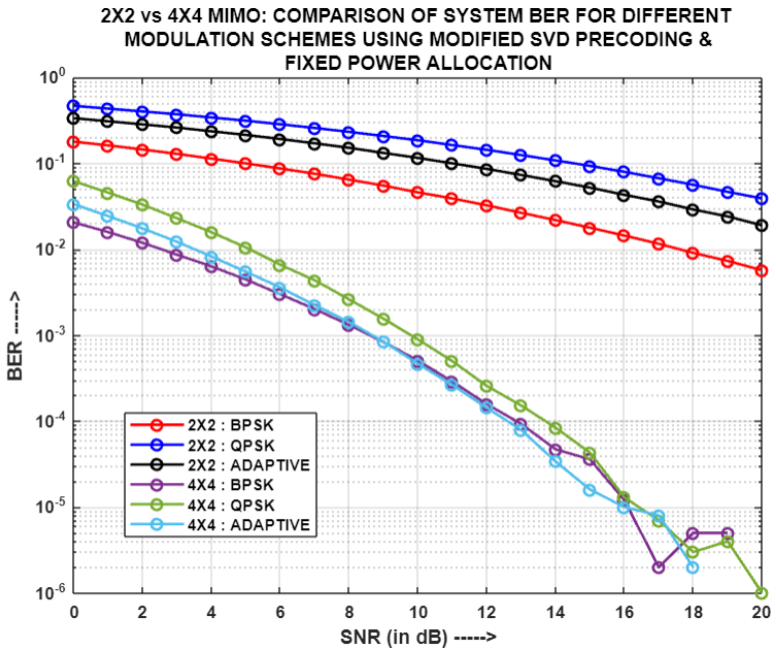

Fig.4.27: (2x2) v/s (4X4) MIMO-NOMA: Comparison of System BER for different modulation schemes using MODIFIED SVD and FPA

Fig.4.23, Fig.4.24, Fig.4.25, Fig.4.26 and Fig.4.27 illustrates the comparison of system BER for different cases of multiple-input-multiple-output (MIMO), i.e. (2x2) and (4x4), using diverse precoding mechanisms respectively, and fixed power allocation (FPA) for employing NOMA principle. It can be seen that for MF, RZF, SVD and MODIFIED SVD precoding schemes, the (4x4) MIMO scenario yields better system BER results than (2x2), for the respective modulation schemes. This is because higher the number of antennas involved in transmission and reception, more will be the number of available channel paths for transfer of information, whereby the signal quality at the receiver enhances. Also, the type of precoding scheme used also plays a crucial role in processing the information signal before transmission so that it can combat the channel effects and reach the receiver in its best form. However, in case of ZF precoding, it is observed that though the number of transmit-receive antennas have been increased but still (4x4) MIMO yields the same performance, with respect to system BER, as its (2x2) counterpart. The reason behind this is that ZF just nullifies the channel effects at the transmitter by multiplying the information signal with the channel's pseudo inverse, whereby the BER is only in accordance to the AWGN noise variance. Therefore, for ZF, both the

MIMO cases produce merged system BERs, for the respective modulation schemes, provided the same set of power coefficient is used for the two cases.

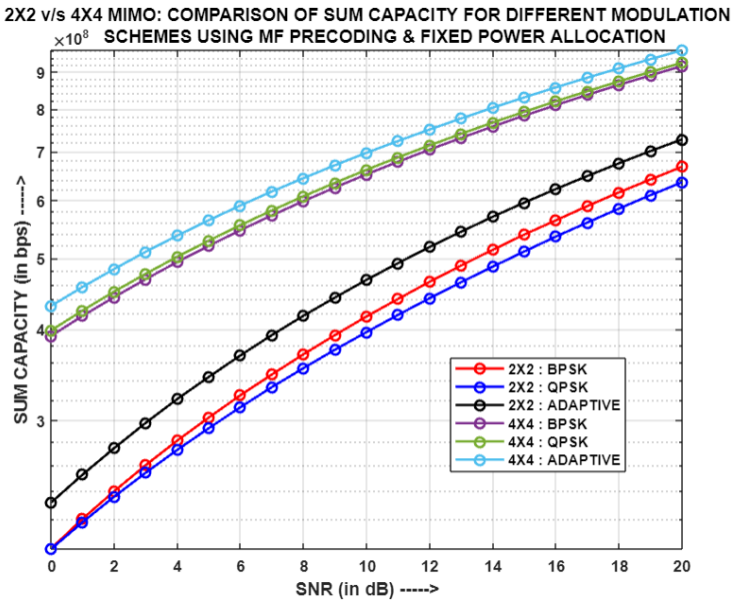

Fig.4.28: (2x2) v/s (4X4) MIMO-NOMA: Comparison of Sum Capacity for different modulation schemes using MF and FPA

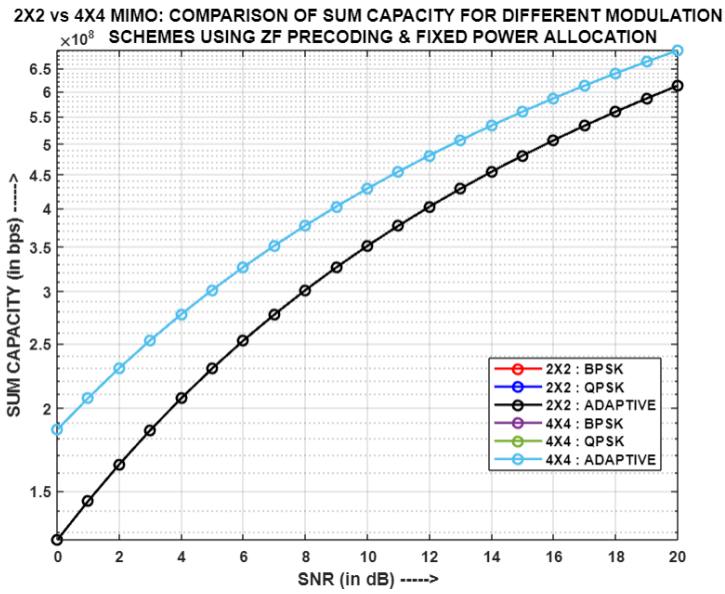

Fig.4.29: (2x2) v/s (4X4) MIMO-NOMA: Comparison of Sum Capacity for different modulation schemes using ZF and FPA

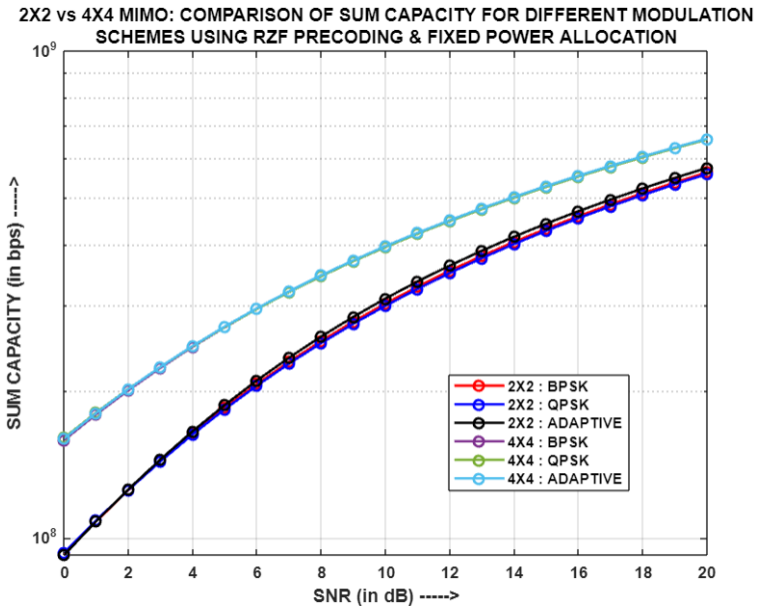

Fig.4.30: (2x2) v/s (4X4) MIMO-NOMA: Comparison of Sum Capacity for different modulation schemes using RZF and FPA

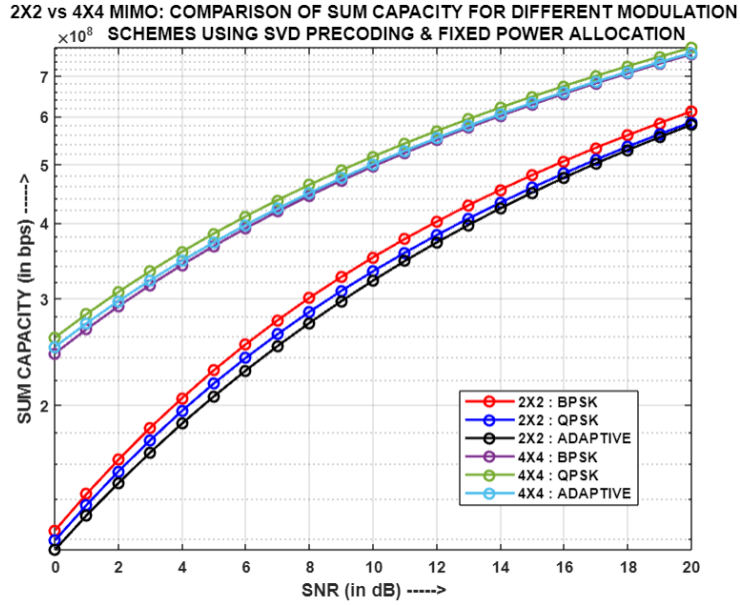

Fig.4.31: (2x2) v/s (4X4) MIMO-NOMA: Comparison of Sum Capacity for different modulation schemes using SVD and FPA

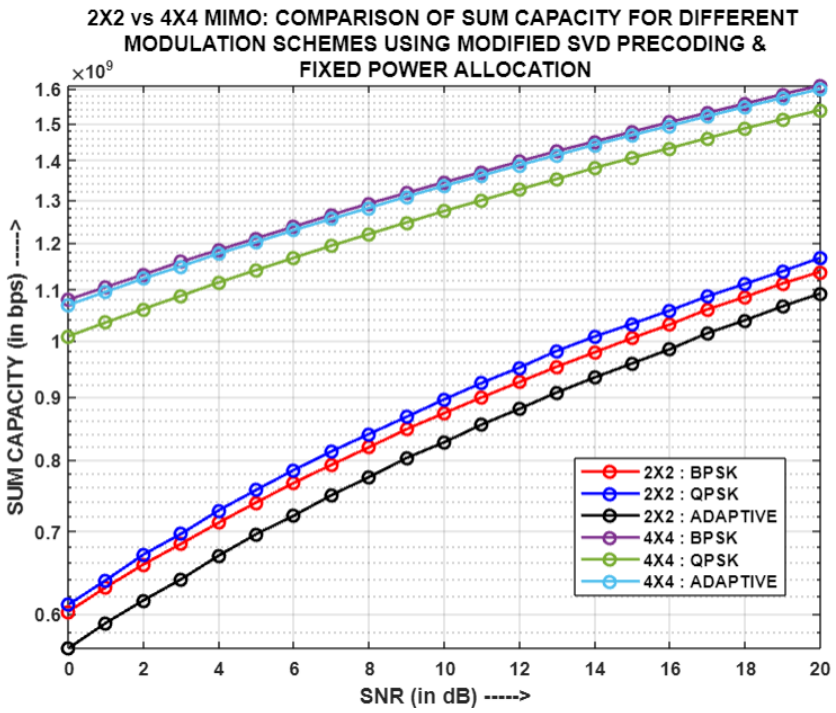

Fig.4.32: (2x2) v/s (4X4) MIMO-NOMA: Comparison of Sum Capacity for different modulation schemes using MODIFIED SVD and FPA

Fig.4.28, Fig.4.29, Fig.4.30, Fig.4.31 and Fig.4.32 depicts the comparison of Sum Capacity for different cases of multiple-input-multiple-output (MIMO), i.e. (2x2) and (4x4), using diverse precoding mechanisms respectively, and fixed power allocation (FPA) for applying NOMA principle. It has been observed that for all the five precoding schemes, (4x4) MIMO yields higher sum capacity than (2x2) MIMO, for the respective modulation schemes. This is because the former provides 16 channel paths for each of the two users in the system, while the latter only provides 4 channel paths per user. Therefore, higher the number of channel paths available to a user, more is the amount of received data, implying an increase in throughput and hence, enhancement in the sum capacity of the system.

4.4.4. Simulation Result Analysis of two-user (2x2)-MIMO-PD-NOMA model for different precoding techniques using COPA:

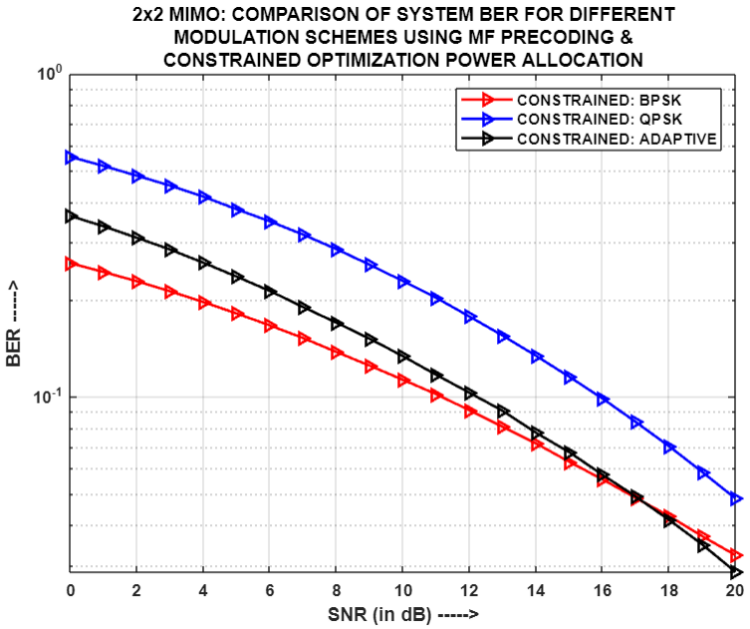

Fig.4.33: For (2x2)-MIMO-NOMA: Comparison of System BER for different modulation schemes using MF and COPA

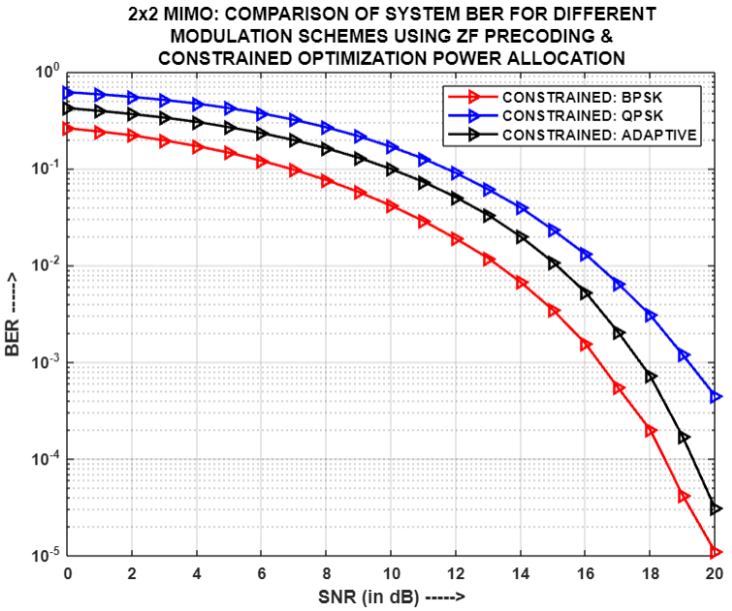

Fig.4.34: For (2x2)-MIMO-NOMA: Comparison of System BER for different modulation schemes using ZF and COPA

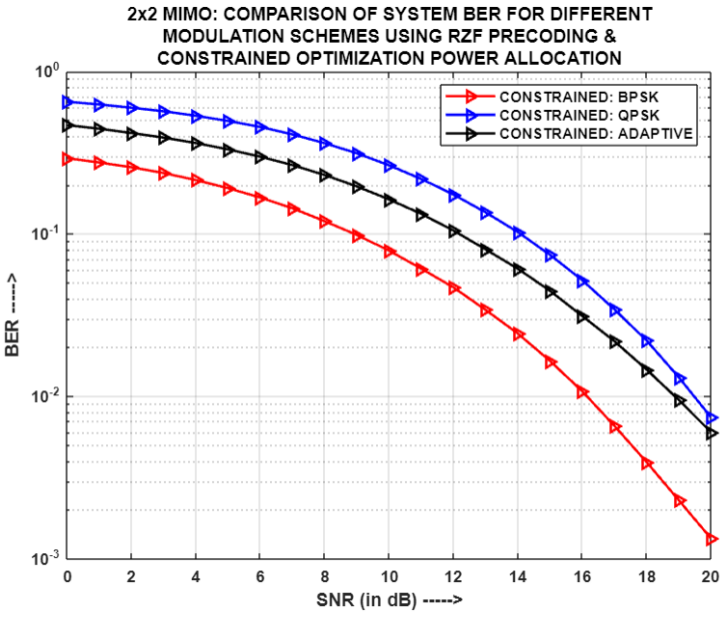

Fig.4.35: For (2x2)-MIMO-NOMA: Comparison of System BER for different modulation schemes using RZF and COPA

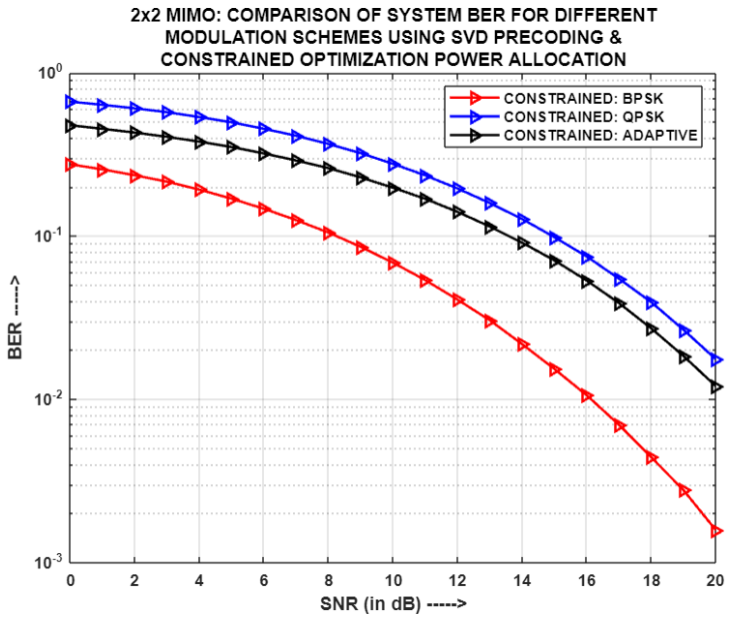

Fig.4.36: For (2x2)-MIMO-NOMA: Comparison of System BER for different modulation schemes using SVD and COPA

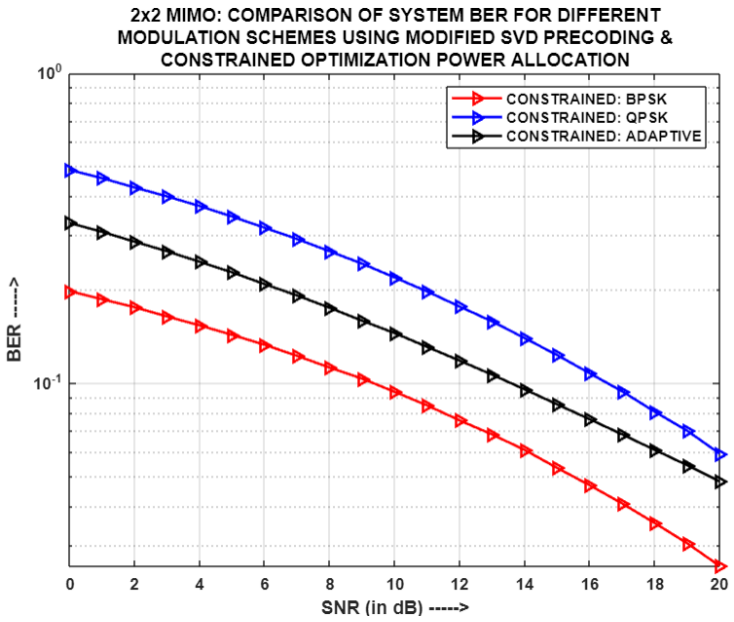

Fig.4.37: For (2x2)-MIMO-NOMA: Comparison of System BER for different modulation schemes using MODIFIED SVD and COPA

The comparison of system BER for different modulation schemes using various precoding techniques, i.e. MF, ZF, RZF, SVD, and MODIFIED SVD respectively, with two antennas per entity in the system and constrained optimization power allocation (COPA) is illustrated in Figures 4.33, 4.34, 4.35, 4.36 and 4.37, respectively. It has been observed that among the five precoding mechanisms, BPSK exhibits the lowest system BER, while QPSK demonstrates the highest. This is due to the fact that BPSK transmits symbols with only one bit, reducing the chances of multiple bit errors at the receiver. Conversely, QPSK transmits two bits simultaneously, leading to an increased probability of bit errors at the receiver. However, since Adaptive modulation combines both BPSK and QPSK, hence it achieves a system BER that falls in between these two modulation schemes. Therefore, in the given scenario, the system BER of Adaptive modulation is satisfactory but does not considerably surpass that of BPSK nor exceeds that of QPSK.

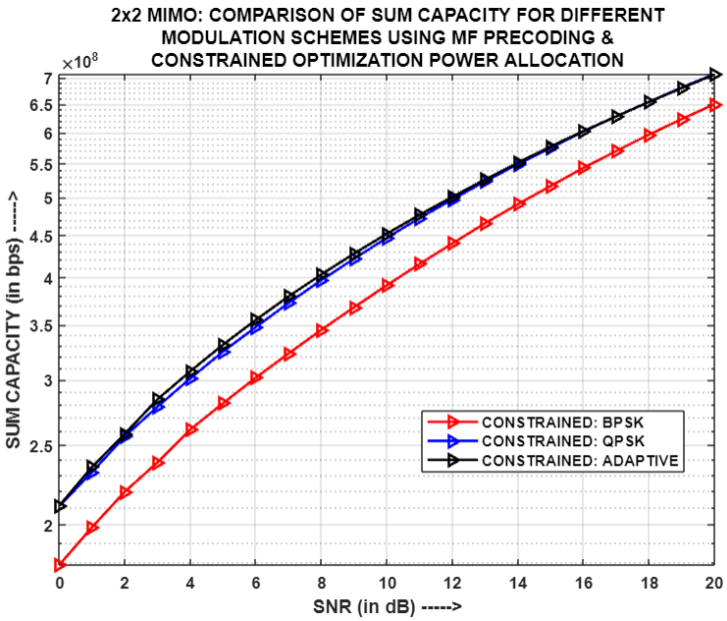

Fig.4.38: For (2x2)-MIMO-NOMA: Comparison of Sum Capacity for different modulation schemes using MF and COPA

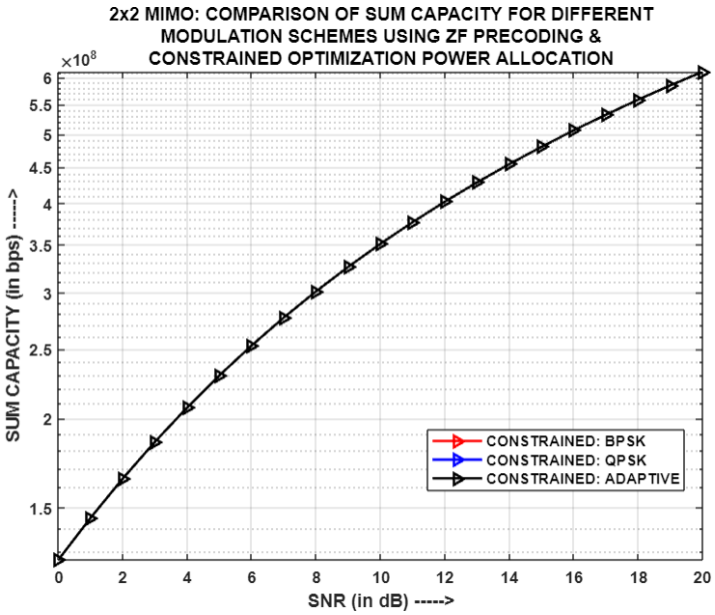

Fig.4.39: For (2x2)-MIMO-NOMA: Comparison of Sum Capacity for different modulation schemes using ZF and COPA

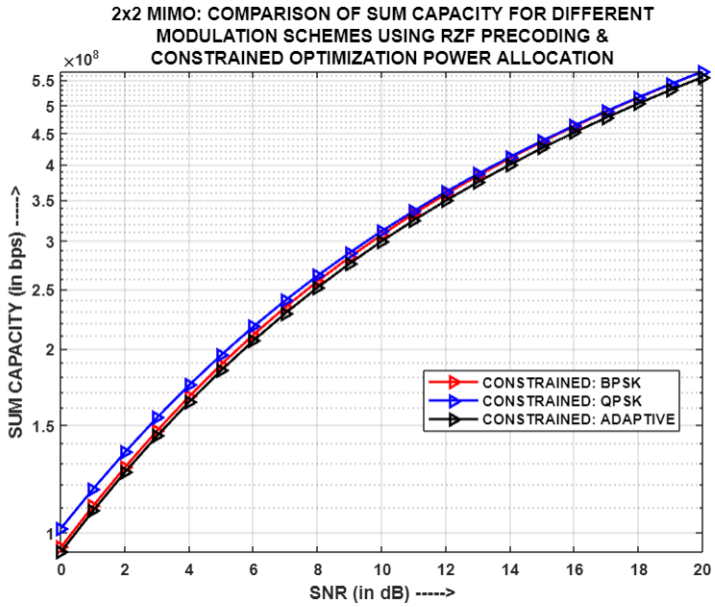

Fig.4.40: For (2x2)-MIMO-NOMA: Comparison of Sum Capacity for different modulation schemes using RZF and COPA

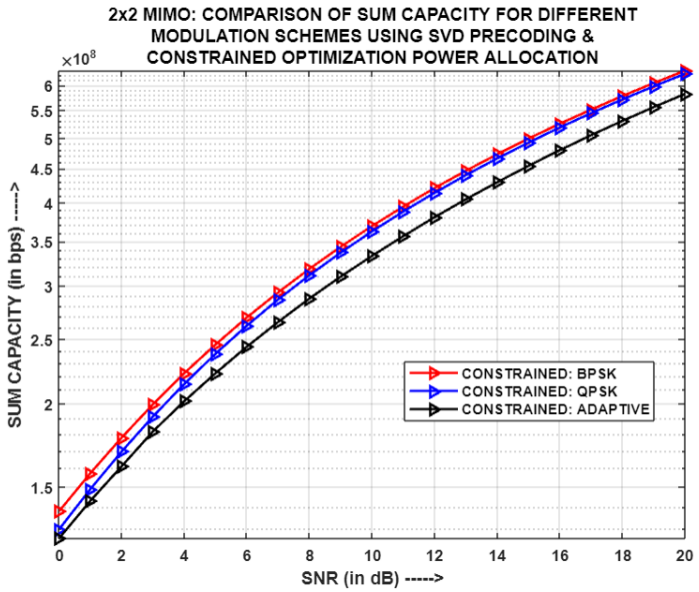

Fig.4.41: For (2x2)-MIMO-NOMA: Comparison of Sum Capacity for different modulation schemes using SVD and COPA

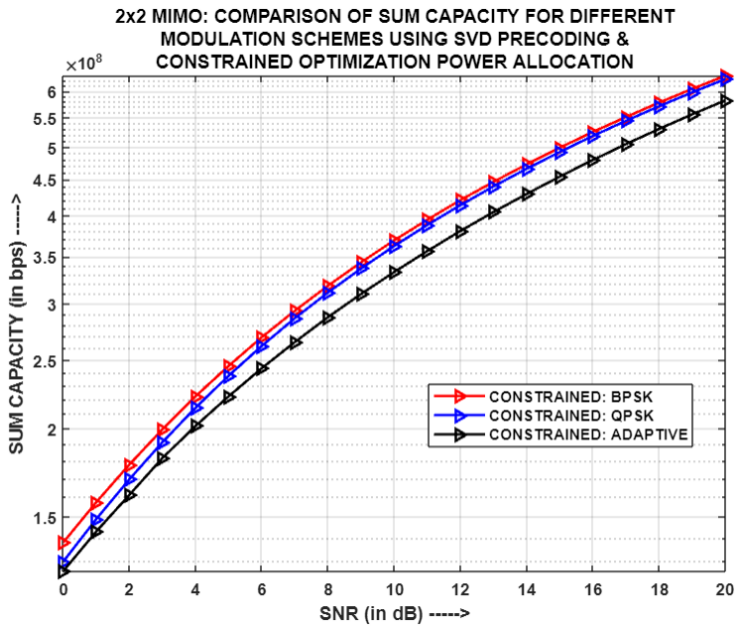

Fig.4.42: For (2x2)-MIMO-NOMA: Comparison of Sum Capacity for different modulation schemes using MODIFIED SVD and COPA

Figures 4.38, 4.39, 4.40, 4.41 and 4.42 display the comparison of Sum Capacity for various modulation schemes utilizing different precoding techniques, i.e. MF, ZF, RZF, SVD, and MODIFIED SVD respectively, with two antennas per entity in the system and using COPA mechanism. It has been witnessed that in case of ZF and RZF precoding mechanisms, the sum capacities for BPSK, QPSK, and Adaptive modulations have almost converged due to similar channel gains and utilization of comparable power allocation coefficient sets for the respective users in the system. However, with MF, SVD, and MODIFIED SVD, slight variations in the sum capacities among the different modulations have been observed. The significant reasons behind this behavior could be the differing channel gains as well as the selection of varied power allocation coefficient sets, across the entire SNR span, for the three modulation schemes. Since the channel gain as well as power coefficients, directly influence the user's throughput and hence the sum capacity, therefore, these variations in sum capacities are noticed for different precoding and modulation schemes.

4.4.5. Simulation Result Analysis of two-user (4x4)-MIMO-PD-NOMA model for different precoding techniques using COPA:

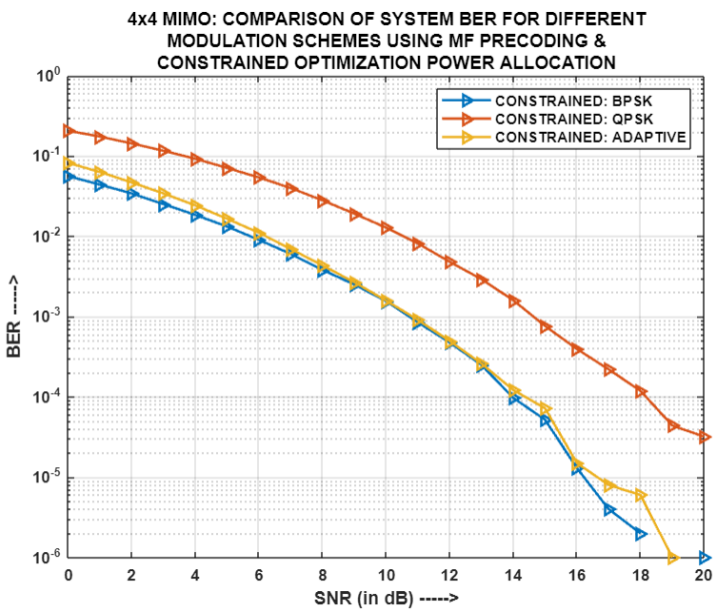

Fig.4.43: For (4x4)-MIMO-NOMA: Comparison of System BER for different modulation schemes using MF and COPA

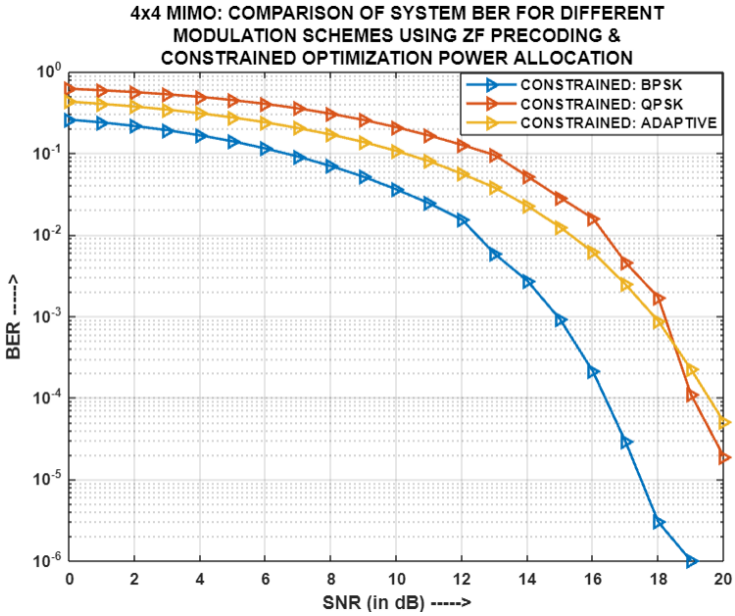

Fig.4.44: For (4x4)-MIMO-NOMA: Comparison of System BER for different modulation schemes using ZF and COPA

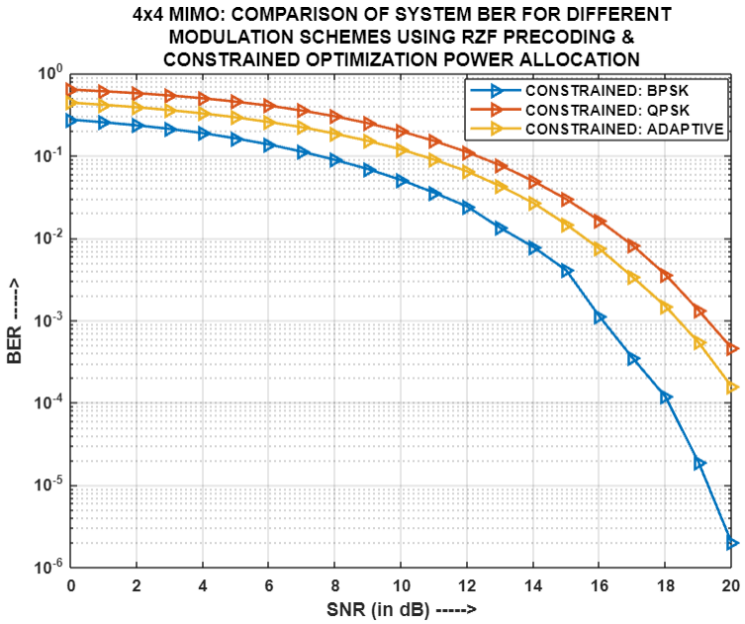

Fig.4.45: For (4x4)-MIMO-NOMA: Comparison of System BER for different modulation schemes using RZF and COPA

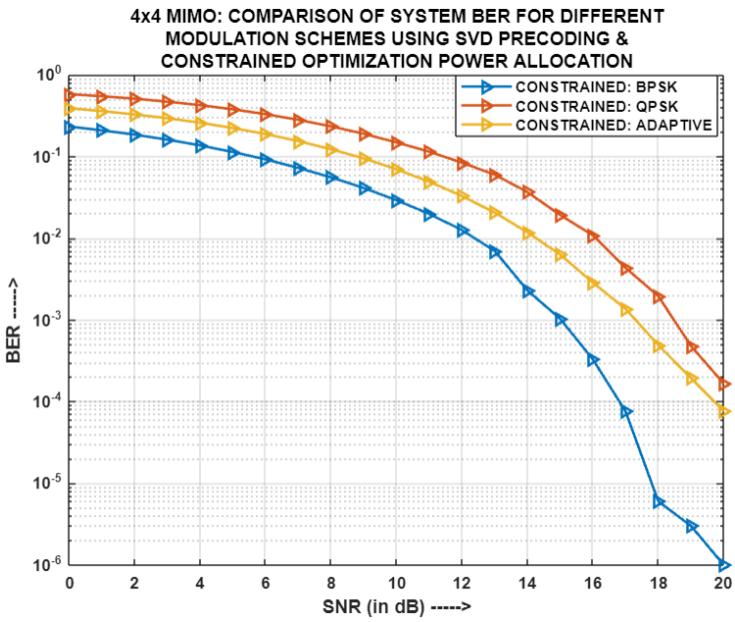

Fig.4.46: For (4x4)-MIMO-NOMA: Comparison of System BER for different modulation schemes using SVD and COPA

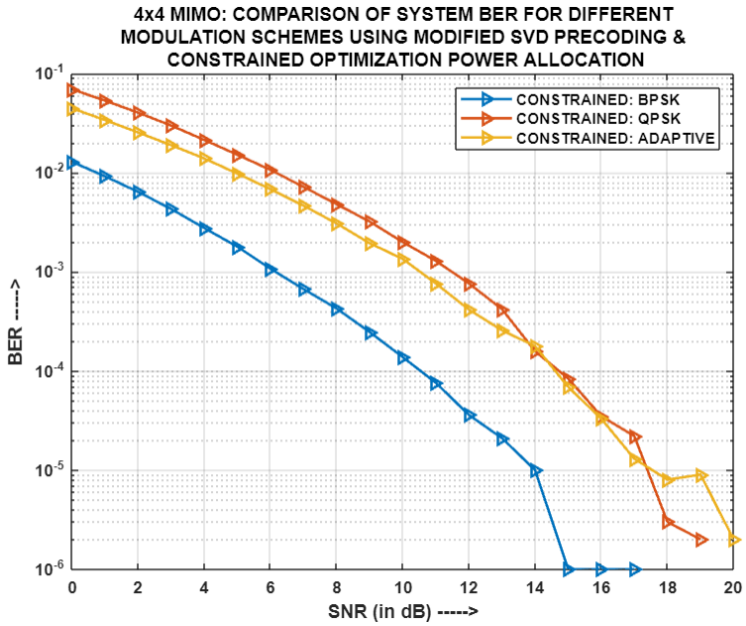

Fig.4.47: For (4x4)-MIMO-NOMA: Comparison of System BER for different modulation schemes using MODIFIED SVD and COPA

Fig.4.43, Fig.4.44, Fig.4.45, Fig.4.46 and Fig.4.47 portrays the comparison of system BER for different modulation schemes using MF, ZF, RZF, SVD, and MODIFIED SVD precoding techniques respectively, with four antennas per entity in the system and COPA mechanism. It has been observed that among ZF, RZF, SVD and MODIFIED SVD precoding mechanisms, BPSK exhibits the least system BER, while QPSK shows the highest. This distinction arises because BPSK transmits one bit per symbol, reducing the likelihood of multiple bit errors at the receiver. In contrast, QPSK transmits two bits simultaneously, increasing the probability of bit errors at the receiver. However, Adaptive modulation, being an amalgamation of both BPSK and QPSK, yields a system BER that lies in between these two modulation schemes, for ZF, RZF, SVD and MODIFIED SVD precoding schemes, respectively. Also, in case of ZF and MODIFIED SVD, it is noticed that the system BER for Adaptive modulation crosses that of QPSK because of utilization of different power coefficient sets for varying SNR values, whereby its respective effect improves the performance of QPSK in the high SNR range. It is because of the dynamic and optimum selection of power allocation coefficient sets, based on COPA, that for MF precoding, the system BERs of BPSK and Adaptive modulations

merge and yield the lowest system BER while QPSK, owing to its nature, produces a comparably higher system BER.

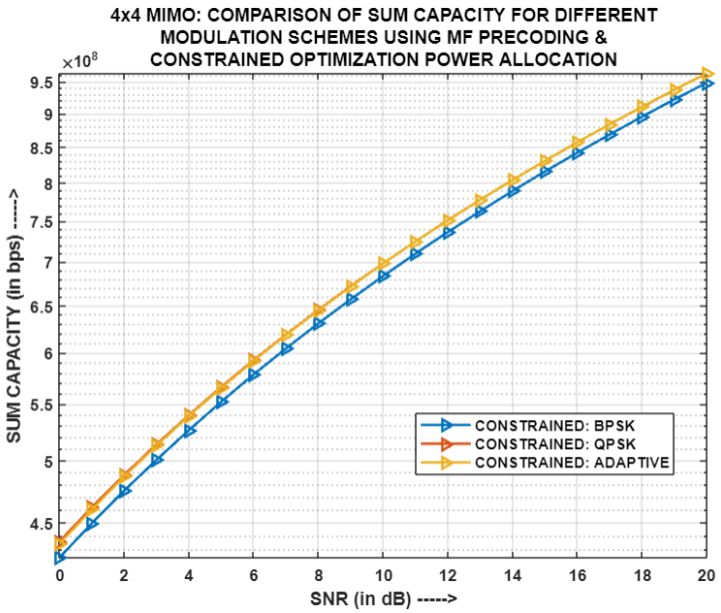

Fig.4.48: For (4x4)-MIMO-NOMA: Comparison of Sum Capacity for different modulation schemes using MF and COPA

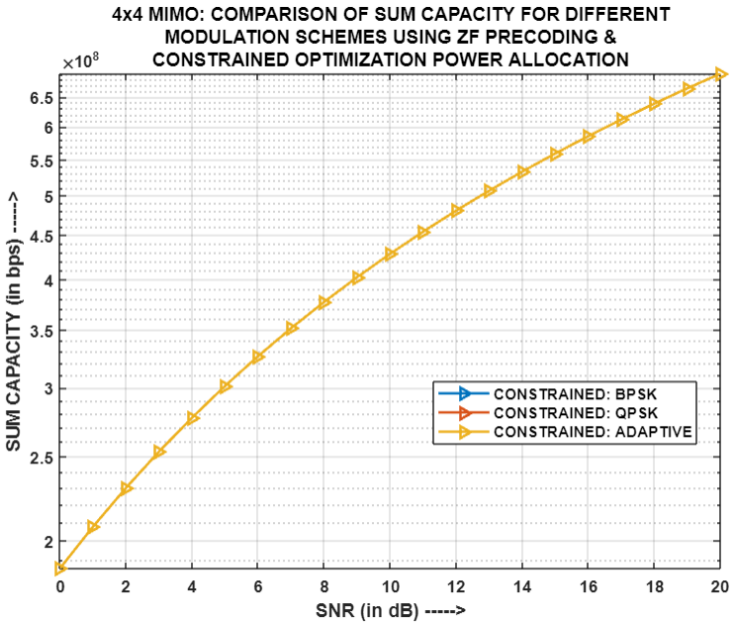

Fig.4.49: For (4x4)-MIMO-NOMA: Comparison of Sum Capacity for different modulation schemes using ZF and COPA

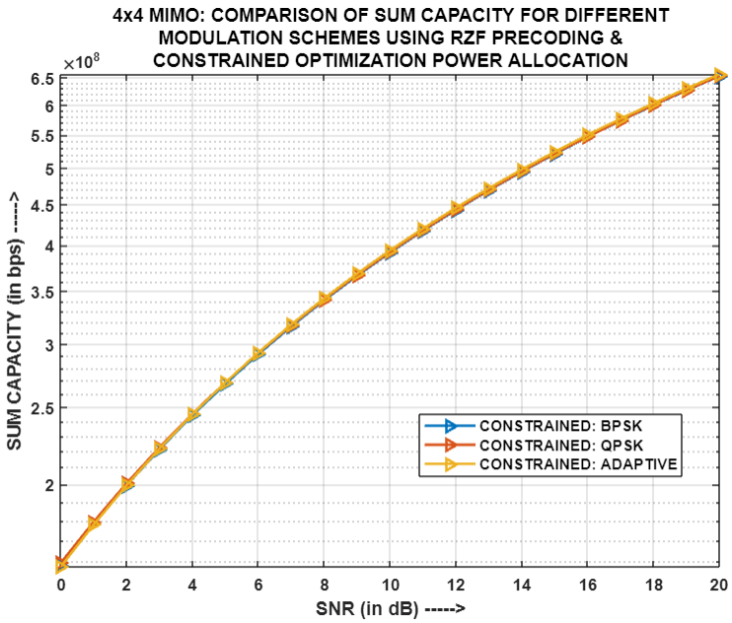

Fig.4.50: For (4x4)-MIMO-NOMA: Comparison of Sum Capacity for different modulation schemes using RZF and COPA

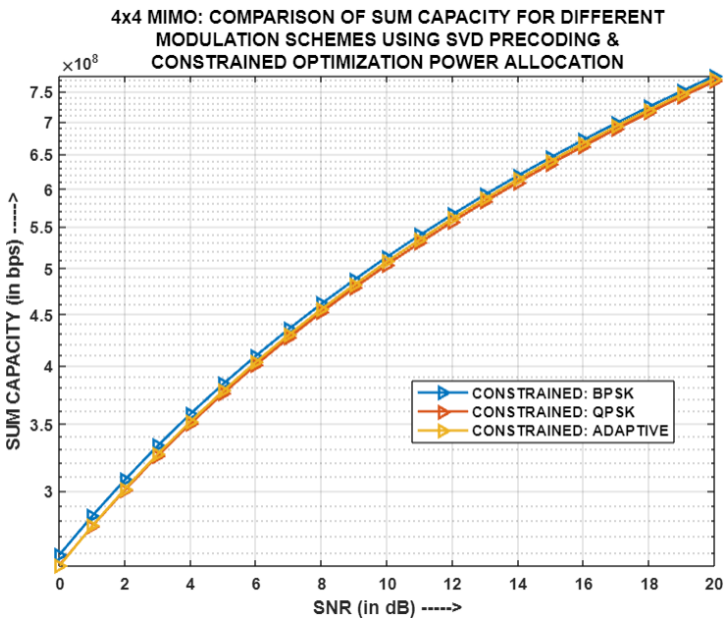

Fig.4.51: For (4x4)-MIMO-NOMA: Comparison of Sum Capacity for different modulation schemes using SVD and COPA

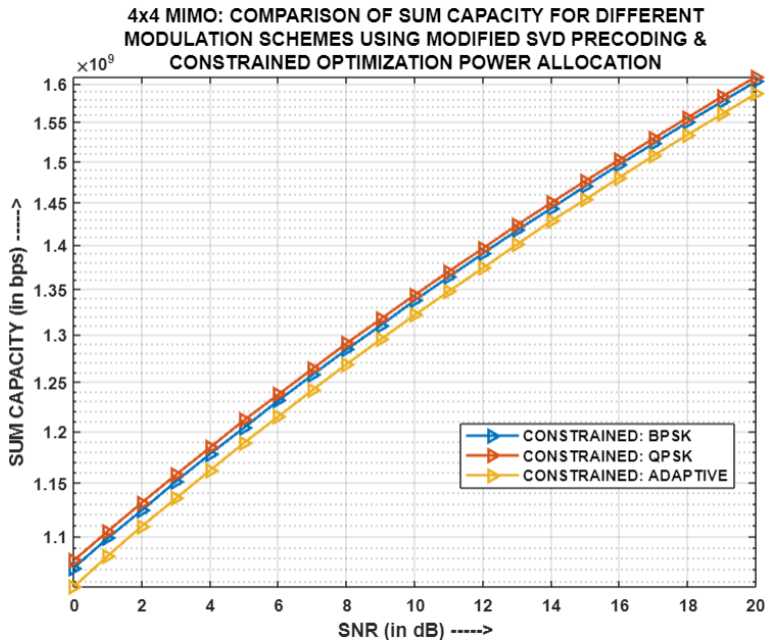

Fig.4.52: For (4x4)-MIMO-NOMA: Comparison of Sum Capacity for different modulation schemes using MODIFIED SVD and COPA

Fig.4.48, Fig.4.49, Fig.4.50, Fig.4.51 and Fig.4.52 presents the comparison of Sum Capacity for different modulation schemes using MF, ZF, RZF, SVD, and MODIFIED SVD precoding techniques respectively, with four antennas per entity in the system and COPA mechanism. It is noteworthy that the sum capacities for BPSK, QPSK, and Adaptive modulations demonstrate a merging trend in case of ZF, RZF and SVD precoding. This convergence can be attributed to similar channel gains and the utilization of comparable power allocation coefficient sets, for the corresponding users. Conversely, when employing MF and MODIFIED SVD, slight variations in the sum capacities are evident among the different modulation schemes. These variations can be attributed to the disparate channel gains as well as selection of slightly different power coefficient sets, associated with each modulation scheme. As channel gain and choice of power coefficients have a direct impact on the user throughput and, subsequently, the sum capacity, therefore, such variations arise across the sum capacities of different precoding and modulation schemes.

4.4.6. Comparative Analysis of simulation results of two-user (2x2) and (4x4) MIMO-PD-NOMA models for different precoding techniques using COPA:

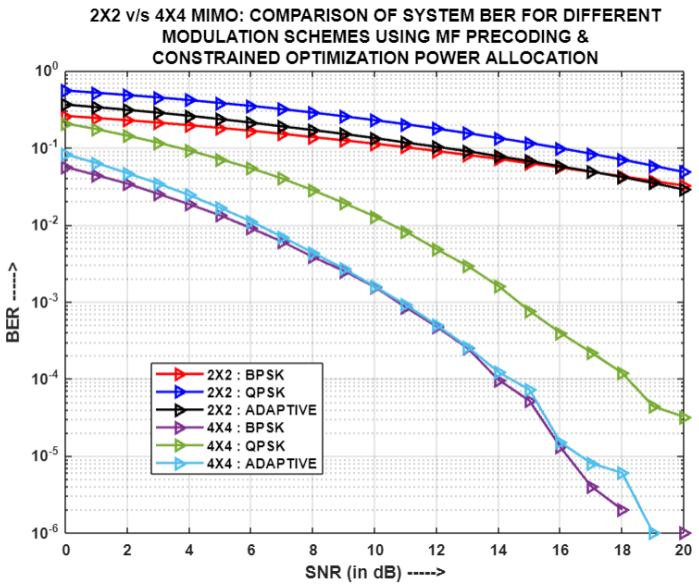

Fig.4.53: (2x2) v/s (4X4) MIMO-NOMA: Comparison of System BER for different modulation schemes using MF and COPA

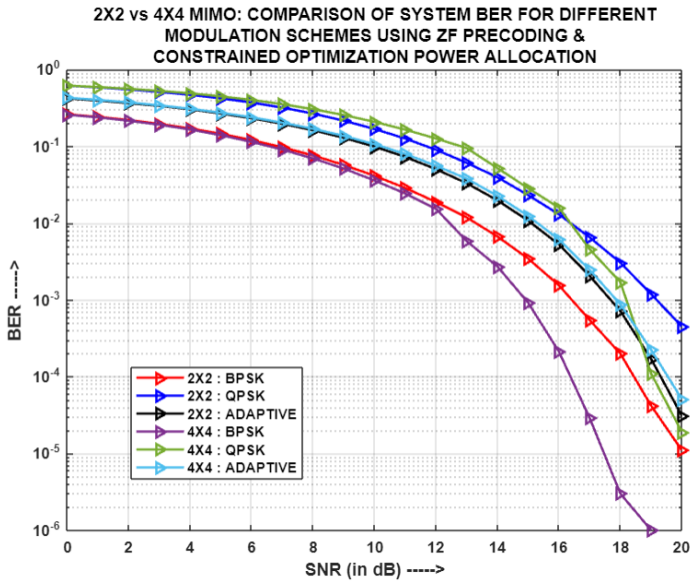

Fig.4.54: (2x2) v/s (4X4) MIMO-NOMA: Comparison of System BER for different modulation schemes using ZF and COPA

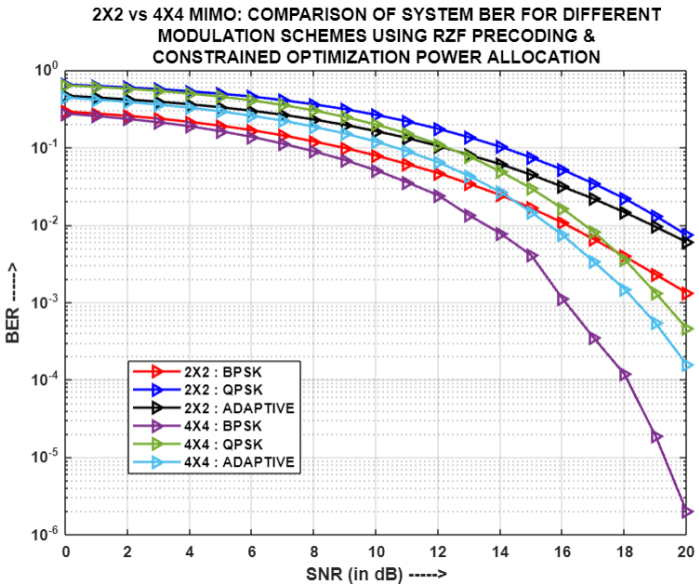

Fig.4.55: (2x2) v/s (4X4) MIMO-NOMA: Comparison of System BER for different modulation schemes using RZF and COPA

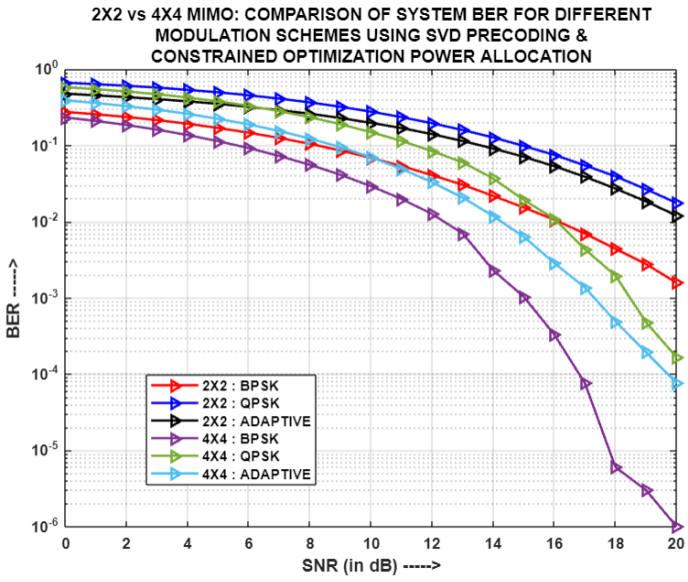

Fig.4.56: (2x2) v/s (4X4) MIMO-NOMA: Comparison of System BER for different modulation schemes using SVD and COPA

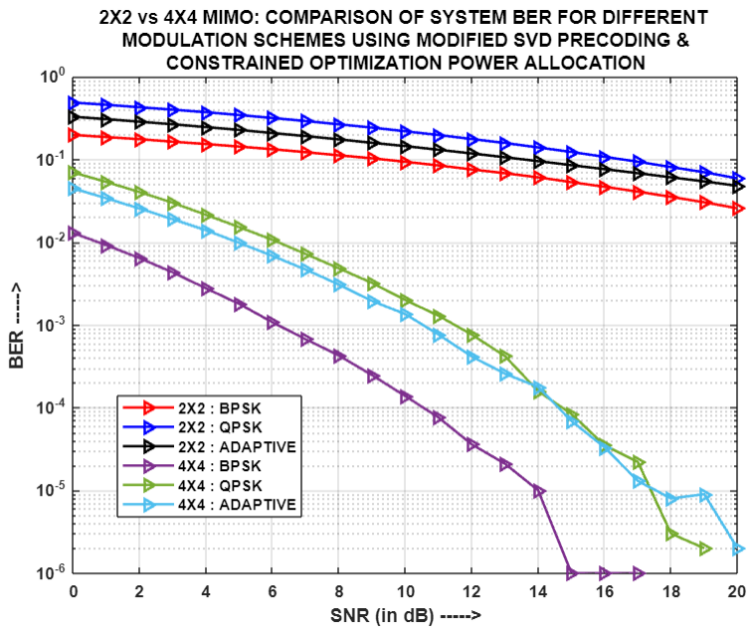

Fig.4.57: (2x2) v/s (4X4) MIMO-NOMA: Comparison of System BER for different modulation schemes using MODIFIED SVD and COPA

Fig.4.53, Fig.4.54, Fig.4.55, Fig.4.56 and Fig.4.57 illustrates the comparison of system BER for different cases of multiple-input-multiple-output (MIMO), i.e. (2x2) and (4x4), using diverse precoding mechanisms respectively, and constrained optimization power allocation (COPA) for employing NOMA principle. It is evident that in the case of MF, RZF, SVD, and MODIFIED SVD precoding schemes, the (4x4) MIMO scenario exhibits improved system BER performance compared to the (2x2) scenario for the corresponding modulation schemes. This improvement can be attributed to the increased number of antennas involved in transmission and reception, resulting in a greater number of available channel paths for information transfer and thereby, enhancing the signal quality at the receiver. Additionally, the choice of precoding scheme also plays a critical role in processing the information signal before transmission, enabling it to effectively combat channel effects and reach the receiver in its optimal form. However, in case of ZF precoding, although for both BPSK and QPSK, (4x4) MIMO yields a better performance than its (2x2) counterpart; but for Adaptive modulation, it is observed that despite increasing the number of transmit-receive antennas, both (4x4) and (2x2) MIMO scenarios generate the same performance in terms of system BER. This can be attributed to ZF's capability to nullify channel effects at the transmitter by multiplying the information signal with the channel's pseudo inverse. As a result, the system BER is

solely influenced by the additive white Gaussian noise (AWGN) variance and the choice of power allocation coefficients sets being used in the system. Therefore, for ZF, in case of BPSK and QPSK, both MIMO cases use different sets of power coefficients and hence, have differing system BER results respectively; while Adaptive modulation coincidentally uses the same power coefficient sets for the two MIMO cases and thus, produce merged system BERs.

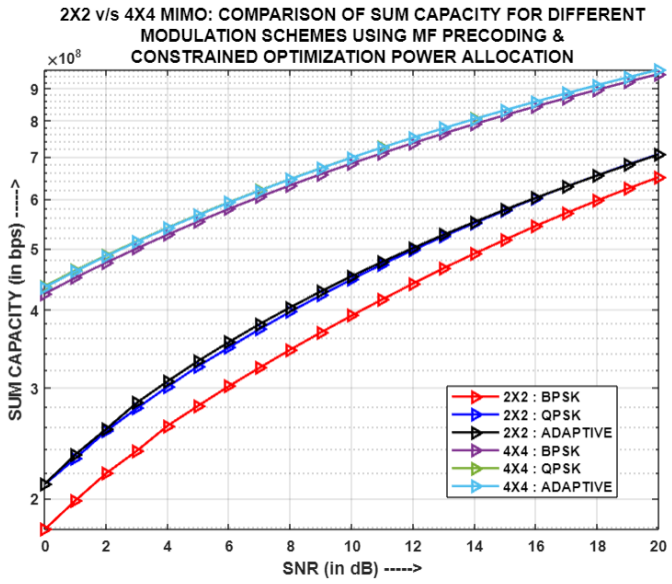

Fig.4.58: (2x2) v/s (4X4) MIMO-NOMA: Comparison of Sum Capacity for different modulation schemes using MF and COPA

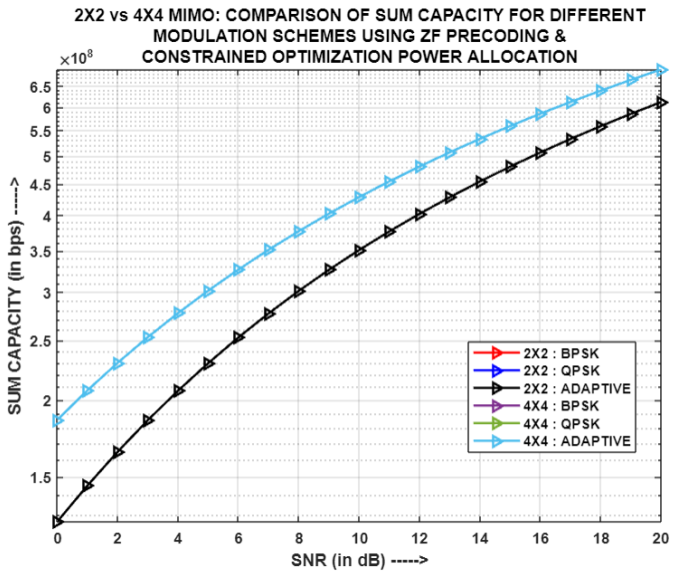

Fig.4.59: (2x2) v/s (4X4) MIMO-NOMA: Comparison of Sum Capacity for different modulation schemes using ZF and COPA

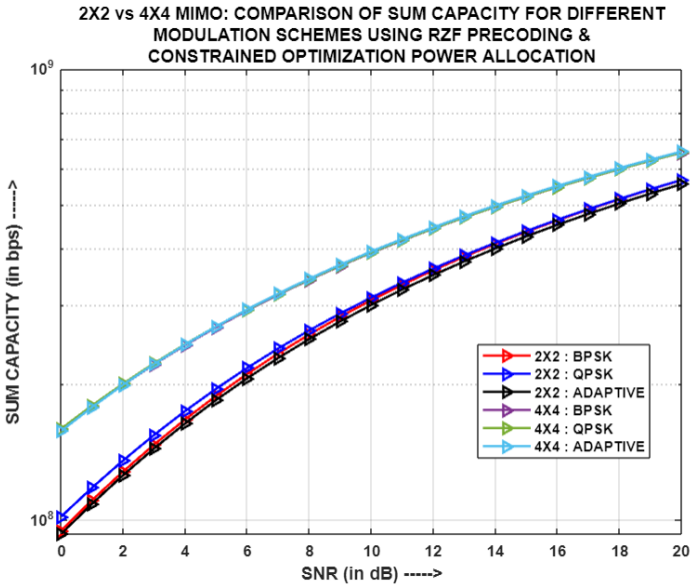

Fig.4.60: (2x2) v/s (4X4) MIMO-NOMA: Comparison of Sum Capacity for different modulation schemes using RZF and COPA

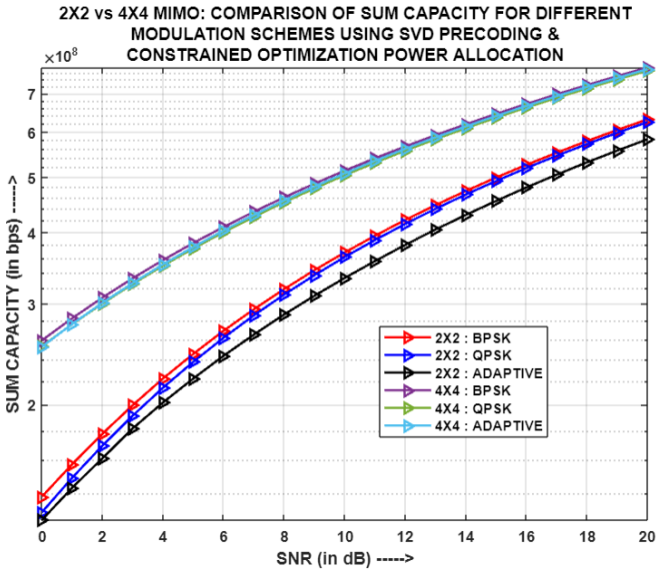

Fig.4.61: (2x2) v/s (4X4) MIMO-NOMA: Comparison of Sum Capacity for different modulation schemes using SVD and COPA

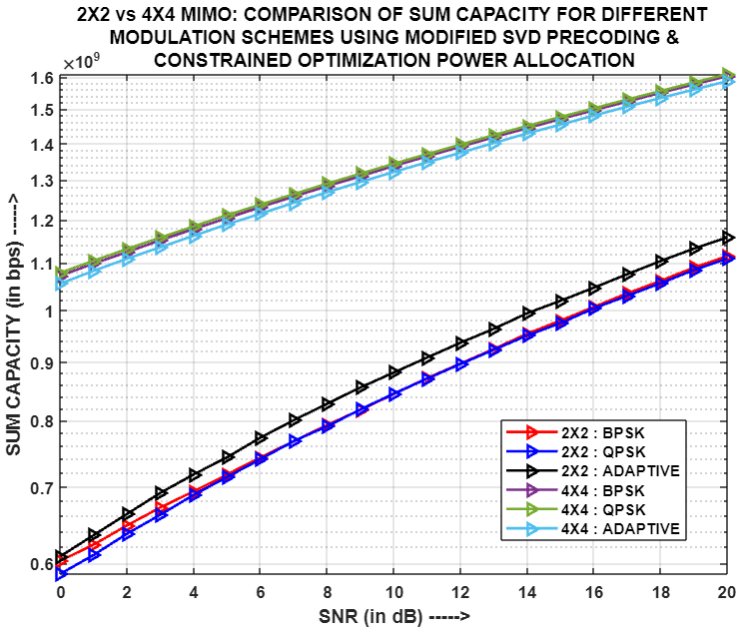

Fig.4.62: (2x2) v/s (4X4) MIMO-NOMA: Comparison of Sum Capacity for different modulation schemes using MODIFIED SVD

Fig.4.58, Fig.4.59, Fig.4.60, Fig.4.61 and Fig.4.62 depicts the comparison of Sum Capacity for different cases of multiple-input-multiple-output (MIMO), i.e. (2x2) and (4x4), using diverse precoding mechanisms respectively, and COPA mechanism for applying NOMA principle. It has been noted that across all five precoding schemes, the (4x4) MIMO configuration consistently exhibits higher sum capacity compared to the (2x2) MIMO configuration for the corresponding modulation schemes. This can be attributed to the fact that the (4x4) MIMO system provides 16 channel paths for each of the two users in the system, whereas the (2x2) MIMO system offers only 4 channel paths per user. As a result, the availability of a greater number of channel paths, per user, allows for a higher amount of received data, leading to increased throughput and thereby enhanced sum capacity.

4.4.7. Simulation Result Analysis of two-user (2x2)-MIMO-PD-NOMA model for different precoding techniques using CON-OPA:

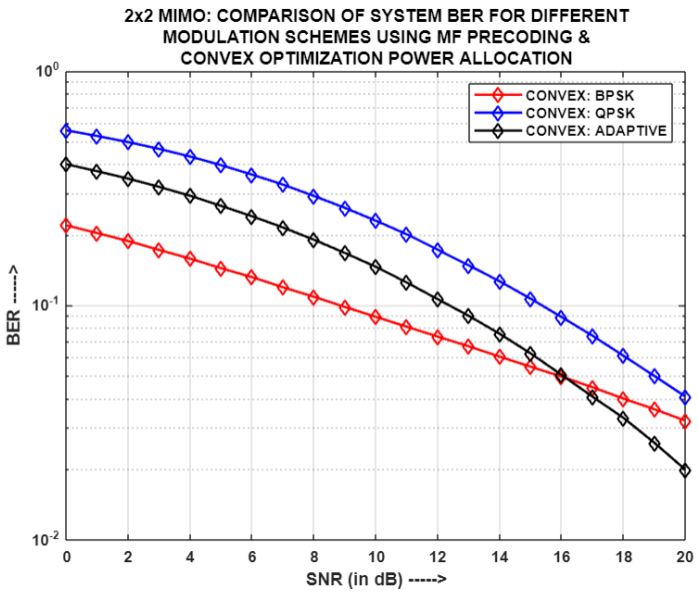

Fig.4.63: For (2x2)-MIMO-NOMA: Comparison of System BER for different modulation schemes using MF and CON-OPA

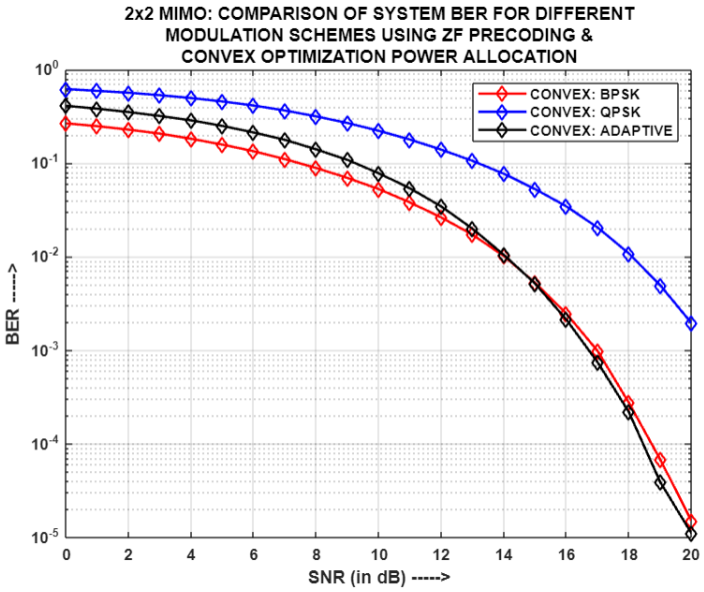

Fig.4.64: For (2x2)-MIMO-NOMA: Comparison of System BER for different modulation schemes using ZF and CON-OPA

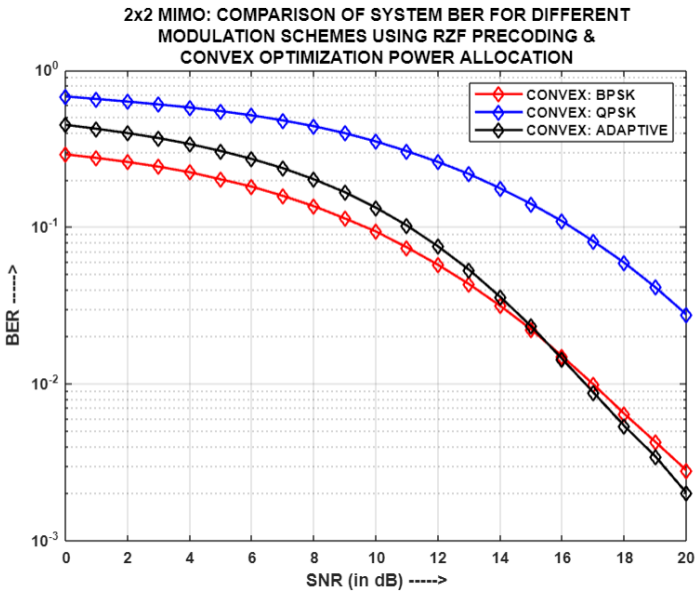

Fig.4.65: For (2x2)-MIMO-NOMA: Comparison of System BER for different modulation schemes using RZF and CON-OPA

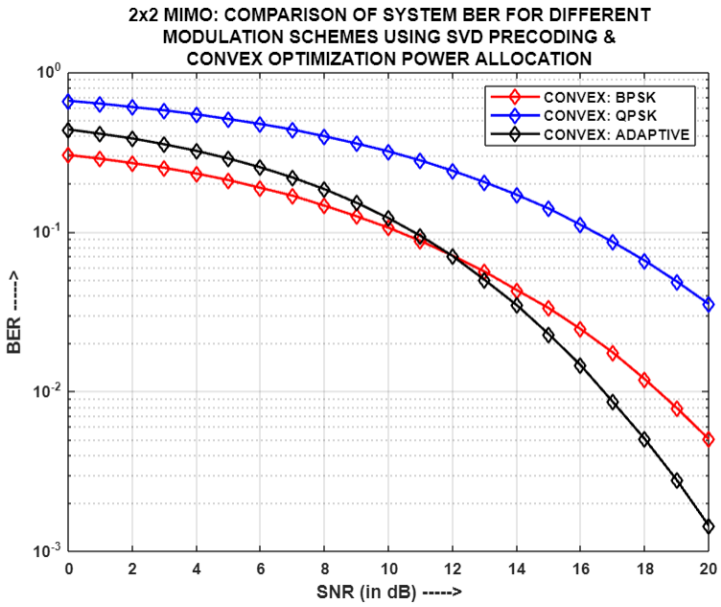

Fig.4.66: For (2x2)-MIMO-NOMA: Comparison of System BER for different modulation schemes using SVD and CON-OPA

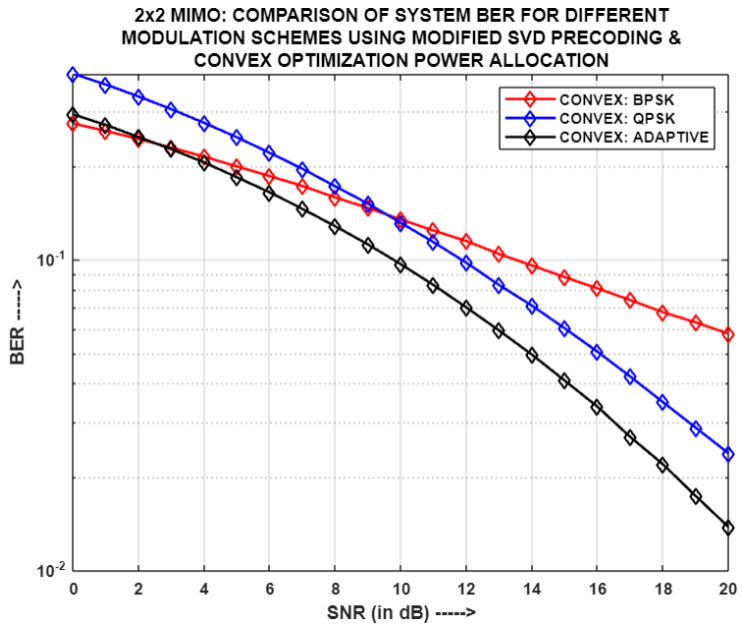

Fig.4.67: For (2x2)-MIMO-NOMA: Comparison of System BER for different modulation schemes using MODIFIED SVD and CON-OPA

The comparison of system BER for different modulation schemes using various precoding techniques, i.e. MF, ZF, RZF, SVD, and MODIFIED SVD respectively, with two antennas per entity in the system and convex optimization power allocation (CON-OPA) is shown in Figures 4.63, 4.64, 4.65, 4.66, and 4.67 respectively. It has been observed that in case of MF, ZF, RZF and SVD respectively, QPSK and BPSK produced the highest and the lowest system BERs respectively, owing to their nature. However, Adaptive modulation happened to yield a system BER that merges with and in some cases, also surpasses the system BER of BPSK. This is because of optimum and dynamic allocation of power coefficients among the users, for the entire SNR span, through convex optimization algorithm, whereby the performance of Adaptive modulation enhances considerably. It is for this very reason that in case of MODIFIED SVD, Adaptive modulation outperforms both BPSK and QPSK, thereby generating the least system BER. Also, because of the choice of the power coefficient sets as well as the dominance of the precoding scheme, even QPSK's performance happened to surpass that of BPSK, in regard to MODIFIED SVD.

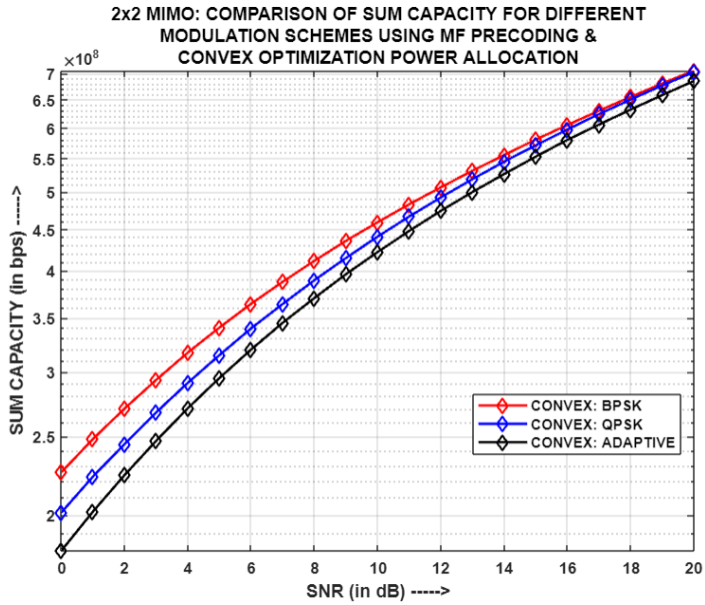

Fig.4.68: For (2x2)-MIMO-NOMA: Comparison of Sum Capacity for different modulation schemes using MF and CON-OPA

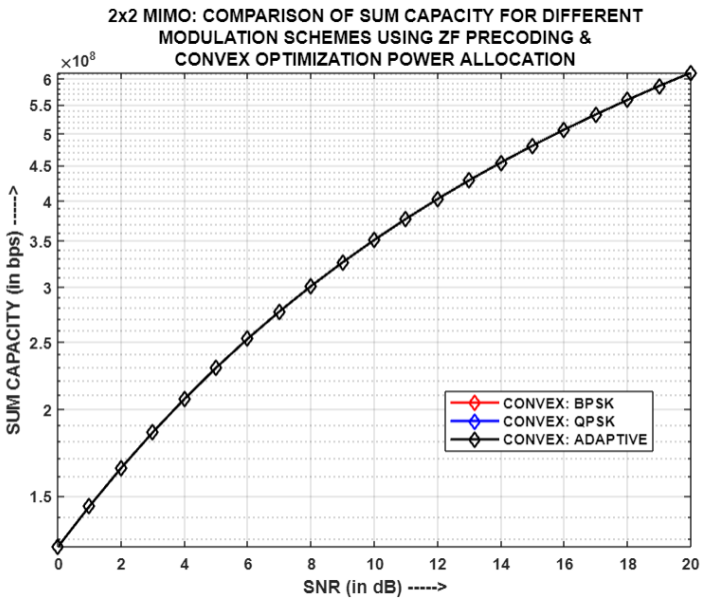

Fig.4.69: For (2x2)-MIMO-NOMA: Comparison of Sum Capacity for different modulation schemes using ZF and CON-OPA

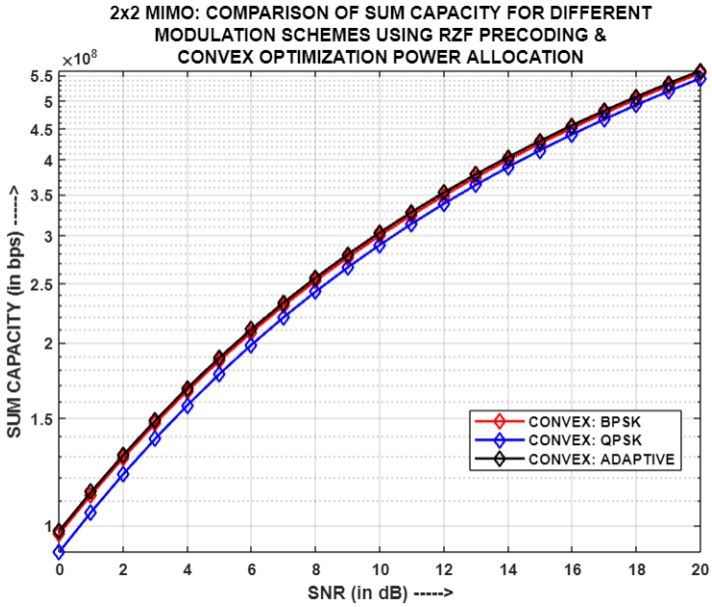

Fig.4.70: For (2x2)-MIMO-NOMA: Comparison of Sum Capacity for different modulation schemes using RZF and CON-OPA

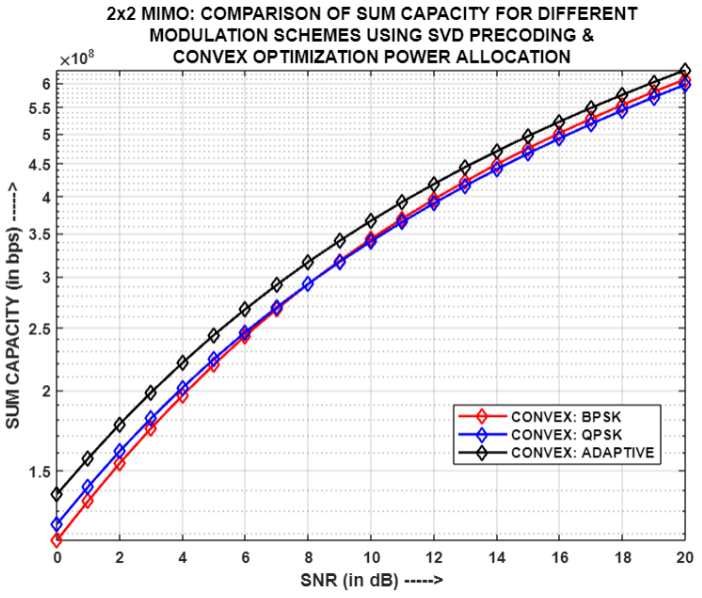

Fig.4.71: For (2x2)-MIMO-NOMA: Comparison of Sum Capacity for different modulation schemes using SVD and CON-OPA

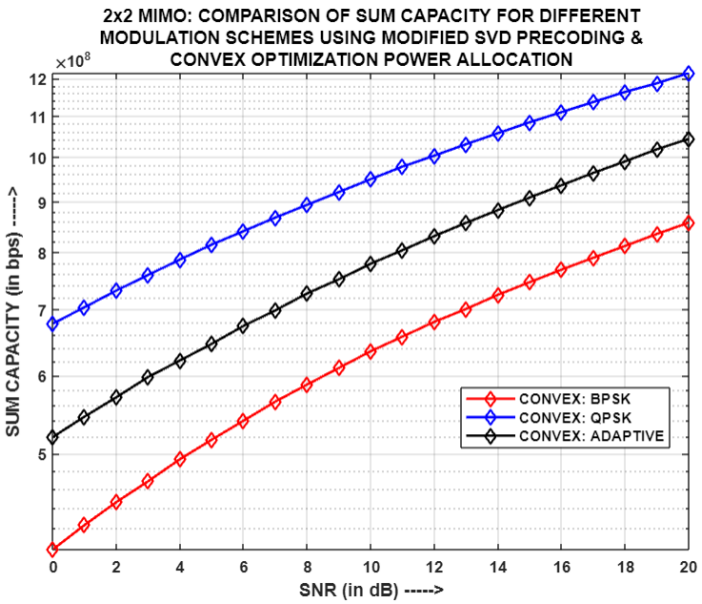

Fig.4.72: For (2x2)-MIMO-NOMA: Comparison of Sum Capacity for different modulation schemes using MODIFIED SVD and CON-OPA

Fig.4.68, Fig.4.69, Fig.4.70, Fig.4.71 and Fig.4.72 portrays the comparison of Sum Capacity for various modulation schemes utilizing different precoding techniques, i.e. MF, ZF, RZF, SVD, and MODIFIED SVD respectively, with two antennas per entity in the system and using CON-OPA mechanism. It has been noticed that when considering ZF and RZF precoding mechanisms, the sum capacities for BPSK, QPSK, and Adaptive modulations exhibit a nearly merged behavior. This convergence is primarily due to the presence of similar channel gains and the utilization of comparable power allocation coefficient sets for the respective users within the system. However, when examining MF, SVD, and MODIFIED SVD, considerable variations in the sum capacities across different modulations have been noticed, especially for MODIFIED SVD. The vital factors contributing to this phenomenon is the usage of different power allocation coefficient sets, for the entire SNR range, and disparate channel gains associated with the three modulation schemes. As the channel gain and choice of power coefficients directly influence the user's throughput and, consequently, the sum capacity, hence these variations manifest themselves in the sum capacities of different precoding and modulation schemes.

4.4.8. Simulation Result Analysis of two-user (4x4)-MIMO-PD-NOMA model for different precoding techniques using CON-OPA:

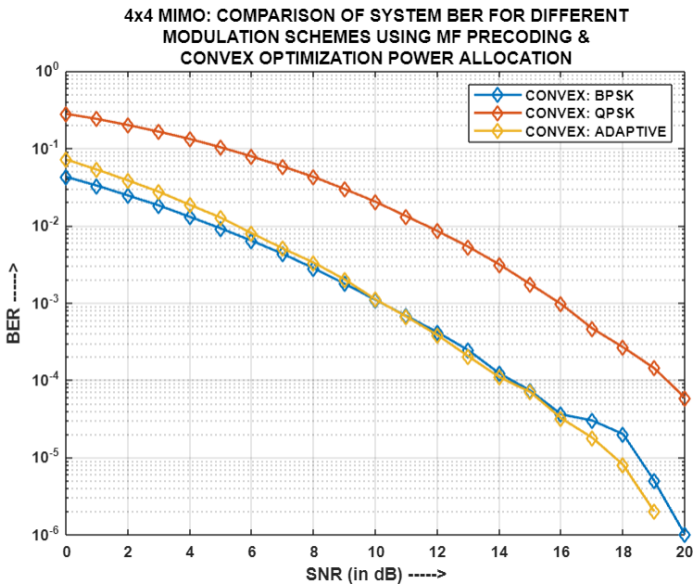

Fig.4.73: For (4x4)-MIMO-NOMA: Comparison of System BER for different modulation schemes using MF and CON-OPA

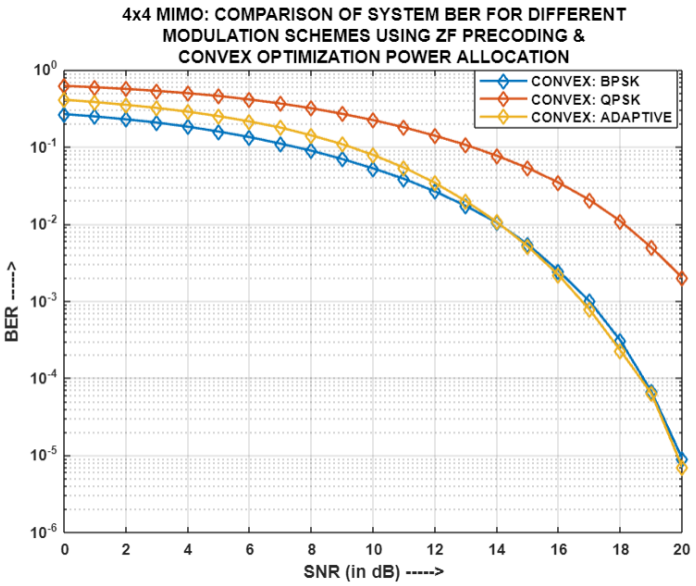

Fig.4.74: For (4x4)-MIMO-NOMA: Comparison of System BER for different modulation schemes using ZF and CON-OPA

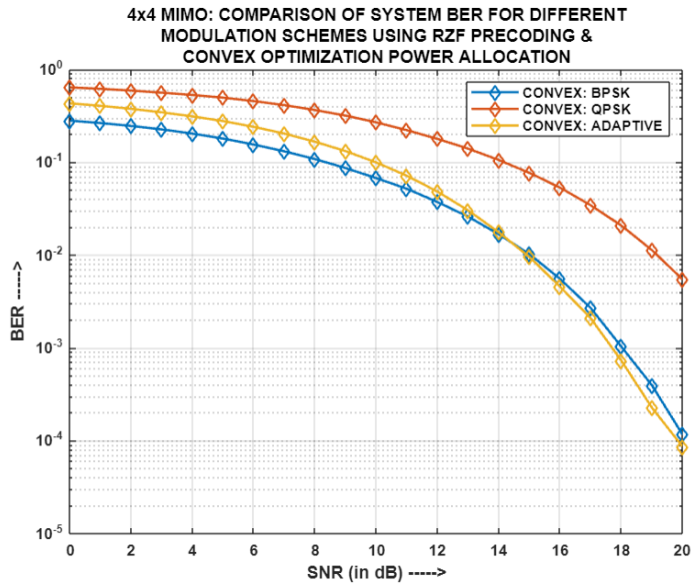

Fig.4.75: For (4x4)-MIMO-NOMA: Comparison of System BER for different modulation schemes using RZF and CON-OPA

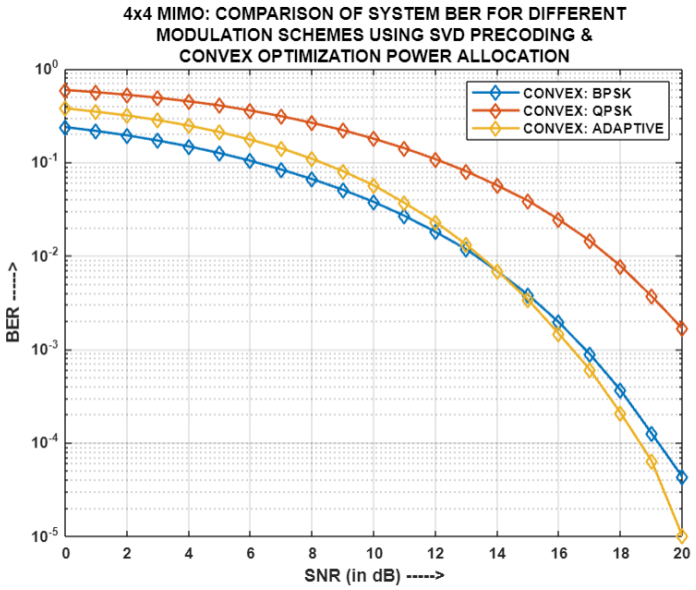

Fig.4.76: For (4x4)-MIMO-NOMA: Comparison of System BER for different modulation schemes using SVD and CON-OPA

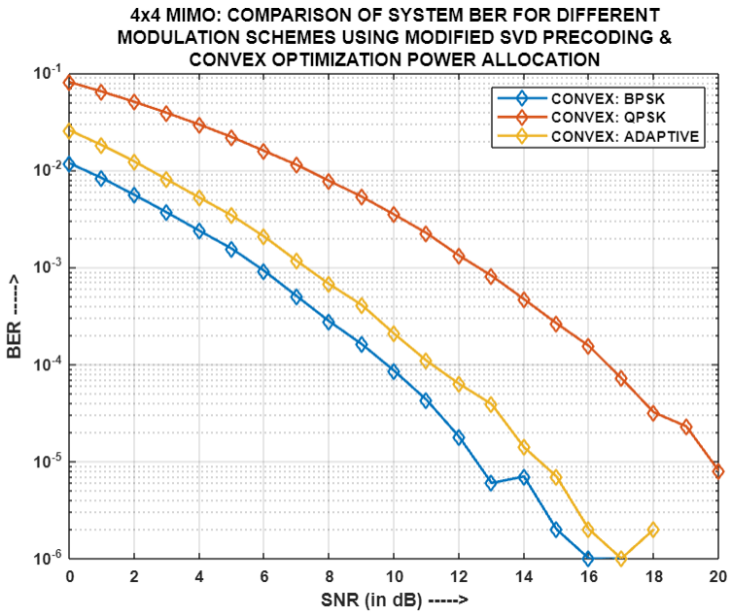

Fig.4.77: For (4x4)-MIMO-NOMA: Comparison of System BER for different modulation schemes using MODIFIED SVD and CON-OPA

Fig.4.73, Fig.4.74, Fig.4.75, Fig.4.76 and Fig.4.77 presents the comparison of system BER for various modulation schemes utilizing different precoding techniques, i.e. MF, ZF, RZF, SVD, and MODIFIED SVD respectively, with four antennas per entity in the system and using CON-OPA mechanism. It has been noted that in the case of MF, ZF, RZF, and SVD precoding techniques, QPSK consistently resulted in the highest system BER, while BPSK persistently yielded the lowest BER. This can be attributed to the inherent characteristics of these modulation schemes. However, it is interesting to observe that Adaptive modulation exhibited a system BER that merged with that of BPSK. This improvement can be credited to the optimal and dynamic allocation of power coefficients among the users, throughout the entire SNR span. Therefore, this power allocation approach, achieved through a convex optimization algorithm, significantly enhanced the performance of Adaptive modulation for the stated precoding schemes. Also, in the case of MODIFIED SVD, as a result of optimum power allocation and predominance of the respective precoding technique, the system BER results of all three modulations were in accordance to the theoretical pattern, i.e., BPSK and QPSK yielding the lowest and highest BERs with that of Adaptive modulation lying in between them, but with improved performance.

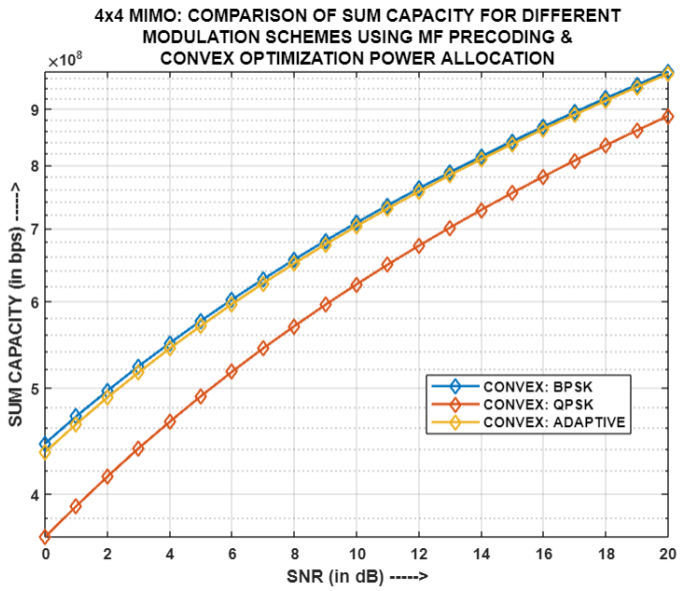

Fig.4.78: For (4x4)-MIMO-NOMA: Comparison of Sum Capacity for different modulation schemes using MF and CON-OPA

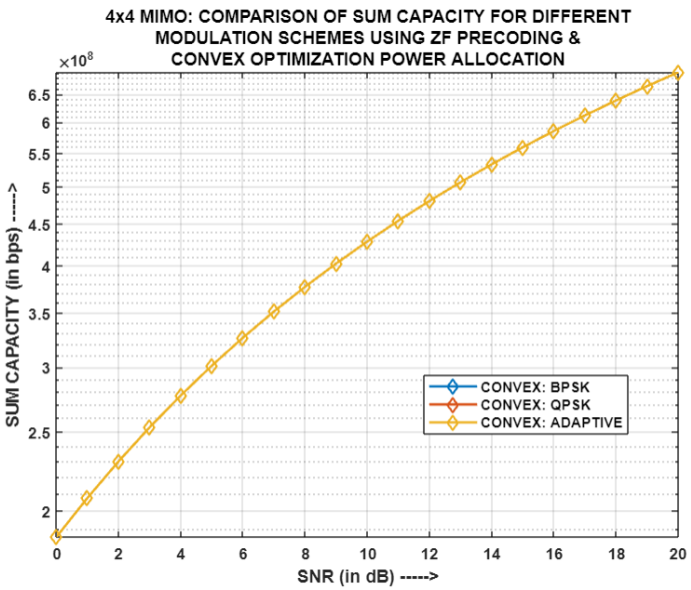

Fig.4.79: For (4x4)-MIMO-NOMA: Comparison of Sum Capacity for different modulation schemes using ZF and CON-OPA

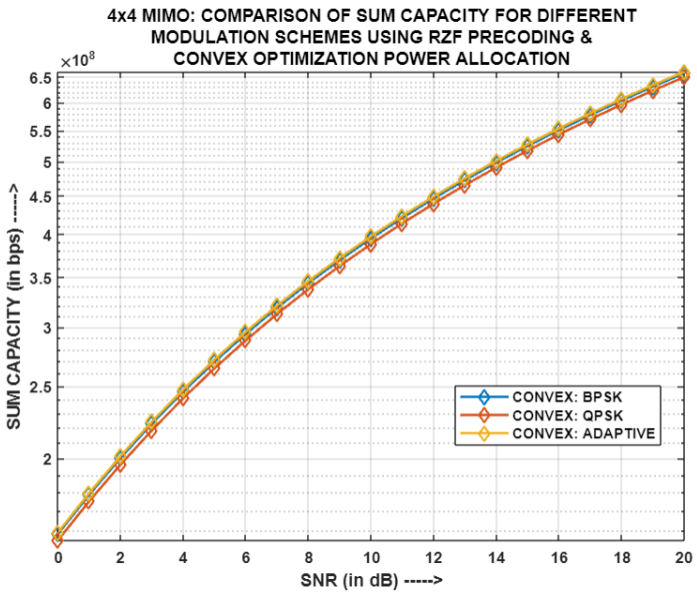

Fig.4.80: For (4x4)-MIMO-NOMA: Comparison of Sum Capacity for different modulation schemes using RZF and CON-OPA

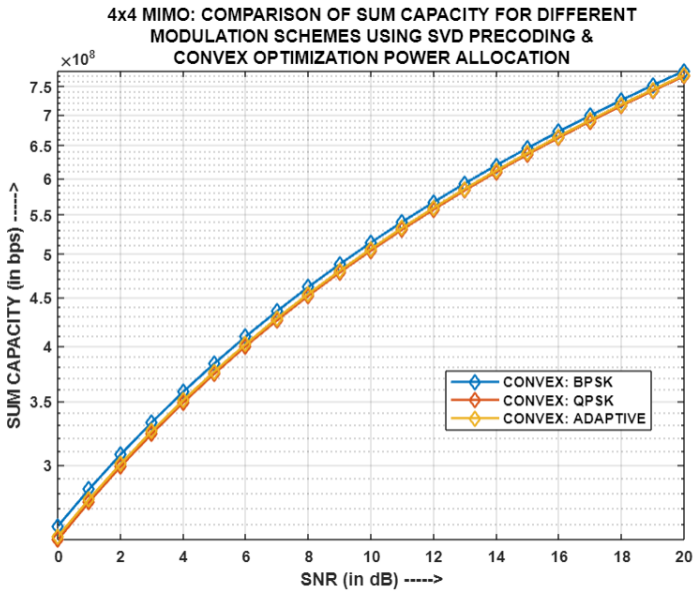

Fig.4.81: For (4x4)-MIMO-NOMA: Comparison of Sum Capacity for different modulation schemes using SVD and CON-OPA

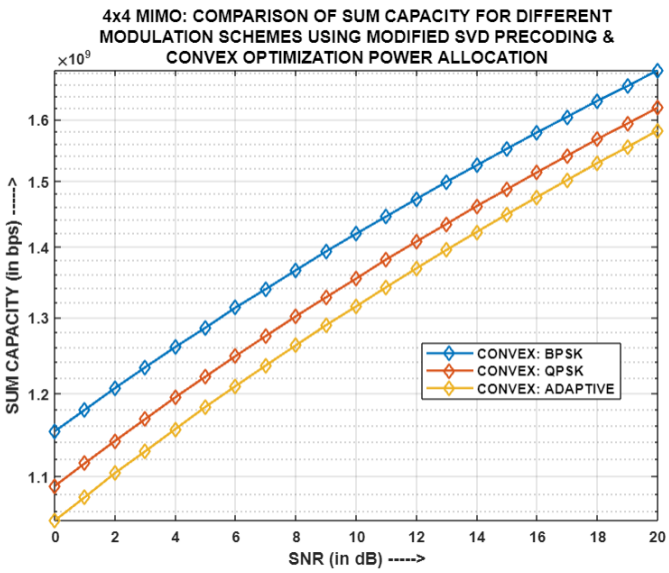

Fig.4.82: For (4x4)-MIMO-NOMA: Comparison of Sum Capacity for different modulation schemes using MODIFIED SVD and CON-OPA

Fig.4.78, Fig.4.79, Fig.4.80, Fig.4.81 and Fig.4.82 presents the comparison of Sum Capacity for different modulation techniques utilizing diverse precoding schemes, i.e. MF, ZF, RZF, SVD, and MODIFIED SVD respectively, with four antennas per entity in the system and using CON-OPA mechanism. It has been observed that in the context of ZF, RZF and SVD precoding mechanisms, the sum capacities for BPSK, QPSK, and Adaptive modulations demonstrate a tendency to converge. This convergence can be primarily attributed to the similarity in channel gains and also slightly, to the utilization of different but comparable power allocation coefficient sets for the respective users in the system. However, notable variations in the sum capacities are evident when considering MF and MODIFIED SVD, particularly for MODIFIED SVD. These variations can be related to the use of different power allocation coefficient sets across the entire SNR range and the presence of disparate channel gains associated with the three modulation schemes. Since the channel gain and the choice of power coefficients directly affects the user's throughput and hence, the sum capacity; therefore, these variations manifest themselves across the sum capacities of different precoding and modulation schemes.

4.4.9. Comparative Analysis of simulation results of two-user (2x2) and (4x4) MIMO-PD-NOMA models for different precoding techniques using CON-OPA:

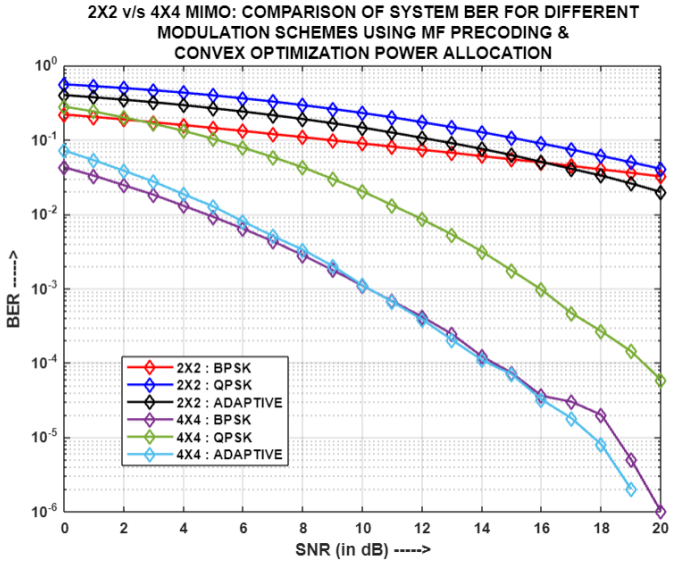

Fig.4.83: (2x2) v/s (4X4) MIMO-NOMA: Comparison of System BER for different modulation schemes using MF and CON-OPA

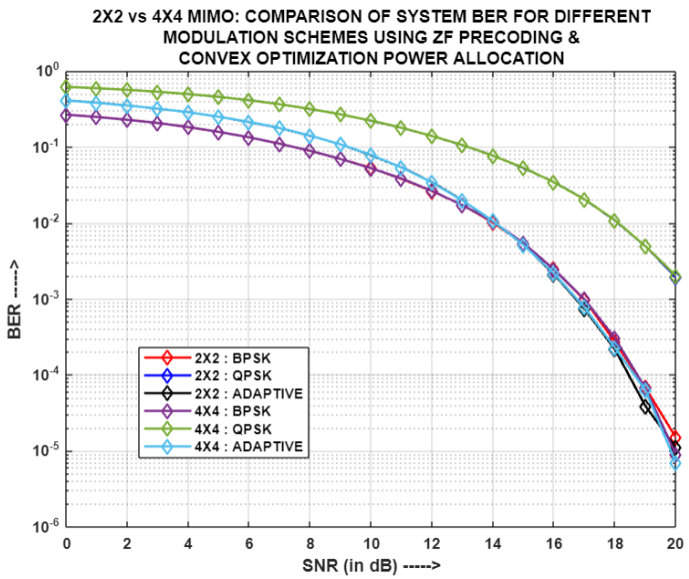

Fig.4.84: (2x2) v/s (4X4) MIMO-NOMA: Comparison of System BER for different modulation schemes using ZF and CON-OPA

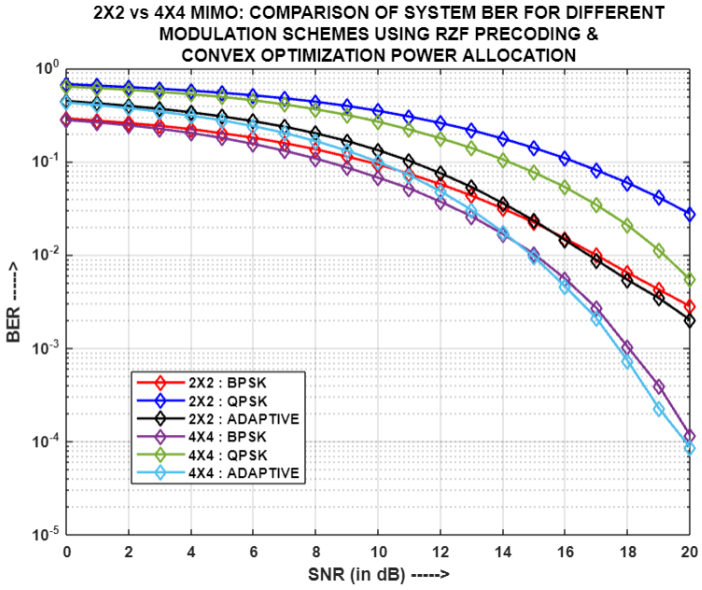

Fig.4.85: (2x2) v/s (4X4) MIMO-NOMA: Comparison of System BER for different modulation schemes using RZF and CON-OPA

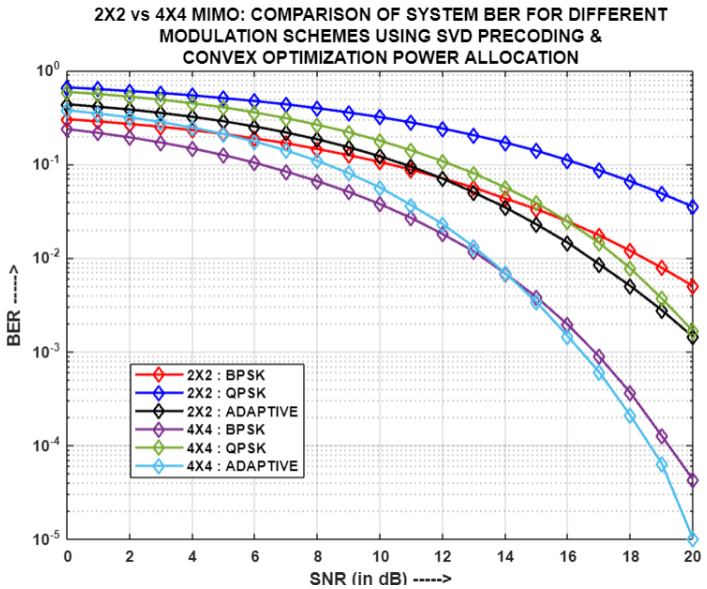

Fig.4.86: (2x2) v/s (4X4) MIMO-NOMA: Comparison of System BER for different modulation schemes using SVD and CON-OPA

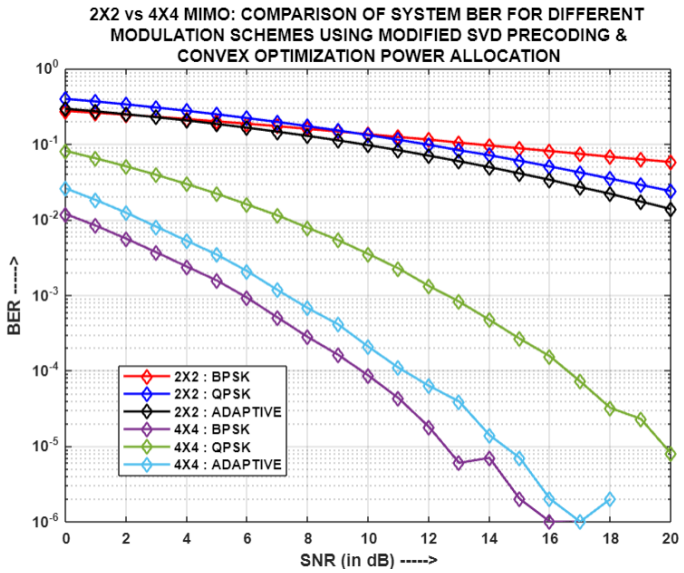

Fig.4.87: (2x2) v/s (4X4) MIMO-NOMA: Comparison of System BER for different modulation schemes using MODIFIED SVD and CON-OPA

Fig.4.83, Fig.4.84, Fig.4.85, Fig.4.86 and Fig.4.87 illustrates the comparison of system BER for different cases of multiple-input-multiple-output (MIMO), i.e. (2x2) and (4x4), using diverse precoding mechanisms respectively, and convex optimization power allocation (CON-OPA) for employing NOMA principle. It is apparent that in the context of MF, RZF, SVD, and MODIFIED SVD precoding schemes, the (4x4) MIMO configuration demonstrates enhanced system BER performance compared to the (2x2) configuration for the corresponding modulation schemes. This improvement can be attributed to the increased number of antennas employed in both transmission and reception, resulting in a greater availability of channel paths for transferring information and ultimately enhancing the quality of the received signal. Furthermore, the selection of the precoding scheme also plays a crucial role in processing the information signal prior to transmission, enabling it to effectively mitigate channel effects and reach the receiver in its optimal state. However, when considering ZF precoding, it is interesting to note that, regardless of the number of transmit-receive antennas, the performance of all three modulation schemes remains the same for both (4x4) and (2x2) MIMO configurations. This can be attributed to the natural capability of ZF precoding to nullify channel effects at

the transmitter by multiplying the information signal with the pseudo inverse of the channel matrix. Consequently, the system BER, in this case, is primarily influenced by the additive white Gaussian noise (AWGN) variance. Therefore, for ZF, both the MIMO configurations produce merged system BERs, for the respective modulation schemes, as comparable sets of power coefficients are used for the two cases and corresponding modulation schemes.

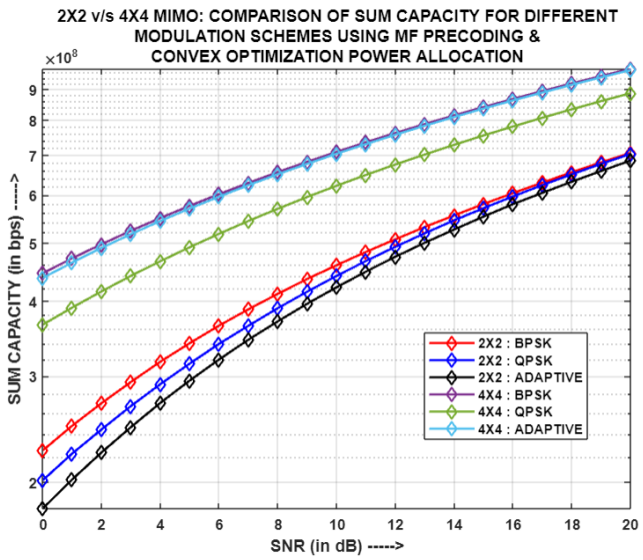

Fig.4.88: (2x2) v/s (4X4) MIMO-NOMA: Comparison of Sum Capacity for different modulation schemes using MF and CON-OPA

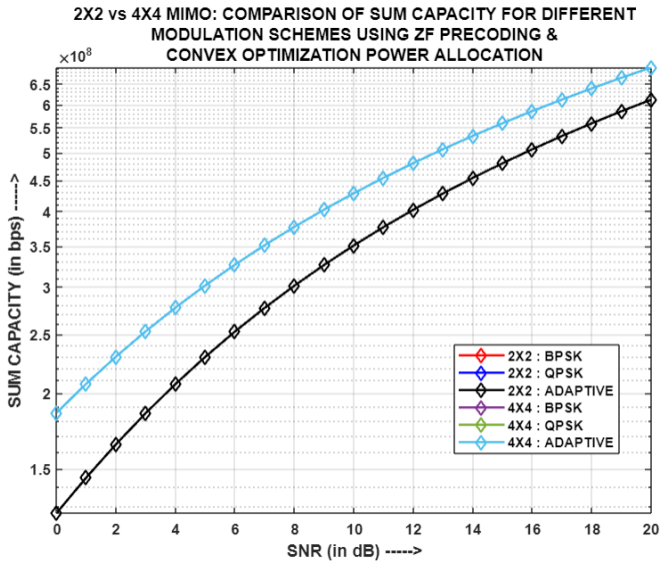

Fig.4.89: (2x2) v/s (4X4) MIMO-NOMA: Comparison of Sum Capacity for different modulation schemes using ZF and CON-OPA

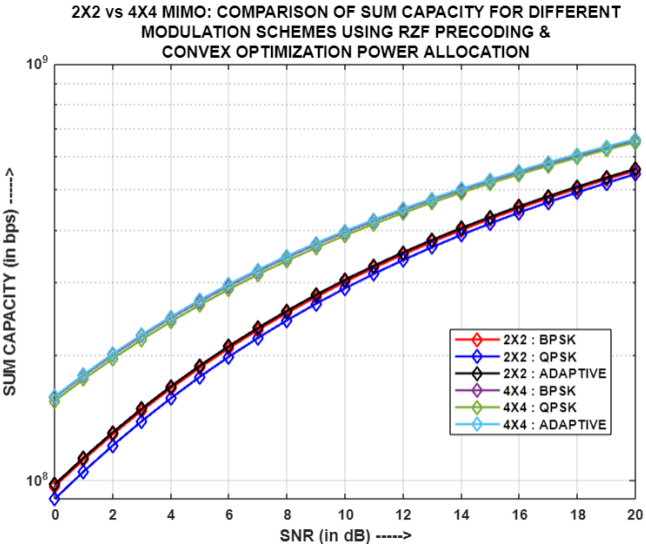

Fig.4.90: (2x2) v/s (4X4) MIMO-NOMA: Comparison of Sum Capacity for different modulation schemes using RZF and CON-OPA

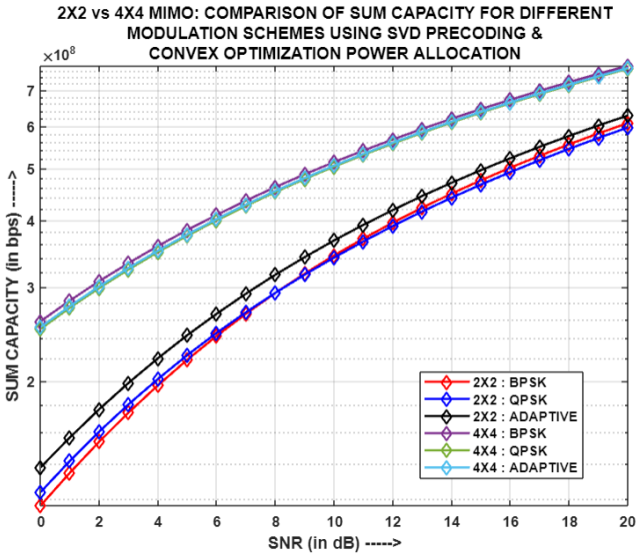

Fig.4.91: (2x2) v/s (4X4) MIMO-NOMA: Comparison of Sum Capacity for different modulation schemes using SVD and CON-OPA

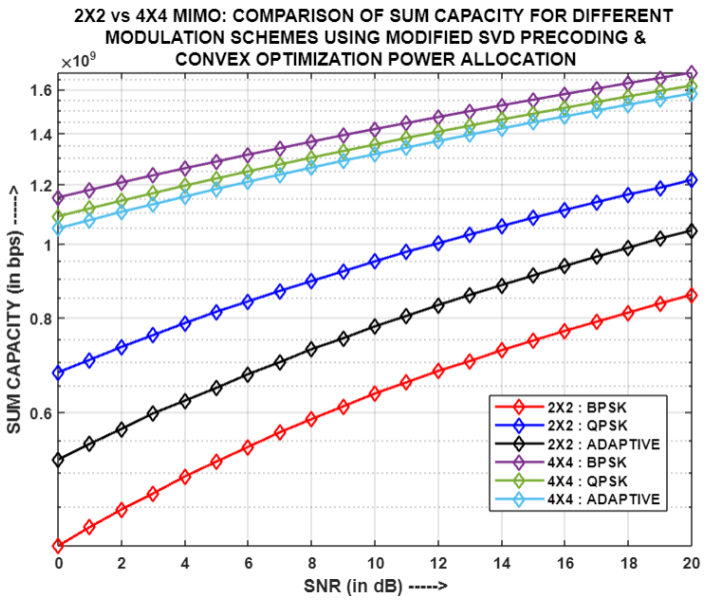

Fig.4.92: (2x2) v/s (4X4) MIMO-NOMA: Comparison of Sum Capacity for different modulation schemes using MODIFIED SVD and CON-OPA

Fig.4.88, Fig.4.89, Fig.4.90, Fig.4.91 and Fig.4.92 represents the comparison of Sum Capacity for different cases of multiple-input-multiple-output (MIMO), i.e. (2x2) and (4x4), using diverse precoding mechanisms respectively, and CON-OPA for applying NOMA principle. It has been witnessed that across all five precoding schemes, the (4x4) MIMO configuration consistently demonstrates superior sum capacity compared to the (2x2) MIMO configuration, for the corresponding modulation schemes. This can be attributed to the fact that the (4x4) MIMO system provides 16 channel paths for each user in the system. In contrast, the (2x2) MIMO system only offers 4 channel paths per user. This greater number of channel paths per user in the (4x4) MIMO configuration allows for a larger volume of received data, thereby resulting in increased throughput and, consequently, enhanced sum capacity.

4.4.10. Simulation Result Analysis of two-user (2x2)-MIMO-PD-NOMA model for different precoding techniques and modulation schemes:

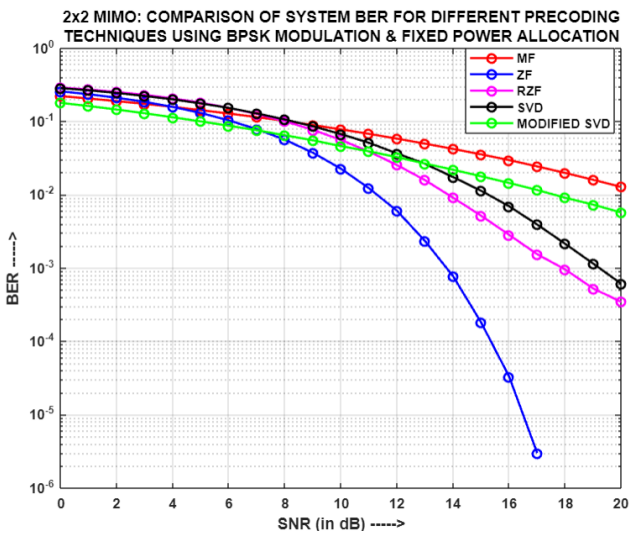

Fig.4.93: For (2x2)-MIMO-NOMA: Comparison of System BER for different precoding techniques using BPSK and FPA

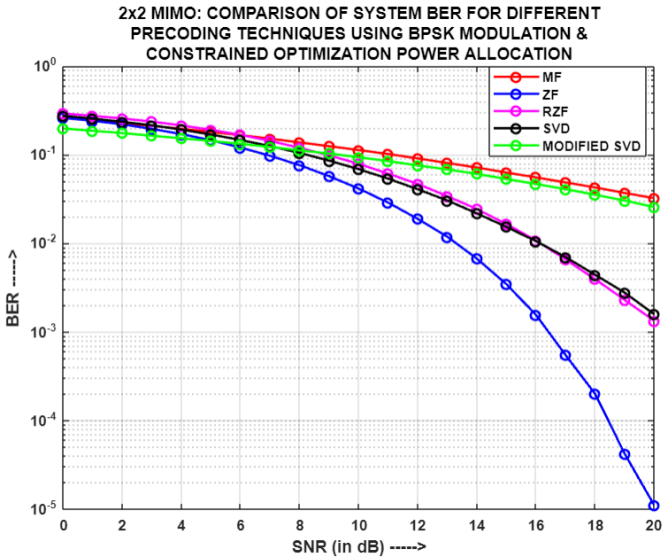

Fig.4.94: For (2x2)-MIMO-NOMA: Comparison of System BER for different precoding techniques using BPSK and COPA

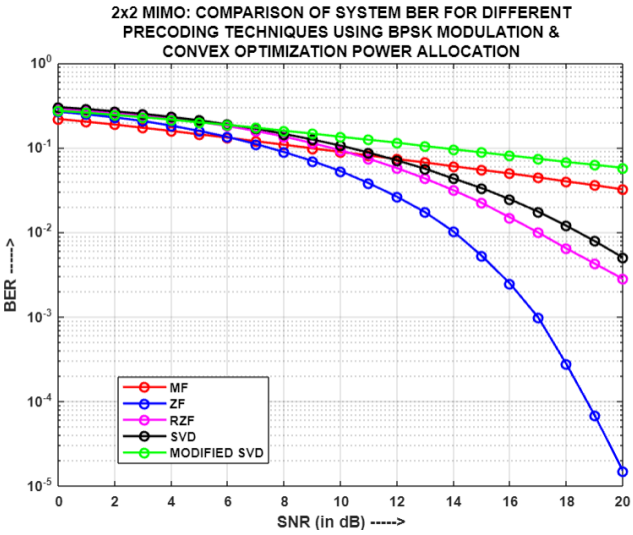

Fig.4.95: For (2x2)-MIMO-NOMA: Comparison of System BER for different precoding techniques using BPSK and CON-OPA

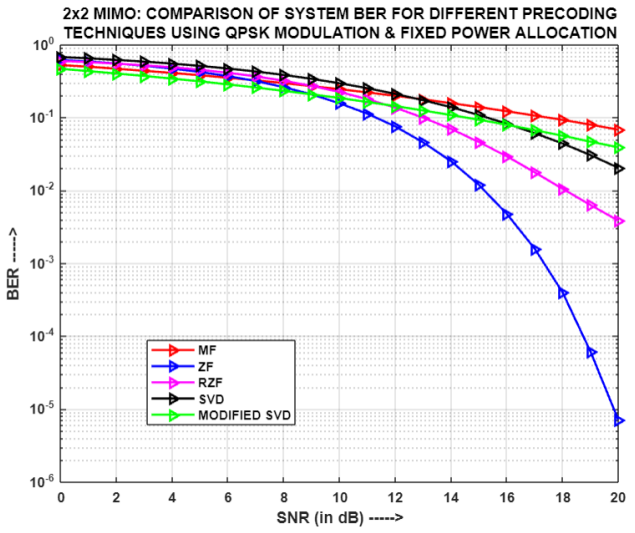

Fig.4.96: For (2x2)-MIMO-NOMA: Comparison of System BER for different precoding techniques using QPSK and FPA

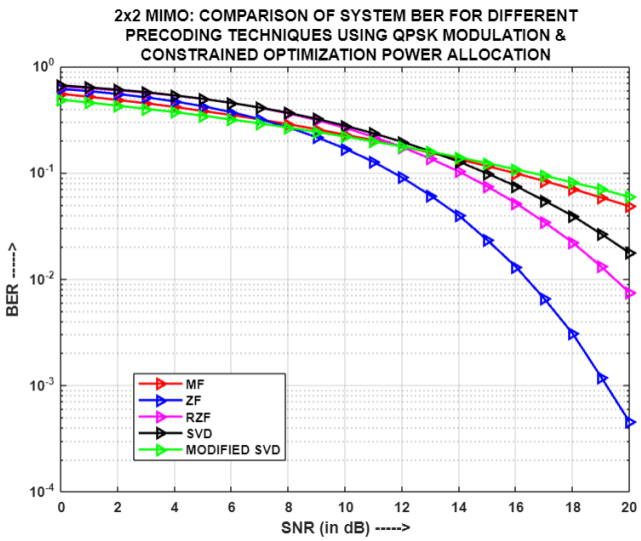

Fig.4.97: For (2x2)-MIMO-NOMA: Comparison of System BER for different precoding techniques using QPSK and COPA

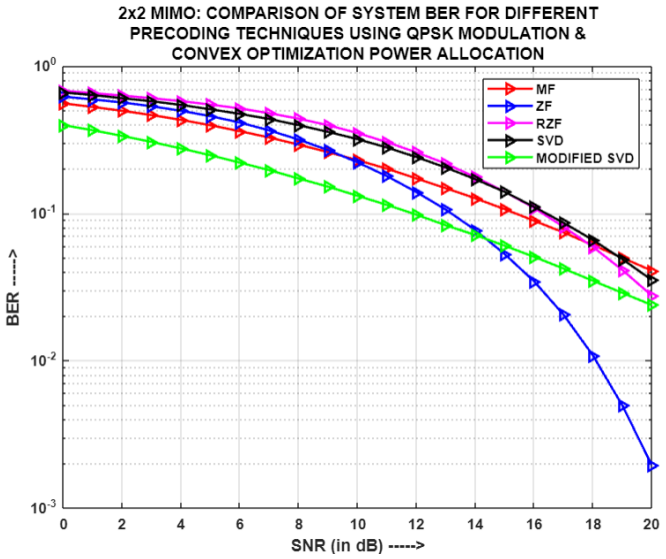

Fig.4.98: For (2x2)-MIMO-NOMA: Comparison of System BER for different precoding techniques using QPSK and CON-OPA

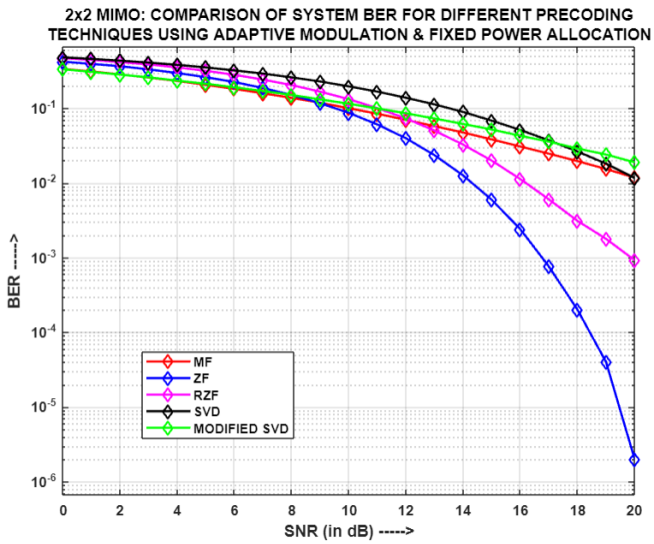

Fig.4.99: For (2x2)-MIMO-NOMA: Comparison of System BER for different precoding techniques using Adaptive Modulation and FPA

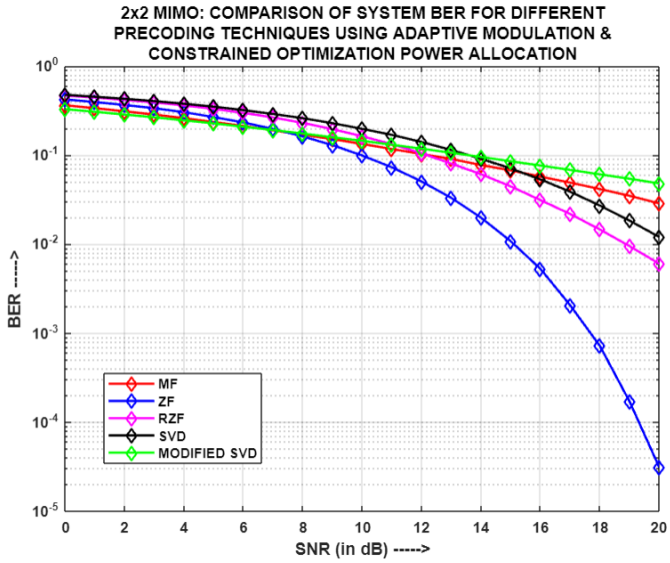

Fig.4.100: For (2x2)-MIMO-NOMA: Comparison of System BER for different precoding techniques using Adaptive Modulation and COPA

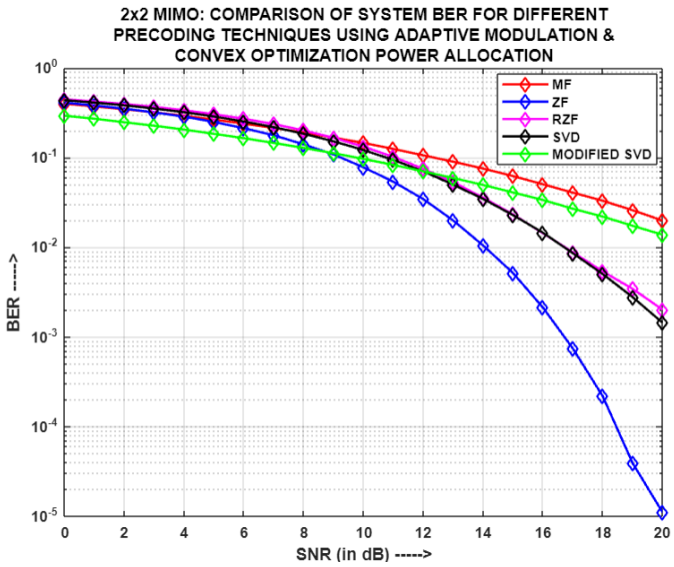

Fig.4.101: For (2x2)-MIMO-NOMA: Comparison of System BER for different precoding techniques using Adaptive Modulation and CON-OPA

Fig.4.93, Fig.4.94, Fig.4.95, Fig.4.96, Fig.4.97, Fig.4.98, Fig.4.99, Fig.4.100 and Fig.4.101 depicts the comparison of system BER for different precoding techniques using BPSK, QPSK and Adaptive modulations and varied power allocation strategies, i.e. FPA, COPA and CON-OPA, respectively, with each entity in the system having two antennas. For all the above cases, ZF produces the least system BER, while MF and MODIFIED SVD, both yield the highest system BER interchangeably, with minute differences between the two. On the contrary, the system BERs of RZF and SVD tend to lie close to each other, thereby mostly residing in the region in between ZF and the other two precoding schemes. ZF yields the best system BER performance because it nullifies the channel effects at the transmitter by multiplying the information signal with the pseudo inverse of the channel matrix. Since RZF is also based on ZF but with a little change in its operation, hence it produces better results than the other three precoding schemes. SVD's system BER performance is comparable to that of RZF, since the precoding and post-coding matrices used in the former precoding scheme, together produce a similar effect on the information signal, as that of RZF. Therefore, for a similar reason MF and MODIFIED SVD yield almost equivalent system BERs. MF produces the highest system BER because it just precodes the information signal with the channel's Hermitian conjugate and hence, in this case, it doesn't seem to effectively orient the information signal, as per the channel, in order to eliminate the

channel effects. On the other hand, MODIFIED SVD doesn't perform that well, in terms of system BER, because in this case, the amplification matrices used for precoding and post-coding, contains low values of channel gain, owing to the less number of channel paths involved in transmission and reception. However, only in Fig.4.98, MODIFIED SVD outperforms the other precoding schemes, except ZF, because of the significant contribution of the selection of optimum power allocation coefficient sets, using convex optimization algorithm, for the corresponding users.

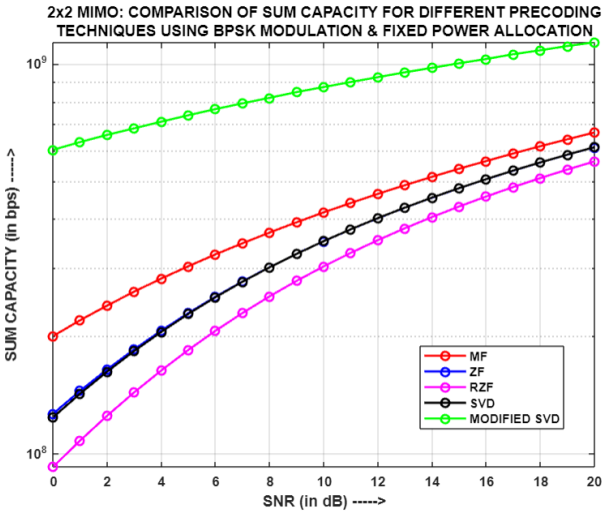

Fig.4.102: For (2x2)-MIMO-NOMA: Comparison of Sum Capacity for different precoding techniques using BPSK and FPA

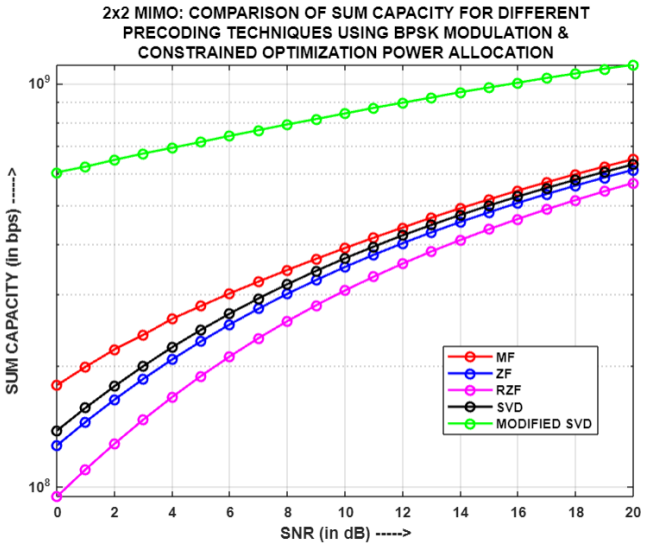

Fig.4.103: For (2x2)-MIMO-NOMA: Comparison of Sum Capacity for different precoding techniques using BPSK and COPA

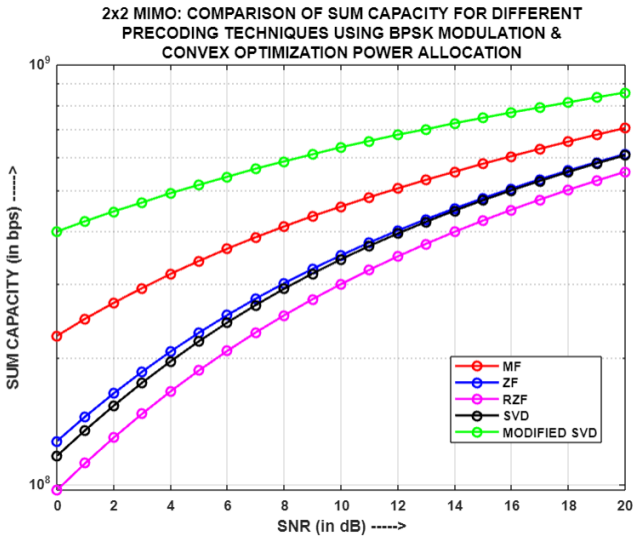

Fig.4.104: For (2x2)-MIMO-NOMA: Comparison of Sum Capacity for different precoding techniques using BPSK and CON-OPA

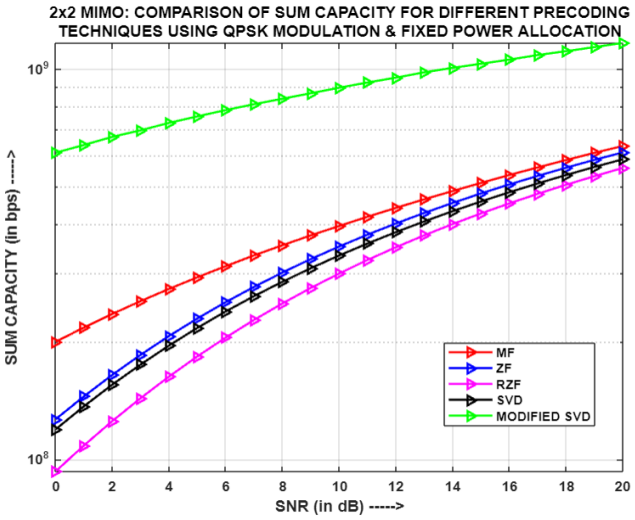

Fig.4.105: For (2x2)-MIMO-NOMA: Comparison of Sum Capacity for different precoding techniques using QPSK and FPA

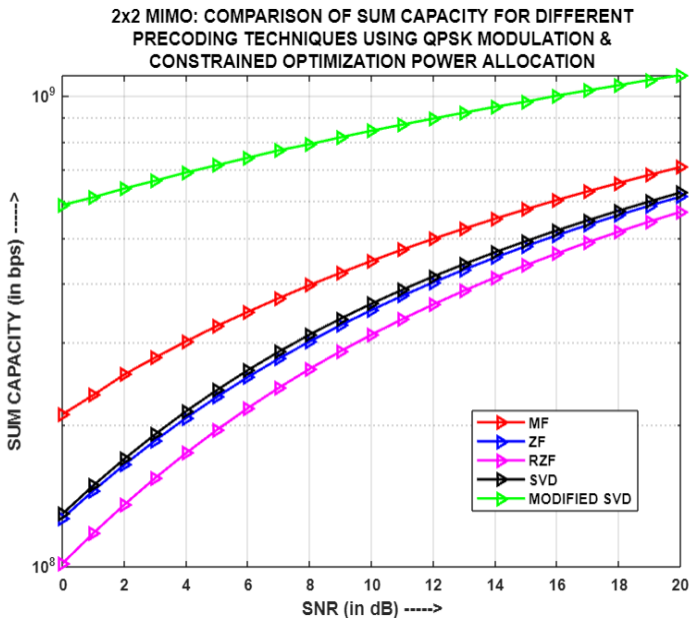

Fig.4.106: For (2x2)-MIMO-NOMA: Comparison of Sum Capacity for different precoding techniques using QPSK and COPA

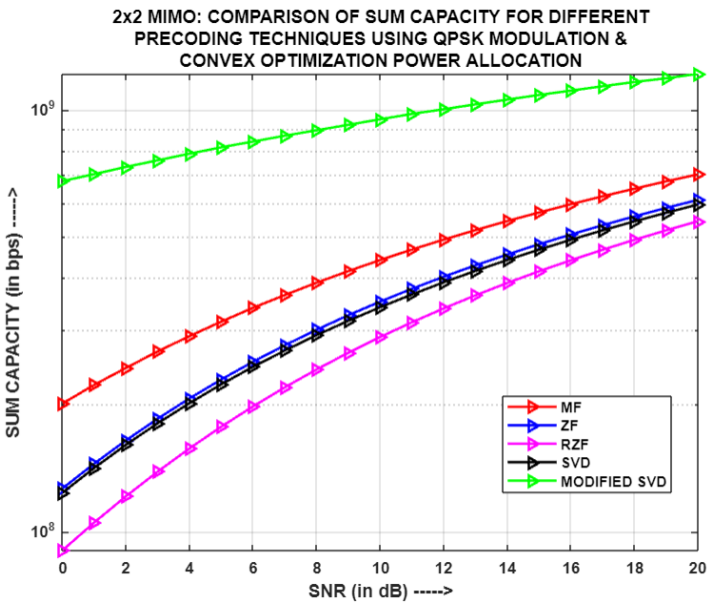

Fig.4.107: For (2x2)-MIMO-NOMA: Comparison of Sum Capacity for different precoding techniques using QPSK and CON-OPA

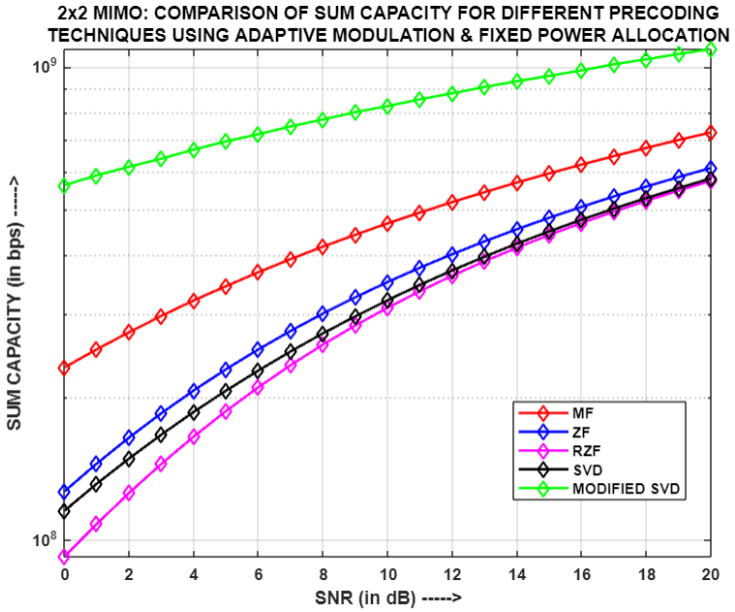

Fig.4.108: For (2x2)-MIMO-NOMA: Comparison of Sum Capacity for different precoding techniques using Adaptive Modulation and FPA

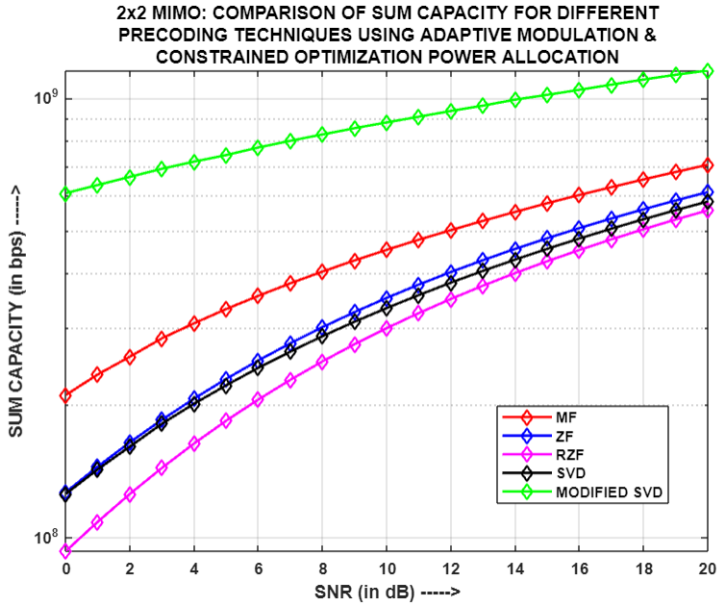

Fig.4.109: For (2x2)-MIMO-NOMA: Comparison of Sum Capacity for different precoding techniques using Adaptive Modulation and COPA

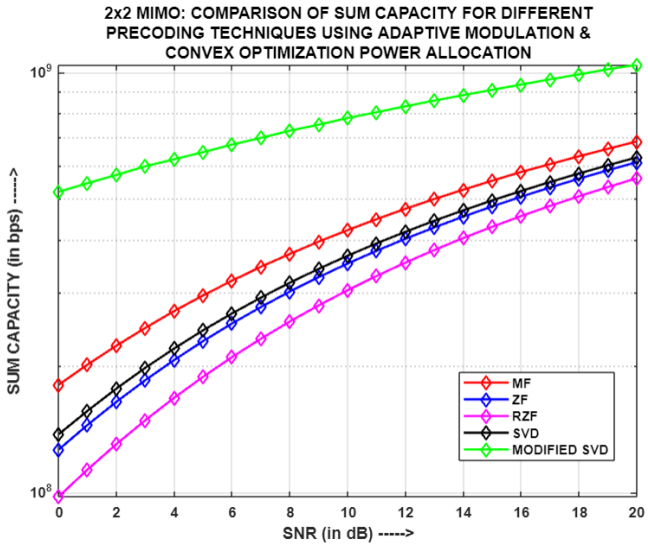

Fig.4.110: For (2x2)-MIMO-NOMA: Comparison of Sum Capacity for different precoding techniques using Adaptive Modulation and CON-OPA

Fig.4.102, Fig.4.103, Fig.4.104, Fig.4.105, Fig.4.106, Fig.4.107, Fig.4.108, Fig.4.109 and Fig.4.110 portrays the comparison of Sum Capacity for different precoding techniques using BPSK, QPSK and Adaptive modulations and varied power allocation strategies, i.e., FPA, COPA and CON-OPA, respectively, with each entity in the system having two antennas. It has been observed that for all the above cases, MODIFIED SVD generates the highest sum capacity, followed by MF, ZF and SVD producing almost merged sum capacities and finally RZF. The primary reason behind such a behaviour is because of the differing effects of the precoding techniques on the channel gain of the respective users that thereby influence their throughputs and subsequently, the sum capacity of the system. Since MODIFIED SVD precoding entails the use of an amplification matrix, both at the transmitter and receiver, which further affects the respective user channel gains and hence, tends to provide considerably high sum capacity, compared to its contemporaries. ZF and SVD yield converged sum capacities because they produce similar values of channel gains for the respective users, whereby their throughputs are comparable and hence, their sum capacities merge or tend to merge.

4.4.11. Simulation Result Analysis of two-user (4x4)-MIMO-PD-NOMA model for different precoding techniques and modulation schemes:

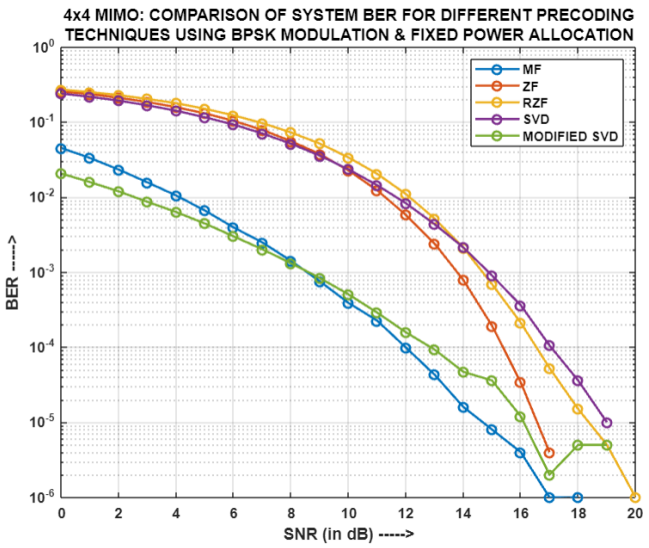

Fig.4.111: For (4x4)-MIMO-NOMA: Comparison of System BER for different precoding techniques using BPSK and FPA

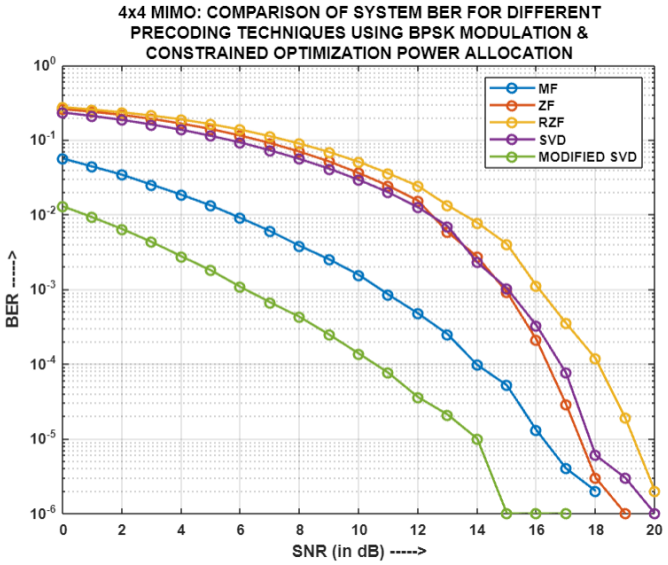

Fig.4.112: For (4x4)-MIMO-NOMA: Comparison of System BER for different precoding techniques using BPSK and COPA

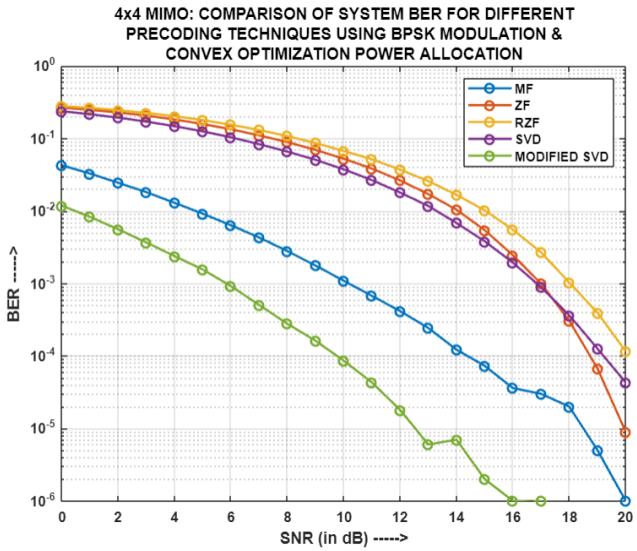

Fig.4.113: For (4x4)-MIMO-NOMA: Comparison of System BER for different precoding techniques using BPSK and CON-OPA

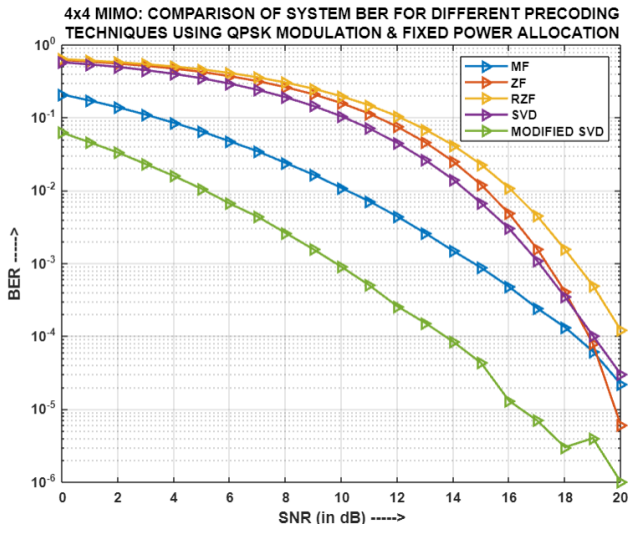

Fig.4.114: For (4x4)-MIMO-NOMA: Comparison of System BER for different precoding techniques using QPSK and FPA

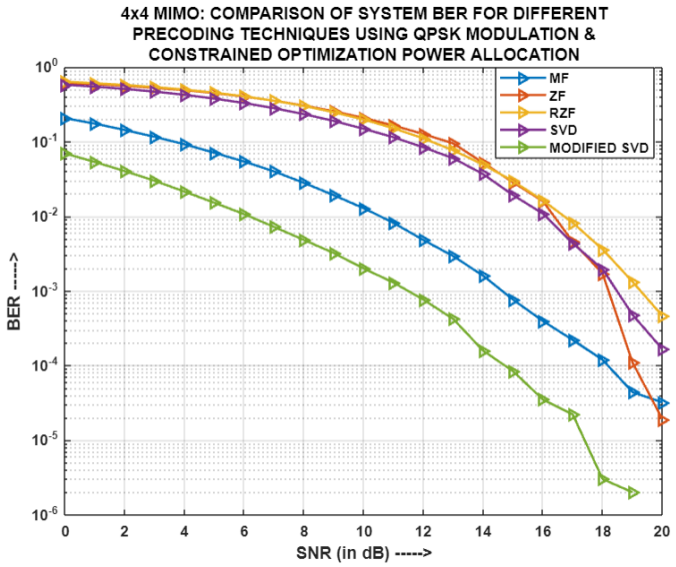

Fig.4.115: For (4x4)-MIMO-NOMA: Comparison of System BER for different precoding techniques using QPSK and COPA

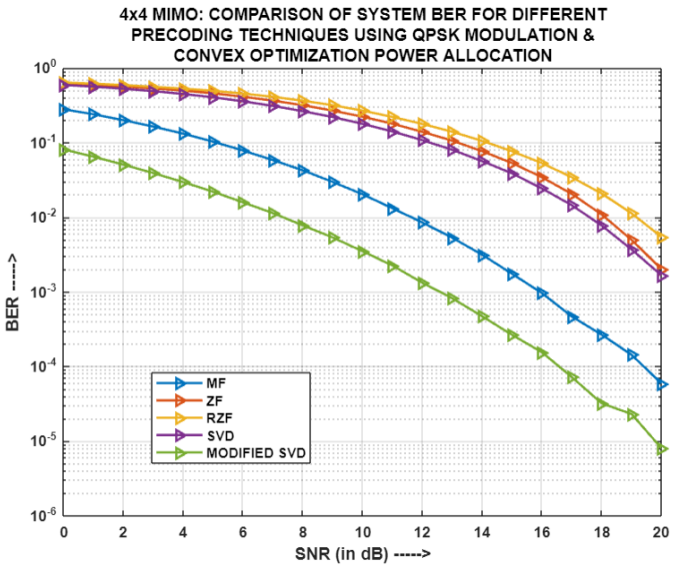

Fig.4.116: For (4x4)-MIMO-NOMA: Comparison of System BER for different precoding techniques using QPSK and CON-OPA

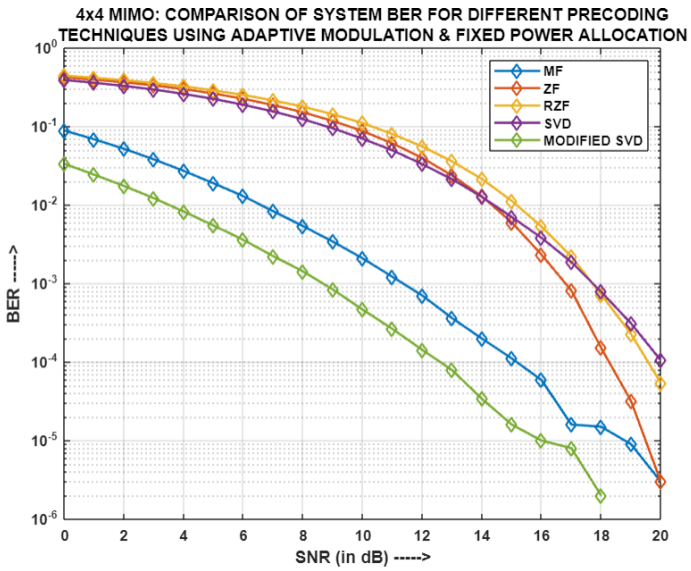

Fig.4.117: For (4x4)-MIMO-NOMA: Comparison of System BER for different precoding techniques using Adaptive Modulation and FPA

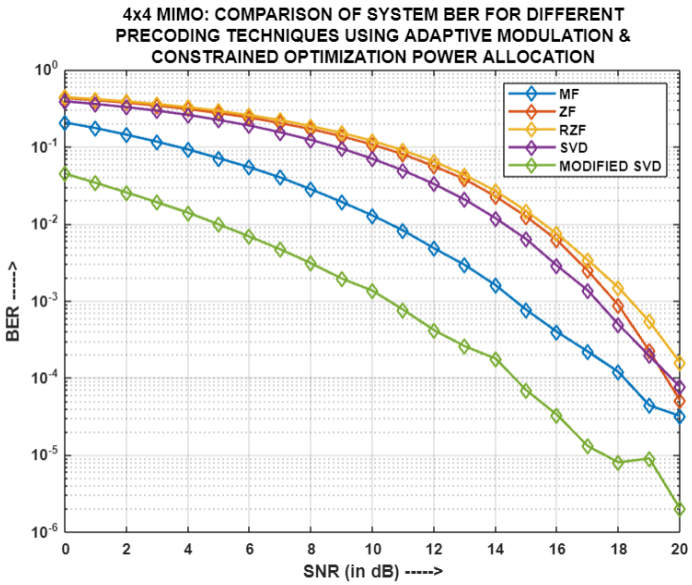

Fig.4.118: For (4x4)-MIMO-NOMA: Comparison of System BER for different precoding techniques using Adaptive Modulation and COPA

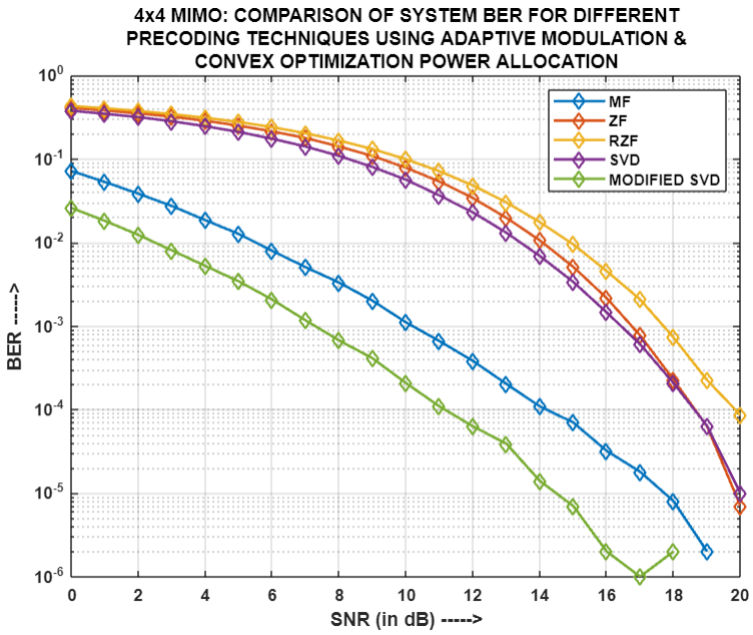

Fig.4.119: For (4x4)-MIMO-NOMA: Comparison of System BER for different precoding techniques using Adaptive Modulation and CON-OPA

Fig.4.111, Fig.4.112, Fig.4.113, Fig.4.114, Fig.4.115, Fig.4.116, Fig.4.117, Fig.4.118 and Fig.4.119 presents the comparison of system BER for different precoding techniques using BPSK, QPSK and Adaptive modulations and varied power allocation strategies, i.e. FPA, COPA and CON-OPA, respectively, with each entity in the system having four antennas. It has been observed that for almost all the cases, MODIFIED SVD yields the least system BER, followed by MF and finally, comparably same system BERs for SVD, ZF and RZF. This is so because in case of MODIFIED SVD precoding, along with the respective precoding and post-coding matrices, a gain matrix formed from the channel gains, is used both at the transmitter and receiver, which considerably enhances the quality of signal reception. MF also produces good enough system BER results, especially in Fig.4.111, wherein it closely surpasses MODIFIED SVD, indicating that due to the presence of additional number of transmission-reception channel paths, it becomes more convenient for the aforementioned precoding scheme to align the information signal as per the channel, so that the signal is received in its optimum form. The rest of the precoding schemes behave similarly, with respect to system BER, because of comparable impact of the precoding techniques on the transmission and reception of the information signal.

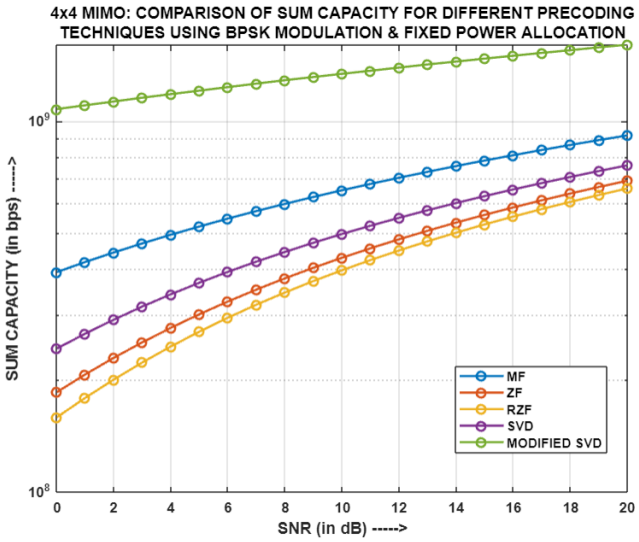

Fig.4.120: For (4x4)-MIMO-NOMA: Comparison of Sum Capacity for different precoding techniques using BPSK and FPA

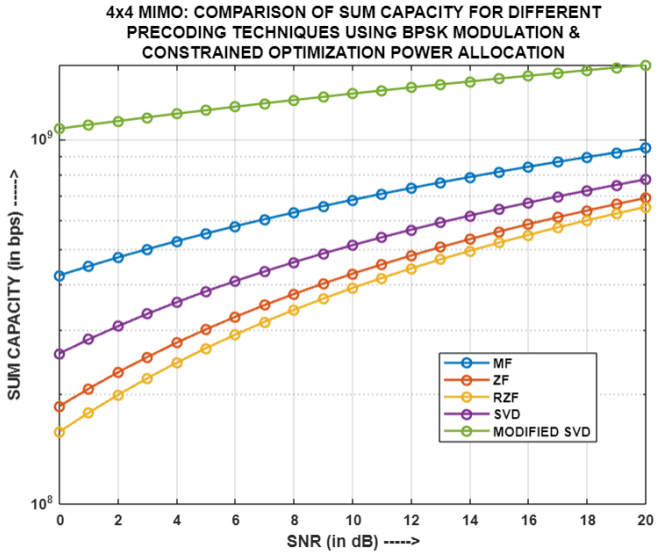

Fig.4.121: For (4x4)-MIMO-NOMA: Comparison of Sum Capacity for different precoding techniques using BPSK and COPA

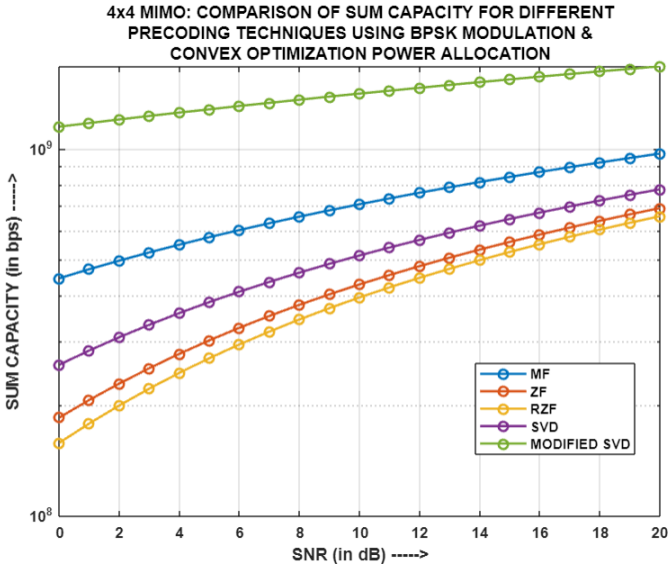

Fig.4.122: For (4x4)-MIMO-NOMA: Comparison of Sum Capacity for different precoding techniques using BPSK and CON-OPA

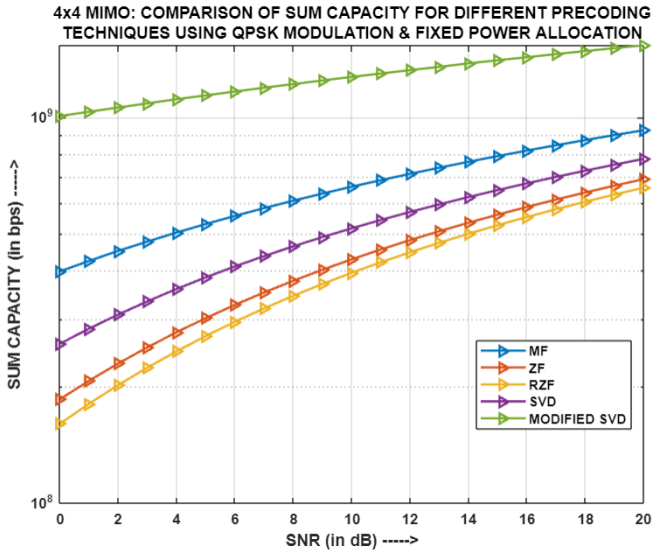

Fig.4.123: For (4x4)-MIMO-NOMA: Comparison of Sum Capacity for different precoding techniques using QPSK and FPA

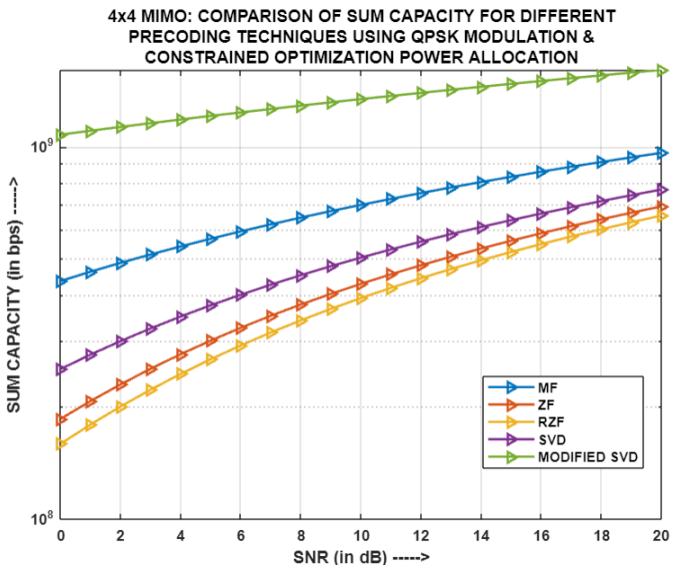

Fig.4.124: For (4x4)-MIMO-NOMA: Comparison of Sum Capacity for different precoding techniques using QPSK and COPA

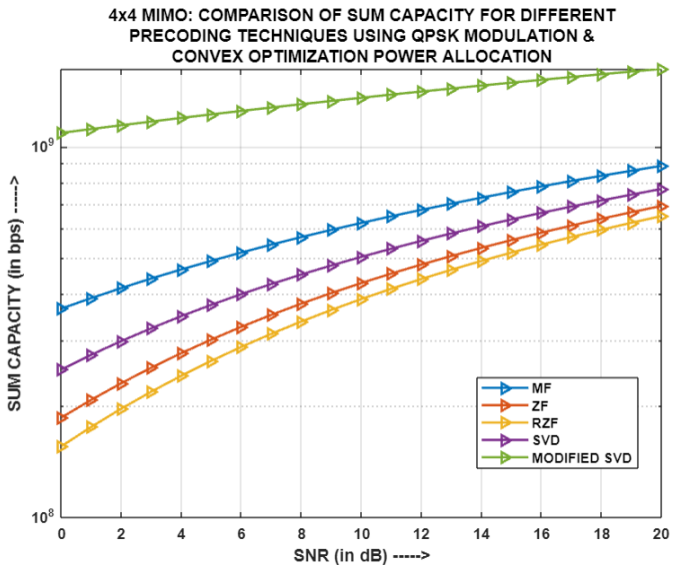

Fig.4.125: For (4x4)-MIMO-NOMA: Comparison of Sum Capacity for different precoding techniques using QPSK and CON-OPA

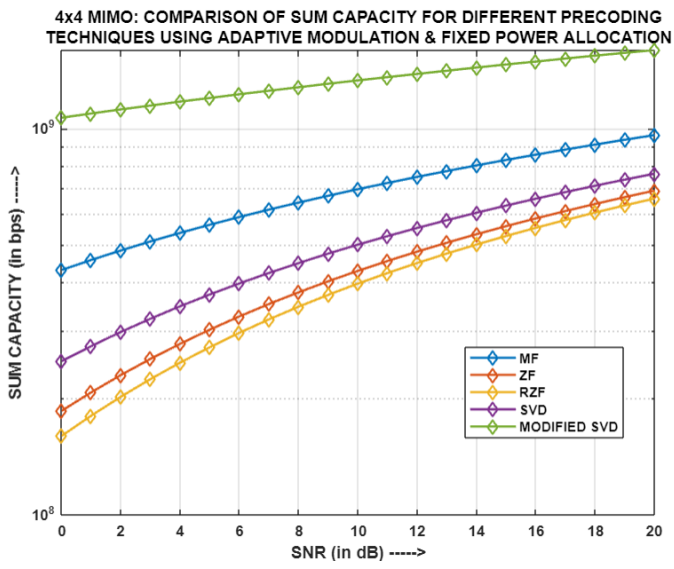

Fig.4.126: For (4x4)-MIMO-NOMA: Comparison of Sum Capacity for different precoding techniques using Adaptive Modulation and FPA

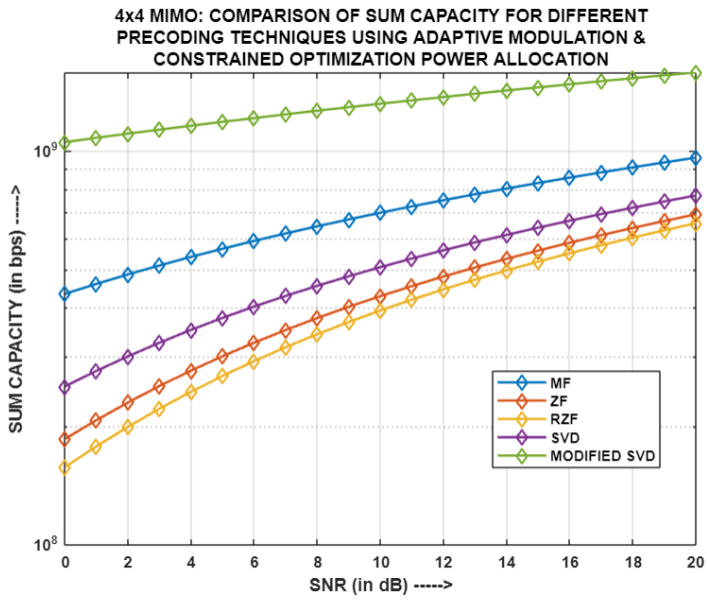

Fig.4.127: For (4x4)-MIMO-NOMA: Comparison of Sum Capacity for different precoding techniques using Adaptive Modulation and COPA

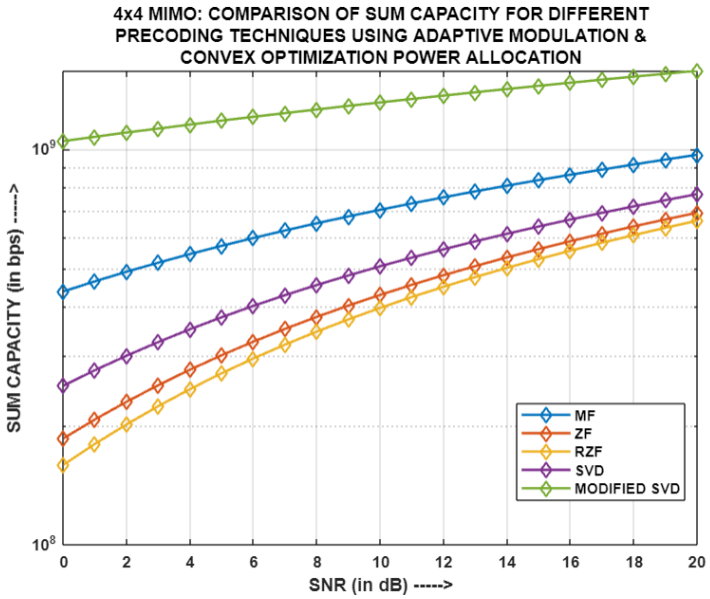

Fig.4.128: For (4x4)-MIMO-NOMA: Comparison of Sum Capacity for different precoding techniques using Adaptive Modulation and CON-OPA

Fig.4.120, Fig.4.121, Fig.4.122, Fig.4.123, Fig.4.124, Fig.4.125, Fig.4.126, Fig.4.127 and Fig.4.128 depicts the comparison of Sum Capacity for different precoding techniques using BPSK, QPSK and Adaptive modulations and varied power allocation strategies, i.e. FPA, COPA and CON-OPA, respectively, with each entity in the system having four antennas. The highest sum capacity is generated by MODIFIED SVD in all the cases mentioned above, followed by MF, SVD, ZF, and finally RZF. This behavior can be attributed to the distinct impacts of the precoding techniques on the channel gain of individual users, which in turn affect their throughputs and ultimately the overall sum capacity of the system. The reason behind MODIFIED SVD's superior performance lies in its utilization of a gain matrix at both the transmitter and receiver, which significantly influences the channel gains and results in a substantially higher sum capacity compared to the other precoding schemes.

4.4.12. Comparative Analysis of simulation results of two-user (2x2) and (4x4) MIMO-PD-NOMA models for different precoding techniques and modulation schemes:

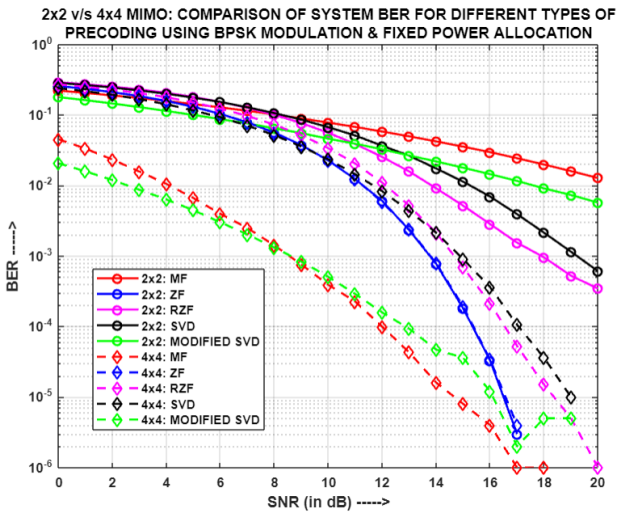

Fig.4.129: (2x2) v/s (4X4) MIMO-NOMA: Comparison of System BER for different precoding schemes using BPSK and FPA

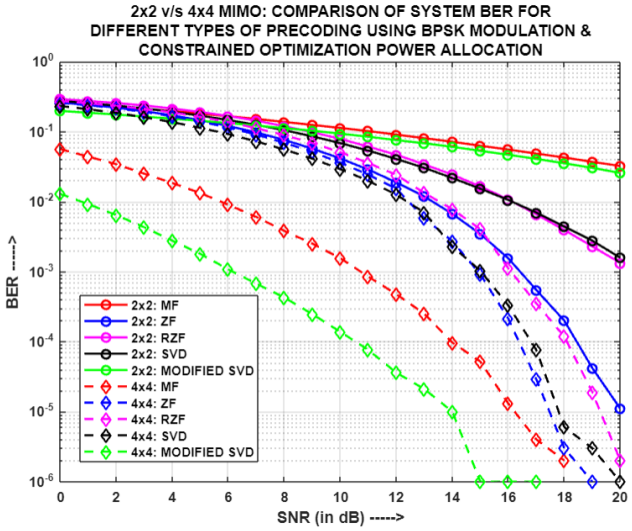

Fig.4.130: (2x2) v/s (4X4) MIMO-NOMA: Comparison of System BER for different precoding schemes using BPSK and COPA

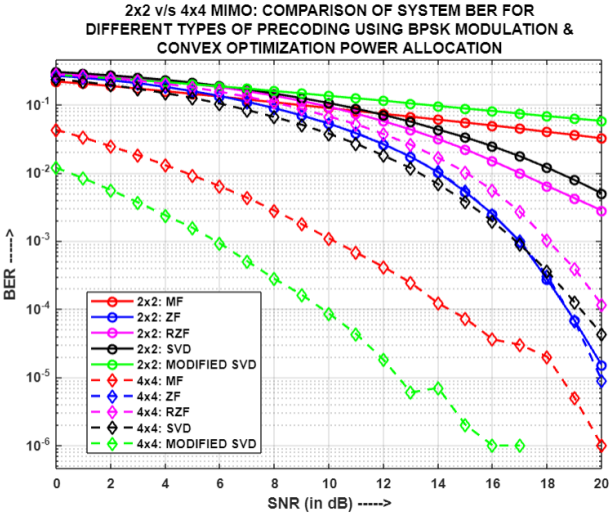

Fig.4.131: (2x2) v/s (4X4) MIMO-NOMA: Comparison of System BER for different precoding schemes using BPSK and CON-OPA

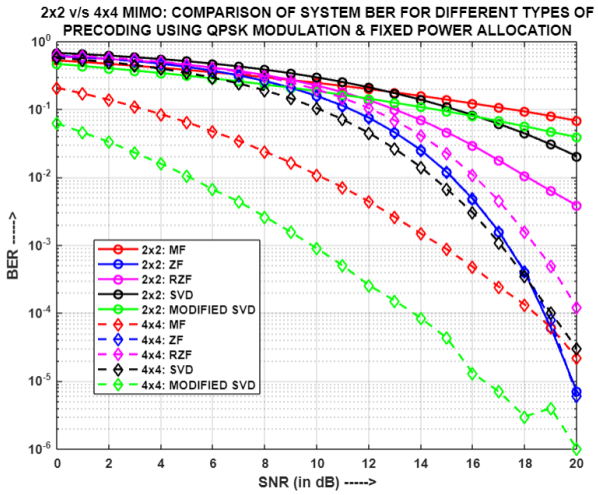

Fig.4.132: (2x2) v/s (4X4) MIMO-NOMA: Comparison of System BER for different precoding schemes using QPSK and FPA

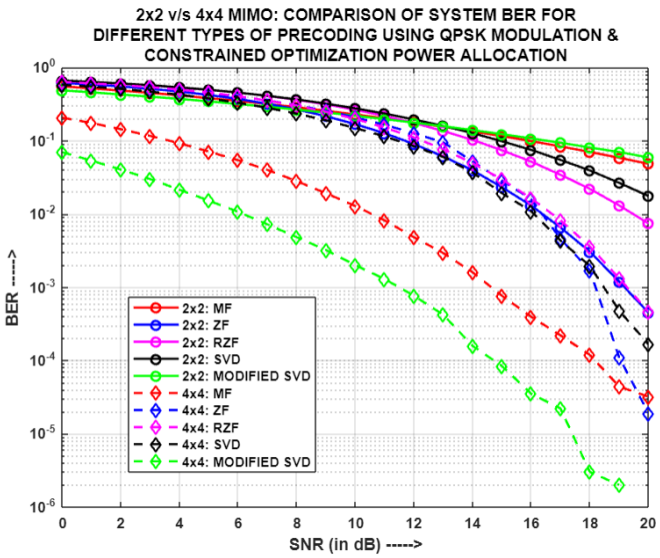

Fig.4.133: (2x2) v/s (4X4) MIMO-NOMA: Comparison of System BER for different precoding schemes using QPSK and COPA

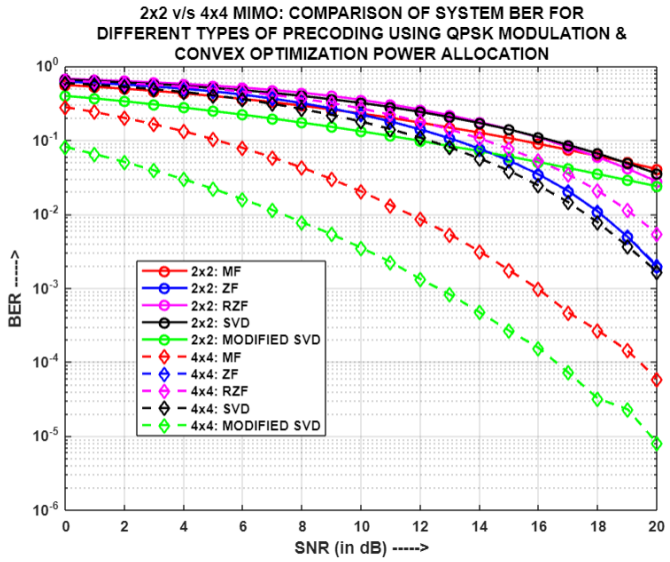

Fig.4.134: (2x2) v/s (4X4) MIMO-NOMA: Comparison of System BER for different precoding schemes using QPSK and CON-OPA

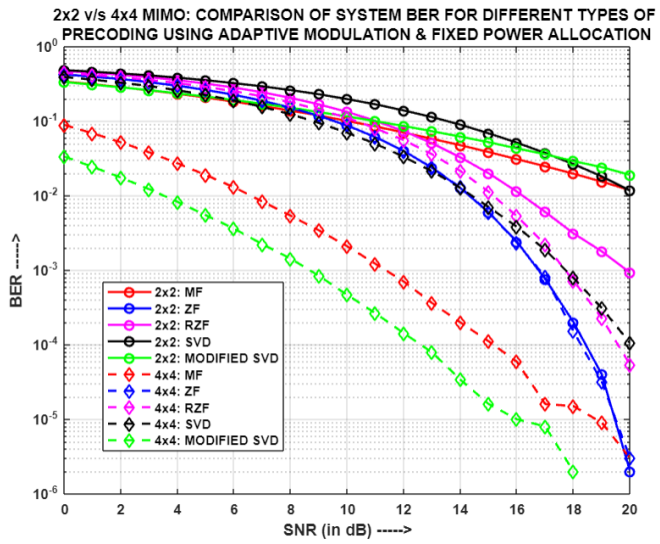

Fig.4.135: (2x2) v/s (4X4) MIMO-NOMA: Comparison of System BER for different precoding schemes using Adaptive Modulation and FPA

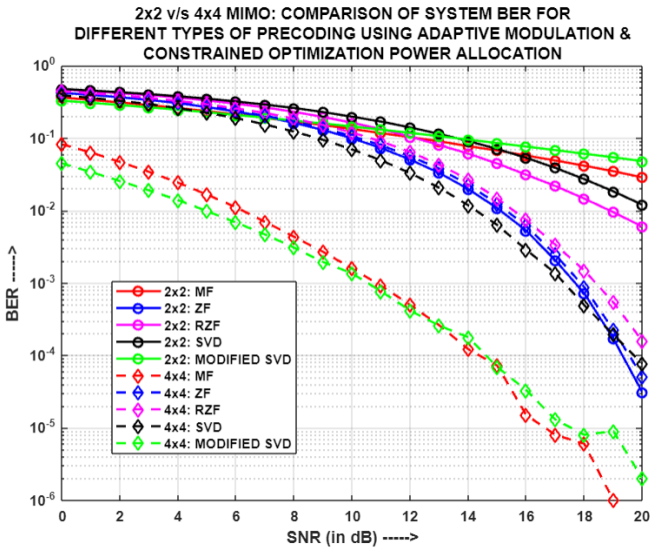

Fig.4.136: (2x2) v/s (4X4) MIMO-NOMA: Comparison of System BER for different precoding schemes using Adaptive Modulation and COPA

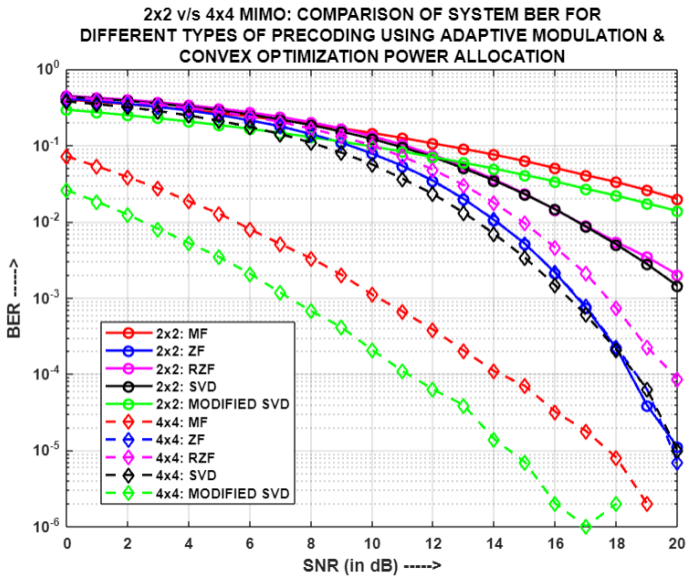

Fig.4.137: (2x2) v/s (4X4) MIMO-NOMA: Comparison of System BER for different precoding schemes using Adaptive Modulation and CON-OPA

Fig.4.129, Fig.4.130, Fig.4.131, Fig.4.132, Fig.4.133, Fig.4.134, Fig.4.135, Fig.4.136 and Fig.4.137 illustrates the comparison of system BER for different cases of multiple-input-multiple-output (MIMO), i.e. (2x2) and (4x4), using diverse precoding mechanisms and power allocation strategies, i.e. FPA, COPA and CON-OPA respectively. It has been witnessed that for all the above cases, MF, RZF, SVD and MODIFIED SVD generates a lower system BER for the (4x4) MIMO configuration in contrast to its (2x2) counterpart. This happens because of additional number of TX-RX antennas, which implies more number of channel paths and hence higher chances of better signal reception. However, in case of ZF, this theory holds true only when different sets of power coefficients are used for (4x4) and (2x2) MIMO configurations. Otherwise, comparable system BERs are produced by ZF, for the two MIMO cases, owing to the generic attribute of ZF, wherein it processes the informational signal with the channel's pseudo inverse and thereby, makes the system BER proportional to the AWGN variance only.

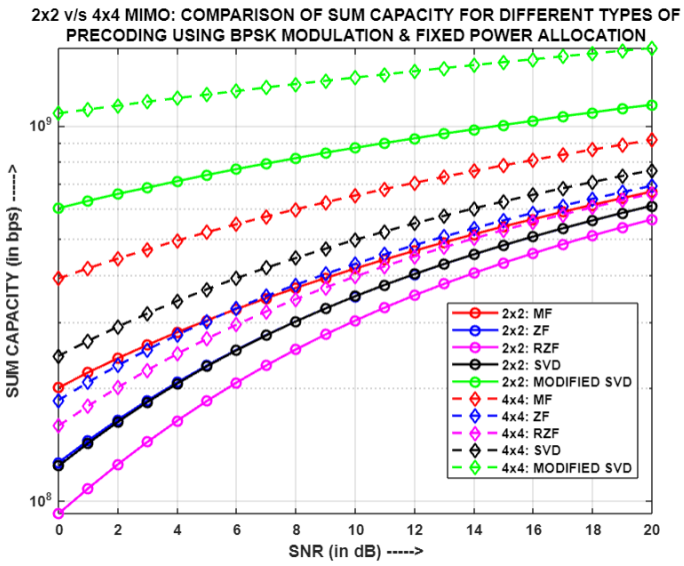

Fig.4.138: (2x2) v/s (4X4) MIMO-NOMA: Comparison of Sum Capacity for different precoding schemes using BPSK and FPA

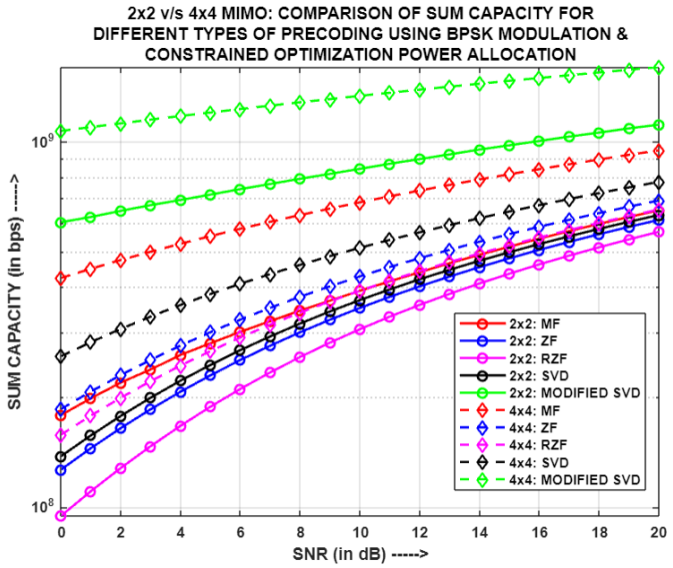

Fig.4.139: (2x2) v/s (4X4) MIMO-NOMA: Comparison of Sum Capacity for different precoding schemes using BPSK and COPA

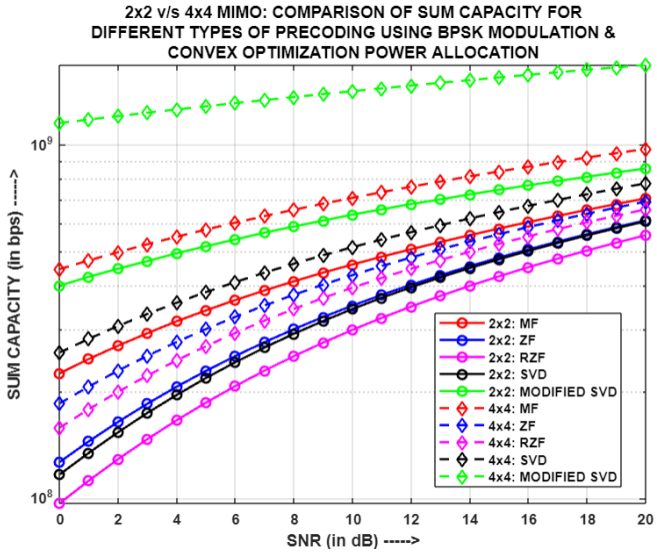

Fig.4.140: (2x2) v/s (4X4) MIMO-NOMA: Comparison of Sum Capacity for different precoding schemes using BPSK and CON-OPA

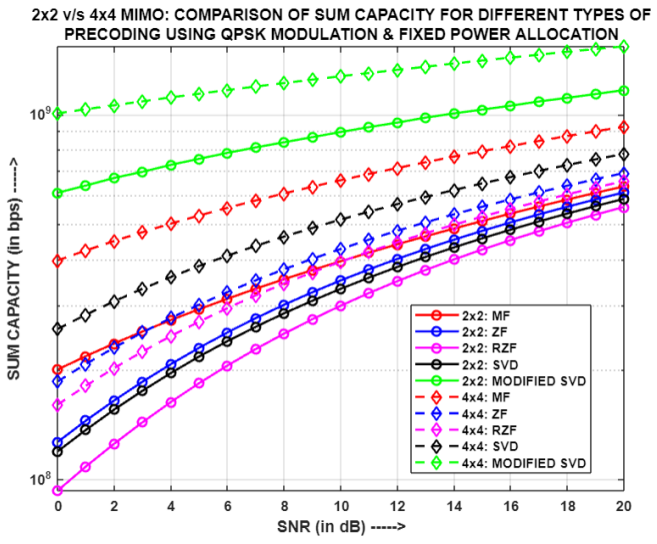

Fig.4.141: (2x2) v/s (4X4) MIMO-NOMA: Comparison of Sum Capacity for different precoding schemes using QPSK and FPA

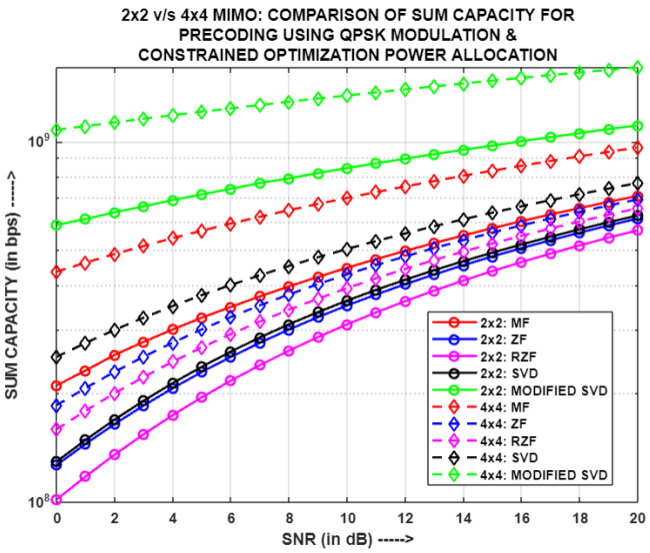

Fig.4.142: (2x2) v/s (4X4) MIMO-NOMA: Comparison of Sum Capacity for different precoding schemes using QPSK and COPA

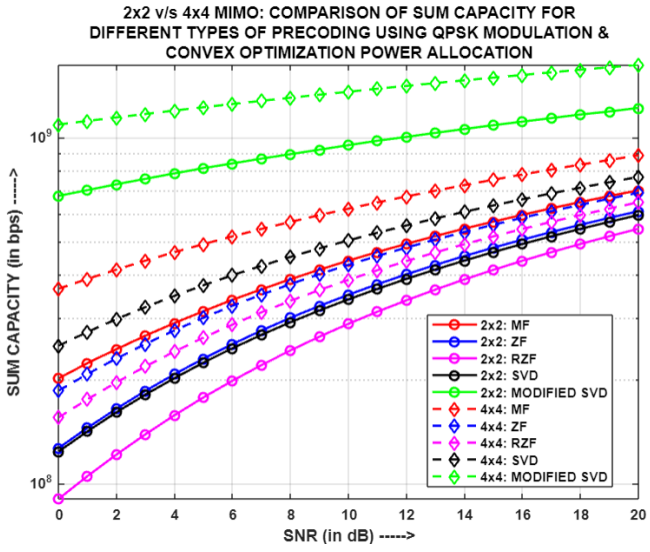

Fig.4.143: (2x2) v/s (4X4) MIMO-NOMA: Comparison of Sum Capacity for different precoding schemes using QPSK and CON-OPA

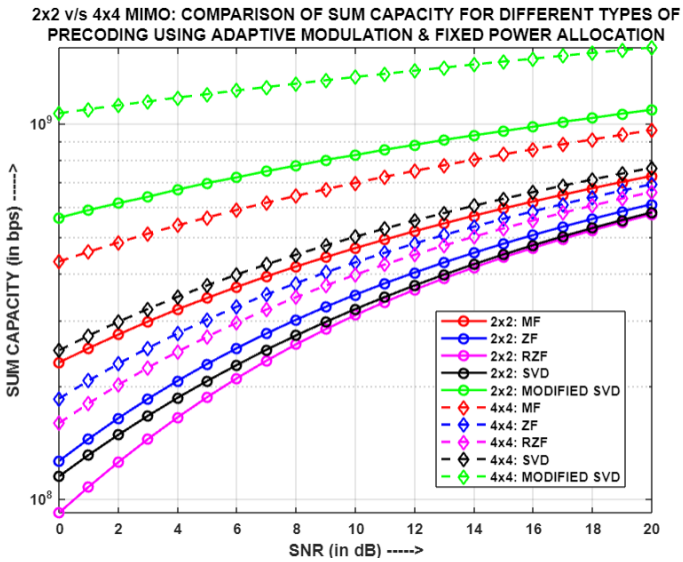

Fig.4.144: (2x2) v/s (4X4) MIMO-NOMA: Comparison of Sum Capacity for different precoding schemes using Adaptive Modulation and FPA

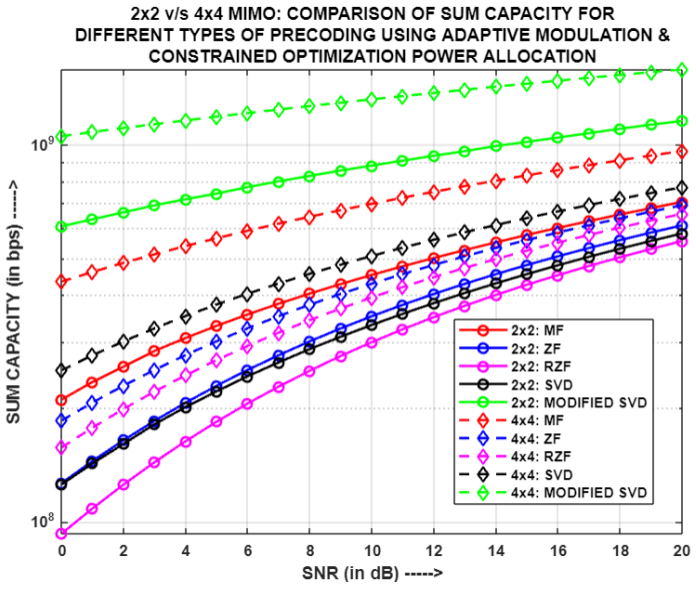

Fig.4.145: (2x2) v/s (4X4) MIMO-NOMA: Comparison of Sum Capacity for different precoding schemes using Adaptive Modulation and COPA

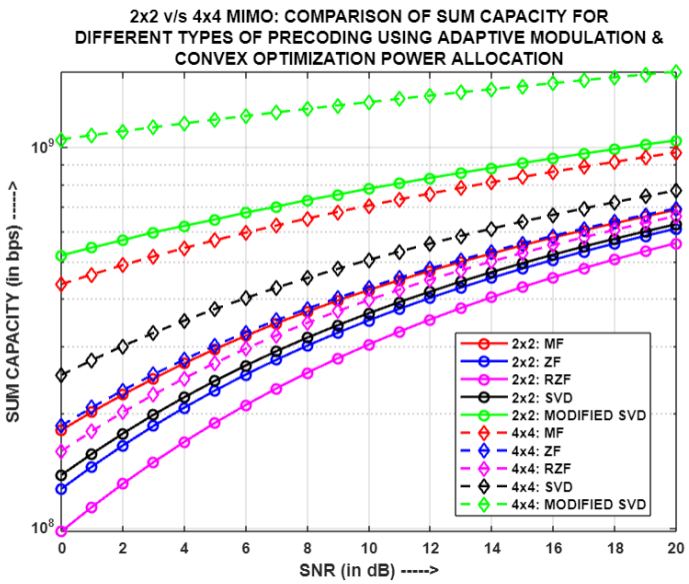

Fig.4.146: (2x2) v/s (4X4) MIMO-NOMA: Comparison of Sum Capacity for different precoding schemes using Adaptive Modulation and CON-OPA

Fig.4.138, Fig.4.139, Fig.4.140, Fig.4.141, Fig.4.142, Fig.4.143, Fig.4.144, Fig.4.145 and Fig.4.146 showcases the comparison of Sum Capacity for different cases of multiple-input-multiple-output (MIMO), i.e. (2x2) and (4x4), using diverse precoding mechanisms and power allocation strategies, i.e. FPA, COPA and CON-OPA respectively. It can be seen that for all the above cases that all the precoding schemes yield a higher sum capacity for the (4x4) MIMO system in comparison to (2x2) MIMO system. This behaviour can be attributed to the fact that along with the influence of the precoding techniques on the channel gains, (4x4) MIMO configuration offers 16 channels to each of its users, while (2x2) MIMO system offers only 4 channels per user. Since channel gain is one the primary factors that directly influences the users' throughput and hence, sum capacity; therefore, such variations in sum capacities are observed for the two MIMO configurations.

4.4.13. Simulation Result Analysis of two-user (2x2)-MIMO-PD-NOMA model for different power allocation strategies and precoding techniques:

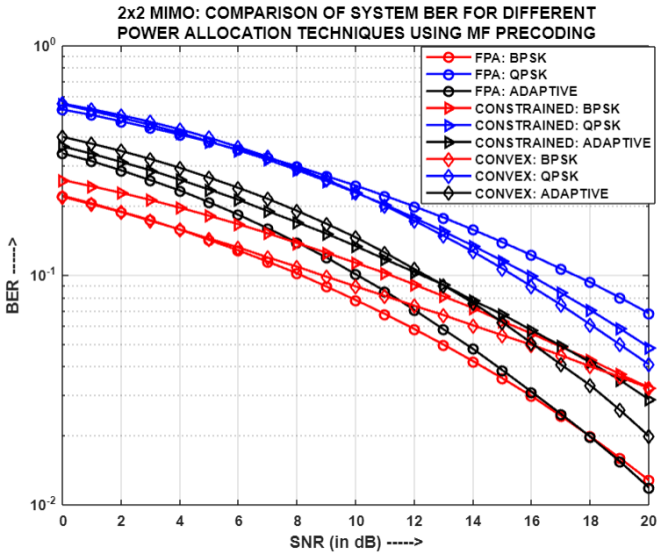

Fig.4.147: For (2x2)-MIMO-NOMA: Comparison of System BER for different power allocation strategies using MF

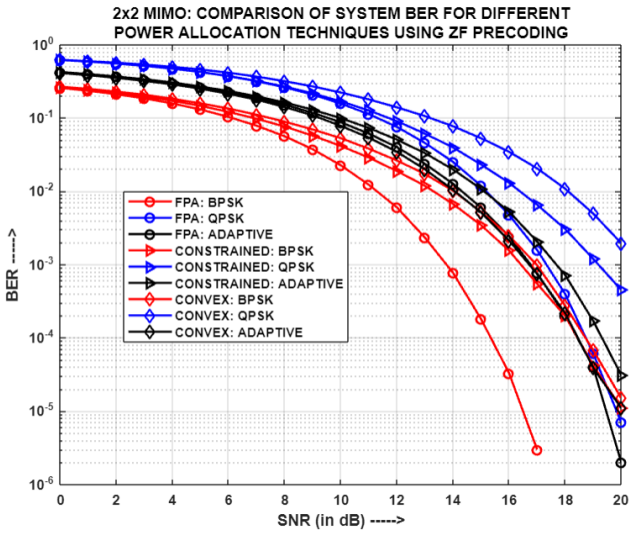

Fig.4.148: For (2x2)-MIMO-NOMA: Comparison of System BER for different power allocation strategies using ZF

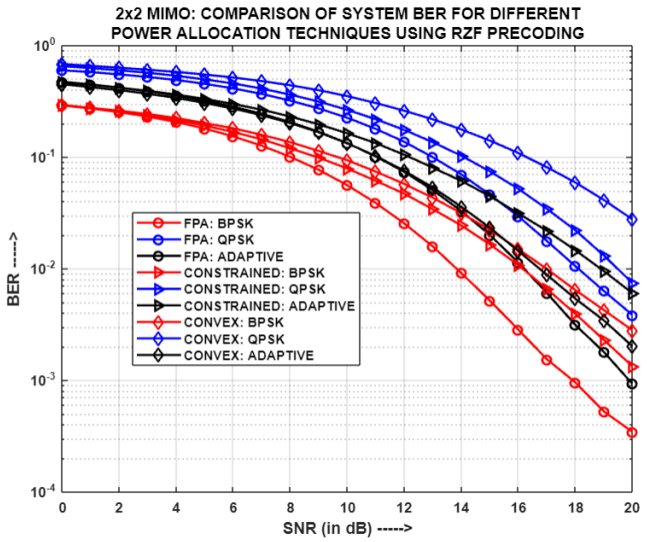

Fig.4.149: For (2x2)-MIMO-NOMA: Comparison of System BER for different power allocation strategies using RZF

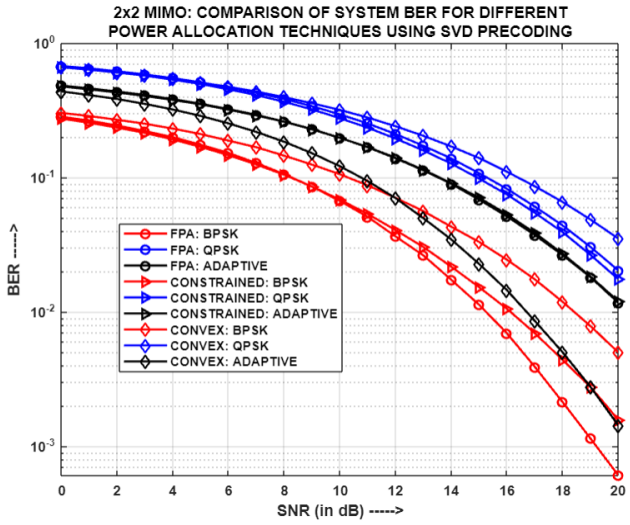

Fig.4.150: For (2x2)-MIMO-NOMA: Comparison of System BER for different power allocation strategies using SVD

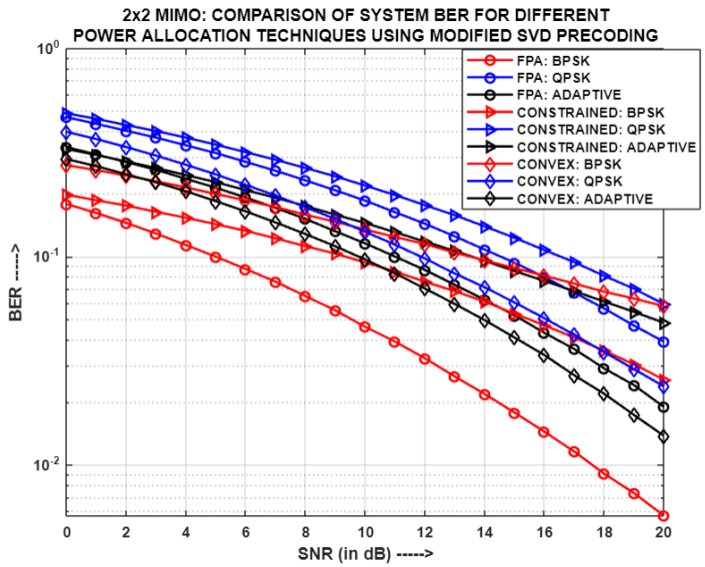

Fig.4.151: For (2x2)-MIMO-NOMA: Comparison of System BER for different power allocation strategies using MODIFIED SVD

Fig.4.147, Fig.4.148, Fig.4.149, Fig.4.150 and Fig.4.151 presents the comparison of system BER for different power allocation (PA) strategies using diverse precoding techniques, i.e. MF, ZF, RZF, SVD and MODIFIED SVD respectively, with each entity in the system having two antennas. For both BPSK and Adaptive modulations in regard to MF, the FPA technique results in the lowest system BER. However, when using QPSK, the CON-OPA mechanism achieves better system BER performance than the other two PA strategies. This is due to the optimal selection of power coefficients, by the respective PA mechanisms, across the entire SNR range. However, for ZF and RZF, FPA yields the least system BER performance in case of all the modulation schemes, implying that the power coefficient set used in FPA is the best choice for power distribution among users, when employing the aforementioned precoding techniques. In case of SVD, for BPSK and QPSK both, FPA yields the least system BER respectively; while for Adaptive modulation, it is CON-OPA mechanism that produces the lowest system BER, as the respective PA strategies make the optimum choice of power coefficients for the entire SNR range. Also, for QPSK, even COPA gives comparable results in accordance to FPA, as the sets of power coefficients selected through the constrained optimization algorithm, are similar to the one used in the latter. Finally, it has been

observed in regard to MODIFIED SVD, that for both QPSK and Adaptive modulations, CON-OPA strategy has outperformed the other two PA mechanisms, in determining the optimum choice of power allocation coefficient sets, with respect to system BER. However, in case of BPSK, FPA still is the best choice in terms of yielding the least system BER.

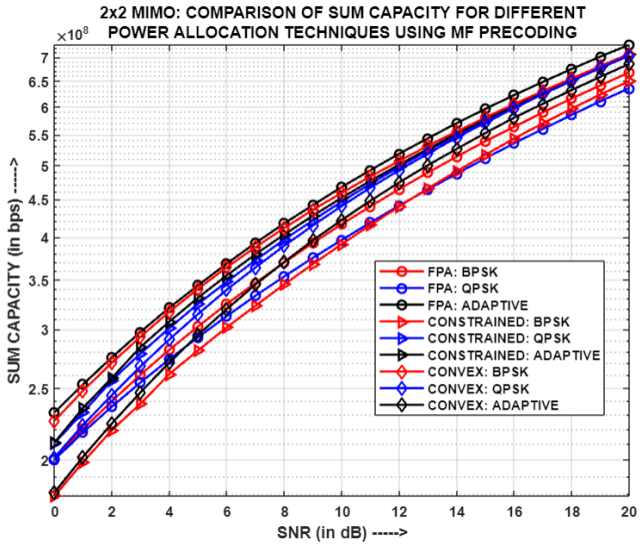

Fig.4.152: For (2x2)-MIMO-NOMA: Comparison of Sum Capacity for different power allocation strategies using MF

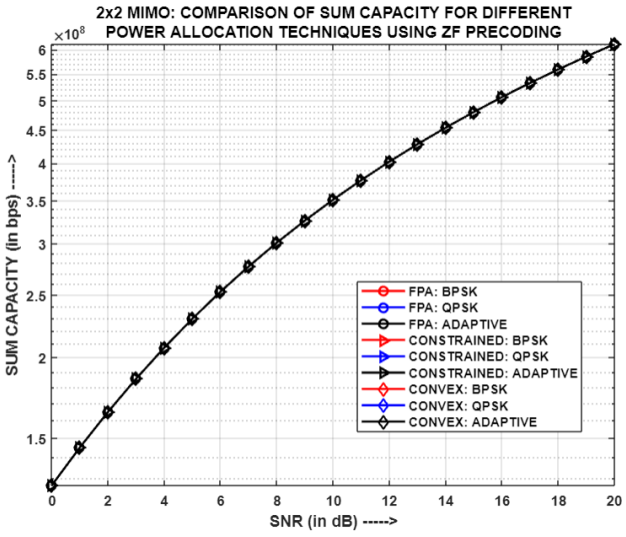

Fig.4.153: For (2x2)-MIMO-NOMA: Comparison of Sum Capacity for different power allocation strategies using ZF

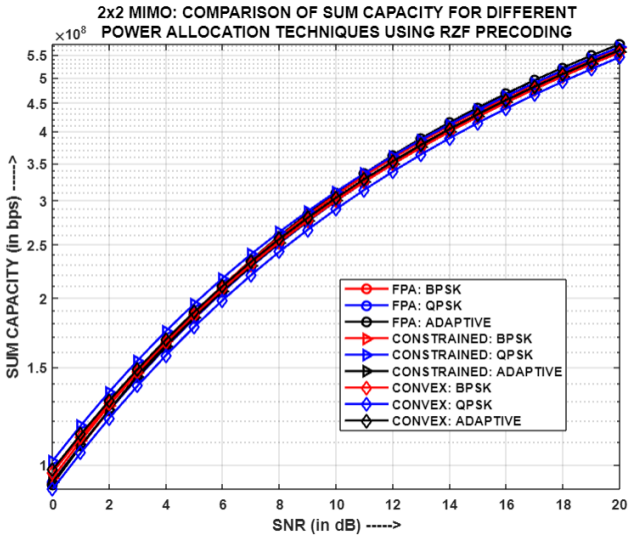

Fig.4.154: For (2x2)-MIMO-NOMA: Comparison of Sum Capacity for different power allocation strategies using RZF

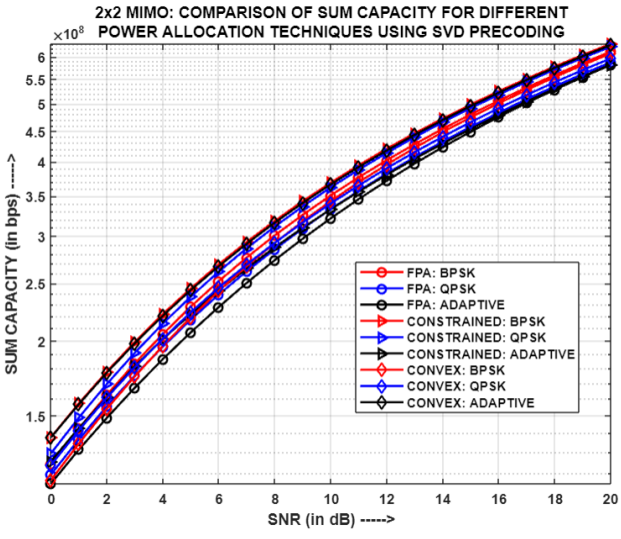

Fig.4.155: For (2x2)-MIMO-NOMA: Comparison of Sum Capacity for different power allocation strategies using SVD

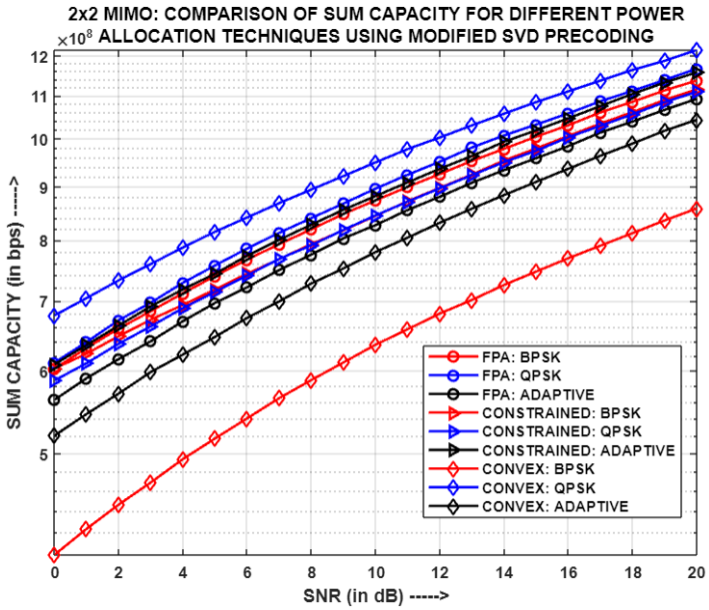

Fig.4.156: For (2x2)-MIMO-NOMA: Comparison of Sum Capacity for different power allocation strategies using MODIFIED SVD

Fig.4.152, Fig.4.153, Fig.4.154, Fig.4.155 and Fig.4.156 portrays the comparison of Sum Capacity for different power allocation strategies using diverse precoding techniques, i.e., MF, ZF, RZF, SVD and MODIFIED SVD respectively, with each entity in the system having two antennas. Apart from MODIFIED SVD, the PA strategies applied to all other precoding schemes happened to yield comparable or slightly different sum capacities because of the dominance of the effect of channel gains on the throughput of the users and hence, on the overall sum capacity of the system. In case of MODIFIED SVD, although FPA and COPA mechanisms generate similar sum capacities, for all the modulation schemes, due to the effect of alike channel gains and comparable power allocation coefficient sets on the user throughput. However, for CON-OPA, vast differences in sum capacities have been observed, indicating to the fact that considerably different sets of power coefficients have been chosen for the different modulation schemes, thereby producing the highest sum capacity for QPSK.

4.4.14. Simulation Result Analysis of two-user (4x4)-MIMO-PD-NOMA model for different power allocation strategies and precoding techniques

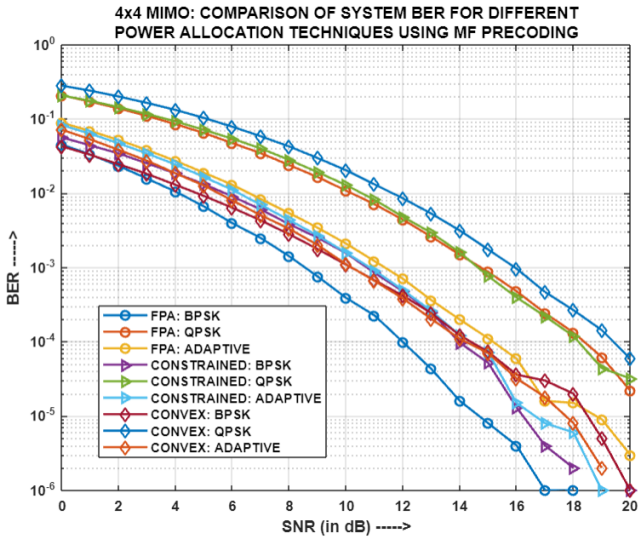

Fig.4.157: For (4x4)-MIMO-NOMA: Comparison of System BER for different power allocation strategies using MF

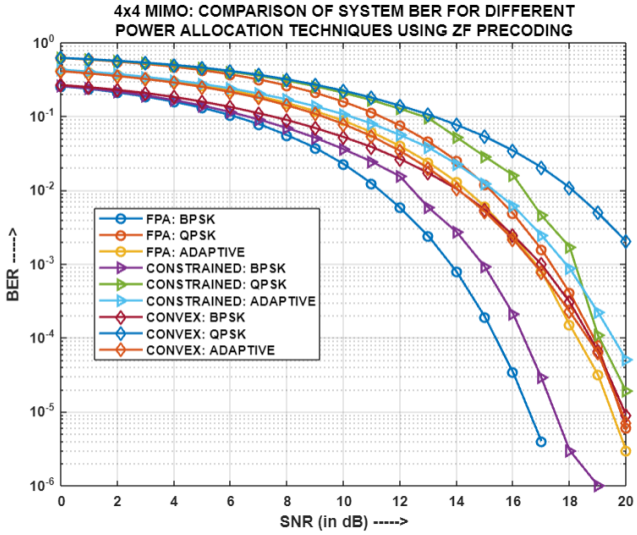

Fig.4.158: For (4x4)-MIMO-NOMA: Comparison of System BER for different power allocation strategies using ZF

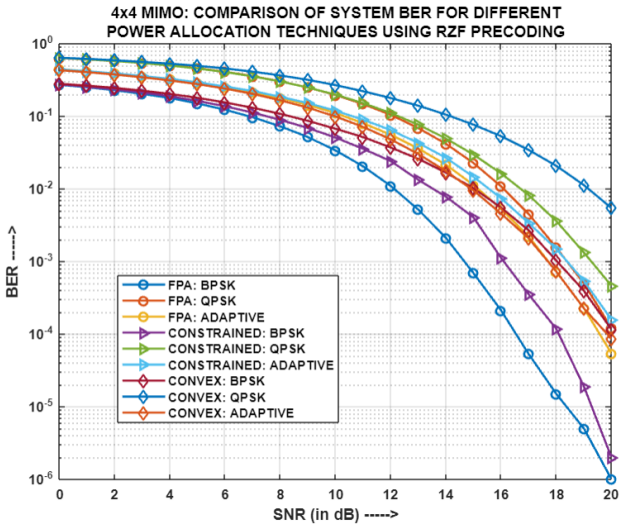

Fig.4.159: For (4x4)-MIMO-NOMA: Comparison of System BER for different power allocation strategies using RZF

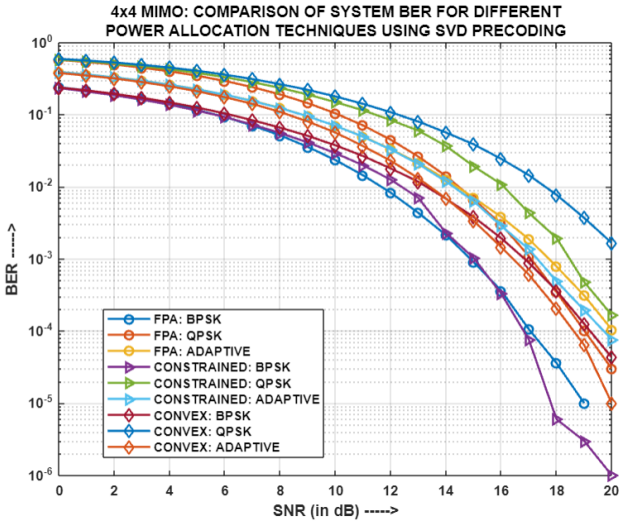

Fig.4.160: For (4x4)-MIMO-NOMA: Comparison of System BER for different power allocation strategies using SVD

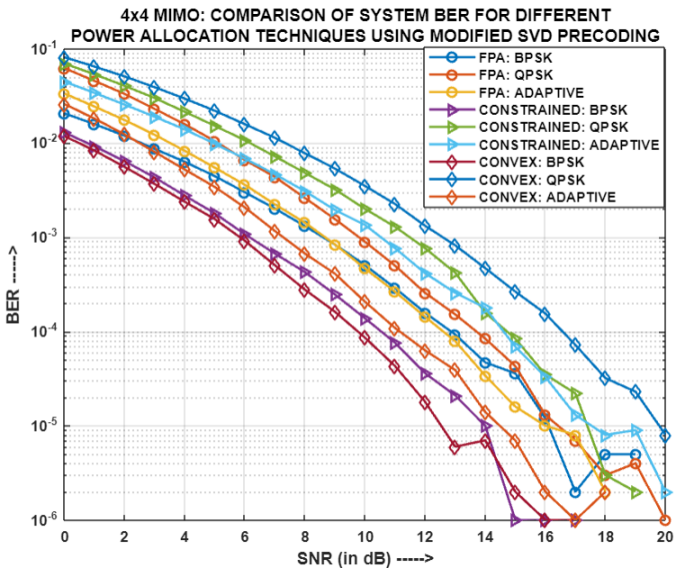

Fig.4.161: For (4x4)-MIMO-NOMA: Comparison of System BER for different power allocation strategies using MODIFIED SVD

Fig.4.157, Fig.4.158, Fig.4.159, Fig.4.160 and Fig.4.161 illustrates the comparison of system BER for different power allocation strategies using diverse precoding techniques, i.e. MF, ZF, RZF, SVD and MODIFIED SVD respectively, with each entity in the system having four antennas. In context of MF, the FPA technique demonstrates the lowest system BER for both BPSK and QPSK modulations. However, in case of Adaptive modulation, the COPA mechanism happens to slightly outperform the other two PA strategies in terms of system BER performance. This can be attributed to the optimal selection of power coefficients by the respective PA mechanisms throughout the entire SNR range. Also, for both QPSK and Adaptive modulations, COPA and CON-OPA mechanisms respectively, tend to produce similar results as to those obtained by the particular aforementioned optimum PA strategies, because of comparable selection of power allocation coefficient sets. In contrast, when it comes to ZF and RZF, the FPA technique demonstrates the lowest system BER performance for all modulation schemes. This indicates that the power coefficient set utilized in FPA is the optimal choice for distributing power among users when employing the respective precoding techniques. In case of SVD, for BPSK, QPSK and Adaptive modulations, COPA, FPA and CON-OPA strategies respectively, generate the least system BER owing to

the use of optimal power coefficient sets for the particular modulation techniques. Finally, in regard to MODIFIED SVD, for both BPSK and Adaptive modulations, CON-OPA mechanism determines the best choice of power coefficient sets, whereby it produces the least system BER; while the power allocation using FPA happened to yield the lowest system BER for QPSK.

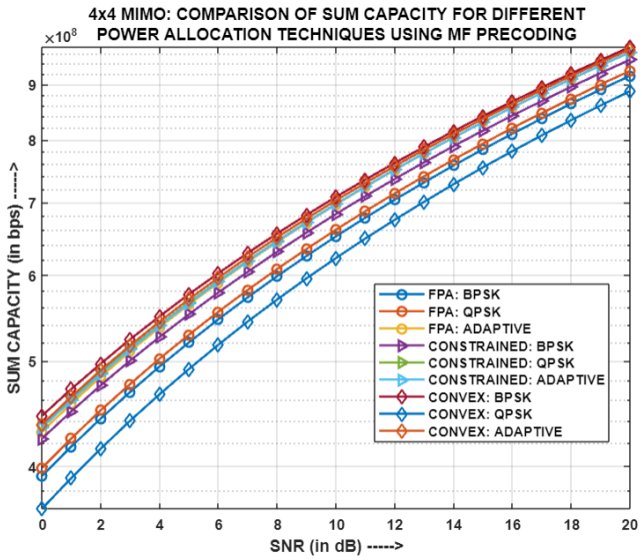

Fig.4.162: For (4x4)-MIMO-NOMA: Comparison of Sum Capacity for different power allocation strategies using MF

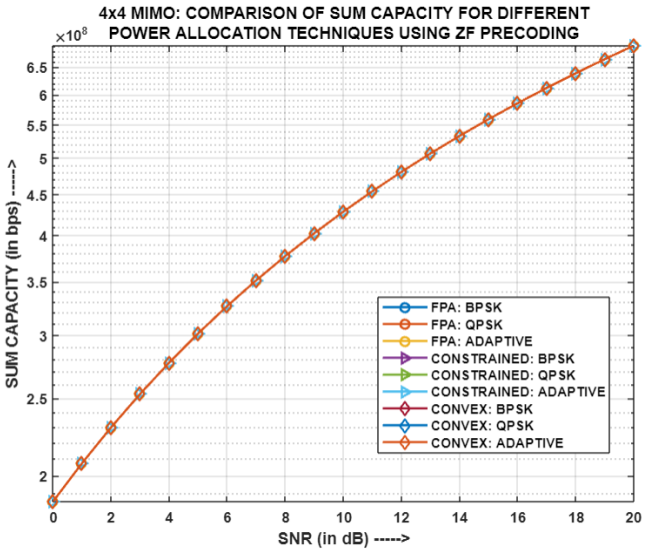

Fig.4.163: For (4x4)-MIMO-NOMA: Comparison of Sum Capacity for different power allocation strategies using ZF

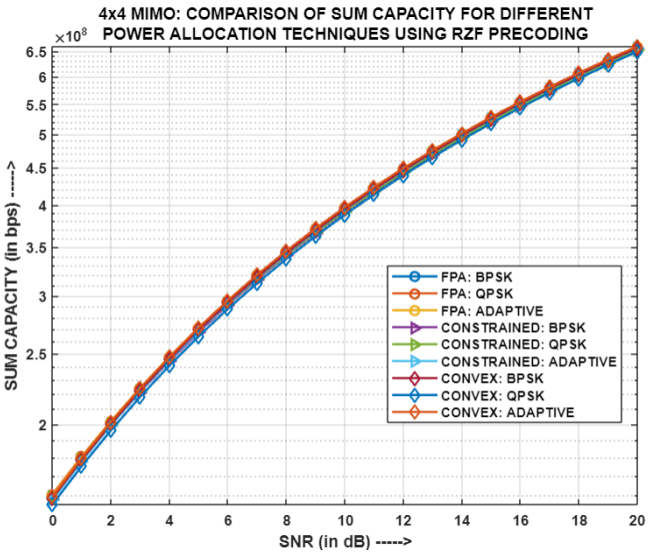

Fig.4.164: For (4x4)-MIMO-NOMA: Comparison of Sum Capacity for different power allocation strategies using RZF

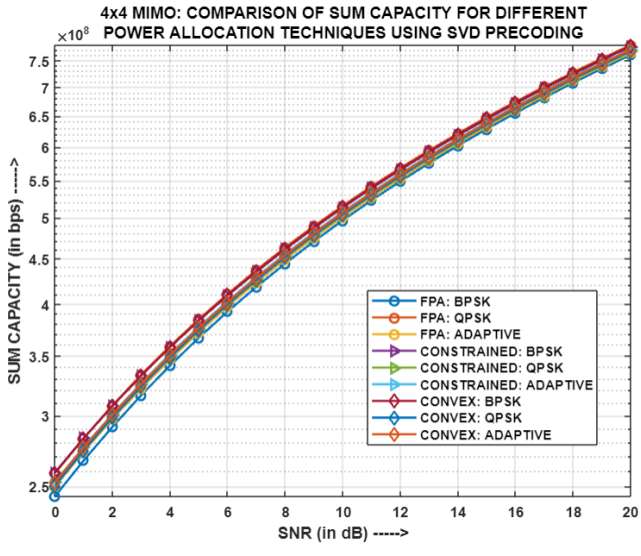

Fig.4.165: For (4x4)-MIMO-NOMA: Comparison of Sum Capacity for different power allocation strategies using SVD

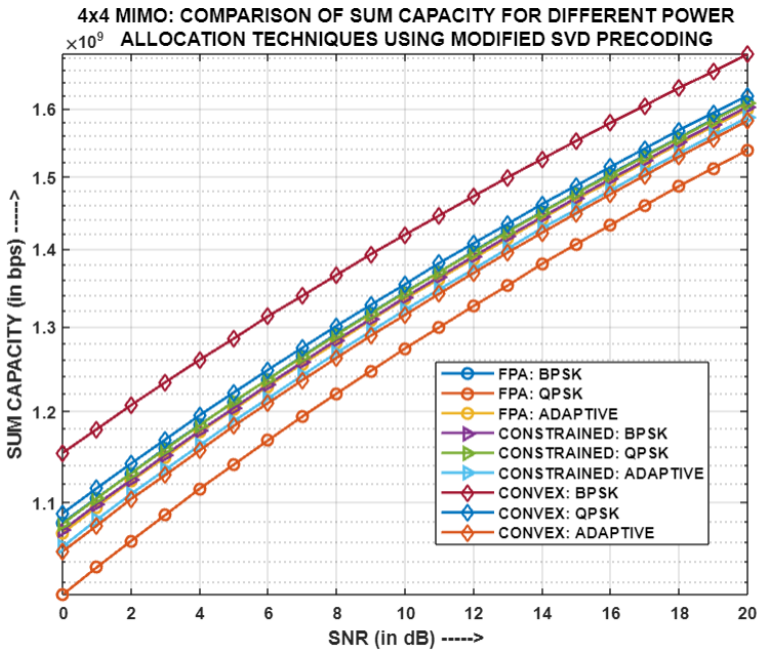

Fig.4.166: For (4x4)-MIMO-NOMA: Comparison of Sum Capacity for different power allocation strategies using MODIFIED SVD

Fig.4.162, Fig.4.163, Fig.4.164, Fig.4.165 and Fig.4.166 showcases the comparison of Sum Capacity for different power allocation strategies using diverse precoding techniques, i.e. MF, ZF, RZF, SVD and MODIFIED SVD respectively, with each entity in the system having four antennas. In case of ZF, RZF and SVD, all the PA strategies implemented produce comparable sum capacities, even though different power allocation coefficient sets have been utilized. This behaviour can be attributed to the significant influence of channel gains on the user throughputs and, consequently, on the overall sum capacity of the system. However, for MF and MODIFIED SVD, considerable difference in the sum capacities have been noticed, especially in the latter, because of strong impact of significantly different usage of power allocation coefficient sets. Therefore, for MODIFIED SVD, CON-OPA mechanism yields the highest sum capacity for BPSK.

Table 4.3: Compilation of Result Analysis for MU-MIMO-PD-NOMA for different Precoding techniques

Precoding Technique	Modulation Scheme	Power Allocation (PA) Strategy	System BER		Sum Capacity		Remarks
			(2x2) MIMO	(4x4) MIMO	(2x2) MIMO	(4x4) MIMO	
MF	BPSK	FPA	Least	Least	Moderate	Low	• BPSK performs well for all PA mechanisms. • In case of (4x4)-MIMO, Adaptive Modulation, using COPA and CON-OPA, surpasses the rest.
		COPA	Least	Least	Low	High	
		CON-OPA	Least	Least	High	High	
	QPSK	FPA	Highest	Highest	Low	Low	
		COPA	Highest	Highest	High	High	
		CON-OPA	Highest	Highest	Moderate	Low	
	Adaptive Modulation	FPA	Moderate	Moderate	High	High	
		COPA	Moderate	Least	High	High	
		CON-OPA	Moderate	Least	Low	High	
ZF	BPSK	FPA	Least	Least	High	High	• BPSK yields optimum performance. • Adaptive Modulation performs comparable to BPSK, when used with CON-OPA.
		COPA	Least	Least	High	High	
		CON-OPA	Least	Least	High	High	
	QPSK	FPA	Highest	Highest	High	High	
		COPA	Highest	Highest	High	High	
		CON-OPA	Highest	Highest	High	High	
	Adaptive Modulation	FPA	Moderate	Moderate	High	High	
		COPA	Moderate	Moderate	High	High	
		CON-OPA	Least	Least	High	High	
RZF	BPSK	FPA	Least	Least	High	High	• BPSK delivers best performance for FPA and COPA. • Adaptive Modulation, with CON-OPA, showcases similar behaviour to BPSK.
		COPA	Least	Least	High	High	
		CON-OPA	Least	Least	High	High	
	QPSK	FPA	Highest	Highest	High	High	
		COPA	Highest	Highest	High	High	
		CON-OPA	Highest	Highest	High	High	
	Adaptive Modulation	FPA	Moderate	Moderate	High	High	
		COPA	Moderate	Moderate	High	High	
		CON-OPA	Least	Least	High	High	
SVD	BPSK	FPA	Least	Least	High	High	• BPSK performs well with FPA and COPA. • Adaptive modulation excels when used with CON-OPA.
		COPA	Least	Least	High	High	
		CON-OPA	Moderate	Least	Moderate	High	
	QPSK	FPA	Highest	Highest	High	High	
		COPA	Highest	Highest	High	High	
		CON-OPA	Highest	Highest	Moderate	High	
	Adaptive Modulation	FPA	Moderate	Moderate	High	High	
		COPA	Moderate	Moderate	Moderate	High	
		CON-OPA	Least	Least	High	High	
MODIFIED SVD	BPSK	FPA	Least	Least	High	High	• BPSK behaves optimally, using all kinds of PA, for (4x4)-MIMO. • Adaptive Modulation performs the best using FPA and (4x4)-MIMO
		COPA	Least	Least	High	High	
		CON-OPA	Highest	Least	Low	High	
	QPSK	FPA	Highest	Highest	High	Low	
		COPA	Highest	Highest	High	High	
		CON-OPA	Moderate	Highest	High	Moderate	
	Adaptive Modulation	FPA	Moderate	Least	Moderate	High	
		COPA	Moderate	Moderate	Moderate	High	
		CON-OPA	Least	Moderate	Moderate	Low	

4.5. DISCUSSION

It is readily apparent from Table that similar to Chapter 3, BPSK, using fixed and constrained power allocation mechanisms respectively, yet again performs optimally, with respect to System BER and Sum Capacity, for all five precoding schemes. However, in some of the cases, it is unexpectedly the Adaptive modulation scheme that outperforms others, mostly using convex optimization power allocation algorithm. Therefore, the choice of power allocation coefficients, to implement the NOMA theory, plays a crucial role in commanding the BER of individual users, wherefrom the system BER is dictated. Moreover, these power coefficients significantly impact the user's throughput, which directly affects the system's sum capacity. In regard to precoding, the effective channel gain is another major factor that influences the throughput of the users, whereby higher effective channel gain enhances the throughput and improves the sum capacity; whereas comparable effective channel gains produce similar sum capacities, even when the precoding and modulation schemes are different. Furthermore, the type of precoding employed also affects the performance of the respective modulation schemes, as appropriate precoding of the transmitter signal considerably improves the signal reception quality, which aids in efficient demodulation. Additionally, the number of transmit-receive antennas used during transmission-reception plays a significant part in reducing the bit error probability at the user receiver as well as increasing the data rates at the respective users.

4.6. CONCLUSION

This chapter thoroughly analyzed the performance of NOMA in conjunction with the proposed precoding scheme, i.e. MODIFIED SVD, as well as existing precoding schemes, i.e. MF, ZF, RZF and SVD, with respect to System BER and Sum Capacity, on grounds of different power allocation strategies, modulation schemes as well as number of transmit-receive(TX-RX) antennas employed in the system. MODIFIED SVD outperformed its contemporaries when the number of TX-RX antennas were increased from (2x2) to (4x4). Hence, the proposed precoding scheme shall perform well for scenarios having (TX-RX) antennas greater than (2x2). Also, the performance of the precoding scheme is undeniably impacted by the

selected power allocation mechanism and the employed modulation technique, along with its inherent ability to counteract the channel impairments and optimize signal transmission. The results obtained in this chapter showcase the superiority of precoding over the cases where no precoding has been employed, like in Chapter 3. The use of precoding in MIMO-NOMA systems considerably enhances the overall system performance. As different precoding schemes require different levels of processing, therefore, the suitable precoding technique is selected based on the application area it needs to be employed. Precoding has been used in millimeter wave (mmWave) communication, interference management, cooperative communication and is a significant part of massive MIMO. Therefore, if the concept of NOMA is also applied to these systems, then with the help of precoding, better quality of signals will be received whereby, the process of successive interference cancellation (SIC) can operate more efficiently, which will reduce the chances of higher bit error probability at the receiver, especially for higher order modulation schemes. Also, the spectral efficiency of the system will increase as multiple users will be served on the same bandwidth. Thus, MIMO-NOMA employing precoding promises reliable and efficient communication among all kinds of user equipments.

Chapter 5 PROPOSITION OF A NOVEL CLUSTERING METHODOLOGY OVER CONVENTIONAL SCHEMES FOR MULTI-USER MIMO-PD-NOMA

5.1. ABSTRACT

Clustering techniques have gained significant attention in the field of wireless communication due to their ability to improve resource allocation, network management, and overall system performance. Since in NOMA, successive interference cancellation (SIC) tends to get more imperfect with increase in the number of users in the network; hence, clustering methodology serves to be beneficial in such scenarios. With the help of clustering, the users are grouped into small clusters, wherein each cluster employs NOMA independently. Therefore, clustering is chosen to be applied to MIMO-NOMA systems. Furthermore, in MIMO-NOMA systems, the interference between clusters is handled through the usage of efficient precoding techniques. This chapter provides a meticulous performance analysis, with respect to system Bit Error Rate (BER), Sum Capacity and Spectral Efficiency (SE), of a downlink MU-MIMO-PD-NOMA system for different clustering methodologies, applying varied precoding schemes. A novel clustering methodology, based on user's channel gain and channel correlation, has been proposed and compared with the conventional clustering techniques like Random clustering (RAN), Best-With-Worst (BWW) clustering and Best-With-Best (BWB) clustering. The MU-MIMO-PD-NOMA system model is explored for two scenarios of MIMO, in which the first scenario deals with two clusters, wherein each entity in the system has two antennas; while the second scenario equips all the entities in the system with four antennas each and handles four cluster of users. A comparative analysis of the results for both the MIMO scenarios is also presented in this chapter. The principle of NOMA requires the total transmission power to be prudently allocated among the users of the respective clusters, therefore different kinds of power allocation strategies are inspected to determine the optimum power allocation mechanism for the aforementioned system models. The power allocation

strategies used are fixed power allocation (FPA) and dynamic power allocation using constrained optimization (COPA) and convex optimization (CON-OPA) algorithms respectively. The complete analysis is carried out under different modulation schemes to scrutinize the effect on the performance of the MU-MIMO-PD-NOMA system.

5.2. SYSTEM MODEL

The following two cases illustrate two different kinds of system models that have been explored in this chapter.

CASE I:

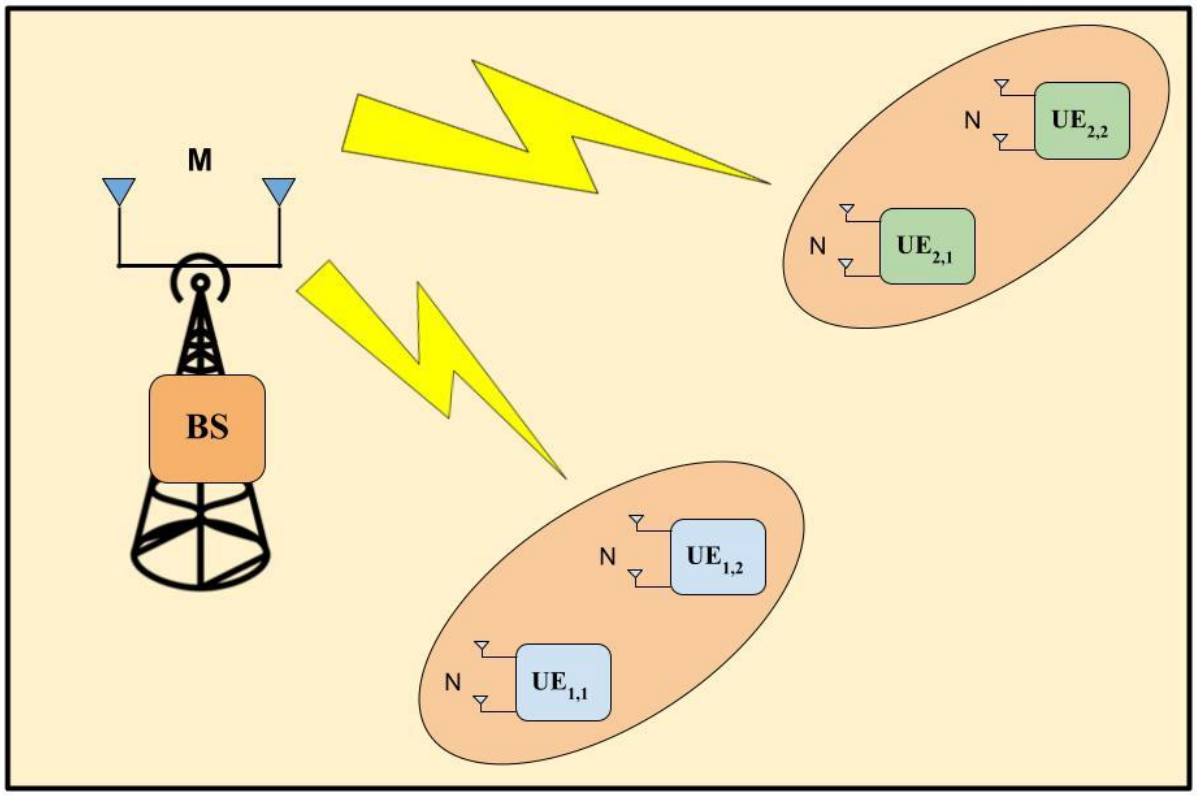

Fig.5.1: Downlink Multi-User (2x2)-MIMO-PD-NOMA System Model with Clustering

Fig.5.1 represents a multi-user (2x2)-MIMO-PD-NOMA system in a single-cell downlink scenario, wherein a single base station (BS), equipped with *M=2* antennas, communicates with *M=2* number of clusters, each having *B=2* user

equipments ($UE_{i,j}$), equipped with $N=2$ antennas each, where $i \in \{1,2\}$ and $j \in \{1,2\}$. The UEs are clustered based on a suitable clustering algorithm. Each cluster employs NOMA principle individually, i.e. only among the users in the respective cluster. The $UE_{i,1}$ is situated closest to the BS, whereas $UE_{i,2}$ is located at the farthest distance from the BS, in the respective cluster. Each $UE_{i,j}$ has (2x2) communication channel paths between the BS and itself. It is assumed that the total transmitter power is P_t and the wireless links experience independent and identically distributed (i.i.d.) Rayleigh fading with Additive White Gaussian Noise (AWGN). The effective channel gains of the UEs in a cluster are sorted as: $|z_{i,1}H_{i,1}p_{i,1}|^2 \geq |z_{i,2}H_{i,2}p_{i,2}|^2$, wherein $H_{i,B}$ indicates the (2x2) Rayleigh fading channel matrix, from the BS to the j^{th} UE in the i^{th} cluster; and $p_{i,B}$ and $z_{i,B}$ are the precoding and post-coding vectors respectively, for the j^{th} UE in the i^{th} cluster.

CASE II:

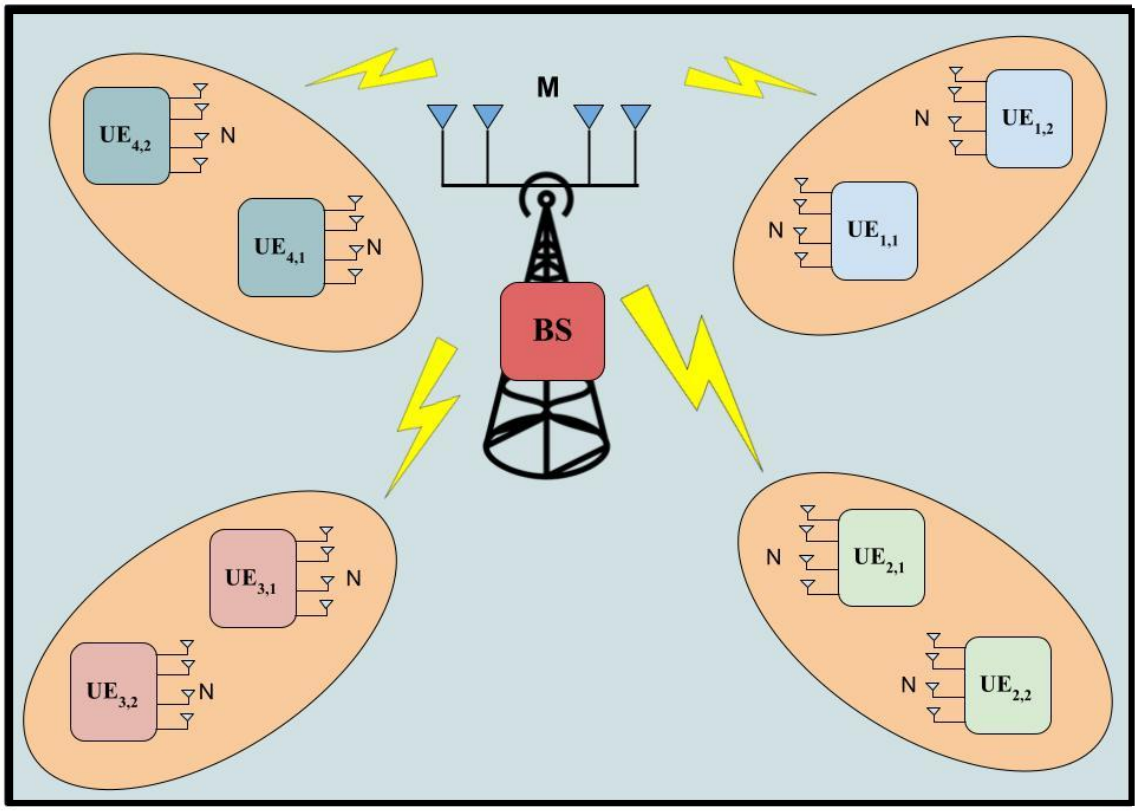

Fig.5.2: Downlink Multi-User (4x4)-MIMO-PD-NOMA System Model with Clustering

Fig.5.2 represents a multi-user (4x4)-MIMO-PD-NOMA system in a single-cell downlink scenario, wherein a single base station (BS), equipped with *M=2* antennas, communicates with *M=4* number of clusters, each having *B=4* user equipments ($UE_{i,j}$), equipped with *N=4* antennas each, where $i \in \{1,2,3,4\}$ and $j \in \{1,2\}$. The UEs are clustered based on a suitable clustering algorithm. Each cluster employs NOMA principle individually, i.e. only among the users in the respective cluster. The $UE_{i,1}$ is situated closest to the BS, whereas $UE_{i,2}$ is located at the farthest distance from the BS, in the respective cluster. Each $UE_{i,j}$ has (4x4) communication channel paths between the BS and itself. It is assumed that the total transmitter power is P_t and the wireless links experience independent and identically distributed (i.i.d.) Rayleigh fading with Additive White Gaussian Noise (AWGN). The effective channel gains of the UEs in a cluster are sorted as: $|z_{i,1}H_{i,1}p_{i,1}|^2 \geq |z_{i,2}H_{i,2}p_{i,2}|^2$, wherein $H_{i,B}$ indicates the (4x4) Rayleigh fading channel matrix, from the BS to the j^{th} UE in the i^{th} cluster; and $p_{i,B}$ and $z_{i,B}$ are the precoding and post-coding vectors respectively, for the j^{th} UE in the i^{th} cluster.

Therefore, $UE_{i,1}$ has the highest channel gain and is hence referred to as the strong user while the other user, in the respective cluster, is labelled as the weak user. At the BS, as per the NOMA principle, the signals for the different users of a cluster, are allocated different fraction of the total power and thereafter superposed to be transmitted over the same channel. The strong user of a cluster is given the least fraction of power compared to other weak users in the respective cluster. Hence, the power allocation order of the UEs in a cluster is as follows: $P_{i,1} < P_{i,2}$. Whenever clustering is implemented in a MU-MIMO-NOMA system, there are primarily two kinds of interference that need to be handled. The first is intra-cluster interference that is looked after through SIC; and the other is inter-cluster interference that is dealt by using an appropriate precoding scheme. Therefore, the superposed signals are precoded and the resultant signals are transmitted through the M antennas of the BS. At the receiving end, each UE receives the transmitted signal through its N antennas, and thereby employs MRC receiver diversity scheme, followed by post-coding, depending on the precoding scheme applied at the transmitter. After that, $UE_{i,1}$ performs SIC to decode and subtract out the information signal intended for $UE_{i,2}$; while $UE_{i,2}$ applies direct decoding to its respective resultant received signal.

5.3. PROPOSED CLUSTERING METHODOLOGY

The proposed clustering methodology groups users based on discrimination of their channel gains and having least channel correlation with each other. Since, this method considers channel correlation as a crucial parameter, along with channel gain, hence, this mechanism has been named Least Channel Correlation (LCC) clustering. In this scheme, all the users are arranged in descending order of their channel gains and divided into *K* groups, where *K* is the number of users required to be in a cluster. Thereafter, the channel correlation coefficient among users from each of the *K* groups is computed, whereby the users having least correlation coefficient values, with respect to one another, are grouped into a cluster. Thus, this clustering methodology clusters/pairs users having considerable differences, both in their channel correlations as well channel gains. The algorithm for LCC clustering mechanism is depicted in the following flowchart:

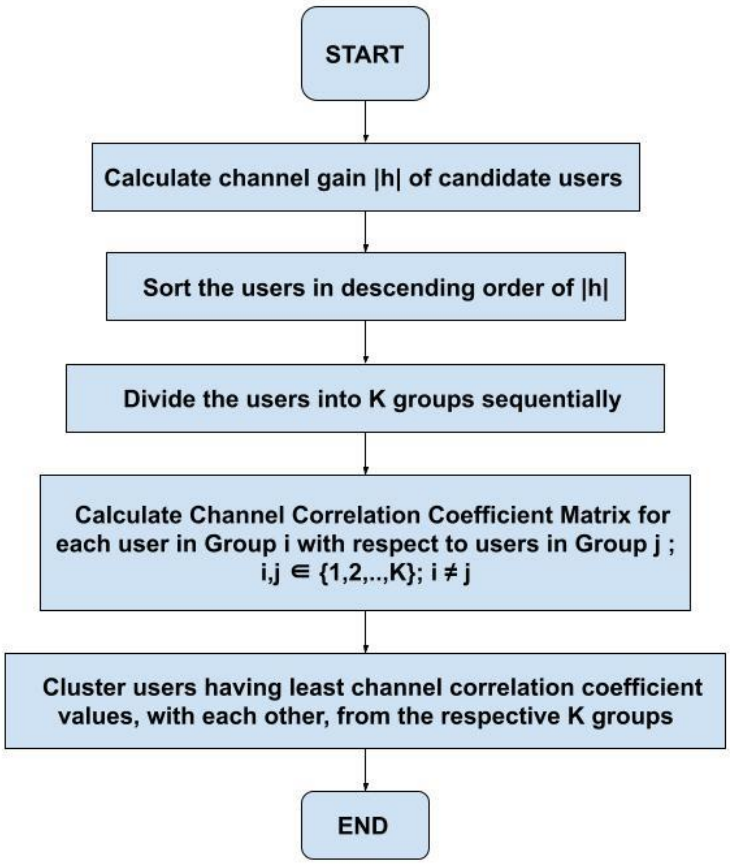

Fig.5.3: FLOWCHART FOR LEAST CHANNEL CORRELATION (LCC) CLUSTERING

5.4. PERFORMANCE ANALYSIS OF SIMULATION MODEL

The following sub-sections present a substantial analysis of simulation results, with respect to system BER, Sum Capacity and Spectral Efficiency (SE), of downlink multi-user (2x2) and (4x4) MIMO-PD-NOMA models for different clustering methodologies, applying diverse precoding schemes, and varied power allocation strategies. The power allocation strategies employed are fixed power allocation (FPA), constrained optimization power allocation (COPA) and convex optimization power allocation (CON-OPA) mechanisms respectively. The simulation is conducted using MATLAB software. Each simulation is performed considerable number of times and their ensemble average is taken to consider the different aspects of fading environment. The clustering methodologies that have been analyzed in the aforementioned system are as follows:

1. Random (RAN) Clustering
2. Best-With-Worst (BWW) Clustering
3. Best-With-Best (BWB) Clustering
4. Least Channel Correlation (LCC) Clustering

The diverse precoding schemes that have been applied to all the above clustering methodologies are as follows:

i) Matched Filter (MF)

ii) Zero-Forcing (ZF)

iii) Regularized Zero-Forcing (RZF)

iv) Singular Value Decomposition (SVD)

v) Modified Singular Value Decomposition, i.e., MODIFIED SVD

All the analysis have been made considering three types of modulation schemes, under Rayleigh fading channel, as follows:

a) BPSK modulation scheme for both near and far user
b) QPSK modulation scheme for both near and far user
c) QPSK modulation for near user and BPSK for far user, i.e., an Adaptive Modulation scheme

The parameters used for simulation in MATLAB, considering downlink multi-user (2x2) and (4x4) MIMO-PD-NOMA models, employing clustering, are enlisted in the following tables, i.e., Table 5.1 and Table 5.2 respectively:

Table 5.1: Simulation Parameters for Downlink Multi-User (2x2)-MIMO-PD-NOMA Model

PARAMETERS	VALUES
Transmitter Power	5 Watt
Number of Transmitter Antenna at the Base Station	2
Number of Receiver Antenna per User Equipment ($UE_{i,j}$)	2
Number of users per cluster	2
Power Allocation Coefficient for near user ($UE_{i,1}$) in all the clusters, when employing FPA	0.2
Power Allocation Coefficient for far user ($UE_{i,2}$) in all the clusters, when employing FPA	0.8
Target Fairness Factor, when employing COPA	0.7
Bandwidth	80 MHz

Table 5.2: Simulation Parameters for Downlink Multi-User (4x4)-MIMO-PD-NOMA Model

PARAMETERS	VALUES
Transmitter Power	5 Watt
Number of Transmitter Antenna at the Base Station	4
Number of Receiver Antenna per User Equipment ($UE_{i,j}$)	4
Number of users per cluster	2
Power Allocation Coefficient for near user ($UE_{i,1}$) in all the clusters, when employing FPA	0.2
Power Allocation Coefficient for far user ($UE_{i,2}$) in all the clusters, when employing FPA	0.8
Target Fairness Factor, when employing COPA	0.7
Bandwidth	80 MHz

5.3.1. Simulation Result Analysis of two-user (2x2)-MIMO-PD-NOMA model for different clustering methodologies using diverse precoding schemes and FPA:

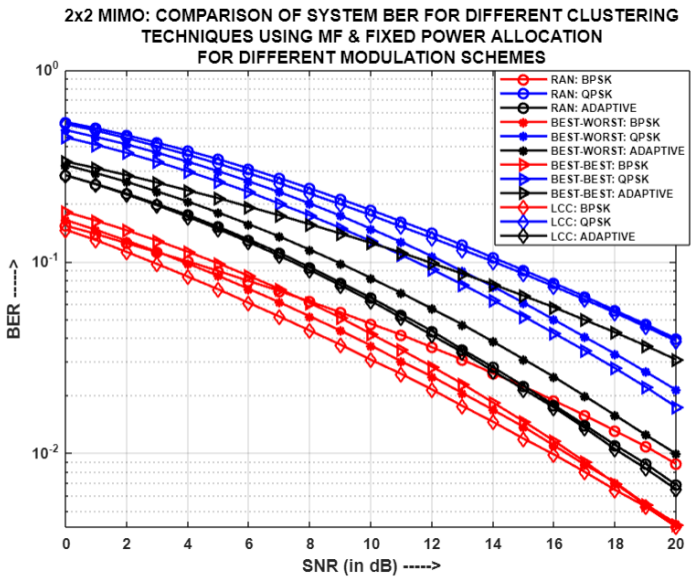

Fig.5.4: For (2x2)-MIMO-NOMA: Comparison of System BER for different clustering techniques using MF and FPA

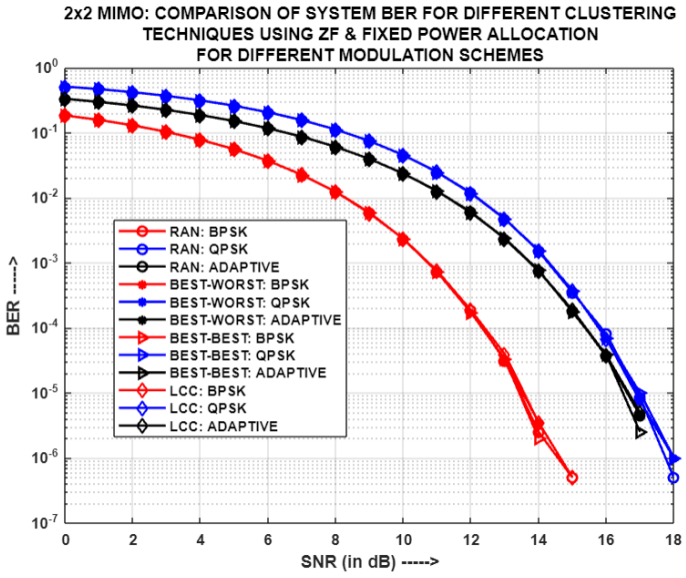

Fig.5.5: For (2x2)-MIMO-NOMA: Comparison of System BER for different clustering techniques using ZF and FPA

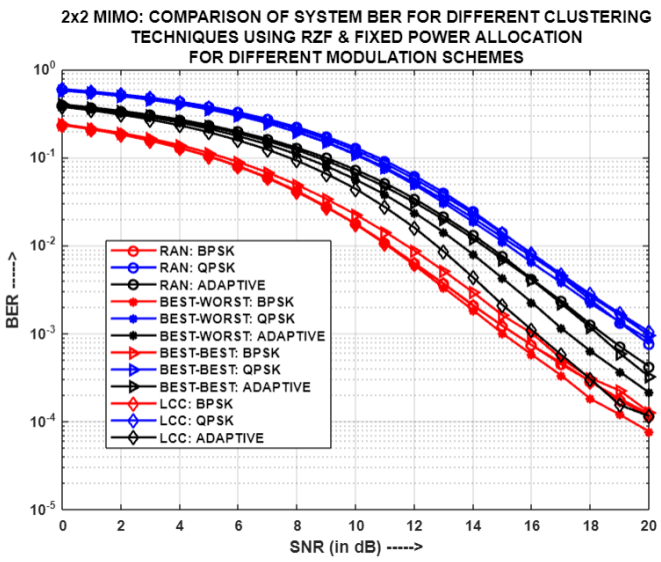

Fig.5.6: For (2x2)-MIMO-NOMA: Comparison of System BER for different clustering techniques using RZF and FPA

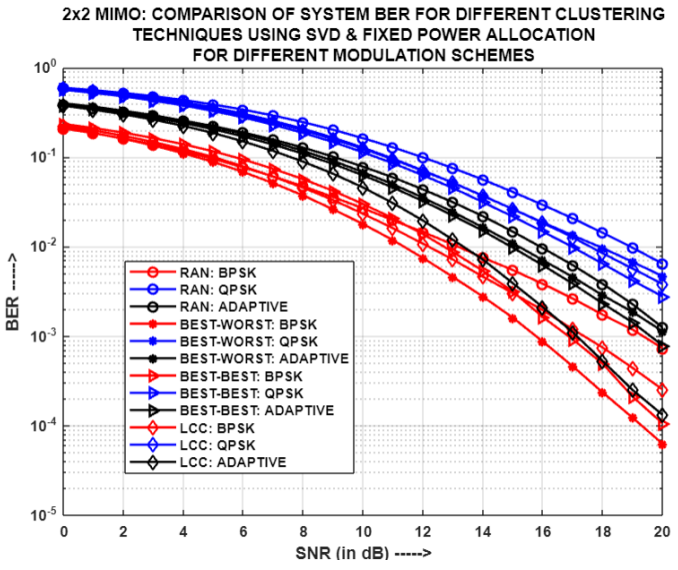

Fig.5.7: For (2x2)-MIMO-NOMA: Comparison of System BER for different clustering techniques using SVD and FPA

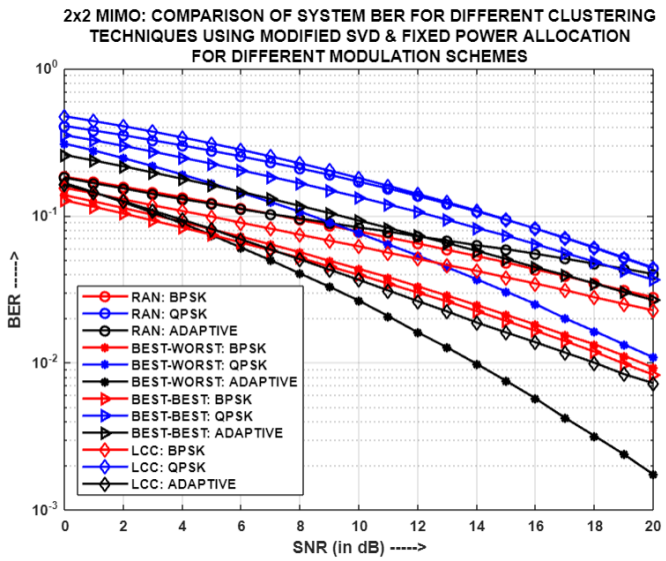

Fig.5.8: For (2x2)-MIMO-NOMA: Comparison of System BER for different clustering techniques using MODIFIED SVD and FPA

Fig.5.4, Fig.5.5, Fig.5.6, Fig.5.7 and Fig.5.8 depicts the comparison of system BER for different clustering methodologies using diverse precoding schemes, i.e. MF, ZF, RZF, SVD and MODIFIED SVD respectively, and fixed power allocation (FPA), with each entity in the system having two antennas. In regard to MF, it has been observed that LCC produces better system BER results for both BPSK and Adaptive modulations, while BWB happens to produce superior performance in case of QPSK's system BER. This is because LCC groups the users on basis of considerably different channel characteristics, whereas BWB pairs the users having differing but adjacent channel gains. Therefore, when applying MF precoding, it is noticeable that for modulation schemes like BPSK and Adaptive mechanism, the more the paired users have diverse channel behaviour, the easier it is to separate out the signals at the respective users, which thereby dictates the system BER performance; whereas for QPSK, although users having consecutive decreasing order channel gains have been paired, but still it produces satisfactory results because the channel gains are significantly different and hence, the strong signal can be distinguished from the weak one at the receiving end. In case of ZF, it is noticed that all the clustering methodologies yield absolutely similar system BERs for the respective modulation schemes. This is because the inherent nature of ZF precoding technique predominates the effectiveness of the different clustering schemes, as long as the same power allocation coefficient sets are used by all the clustering mechanisms. In

context of RZF, following the same reason as that of ZF, both BPSK and QPSK, yield almost comparable system BERs for all the clustering techniques. However, in case of Adaptive modulation, LCC outperforms the other three clustering mechanisms as it pairs the users in an optimal way, through exploration of their channel characteristics, such that the overall system BER enhances. It is for this very reason that even in case of SVD, for Adaptive modulation scheme, LCC yields the least system BER. However, for BPSK and QPSK, in regard to SVD precoding technique, BWW and BWB clustering mechanisms yield the lowest system BER respectively, as all the users in the system are paired, in the most advantageous way, with users having different channel gains. Also, LCC and BWB mechanism yield comparable results for QPSK because of quite similar pairing of users. Finally, for MODIFIED SVD, BWW clustering mechanism yields the best system BER results for both QPSK and Adaptive modulations; while for BPSK, both BWW and BWB clustering methodologies generate comparable results.

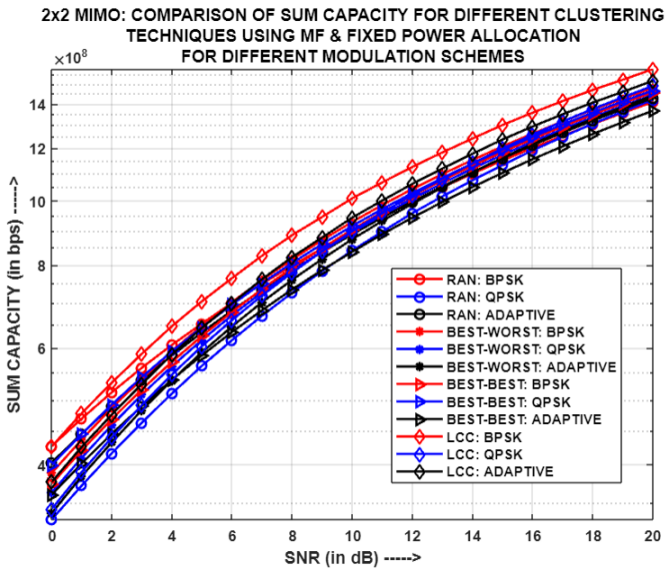

Fig.5.9: For (2x2)-MIMO-NOMA: Comparison of Sum Capacity for different clustering techniques using MF and FPA

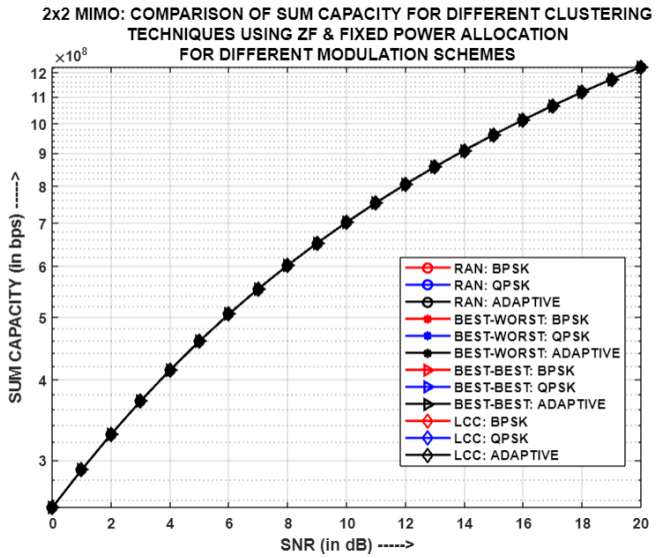

Fig.5.10: For (2x2)-MIMO-NOMA: Comparison of Sum Capacity for different clustering techniques using ZF and FPA

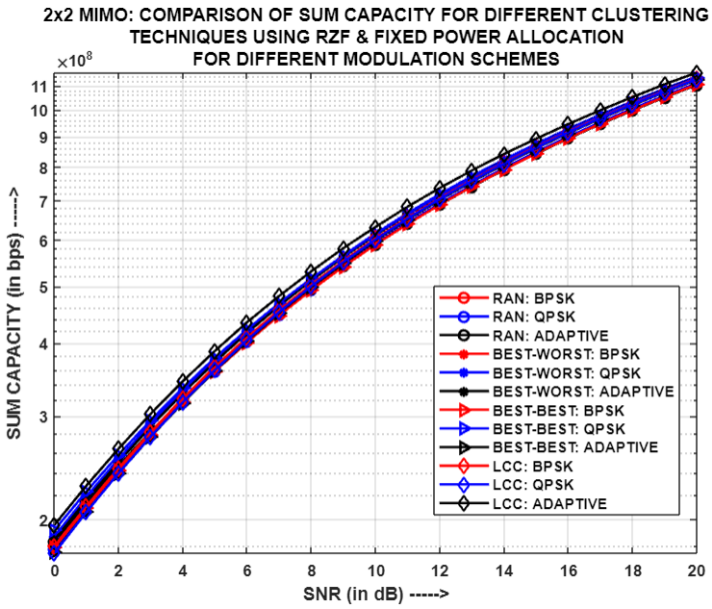

Fig.5.11: For (2x2)-MIMO-NOMA: Comparison of Sum Capacity for different clustering techniques using RZF and FPA

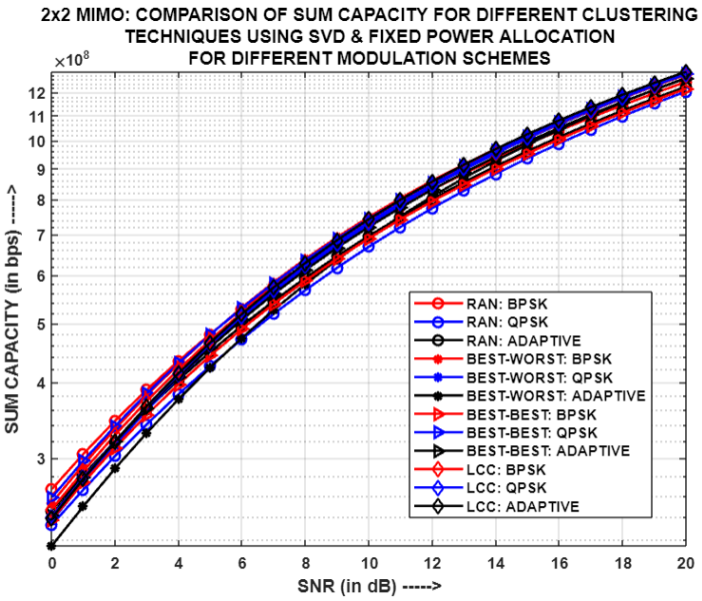

Fig.5.12: For (2x2)-MIMO-NOMA: Comparison of Sum Capacity for different clustering techniques using SVD and FPA

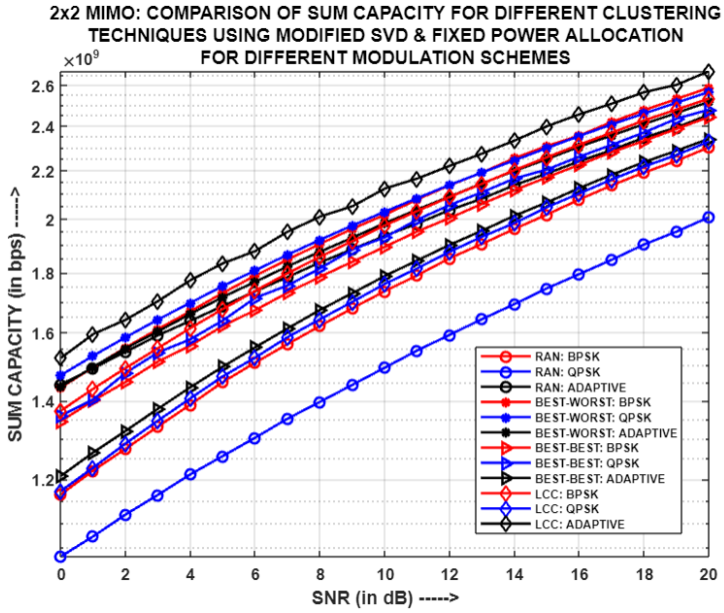

Fig.5.13: For (2x2)-MIMO-NOMA: Comparison of Sum Capacity for different clustering techniques using MODIFIED SVD and FPA

Fig.5.9, Fig.5.10, Fig.5.11, Fig.5.12 and Fig.5.13 portrays the comparison of Sum Capacity for different clustering methodologies using diverse precoding schemes, i.e. MF, ZF, RZF, SVD and MODIFIED SVD respectively, and FPA, with each entity in the system having two antennas. In case of MF, ZF, RZF and SVD, almost comparable sum capacities are produced by all the clustering methodologies because the effect of the employed precoding technique and the usage of the same power allocation coefficient set, overshadows the sole impact of the respective channel gain, on the user's throughput, which thereby influences the sum capacity of the system. Therefore, similar sum capacities are generated by all the clustering methodologies for the aforementioned precoding schemes respectively. However, for MODIFIED SVD, considerable differences in the sum capacities have been observed for the different clustering mechanisms. This is because of the fact that MODIFIED SVD uses an amplification matrix, both for the precoding and post-coding matrices, which thereby affects the user's resultant channel gain significantly. Therefore, depending on the way the users are clustered, accordingly the amplification matrices are designed and hence, the user's resultant channel gain and throughput are computed respectively. Since, throughput has a direct impact on the overall system's sum capacity, consequently variations in the sum capacities are noticeable for different clustering techniques using MODIFIED SVD. Thus, LCC clustering employing Adaptive modulation yields the highest sum capacity for the above mentioned precoding scheme.

5.3.2. Simulation Result Analysis of two-user (4x4)-MIMO-PD-NOMA model for different clustering methodologies using diverse precoding schemes and FPA:

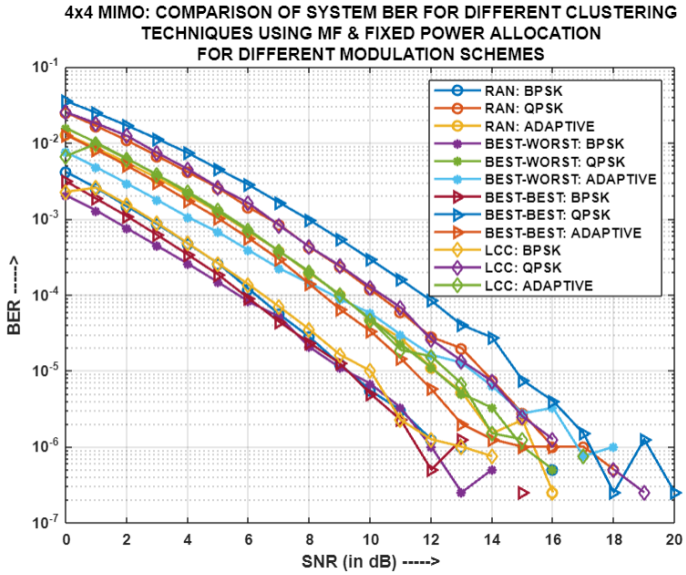

Fig.5.14: For (4x4)-MIMO-NOMA: Comparison of System BER for different clustering techniques using MF and FPA

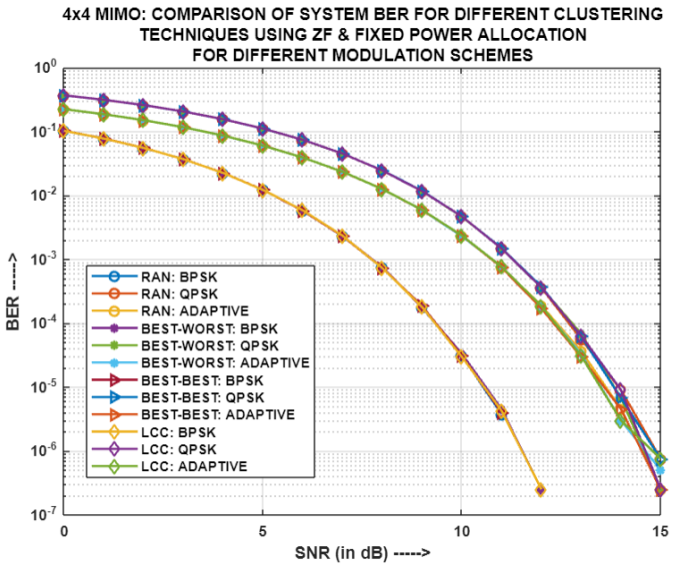

Fig.5.15: For (4x4)-MIMO-NOMA: Comparison of System BER for different clustering techniques using ZF and FPA

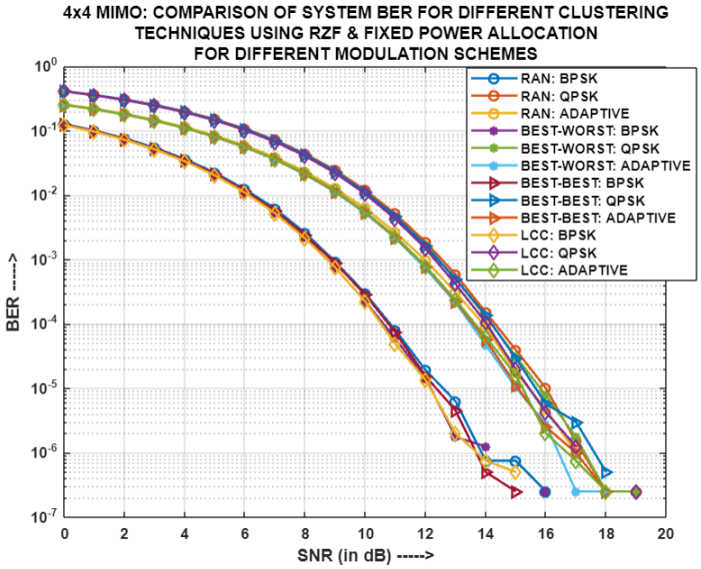

Fig.5.16: For (4x4)-MIMO-NOMA: Comparison of System BER for different clustering techniques using RZF and FPA

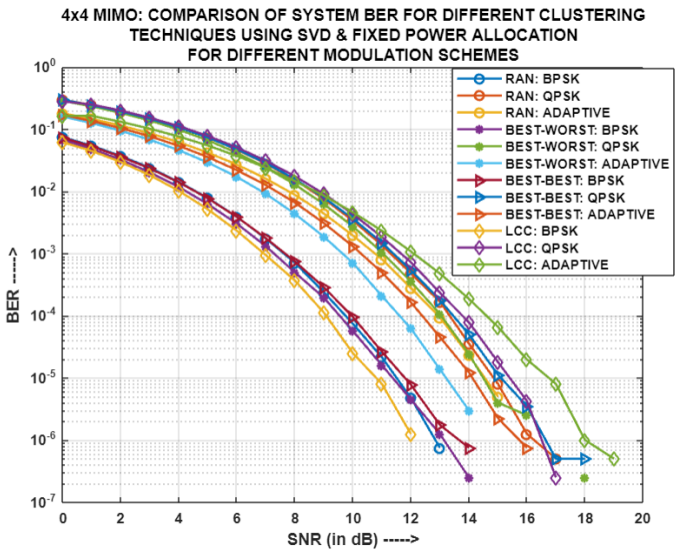

Fig.5.17: For (4x4)-MIMO-NOMA: Comparison of System BER for different clustering techniques using SVD and FPA

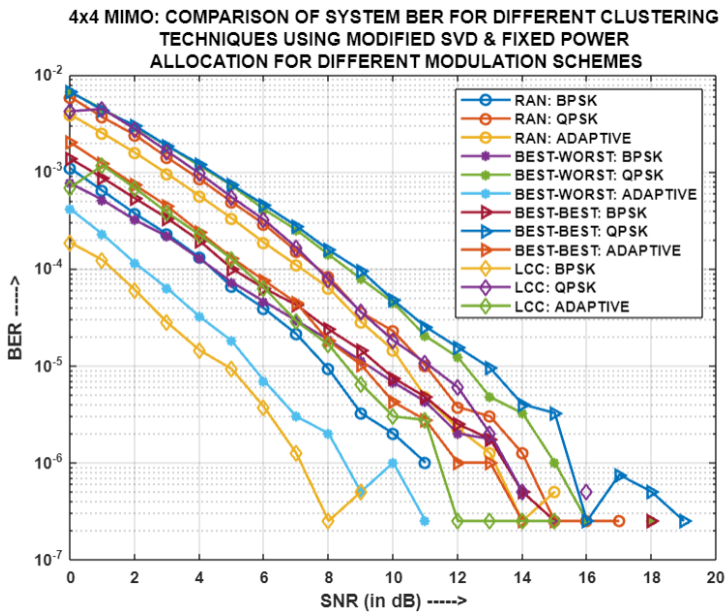

Fig.5.18: For (4x4)-MIMO-NOMA: Comparison of System BER for different clustering techniques using MODIFIED SVD and FPA

Fig.5.14, Fig.5.15, Fig.5.16, Fig.5.17 and Fig.5.18 presents the comparison of system BER for different clustering methodologies using diverse precoding schemes, i.e. MF, ZF, RZF, SVD and MODIFIED SVD respectively, and fixed power allocation (FPA), with each entity in the system having four antennas. In case of MF, for BPSK and Adaptive modulation schemes respectively, all the employed clustering mechanisms yield comparable system BER results because of similar pairing of users and usage of the same power allocation coefficient set across the different clustering schemes. However, for QPSK, BWW mechanism generates the minimum system BER because of significant difference among the channel gains of the users in all the respective clusters, which makes it very convenient to differentiate the strong and weak signals respectively, at the receiving end. On the other hand, for ZF and RZF, it is observed that all the clustering methodologies yield absolutely similar system BERs for the respective modulation schemes. This occurs because the fundamental nature of the ZF and RZF precoding techniques surpasses the influence of the different clustering schemes, as long as they utilize the same power allocation coefficient sets across all the clustering methodologies. In context of SVD, for both QPSK and Adaptive modulations, BWW yields the least system

BER; while LCC generates the lowest system BER for BPSK as well as the whole comparative system. This is because in the former case of QPSK and Adaptive schemes, BWW performed well as the users had significant differences in their channel gains, even when their channel correlation was close enough; whereas for BPSK, the users' channel correlation was the least along with considerable difference in their channel gains, whereby LCC outperformed its contemporaries. Finally, in context of MODIFIED SVD, BPSK with LCC clustering yields the lowest system BER compared to all. Also, LCC supersedes other clustering mechanisms for QPSK in particular. It is for the same reason of clustering users based on a balance between their channel correlations and gains. However, for Adaptive modulation, BWW performs the best as the users had close channel correlation but considerably varied channel gains.

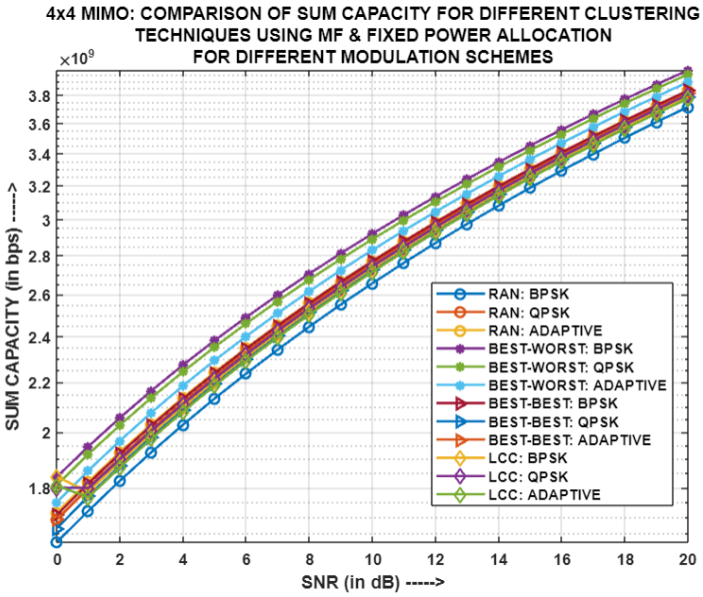

Fig.5.19: For (4x4)-MIMO-NOMA: Comparison of Sum Capacity for different clustering techniques using MF and FPA

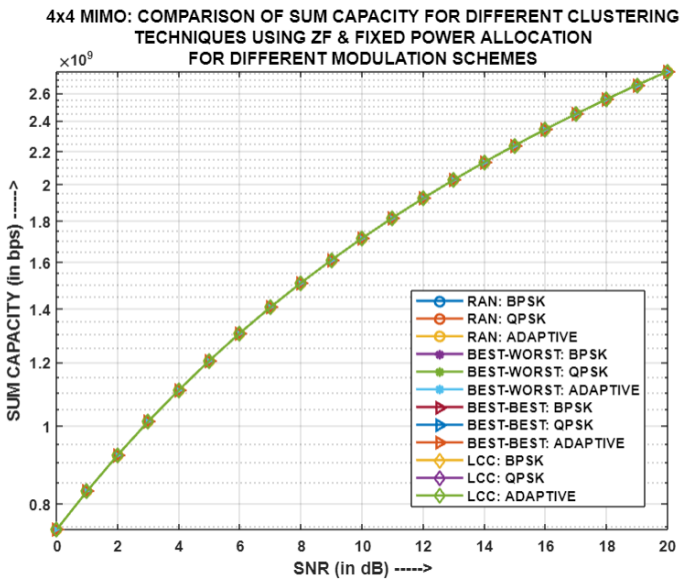

Fig.5.20: For (4x4)-MIMO-NOMA: Comparison of Sum Capacity for different clustering techniques using ZF and FPA

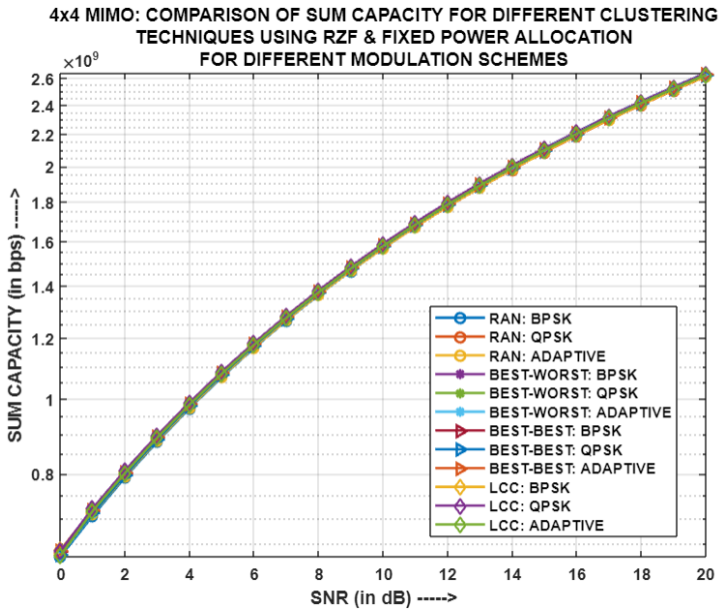

Fig.5.21: For (4x4)-MIMO-NOMA: Comparison of Sum Capacity for different clustering techniques using RZF and FPA

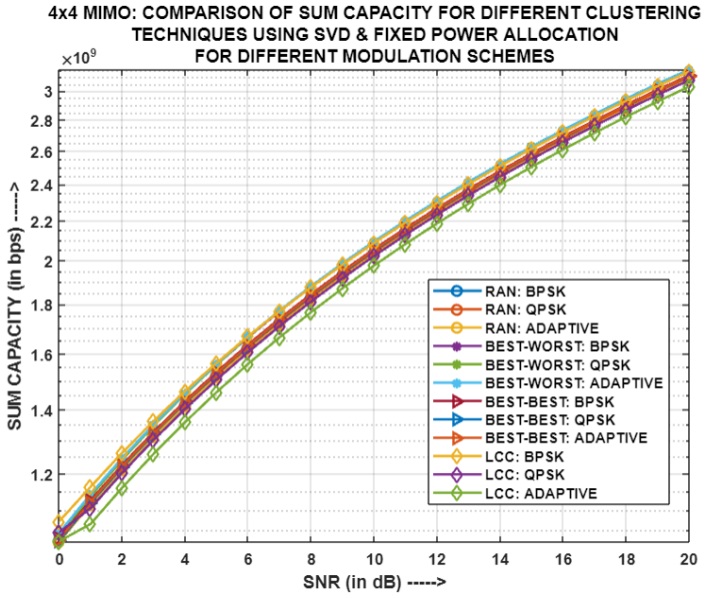

Fig.5.22: For (4x4)-MIMO-NOMA: Comparison of Sum Capacity for different clustering techniques using SVD and FPA

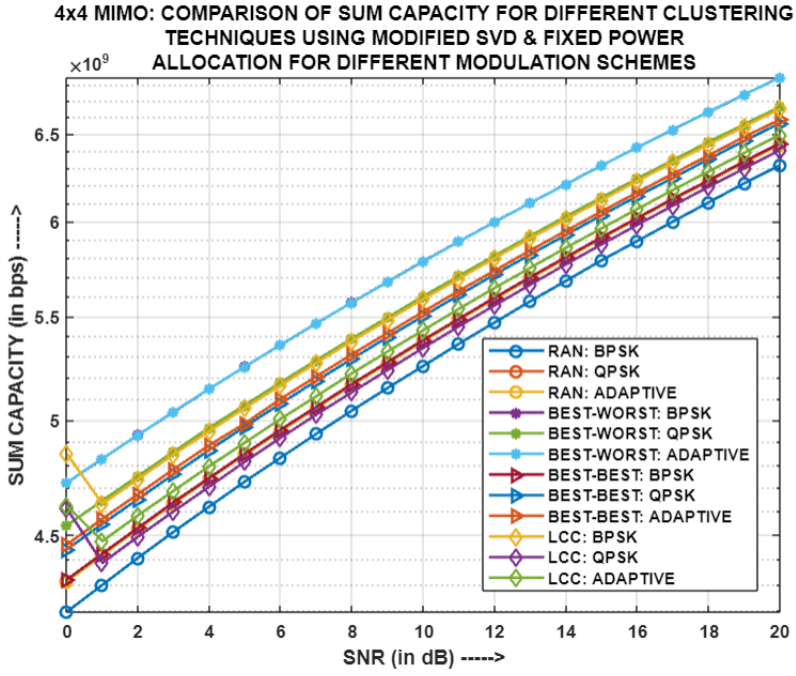

Fig.5.23: For (4x4)-MIMO-NOMA: Comparison of Sum Capacity for different clustering techniques using MODIFIED SVD and FPA

Fig.5.19, Fig.5.20, Fig.5.21, Fig.5.22 and Fig.5.23 showcases the comparison of Sum Capacity for different clustering methodologies using diverse precoding schemes, i.e. MF, ZF, RZF, SVD and MODIFIED SVD respectively, and FPA, with each entity in the system having four antennas. All clustering methodologies, for MF, ZF, RZF and SVD, result in comparable capacities. This is primarily because the impact of the employed precoding technique and the use of the same power allocation coefficient set supersedes the influence of channel gain on the users' throughput, which ultimately affects the system's sum capacity. As a result, similar sum capacities are achieved by all clustering methodologies for the respective precoding schemes mentioned. However, when it comes to MODIFIED SVD, significant differences in sum capacities are observed among the different clustering mechanisms. This disparity arises due to the utilization of a gain matrix in MODIFIED SVD, which affects both the precoding and post-coding matrices, resulting in a significant impact on the user's resultant channel gain. Consequently, the design of the amplification matrices depends on the clustering of users, which in turn influences the user's resultant channel gain and throughput. Since throughput directly impacts the overall system's sum capacity, noticeable variations in sum capacities are evident when different clustering techniques are applied with MODIFIED SVD. Therefore, BWW clustering employing BPSK and Adaptive modulations respectively, yield the highest sum capacity for the aforementioned precoding scheme. The merging of sum capacities is because of similar pairing of users and use of the same power allocation coefficient set.

5.3.3. Simulation Result Analysis of two-user (2x2)-MIMO-PD-NOMA model for different clustering methodologies using diverse precoding schemes and COPA:

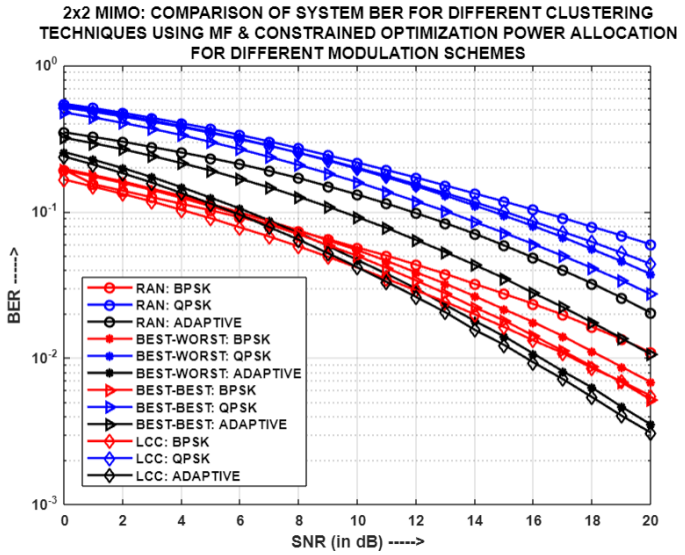

Fig.5.24: For (2x2)-MIMO-NOMA: Comparison of System BER for different clustering techniques using MF and COPA

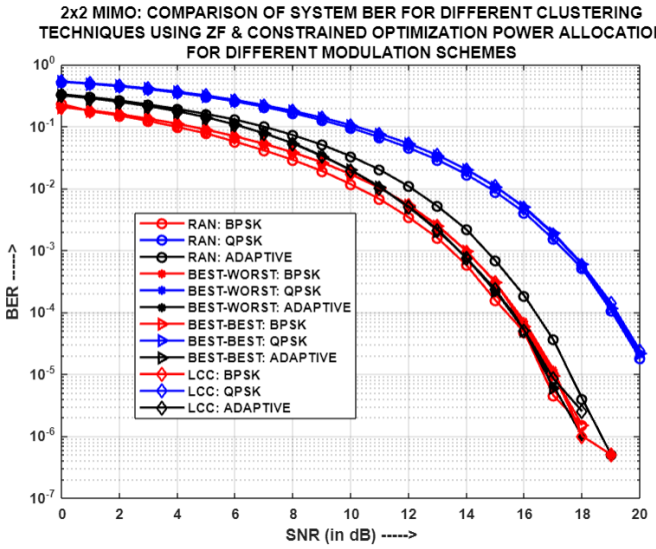

Fig.5.25: For (2x2)-MIMO-NOMA: Comparison of System BER for different clustering techniques using ZF and COPA

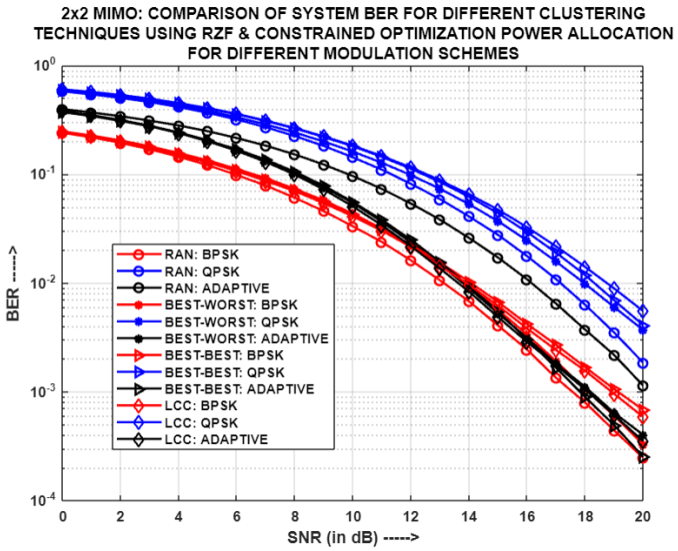

Fig.5.26: For (2x2)-MIMO-NOMA: Comparison of System BER for different clustering techniques using RZF and COPA

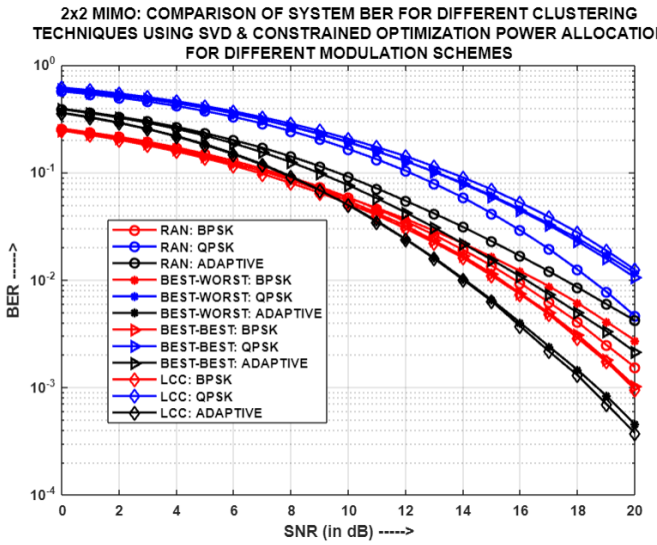

Fig.5.27: For (2x2)-MIMO-NOMA: Comparison of System BER for different clustering techniques using SVD and COPA

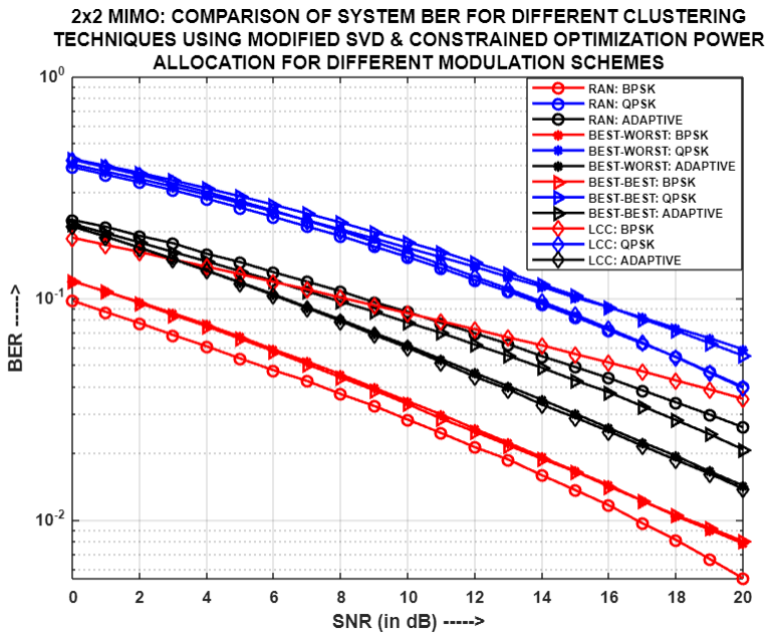

Fig.5.28: For (2x2)-MIMO-NOMA: Comparison of System BER for different clustering techniques using MODIFIED SVD and COPA

Fig.5.24, Fig.5.25, Fig.5.26, Fig.5.27 and Fig.5.28 demonstrates the comparison of system BER for different clustering methodologies using diverse precoding schemes, i.e. MF, ZF, RZF, SVD and MODIFIED SVD respectively, and constrained optimization power allocation (COPA), with each entity in the system having two antennas. In context of MF, for both BPSK and Adaptive modulations, LCC outperformed the other clustering methodologies as it optimally clustered users based on their channel correlations and gains, and depending on that the COPA mechanism selected the most suitable power allocation coefficient sets for the user pairs. For ZF and RZF, in case of Adaptive modulation, LCC performed exceedingly well, with respect to system BER, as the COPA mechanism selected differing sets of power allocation coefficients, for the entire SNR range, owing to the pairing of users based on their channel gains and correlation. However, for BPSK and QPSK, related to ZF, all the clustering methodologies yielded comparable performances, since the users were grouped similarly and the COPA mechanism selected the same sets of power allocation coefficient for the user pairs. In case of SVD precoding, LCC and BWW, both yield merged least system BER for BPSK and Adaptive modulations. This implies that the users that were paired based on their channel gains by BWW, also happened to have least channel correlation as per LCC. Finally, in

regard to MODIFIED SVD, although LCC provides the lowest system BER for both QPSK and Adaptive modulations respectively, but it has been observed that for BPSK, Random clustering performs better than the other clustering mechanisms. The credit to such a performance primarily goes to the precoding technique, efficient SIC and also the coincidental pairing of users having significant differences in their channel characteristics.

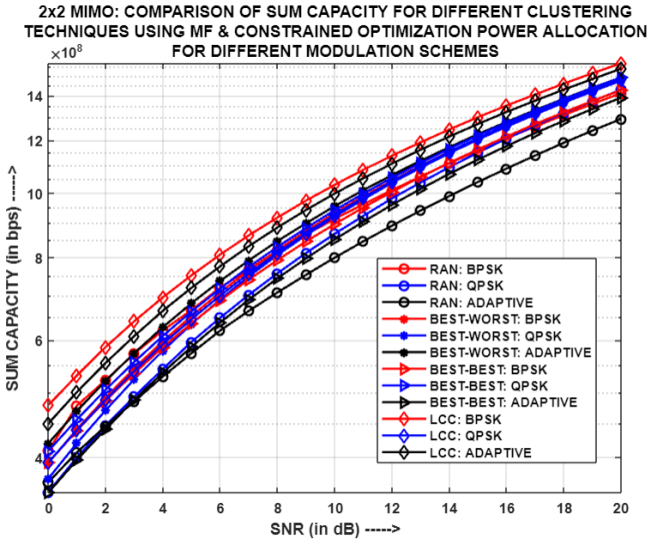

Fig.5.29: For (2x2)-MIMO-NOMA: Comparison of Sum Capacity for different clustering techniques using MF and COPA

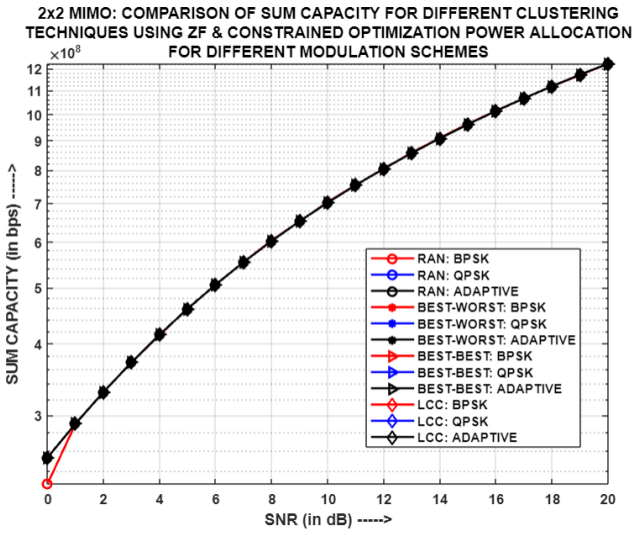

Fig.5.30: For (2x2)-MIMO-NOMA: Comparison of Sum Capacity for different clustering techniques using ZF and COPA

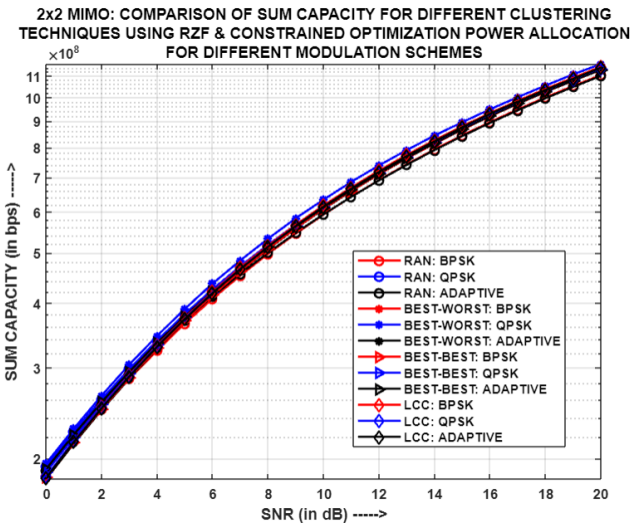

Fig.5.31: For (2x2)-MIMO-NOMA: Comparison of Sum Capacity for different clustering techniques using RZF and COPA

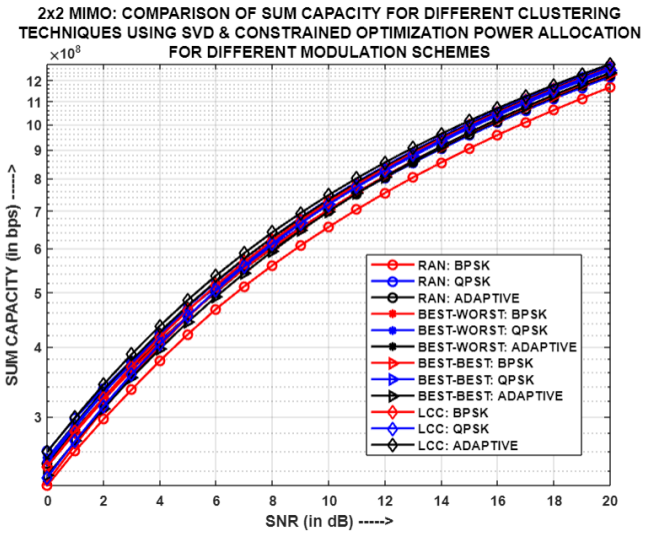

Fig.5.32: For (2x2)-MIMO-NOMA: Comparison of Sum Capacity for different clustering techniques using SVD and COPA

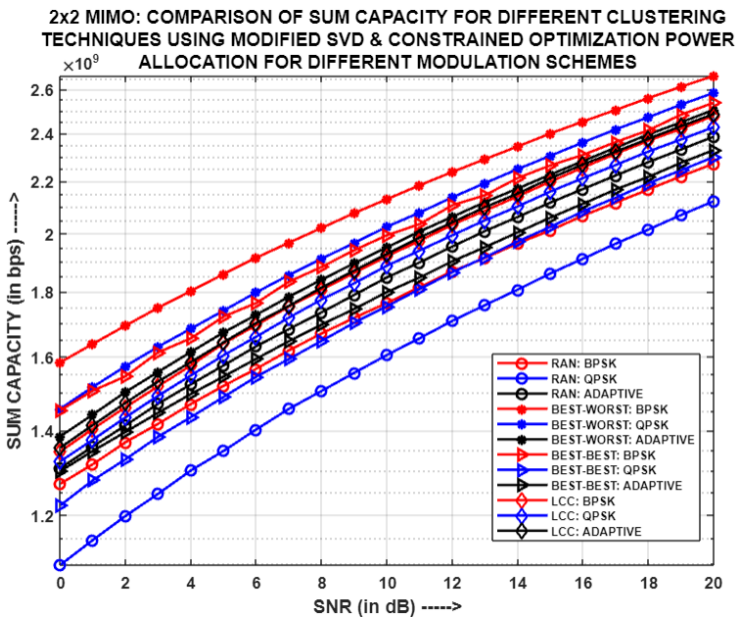

Fig.5.33: For (2x2)-MIMO-NOMA: Comparison of Sum Capacity for different clustering techniques using MODIFIED SVD and COPA

Fig.5.29, Fig.5.30, Fig.5.31, Fig.5.32 and Fig.5.33 represents the comparison of Sum Capacity for different clustering methodologies using diverse precoding schemes, i.e. MF, ZF, RZF, SVD and MODIFIED SVD respectively, and COPA, with each entity in the system having two antennas. In regard to ZF, RZF and SVD, all the employed clustering methodologies yield comparable sum capacities. This is primarily due to the dominant influence of the chosen precoding technique and the use of similar power allocation coefficient sets, for all the clustering schemes across the varied clusters, which overshadows the impact of channel gain on the user throughput. As a result, equivalent sum capacities are achieved by all clustering methodologies for the respective precoding schemes. On the contrary, in case of MF, difference in sum capacities for different clustering mechanisms have been observed because of the selection of different power coefficient sets for the different clustering methodologies, across all the clusters. Also, when considering MODIFIED SVD, significant disparities in sum capacities are witnessed among the different clustering mechanisms. This discrepancy arises from the utilization of a gain matrix in MODIFIED SVD, which affects both the precoding and post-coding matrices, leading to a notable impact on the user's resultant channel gain. Consequently, the

design of the amplification matrices depends on the clustering of users, which thereby influences the user's resultant channel gain and throughput. Since throughput directly affects the overall system's sum capacity; hence, noteworthy variations in sum capacities become evident when different clustering techniques are employed with MODIFIED SVD. Therefore, the BWW clustering approach, applying BPSK modulation, produces the highest sum capacity for the above stated precoding scheme.

5.3.4. Simulation Result Analysis of two-user (4x4)-MIMO-PD-NOMA model for different clustering methodologies using diverse precoding schemes and COPA:

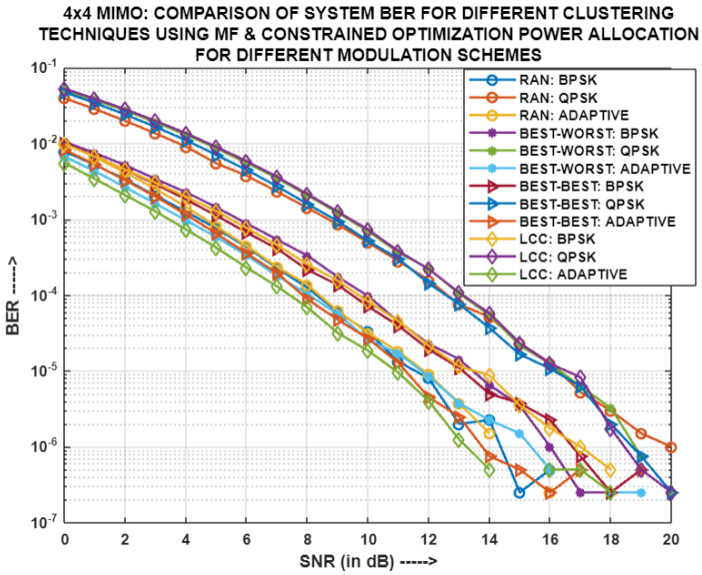

Fig.5.34: For (4x4)-MIMO-NOMA: Comparison of System BER for different clustering techniques using MF and COPA

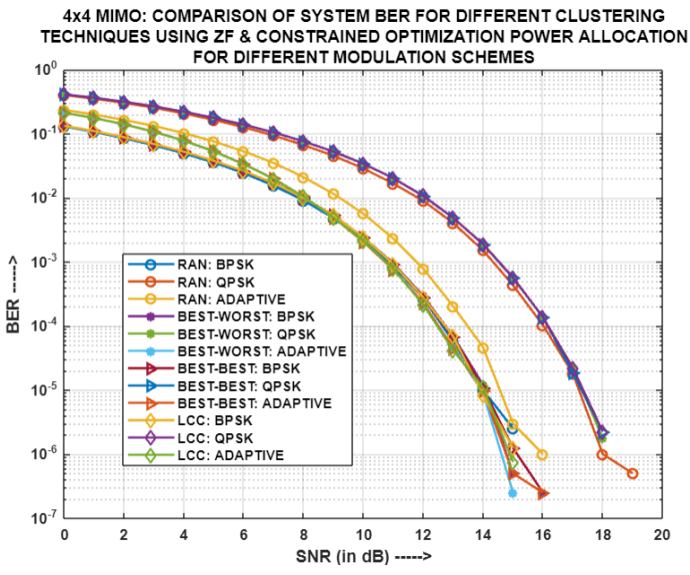

Fig.5.35: For (4x4)-MIMO-NOMA: Comparison of System BER for different clustering techniques using ZF and COPA

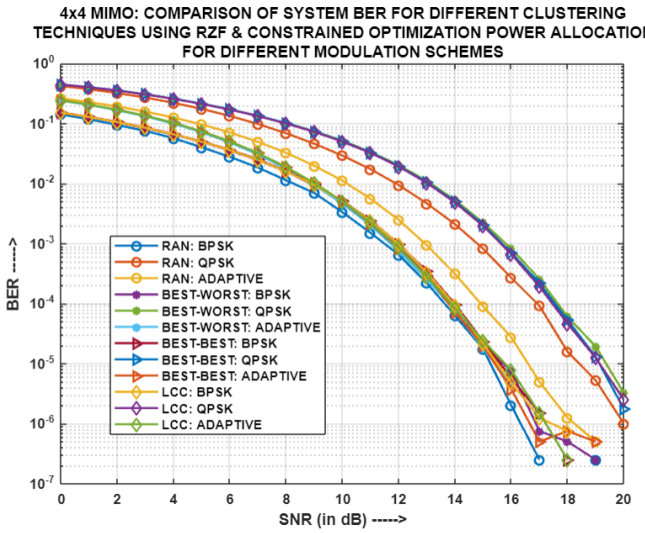

Fig.5.36: For (4x4)-MIMO-NOMA: Comparison of System BER for different clustering techniques using RZF and COPA

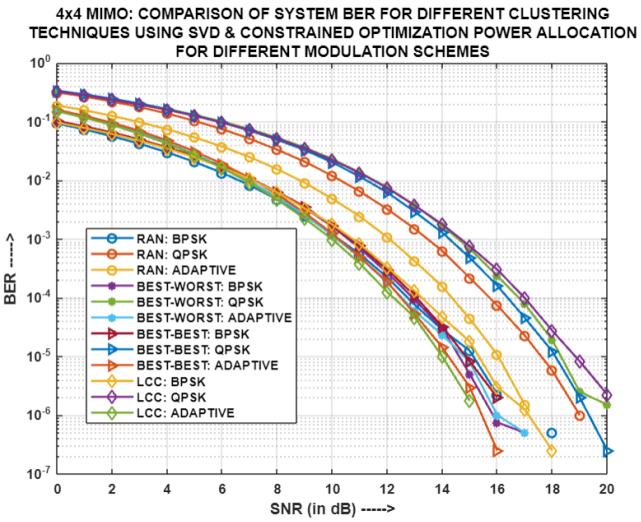

Fig.5.37: For (4x4)-MIMO-NOMA: Comparison of System BER for different clustering techniques using SVD and COPA

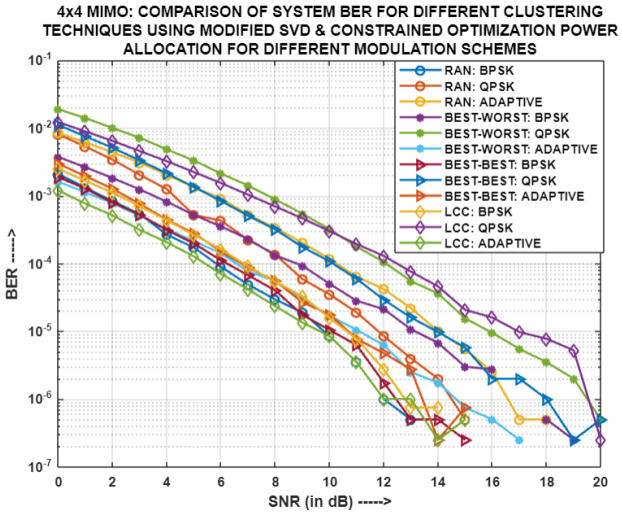

Fig.5.38: For (4x4)-MIMO-NOMA: Comparison of System BER for different clustering techniques using MODIFIED SVD and COPA

Fig.5.34, Fig.5.35, Fig.5.36, Fig.5.37 and Fig.5.38 displays the comparison of system BER for different clustering methodologies using diverse precoding schemes, i.e. MF, ZF, RZF, SVD and MODIFIED SVD respectively, and constrained optimization power allocation (COPA), with each entity in the system having four antennas. It has been observed that for MF, LCC yields the system BER for QPSK and Adaptive modulations; whereas for ZF and RZF, LCC generates the

lowest system BER for all the modulation schemes. This is because of the optimum pairing of users, based on which the convex optimization algorithm allocates powers among the users and thereby, it influences the efficient distinction of the respective users' information at the receiver, whereby the BER performance is dictated. In case of SVD, although comparable system BER results are obtained for all clustering methodologies, for BPSK and QPSK respectively, however LCC with Adaptive modulation outperforms its contemporaries and provides the lowest system BER. This is because of the dominance of LCC clustering which aids in optimal power allocation among the user-pairs, through COPA mechanism and thereby anchors the performance of the system. Finally, in context of MODIFIED SVD, it is noteworthy that LCC achieves the least system BER for both BPSK and Adaptive modulations. However, interestingly, for QPSK, Random clustering supersedes other clustering mechanisms. This improved performance can be attributed to the combination of the precoding technique, efficient successive interference cancellation (SIC), and the fortuitous pairing of users with notable differences in their channel characteristics.

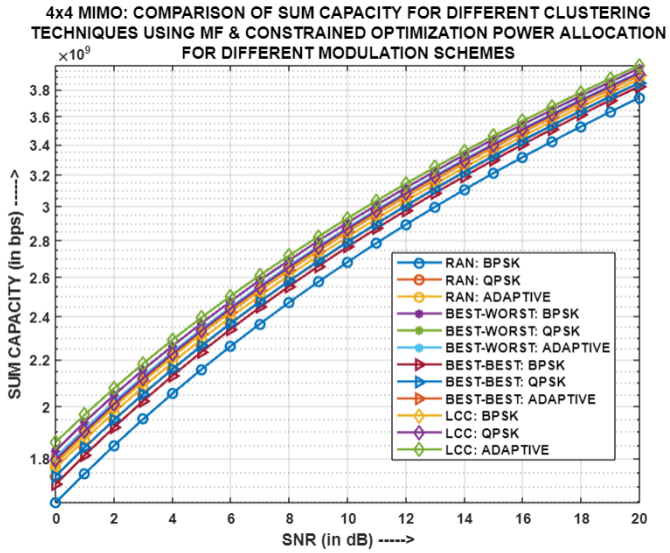

Fig.5.39: For (4x4)-MIMO-NOMA: Comparison of Sum Capacity for different clustering techniques using MF and COPA

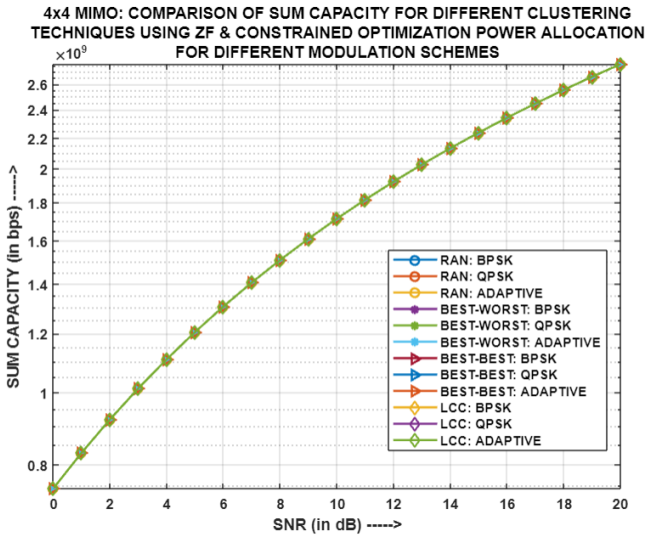

Fig.5.40: For (4x4)-MIMO-NOMA: Comparison of Sum Capacity for different clustering techniques using ZF and COPA

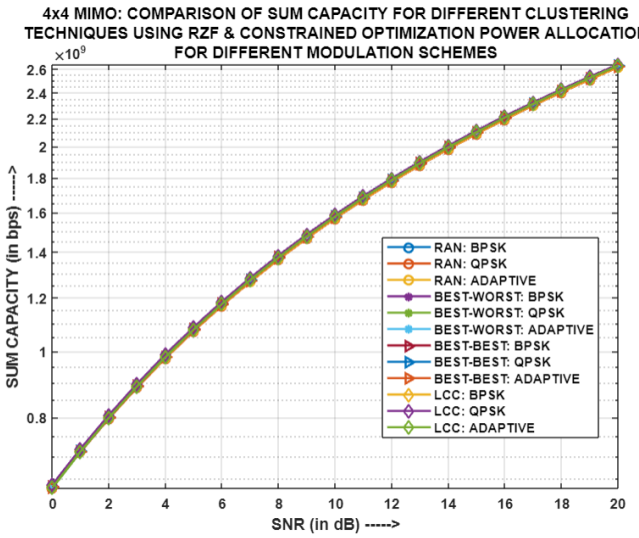

Fig.5.41: For (4x4)-MIMO-NOMA: Comparison of Sum Capacity for different clustering techniques using RZF and COPA

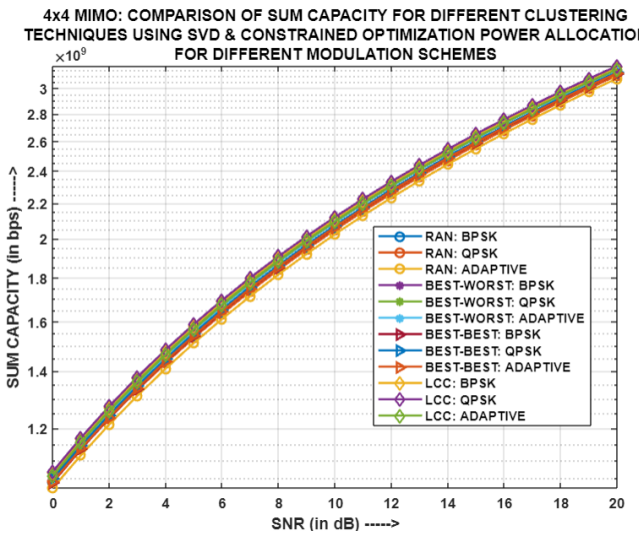

Fig.5.42: For (4x4)-MIMO-NOMA: Comparison of Sum Capacity for different clustering techniques using SVD and COPA

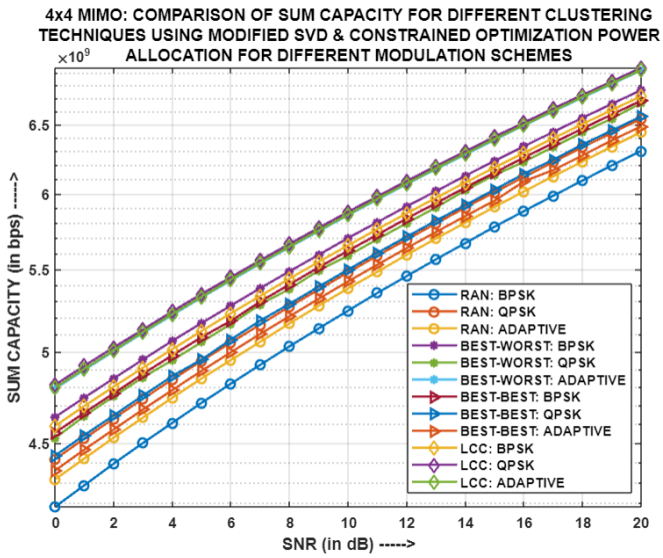

Fig.5.43: For (4x4)-MIMO-NOMA: Comparison of Sum Capacity for different clustering techniques using MODIFIED SVD and COPA

Fig.5.39, Fig.5.40, Fig.5.41, Fig.5.42 and Fig.5.43 depicts the comparison of Sum Capacity for different clustering methodologies using diverse precoding schemes, i.e. MF, ZF, RZF, SVD and MODIFIED SVD respectively, and COPA, with each entity in the system having four antennas. For ZF, RZF, and SVD respectively, all the clustering methodologies yield comparable sum capacities. This is primarily

because the chosen precoding technique and the usage of similar power allocation coefficient sets, across different clustering schemes as well as clusters, dominate the impact of channel gain on the user throughput. Consequently, all these clustering methodologies achieve similar sum capacities for their respective precoding schemes. On the other hand, MF clustering exhibits slight differences in sum capacities among different clustering mechanisms due to the use of distinct power coefficient sets across the employed clustering schemes. However, in case of MODIFIED SVD, significant variations in sum capacities are observed across different clustering methodologies. This is attributed to the utilization of an amplification matrix, affecting both precoding and post-coding matrices, thereby resulting in a notable impact on the user's channel gain. The design of amplification matrices depends on user clustering, hence, influencing their channel gain and throughput. Since users' throughput directly affects the overall sum capacity, therefore, variations in sum capacities arise when employing different clustering techniques with MODIFIED SVD. Therefore, LCC clustering, employing QPSK and Adaptive modulations respectively, yield merged but highest sum capacity for the above-mentioned precoding scheme. The merging of sum capacities attributes to similar grouping of users and use of same sets of power allocation coefficients.

5.3.5. Simulation Result Analysis of two-user (2x2)-MIMO-PD-NOMA model for different clustering methodologies using diverse precoding schemes and CON-OPA:

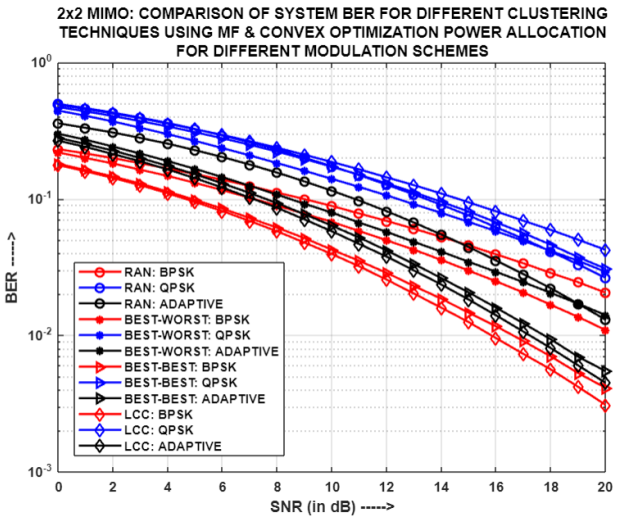

Fig.5.44: For (2x2)-MIMO-NOMA: Comparison of System BER for different clustering techniques using MF and CON-OPA

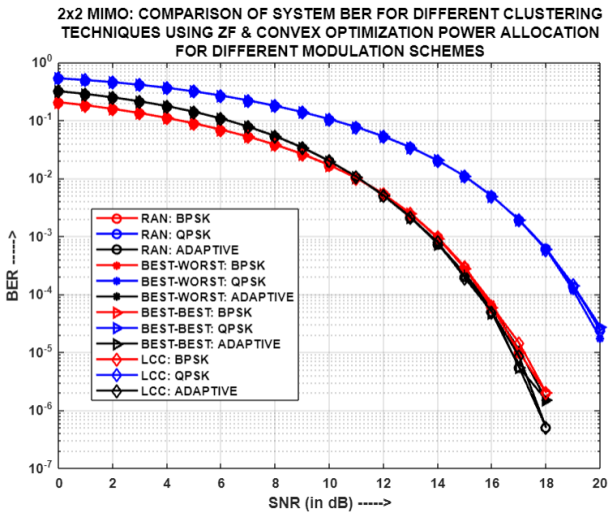

Fig.5.45: For (2x2)-MIMO-NOMA: Comparison of System BER for different clustering techniques using ZF and CON-OPA

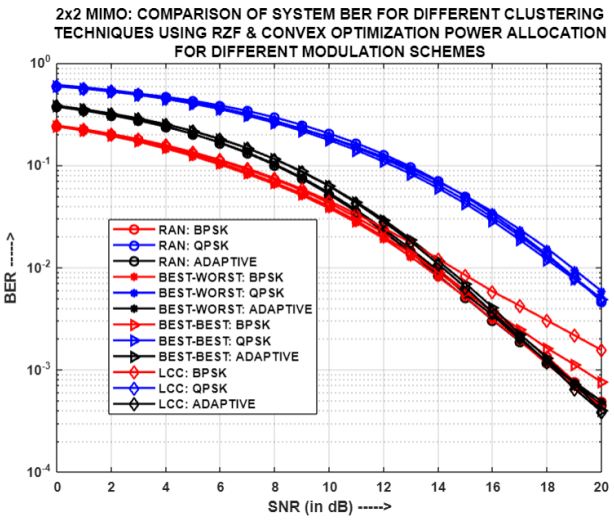

Fig.5.46: For (2x2)-MIMO-NOMA: Comparison of System BER for different clustering techniques using RZF and CON-OPA

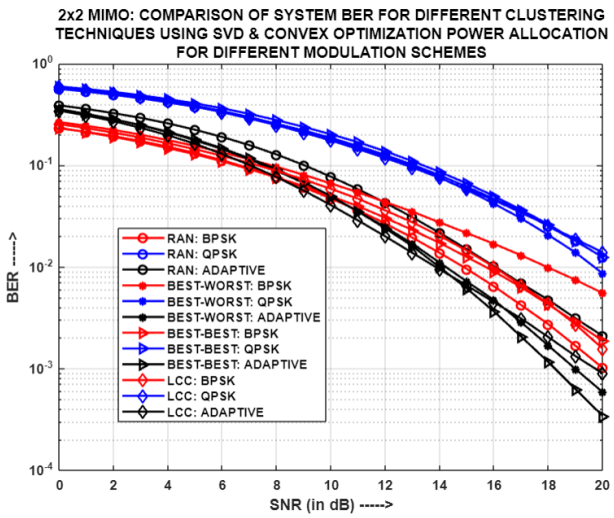

Fig.5.47: For (2x2)-MIMO-NOMA: Comparison of System BER for different clustering techniques using SVD and CON-OPA

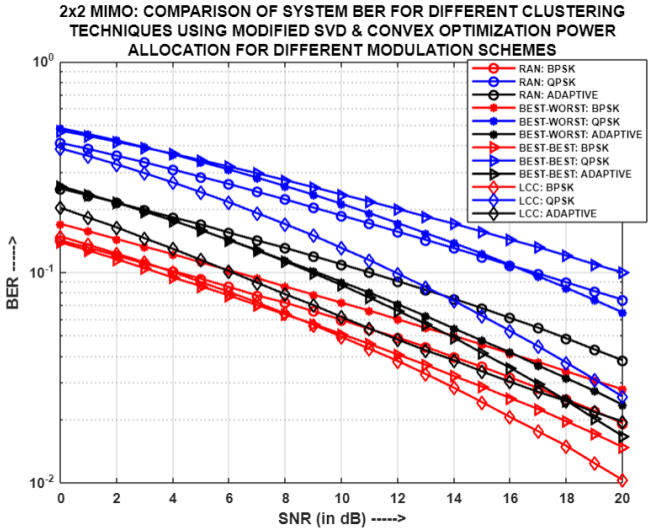

Fig.5.48: For (2x2)-MIMO-NOMA: Comparison of System BER for different clustering techniques using MODIFIED SVD and CON-OPA

Fig.5.44, Fig.5.45, Fig.5.46, Fig.5.47 and Fig.5.48 depicts the comparison of system BER for different clustering methodologies using diverse precoding schemes, i.e. MF, ZF, RZF, SVD and MODIFIED SVD respectively, and convex optimization power allocation (CON-OPA), with each entity in the system having two antennas. It can be seen that for MF, LCC yields the least system BER for both BPSK and

Adaptive modulations, because of its capability to pair users based on their channel gains as well as channel correlations, which thereby leads to optimum power allocation among the user-pairs through convex optimization algorithm. However, in case of ZF and RZF, all the clustering methodologies produce almost comparable system BERs for all the modulation schemes respectively, as the users are paired in a similar way and also, the CON-OPA strategy determines alike sets of power allocation coefficients for the user-pairs. In context of SVD, it is interesting to note that for Adaptive modulation scheme, both LCC and BWB yield the least system BERs for varying SNR values. This is because of the dynamic selection of power allocation coefficient sets, using convex optimization algorithm, for different range of SNR. Finally, in regard to MODIFIED SVD, LCC generates the least system BER for all the modulation schemes respectively, thereby outperforming its competing clustering methodologies through its efficient mechanism of pairing of users based on a balance between channel gains and channel correlations.

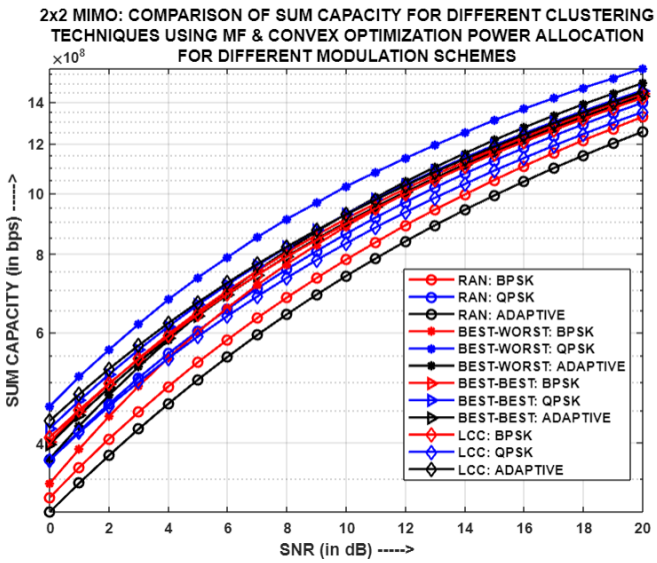

Fig.5.49: For (2x2)-MIMO-NOMA: Comparison of Sum Capacity for different clustering techniques using MF and CON-OPA

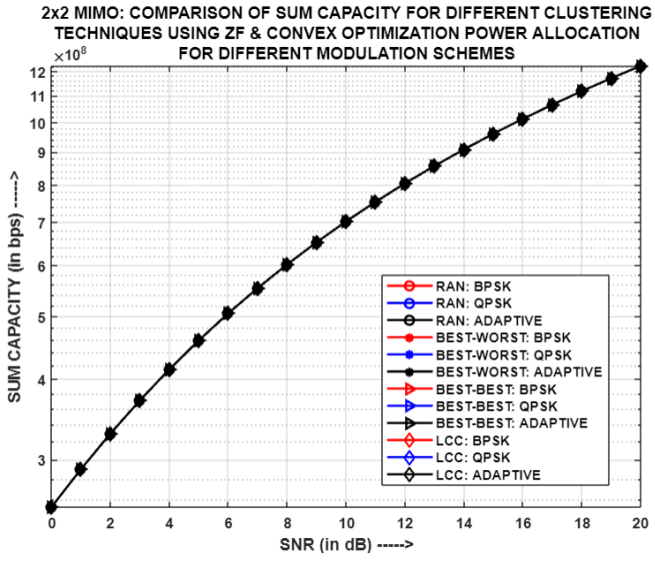

Fig.5.50: For (2x2)-MIMO-NOMA: Comparison of Sum Capacity for different clustering techniques using ZF and CON-OPA

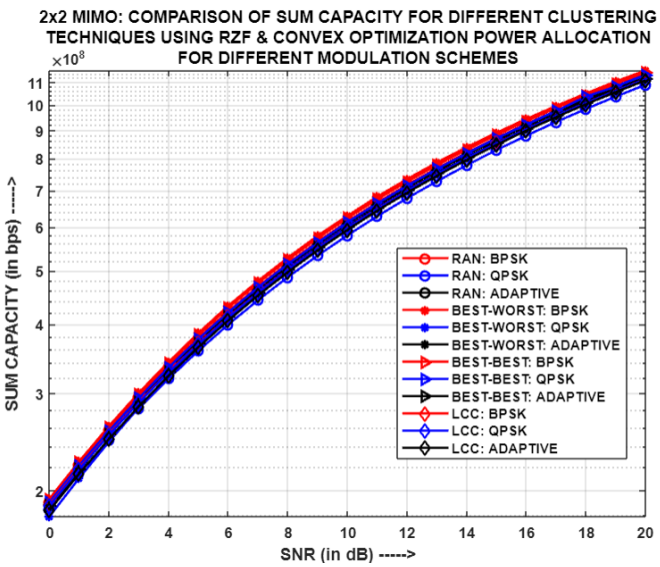

Fig.5.51: For (2x2)-MIMO-NOMA: Comparison of Sum Capacity for different clustering techniques using RZF and CON-OPA

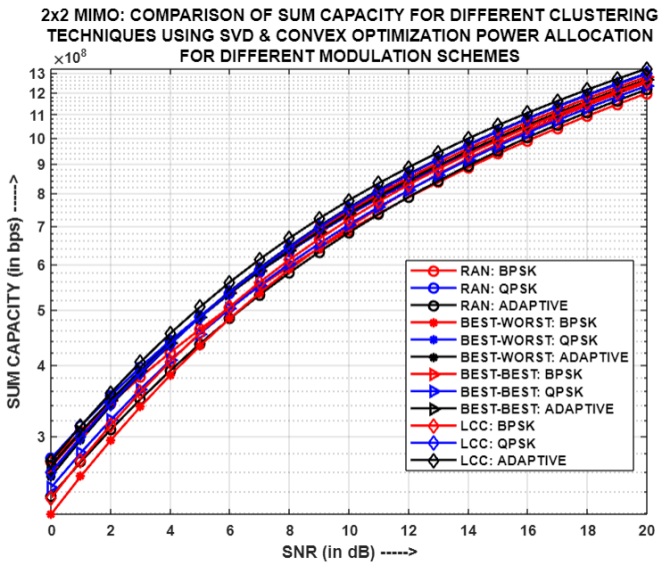

Fig.5.52: For (2x2)-MIMO-NOMA: Comparison of Sum Capacity for different clustering techniques using SVD and CON-OPA

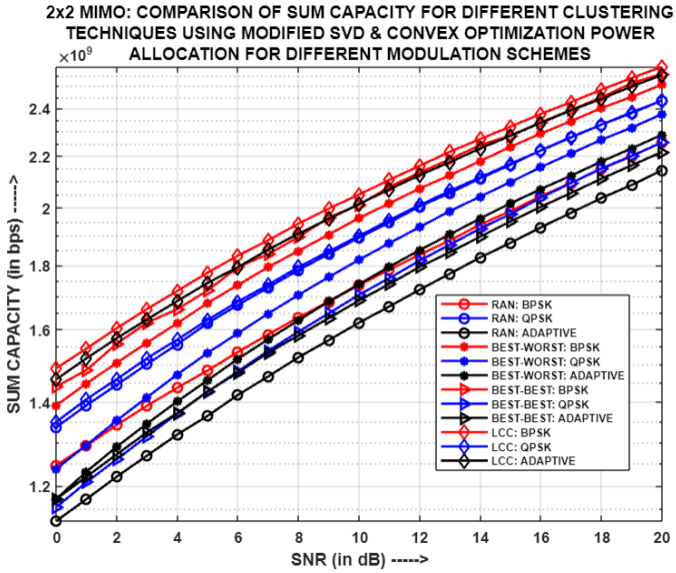

Fig.5.53: For (2x2)-MIMO-NOMA: Comparison of Sum Capacity for different clustering techniques using MODIFIED SVD and CON-OPA

Fig.5.49, Fig.5.50, Fig.5.51, Fig.5.52 and Fig.5.53 showcases the comparison of Sum Capacity for different clustering methodologies using diverse precoding schemes, i.e., MF, ZF, RZF, SVD and MODIFIED SVD respectively, and CON-OPA, with each entity in the system having two antennas. The clustering methodologies employed for ZF, RZF, and SVD respectively, produce comparable

sum capacities. This is mainly due to the influence of the chosen precoding technique and the utilization of similar power allocation coefficient sets across the various clustering schemes and clusters, which overshadow the influence of the channel gain on the user throughput. As a result, all these clustering methodologies achieve similar sum capacities for their respective precoding schemes. On the other hand, MF clustering shows contrasting sum capacities among the different clustering mechanisms, owing to the use of different power coefficient sets across all the clustering schemes, due to CON-OPA mechanism. However, significant variations in sum capacities are observed for different clustering methodologies, when employing MODIFIED SVD. This is because of the use of a gain matrix that affects both the precoding and post-coding matrices, leading to a notable impact on the user's channel gain. The design of amplification matrices depends on user clustering, which in turn influences their channel gain and throughput. Since user throughput directly impacts the overall sum capacity; hence, variations in sum capacities arise when applying different clustering techniques with MODIFIED SVD. Therefore, LCC clustering employing BPSK and Adaptive modulations respectively, yield comparable and highest sum capacity for the aforementioned precoding scheme. The merging of sum capacities attributes to similar grouping of users.

5.3.6. Simulation Result Analysis of two-user (4x4)-MIMO-PD-NOMA model for different clustering methodologies using diverse precoding schemes and CON-OPA:

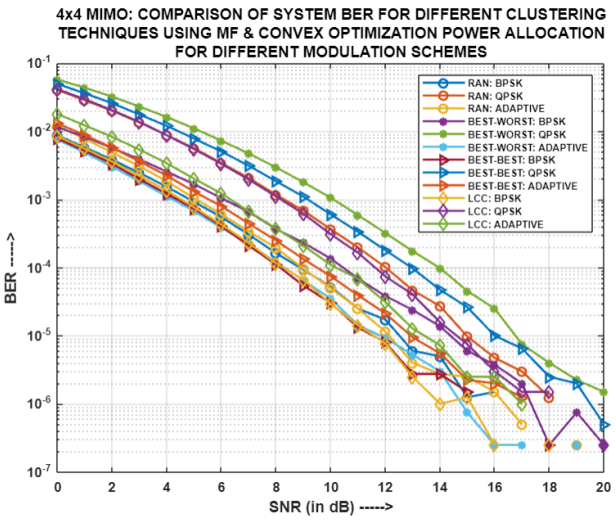

Fig.5.54: For (4x4)-MIMO-NOMA: Comparison of System BER for different clustering techniques using MF and CON-OPA

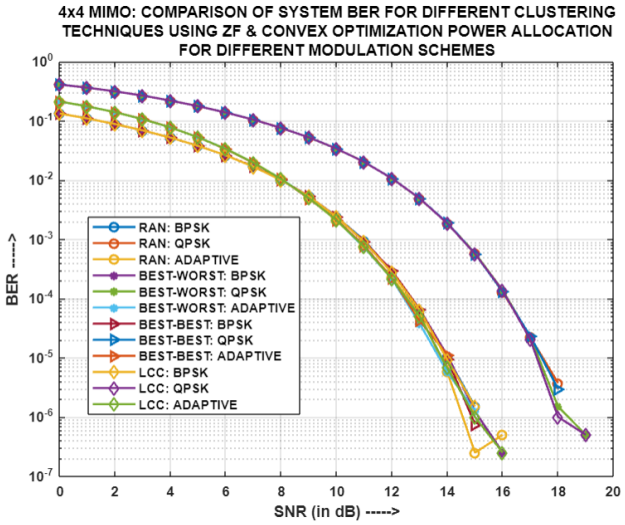

Fig.5.55: For (4x4)-MIMO-NOMA: Comparison of System BER for different clustering techniques using ZF and CON-OPA

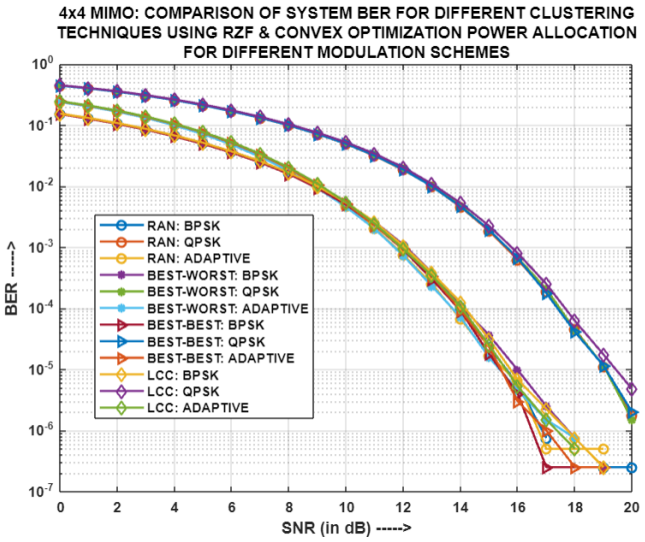

Fig.5.56: For (4x4)-MIMO-NOMA: Comparison of System BER for different clustering techniques using RZF and CON-OPA

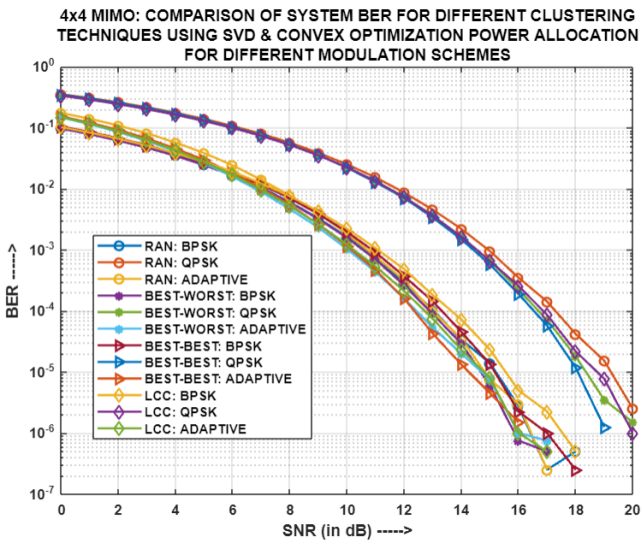

Fig.5.57: For (4x4)-MIMO-NOMA: Comparison of System BER for different clustering techniques using SVD and CON-OPA

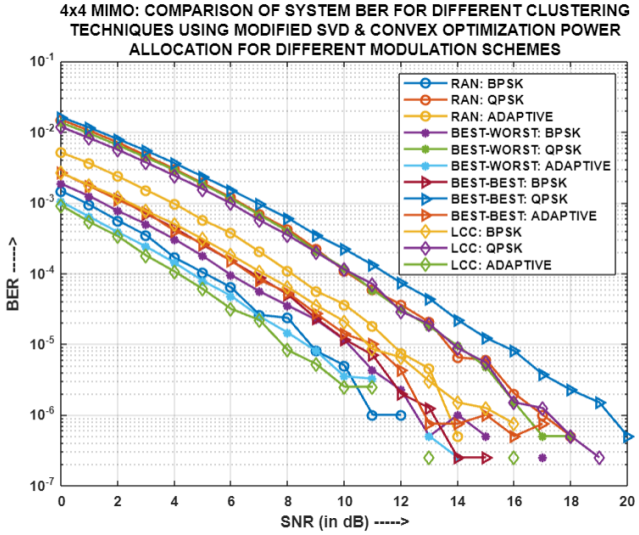

Fig.5.58: For (4x4)-MIMO-NOMA: Comparison of System BER for different clustering techniques using MODIFIED SVD and CON-OPA

Fig.5.54, Fig.5.55, Fig.5.56, Fig.5.57 and Fig.5.58 portrays the comparison of system BER for different clustering methodologies using diverse precoding schemes, i.e. MF, ZF, RZF, SVD and MODIFIED SVD respectively, and convex optimization power allocation (CON-OPA), with each entity in the system having four antennas. It has been witnessed that for MF, LCC generates the lowest system

BER for both BPSK and QPSK respectively; while for Adaptive modulation, BWW yields the best system BER performance. This is because in the former two modulation cases, the user pairs had considerable differences in their channel gains as well channel correlations, which made it convenient to separate out the information signals at the receiver; whereas in the latter case, the users had similar channel correlations and hence, pairing them on basis of their channel gains turned out to be the optimum choice. Nevertheless, when it comes to ZF, RZF and SVD, all clustering methodologies yield nearly identical system BERs for each modulation scheme. This resemblance arises from the pairing of users in a similar manner and the usage of comparable sets of power allocation coefficients for the user-pairs, which are determined through the CON-OPA mechanism. However, in context of MODIFIED SVD, LCC yields the least system BER for both QPSK and Adaptive modulations due to optimal user-pairing and hence, power distribution among the user-pairs, through CON-OPA strategy.

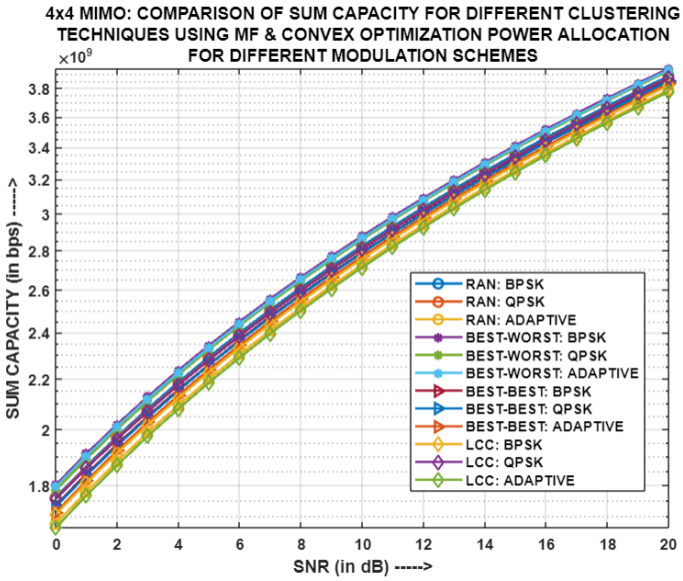

Fig.5.59: For (4x4)-MIMO-NOMA: Comparison of Sum Capacity for different clustering techniques using MF and CON-OPA

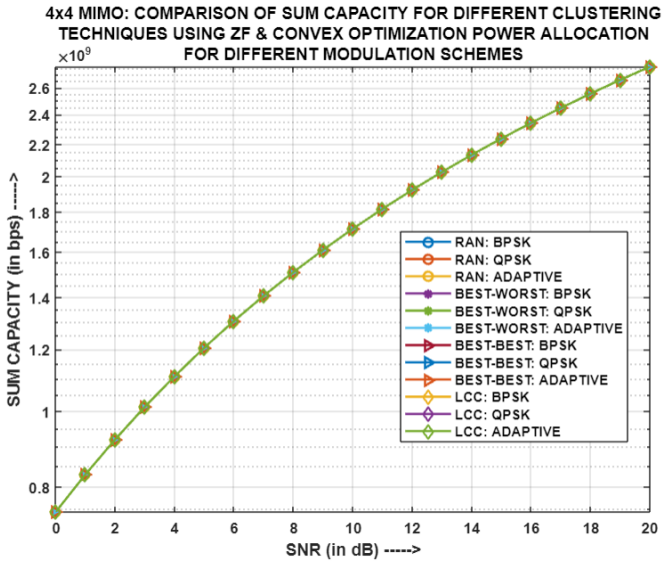

Fig.5.60: For (4x4)-MIMO-NOMA: Comparison of Sum Capacity for different clustering techniques using ZF and CON-OPA

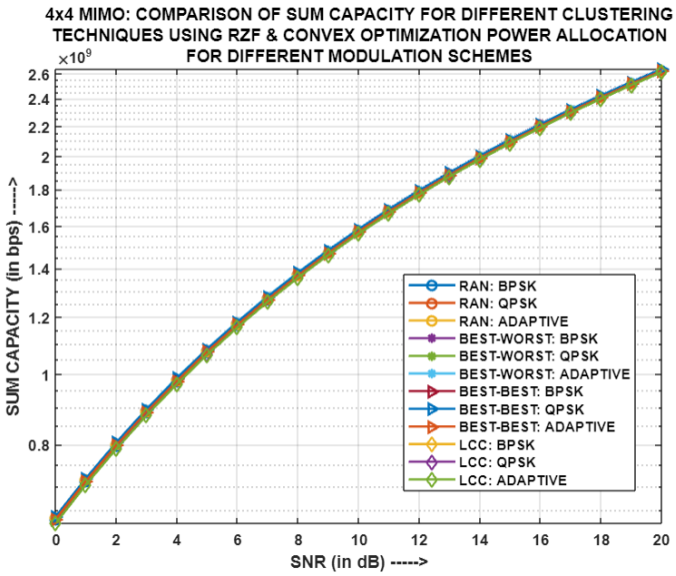

Fig.5.61: For (4x4)-MIMO-NOMA: Comparison of Sum Capacity for different clustering techniques using RZF and CON-OPA

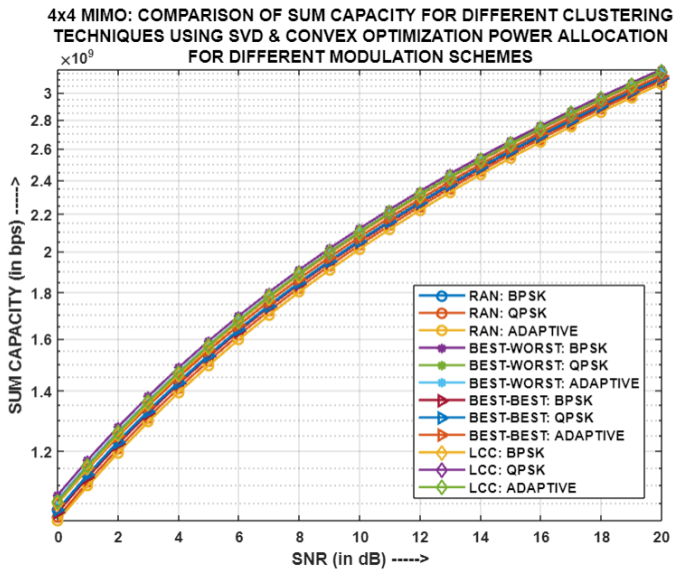

Fig.5.62: For (4x4)-MIMO-NOMA: Comparison of Sum Capacity for different clustering techniques using SVD and CON-OPA

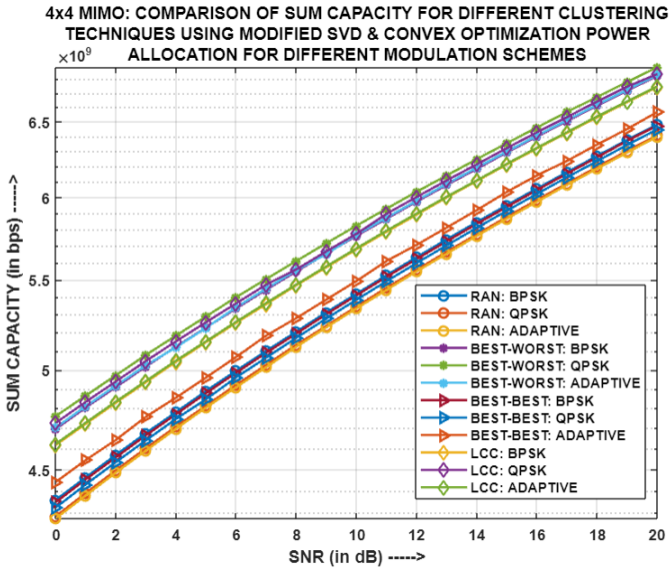

Fig.5.63: For (4x4)-MIMO-NOMA: Comparison of Sum Capacity for different clustering techniques using MODIFIED SVD and CON-OPA

Fig.5.59, Fig.5.60, Fig.5.61, Fig.5.62 and Fig.5.63 presents the comparison of Sum Capacity for different clustering methodologies using diverse precoding schemes, i.e. MF, ZF, RZF, SVD and MODIFIED SVD respectively, and CON-OPA, with each entity in the system having four antennas. The clustering methodologies applied to MF, ZF, RZF, and SVD respectively, result in merged sum

capacities. This can be attributed to the impact of the chosen precoding technique and the use of comparable power allocation coefficient sets across the different clustering schemes. These factors seem to have a stronger influence on the user's throughput than the respective channel gains. As users' throughput is responsible to determine the sum capacity of the system, hence consequently, all clustering methodologies yield comparable sum capacities for their respective precoding schemes. On the other hand, when utilizing MODIFIED SVD, notable differences in sum capacities can be observed among different clustering methodologies. This is because of the default introduction of a gain matrix that affects both the precoding and post-coding matrices, resulting in a significant impact on the channel gain experienced by the users. The design of these amplification matrices is dependent on the clustering of users, which in turn influences their channel gain and subsequently, their throughput. As user throughput directly affects the overall sum capacity of the system, variations in sum capacities become apparent when employing different clustering techniques with MODIFIED SVD. Thus, LCC clustering with QPSK and BWW clustering with QPSK and Adaptive modulations, yield merged but highest sum capacity for the above stated precoding scheme. The merging of sum capacities attributes to similar grouping of users.

5.3.7. Simulation Result Analysis of two-user (2x2)-MIMO-PD-NOMA model for different power allocation strategies and clustering methodologies:

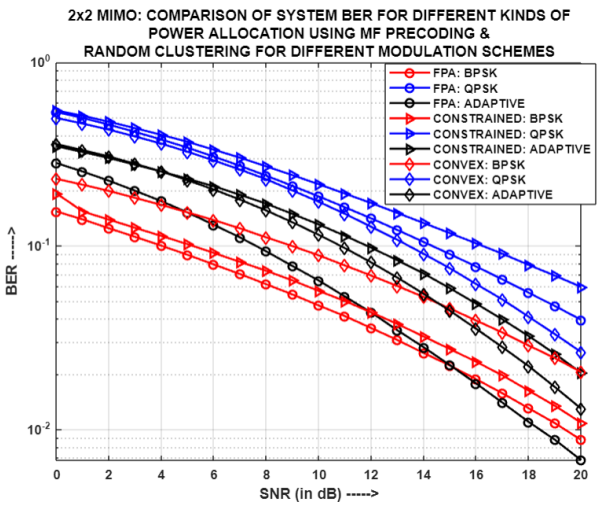

Fig.5.64: For (2x2)-MIMO-NOMA: Comparison of System BER for different power allocation strategies using MF and Random clustering

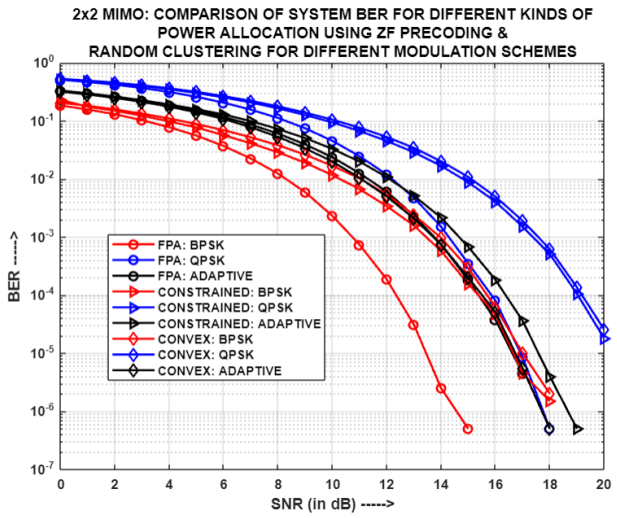

Fig.5.65: For (2x2)-MIMO-NOMA: Comparison of System BER for different power allocation strategies using ZF and Random clustering

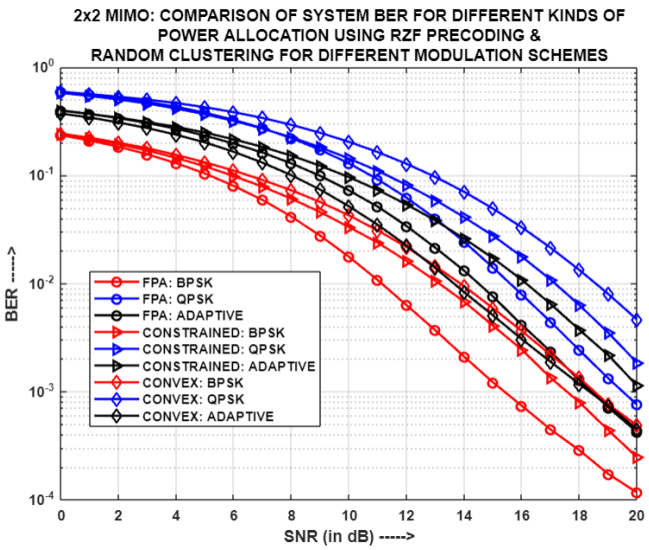

Fig.5.66: For (2x2)-MIMO-NOMA: Comparison of System BER for different power allocation strategies using RZF and Random clustering

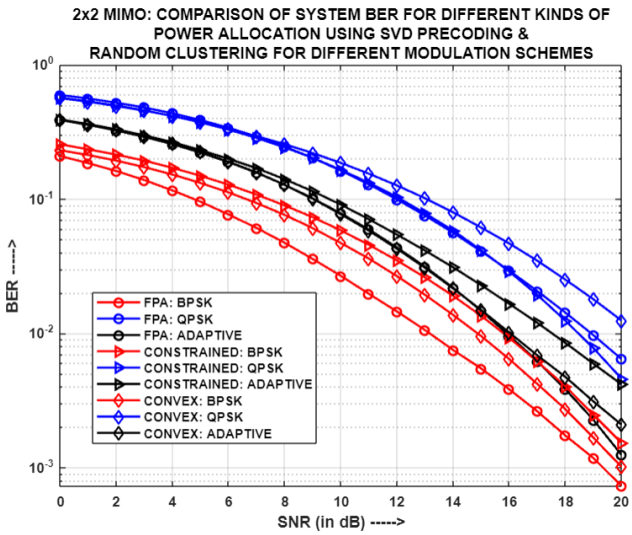

Fig.5.67: For (2x2)-MIMO-NOMA: Comparison of System BER for different power allocation strategies using SVD and Random clustering

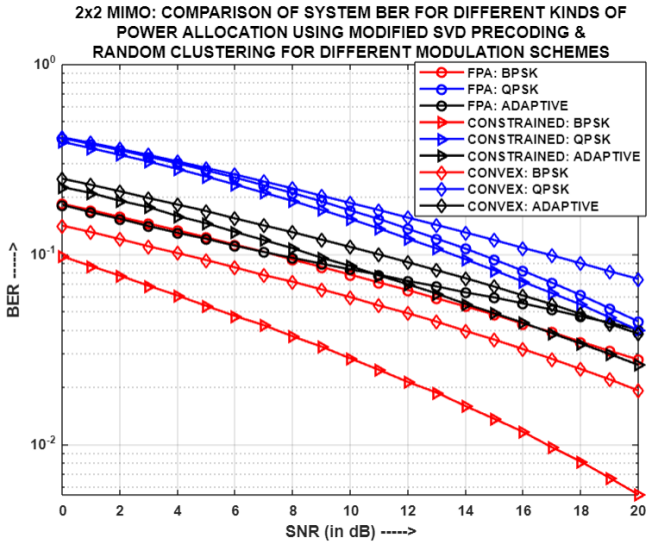

Fig.5.68: For (2x2)-MIMO-NOMA: Comparison of System BER for different power allocation strategies using MODIFIED SVD and Random clustering

Fig.5.64, Fig.5.65, Fig.5.66, Fig.5.67 and Fig.5.68 depicts the comparison of system BER for different power allocation strategies using varied precoding techniques and Random clustering, with each entity in the system having two antennas each. It has been observed that for MF, FPA gives better system BER performance for both BPSK and Adaptive modulations, while CON-OPA excels in

case of QPSK. However, in context of ZF and RZF, for both BPSK and QPSK, FPA produces the least system BER results. On the contrary, in case of Adaptive modulation, CON-OPA yields merged system BER along with FPA for ZF, whereas for RZF, it's just CON-OPA that generates the lowest system BER. On the other hand, for SVD, it is seen that FPA produces the minimum system BER for BPSK, while CON-OPA and COPA yield better system BER performance for QPSK and Adaptive modulations respectively. In regard to MODIFIED SVD, COPA produces the least system BER for BPSK and Adaptive modulations respectively; whereas for Adaptive modulation, FPA and COPA yield optimum system BER for varying range of SNR. For all the above cases, the reason behind different power allocation strategies producing optimum performance for the same modulation scheme but different precoding technique, is primarily because of the impact of the different precoding schemes as well as the manner in which the users are paired. In random clustering, users are arbitrarily paired, where at times, coincidentally, users with considerably different channel gains might be paired, while again there is a possibility that users with similar channel characteristics can also be grouped together. The pairing scheme of users is important as the COPA and CON-OPA mechanisms utilize the channel gain of these users in computing their throughputs and hence, the sum capacity of the respective clusters, to determine the suitable power allocation coefficient sets for them.

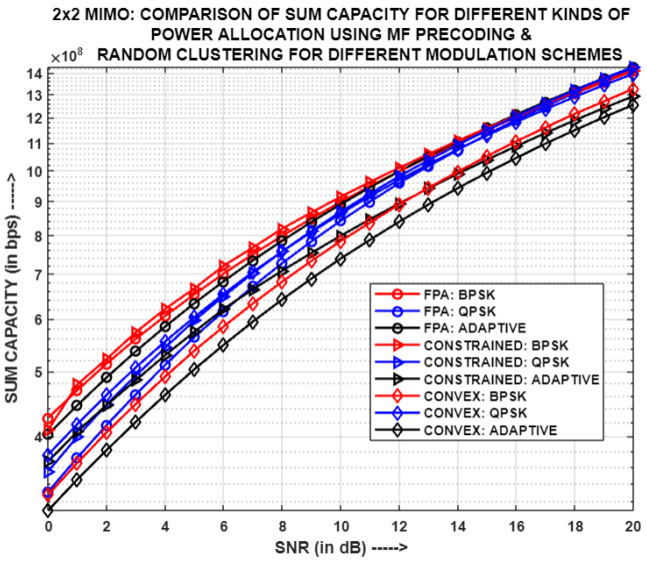

Fig.5.69: For (2x2)-MIMO-NOMA: Comparison of Sum Capacity for different power allocation strategies using MF and Random clustering

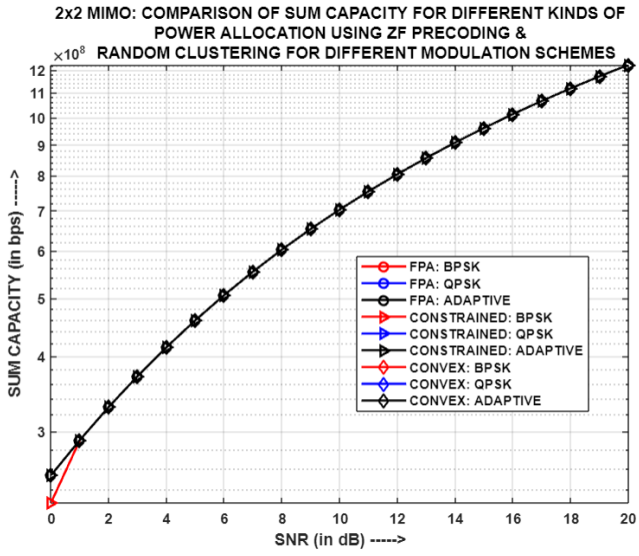

Fig.5.70: For (2x2)-MIMO-NOMA: Comparison of Sum Capacity for different power allocation strategies using ZF and Random clustering

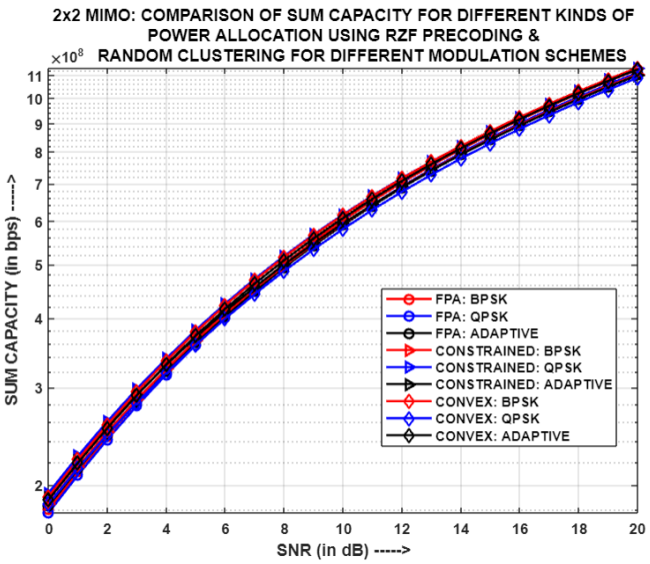

Fig.5.71: For (2x2)-MIMO-NOMA: Comparison of Sum Capacity for different power allocation strategies using RZF and Random clustering

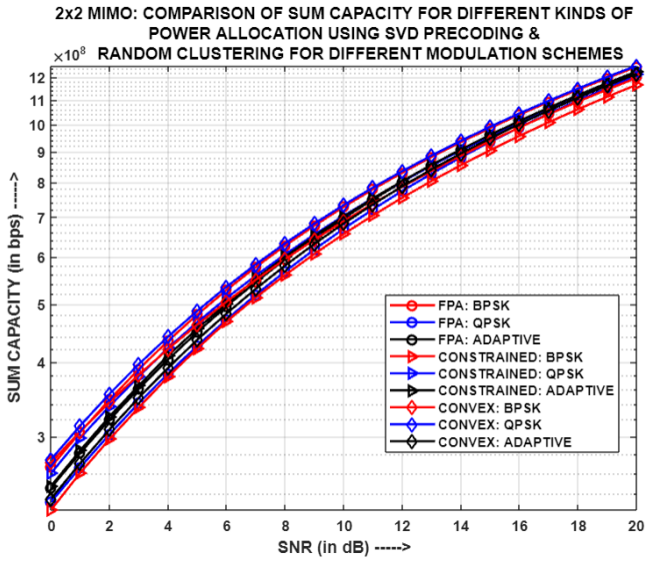

Fig.5.72: For (2x2)-MIMO-NOMA: Comparison of Sum Capacity for different power allocation strategies using SVD and Random clustering

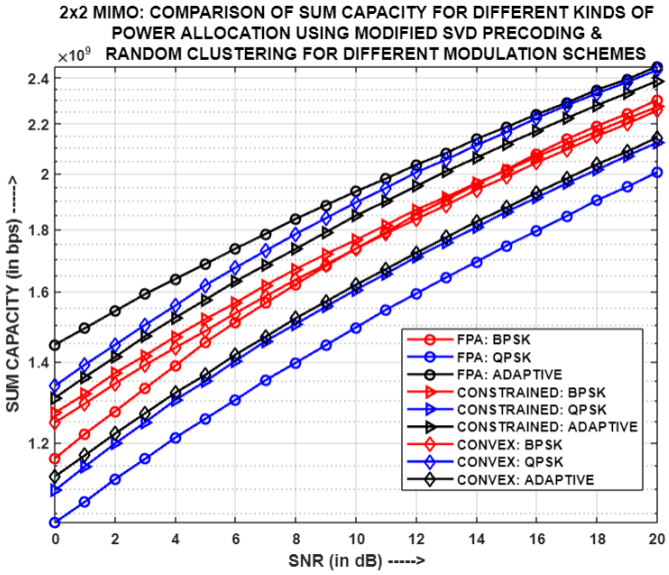

Fig.5.73: For (2x2)-MIMO-NOMA: Comparison of Sum Capacity for different power allocation strategies using MODIFIED SVD and Random clustering

Fig.5.69, Fig.5.70, Fig.5.71, Fig.5.72 and Fig.5.73 portrays the comparison of Sum Capacity for different power allocation strategies using varied precoding techniques and Random clustering, with each entity in the system having two antennas each.

The power allocation (PA) strategies utilized for ZF, RZF, and SVD, respectively, generate comparable sum capacities. This is primarily due to the influence of the chosen precoding technique, alike user channel gains and the utilization of similar sets of power allocation coefficients across the different PA mechanisms. However, when it comes to MF, slightly contrasting sum capacities are observed among the different PA mechanisms and modulation schemes. This is because of the utilization of different sets of power coefficients by the varied PA strategies, across the entire SNR range. On the other hand, significant variations in sum capacities are witnessed for different PA schemes, when MODIFIED SVD is employed. The reason behind such behaviour attributes to the selection of differing sets of power coefficients by the varied PA mechanisms and also the incorporation of a gain matrix that affects both the precoding and post-coding matrices, resulting in a notable influence on the user's resultant channel gain. The design of amplification matrices depends on user clustering, which in turn affects their channel gain and throughput. Since user throughput directly impacts the overall sum capacity, hence, variations in sum capacities arise when different PA techniques are applied with MODIFIED SVD. Therefore, Adaptive modulation, along with FPA, produces the highest sum capacity for MODIFIED SVD.

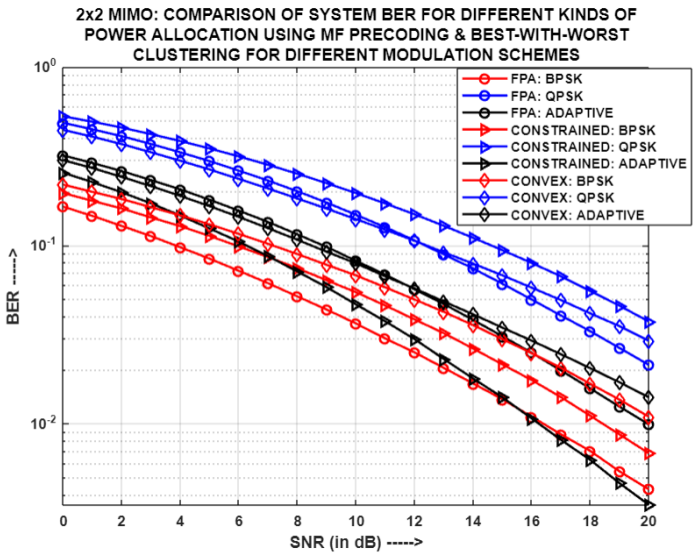

Fig.5.74: For (2x2)-MIMO-NOMA: Comparison of System BER for different power allocation strategies using MF and BWW clustering

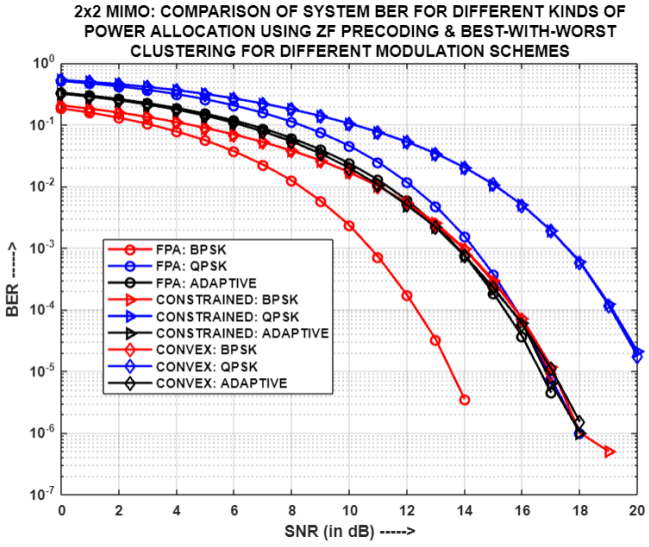

Fig.5.75: For (2x2)-MIMO-NOMA: Comparison of System BER for different power allocation strategies using ZF and BWW clustering

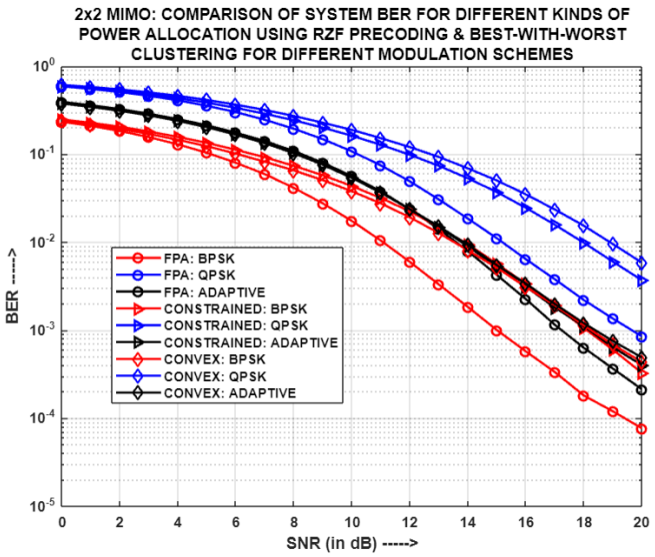

Fig.5.76: For (2x2)-MIMO-NOMA: Comparison of System BER for different power allocation strategies using RZF and BWW clustering

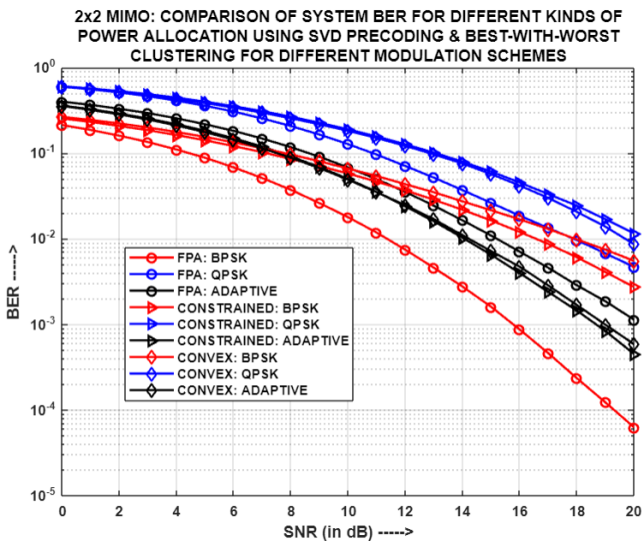

Fig.5.77: For (2x2)-MIMO-NOMA: Comparison of System BER for different power allocation strategies using SVD and BWW clustering

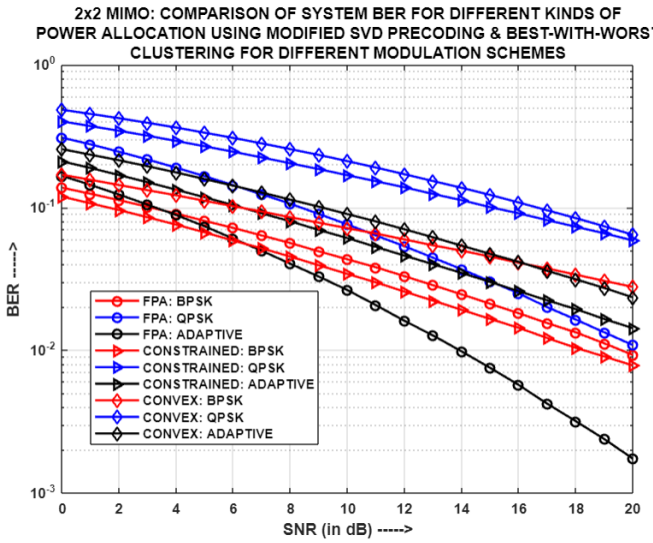

Fig.5.78: For (2x2)-MIMO-NOMA: Comparison of System BER for different power allocation strategies using MODIFIED SVD and BWW clustering

Fig.5.74, Fig.5.75, Fig.5.76, Fig.5.77 and Fig.5.78 showcases the comparison of system BER for different power allocation strategies using varied precoding techniques and Best-With-Worst (BWW) clustering, with each entity in the system having two antennas each. It is noticeable that for MF, FPA and CON-OPA

interchangeably, for different SNR range, produce optimum system BER for QPSK, while FPA and COPA yield the least system BER for BPSK and Adaptive modulations respectively. In case of ZF and RZF, it is noteworthy that FPA generates the least system BER for all the modulation schemes respectively. Also, in case of Adaptive modulation for ZF, COPA and CON-OPA yield comparable system BERs as to FPA, indicating the selection of the same power allocation coefficient set. On the contrary, for SVD, FPA generates the lowest system BER for both BPSK and QPSK respectively; whereas COPA and CON-OPA produce merged optimum system BERs for Adaptive modulation scheme. The merging of system BERs is because of the fact that both the power allocation mechanisms happen to dynamically select the same power coefficient sets for the respective user-pairs in the system. Finally, in regard to MODIFIED SVD, it is interesting to observe that FPA gives rise to the minimum system BER for both QPSK and Adaptive modulations, while COPA yields the least system BER for BPSK. The reason behind different power allocation strategies leading to optimal performance for the same modulation scheme, but different precoding technique, in the aforementioned cases is due to the influence of the respective precoding techniques and the pairing scheme of users. In BWW clustering, users are paired based on them having considerably different channel gains. However, at times it happens that the difference in channel gains of paired users is nominal. The pairing scheme of users play a crucial role because the COPA and CON-OPA mechanisms use the channel gain of these users to calculate their throughputs and, consequently, the sum capacity of the respective clusters. This information is then used to determine the appropriate sets of power allocation coefficients for the user-pairs.

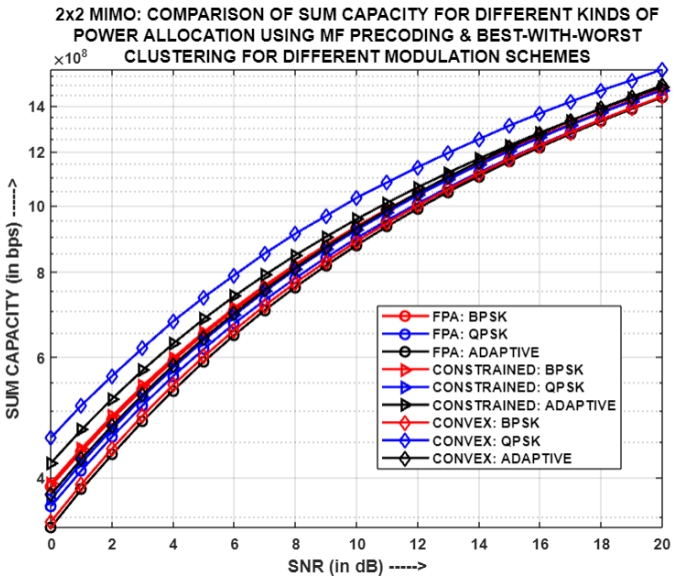

Fig.5.79: For (2x2)-MIMO-NOMA: Comparison of Sum Capacity for different power allocation strategies using MF and BWW clustering

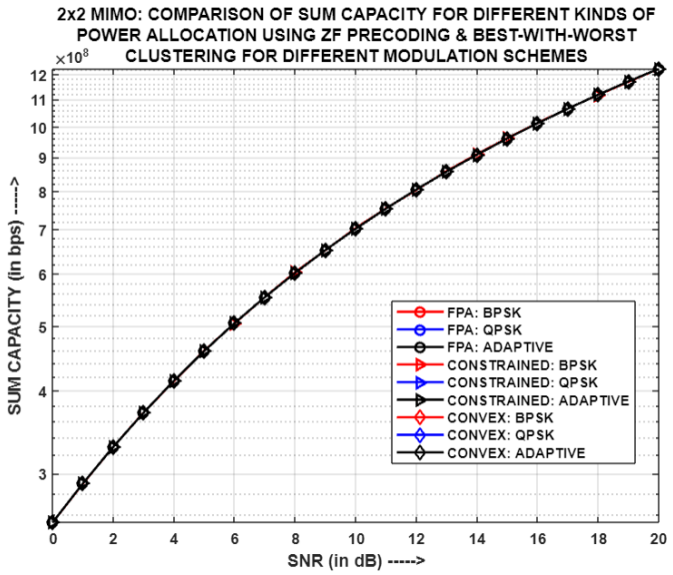

Fig.5.80: For (2x2)-MIMO-NOMA: Comparison of Sum Capacity for different power allocation strategies using ZF and BWW clustering

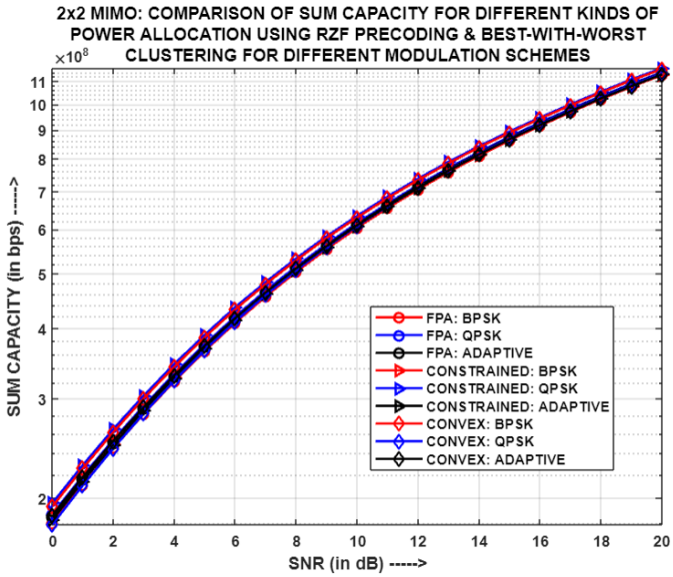

Fig.5.81: For (2x2)-MIMO-NOMA: Comparison of Sum Capacity for different power allocation strategies using RZF and BWW clustering

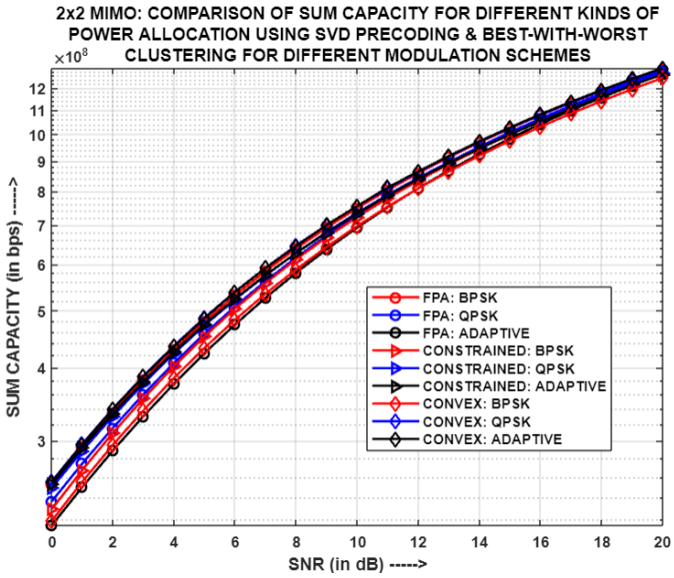

Fig.5.82: For (2x2)-MIMO-NOMA: Comparison of Sum Capacity for different power allocation strategies using SVD and BWW clustering

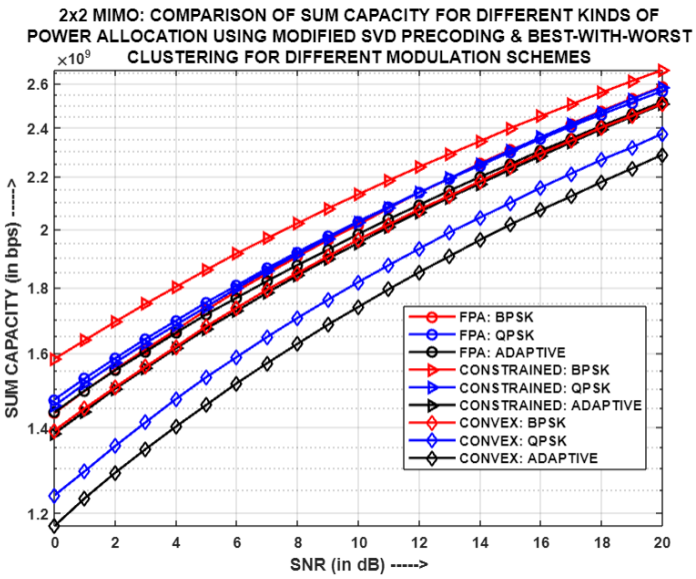

Fig.5.83: For (2x2)-MIMO-NOMA: Comparison of Sum Capacity for different power allocation strategies using MODIFIED SVD and BWW clustering

Fig.5.79, Fig.5.80, Fig.5.81, Fig.5.82 and Fig.5.83 presents the comparison of Sum Capacity for different power allocation strategies using varied precoding techniques and BWW clustering, with each entity in the system having two antennas each. The power allocation (PA) strategies employed for ZF, RZF, and SVD, respectively, yield comparable sum capacities. This similarity is primarily due to the influence of the chosen precoding technique, alike user channel gains, and the utilization of almost similar sets of power allocation coefficients across the various PA mechanisms. However, when it comes to MF, slight variations in total capacities are observed among the different PA mechanisms and modulation schemes. This can be attributed to the utilization of different sets of power coefficients by the diverse PA strategies across the entire SNR range. On the other hand, significant variations in sum capacities are observed for different PA schemes, when MODIFIED SVD precoding is used. This behavior is due to the selection of different sets of power coefficients by the various PA mechanisms, as well as the incorporation of a gain matrix that impacts both the precoding and post-coding matrices, leading to a notable influence on the resulting channel gain of the users. The design of amplification matrices depends on user clustering, which in turn affects their channel gain and throughput. Since user throughput directly affects the overall sum capacity, therefore, variations in sum capacities arise when different PA techniques are

applied with MODIFIED SVD. Thus, BPSK modulation, along with COPA, produces the highest sum capacity for MODIFIED SVD.

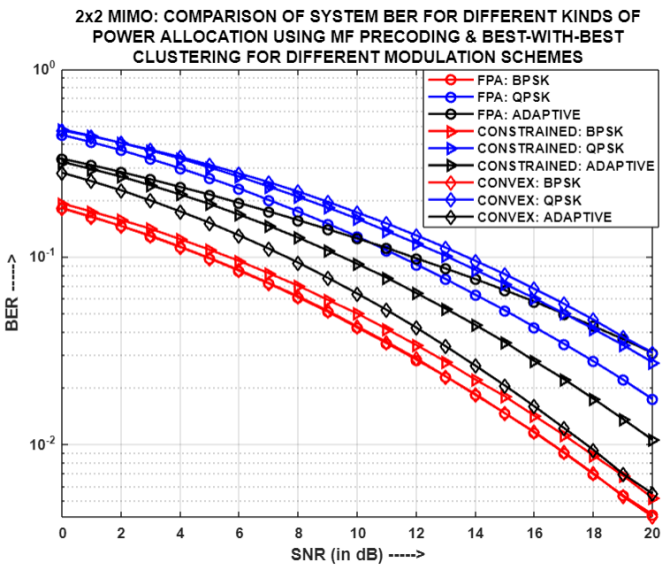

Fig.5.84: For (2x2)-MIMO-NOMA: Comparison of System BER for different power allocation strategies using MF and BWB clustering

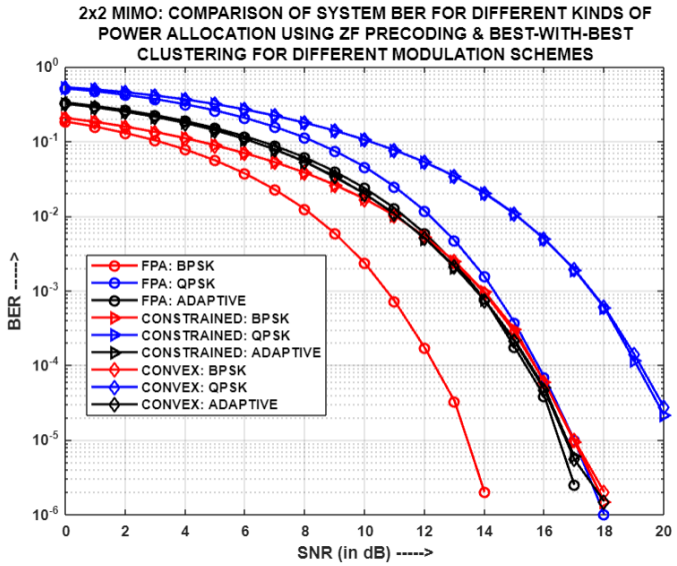

Fig.5.85: For (2x2)-MIMO-NOMA: Comparison of System BER for different power allocation strategies using ZF and BWB clustering

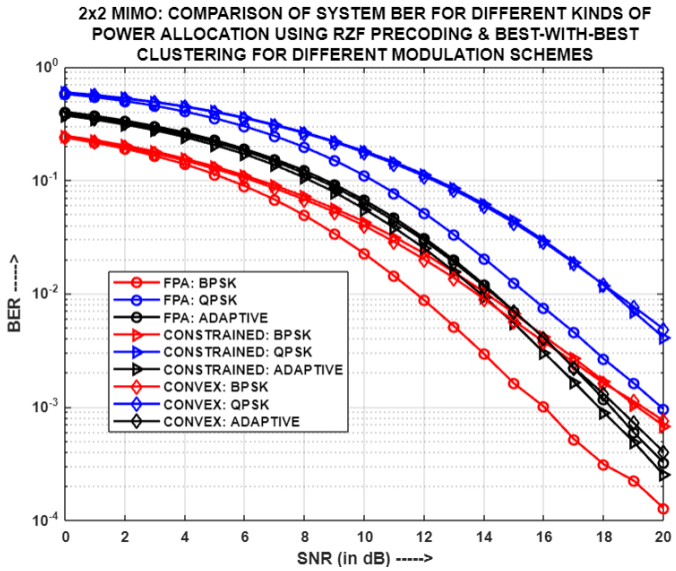

Fig.5.86: For (2x2)-MIMO-NOMA: Comparison of System BER for different power allocation strategies using RZF and BWB clustering

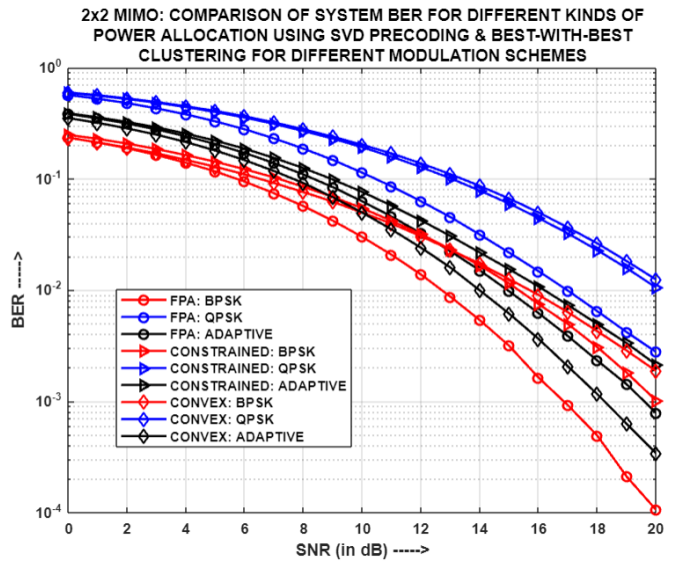

Fig.5.87: For (2x2)-MIMO-NOMA: Comparison of System BER for different power allocation strategies using SVD and BWB clustering

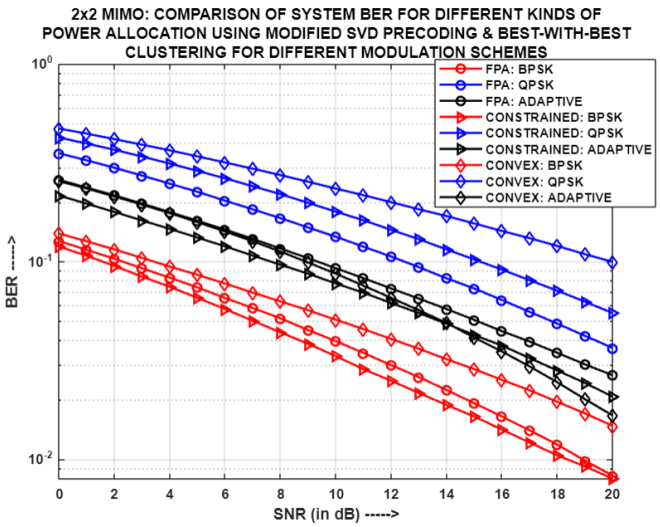

Fig.5.88: For (2x2)-MIMO-NOMA: Comparison of System BER for different power allocation strategies using MODIFIED SVD and BWB clustering

Fig.5.84, Fig.5.85, Fig.5.86, Fig.5.87 and Fig.5.88 illustrates the comparison of system BER for different power allocation strategies using varied precoding techniques and Best-With-Best (BWB) clustering, with each entity in the system having two antennas each. It can be seen that for MF, when employing QPSK and Adaptive modulations, FPA and CON-OPA yields the least system BER respectively; while for BPSK, FPA and CON-OPA generate a merged least system BER for BPSK. The convergence of system BERs occur because both the power allocation mechanisms coincidentally and dynamically select the same power coefficient sets for the corresponding user-pairs in the system. It is important to highlight that in the case of ZF and RZF, the FPA consistently achieves the lowest system BER for all the modulation schemes respectively. Additionally, when it comes to Adaptive modulation with ZF and RZF, both the COPA and CON-OPA strategies yield comparable system BERs, alike FPA. This suggests that they select the same power allocation coefficient set, resulting in similar performance. In context of SVD, FPA produces the least system BER for both BPSK and QPSK respectively. However, in case of Adaptive modulation, CON-OPA yields the minimum system BER. Finally, in regard to MODIFIED SVD, COPA and FPA achieves the lowest system BER for BPSK and QPSK respectively; whereas COPA and CON-OPA, interchangeably, for varying SNR range, generate the least system

BER for Adaptive modulation scheme. It can be inferred from all the above cases that the variation in power allocation strategies resulting in optimal performance for the same modulation scheme, but with different precoding techniques, can be attributed to the combined influence of the respective precoding technique and the pairing scheme of users. In BWB, the users are paired based on the decreasing order of consecutive channel gains. Therefore, it becomes a matter of probability, wherein at times, users that are paired might have significant difference in their channel gains or the difference can be nominal. It all depends on the channel characteristics at that instant of time. The pairing scheme plays a critical role as the COPA and CON-OPA mechanisms leverage the channel gain of the users to calculate their throughputs and, consequently, the sum capacity of the clusters. This information is then utilized to determine the suitable sets of power allocation coefficients for the user-pairs, through the respective algorithms.

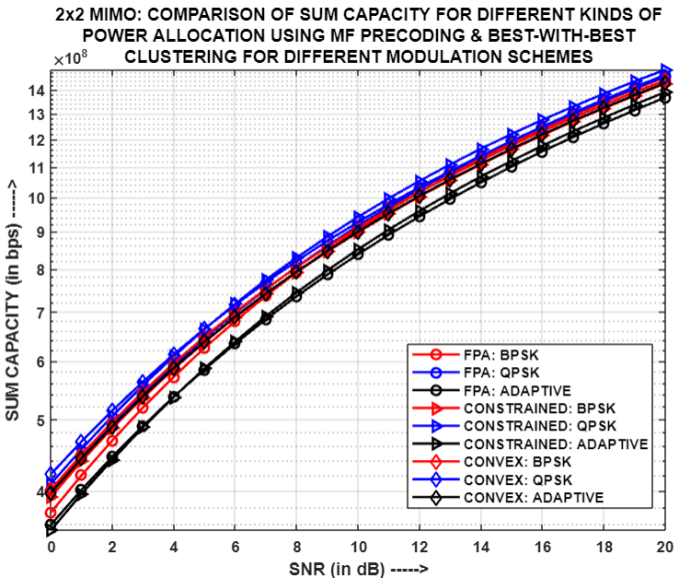

Fig.5.89: For (2x2)-MIMO-NOMA: Comparison of Sum Capacity for different power allocation strategies using MF and BWB clustering

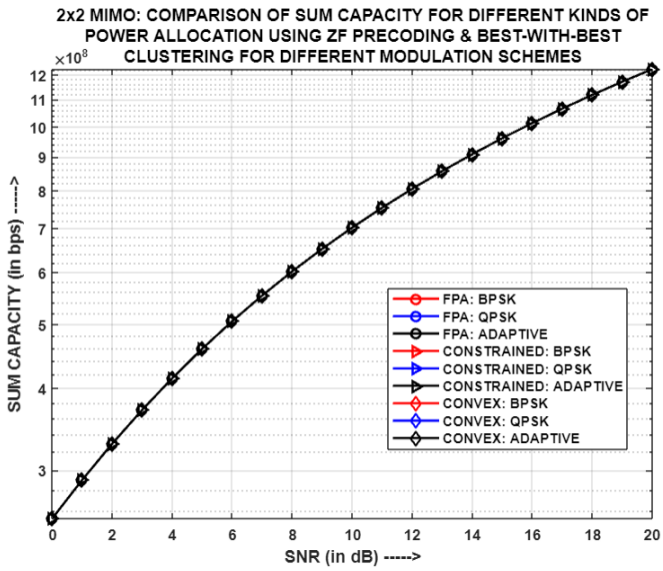

Fig.5.90: For (2x2)-MIMO-NOMA: Comparison of Sum Capacity for different power allocation strategies using ZF and BWB clustering

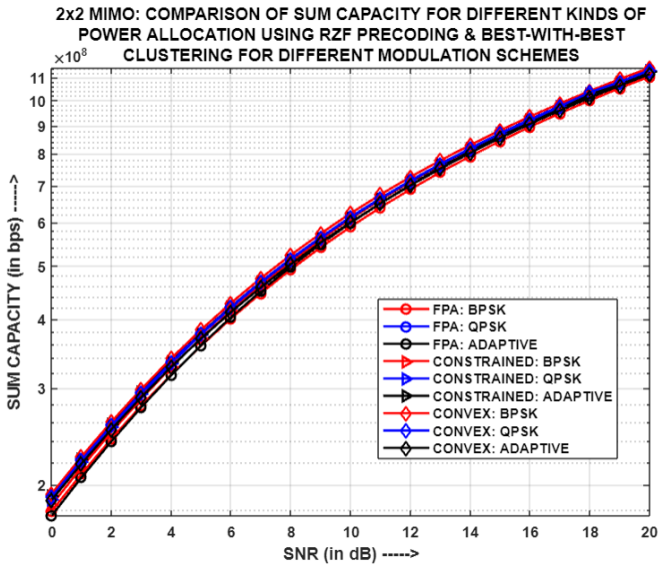

Fig.5.91: For (2x2)-MIMO-NOMA: Comparison of Sum Capacity for different power allocation strategies using RZF and BWB clustering

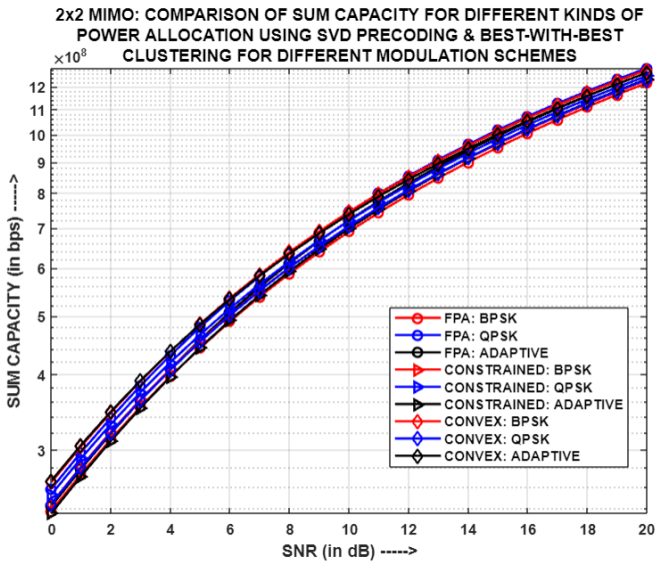

Fig.5.92: For (2x2)-MIMO-NOMA: Comparison of Sum Capacity for different power allocation strategies using SVD and BWB clustering

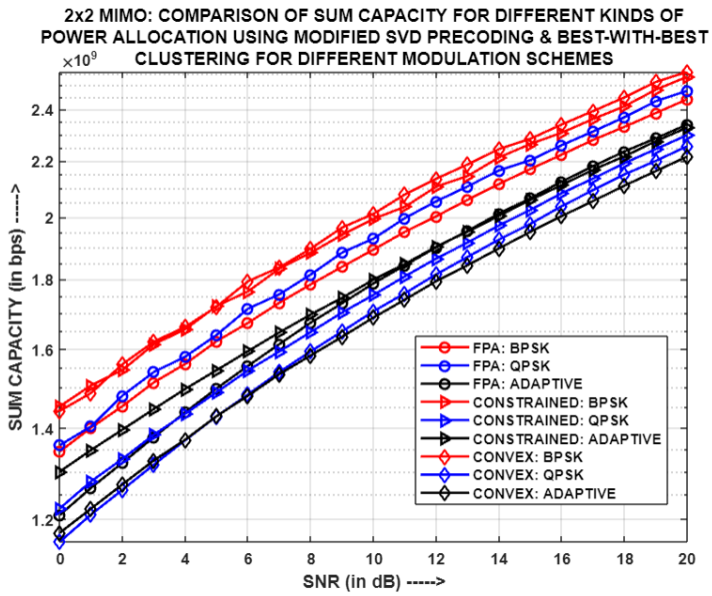

Fig.5.93: For (2x2)-MIMO-NOMA: Comparison of Sum Capacity for different power allocation strategies using MODIFIED SVD and BWB clustering

Fig.5.89, Fig.5.90, Fig.5.91, Fig.5.92 and Fig.5.93 portrays the comparison of Sum Capacity for different power allocation strategies using varied precoding techniques and BWB clustering, with each entity in the system having two antennas each. The

power allocation (PA) strategies employed for ZF, RZF, and SVD, respectively, yield comparable sum capacities. This is mainly due to the impact of the chosen precoding technique, the similarity in user channel gains, and the use of alike sets of power allocation coefficients across the different PA mechanisms. However, when it comes to MF, slight differences in sum capacities are observed among the various PA mechanisms and modulation schemes. This is because each PA strategy employs different sets of power coefficients across the entire SNR range. On the contrary, noteworthy variations in sum capacities are observed when MODIFIED SVD is used with different PA schemes. This behavior can be attributed to the selection of distinct power coefficient sets by the diverse PA mechanisms, as well as the incorporation of a gain matrix that affects both the precoding and post-coding matrices, leading to a notable influence on the resulting channel gain for each user. The design of amplification matrices depends on user clustering, which in turn impacts their channel gain and throughput. As user throughput directly affects the overall sum capacity, hence, variations in sum capacities arise when different PA techniques are applied with MODIFIED SVD. Thus, both COPA and CON-OPA yield almost merged but highest sum capacity for BPSK modulation, employing the aforementioned precoding scheme.

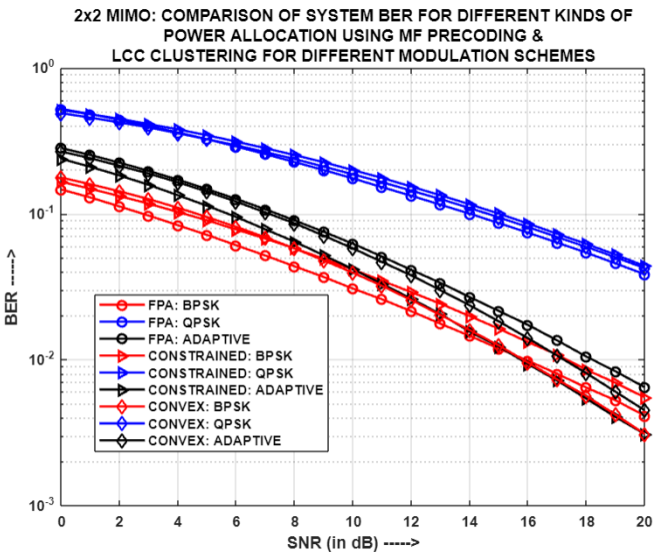

Fig.5.94: For (2x2)-MIMO-NOMA: Comparison of System BER for different power allocation strategies using MF and LCC clustering

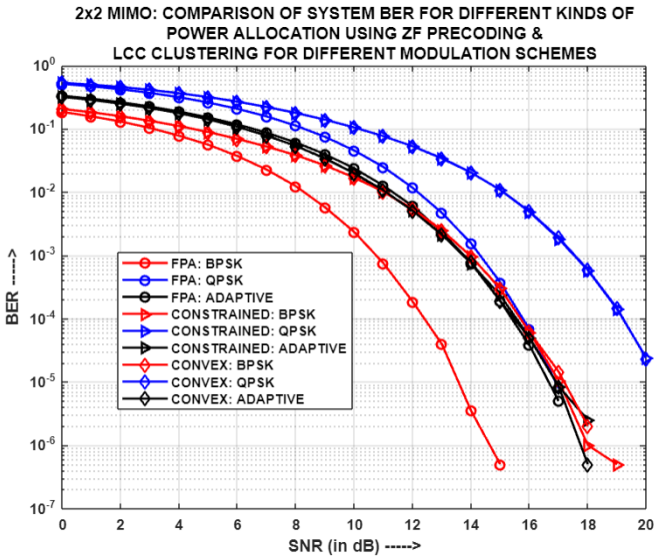

Fig.5.95: For (2x2)-MIMO-NOMA: Comparison of System BER for different power allocation strategies using ZF and LCC clustering

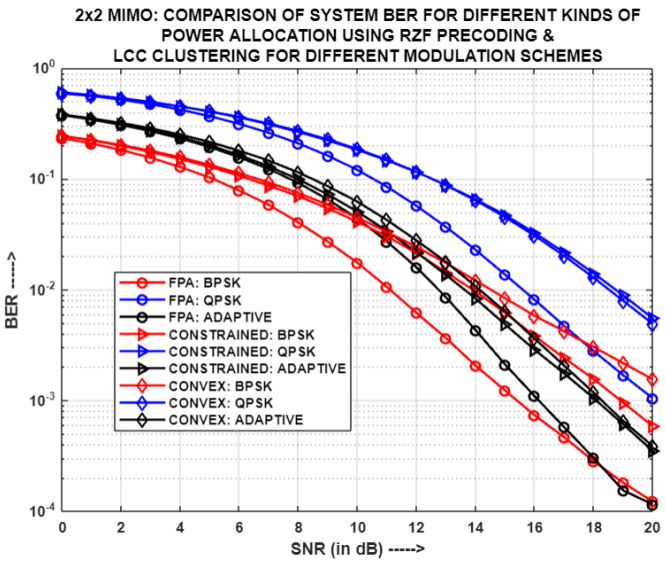

Fig.5.96: For (2x2)-MIMO-NOMA: Comparison of System BER for different power allocation strategies using RZF and LCC clustering

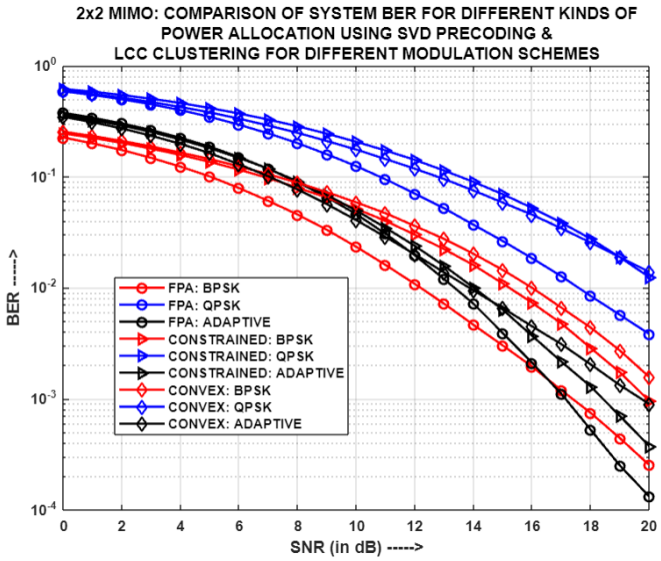

Fig.5.97: For (2x2)-MIMO-NOMA: Comparison of System BER for different power allocation strategies using SVD and LCC clustering

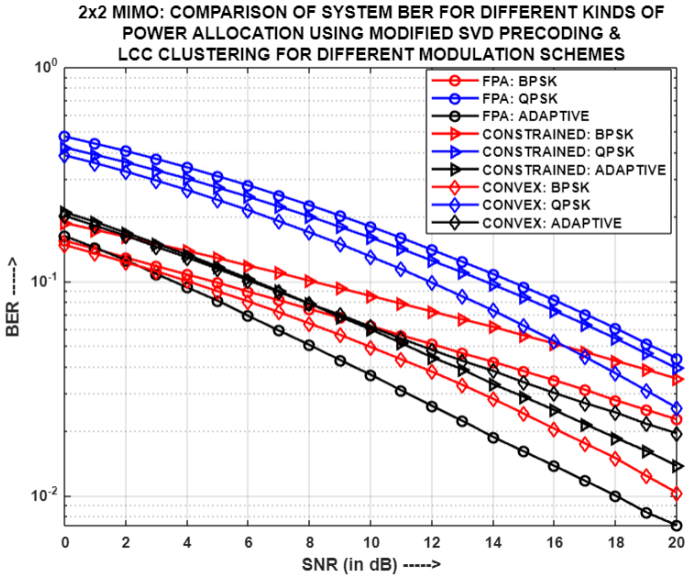

Fig.5.98: For (2x2)-MIMO-NOMA: Comparison of System BER for different power allocation strategies using MODIFIED SVD and LCC clustering

Fig.5.94, Fig.5.95, Fig.5.96, Fig.5.97 and Fig.5.98 depicts the comparison of system BER for different power allocation (PA) strategies using varied precoding techniques and LCC clustering, with each entity in the system having two antennas each. It has been noticed that for MF, FPA and COPA yield the least system BER for BPSK and Adaptive Modulation respectively. However, for QPSK, all the PA

mechanisms generate a merged system BER, implying comparable selection of power allocation coefficient sets, for the entire SNR range. It is worth emphasizing that in the scenarios involving ZF, RZF and SVD, FPA consistently achieves the lowest system BER across all modulation schemes respectively. Moreover, in the context of Adaptive modulation with ZF, both the COPA and CON-OPA strategies yield system BERs that are comparable to FPA. This similarity suggests that they select the same set of power allocation coefficients, leading to similar performance outcomes. However, in case of MODIFIED SVD, CON-OPA yields the least system BER for both BPSK and QPSK, while for Adaptive modulation scheme, FPA generates the lowest system BER. For all the above cases, the diverse selection of power allocation strategies, resulting in optimal performance for the same modulation scheme but different precoding techniques, can be attributed to the impact of the respective precoding techniques and the pairing scheme of users. In LCC, the users are paired based on both channel gain and channel correlation, whereby users with considerably different channel characteristics are usually paired. The pairing scheme of users plays a vital role as the COPA and CON-OPA mechanisms utilize the channel gain of these users to compute their throughputs and, consequently, the sum capacity of the respective clusters. This information is then employed to determine the suitable sets of power allocation coefficients for the user-pairs, through the particular algorithms.

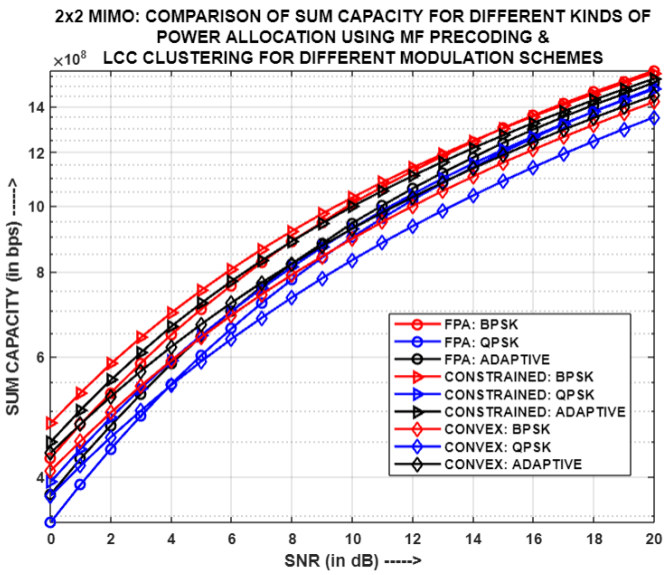

Fig.5.99: For (2x2)-MIMO-NOMA: Comparison of Sum Capacity for different power allocation strategies using MF and LCC clustering

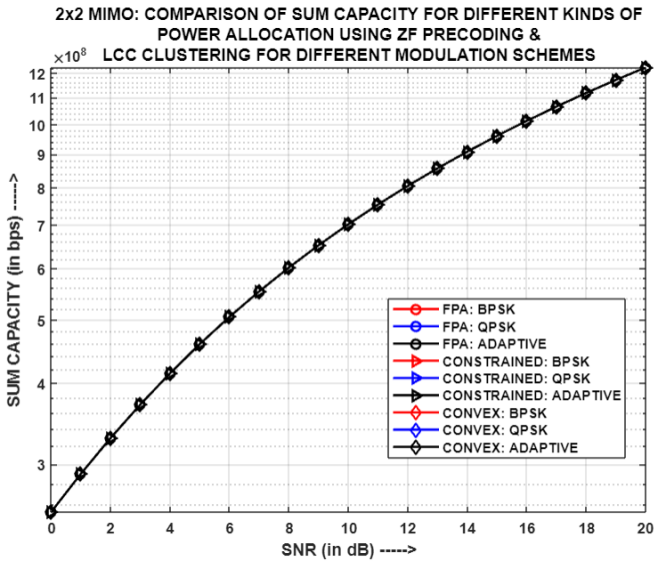

Fig.5.100: For (2x2)-MIMO-NOMA: Comparison of Sum Capacity for different power allocation strategies using ZF and LCC clustering

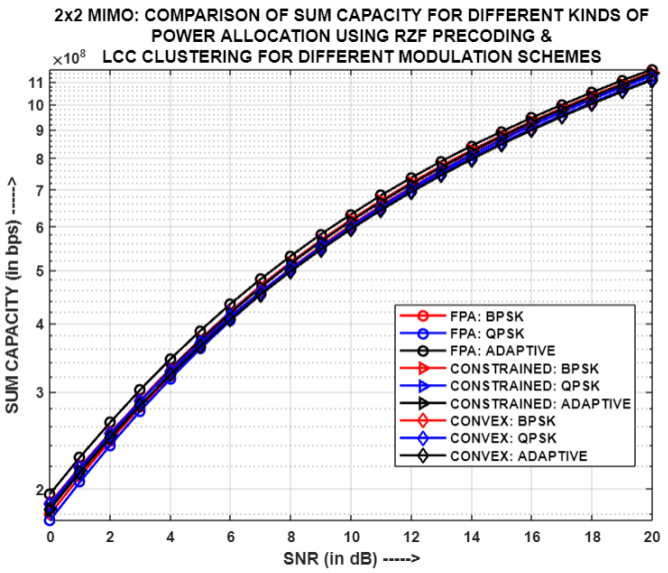

Fig.5.101: For (2x2)-MIMO-NOMA: Comparison of Sum Capacity for different power allocation strategies using RZF and LCC clustering

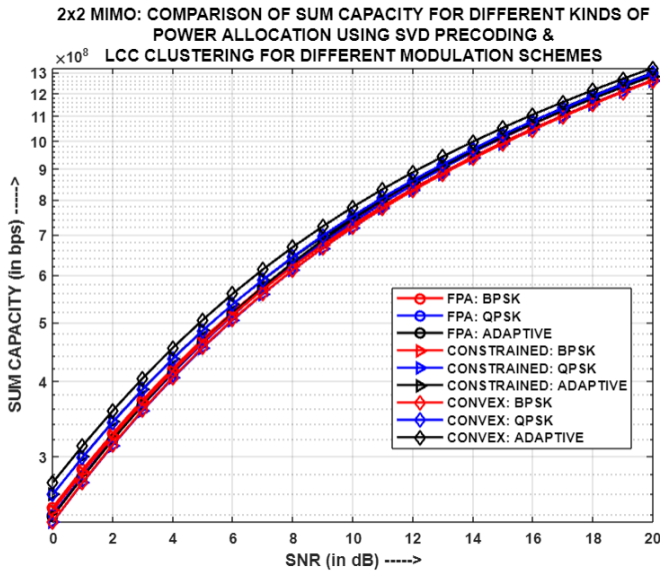

Fig.5.102: For (2x2)-MIMO-NOMA: Comparison of Sum Capacity for different power allocation strategies using SVD and LCC clustering

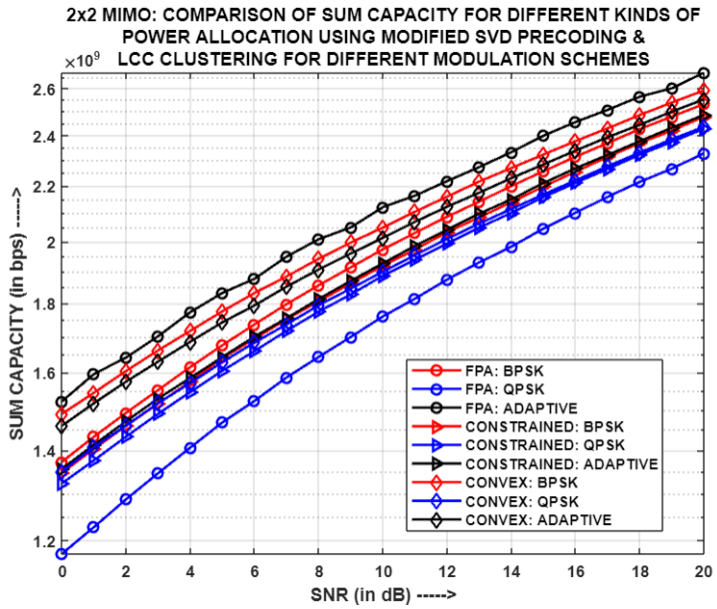

Fig.5.103: For (2x2)-MIMO-NOMA: Comparison of Sum Capacity for different power allocation strategies using MODIFIED SVD and LCC clustering

Fig.5.99, Fig.5.100, Fig.5.101, Fig.5.102 and Fig.5.103 displays the comparison of Sum Capacity for different power allocation strategies using varied precoding techniques and LCC clustering, with each entity in the system having two antennas each. The power allocation (PA) strategies employed for ZF, RZF, and SVD yield

comparable sum capacities. This alikeness arises primarily from the influence of the chosen precoding technique, the similarity in user channel gains, and the utilization of close enough power allocation coefficient sets across the different PA mechanisms. However, when it comes to MF, slight variations in sum capacities are observed among the different PA mechanisms and modulation schemes. This discrepancy is attributed to the usage of different sets of power coefficients by the various PA strategies across the entire SNR range. On the contrary, significant differences in sum capacities are observed for different PA schemes, when MODIFIED SVD precoding scheme is applied. This behavior can be explained by the selection of distinct sets of power coefficients for the diverse PA mechanisms and the incorporation of a gain matrix that affects both the precoding and post-coding matrices, leading to a noticeable impact on the resulting channel gain of the users. The design of amplification matrices depends on user clustering, which in turn influences their channel gain and throughput. As user throughput directly affects the overall total capacity, thus, variations in sum capacities arise when different PA techniques are applied with MODIFIED SVD. Thus, Adaptive modulation, along with FPA, produces the highest sum capacity for MODIFIED SVD.

5.3.8. Simulation Result Analysis of two-user (4x4)-MIMO-PD-NOMA model for different power allocation strategies and clustering methodologies:

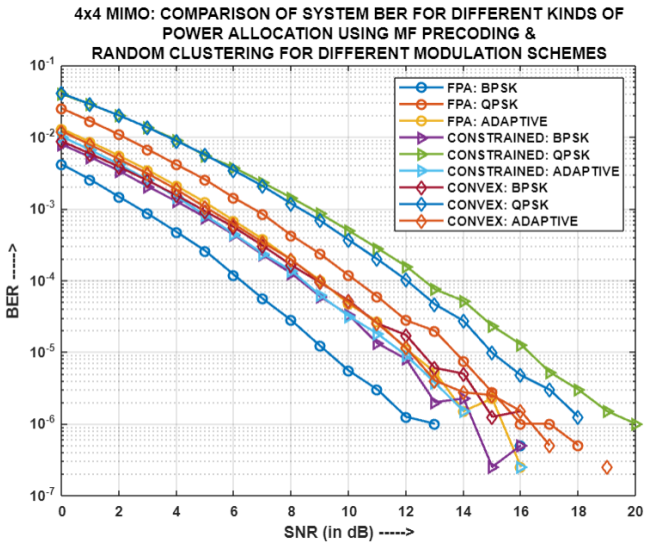

Fig.5.104: For (4x4)-MIMO-NOMA: Comparison of System BER for different power allocation strategies using MF and Random clustering

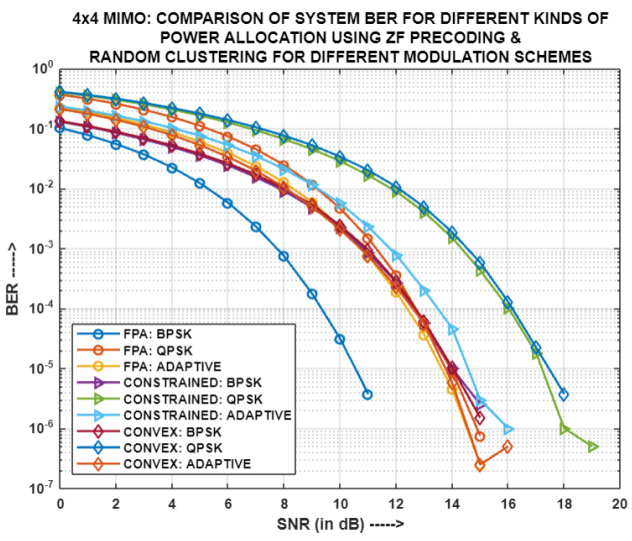

Fig.5.105: For (4x4)-MIMO-NOMA: Comparison of System BER for different power allocation strategies using ZF and Random clustering

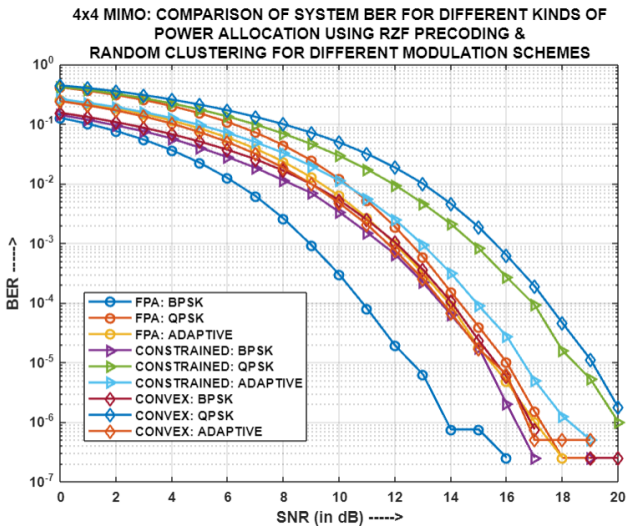

Fig.5.106: For (4x4)-MIMO-NOMA: Comparison of System BER for different power allocation strategies using RZF and Random clustering

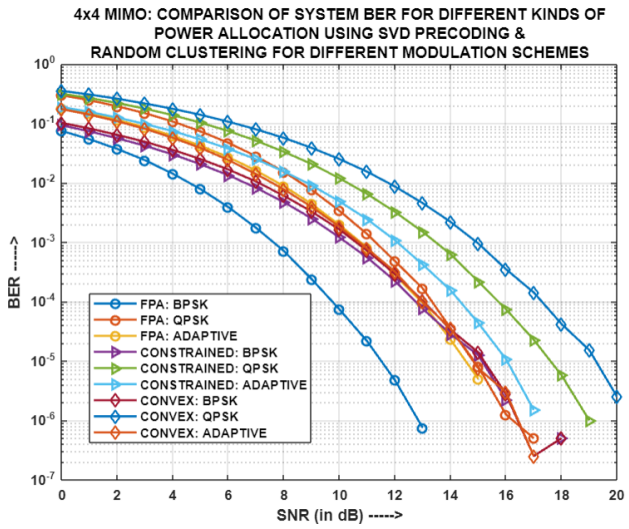

Fig.5.107: For (4x4)-MIMO-NOMA: Comparison of System BER for different power allocation strategies using SVD and Random clustering

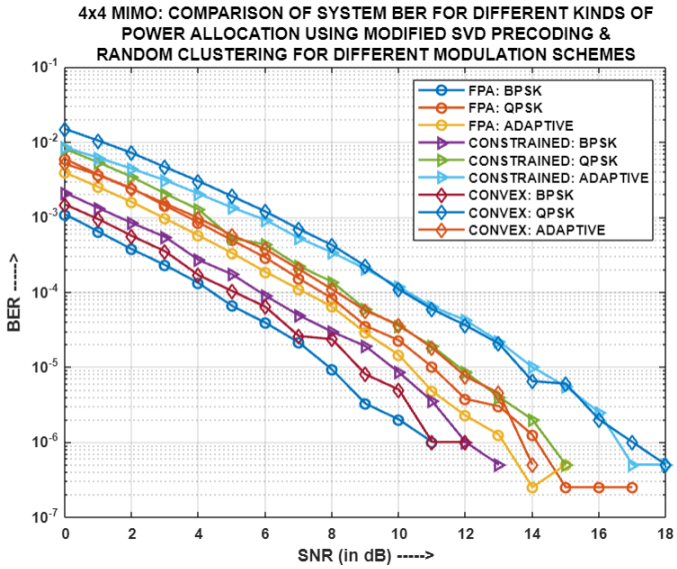

Fig.5.108: For (4x4)-MIMO-NOMA: Comparison of System BER for different power allocation strategies using MODIFIED SVD and Random clustering

Fig.5.104, Fig.5.105, Fig.5.106, Fig.5.107 and Fig.5.108 showcases the comparison of system BER for different power allocation (PA) strategies using varied precoding techniques and Random clustering, with each entity in the system having four antennas each. It has been observed that for MF, FPA gives better system BER performance for both BPSK and QPSK; while for Adaptive modulation, all the PA

strategies yield comparable system BERs. The merging of system BERs is because of the fact that the power allocation mechanisms happen to select the same power coefficient sets for the respective user-pairs in the system. In context of ZF, RZF and SVD, FPA produces the least system BER for BPSK and QPSK respectively. However, for Adaptive modulation, in case of ZF, RZF and SVD, all the PA strategies yield comparable system BERs. On the contrary, in regard to MODIFIED SVD, FPA achieves the least system BER for all the three modulation schemes respectively. For all the above cases, the reason behind different power allocation strategies producing optimum performance for the same modulation scheme but different precoding technique, is primarily because of the impact of the different precoding schemes as well as the manner in which the users are paired. In random clustering, users are paired in an arbitrary manner. As a result, there are instances where users with significantly different channel gains may be coincidentally paired. Conversely, there is also a possibility of grouping together users with similar channel characteristics. The pairing scheme of users is important as the COPA and CON-OPA mechanisms utilize the channel gain of these users in computing their throughputs and hence, the sum capacity of the respective clusters, to determine the suitable power allocation coefficient sets for them.

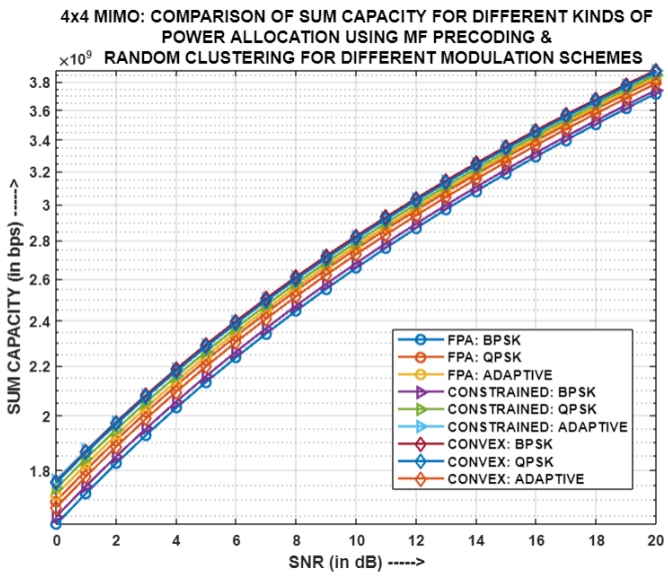

Fig.5.109: For (4x4)-MIMO-NOMA: Comparison of Sum Capacity for different power allocation strategies using MF and Random clustering

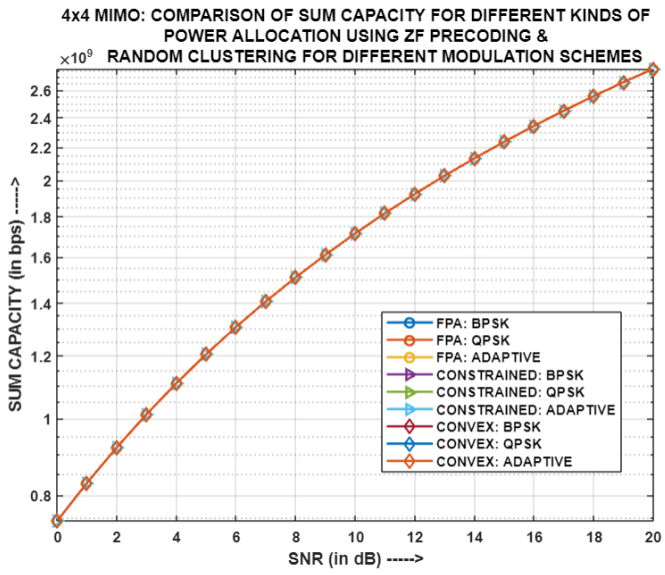

Fig.5.110: For (4x4)-MIMO-NOMA: Comparison of Sum Capacity for different power allocation strategies using ZF and Random clustering

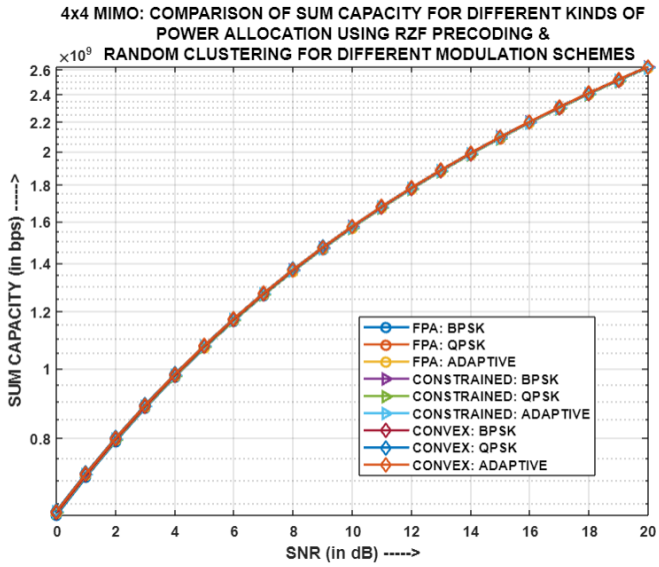

Fig.5.111: For (4x4)-MIMO-NOMA: Comparison of Sum Capacity for different power allocation strategies using RZF and Random clustering

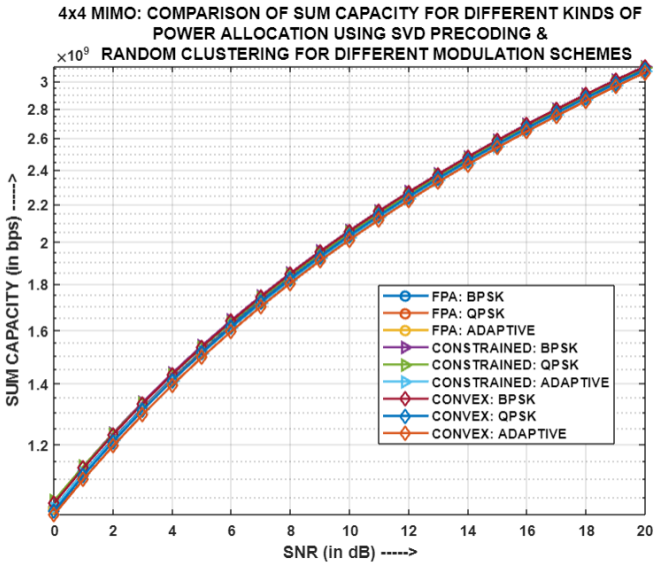

Fig.5.112: For (4x4)-MIMO-NOMA: Comparison of Sum Capacity for different power allocation strategies using SVD and Random clustering

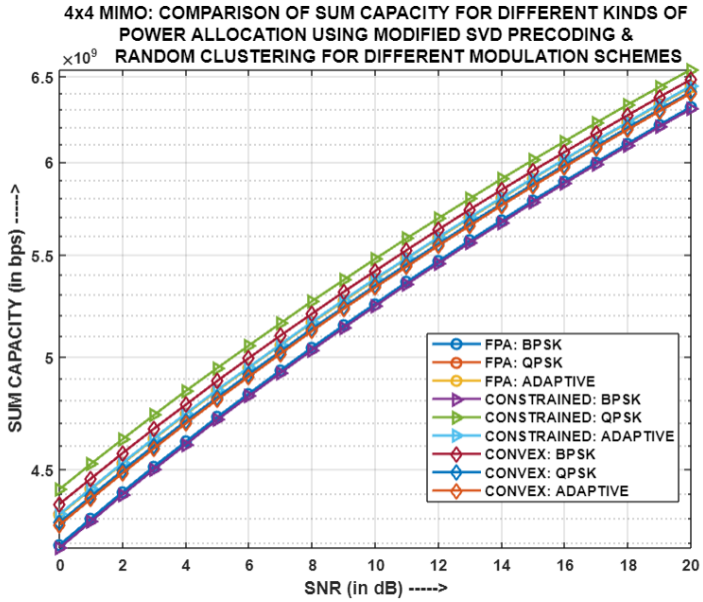

Fig.5.113: For (4x4)-MIMO-NOMA: Comparison of Sum Capacity for different power allocation strategies using MODIFIED SVD and Random clustering

Fig.5.109, Fig.5.110, Fig.5.111, Fig.5.112 and Fig.5.113 illustrates the comparison of Sum Capacity for different power allocation strategies using varied precoding techniques and Random clustering, with each entity in the system having

four antennas each. The power allocation (PA) strategies utilized for ZF, RZF, and SVD, respectively, generate comparable sum capacities. This is primarily due to the influence of the chosen precoding technique, alike user channel gains and the utilization of similar sets of power allocation coefficients across the different PA mechanisms. However, when it comes to MF, slightly contrasting sum capacities are observed among the different PA mechanisms and modulation schemes. This is because of the utilization of different sets of power coefficients by the varied PA strategies, across the entire SNR range. On the other hand, significant variations in sum capacities are witnessed for different PA schemes, when MODIFIED SVD is employed. The reason behind such behaviour attributes to the selection of differing sets of power coefficients by the varied PA mechanisms and also the incorporation of a gain matrix that affects both the precoding and post-coding matrices, resulting in a notable influence on the user's resultant channel gain. The design of amplification matrices depends on user clustering, which in turn affects their channel gain and throughput. Since user throughput directly impacts the overall sum capacity, hence, variations in sum capacities arise when different PA techniques are applied with MODIFIED SVD. Therefore, QPSK modulation, along with COPA, produces the highest sum capacity for MODIFIED SVD.

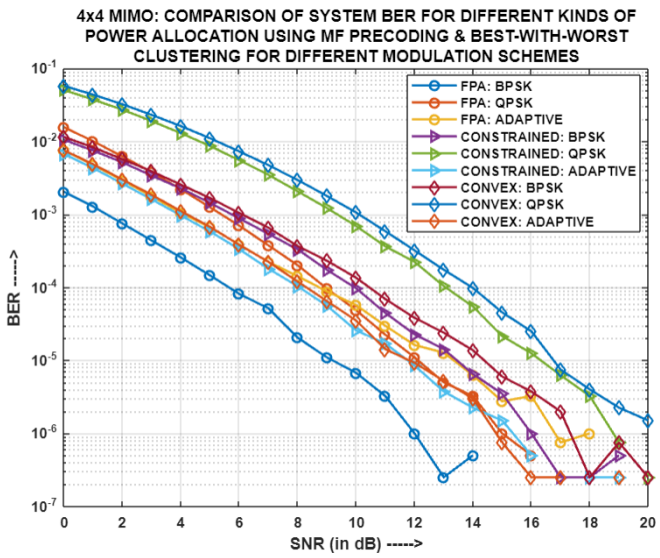

Fig.5.114: For (4x4)-MIMO-NOMA: Comparison of System BER for different power allocation strategies using MF and BWW clustering

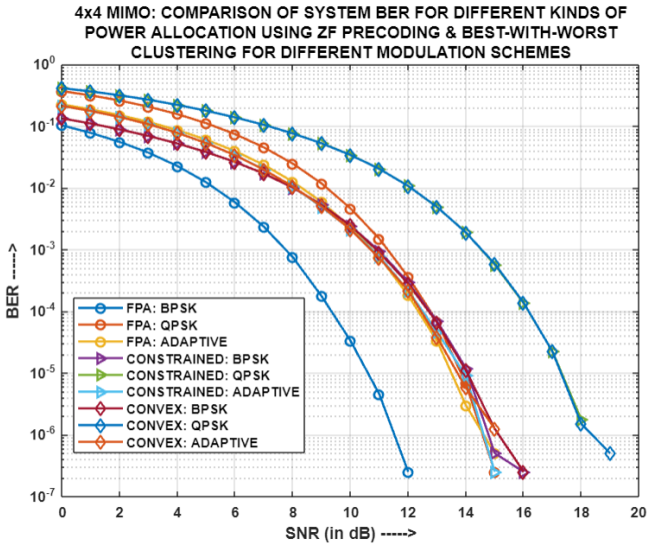

Fig.5.115: For (4x4)-MIMO-NOMA: Comparison of System BER for different power allocation strategies using ZF and BWW clustering

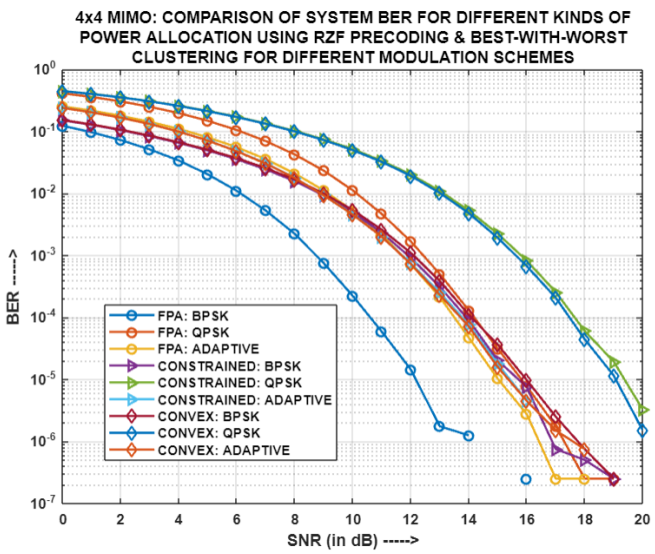

Fig.5.116: For (4x4)-MIMO-NOMA: Comparison of System BER for different power allocation strategies using RZF and BWW clustering

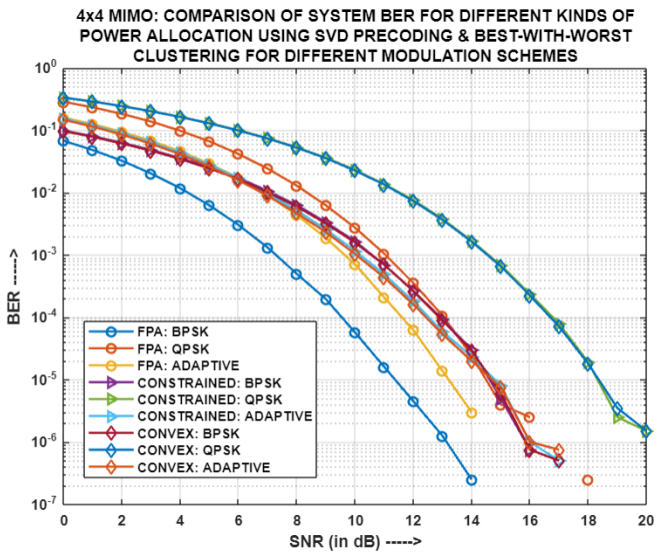

Fig.5.117: For (4x4)-MIMO-NOMA: Comparison of System BER for different power allocation strategies using SVD and BWW clustering

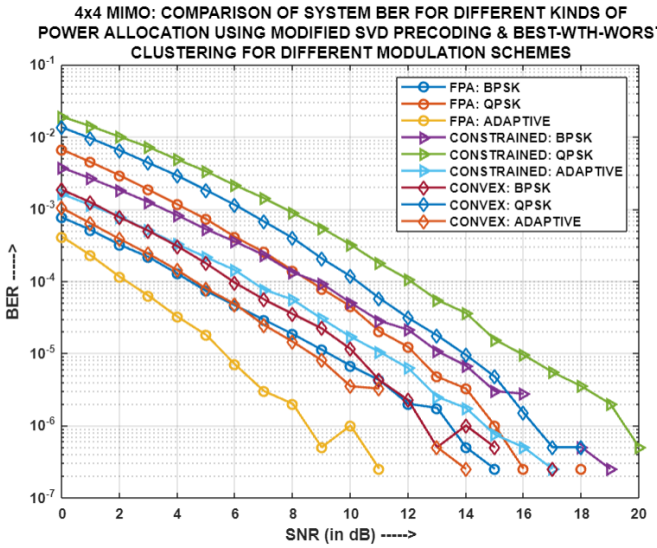

Fig.5.118: For (4x4)-MIMO-NOMA: Comparison of System BER for different power allocation strategies using MODIFIED SVD and BWW clustering

Fig.5.114, Fig.5.115, Fig.5.116, Fig.5.117 and Fig.5.118 depicts the comparison of system BER for different power allocation strategies using varied precoding techniques and BWW clustering, with each entity in the system having four antennas each. It is noticeable that for MF, FPA produces the optimum system BER for BPSK and QPSK respectively; while COPA and CON-OPA yield merged

but least system BERs for Adaptive modulation. The merging of system BERs is because of the fact that both the power allocation mechanisms happen to dynamically select the same power coefficient sets for the respective user-pairs in the system. It is worth highlighting that in the case of ZF and RZF, FPA consistently achieves the lowest system BER for BPSK and QPSK respectively. Furthermore, when it comes to Adaptive modulation with ZF and RZF, both the COPA and CON-OPA strategies produce system BERs that are comparable to FPA. This suggests that they select the similar set of power allocation coefficients, for the entire SNR range, resulting in similar performance. On the contrary, for SVD and MODIFIED SVD, FPA generates the least system BER for all the modulation schemes respectively. The differing power allocation strategies leading to optimal performance for the same modulation scheme, but with different precoding techniques, in the above mentioned cases, can be attributed to the combined influence of the respective precoding techniques and the pairing scheme of users. In BWW clustering, users are paired based on having significantly different channel gains. However, there are instances where the difference in channel gains between paired users is nominal. The pairing scheme of users play a crucial role as the COPA and CON-OPA mechanisms utilize the channel gain of these users to calculate their throughputs and, consequently, the sum capacity of the respective clusters. This information is then employed to determine the suitable sets of power allocation coefficients for the user-pairs.

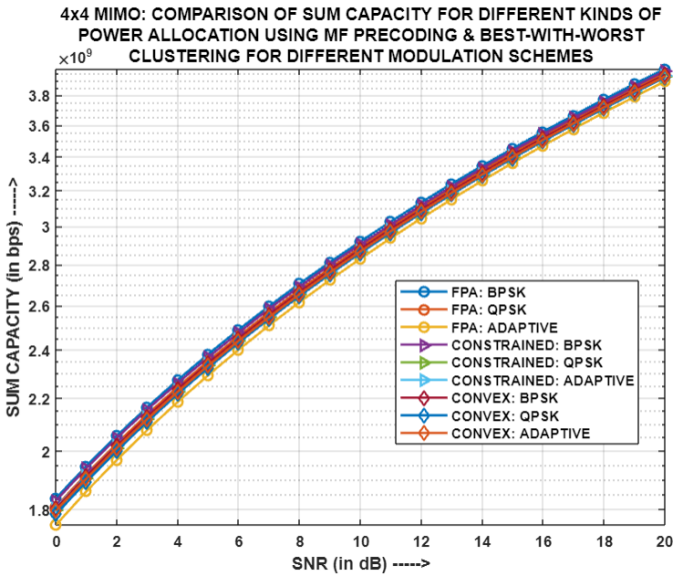

Fig.5.119: For (4x4)-MIMO-NOMA: Comparison of Sum Capacity for different power allocation strategies using MF and BWW clustering

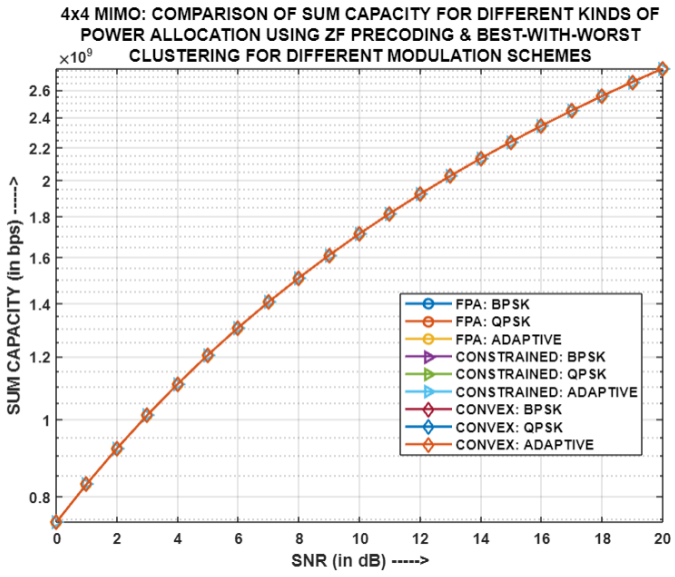

Fig.5.120: For (4x4)-MIMO-NOMA: Comparison of Sum Capacity for different power allocation strategies using ZF and BWW clustering

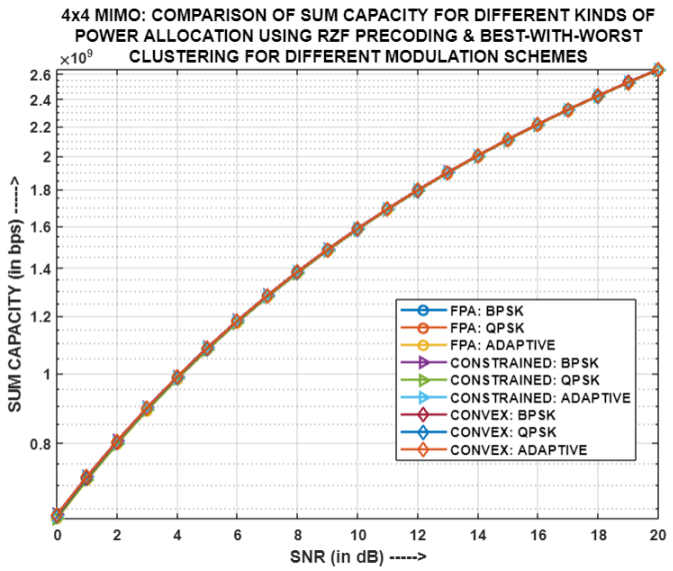

Fig.5.121: For (4x4)-MIMO-NOMA: Comparison of Sum Capacity for different power allocation strategies using RZF and BWW clustering

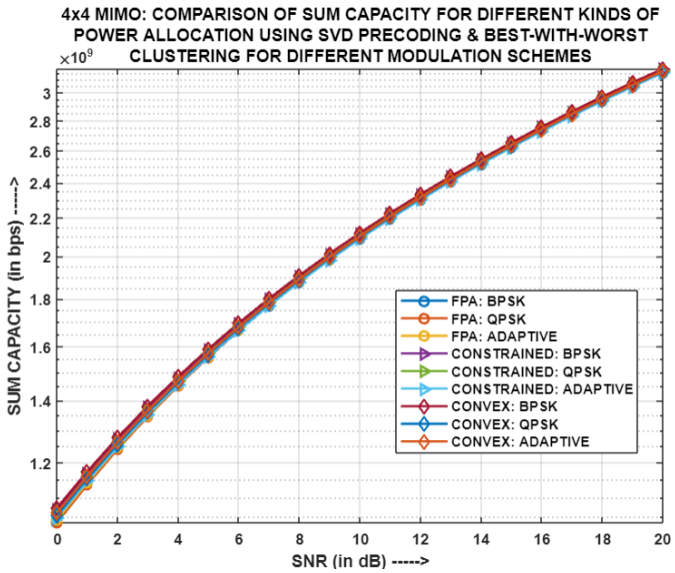

Fig.5.122: For (4x4)-MIMO-NOMA: Comparison of Sum Capacity for different power allocation strategies using SVD and BWW clustering

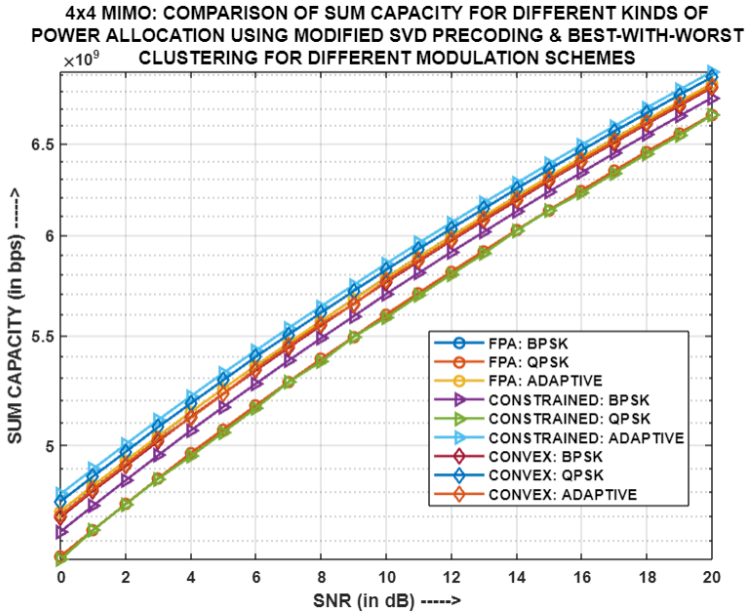

Fig.5.123: For (4x4)-MIMO-NOMA: Comparison of Sum Capacity for different power allocation strategies using MODIFIED SVD and BWW clustering

Fig.5.119, Fig.5.120, Fig.5.121, Fig.5.122 and Fig.5.123 presents the comparison of Sum Capacity for different power allocation strategies using varied precoding techniques and BWW clustering, with each entity in the system having

four antennas each. The power allocation (PA) strategies employed for ZF, RZF, and SVD, respectively, yield comparable sum capacities. This similarity is primarily due to the influence of the chosen precoding technique, alike user channel gains, and the utilization of almost similar sets of power allocation coefficients across the various PA mechanisms. However, when it comes to MF, slight variations in total capacities are observed among the different PA mechanisms and modulation schemes. This can be attributed to the utilization of different sets of power coefficients by the diverse PA strategies across the entire SNR range. On the other hand, significant variations in sum capacities are observed for different PA schemes, when MODIFIED SVD precoding is used. This behavior is due to the selection of different sets of power coefficients by the various PA mechanisms, as well as the incorporation of a gain matrix that impacts both the precoding and post-coding matrices, leading to a notable influence on the resulting channel gain of the users. The design of amplification matrices depends on user clustering, which in turn affects their channel gain and throughput. Since user throughput directly affects the overall sum capacity, therefore, variations in sum capacities arise when different PA techniques are applied with MODIFIED SVD. Thus, Adaptive and QPSK modulations, along with COPA and CON-OPA respectively, produces merged and highest sum capacity for MODIFIED SVD. The merging of sum capacities is attributed to comparable user-pairing, alike user channel gains and selection of similar power coefficient sets, for the respective clusters, by the particular PA mechanisms.

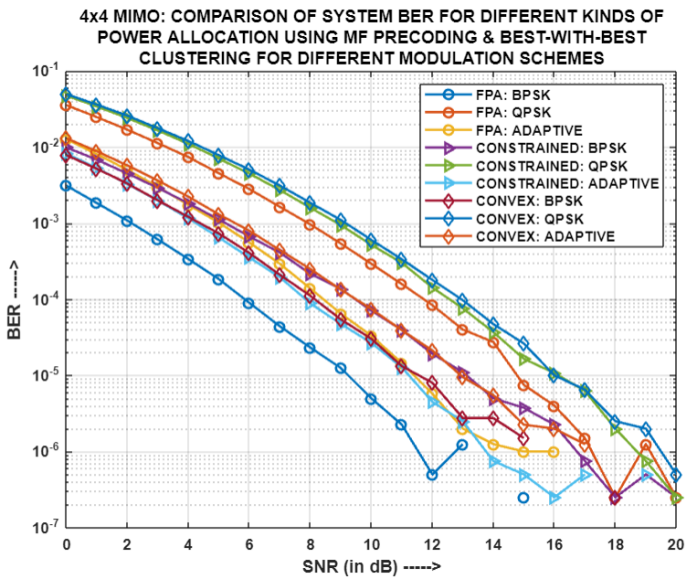

Fig.5.124: For (4x4)-MIMO-NOMA: Comparison of System BER for different power allocation strategies using MF and BWB clustering

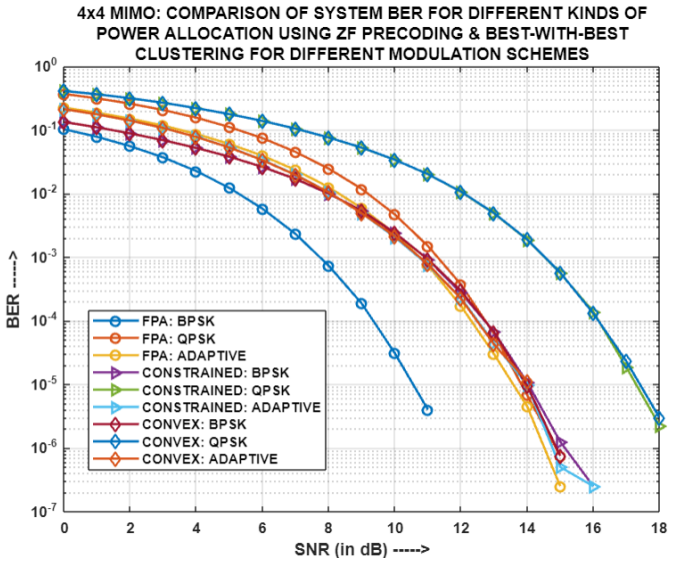

Fig.5.125: For (4x4)-MIMO-NOMA: Comparison of System BER for different power allocation strategies using ZF and BWB clustering

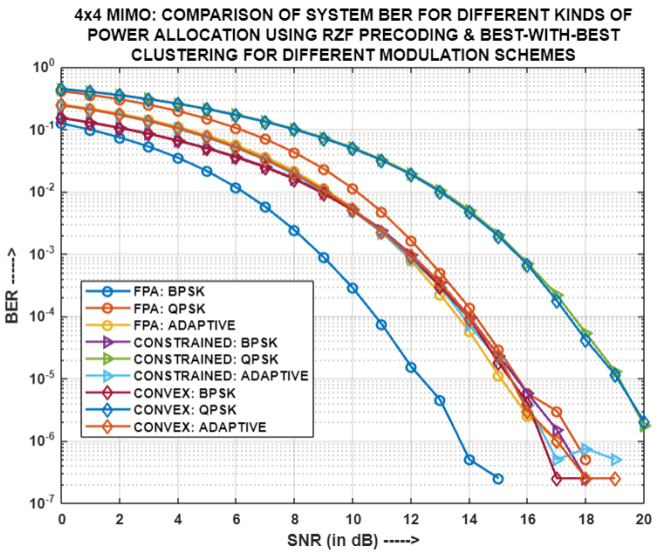

Fig.5.126: For (4x4)-MIMO-NOMA: Comparison of System BER for different power allocation strategies using RZF and BWB clustering

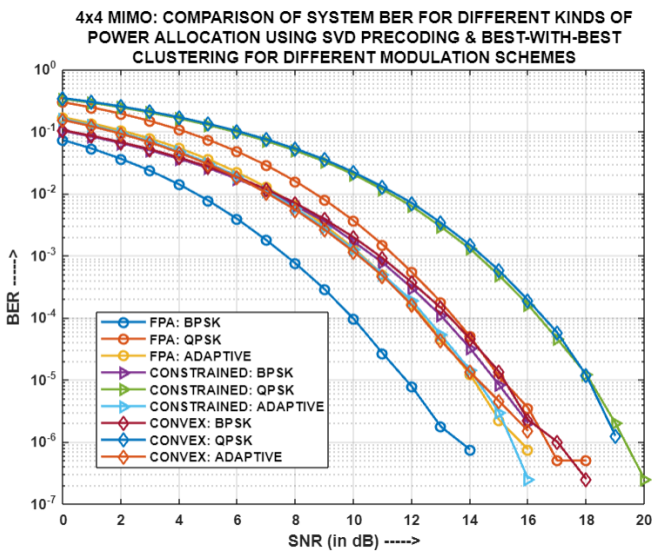

Fig.5.127: For (4x4)-MIMO-NOMA: Comparison of System BER for different power allocation strategies using SVD and BWB clustering

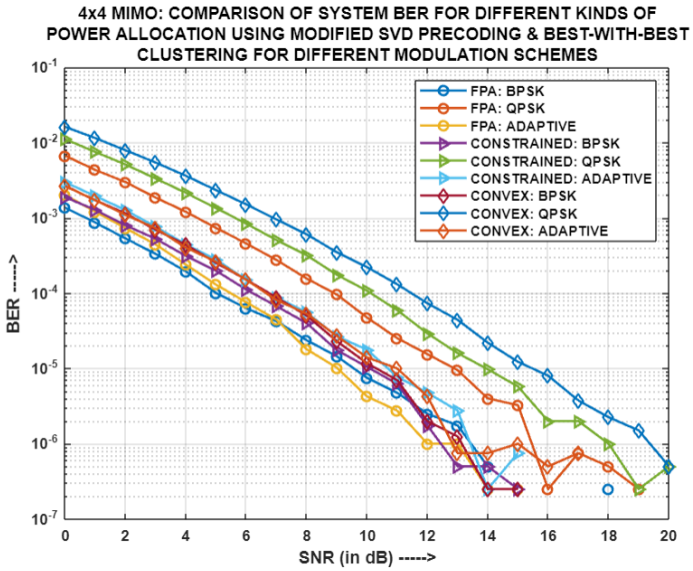

Fig.5.128: For (4x4)-MIMO-NOMA: Comparison of System BER for different power allocation strategies using MODIFIED SVD and BWB clustering

Fig.5.124, Fig.5.125, Fig.5.126, Fig.5.127 and Fig.5.128 displays the comparison of system BER for different power allocation (PA) strategies using varied precoding techniques and BWB clustering, with each entity in the system having four antennas

each. It can be seen that for MF, when employing BPSK and QPSK modulations, FPA yields the least system BER respectively; while for Adaptive modulation scheme, FPA and COPA generate a merged least system BER for BPSK. The convergence of system BERs occur because the COPA mechanism coincidentally selects the same power coefficient sets for the corresponding user-pairs in the system, as used by FPA. It is important to highlight that in the case of ZF, RZF, SVD and MODIFIED SVD, FPA consistently achieves the lowest system BER for BPSK and QPSK modulation schemes respectively. Additionally, when it comes to Adaptive modulation for the above-mentioned precoding schemes respectively, all the PA strategies yield comparable system BERs. This suggests that they select the same power allocation coefficient sets, for the entire SNR range, resulting in similar performance. Based on the above-mentioned cases, it can be culminated that the variation in power allocation strategies, leading to optimal performance for the same modulation scheme but with different precoding techniques, can be credited to the joint influence of the specific precoding technique and the pairing scheme of users. In case of BWB clustering, users are paired based on the decreasing order of consecutive channel gains. As a result, the pairing outcome is such that there can be instances where paired users have either a significant difference or a minimal difference in their channel gains. This variability is determined by the channel characteristics at a given moment. The pairing scheme of users play a critical role in this context, as the COPA and CON-OPA mechanisms utilize the channel gain of the users to calculate their throughputs and, subsequently, the sum capacity of the clusters. This information is then used by the respective algorithms to determine the appropriate sets of power allocation coefficients for the user-pairs.

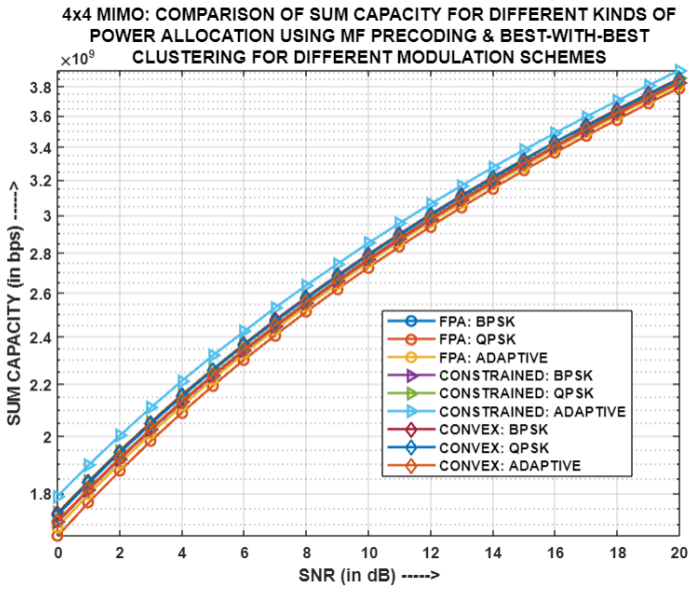

Fig.5.129: For (4x4)-MIMO-NOMA: Comparison of Sum Capacity for different power allocation strategies using MF and BWB clustering

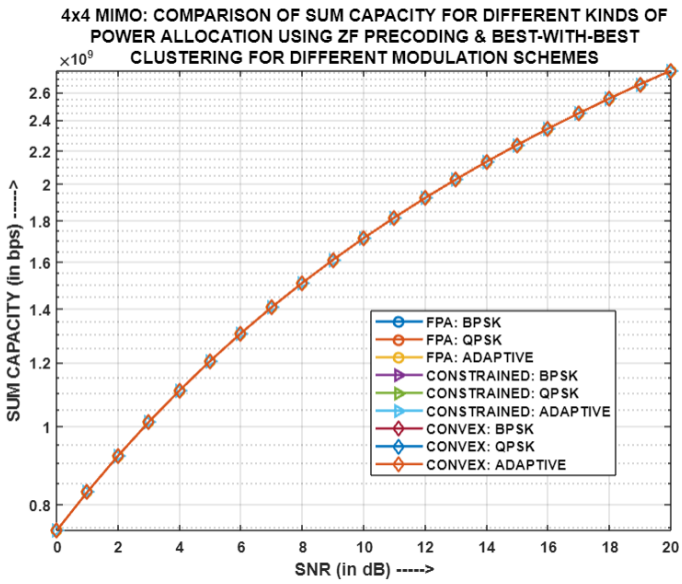

Fig.5.130: For (4x4)-MIMO-NOMA: Comparison of Sum Capacity for different power allocation strategies using ZF and BWB clustering

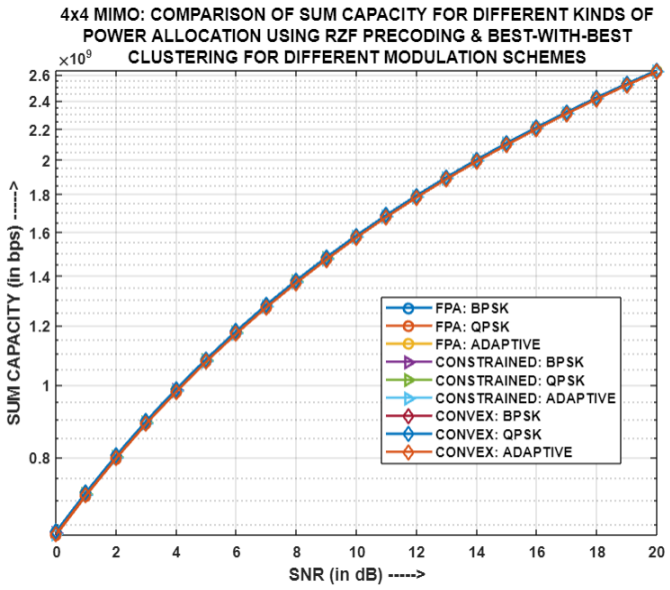

Fig.5.131: For (4x4)-MIMO-NOMA: Comparison of Sum Capacity for different power allocation strategies using RZF and BWB clustering

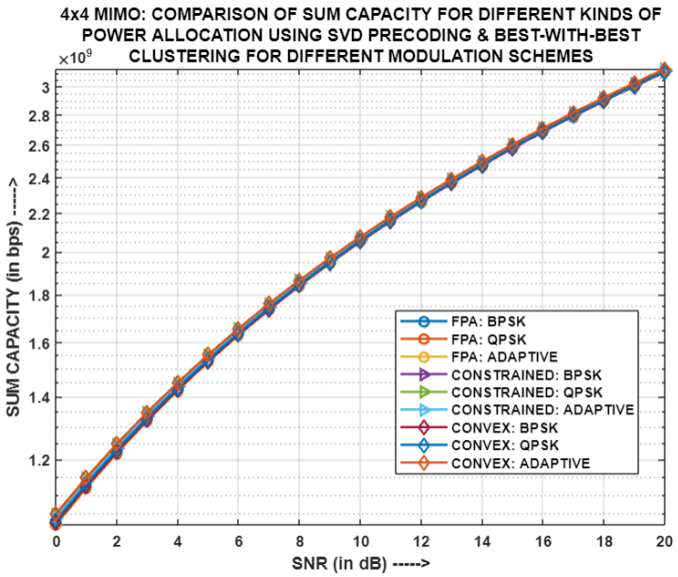

Fig.5.132: For (4x4)-MIMO-NOMA: Comparison of Sum Capacity for different power allocation strategies using SVD and BWB clustering

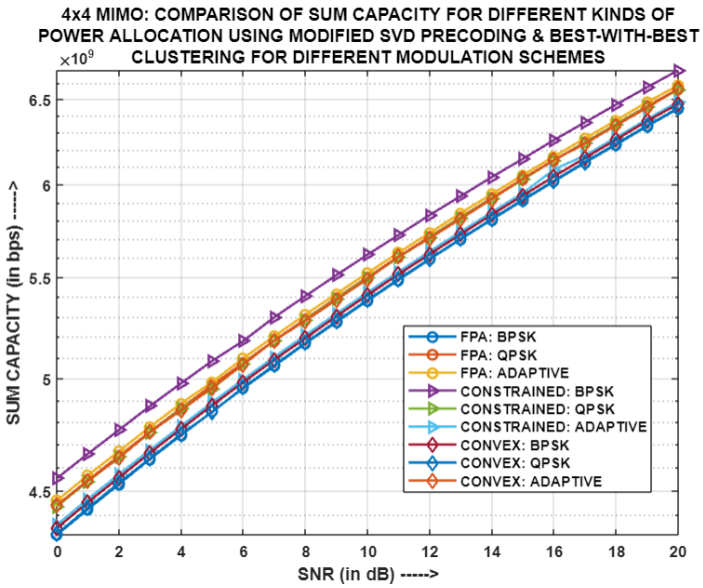

Fig.5.133: For (4x4)-MIMO-NOMA: Comparison of Sum Capacity for different power allocation strategies using MODIFIED SVD and BWB clustering

Fig.5.129, Fig.5.130, Fig.5.131, Fig.5.132 and Fig.5.133 showcases the comparison of Sum Capacity for different power allocation strategies using varied precoding techniques and BWB clustering, with each entity in the system having four antennas each. The power allocation (PA) strategies employed for ZF, RZF, and SVD, respectively, yield comparable sum capacities. This is mainly due to the impact of the chosen precoding technique, the similarity in user channel gains, and the use of alike sets of power allocation coefficients across the different PA mechanisms. However, when it comes to MF, slight differences in sum capacities are observed among the various PA mechanisms and modulation schemes. This is because each PA strategy employs different sets of power coefficients across the entire SNR range. On the contrary, noteworthy variations in sum capacities are observed when MODIFIED SVD is used with different PA schemes. This behavior can be attributed to the selection of distinct power coefficient sets by the diverse PA mechanisms, as well as the incorporation of a gain matrix that affects both the precoding and post-coding matrices, leading to a notable influence on the resulting channel gain for each user. The design of amplification matrices depends on user clustering, which in turn impacts their channel gain and throughput. As user throughput directly affects the overall sum capacity, hence, variations in sum capacities arise when different PA techniques are applied with MODIFIED SVD.

Thus, COPA yields the highest sum capacity for BPSK modulation, employing the aforementioned precoding scheme.

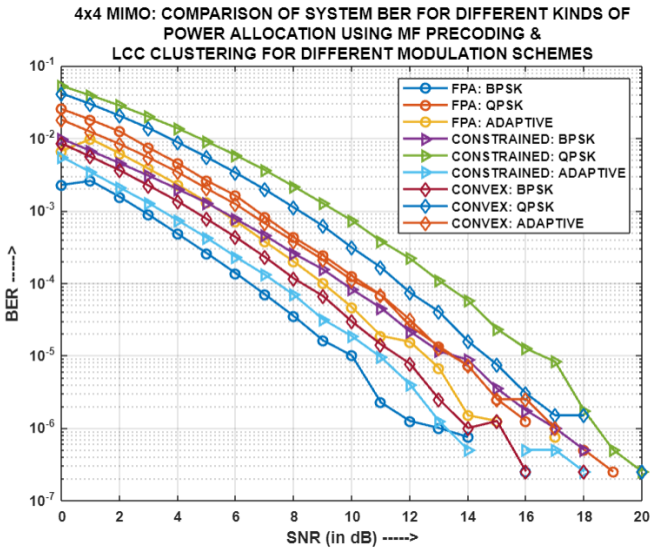

Fig.5.134: For (4x4)-MIMO-NOMA: Comparison of System BER for different power allocation strategies using MF and LCC clustering

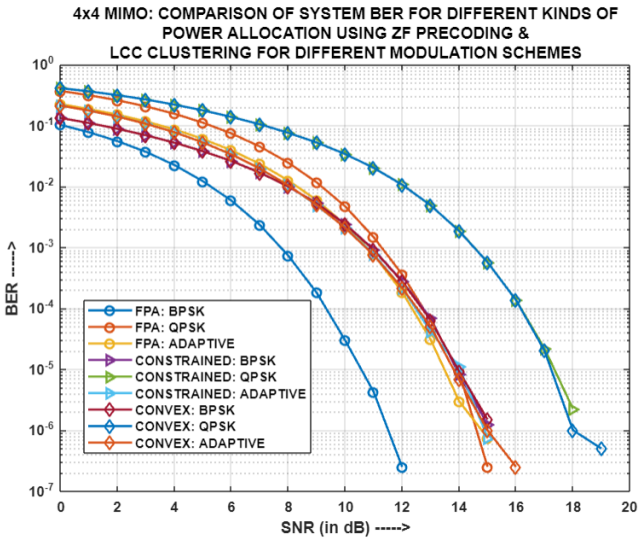

Fig.5.135: For (4x4)-MIMO-NOMA: Comparison of System BER for different power allocation strategies using ZF and LCC clustering

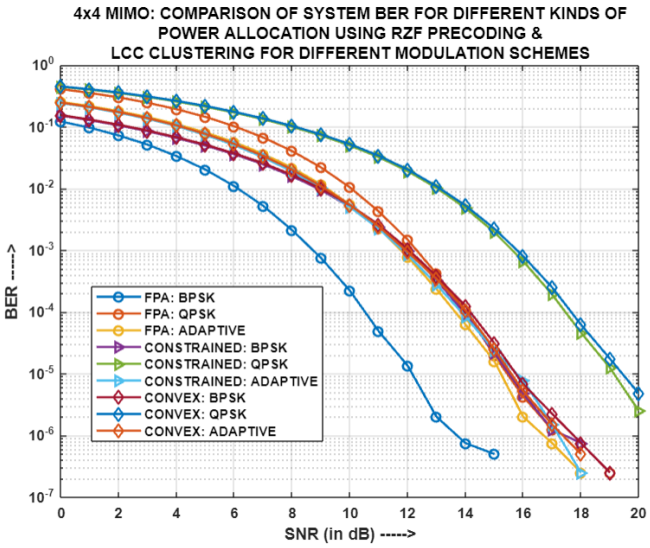

Fig.5.136: For (4x4)-MIMO-NOMA: Comparison of System BER for different power allocation strategies using RZF and LCC clustering

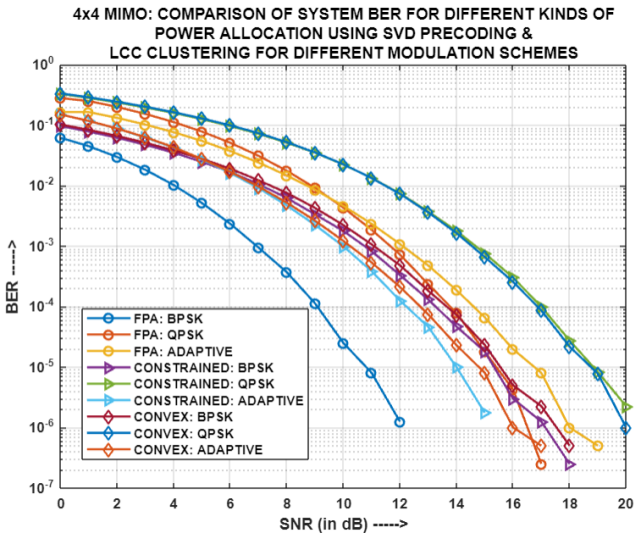

Fig.5.137: For (4x4)-MIMO-NOMA: Comparison of System BER for different power allocation strategies using SVD and LCC clustering

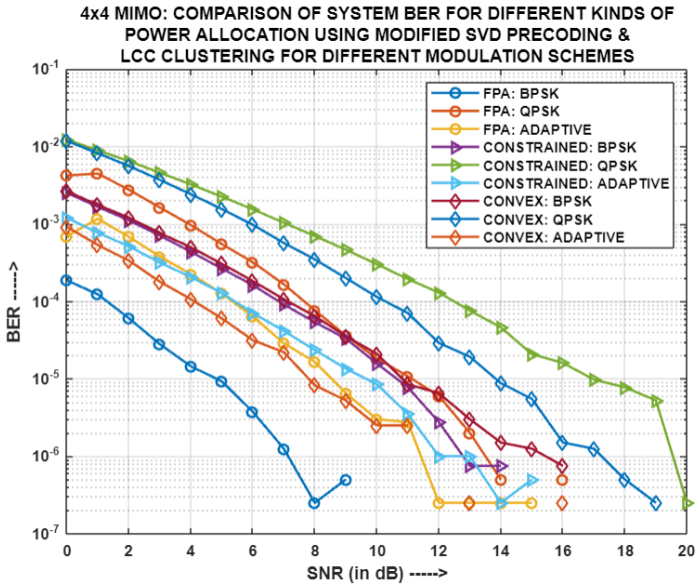

Fig.5.138: For (4x4)-MIMO-NOMA: Comparison of System BER for different power allocation strategies using MODIFIED SVD and LCC clustering

Fig.5.134, Fig.5.135, Fig.5.136, Fig.5.137 and Fig.5.138 represents the comparison of system BER for different power allocation strategies using varied precoding techniques and LCC clustering, with each entity in the system having four antennas each. It has been interesting to observe that for MF and SVD, FPA yields the least system BER for BPSK and QPSK respectively; while COPA generates the lowest system BER for Adaptive modulation. It is noteworthy that in the scenarios involving ZF and RZF, FPA consistently achieves the lowest system BER across all modulation schemes respectively. Moreover, in the context of Adaptive modulation with ZF and RZF, both the COPA and CON-OPA strategies yield system BERs that are comparable to FPA. This similarity suggests that they dynamically select the same set of power allocation coefficients, leading to similar performance outcomes. However, in case of MODIFIED SVD, FPA yields the least system BER for both BPSK and QPSK respectively; while for Adaptive modulation scheme, CON-OPA generates the lowest system BER. The varying selection of power allocation strategies, leading to optimal performance for the same modulation scheme but different precoding techniques in the aforementioned cases, can be attributed to the influence of the respective precoding techniques and the pairing scheme of users. In LCC clustering, users are paired based on both their channel gain and channel correlation, resulting in the pairing of users with significantly different channel

characteristics. The pairing scheme of users plays a crucial role as the COPA and CON-OPA mechanisms utilize the channel gain of these users to calculate their throughputs and, hence, the sum capacity of the respective clusters. This information is then utilized by the specific algorithms to determine the appropriate sets of power allocation coefficients for the user-pairs.

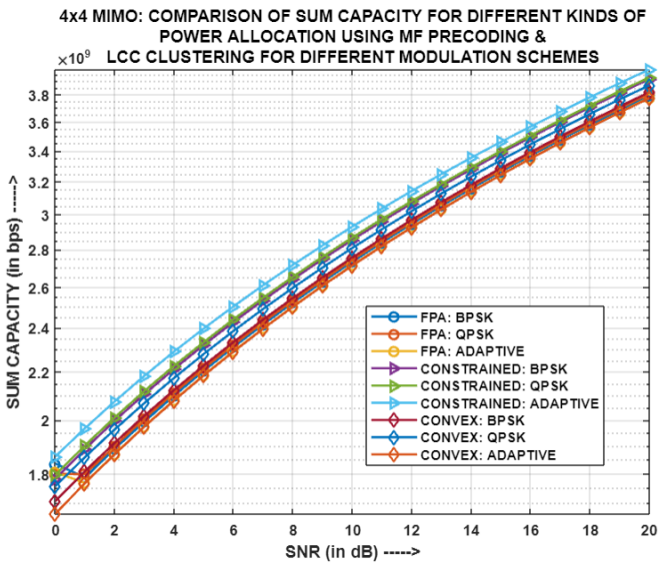

Fig.5.139: For (4x4)-MIMO-NOMA: Comparison of Sum Capacity for different power allocation strategies using MF and LCC clustering

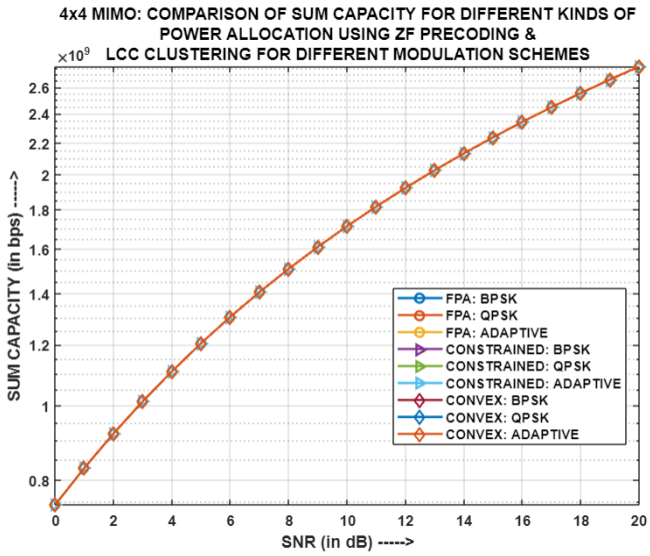

Fig.5.140: For (4x4)-MIMO-NOMA: Comparison of Sum Capacity for different power allocation strategies using ZF and LCC clustering

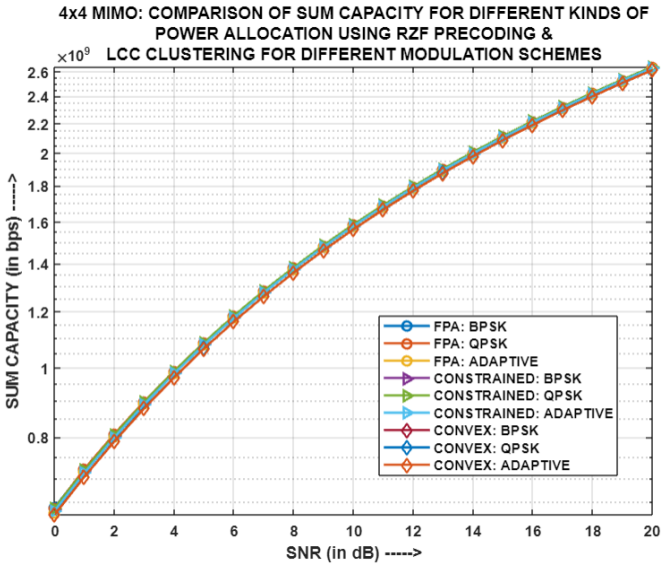

Fig.5.141: For (4x4)-MIMO-NOMA: Comparison of Sum Capacity for different power allocation strategies using RZF and LCC clustering

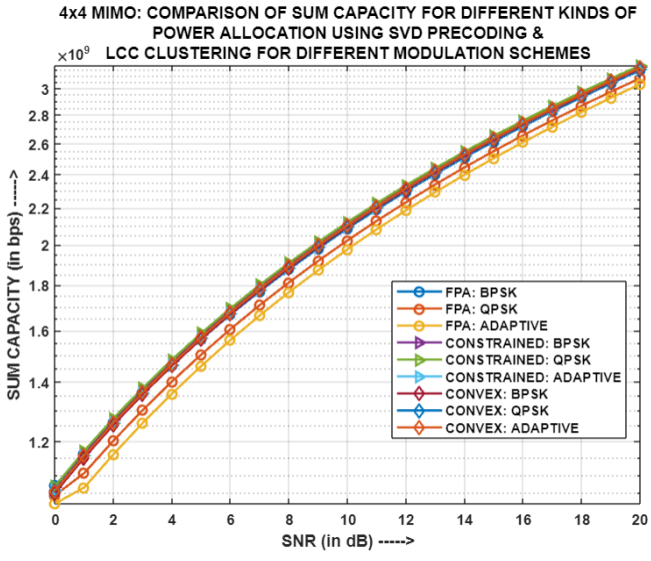

Fig.5.142: For (4x4)-MIMO-NOMA: Comparison of Sum Capacity for different power allocation strategies using SVD and LCC clustering

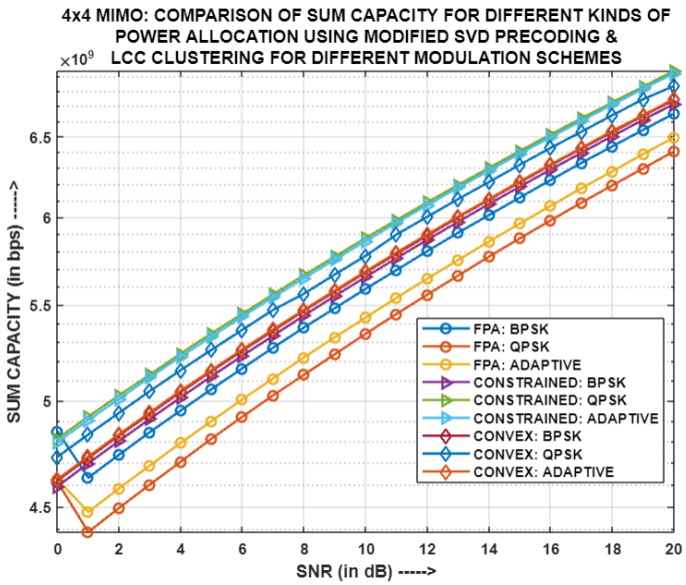

Fig.5.143: For (4x4)-MIMO-NOMA: Comparison of Sum Capacity for different power allocation strategies using MODIFIED SVD and LCC clustering

Fig.5.139, Fig.5.140, Fig.5.141, Fig.5.142 and Fig.5.135 depicts the comparison of Sum Capacity for different power allocation strategies using varied precoding techniques and LCC clustering, with each entity in the system having four antennas each. The power allocation (PA) strategies employed for ZF, RZF, and SVD yield comparable sum capacities. This alikeness arises primarily from the influence of the chosen precoding technique, the similarity in user channel gains, and the utilization of close enough power allocation coefficient sets across the different PA mechanisms. However, when it comes to MF, slight variations in sum capacities are observed among the different PA mechanisms and modulation schemes. This discrepancy is attributed to the usage of different sets of power coefficients by the various PA strategies across the entire SNR range. On the contrary, significant differences in sum capacities are observed for different PA schemes, when MODIFIED SVD precoding scheme is utilized. This behavior can be explained by the selection of distinct sets of power coefficients for the diverse PA mechanisms and the incorporation of a gain matrix that affects both the precoding and post-coding matrices, leading to a noticeable impact on the resulting channel gain of the users. The design of amplification matrices depends on user clustering, which in turn influences their channel gain and throughput. As user throughput directly affects the overall total capacity, thus, variations in sum capacities arise when different PA

techniques are applied with MODIFIED SVD. Thus, QPSK and Adaptive modulation schemes, along with COPA respectively, produces merged but highest sum capacity for MODIFIED SVD. The merging of sum capacities is because of comparable user-pairing, alike user channel gains and selection of similar power coefficient sets, for the respective clusters, by the particular PA mechanisms.

5.3.9. Comparative Analysis of simulation results of two-user (2x2) and (4x4) MIMO-PD-NOMA models for different clustering methodologies, modulation schemes and power allocation strategies:

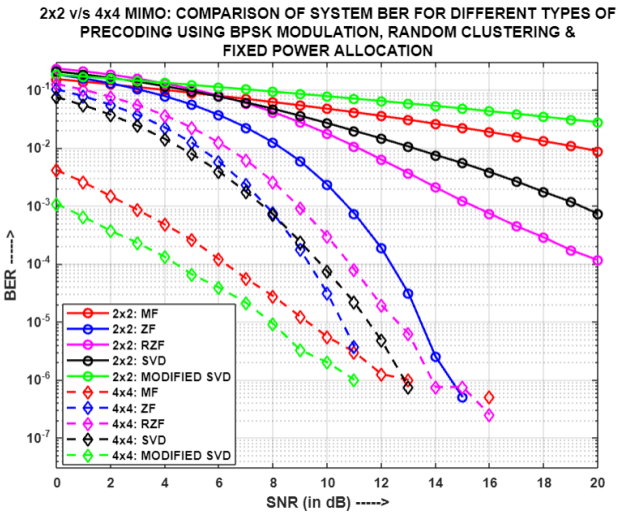

Fig.5.144: (2x2) v/s (4X4) MIMO-NOMA: Comparison of System BER for different precoding schemes using BPSK, Random clustering and FPA

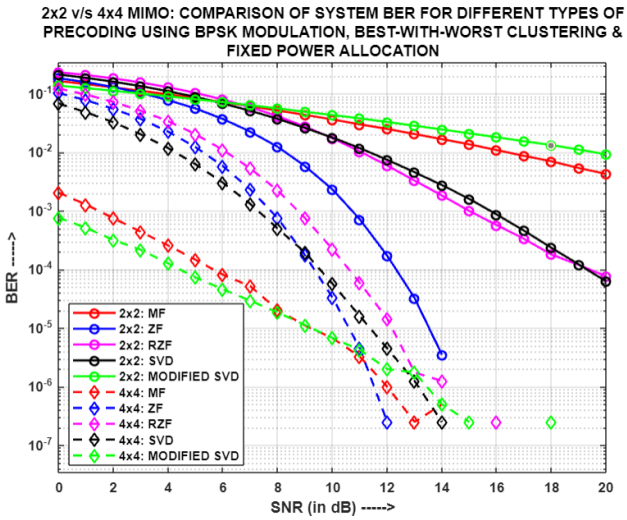

Fig.5.145: (2x2) v/s (4X4) MIMO-NOMA: Comparison of System BER for different precoding schemes using BPSK, BWW clustering and FPA

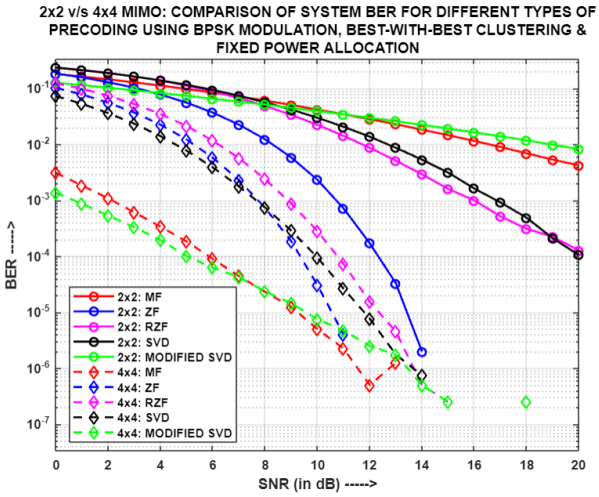

Fig.5.146: (2x2) v/s (4X4) MIMO-NOMA: Comparison of System BER for different precoding schemes using BPSK, BWB clustering and FPA

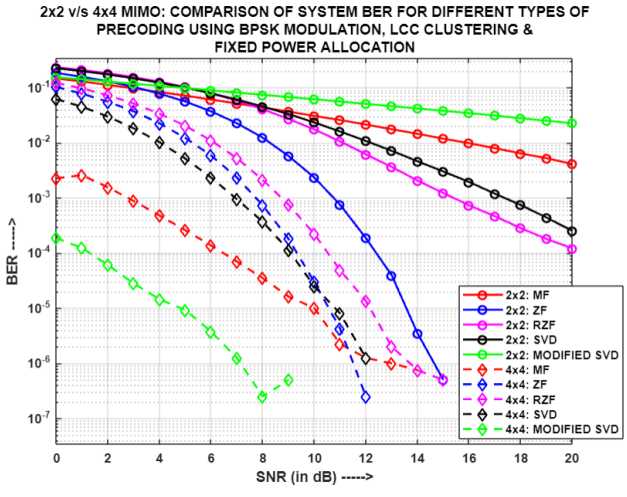

Fig.5.147: (2x2) v/s (4X4) MIMO-NOMA: Comparison of System BER for different precoding schemes using BPSK, LCC clustering and FPA

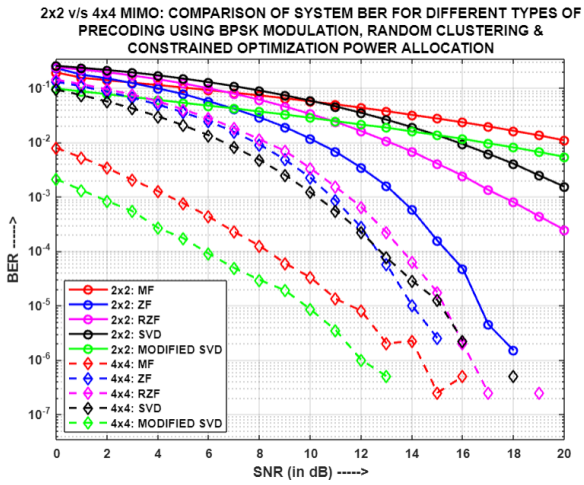

Fig.5.148: (2x2) v/s (4X4) MIMO-NOMA: Comparison of System BER for different precoding schemes using BPSK, Random clustering and COPA

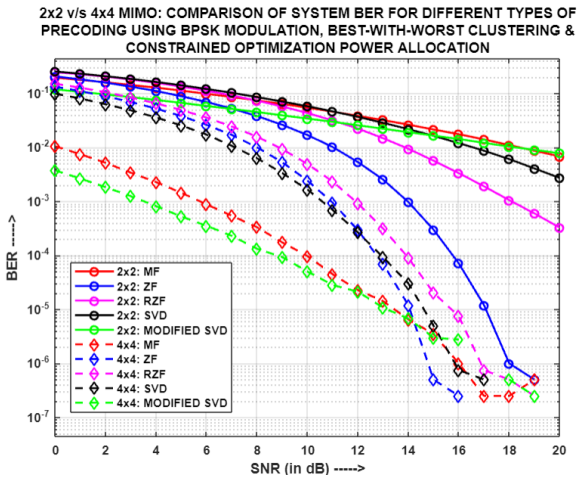

Fig.5.149: (2x2) v/s (4X4) MIMO-NOMA: Comparison of System BER for different precoding schemes using BPSK, BWW clustering and COPA

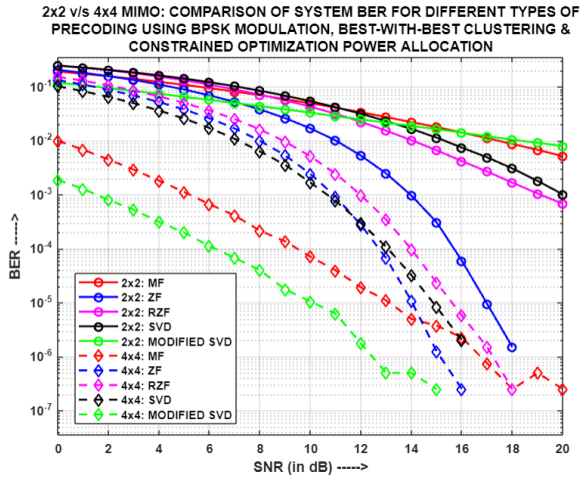

Fig.5.150: (2x2) v/s (4X4) MIMO-NOMA: Comparison of System BER for different precoding schemes using BPSK, BWB clustering and COPA

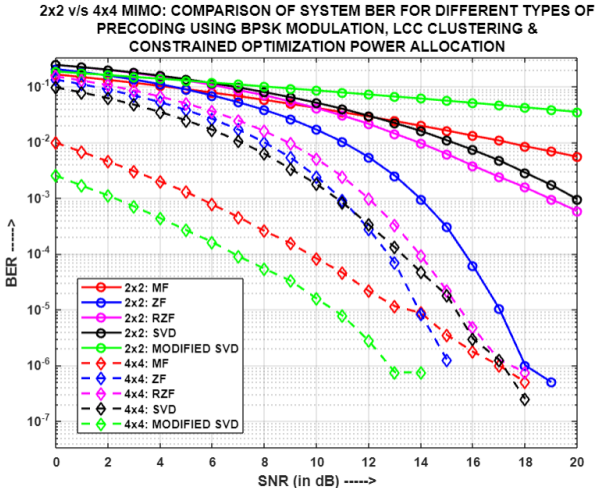

Fig.5.151: (2x2) v/s (4X4) MIMO-NOMA: Comparison of System BER for different precoding schemes using BPSK, LCC clustering and COPA

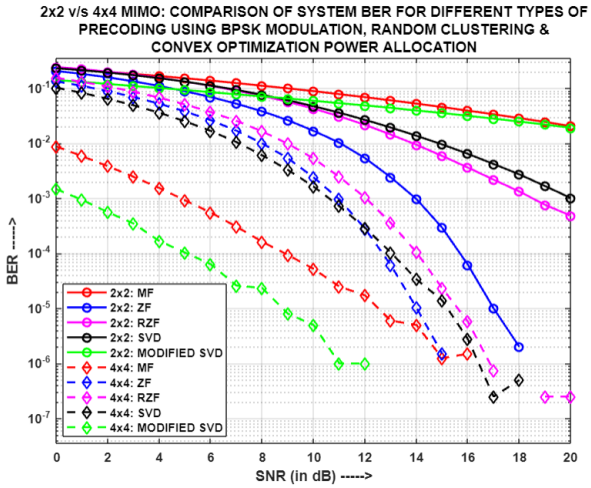

Fig.5.152: (2x2) v/s (4X4) MIMO-NOMA: Comparison of System BER for different precoding schemes using BPSK, Random clustering and CON-OPA

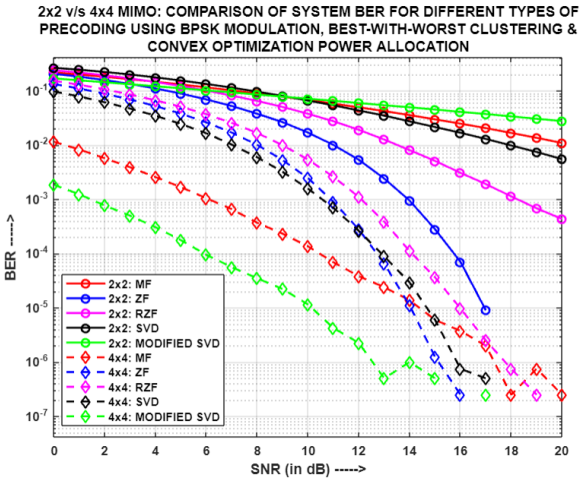

Fig.5.153: (2x2) v/s (4X4) MIMO-NOMA: Comparison of System BER for different precoding schemes using BPSK, BWW clustering and CON-OPA

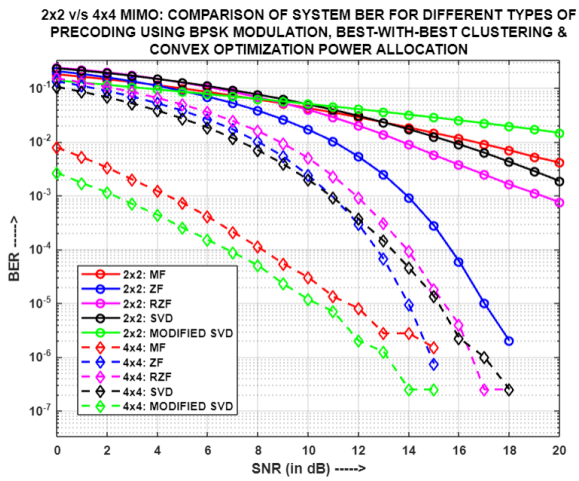

Fig.5.154: (2x2) v/s (4X4) MIMO-NOMA: Comparison of System BER for different precoding schemes using BPSK, BWB clustering and CON-OPA

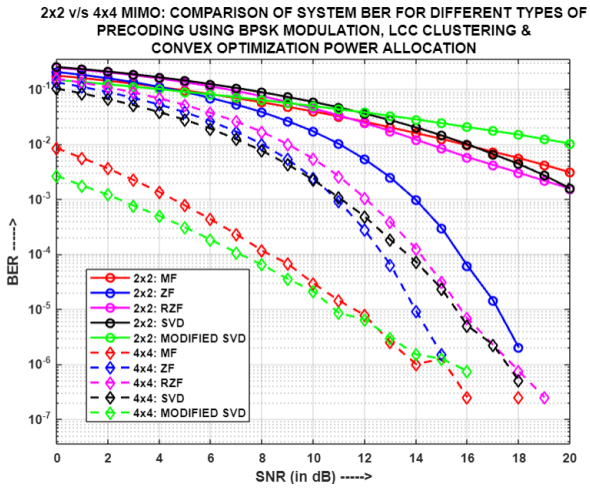

Fig.5.155: (2x2) v/s (4X4) MIMO-NOMA: Comparison of System BER for different precoding schemes using BPSK, LCC clustering and CON-OPA

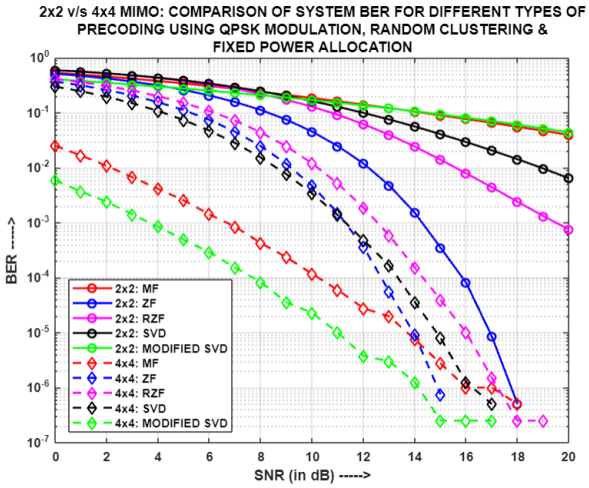

Fig.5.156: (2x2) v/s (4X4) MIMO-NOMA: Comparison of System BER for different precoding schemes using QPSK, Random clustering and FPA

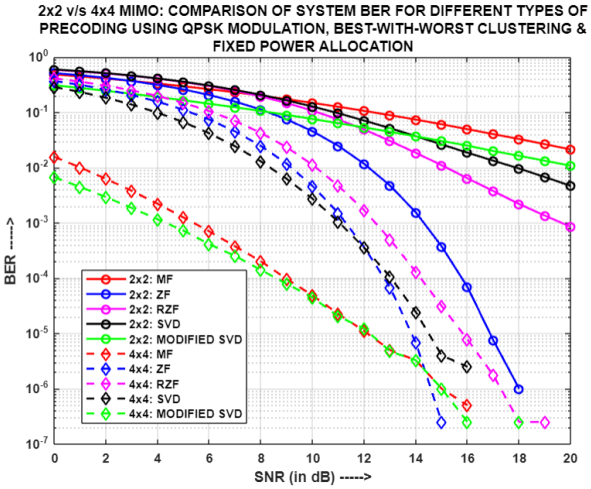

Fig.5.157: (2x2) v/s (4X4) MIMO-NOMA: Comparison of System BER for different precoding schemes using QPSK, BWW clustering and FPA

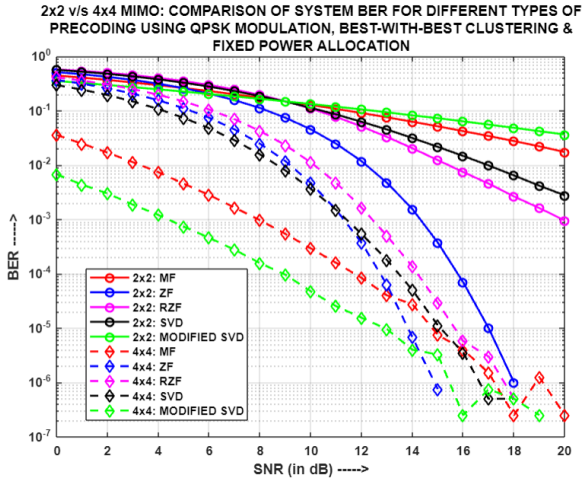

Fig.5.158: (2x2) v/s (4X4) MIMO-NOMA: Comparison of System BER for different precoding schemes using QPSK, BWB clustering and FPA

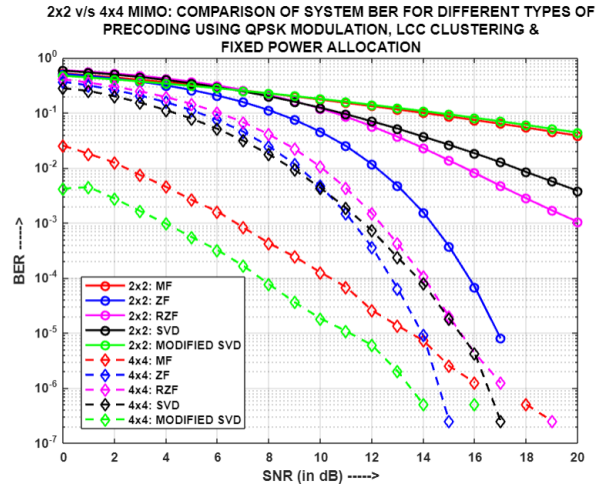

Fig.5.159: (2x2) v/s (4X4) MIMO-NOMA: Comparison of System BER for different precoding schemes using QPSK, LCC clustering and FPA

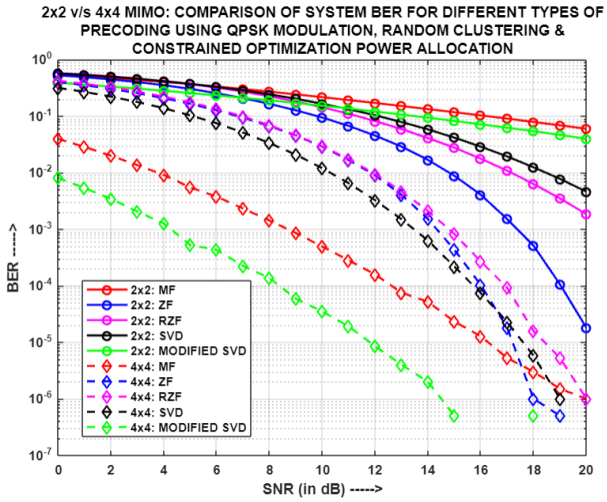

Fig.5.160: (2x2) v/s (4X4) MIMO-NOMA: Comparison of System BER for different precoding schemes using QPSK, Random clustering and COPA

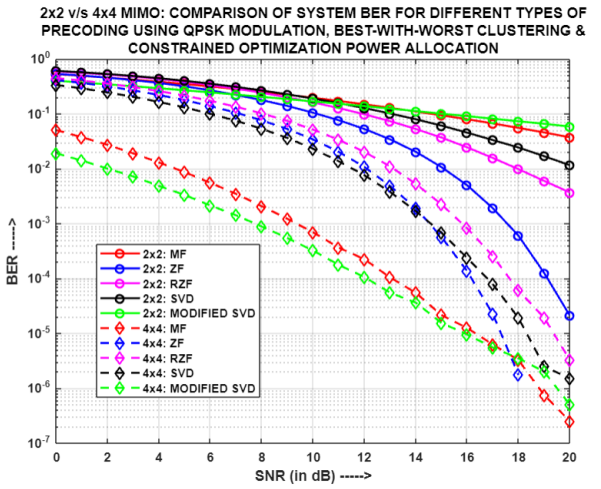

Fig.5.161: (2x2) v/s (4X4) MIMO-NOMA: Comparison of System BER for different precoding schemes using QPSK, BWW clustering and COPA

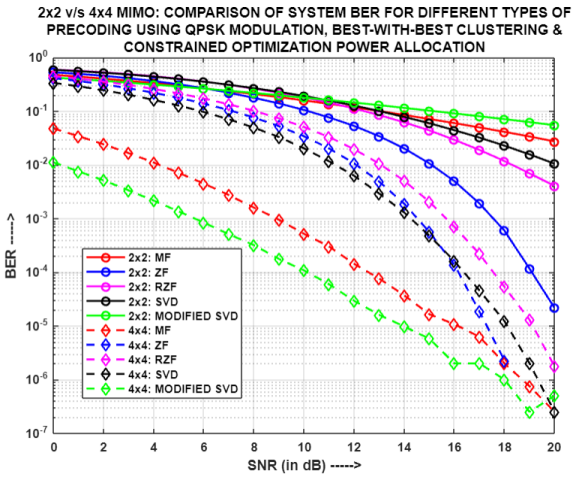

Fig.5.162: (2x2) v/s (4X4) MIMO-NOMA: Comparison of System BER for different precoding schemes using QPSK, BWB clustering and COPA

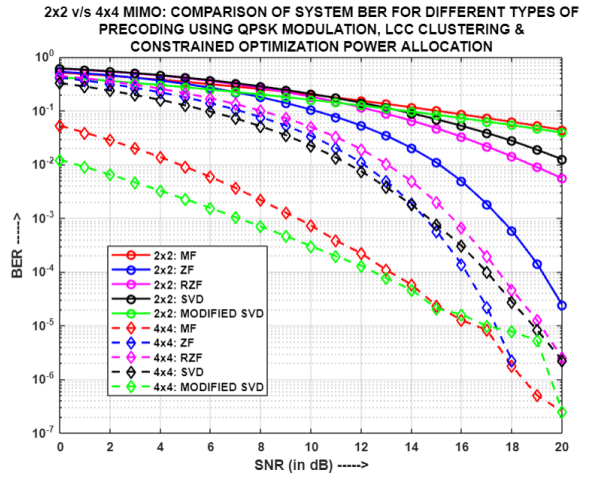

Fig.5.163: (2x2) v/s (4X4) MIMO-NOMA: Comparison of System BER for different precoding schemes using QPSK, LCC clustering and COPA

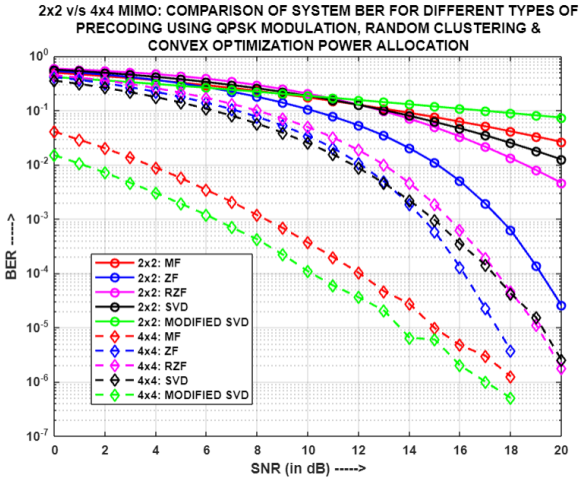

Fig.5.164: (2x2) v/s (4X4) MIMO-NOMA: Comparison of System BER for different precoding schemes using QPSK, Random clustering and CON-OPA

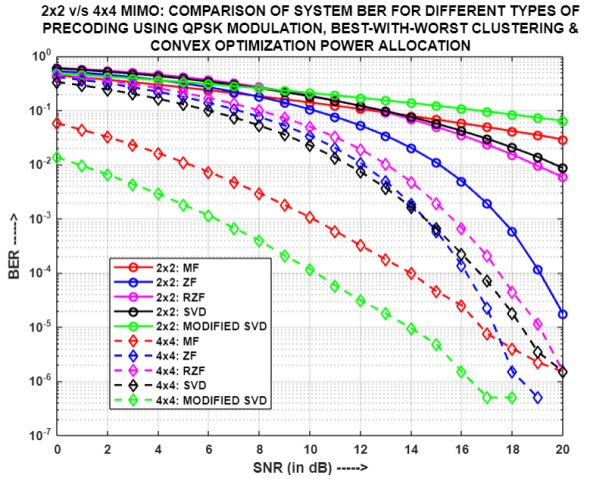

Fig.5.165: (2x2) v/s (4X4) MIMO-NOMA: Comparison of System BER for different precoding schemes using QPSK, BWW clustering and CON-OPA

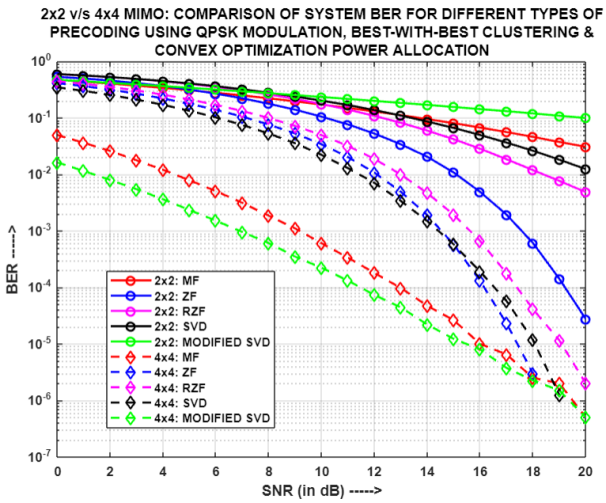

Fig.5.166: (2x2) v/s (4X4) MIMO-NOMA: Comparison of System BER for different precoding schemes using QPSK, BWB clustering and CON-OPA

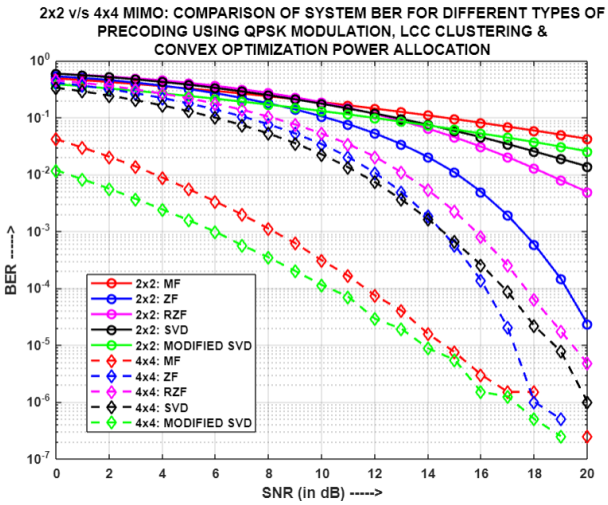

Fig.5.167: (2x2) v/s (4X4) MIMO-NOMA: Comparison of System BER for different precoding schemes using QPSK, LCC clustering and CON-OPA

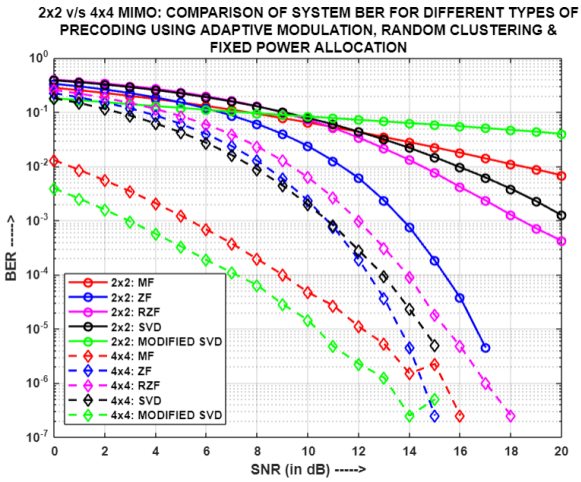

Fig.5.168: (2x2) v/s (4X4) MIMO-NOMA: Comparison of System BER for different precoding schemes using Adaptive, Random clustering and FPA

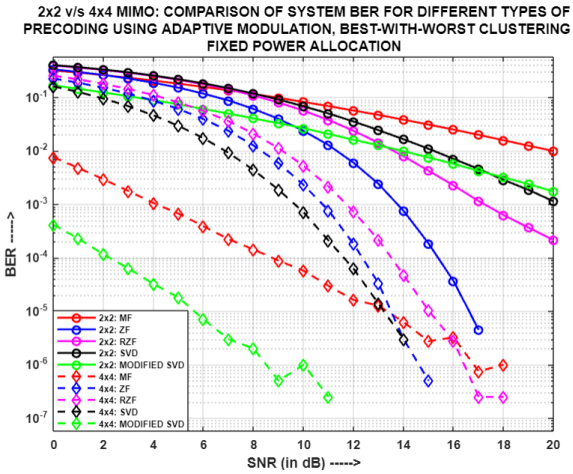

Fig.5.169: (2x2) v/s (4X4) MIMO-NOMA: Comparison of System BER for different precoding schemes using Adaptive, BWW clustering and FPA

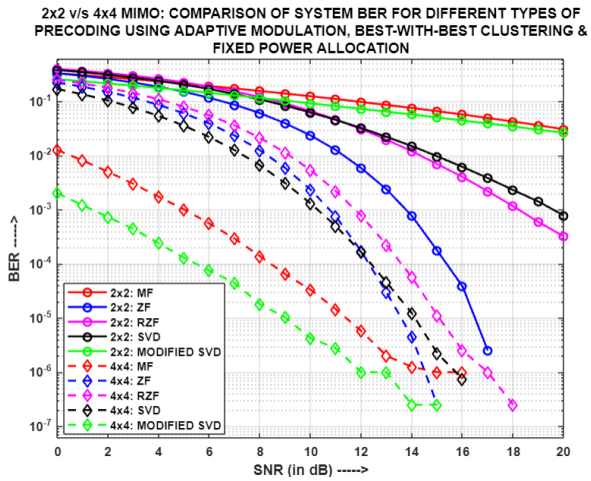

Fig.5.170: (2x2) v/s (4X4) MIMO-NOMA: Comparison of System BER for different precoding schemes using Adaptive, BWB clustering and FPA

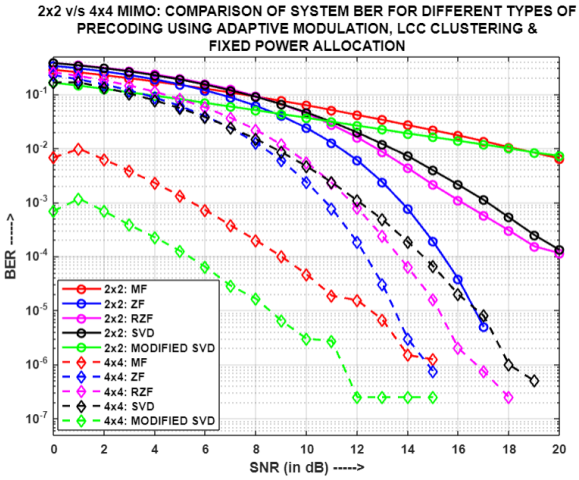

Fig.5.171: (2x2) v/s (4X4) MIMO-NOMA: Comparison of System BER for different precoding schemes using Adaptive, LCC clustering and FPA

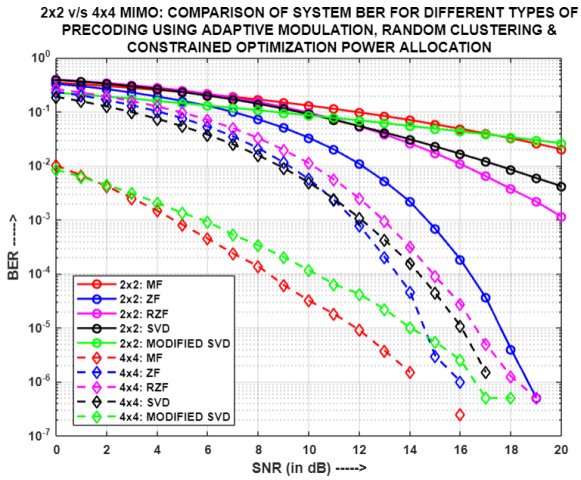

Fig.5.172: (2x2) v/s (4X4) MIMO-NOMA: Comparison of System BER for different precoding schemes using Adaptive, Random clustering and COPA

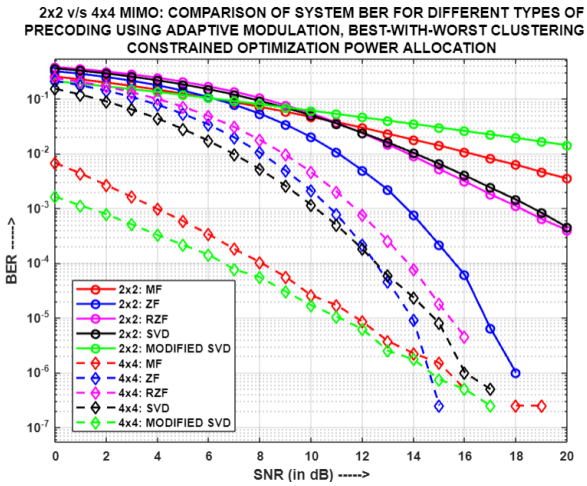

Fig.5.173: (2x2) v/s (4X4) MIMO-NOMA: Comparison of System BER for different precoding schemes using Adaptive, BWW clustering and COPA

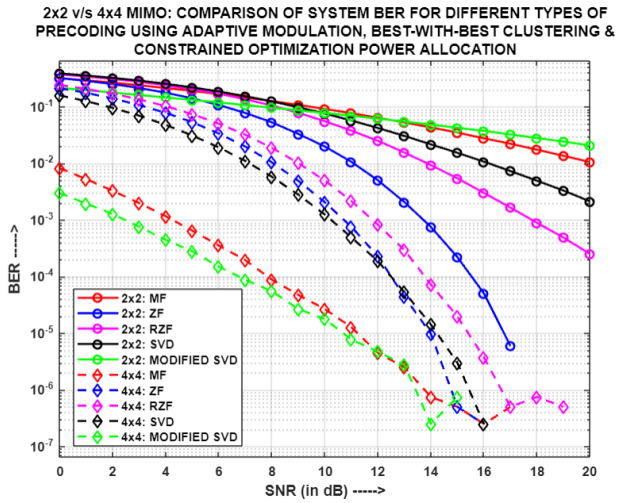

Fig.5.174: (2x2) v/s (4X4) MIMO-NOMA: Comparison of System BER for different precoding schemes using Adaptive, BWB clustering and COPA

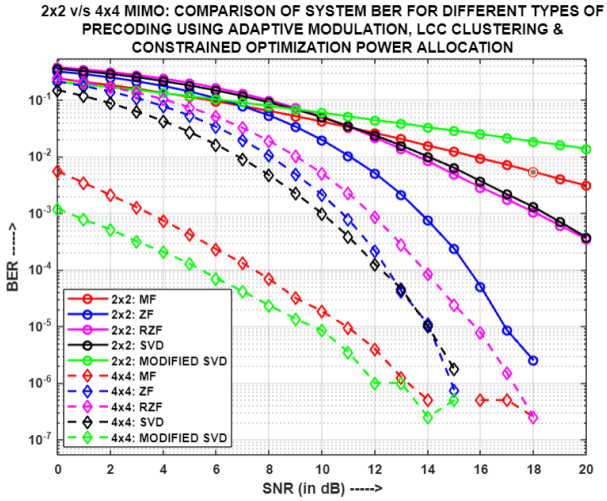

Fig.5.175: (2x2) v/s (4X4) MIMO-NOMA: Comparison of System BER for different precoding schemes using Adaptive, LCC clustering and COPA

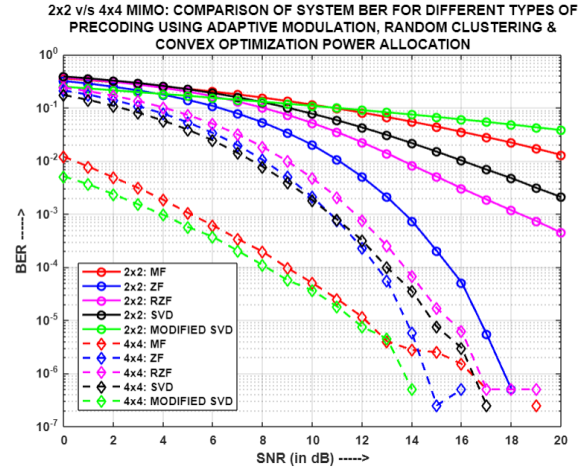

Fig.5.176: (2x2) v/s (4X4) MIMO-NOMA: Comparison of System BER for different precoding schemes using Adaptive, Random clustering and CON-OPA

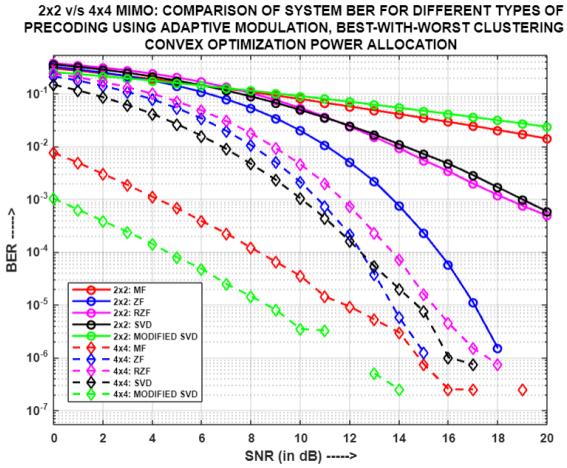

Fig.5.177: (2x2) v/s (4X4) MIMO-NOMA: Comparison of System BER for different precoding schemes using Adaptive, BWW clustering and CON-OPA

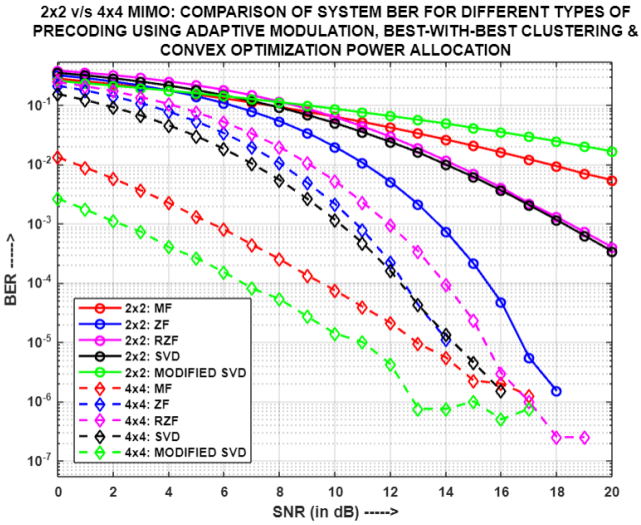

Fig.5.178: (2x2) v/s (4X4) MIMO-NOMA: Comparison of System BER for different precoding schemes using Adaptive, BWB clustering and CON-OPA

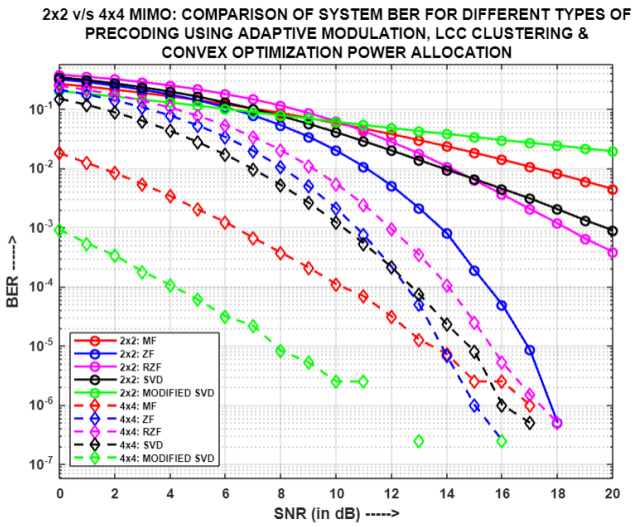

Fig.5.179: (2x2) v/s (4X4) MIMO-NOMA: Comparison of System BER for different precoding schemes using Adaptive, LCC clustering and CON-OPA

Fig.5.144, Fig.5.145, Fig.5.146, Fig.5.147, Fig.5.148, Fig.5.149, Fig.5.150, Fig.5.151, Fig.5.152, Fig.5.153, Fig.5.154 and Fig.5.155 illustrates the comparison of system BER for different configurations of multiple-input-multiple-output (MIMO), i.e. (2x2) and (4x4), using diverse clustering methodologies, i.e. Random, BWW, BWB and LCC clustering respectively, and power allocation strategies, i.e. FPA, COPA and CON-OPA in particular, employing BPSK modulation for all the precoding techniques. Figures 5.156 to 5.167 provide a visual comparison of the system BER for the same two configurations of MIMO, i.e. (2x2) and (4x4), using the aforementioned clustering methodologies and power allocation strategies respectively, and applying QPSK modulation for all the precoding techniques. Figures 5.168 to 5.179 showcases the comparison of the system BER for the above two configurations of MIMO, i.e. (2x2) and (4x4), using the aforesaid clustering mechanisms and power allocation strategies respectively, and utilizing Adaptive modulation scheme for all the precoding techniques. It is observed that for all precoding techniques, the system BERs for (4x4) MIMO configuration outperforms that of (2x2) MIMO system, in case of all the respective clustering methodologies, employing different power allocation mechanisms. This behavior attributes to the fact that in case of (4x4) MIMO, all the users in the clusters are equipped with more number of antennas as compared to the (2x2) MIMO scenario. Hence, higher the number of TX-RX antennas involved in the transmission-reception of information,

more are number of available channel paths to the user, whereby the chances of receiving the correct signal enhances and also, leads to reception of a better quality signal. The receiving of a signal in its optimal form also depends on the precoding scheme used. Like for all the above cases, MODIFIED SVD, for the (4x4) MIMO scenario, yields the least system BER for all the respective clustering methodologies, power allocation strategies and even varied modulation schemes. This happens because of the dominance of the stated precoding scheme as it transmits and receives the information signal, with proper amplification in regard to the channel gain. Therefore, MODIFIED SVD outperforms its contemporaries, for enhanced number of TX-RX antennas.

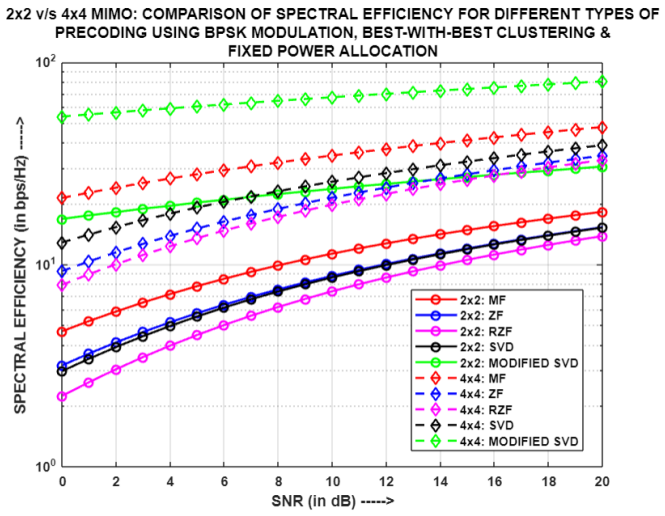

Fig.5.180: (2x2) v/s (4X4) MIMO-NOMA: Comparison of Sum Capacity for different precoding schemes using BPSK, Random clustering and FPA

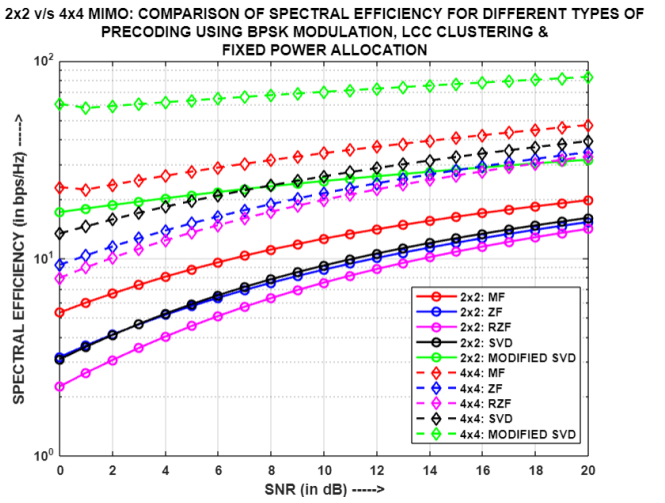

Fig.5.181: (2x2) v/s (4X4) MIMO-NOMA: Comparison of Sum Capacity for different precoding schemes using BPSK, BWW clustering and FPA

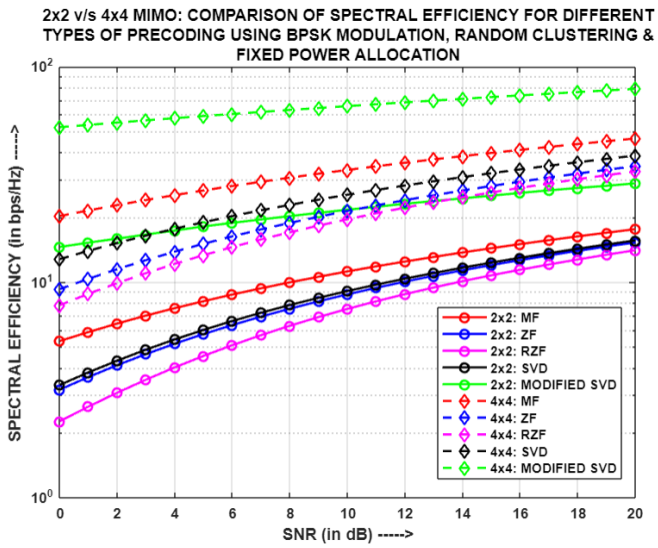

Fig.5.182: (2x2) v/s (4X4) MIMO-NOMA: Comparison of Sum Capacity for different precoding schemes using BPSK, BWB clustering and FPA

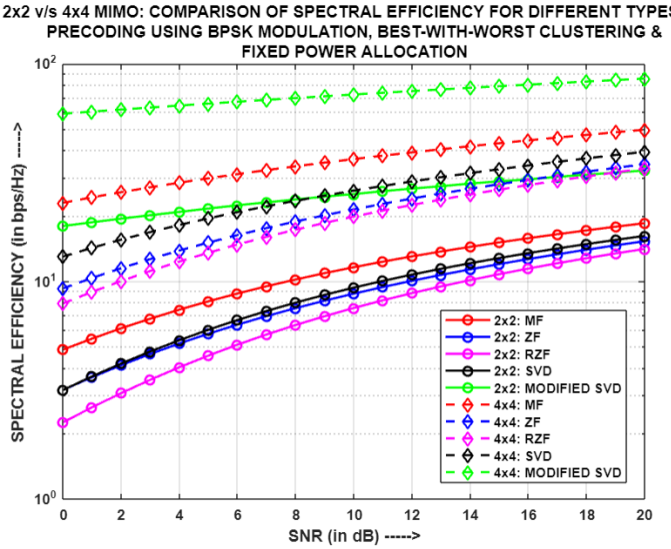

Fig.5.183: (2x2) v/s (4X4) MIMO-NOMA: Comparison of Sum Capacity for different precoding schemes using BPSK, LCC clustering and FPA

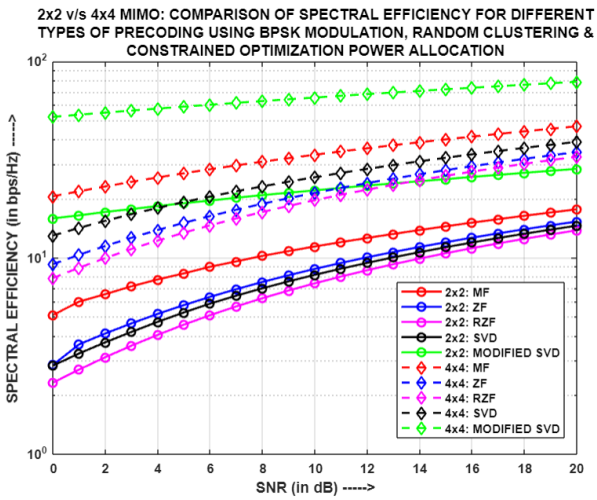

Fig.5.184: (2x2) v/s (4X4) MIMO-NOMA: Comparison of Sum Capacity for different precoding schemes using BPSK, Random clustering and COPA

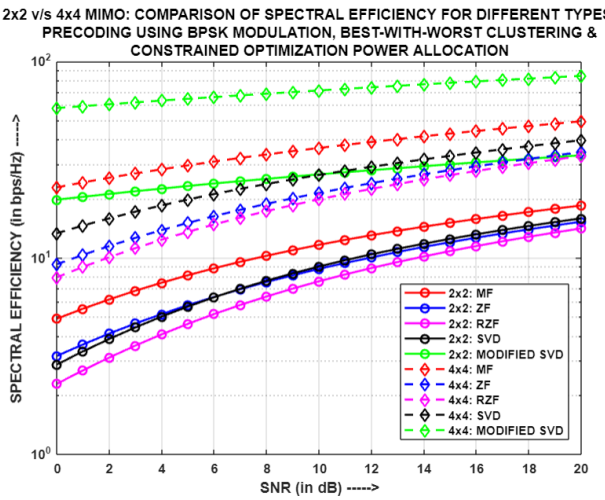

Fig.5.185: (2x2) v/s (4X4) MIMO-NOMA: Comparison of Sum Capacity for different precoding schemes using BPSK, BWW clustering and COPA

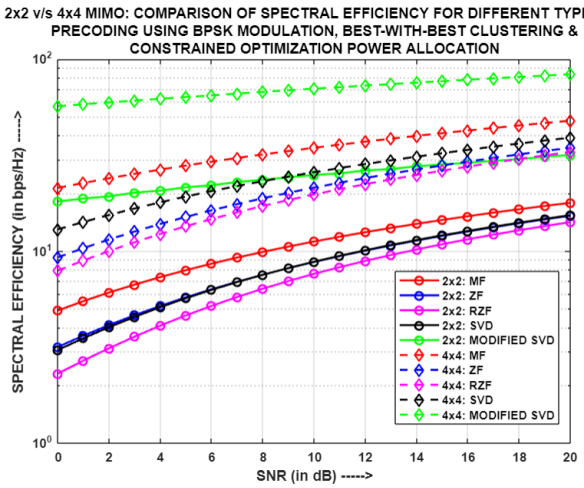

Fig.5.186: (2x2) v/s (4X4) MIMO-NOMA: Comparison of Sum Capacity for different precoding schemes using BPSK, BWB clustering and COPA

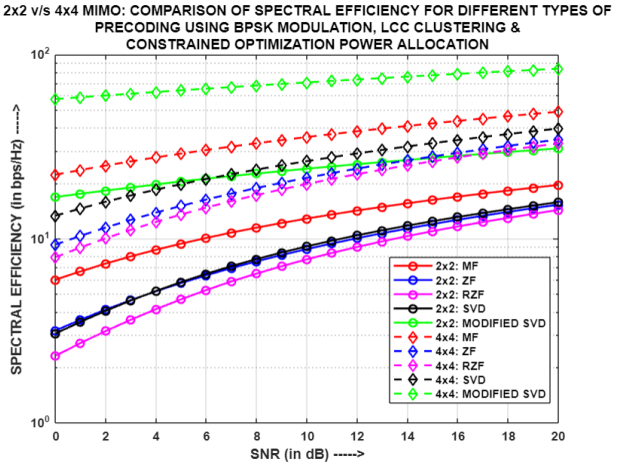

Fig.5.187: (2x2) v/s (4X4) MIMO-NOMA: Comparison of Sum Capacity for different precoding schemes using BPSK, LCC clustering and COPA

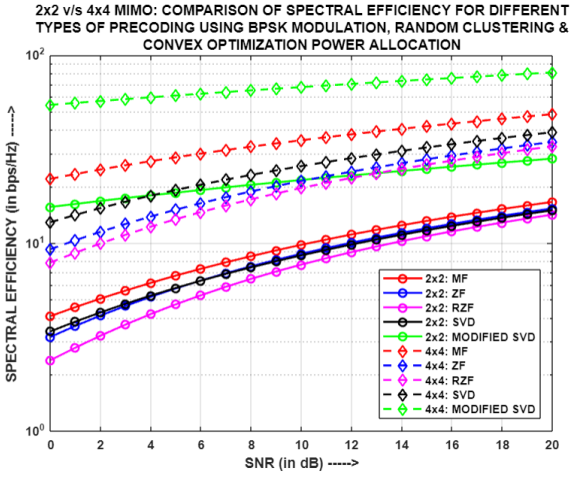

Fig.5.188: (2x2) v/s (4X4) MIMO-NOMA: Comparison of Sum Capacity for different precoding schemes using BPSK, Random clustering and CON-OPA

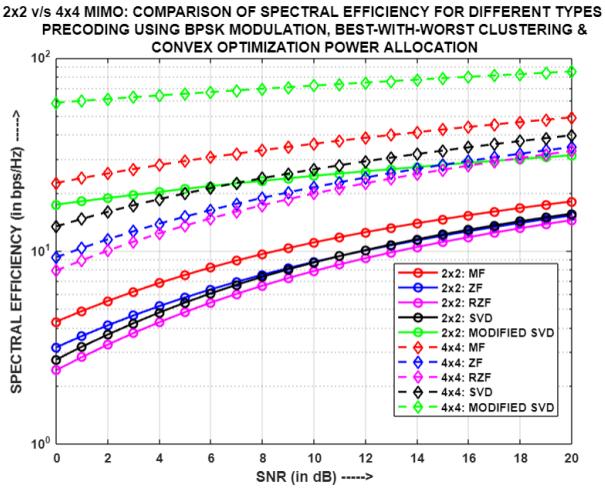

Fig.5.189: (2x2) v/s (4X4) MIMO-NOMA: Comparison of Sum Capacity for different precoding schemes using BPSK, BWW clustering and CON-OPA

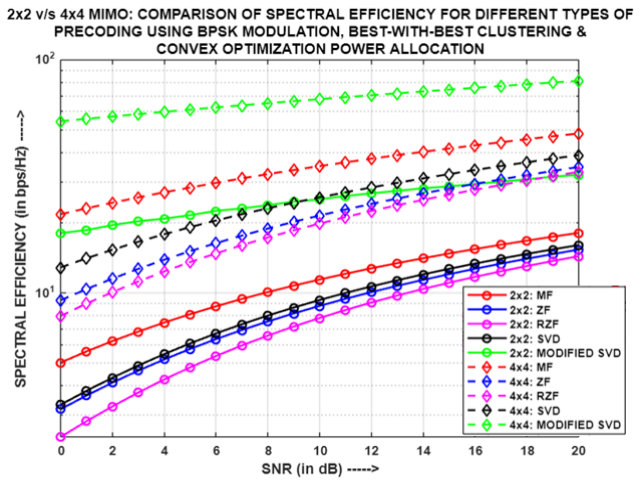

Fig.5.190: (2x2) v/s (4X4) MIMO-NOMA: Comparison of Sum Capacity for different precoding schemes using BPSK, BWB clustering and CON-OPA

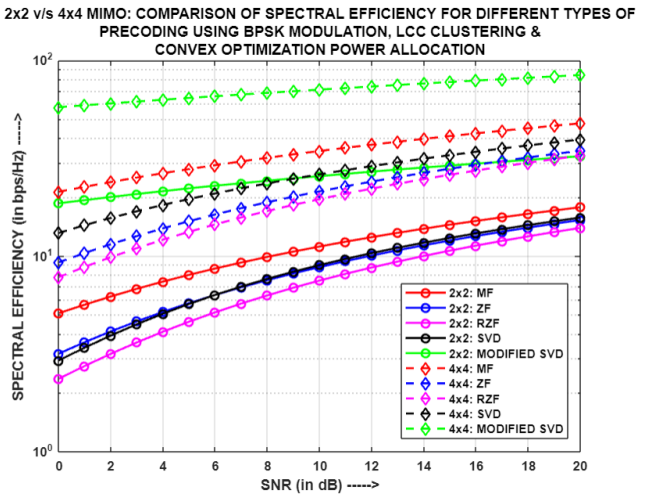

Fig.5.191: (2x2) v/s (4X4) MIMO-NOMA: Comparison of Sum Capacity for different precoding schemes using BPSK, LCC clustering and CON-OPA

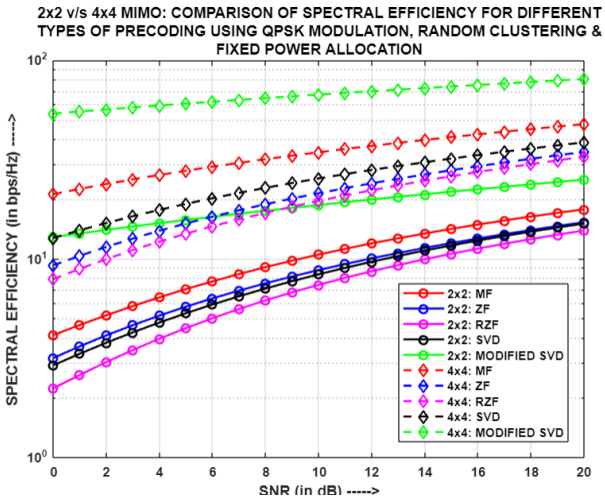

Fig.5.192: (2x2) v/s (4X4) MIMO-NOMA: Comparison of Sum Capacity for different precoding schemes using QPSK, Random clustering and FPA

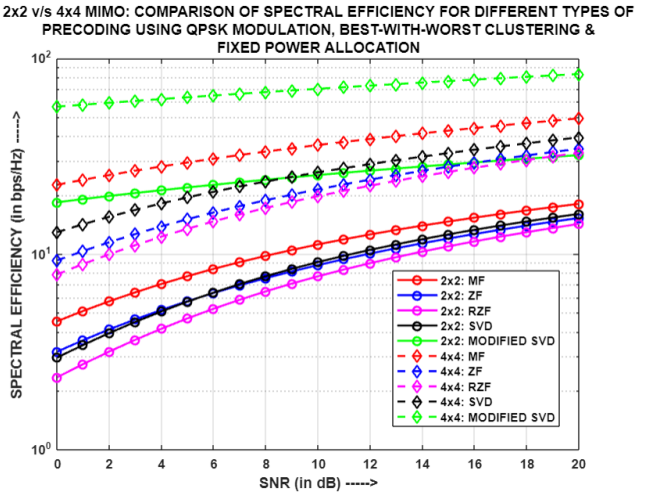

Fig.5.193: (2x2) v/s (4X4) MIMO-NOMA: Comparison of Sum Capacity for different precoding schemes using QPSK, BWW clustering and FPA

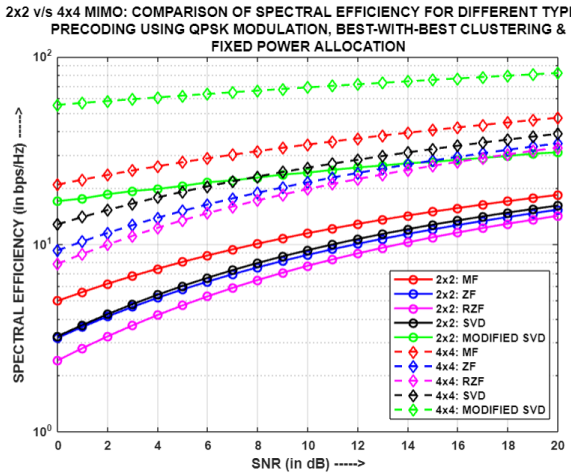

Fig.5.194: (2x2) v/s (4X4) MIMO-NOMA: Comparison of Sum Capacity for different precoding schemes using QPSK, BWB clustering and FPA

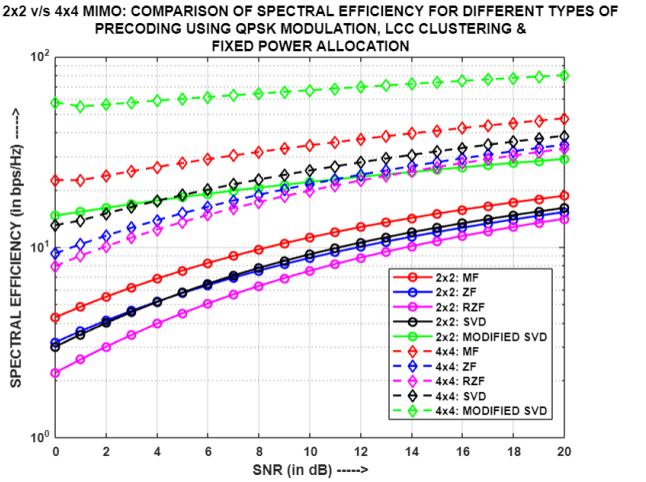

Fig.5.195: (2x2) v/s (4X4) MIMO-NOMA: Comparison of Sum Capacity for different precoding schemes using QPSK, LCC clustering and FPA

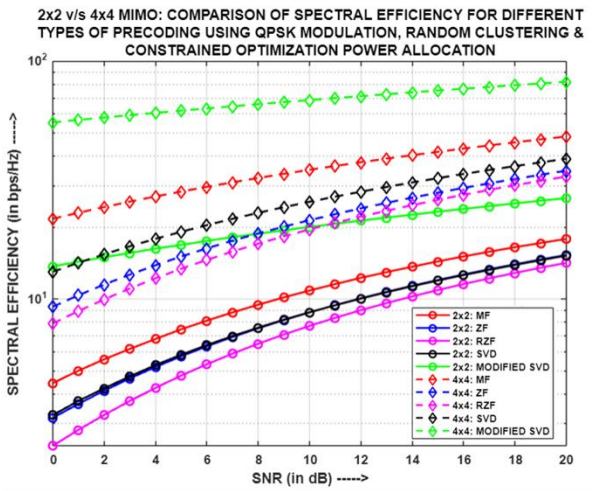

Fig.5.196: (2x2) v/s (4X4) MIMO-NOMA: Comparison of Sum Capacity for different precoding schemes using QPSK, Random clustering and COPA

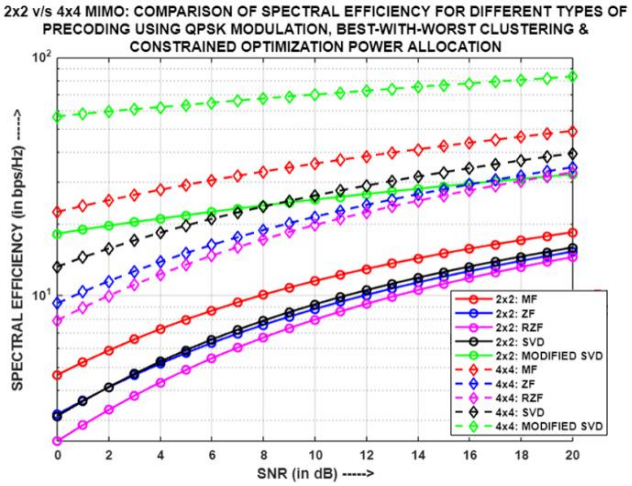

Fig.5.197: (2x2) v/s (4X4) MIMO-NOMA: Comparison of Sum Capacity for different precoding schemes using QPSK, BWW clustering and COPA

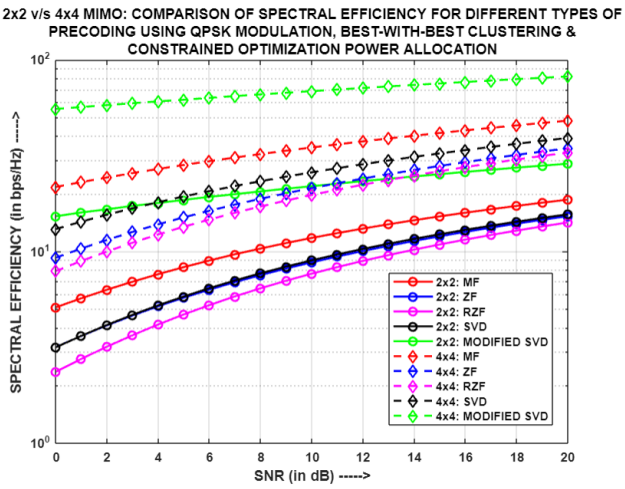

Fig.5.198: (2x2) v/s (4X4) MIMO-NOMA: Comparison of Sum Capacity for different precoding schemes using QPSK, BWB clustering and COPA

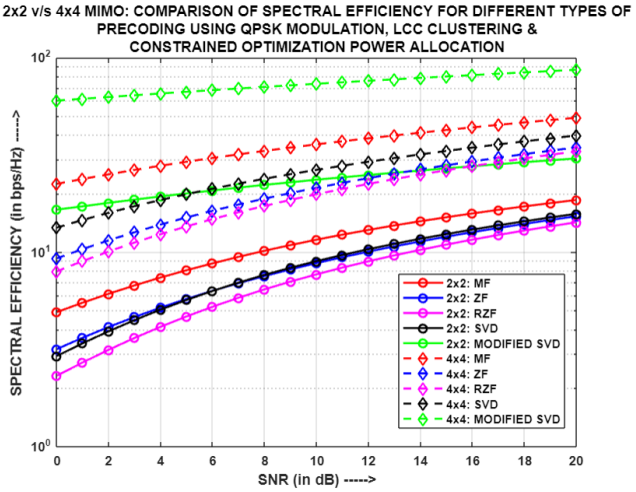

Fig.5.199: (2x2) v/s (4X4) MIMO-NOMA: Comparison of Sum Capacity for different precoding schemes using QPSK, LCC clustering and COPA

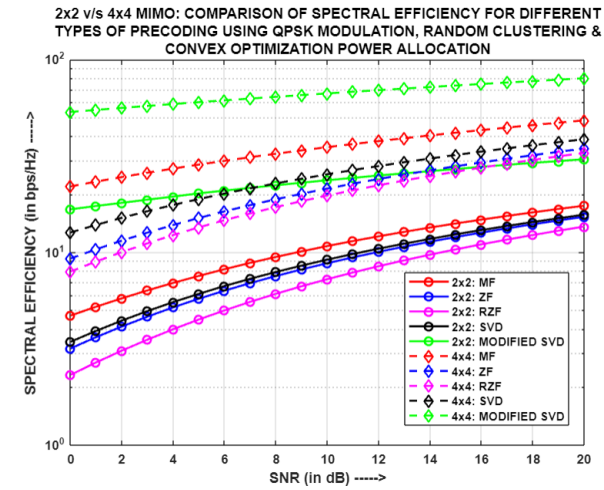

Fig.5.200: (2x2) v/s (4X4) MIMO-NOMA: Comparison of Sum Capacity for different precoding schemes using QPSK, Random clustering and CON-OPA

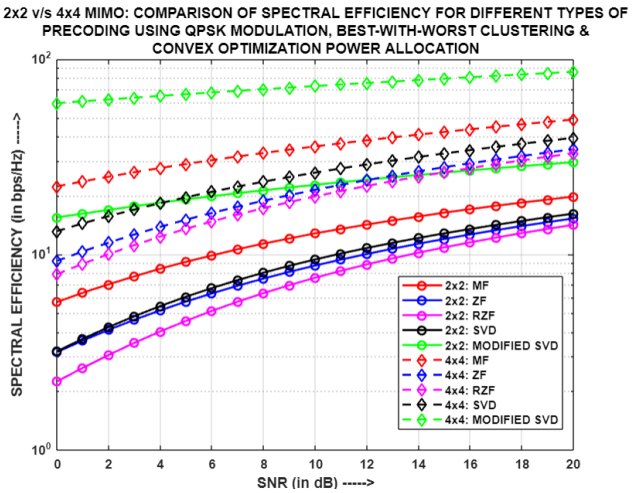

Fig.5.201: (2x2) v/s (4X4) MIMO-NOMA: Comparison of Sum Capacity for different precoding schemes using QPSK, BWW clustering and CON-OPA

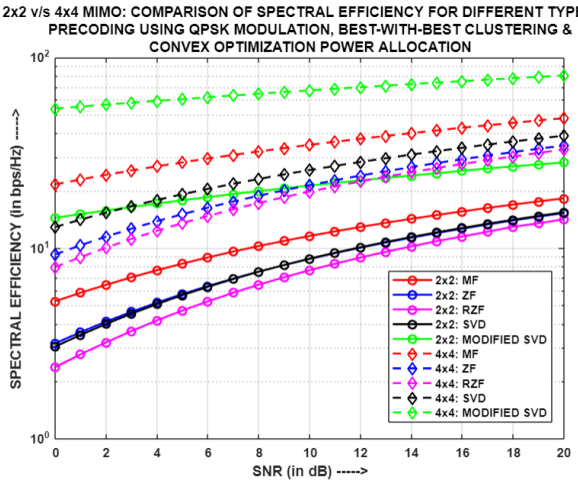

Fig.5.202: (2x2) v/s (4X4) MIMO-NOMA: Comparison of Sum Capacity for different precoding schemes using QPSK, BWB clustering and CON-OPA

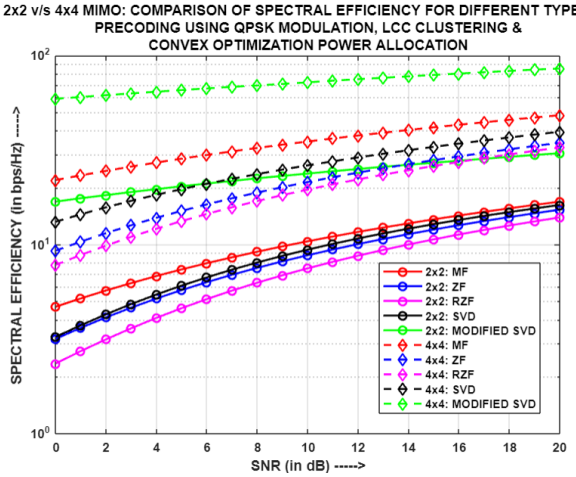

Fig.5.203: (2x2) v/s (4X4) MIMO-NOMA: Comparison of Sum Capacity for different precoding schemes using QPSK, LCC clustering and CON-OPA

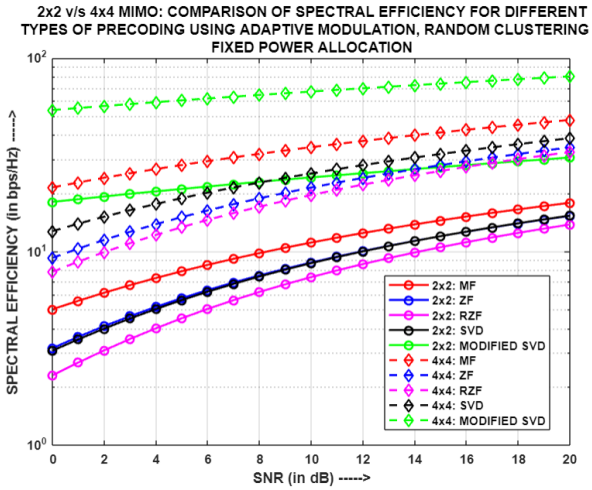

Fig.5.204: (2x2) v/s (4X4) MIMO-NOMA: Comparison of Sum Capacity for different precoding schemes using Adaptive, Random clustering and FPA

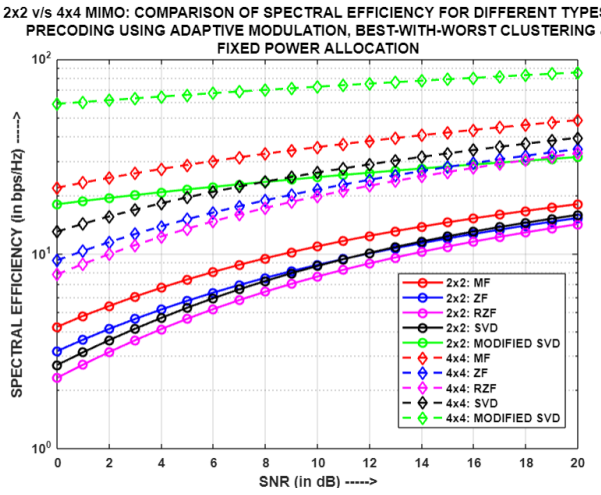

Fig.5.205: (2x2) v/s (4X4) MIMO-NOMA: Comparison of Sum Capacity for different precoding schemes using Adaptive, BWW clustering and FPA

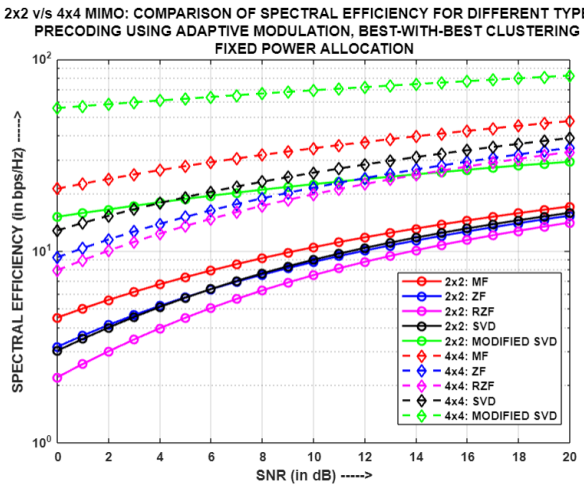

Fig.5.206: (2x2) v/s (4X4) MIMO-NOMA: Comparison of Sum Capacity for different precoding schemes using Adaptive, BWB clustering and FPA

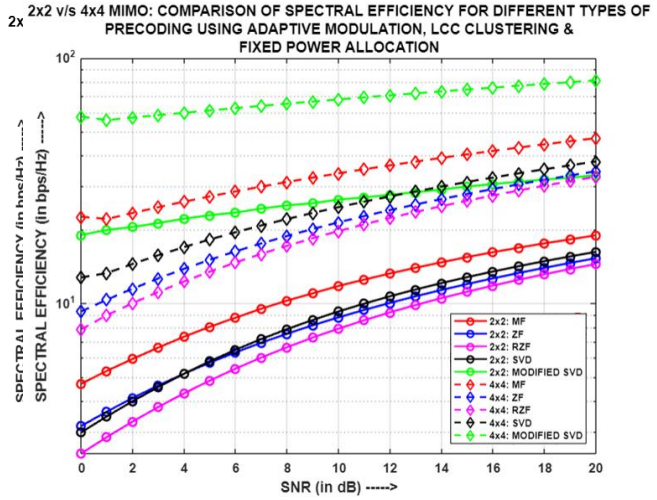

Fig.5.207: (2x2) v/s (4X4) MIMO-NOMA: Comparison of Sum Capacity for different precoding schemes using Adaptive, LCC clustering and FPA

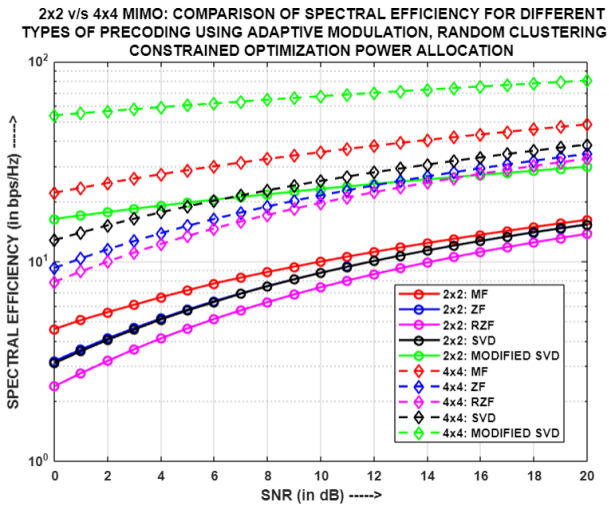

Fig.5.208: (2x2) v/s (4X4) MIMO-NOMA: Comparison of Sum Capacity for different precoding schemes using Adaptive, Random clustering and COPA

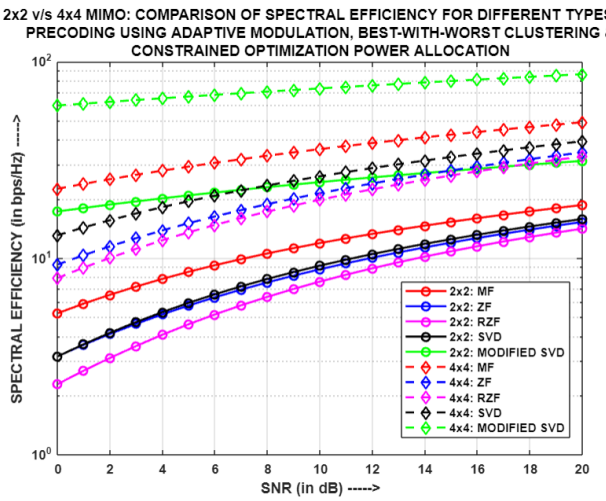

Fig.5.209: (2x2) v/s (4X4) MIMO-NOMA: Comparison of Sum Capacity for different precoding schemes using Adaptive, BWW clustering and COPA

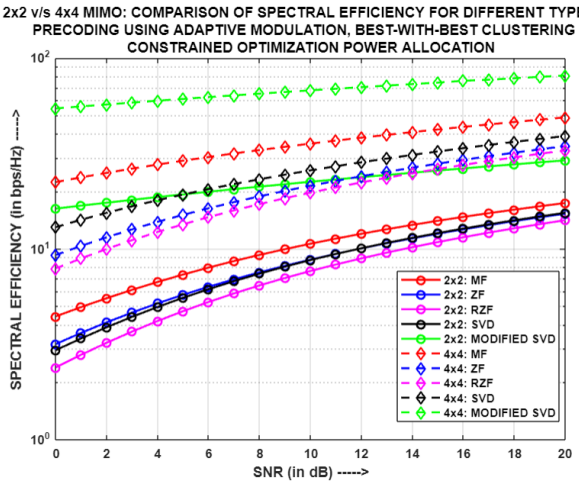

Fig.5.210: (2x2) v/s (4X4) MIMO-NOMA: Comparison of Sum Capacity for different precoding schemes using Adaptive, BWB clustering and COPA

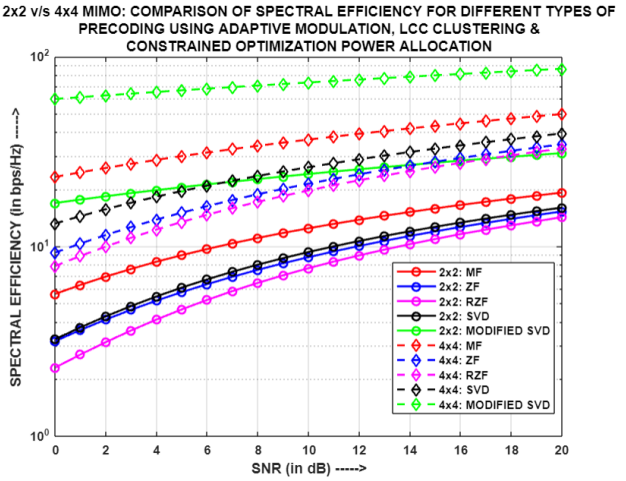

Fig.5.211: (2x2) v/s (4X4) MIMO-NOMA: Comparison of Sum Capacity for different precoding schemes using Adaptive, LCC clustering and COPA

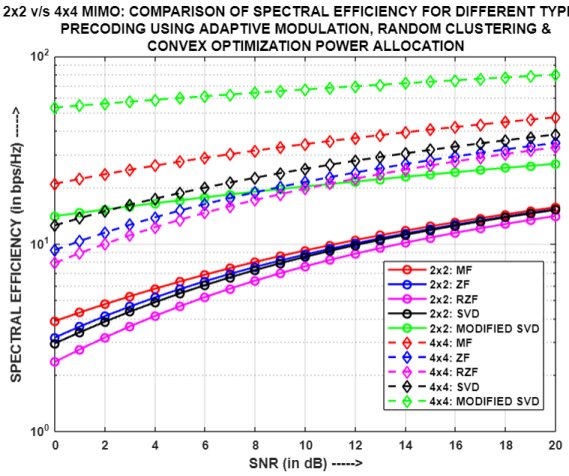

Fig.5.212: (2x2) v/s (4X4) MIMO-NOMA: Comparison of Sum Capacity for different precoding schemes using Adaptive, Random clustering and CON-OPA

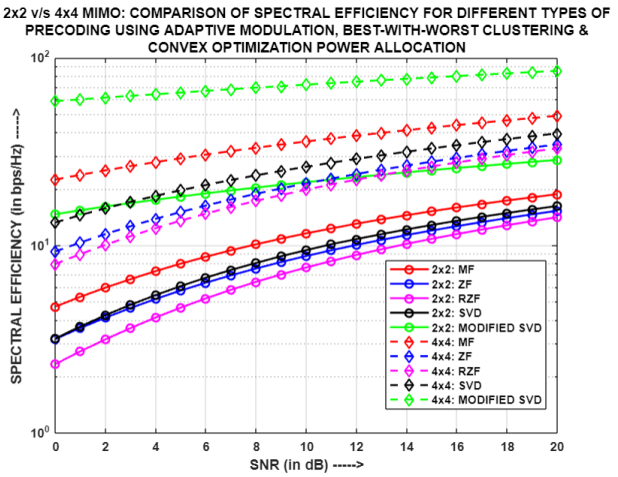

Fig.5.213: (2x2) v/s (4X4) MIMO-NOMA: Comparison of Sum Capacity for different precoding schemes using Adaptive, BWW clustering and CON-OPA

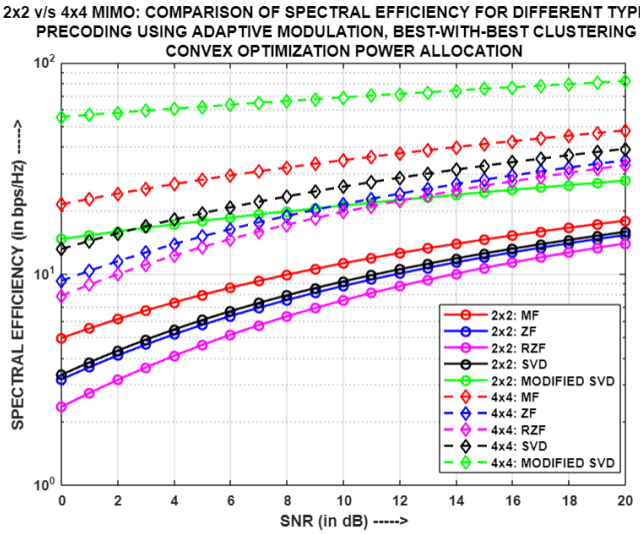

Fig.5.214: (2x2) v/s (4X4) MIMO-NOMA: Comparison of Sum Capacity for different precoding schemes using Adaptive, BWB clustering and CON-OPA

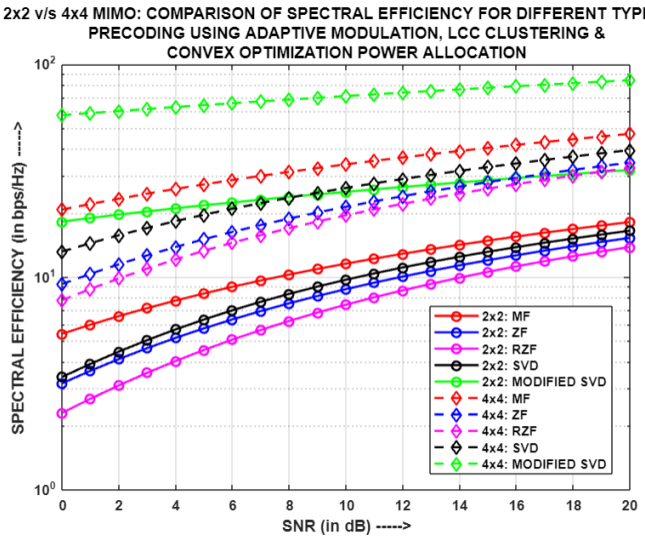

Fig.5.215: (2x2) v/s (4X4) MIMO-NOMA: Comparison of Sum Capacity for different precoding schemes using Adaptive, LCC clustering and CON-OPA

Fig.5.180, Fig.5.181, Fig.5.182, Fig.5.183, Fig.5.184, Fig.5.185, Fig.5.186, Fig.5.187, Fig.5.188, Fig.5.189, Fig.5.190 and Fig.5.191 depicts the comparison of Spectral Efficiency (SE) for different configurations of multiple-input-multiple-output (MIMO), i.e. (2x2) and (4x4), using varied clustering methodologies, i.e. Random, BWW, BWB and LCC clustering respectively, and power allocation strategies, i.e. FPA, COPA and CON-OPA in particular, employing BPSK modulation for all the precoding techniques. Figures 5.192 to 5.203 provide a visual representation of the Spectral Efficiency for the same two configurations of MIMO, i.e. (2x2) and (4x4), using the above-mentioned clustering methodologies and power allocation strategies respectively, and applying QPSK modulation for all the precoding techniques. Figures 5.204 to 5.215 portrays the comparison of the Spectral Efficiency for the above two configurations of MIMO, i.e. (2x2) and (4x4), using the above-stated clustering mechanisms and power allocation strategies respectively, and utilizing Adaptive modulation scheme for all the precoding techniques. It is witnessed that for all the above cases, the Spectral Efficiency considerably increases for (4x4) MIMO configuration, compared to (2x2) MIMO system. This is because for the former, there are four clusters and each user in the respective cluster has 16 available channel paths; while in case of latter, there are two clusters, wherein each

user has 4 available channel paths. For both the configurations, each cluster has two users. It is clearly evident that (4x4) MIMO system is able to serve more number of users and also provide more data to each of the user in the respective cluster due to the availability of additional number of channel paths per user. However, for a (2x2) MIMO system, less number of users are served and comparatively less data is sent to each user. It is for this reason that for all the clustering methodologies, the (4x4) MIMO system yields a higher spectral efficiency than that produced by the (2x2) MIMO system, for all the respective precoding techniques and power allocation strategies. The precoding scheme used also plays a vital role in strengthening the channel gain of the user, which thereby influences the user's throughput and hence, sum capacity of the overall system. As spectral efficiency is a parameter that indicates the efficient usage of the available bandwidth, therefore, for all the aforementioned cases, (4x4) MIMO with MODIFIED SVD precoding, generated the highest SE, across different clustering methodologies, power allocation strategies and modulation schemes respectively. In fact, MODIFIED SVD precoding, for a (4x4) MIMO system, elevated the SE by almost 10 times the SE obtained in a (2x2) MIMO system. This behaviour attributes to the characteristic traits of the above stated precoding scheme that makes use of an amplification matrix, both at the transmitter and receiver, i.e., with the precoding and post-coding matrices respectively, which thereby enhances the channel gain and subsequently, throughput of the respective user. Therefore, MODIFIED SVD, with respect to spectral efficiency, supersedes its contemporaries, for both the MIMO configurations.

Table 5.3: Compilation of Result Analysis for MU-MIMO-PD-NOMA for different Clustering techniques

Precoding Technique	Modulation Scheme	Power Allocation Strategy	Best Clustering Method w.r.t				Remarks
			System BER		Sum Capacity		
			(2x2) MIMO	(4x4) MIMO	(2x2) MIMO	(4x4) MIMO	
MF	BPSK	FPA	LCC	All	LCC	BWW	• For BPSK, LCC mostly yields optimum results. • In case of QPSK and Adaptive, LCC and BWW seem to be more suitable for both.
		COPA	LCC	All	LCC	LCC	
		CON-OPA	LCC	LCC	All	All	
	QPSK	FPA	BWB	BWW	All	BWW	
		COPA	LCC	All	All	LCC	
		CON-OPA	BWW	All	BWW	All	
	Adaptive Modulation	FPA	LCC, BWW	BWB	All	BWW	
		COPA	BWB	LCC	LCC	LCC	
		CON-OPA	LCC	BWW	LCC	All	
ZF	BPSK	FPA	All	All	All	All	• All clustering techniques happen to yield comparable results. • In case of Adaptive using COPA, RAN isn't suitable for (2x2)-MIMO.
		COPA	All	All	All	All	
		CON-OPA	All	All	All	All	
	QPSK	FPA	All	All	All	All	
		COPA	All	All	All	All	
		CON-OPA	All	All	All	All	
	Adaptive Modulation	FPA	All	All	All	All	
		COPA	All, except RAN	All	All	All	
		CON-OPA	All	All	All	All	
RZF	BPSK	FPA	BWW	All	All	All	• All clustering techniques produce comparable sum capacities for all the cases and similar system BER for majority of the cases..
		COPA	RAN	All	All	All	
		CON-OPA	All	All	All	All	
	QPSK	FPA	All	All	All	All	
		COPA	RAN	RAN	All	All	
		CON-OPA	All	All	All	All	
	Adaptive Modulation	FPA	LCC	All	All	All	
		COPA	All, except RAN	All, except RAN	All	All	
		CON-OPA	All	All	All	All	
SVD	BPSK	FPA	BWW	LCC	All	All	• LCC using CON-OPA yield good enough results for BPSK, while LCC with CON-OPA produces optimum results for Adaptive Modulation.
		COPA	LCC	All	All	All	
		CON-OPA	RAN	All	LCC	All	
	QPSK	FPA	BWB	BWW	All	All	
		COPA	RAN	RAN	All	All	
		CON-OPA	All	All	All		
	Adaptive Modulation	FPA	LCC	BWW	All	All	
		COPA	LCC	LCC	All	All	
		CON-OPA	LCC,BWB	All	All	All	
MODIFIED SVD	BPSK	FPA	BWB	LCC	BWW	BWW	• LCC with CON-OPA turns out to be the optimum choice for all three modulation schemes, for both (2x2) and (4x4) MIMO.
		COPA	RAN	BWB	BWW	LCC	
		CON-OPA	LCC	LCC	LCC	LCC	
	QPSK	FPA	BWW	LCC	BWW	BWW	
		COPA	LCC	RAN	BWW	LCC	
		CON-OPA	LCC	LCC	LCC	LCC	
	Adaptive Modulation	FPA	BWW	BWW	LCC	BWW	
		COPA	LCC,BWW	LCC	LCC	LCC	
		CON-OPA	LCC	LCC	LCC	LCC	

5.5. DISCUSSION

It is evident from Table that depending on the employed precoding scheme and power allocation mechanism, the chosen clustering methodology keeps changing for the respective modulation scheme. This is because, except for RAN, the other clustering methods' algorithm primarily depends on the corresponding user's effective channel gain. As it has been stated in Chapter 4, the effective channel gain depends on the applied precoding and post-coding matrices, along with the general channel gain of the users. Therefore, depending on the way users are grouped, their respective throughputs will vary and hence, the sum capacity of the system gets affected. If users in the respective clusters have considerable differences in their effective channel gains for different cases of clustering, then their overall sum capacities diverge; whereas if the users in the corresponding clusters have similar effective channel gains for the varied clustering methods, then the resultant sum capacities merge, like in case of ZF, RZF and SVD. Furthermore, depending on the number of transmit-receive antennas employed in the system, the general channel gain varies and hence, the algorithm of clustering methodology is impacted. Additionally, the selected clustering technique affects the power allocation among users, which is required to employ the NOMA principle. The power coefficients not only affect the users' throughput but also plays a significant role in dictating the BER of individual users, wherefrom the BER of the overall system is determined. The precoding scheme is responsible for enhancing the quality of signal reception as well as handling interference among the clusters.

5.6. CONCLUSION

This chapter profoundly analyzed the performance of NOMA, in combination with a proposed clustering methodology, i.e. LCC, and other conventional clustering techniques, i.e. RAN, BWW and BWB, with respect to system BER, Sum Capacity and Spectral Efficiency, on grounds of different power allocation strategies, precoding techniques, modulation schemes and the number of transmit-receive (TX-RX) antennas used in the system. LCC outperformed its contemporaries, especially for MODIFIED SVD precoding scheme and using convex optimization power allocation (CON-OPA) to apply NOMA. Therefore, the proposed clustering method in conjunction with MODIFIED SVD precoding scheme and CON-OPA mechanism can optimally serve scenarios with more than two users per cluster and in order to

enhance the overall system performance, more number of TX-RX antennas needs to be employed. Precoding and clustering go hand-in-hand whereby, the appropriate choice of precoding scheme for the chosen clustering method is essential for handling inter-cluster interference as well as for better signal reception. The choice of clustering technique depends on the application area. Clustering has been used in cooperative communication, network management, wireless sensor networks and such like. If clustering is employed with a suitable precoding scheme and NOMA, then the performance of the overall system can be improved. As per the characteristic trait of NOMA, all the users in a single cluster can be served on the same bandwidth, whereby the spectral efficiency would considerably increase. Additionally, due to the effectiveness of the precoding scheme, inter-cluster interference will be mitigated and signals will be received in their optimal form by the users in the respective clusters. Better the quality of signal reception, more accurate will be the process of successive interference cancellation (SIC), leading to minimized chances of higher bit error probability at the corresponding user, especially for higher order modulation schemes. Therefore, clustering enhances the scalability of wireless communication systems by dividing the cell into small groups of users, thereby making it more convenient to handle. This scalability is particularly crucial in scenarios with a high density of devices or in Internet of Things (IoT) applications. Thus, MIMO-NOMA with clustering and precoding seems to be a promising and robust approach towards efficient communication among all kinds of user equipments.

Chapter 6 REAL-TIME EXPERIMENTATION OF MU-MIMO-PD-NOMA USING WARP: A SOFTWARE DEFINED RADIO KIT

6.1. ABSTRACT

MIMO-NOMA systems have so far been analyzed on a simulation platform, wherein they excelled as per respective choices. However, in order to completely understand their feasibility and effectiveness as a promising technology for the future, MIMO-NOMA systems need to be exposed to the real-time environment. This chapter highlights the real-time test-bed implementation of two-user MIMO-PD-NOMA system using a software defined radio (SDR) kit, named Wireless Access Research Platform (WARP) v3 radio frequency (RF) transceiver system, that employs Orthogonal Frequency Division Multiplexing (OFDM) technology for robust performance. A (2x2)-MIMO-OFDM system is also physically implemented on the WARP v3 kit and the obtained Constellation Diagrams are thoroughly analyzed, both for without precoding and with different types of precoding schemes respectively, using diverse combination of TX RF gain and Automatic Gain Control (AGC) levels. The performance of two-user MIMO-OFDM-PD-NOMA, using varied precoding techniques, is scrutinized for different positions of the users and thereby the optimum position of the users, in terms of system bit error rate (BER) and Spectral Efficiency (SE), is determined experimentally. At the optimum location of users, the performance of the varied precoding schemes, for the two-user MIMO-OFDM-PD-NOMA system, is compared and inspected based on the system BER and Sum Capacity. Fixed power allocation (FPA) strategy is used to employ the NOMA principle. A novel precoding scheme, which is a modified version of SVD, was also experimentally applied along with the existing precoding schemes like MF, ZF, RZF and SVD, to the aforementioned system. All the experiments and analysis were conducted for different modulation schemes, in the 2.4GHz band. It has also been experimentally verified that MIMO-NOMA has higher spectral efficiency over MIMO-without-NOMA, both using OFDM. Nevertheless, a brief overview of WARP and its functionality have also been presented in this chapter.

6.2. WIRELESS OPEN-ACCESS RESEARCH PLATFORM (WARP)

The Wireless Open-Access Research Platform (WARP) is a scalable and extensible programmable wireless platform, built from the ground up to prototype advanced wireless networks. WARP combines high-performance programmable hardware with an open-source repository of reference designs and support materials.

The following sub-sections give a profound insight of the various aspects of WARP.

6.2.1. WARP: A Custom Research Platform

The Wireless Open-Access Research Platform (WARP) is widely recognized as a platform for advanced wireless algorithm and application research. It serves as a scalable and programmable wireless platform for modeling advanced wireless networks. The platform comprises four essential components: custom hardware, platform support packages, an open access repository, and research applications. These elements collectively create a flexible wireless testbed that can be utilized by students and faculty[66].

WARP was developed by the research team at RICE University and is distributed by Mango Communication. It operates within the frequency range of 2.4 GHz to 2.5 GHz, and can also transmit within the 5.875 GHz range with a bandwidth of 40 MHz. The central component of the WARP node is a Xilinx FPGA board, which provides the necessary processing resources for each node.

While there are other wireless testbeds and commercial products available that offer some similar capabilities to WARP, they fall short in certain aspects. For instance, the GNU Radio project provides a flexible wireless development platform that includes an open-source framework for implementing wireless algorithms in software[67]. However, due to the majority of processing being handled by a host PC, current GNU Radio systems are unable to achieve the same high-throughput and wide-band communications capabilities offered by WARP. Commercial platforms like those from Sundance[68] and Lyrtech[69] provide RF capabilities similar to

WARP, but they lack an open framework for implementing algorithms at both the physical and MAC layers, which is a crucial feature of WARP.

WARP stands out for its distinctive blend of high-performance programmable radio interfaces and open-access frameworks, facilitating research in wireless architecture, physical layer, and network protocols. The effectiveness of WARP in implementing diverse wireless protocols, such as 802.11 g/n PHY and MAC, and achieving real-time performance has made it widely adopted in the research community. Additionally, WARP supports Multiple-Input Multiple-Output (MIMO) technology by incorporating multiple RF interfaces. Thus, WARP has been selected as the wireless research tool for real-time over-the-air transmission and reception, for the experiments conducted in this thesis.

6.2.2. WARP: A Software Defined Radio (SDR) Kit

Software-Defined Radio (SDR) is a programmable transceiver kit that offers the potential to operate on various wireless communication protocols without the need to change or update the associated hardware[70]. Designed to provide a cost-effective and flexible solution, SDR enables the implementation of a wide range of wireless protocols through software. In recent years, SDR has gained significant acceptance due to its ability to realize diverse applications without extensive efforts in integrating different components. This device empowers engineers to incorporate additional features into communication systems and implement numerous signal processing elements or protocols without altering the original hardware or system architecture. It provides a customizable and portable communication platform for various applications, including the prototyping and implementation of wireless protocols with their respective performance evaluations. Furthermore, it can interface with a separate hardware module to facilitate communication over a real channel.

In order to implement radio communication using SDR, previous radio components such as filters, modulation, demodulation, detectors, amplifiers, and mixers have been implemented in software[71]. The motherboard is positioned between the daughter board (RF front-end or TX RF) and the host computer (software) at both the transmitter and receiver ends. Analog-to-digital converters

(ADCs) and digital-to-analog converters (DACs) are employed to convert data formats between analog and digital. Field Programmable Gate Array (FPGA) technology aids in executing high-bandwidth mathematical calculations such as decimation, modulation/demodulation, digital down-conversion, digital up-conversion, and interpolation processes. Wired Ethernet is utilized to transmit and receive data between the motherboard and the host computer[72].

The architecture of SDR at the transmitter and receiver is shown in the following figure:

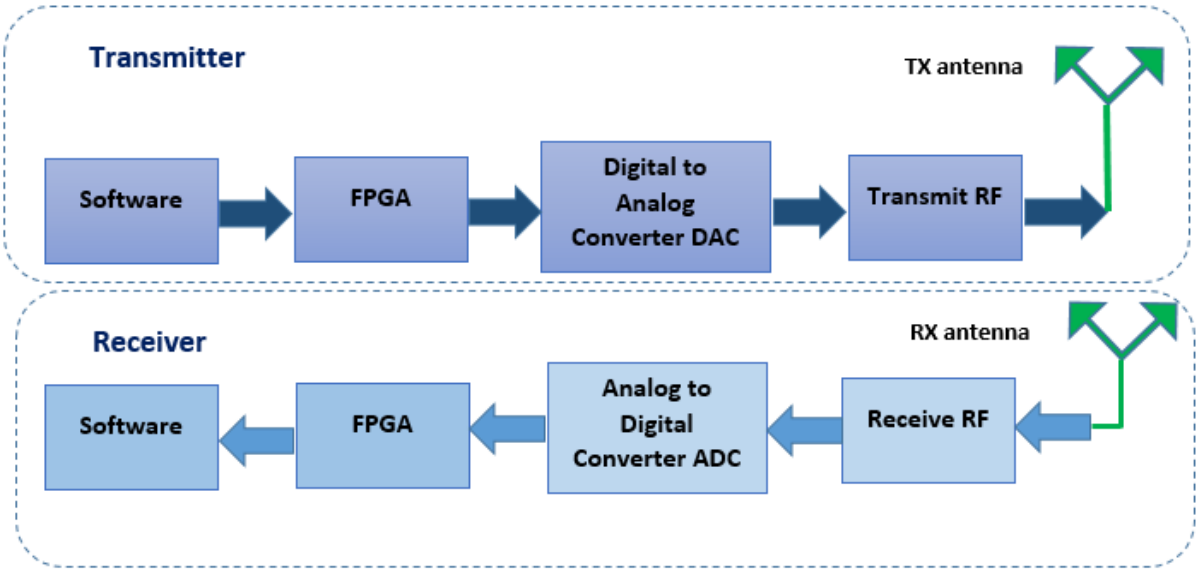

Fig.6.1: Basic Architecture of SDR

The hardware for software-defined radio (SDR) can be approached through three techniques, namely digital signal processors (DSPs), Field Programmable Gate Arrays (FPGAs), and utilizing a General Purpose Processor (GPP) in a conventional computer[73]. WARP serves as an example of an SDR that is implemented on an FPGA hardware platform and relies on the embedded processors integrated on the board. An FPGA is a collection of programmable logic blocks, including general logic, memory, and multiplier blocks, surrounded by a programmable routing fabric. This circuit has the capability to implement any design or function, with the advantage of easy updates. The FPGA's architecture enables the execution of multiple computational operations in parallel, resulting in significant data throughput at relatively low clock rates.

The latest version of WARP, i.e. WARP v3, is equipped with a powerful FPGA for signal processing, providing a higher processing capacity compared to software-based SDR platforms.

6.2.3. WARP v3 BOARD

The latest generation of WARP hardware is WARP v3, which combines a high-performance FPGA, two versatile RF interfaces, and various peripherals to support fast prototyping of customized wireless designs[74]. WARP v3 features a Xilinx Virtex-6 LX240T FPGA, equipped with two MicroBlaze processors and a Gigabit Ethernet peripheral. This configuration enables the FPGA to achieve high symbol rates while conducting all signal processing tasks internally.

The subsequent diagrams illustrate the modular and layered architecture of WARP v3 Board, thereby showcasing the hardware components involved in it [75].

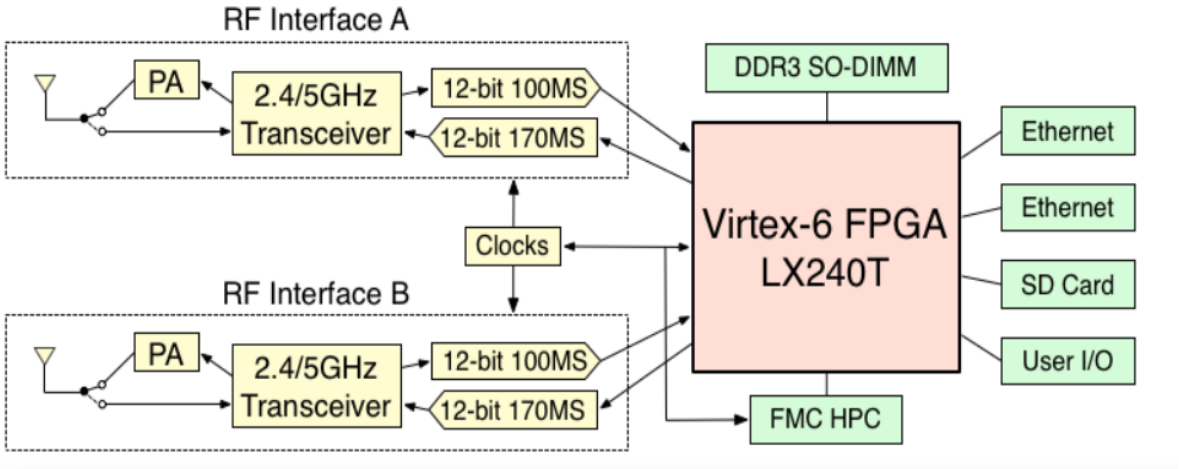

Fig.6.2: Block Diagram of WARP v3

Fig.6.3(a): WARP v3 Board

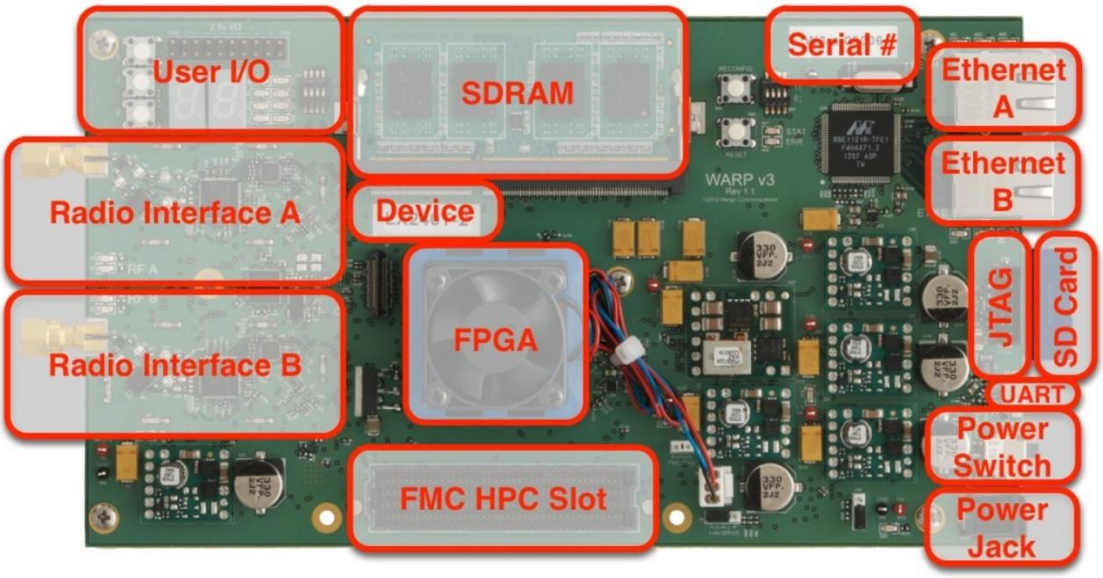

Fig.6.3(b): Labelled Picture of WARP v3

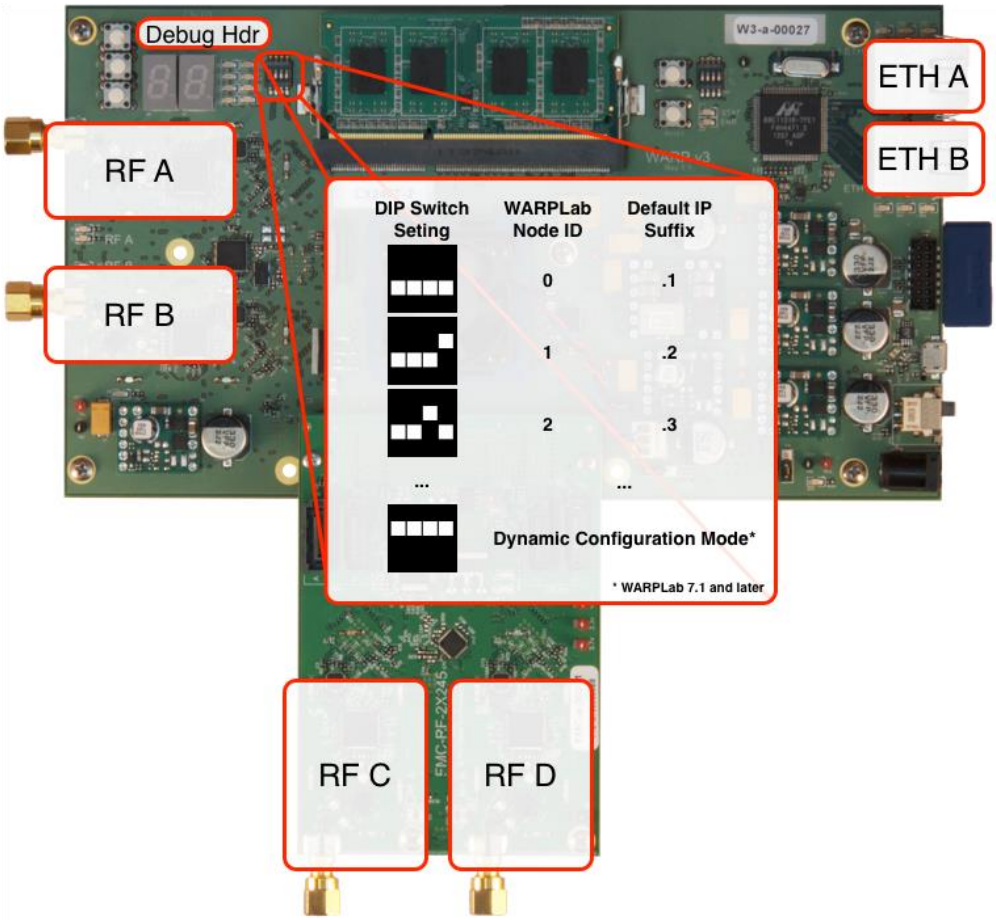

Fig.6.4: WARP v3 Board with FMC

6.2.3.1. Key Hardware Components of WARP v3 Board

The primary hardware components of WARP v3 Board are presented in the following list, accompanied by a brief description of their respective responsibilities[76].

- **User I/O:** This set of interactive elements includes push buttons, LEDs, hexadecimal displays, dip switches, and debug header pins. They allow users to interact with the board by reading values from switches and buttons, and writing values to displays and LEDs. The debug header serves multiple purposes, such as enabling one WARP board to trigger actions on another board via a wire connection.
- **Radio Interfaces A and B:** These interfaces incorporate radios that enable communication in the 2.4 GHz and 5 GHz bands. For each radio interface, the

FPGA delivers digital I and Q values to digital-to-analog converters, which then transmit the signals wirelessly through up conversion. The reverse process occurs for wireless reception, where analog I and Q streams are converted by analog-to-digital converters and delivered to the FPGA. On the board and in reference designs, the interfaces are labeled as "RF A" and "RF B".

- **SDRAM:** This DDR3 SO-DIMM provides additional memory beyond the block RAM within the FPGA. The WARP v3 board includes a pre-tested 2GB SO-DIMM.
- **Device label:** This label displays the FPGA device used on the WARP v3 board. It is referenced in various development processes, such as exporting a peripheral core from Xilinx System Generator, thereby providing convenient lookup.
- **Virtex-6 FPGA:** Located under the fan, the FPGA functions as the central processing system for the WARP board.
- **FMC HPC Slot:** The FPGA Mezzanine Card High Pin Count slot allows connectivity to existing hardware ecosystems and potential WARP-specific modules in the future[77].
- **Serial Number:** This unique serial number identifies the WARP board and is programmed into an EEPROM on the board before shipping. Software running on the hardware can access this information.
- **Ethernet A/B:** These two 10/100/1000 Ethernet ports establish high-speed connections between the board and a wired network. On the WARP v3 board and in reference designs, the ports are labeled as "ETH A" and "ETH B".
- **JTAG:** The JTAG connector permits direct programming of the Virtex-6 FPGA using a Digilent or Xilinx JTAG cable.
- **SD Card:** An alternative programming method to JTAG is utilizing the SD card. It allows programs to be stored in non-volatile memory, which automatically downloads and executes when the SD card is inserted.
- **UART:** The micro-USB connector on the board enables programs on the board to send messages to a computer terminal.
- **Power Switch:** This switch controls the power supply to the board. The "off" position is furthest from the power jack, while the "on" position is closest to the power jack.
- **Power Jack:** The power jack is where the 12V power supply, provided with

the WARP v3 hardware, should be connected. It is important to note that the power switch should be in the "off" position when inserting or removing the power plug. This ensures proper sequencing of power regulators on the board.

The board resources for WARP v3 are showcased in the following Table 6.1[75]:

Table 6.1: Resources of WARP v3 Board

RESOURCE	FEATURES
Memory	• DDR3 SO-DIMM Slot
Ethernet	• Two Gigabit interfaces
Multi-Gigabit Transceivers	• 2.4/5GHz transceiver (40MHz RF bandwidth) • 12-bit 170 MSps DAcs, 12-bit 100MSps ADCs
MGT Clocking	• Dual-band PA (20 dBm, TX power) • Shared Clocking MIMO applications
UART	• FMC HPC expansion slot
User I/O	• 2 Seven Segment Displays • 12 LEDs • 4 Push buttons • 4 bit DIP switch • USB-UART • 16-bit 2.5v I/O header

6.2.3.2. Basic Design Structure of WARP v3 Board

In order to develop custom applications on WARP, it is necessary to utilize Xilinx design tools. All WARP reference designs are constructed using the Xilinx Embedded Development Kit (EDK), which allows the creation of designs incorporating both a processor for running custom software and custom hardware

cores for real-time processing and connection to off-chip hardware.

The EDK consists of two primary tools as follows:

- **Xilinx Platform Studio (XPS):** This tool integrates the hardware cores of a design, including the MicroBlaze processor, memory, peripherals, and interfaces for off-chip hardware.
- **Xilinx Software Development Kit (SDK):** It provides a comprehensive suite of software compilation and debugging tools for the MicroBlaze processor.

The basic structure of WARP reference design is depicted in Fig.6.6[75]:

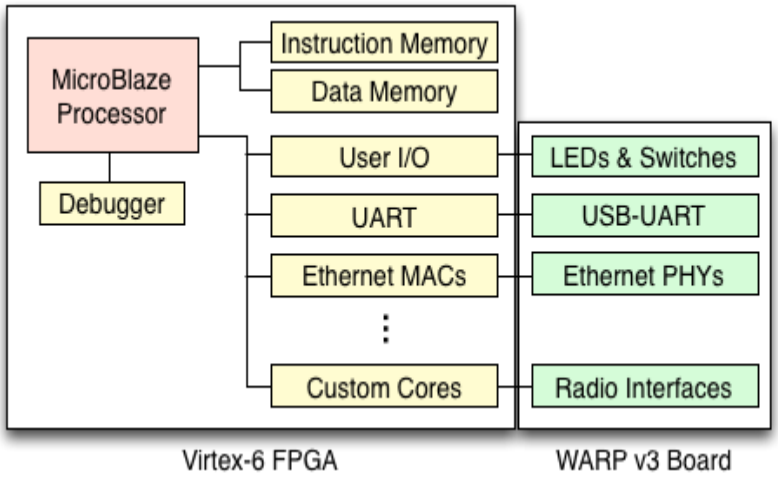

Fig.6.5: Basic Structure of WARP Reference Design

The main components of this architecture include:

- **MicroBlaze Soft Processor:** The MicroBlaze is a processor core implemented within the FPGA fabric and is provided by Xilinx as part of the EDK.
- **Memories:** The Virtex-6 FPGA incorporates numerous "block RAMs" or internal RAM blocks that can be interconnected to create memory areas of various sizes accessible to the MicroBlaze. These block RAMs are utilized for caching, instruction storage, and data storage.
- **Processor bus:** A standard bus connects the MicroBlaze to each core in the system. Current reference designs employ the PLB bus, while future designs

will transition to the newer AXI standard.

- **Peripheral cores:** This collection encompasses various peripheral cores that constitute each hardware design. Some are supplied by Xilinx, such as the UART and Ethernet MAC, while others have been designed specifically for WARP v3, such as the user I/O and radio interface cores.
- **Off-chip resources:** These blocks represent additional hardware components on WARP v3, apart from the FPGA, such as the radio interfaces, FTDI USB-UART transceiver, and Marvell Ethernet PHYs.

The implementation of the MicroBlaze processor and connected cores is achieved in the FPGA fabric using XPS. The outcome of the XPS flow is a "bitstream" that represents the fully synthesized and implemented hardware design. This bitstream incorporates the MicroBlaze, standard peripheral cores, custom cores, I/O assignments, and clock configurations. However, the MicroBlaze instruction and data memories remain empty within this bitstream.

The XPS-generated bitstream, along with its corresponding hardware specification, serves as the initial step in an SDK project. The SDK compiles custom code for the MicroBlaze, as well as drivers for the various cores included in the XPS hardware design. The result of this process is an "elf" file, the software binary, which is prepared for execution by the MicroBlaze. The elf binary is then combined with the XPS-generated bitstream to program the FPGA with the final hardware and software design.

6.2.4. Integration of WARP SDR Kit with WARPLab Framework

WARP has the ability to establish communication with a host computer via Ethernet connections. The experiments conducted on WARP utilize the WARPLab framework, which enables efficient prototyping of physical layer algorithms by combining the user-friendly nature of MATLAB with the capabilities of WARP. WARPLab serves as a framework for rapid prototyping of physical layer functionalities, facilitating the coordination of various configurations of single and multi-antenna transmit and receive nodes. The extensibility of this framework allows users to develop and deploy extensive arrays of nodes to fulfill diverse application

or research requirements.

The implementation of the WARPLab framework is represented by the WARPLab reference design, which facilitates the construction and testing of numerous physical layer designs. This reference design seamlessly integrates MATLAB and FPGA implementations of WARPLab framework modules, offering a high level of flexibility and adaptability. While MATLAB is utilized in the reference design for node control and signal processing, it also enables applications with stringent latency requirements to offload time-critical processing tasks into the FPGA.

The WARPLab framework includes the necessary software components to facilitate convenient interaction with WARP nodes directly from the MATLAB workspace. This software encompasses FPGA code and MATLAB m-code functions, all of which are accessible in the WARP repository[78].

❖ **Hardware Requirements:**

- The utilized version of WARPLab is WARPLab 7, which is compatible with WARP v3 hardware.
- For the 2-radio WARPLab reference design, WARP v3 nodes makes use of the on-board integrated RF interfaces.
- For the 4-radio WARPLab reference design, WARP v3 nodes must be equipped with the FMC-RF-2X245 radio FMC module, in order to provide two more RF interfaces, additional to the ones on-board.

❖ **Software Requirements:**

- MATLAB 2011a or later is required.

❖ **Baseband Buffers Module Implementation:**

The WARPLab Reference Design incorporates a Baseband module responsible for buffering incoming and outgoing samples from radio interfaces. It supports up to 4 interfaces, including I/Q and RSSI. On WARP v3 hardware, each buffer can accommodate over 215 samples.

The generic WARPLab setup wherein multiple WARP nodes are connected to a host PC via an Ethernet switch, is illustrated in the following figure[79]:

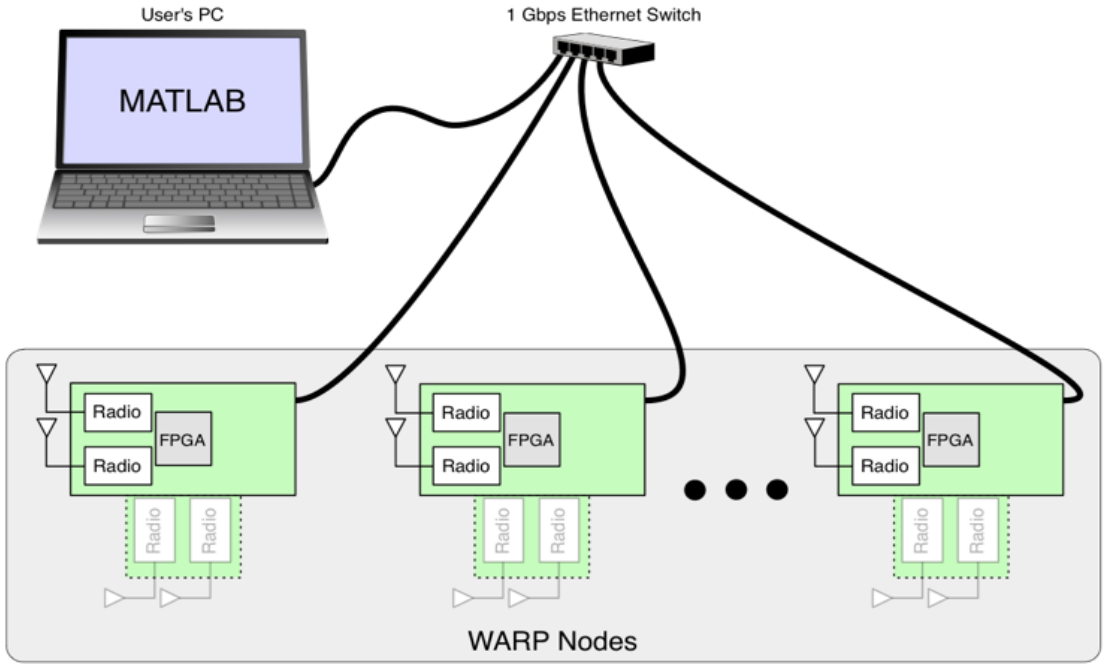

Fig.6.6: Generic Experimental Set-Up using WARP

The following sub-sections discuss some of the significant functionalities, offered by WARPLab 7, that have been used while conducting the experiments of this thesis.

6.2.4.1. TRANSMITTER (TX) and RECEIVER (RX) GAIN

The TX path applies gain at three amplifiers: TX Base Band (TX BB), TX RF, and TX RF PA (Power Amplifier). The TX RF PA is always fixed at 30 dB gain. The TX BB and TX RF amplifiers are adjusted digitally, and the range of gains are as follows:

1. TX BB: In [0, 3] (coarse gain)
2. TX RF: In [0, 63] (fine gain)

The RX path applies gain at two amplifiers: RX Base Band (RX BB) and RX RF. RX amplifiers are also adjusted digitally and the range of gains offered are as follows:

1. RX BB: In [0, 31] (fine gain)
2. RX RF: In [0, 3] (coarse gain)

The TX and RX gain function description as per WARPLab 7 are as follows[80]:

- **tx_gain:** Sets the gains for the variable gain amplifiers in the MAX2829 Tx path.

  Arguments: (int BB_GAIN, int RF_GAIN)

  BB_GAIN: Must be integer in [0,1,2,3] for approx [-5, -3, -1.5, 0]dB baseband gain
  RF_GAIN: Must be integer in [0:63] for approx [0:31]dB RF gain

  Returns: none

  BB_GAIN and RF_GAIN must be scalars (same values for all specified interfaces) or 1-D vectors (one value per interface) with length equal to the length of the interface ID vector

- **rx_gain:** Sets the gains for the variable gain amplifiers in the MAX2829 Rx path.

  Arguments: (int RF_GAIN, int BB_GAIN)

  RF_GAIN: Must be integer in [1,2,3] for approx [0,15,30]dB RF gain
  BB_GAIN: Must be integer in [0:31] for approx [0:63]dB baseband gain

  Returns: none

  BB_GAIN and RF_GAIN must be scalars (same values for all specified interfaces) or 1-D vectors (one value per interface) with length equal to the length of the interface ID vector

6.2.4.2. AUTOMATIC GAIN CONTROL (AGC)

WARPLab includes the option to automatically adjust receiver gains based on the power and structure of an incoming waveform[81].

- **Gain Selection based on RSSI and Received I/Q:**

The transceiver used in WARP's radios, the MAX2829, incorporates two stages of RX gain. The first stage is a low noise amplifier (LNA) that can provide up to 30 dB of amplification, while the second stage is a baseband gain that can provide an additional amplification of up to 63 dB. When combined, these two gain stages can provide a total gain of up to 93 dB to the received signal. The AGC (Automatic Gain Control) core included with WARPLAB operates in three sequential stages to select the appropriate gains:

a) Initially, the AGC triggers the selection of the LNA gain based on the Receive Signal Strength Indicator (RSSI) signal provided by the transceiver. The digital RSSI measurement is first converted into an estimate of received power in dBm. Using this value, the AGC chooses one of three possible LNA gain settings that minimize the Error Vector Magnitude (EVM). The MAX2829 datasheet provides graphs illustrating the EVM for each LNA gain setting as a function of receiver power.

b) Adjusting the LNA gain affects the RSSI measurement. After the RSSI has settled from the previous LNA gain adjustment, its value is re-read and used to make an initial coarse update to the baseband gain stage.

c) Once both the LNA gain and the baseband gain have been adjusted based on the RSSI, the AGC makes a final refinement of the baseband gain using the waveform's I and Q values. Prior to this stage, the waveform cannot be relied upon for accurate power measurement as it may be saturating the radio's ADCs. Refining the baseband gain using the I and Q values introduces a waveform dependence. During the inspection of the I/Q waveform, the magnitude of the signal must exhibit periodicity in 16 40-MHz samples. This requirement can be met by a series of 20 MHz-wide 802.11 Short Training Symbols (STS).

➢ AGC Function description:

agc_target : This command in WARPLab adjusts the target gain of the AGC. A lower (i.e. "more negative") value will produce a smaller signal at the ADCs and vice versa.

Set the AGC target.

Arguments: (int32 target) target: target receive power (in dBm) default value: -16

Returns: none

This command is the best way to adjust AGC behaviour to apply more or less gain. For example, a target of -8dBm will apply more gain than a target of -11dBm, so the waveform will be larger at the inputs of the I and Q ADCs.

6.2.5. OFDM System Design on WARP

The block diagram depicting the implementation of OFDM technique, for a generic number of transmitter (TX) and receiver (RX) antennas, on the WARP module is shown as follows:

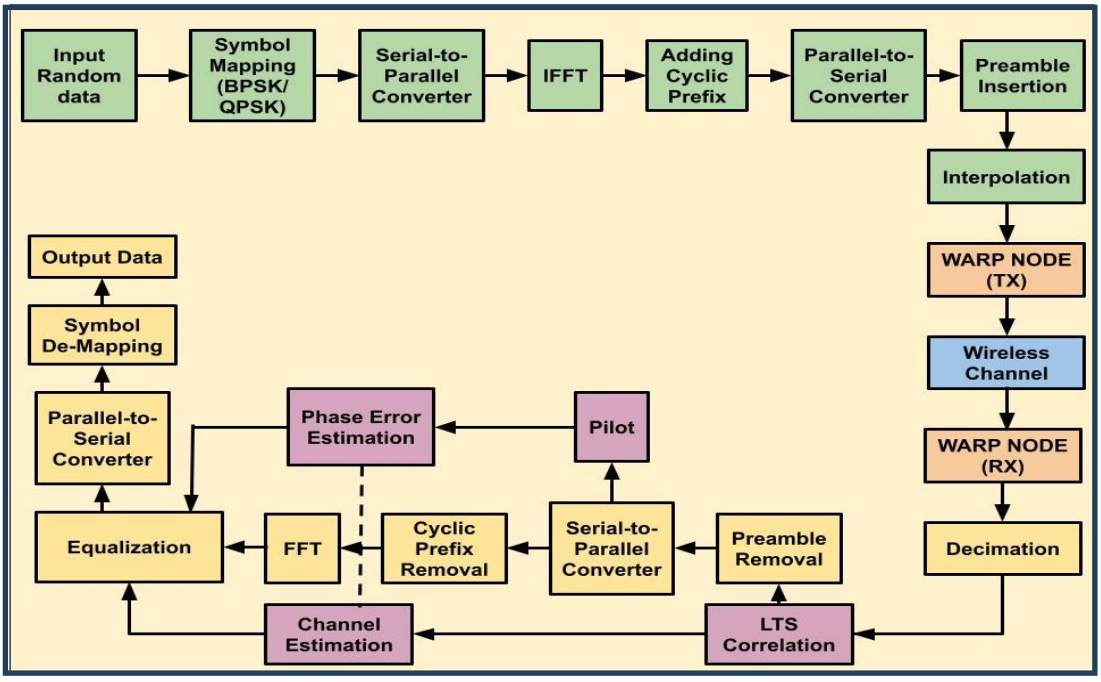

Fig.6.7: Block Diagram of OFDM System Design on WARP

The implementation of OFDM System on WARP takes place in the following steps[82]:

❖ At the Transmitter Side:

- The transmit data bit is mapped into values as per the type of modulation scheme used, i.e., for BPSK and QPSK, the bit sequences consisting of bits 1 and 0, are mapped to values ±1 and four complex values ±0.7071±i 0.7071, respectively, where $i = \sqrt{-1}$.
- Thereafter, the serial-to-parallel block converts the entire data sequence into a matrix of size (N_{data} x N_{sym}); wherein N_{data} is the number of data symbols in a single OFDM symbol, while N_{sym} refers to the total number of OFDM symbols that will be transmitted in a single transmission. In this thesis, 64 sub-carriers are used, out of which 48 sub-carriers are assigned for data symbols, 4 sub-carriers for pilots and the rest are set to zero for Doppler estimation purposes.
- Next, the data symbols and pilots are applied to the IFFT block, whereby, 64-point IFFT is performed on it.
- The output of the IFFT block is converted into serial form by parallel-to-serial converter, followed by addition of cyclic prefix to each OFDM symbol.
- In order to synchronize and estimate the channel, a preamble is added to the overall OFDM frame[83]. The preamble contains two parts: Long Training Sequence (LTS) and Short Training Sequence (STS). The STS and LTS help in packet detection and synchronization applications and also estimate the time and frequency offsets between the receiver and transmitter.

- Following that, the signal is subjected to interpolation to enhance the sampling rate. The interpolation process entails up-sampling and low-pass-filtering (LPF). Subsequently, the signal is modulated onto a higher frequency carrier signal, and it is simultaneously transmitted through all the transmitting antennas.

❖ At the Receiver Side:

- The received signal is decimated. The decimation process involves low-pass filtering and down-sampling.
- Thereafter, the received signal will be cross-correlated with the LTS reference using the following expression[84]:

$$C(n) = \sum_{i=0}^{M} \sum_{j=0}^{N} y(iN + j + n) l^{*}(iN + j) \qquad (6.1)$$

where, y is the total received preamble;

l is one unit LTS;

N is OFDM data length; and,

M is number of cross-correlated LTS.

The cross-correlation process is performed for synchronization process so that the start of each frame can be determined.

- The next step is the removal of cyclic prefix for each OFDM symbol, followed by 64-point FFT.
- The FFT process is followed by Doppler frequency estimation and correction.
- After that, equalization is applied to combat the effects of channel impairments undergone by the signal during transmission through the channel. This is essential to ensure accurate and reliable signal detection[85].

- Finally, the data symbols are converted to the respective bit sequence, through the process of de-mapping as per the employed modulation scheme.

❖ OFDM Frame Design:

The frame design for communication utilizing WARP depends on various parameters. For instance, the follwing experiments in this thesis have utilized a buffer size of 2^16 or 65536 samples in WARP, and the system's sampling rate is set to 40 MHz. This frame design process aims to align the signal structure with the WARP specifications. Each frame should include a field dedicated to accommodating delay margin. The primary sources of delay are propagation delay and data acquisition in WARP, which are assigned as 896 samples. This delay is placed at the end of the frame in the form of zeros, hence referred to as zero padding. Furthermore, all the OFDM symbols not only consist of data but also cyclic-prefix, pilot or training symbols, and virtual subcarriers. The subsequent figure illustrates the frame design for OFDM communication on WARP[84]:

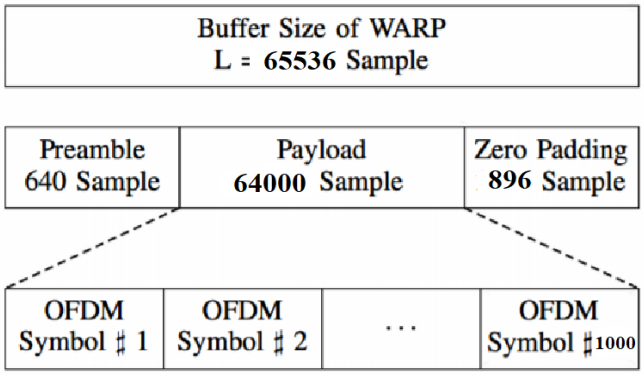

Fig.6.8: OFDM Frame Structure on WARP

❖ CFO, Phase Error and SFO:

Generally, a wireless transmitter and receiver operate with independent clocks, thereby leading to three distinct degradation issues that need to be addressed by the receiver. These are as follows[86]:

a) **Carrier Frequency Offset (CFO):** The difference in frequency between the transmitter and receiver clocks can result in a frequency offset. This offset can cause

the received signal to deviate from its intended frequency, leading to distortion and degradation in signal quality. Therefore, unless CFO is corrected, it will de-orthogonalize the OFDM subcarriers and cause inter-carrier interference (ICI). Thus, CFO is typically corrected in the time domain via multiplication with a digital carrier whose frequency negates the CFO estimate.

b) **Phase Error:** Once the Carrier Frequency Offset (CFO) is corrected in the time domain, there often remains a residual phase error component that needs to be addressed in the frequency domain and continuously tracked over time. To accomplish this, OFDM systems utilize multiple pilot subcarriers. These pilot subcarriers contain known reference signals that enable the correction system. In an OFDM symbol, all the data subcarriers are subjected to a phase rotation to align with any remaining phase rotation observed in the pilot subcarriers. By applying this phase correction, the receiver ensures that the data subcarriers maintain the correct phase relationship, compensating for any residual rotation that may have occurred during transmission. By continually tracking and adjusting the phase based on the pilot subcarriers, the receiver can mitigate the effects of the residual phase error and maintain the integrity of the transmitted data in the presence of frequency and phase variations.

c) **Sampling Frequency Offset (SFO):** The presence of different sampling clocks at the receiver and transmitter causes the temporal duration of a sample to vary slightly between them. As a result, over time, the relative durations of samples will drift apart from each other during reception. This drift introduces larger phase errors, particularly for the outer subcarriers in an OFDM system. To address this issue, each data subcarrier within each OFDM symbol undergoes a unique phase rotation based on its subcarrier index. The phase rotation applied to each subcarrier compensates for the drift and helps align the received subcarriers with the correct timing and phase reference. By individually phase-rotating the data subcarriers according to their specific subcarrier index, the receiver can effectively mitigate the impact of sample duration differences and reduce the phase errors introduced by the drifting sample periods. This enables accurate and reliable demodulation and decoding of the transmitted data in an OFDM system.

6.3. EXPERIMENTAL SETUP

The following sub-sections demonstrates the process of setting up as well as performing the respective experiments.

6.3.1. Requirements for Experimental Setup

- One WARP v3 Board
- 12V DC Power Supply
- One FMC-RF2X245 module
- Four Antennas
- JTAG
- Ethernet Switch
- Xilinx iMPACT Software
- MATLAB 2014a Software

6.3.2. Steps for Experimental Setup

The FMC-RF2X245 module is attached to the WARP v3 board and thereafter the system is employed with four antennas, wherein two antennas serve as transmitters while the other two operate as receivers. The FMC-RF2X245 module is a dual-radio FPGA Mezzanine Card (FMC) daughterboard that expands the capabilities of WARP v3 board from 2 to 4 RF chains.

The following block diagram is a visual representation of the experimental setup:

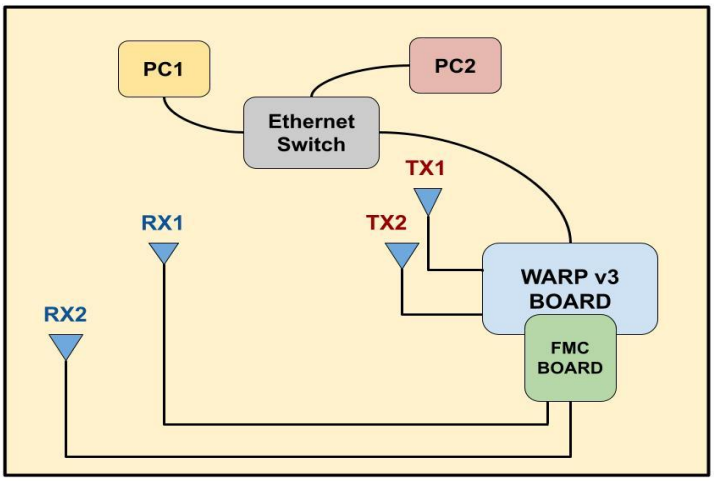

Fig.6.9: Block Diagram of the Experimental Setup on WARP v3

The following steps are subsequently performed to program the WARP v3 board and make it ready for the real-time experiments[87]:

- The power jack is connected to the power port of the WARP v3 board and toggle the power switch to the "ON" position.
- A JTAG cable is used to connect the JTAG connector of the board to the USB port of PC1.
- The Xilinx iMPACT application is opened on PC1. This software facilitates communication, including FPGA configuration, between the computer running iMPACT and the devices on the WARP FPGA board arranged in a **scan chain**. The scan chain involves serial data flowing from the output of each device to the input of its nearest downstream neighbour. The first and last devices in the chain are connected back to the PC via dedicated USB boundary scan circuitry on the WARP FPGA board. Establishing communication through this link is a crucial initial step in utilizing the WARP hardware.
- The FPGA icon is right-clicked and **Initialize Chain** is selected.
- Since 4 RF nodes have been used, hence **4RF bitstream** is used to program the FPGA board. If only 2 RF nodes had been used, then the FPGA would be programmed using 2RF bitstream.
- Then, again after right-clicking on the FPGA icon, **Program** is chosen.
- Finally, iMPACT is closed.
- The basic communication link among the two PCs and the WARP v3 FPGA board, is achieved through Ethernet cables which are connected to an Ethernet switch, for FPGA device configuration, i.e. downloading a program to it. Thereafter, the MATLAB software on PC2 programs the WARP v3 board, on basis of the respective experiment, through the Ethernet switch.

6.3.3. Description of Experimental Setup

The following two cases illustrate different kinds of experiments that have been performed on WARP v3 board.

CASE I:

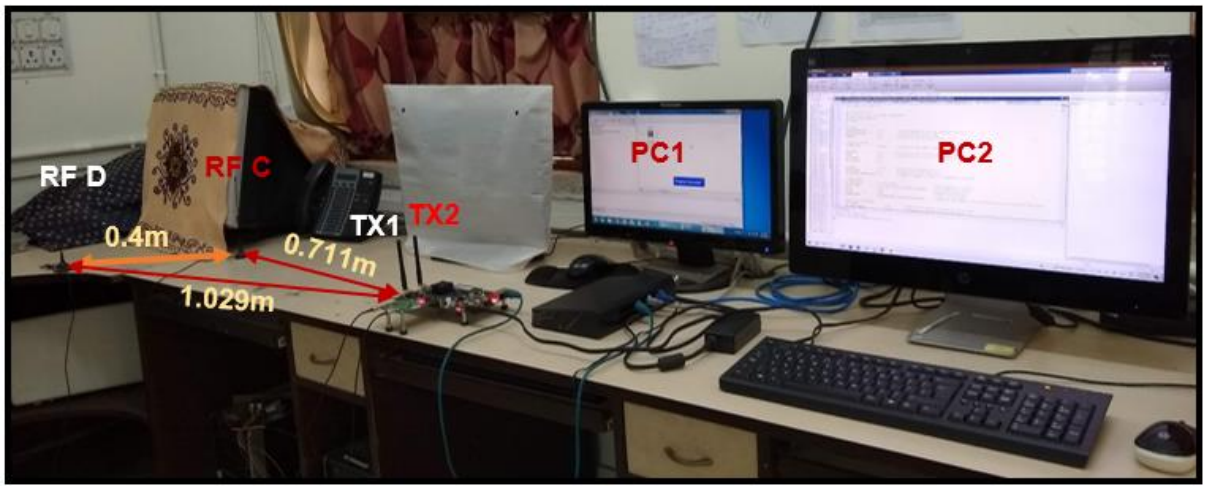

Fig.6.10: Experimental Setup of (2x2)-MIMO model

Fig.6.10 depicts the real-time test-bed implementation of (2x2)-MIMO using WARP v3 board and other necessary software. As it can be seen, two of the antennas (TX1 and TX2) of the WARP transceiver board have been setup as transmitters, while the other two antennas (RF C and RF D) are configured as receivers; wherein the distance between RF C and RF D is set to 0.4m. The distance between the receiving antennas needs to be determined crucially and should be greater than atleast half the operating wavelength, in order to employ diversity among the receiving antennas. In this experiment, RF C and RF D have been placed 40cm apart as it has been practically observed that this is the minimum distance for which the antennas have less interference with each other, whereby they are able to perform diversity effectively. RF C is placed at an approximate distance of 0.711m from the transmitting antennas, while RF D is situated at a rough distance of 1.029m from the transmitting antennas. This (2x2)-MIMO system is experimentally analysed for without and with different precoding schemes, on grounds of Constellation Diagram for BPSK and QPSK modulations respectively, for different values of TX RF Gain and AGC levels.

The following table states the parameters used in conducting the above experiment:

Table 6.2: Experimental Parameters for (2x2)-MIMO model

PARAMETERS	VALUES
Number of Transmitter Antenna	2
Number of Receiver Antenna	2
RF Gain	10, 20
AGC Level	-17, -19, -21
Channel ID	1
Frequency Range	Centre Frequency: 2.412 GHz Start Frequency: 2.401 GHz Stop Frequency: 2.423 GHz
Number of OFDM Symbols	1000
Number of OFDM subcarriers	64
Cyclic Prefix Length	16

CASE II:

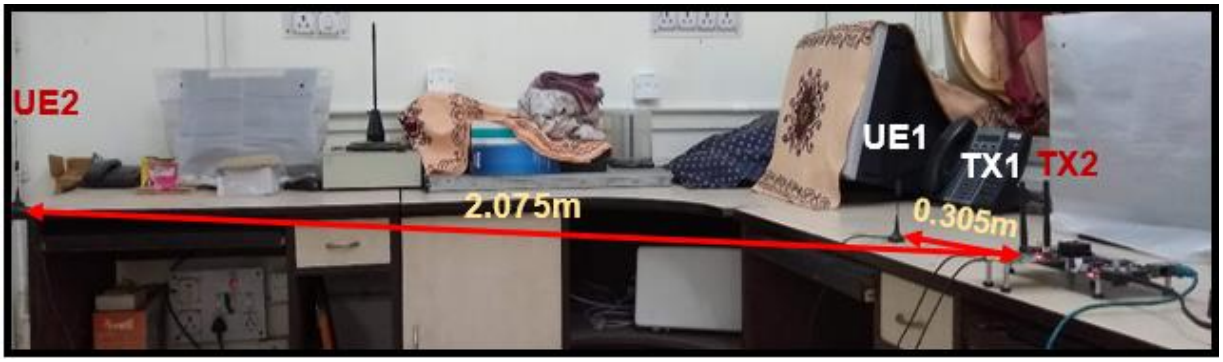

Fig.6.11: Experimental Setup of Downlink two-user (2x2)-MIMO-PD-NOMA model at **distance combination A**

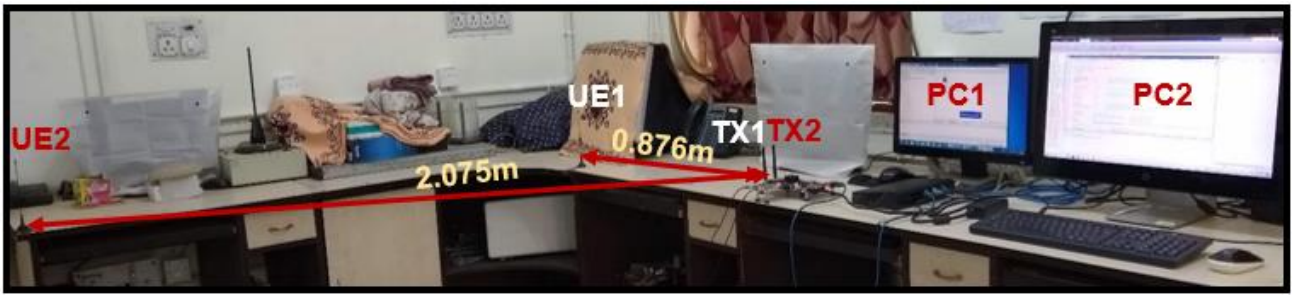

Fig.6.12: Experimental Setup of Downlink two-user (2x2)-MIMO-PD-NOMA model at **distance combination B**

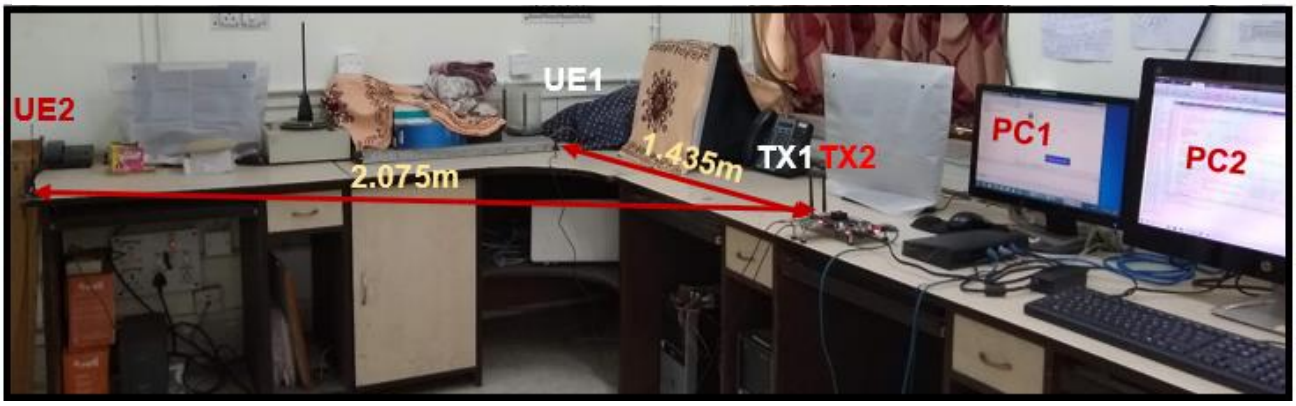

Fig.6.13: Experimental Setup of Downlink two-user (2x2)-MIMO-PD-NOMA model at **distance combination C**

Fig.6.11, Fig.6.12 and Fig.6.13 showcases the real-time test-bed for two-user MIMO-PD-NOMA implementation at different distance combinations, i.e. A, B and C, for near and far user respectively. It can be noticed that two of the antennas (TX1 and TX2) of the WARP transceiver board have been assigned as transmitters of the base station (BS), while the other two antennas represent two separate users (UE1 and UE2) respectively. Therefore, this is an overall (2x2)-MIMO-PD-NOMA system with the BS having two antennas and the two users having single antenna each. The antennas of the two users are placed considerable distance apart from each other so as to ascertain the concept of PD-NOMA, wherein suitable power allocation coefficients are applied depending upon the respective distance of the users from the BS. In this experiment, UE1 denotes the “near user”, while UE2 is the “far user”; and fixed power allocation mechanism has been applied for all the cases. The aforementioned MIMO-PD-NOMA system is experimentally scrutinized for different distance combinations of the two users in order to determine the optimum distance combination, with respect to system BER and Spectral Efficiency, across

different precoding and modulation schemes. For distance combinations A, B and C, UE1 is located at a distance of 0.305m, 0.876m and 1.435m respectively, from the BS; whereas the UE2 is placed at a distance of 2.075m, across all the three distance combinations, as this is the farthest distance possible in order to satisfy PD-NOMA criteria. At the optimum distance combination, the performance of MIMO-PD-NOMA system is experimentally inspected for varied precoding schemes correspondingly, across BPSK, QPSK and Adaptive modulations.

The following table showcases the parameters employed in performing the above experiments:

Table 6.3: Experimental Parameters for Downlink (2x2)-MIMO-PD-NOMA model

PARAMETERS	VALUES
Number of Transmitter Antenna	2
Number of Receiver Antenna	2
Distance Combination A (DIST A)	UE1: 0.305m, UE2: 2.075m
Distance Combination B (DIST B)	UE1: 0.876m, UE2: 2.075m
Distance Combination C (DIST C)	UE1: 1.435m, UE2: 2.075m
Power allocation factor for UE1	0.2
Power allocation factor for UE2	0.8
RF Gain	0-30
AGC Level	-19
Channel ID	1
Frequency Range	Centre Frequency: 2.412 GHz Start Frequency: 2.401 GHz Stop Frequency: 2.423 GHz
Number of OFDM Symbols	1000
Number of OFDM subcarriers	64
Cyclic Prefix Length	16

The subsequent table shows the corresponding power values for the TX RF Gain range used in the aforementioned experiments[63]:

Table 6.4: Power Values for corresponding TX RF Gain

RF GAIN	POWER (in dBm)
0	-33.03
1	-32.85
2	-32.59
3	-32.6
4	-31.53
5	-31.6
6	-30.64
7	-30.57
8	-29.56
9	-29.52
10	-28.45
11	-28.6
12	-27.35
13	-27.34
14	-26.47
15	-26.41
16	-25.34
17	-25.32
18	-24.35
19	-24.45
20	-23.49
21	-23.49
22	-22.54
23	-22.42
24	-21.42
25	-21.54
26	-20.63
27	-20.77
28	-19.64
29	-19.61
30	-18.57

6.4. EXPERIMENTAL RESULTS

The following sub-sections present a broad analysis of the experimental results, with respect to Constellation Diagram, system BER, Sum Capacity and Spectral Efficiency (SE), for a downlink two-user MIMO-PD-NOMA system using OFDM, employing different precoding techniques and varied modulation schemes, at particular distances. The power allocation strategy employed for exhibiting NOMA principle is fixed power allocation (FPA). Additionally, a (2x2)-MIMO setup has also been experimentally analyzed, on grounds of Constellation Diagram, for without and with various precoding schemes, using different combination of TX RF Gain and Automatic Gain Control (AGC) levels. All the experiments have been performed multiple number of times to take their ensemble average for considering different aspects of the real-time environment. The experiment has been conducted on WARP v3 board, in the 2.4 GHz band.

The diverse precoding schemes that have been applied to the above cases are as follows:

i) Matched Filter (MF)

ii) Zero-Forcing (ZF)

iii) Regularized Zero-Forcing (RZF)

iv) Singular Value Decomposition (SVD)

v) Modified Singular Value Decomposition, i.e., MODIFIED SVD

All the analysis regarding Constellation Diagram, system BER, Sum Capacity and Spectral Efficiency (SE) have been made considering three types of modulation schemes, for a real-time environment, as follows:

a) BPSK modulation scheme for both near and far user
b) QPSK modulation scheme for both near and far user
c) QPSK modulation for near user and BPSK for far user, i.e., an Adaptive Modulation scheme

6.4.1. Comparative Analysis of (2x2)-MIMO for without precoding and with varied precoding schemes using different combination of TX RF GAIN and AGC levels:

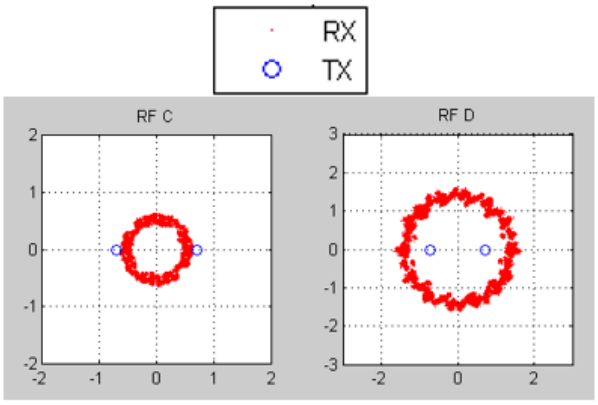

Fig.6.14: Constellation Diagram for BPSK modulation under no precoding at TX RF Gain = 20, AGC level = -17

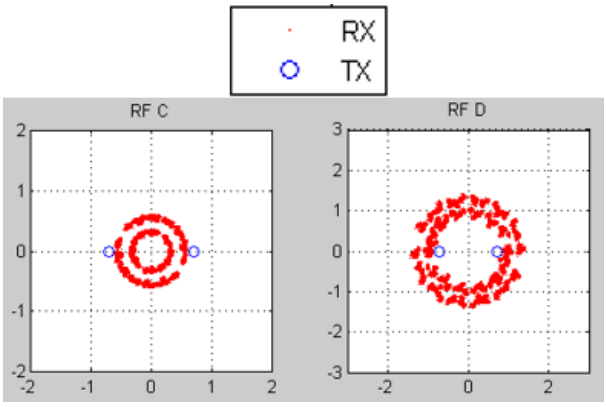

Fig.6.15: Constellation Diagram for BPSK modulation under no precoding at TX RF Gain = 20, AGC level = -19

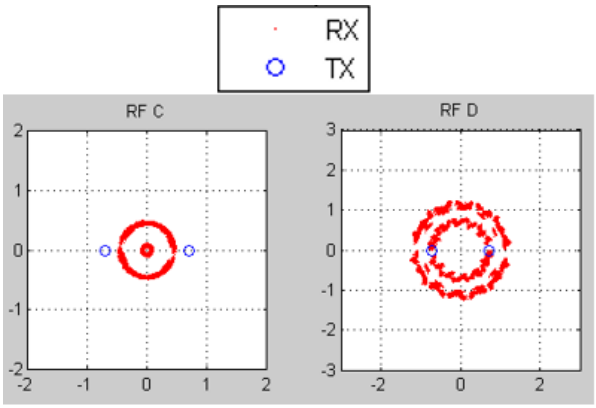

Fig.6.16: Constellation Diagram for BPSK modulation under no precoding at TX RF Gain = 20, AGC level = -21

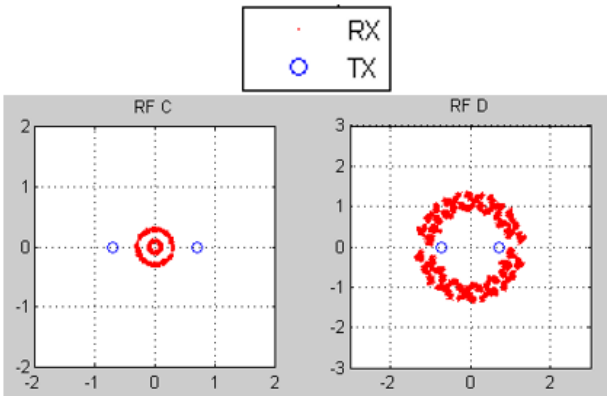

Fig.6.17: Constellation Diagram for BPSK modulation under no precoding at TX RF Gain = 10, AGC level = -17

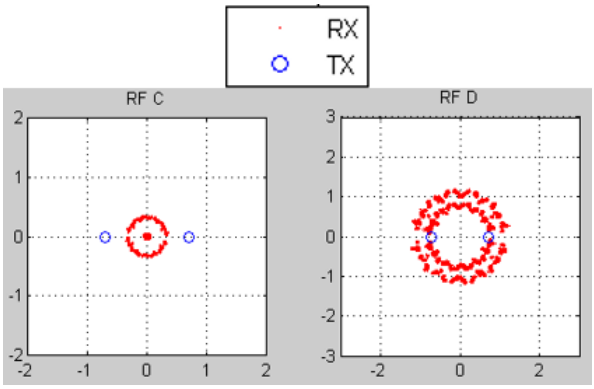

Fig.6.18: Constellation Diagram for BPSK modulation under no precoding at TX RF Gain = 10, AGC level = -19

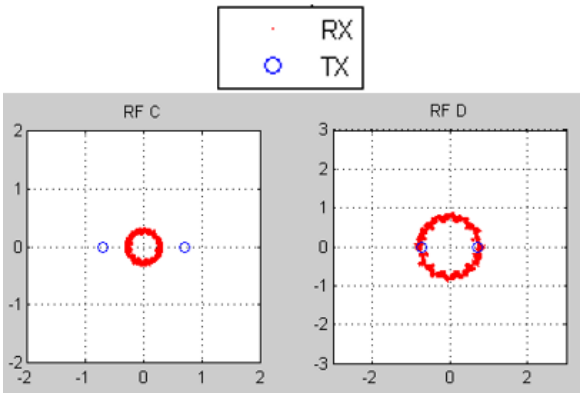

Fig.6.19: Constellation Diagram for BPSK modulation under no precoding at TX RF Gain = 10, AGC level = -21

Fig.6.14, Fig.6.15 and Fig.6.16 depicts the Constellation Diagrams for BPSK modulation at the two receiving antennas, i.e. RF C and RF D respectively, without employing any precoding scheme and setting the TX RF Gain to 20 while changing the AGC levels from -17 to -21, through a step of two. Fig.6.17, Fig.6.18 and Fig.6.19 portrays the Constellation Diagrams for BPSK modulation and a similar above scenario, with only difference being in the TX RF Gain which is set to 10, while adjusting the AGC levels from -17 to -21, through a step of two. It has been observed that when the TX RF Gain is set to 20 and the AGC level is varied from -17 to -21, the RX constellations at both RF C and RF D, consistently shrink in size and try to separate out as two concentric rings, as the AGC levels are decreased. On the other hand, when the TX RF Gain is reduced to 10 and the AGC levels are changed from -17 to -21, it is seen that the two concentric rings of cluster points almost separate out at -17 itself, and by the time the AGC level is decreased to -21, the concentric rings completely merge into a shrunken single circle, with its center lying in between the two TX constellation points. Since, the RX constellation points are more concentrated at RF C than at RF D, therefore, at the former the two individual concentric circles are obtained sooner than at the latter. The two concentric rings of constellation points actually denote the RX cluster of points for the two TX constellation points respectively. However, for all the above cases, the acquired RX constellations are nowhere close to or similar to the TX constellations because no precoding scheme has been utilized whereby, the channel imperfections reside in the received signal, thereby generating a Gaussian cloud of noise for the RX constellations.

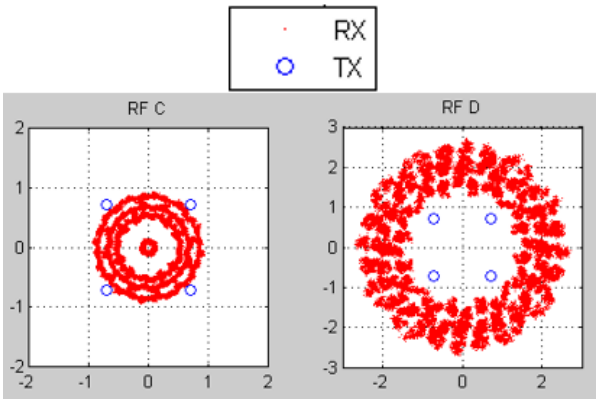

Fig.6.20: Constellation Diagram for QPSK modulation under no precoding at TX RF Gain = 20, AGC level = -17

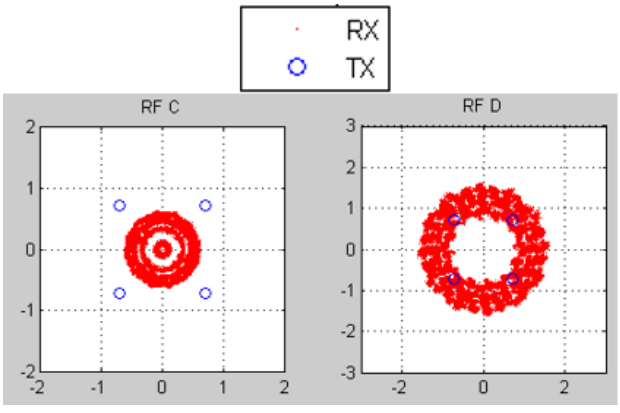

Fig.6.21: Constellation Diagram for QPSK modulation under no precoding at TX RF Gain = 20, AGC level = -19

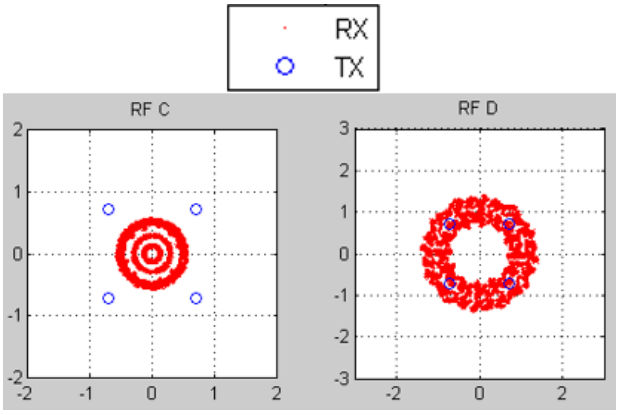

Fig.6.22: Constellation Diagram for QPSK modulation under no precoding at TX RF Gain = 20, AGC level = -21

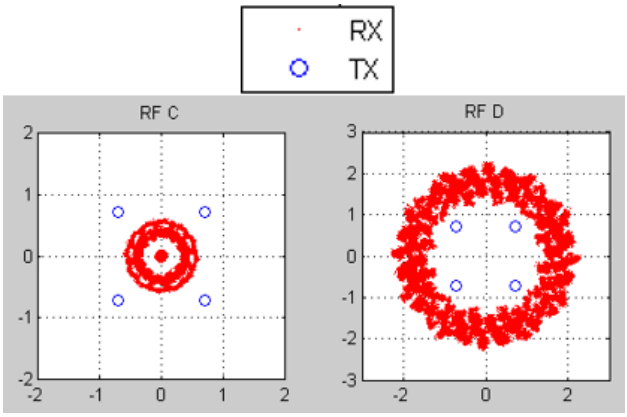

Fig.6.23: Constellation Diagram for QPSK modulation under no precoding at TX RF Gain = 10, AGC level = -17

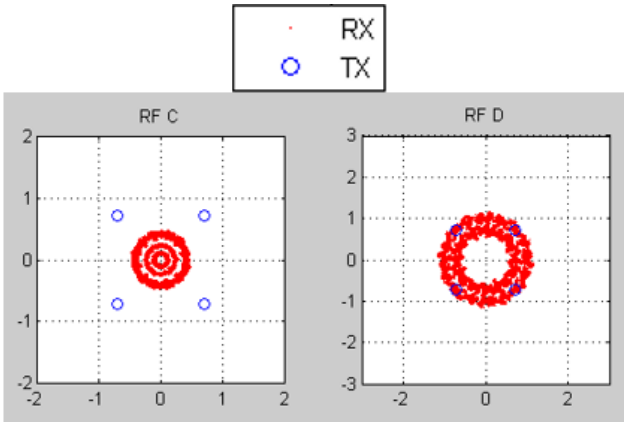

Fig.6.24: Constellation Diagram for QPSK modulation under no precoding at TX RF Gain = 10, AGC level = -19

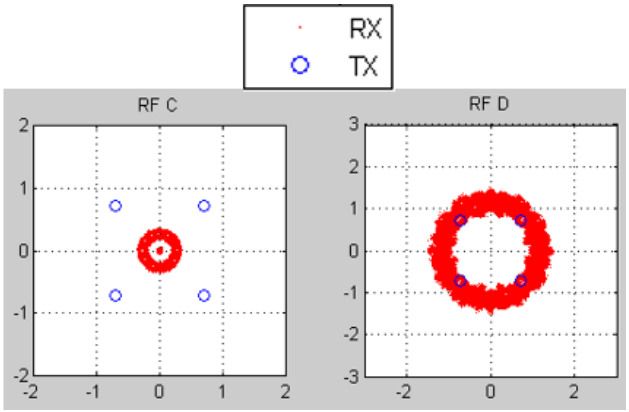

Fig.6.25: Constellation Diagram for QPSK modulation under no precoding at TX RF Gain = 10, AGC level = -21

Figures 6.20, 6.21, and 6.22 represent the Constellation Diagrams for QPSK modulation at the two receiving antennas, RF C and RF D, respectively. These diagrams showcase the scenario without utilizing any precoding scheme. The TX RF Gain is set to 20, and the AGC levels are adjusted from -17 to -21 in steps of two. On the other hand, Figures 6.23, 6.24, and 6.25 displays the Constellation Diagrams for QPSK modulation in a similar scenario as described above. The only difference is that the TX RF Gain is set to 10, while the AGC levels are adjusted from -17 to -21 in steps of two. When the TX RF Gain is set to 20 and the AGC levels are adjusted from -17 to -21, it has been witnessed that the RX constellations at both RF C and RF D exhibit a consistent pattern. They tend to shrink in size and separate into four concentric rings as the AGC levels decrease. On the contrary, when the TX RF Gain is decreased to 10 and the AGC level is changed from -17 to -21, a different behavior is observed. At -19, the four concentric rings of cluster

points almost tend to separate out at RF C, and as the AGC level is further decreased to -21, the concentric rings merge completely into a shrunken single circle. The center of this circle lies at the center of the four TX constellation points. The concentration of RX constellation points is higher at RF C compared to RF D, resulting in the formation of the four individual concentric circles occurring earlier at RF C than at RF D. It is important to note that the four concentric rings of constellation points represent the RX cluster of points corresponding to the four TX constellation points. However, in all the above mentioned cases, the acquired RX constellations differ significantly from the TX constellations. This disparity occurs because no precoding scheme is employed, thereby allowing channel imperfections to manifest in the received signal and generate a Gaussian cloud of noise within the RX constellations.

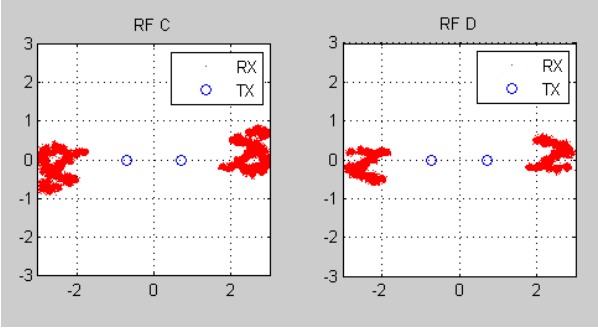

Fig.6.26: Constellation Diagram for BPSK modulation under MF precoding at TX RF Gain = 20, AGC level = -17

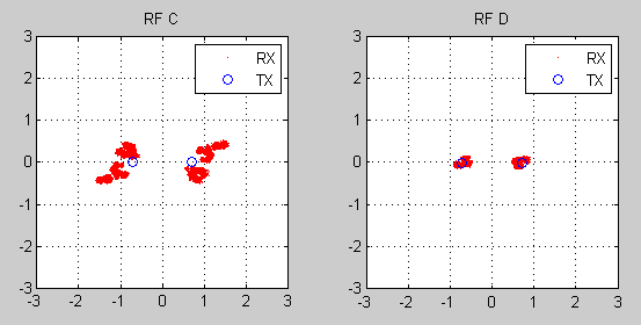

Fig.6.27: Constellation Diagram for BPSK modulation under MF precoding at TX RF Gain = 20, AGC level = -19

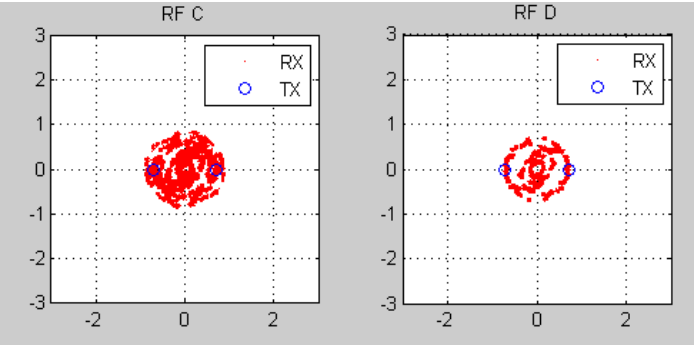

Fig.6.28: Constellation Diagram for BPSK modulation under MF precoding at TX RF Gain = 20, AGC level = -21

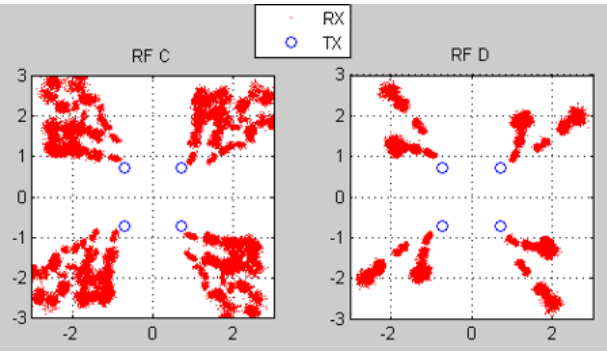

Fig.6.29: Constellation Diagram for QPSK modulation under MF precoding at TX RF Gain = 20, AGC level = -17

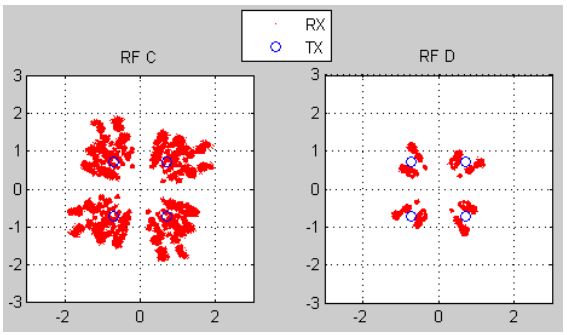

Fig.6.30: Constellation Diagram for QPSK modulation under MF precoding at TX RF Gain = 20, AGC level = -19

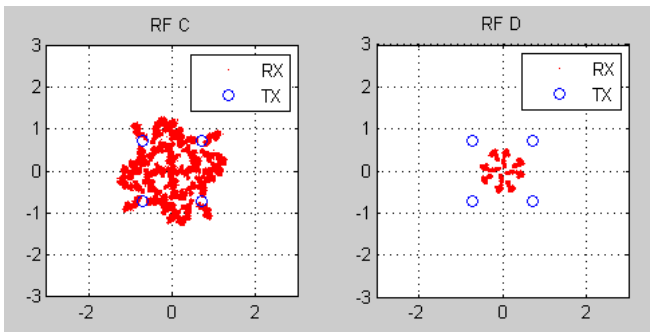

Fig.6.31: Constellation Diagram for QPSK modulation under MF precoding at TX RF Gain = 20, AGC level = -21

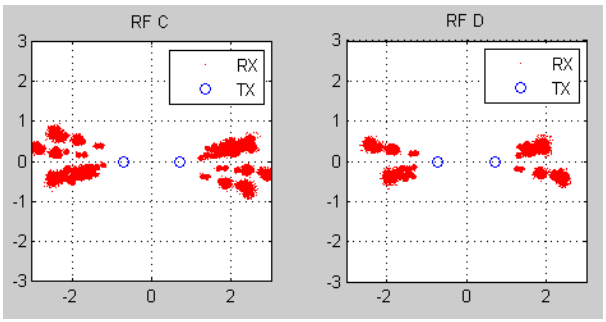

Fig.6.32: Constellation Diagram for BPSK modulation under MF precoding at TX RF Gain = 10, AGC level = -17

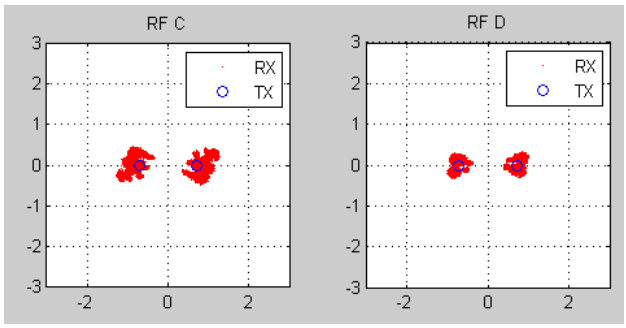

Fig.6.33: Constellation Diagram for BPSK modulation under MF precoding at TX RF Gain = 10, AGC level = -19

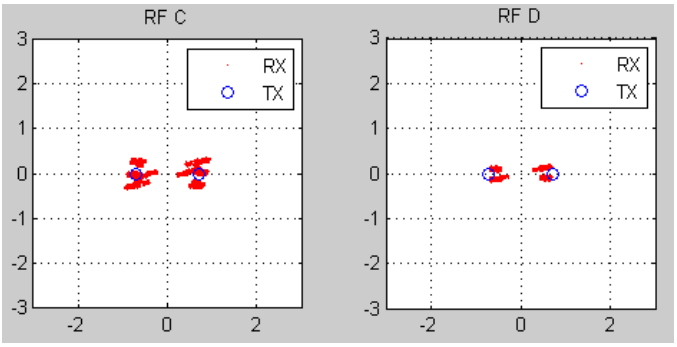

Fig.6.34: Constellation Diagram for BPSK modulation under MF precoding at TX RF Gain = 10, AGC level = -21

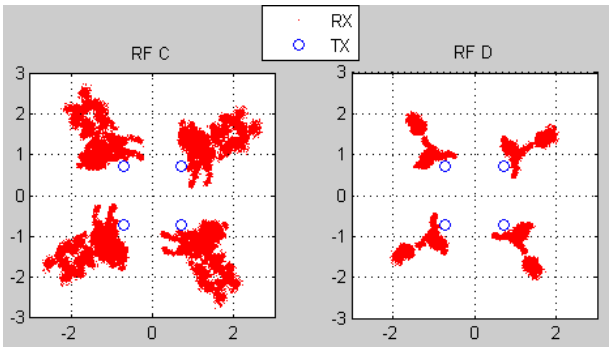

Fig.6.35: Constellation Diagram for QPSK modulation under MF precoding at TX RF Gain = 10, AGC level = -17

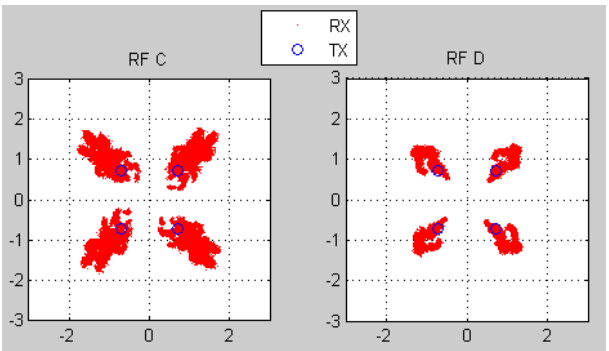

Fig.6.36: Constellation Diagram for QPSK modulation under MF precoding at TX RF Gain = 10, AGC level = -19

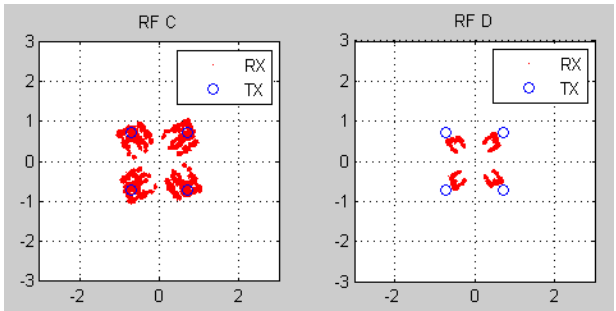

Fig.6.37: Constellation Diagram for QPSK modulation under MF precoding at TX RF Gain = 10, AGC level = -21

Fig.6.26, Fig.6.27, Fig.6.28, Fig.6.29, Fig.30 and Fig.6.31 illustrates the Constellation Diagrams for BPSK and QPSK modulations respectively, at the two receiving antennas, RF C and RF D correspondingly, with the use of MF precoding scheme and setting the TX RF Gain to 20 while changing the AGC levels from -17 to -21, through a step of two. Figures 6.32 to 6.37 presents the Constellation Diagrams for BPSK and QPSK modulations respectively, and an alike scenario as above, with only difference being in the TX RF Gain which is set to 10, while adjusting the AGC levels from -17 to -21, through a step of two. It has been observed that for both the values of TX RF Gain, when the AGC level is varied from -17 to -21, the RX constellation points tend to cluster and try to approach their respective TX constellation points and succeed in doing so at -19 level of AGC. Beyond -19, the RX constellation points tend to surpass their respective TX constellation points and aim to merge at the center of the constellation diagram. Also, for TX RF Gain value of 20, the RX constellation points are a bit more scattered in comparison to that obtained for RF gain value of 10, implying that higher the TX power, more are the chances of the effect of interference among the transmitted signals and hence, this affects the reception of signals. It is interesting to note that the reception of signal is better at RF D than at RF C, for this particular precoding scheme and the respective scenarios, essentially due to the diversity nature of antennas, wherein different antennas perceive signals differently depending upon their position, antenna characteristics as well as the fading environment. The above stated observations apply for both the employed modulation schemes respectively.

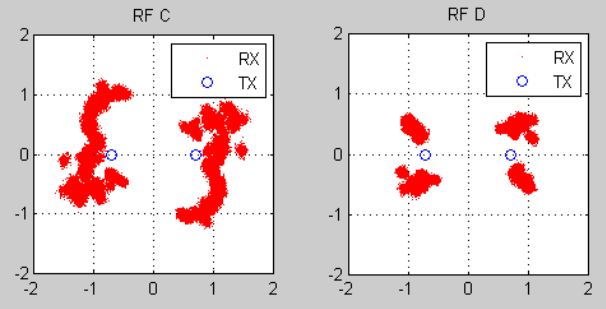

Fig.6.38: Constellation Diagram for BPSK modulation under ZF precoding at TX RF Gain = 20, AGC level = -17

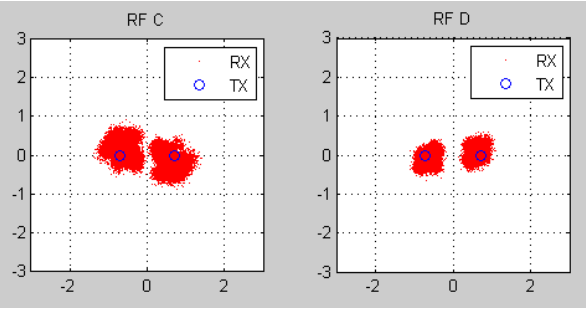

Fig.6.39: Constellation Diagram for BPSK modulation under ZF precoding at TX RF Gain = 20, AGC level = -19

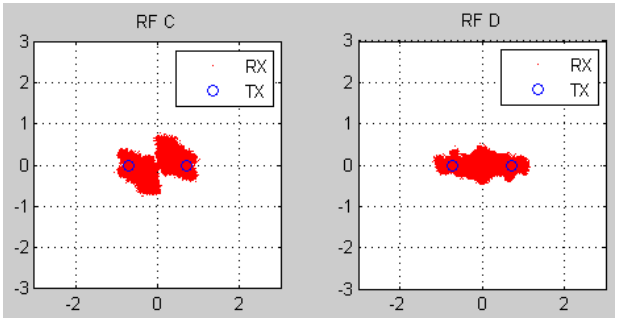

Fig.6.40: Constellation Diagram for BPSK modulation under ZF precoding at TX RF Gain = 20, AGC level = -21

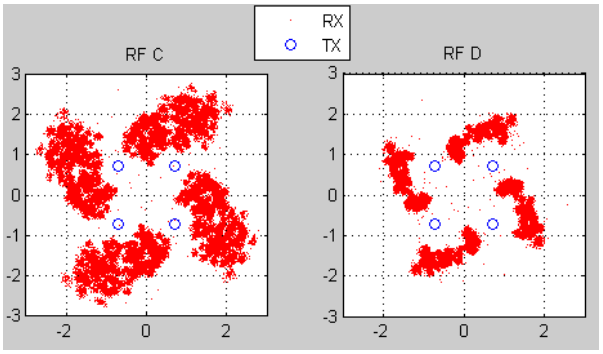

Fig.6.41: Constellation Diagram for QPSK modulation under ZF precoding at TX RF Gain = 20, AGC level = -17

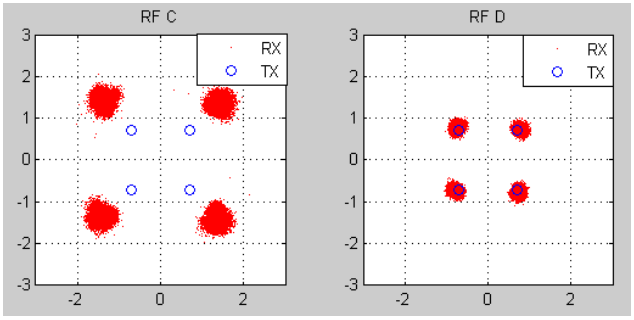

Fig.6.42: Constellation Diagram for QPSK modulation under ZF precoding at TX RF Gain = 20, AGC level = -19

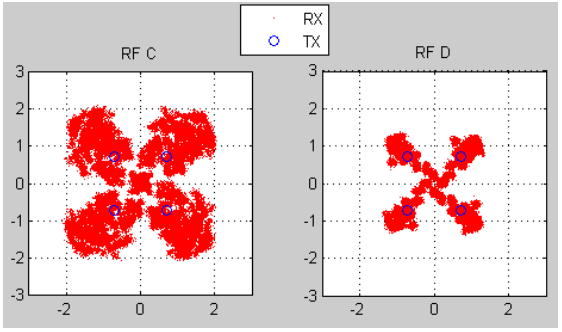

Fig.6.43: Constellation Diagram for QPSK modulation under ZF precoding at TX RF Gain = 20, AGC level = -21

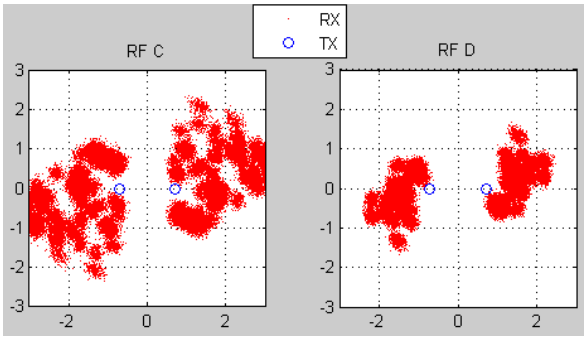

Fig.6.44: Constellation Diagram for BPSK modulation under ZF precoding at TX RF Gain = 10, AGC level = -17

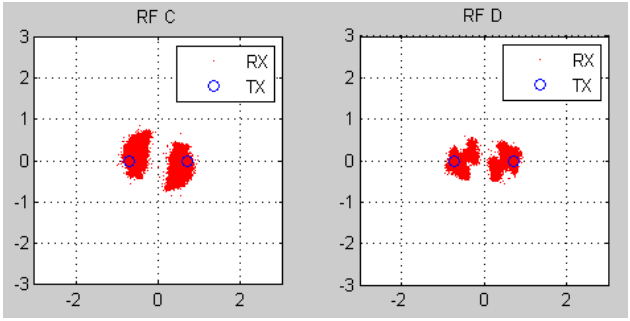

Fig.6.45: Constellation Diagram for BPSK modulation under ZF precoding at TX RF Gain = 10, AGC level = -19

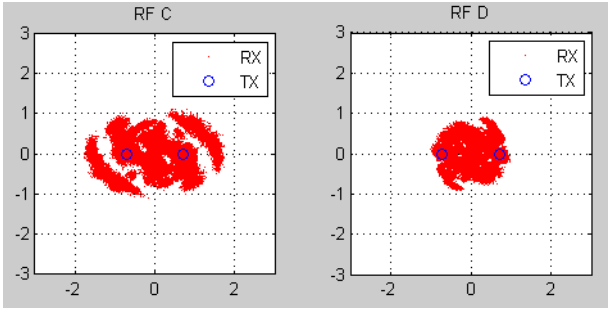

Fig.6.46: Constellation Diagram for BPSK modulation under ZF precoding at TX RF Gain = 10, AGC level = -21

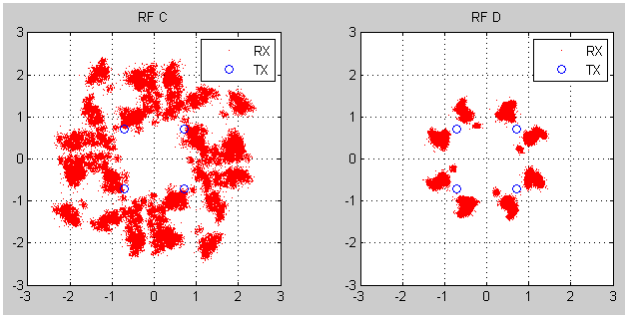

Fig.6.47: Constellation Diagram for QPSK modulation under ZF precoding at TX RF Gain = 10, AGC level = -17

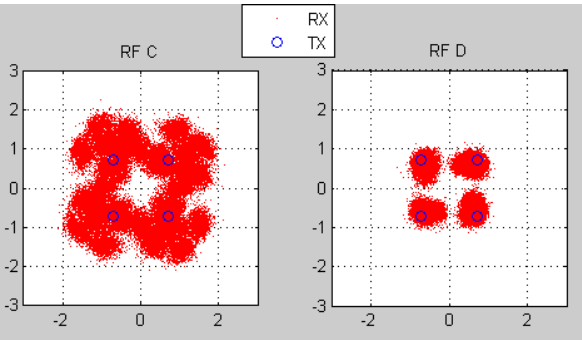

Fig.6.48: Constellation Diagram for QPSK modulation under ZF precoding at TX RF Gain = 10, AGC level = -19

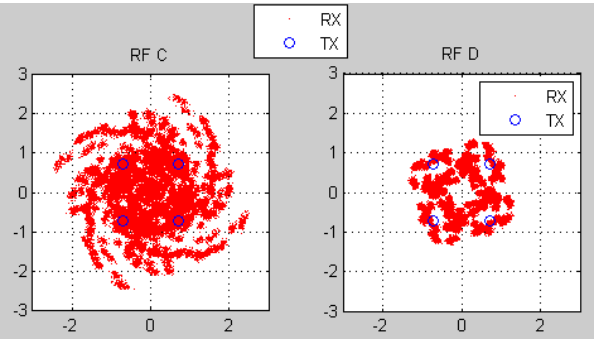

Fig.6.49: Constellation Diagram for QPSK modulation under ZF precoding at TX RF Gain = 10, AGC level = -21

Fig.6.38, Fig.6.39, Fig.6.40, Fig.6.41, Fig.6.42 and Fig.6.43 displays the Constellation Diagrams for BPSK and QPSK modulations respectively, at the two receiving antennas, RF C and RF D correspondingly, with the use of ZF precoding scheme and setting the TX RF Gain to 20 while changing the AGC levels from -17 to -21, through a step of two. Figures 6.44 to 6.49 projects the Constellation Diagrams for BPSK and QPSK modulations respectively, and a similar scenario as above, with only difference being in the TX RF Gain which is set to 10, while adjusting the AGC levels from -17 to -21, through a step of two. Observations have shown that when the AGC level is adjusted from -17 to -21 for both TX RF Gain values, the RX constellation points tend to cluster together and approach their corresponding TX constellation points. This convergence is most successful at an AGC level of -19. Beyond -19, the RX constellation points exceed their TX counterparts and aim to merge at the center of the constellation diagram. Interestingly, when the TX RF Gain value is set to 20, the RX constellation points exhibit more precise clustering at the respective TX constellation points, compared to the case when TX RF Gain value is 10. This implies that although higher TX power increases the likelihood of interference among transmitted signals, but still in regard to ZF precoding, higher TX power is more suitable to overpower the effect of noise that gets incorporated in the received signal, due to the inherent nature of ZF precoding and hence, becomes more prominent in low power signals. It is also worth noting that, considering the diversity nature of antennas, the reception of signals is better at RF D compared to RF C, for this particular precoding scheme and respective scenarios. This is predominantly due to the fact that different antennas perceive signals differently based on their position, antenna characteristics, and the fading environment. These observations are applicable to both employed modulation

schemes, respectively.

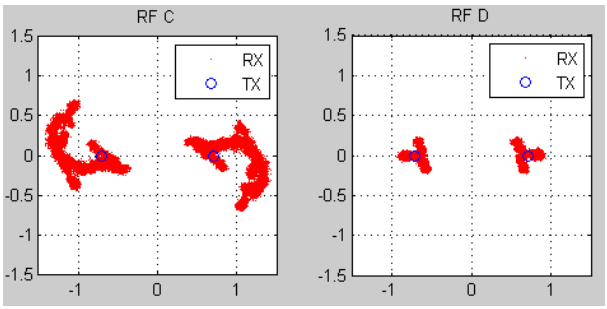

Fig.6.50: Constellation Diagram for BPSK modulation under RZF precoding at TX RF Gain = 20, AGC level = -17

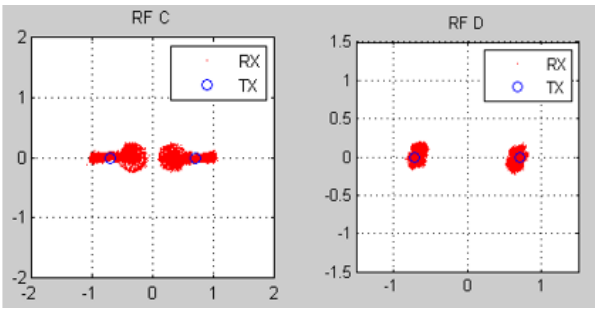

Fig.6.51: Constellation Diagram for BPSK modulation under RZF precoding at TX RF Gain = 20, AGC level = -19

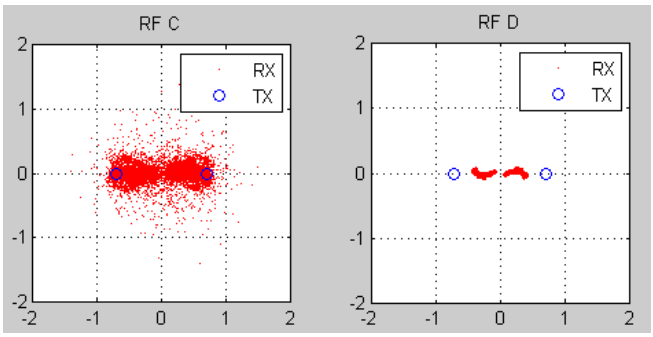

Fig.6.52: Constellation Diagram for BPSK modulation under RZF precoding at TX RF Gain = 20, AGC level = -21

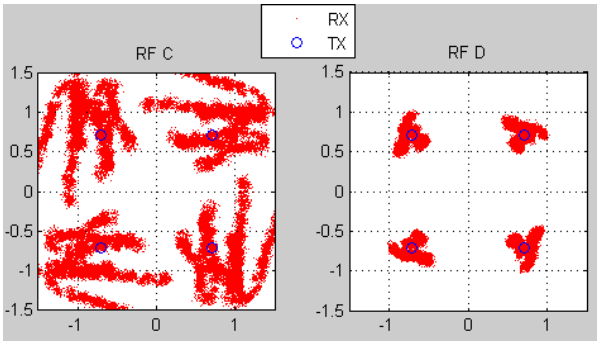

Fig.6.53: Constellation Diagram for QPSK modulation under RZF precoding at TX RF Gain = 20, AGC level = -17

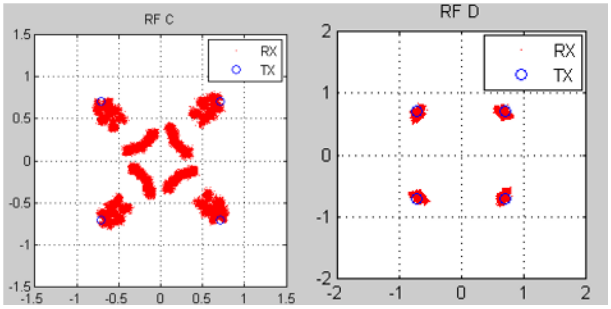

Fig.6.54: Constellation Diagram for QPSK modulation under RZF precoding at TX RF Gain = 20. AGC level = -19

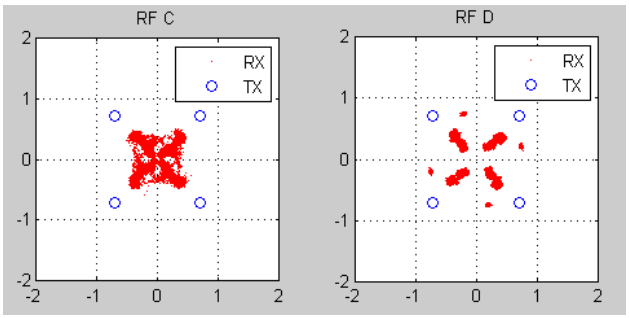

Fig.6.55: Constellation Diagram for QPSK modulation under RZF precoding at TX RF Gain = 10, AGC level = -21

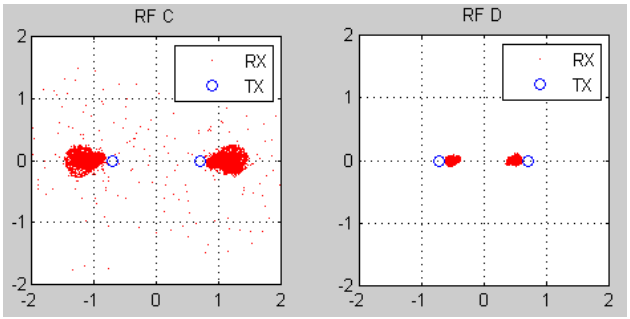

Fig.6.56: Constellation Diagram for BPSK modulation under RZF precoding at TX RF Gain = 10, AGC level = -17

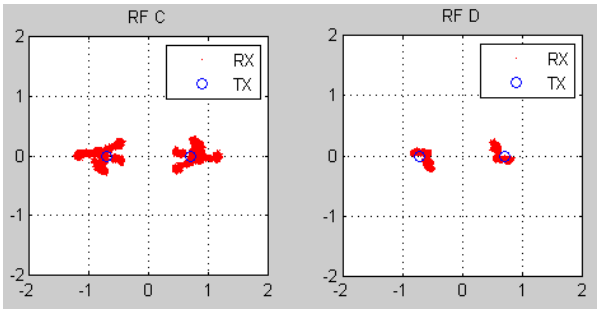

Fig.6.57: Constellation Diagram for BPSK modulation under RZF precoding at TX RF Gain = 10, AGC level = -19

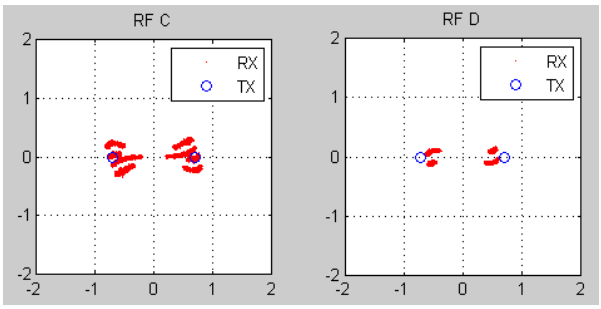

Fig.6.58: Constellation Diagram for BPSK modulation under RZF precoding at TX RF Gain = 10, AGC level = -21

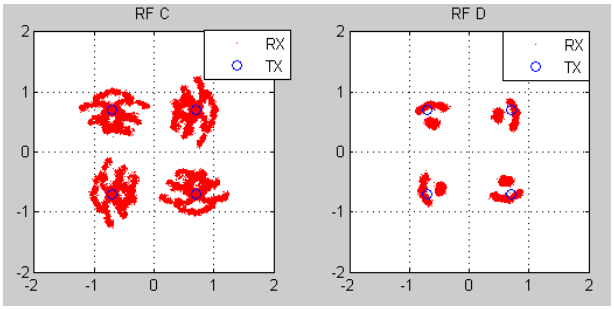

Fig.6.59: Constellation Diagram for QPSK modulation under RZF precoding at TX RF Gain = 10, AGC level = -17

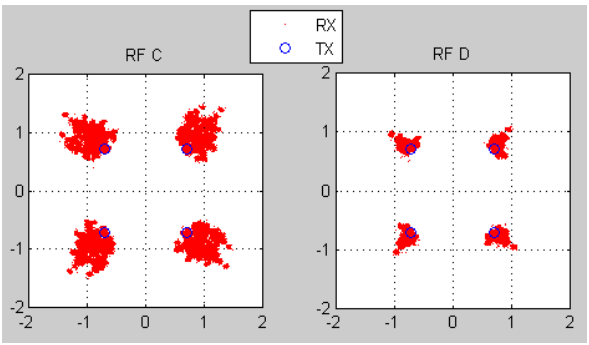

Fig.6.60: Constellation Diagram for QPSK modulation under RZF precoding at TX RF Gain = 10, AGC level = -19

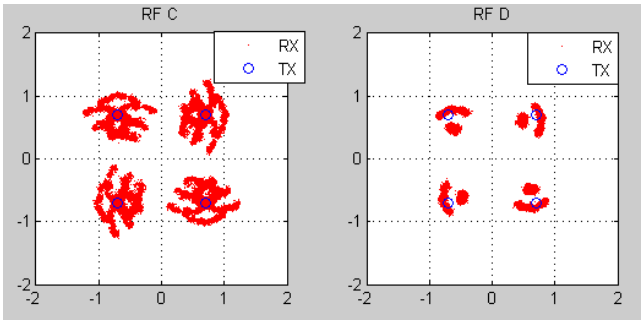

Fig.6.61: Constellation Diagram for QPSK modulation under RZF precoding at TX RF Gain = 10, AGC level = -21

Fig.6.50, Fig.6.51, Fig.6.52, Fig.6.53, Fig.6.54 and Fig.6.55 depicts the Constellation Diagrams for BPSK and QPSK modulations respectively, at the two receiving antennas, RF C and RF D correspondingly, with the utilization of RZF precoding scheme and setting the TX RF Gain to 20 while changing the AGC levels from -17 to -21, through a step of two. Figures 6.56 to 6.61 represents the Constellation Diagrams for BPSK and QPSK modulations respectively, and an alike scenario as above, with only difference being in the TX RF Gain which is set to 10, while adjusting the AGC levels from -17 to -21, through a step of two. In case of RZF precoding too, observations reveal that when the AGC level is adjusted from -17 to -21 for both TX RF Gain values, the RX constellation points exhibit a tendency to cluster and approach their corresponding TX constellation points. This convergence is notably achieved at an AGC level of -19. However, beyond -19, the RX constellation points begin to surpass their corresponding TX constellation points

and strive to merge at the center of the constellation diagram. Additionally, when comparing TX RF Gain value of 20 to TX RF Gain value of 10, it is evident that the RX constellation points are a bit more largely clustered in the former, especially for AGC level -17. This implies that as the TX power increases, the likelihood of interference among transmitted signals rises, consequently impacting signal reception. Interestingly, for the given precoding scheme and respective scenarios, the reception of signals is superior at RF D compared to RF C. This discrepancy can be primarily attributed to the diverse nature of antennas, wherein different antennas perceive signals differently based on their position, antenna characteristics, and the prevailing fading environment. It is worth noting that the aforementioned observations apply to both employed modulation schemes.

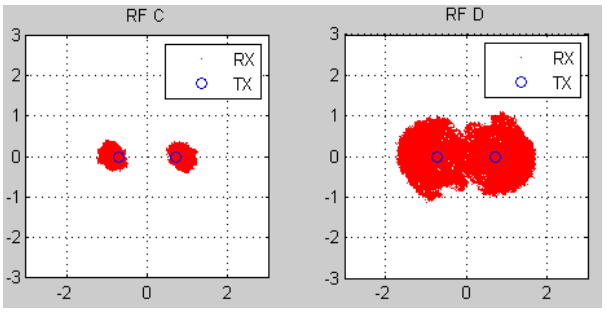

Fig.6.62: Constellation Diagram for BPSK modulation under SVD precoding at TX RF Gain = 20, AGC level = -17

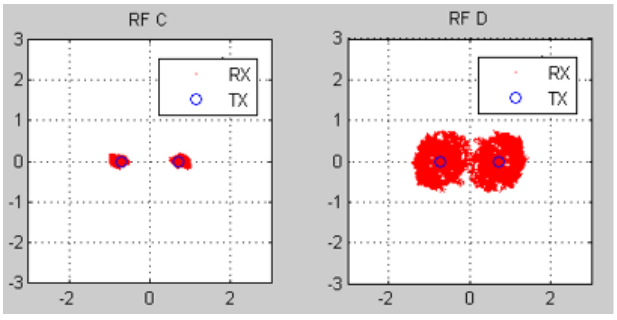

Fig.6.63: Constellation Diagram for BPSK modulation under SVD precoding at TX RF Gain = 20, AGC level = -19

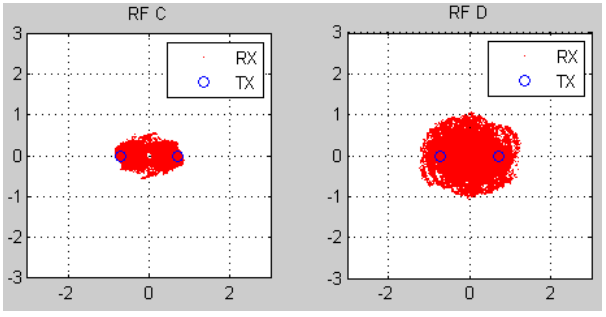

Fig.6.64: Constellation Diagram for BPSK modulation under SVD precoding at TX RF Gain = 20, AGC level = -21

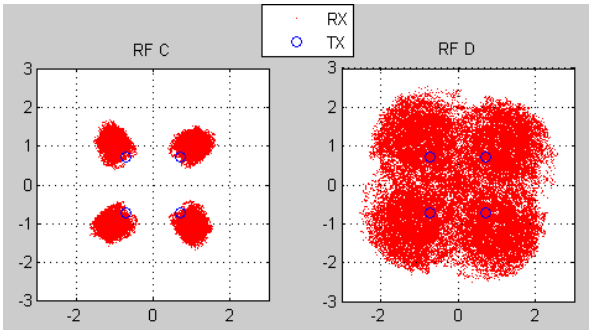

Fig.6.65: Constellation Diagram for QPSK modulation under SVD precoding at TX RF Gain = 20, AGC level = -17

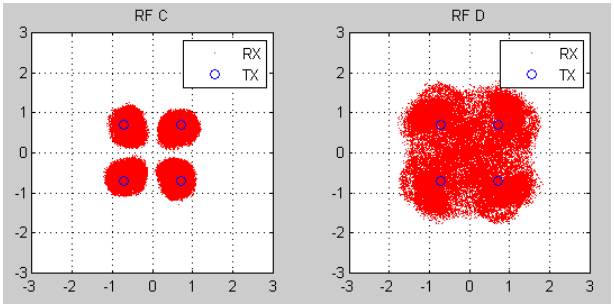

Fig.6.66: Constellation Diagram for QPSK modulation under SVD precoding at TX RF Gain = 20, AGC level = -19

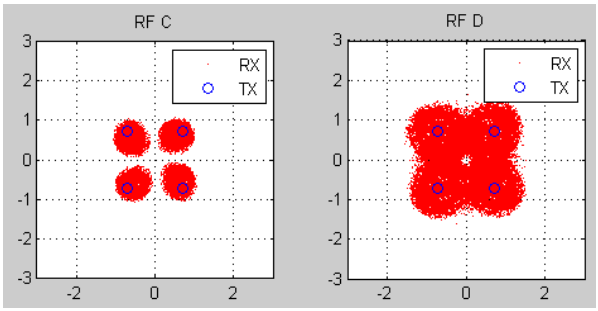

Fig.6.67: Constellation Diagram for QPSK modulation under SVD precoding at TX RF Gain = 20, AGC level = -21

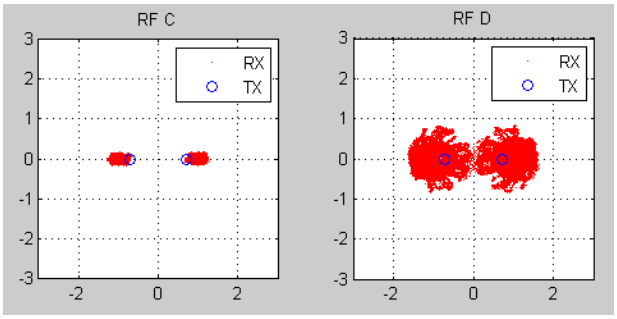

Fig.6.68: Constellation Diagram for BPSK modulation under SVD precoding at TX RF Gain = 10, AGC level = -17

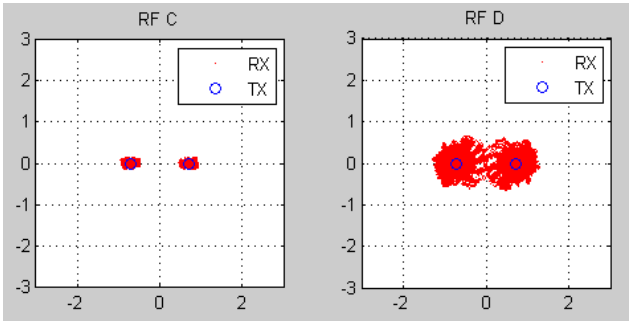

Fig.6.69: Constellation Diagram for BPSK modulation under SVD precoding at TX RF Gain = 10, AGC level = -19

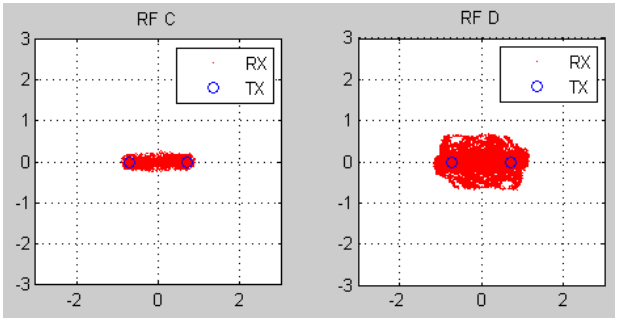

Fig.6.70: Constellation Diagram for BPSK modulation under SVD precoding at TX RF Gain = 10, AGC level = -21

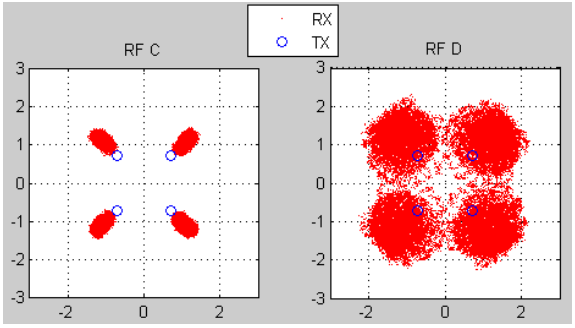

Fig.6.71: Constellation Diagram for QPSK modulation under SVD precoding at TX RF Gain = 10, AGC level = -17

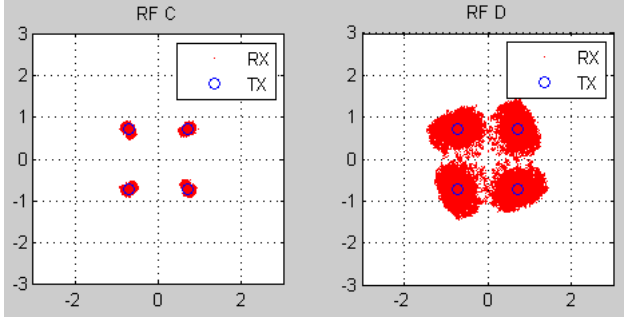

Fig.6.72: Constellation Diagram for QPSK modulation under SVD precoding at TX RF Gain = 10, AGC level = -19

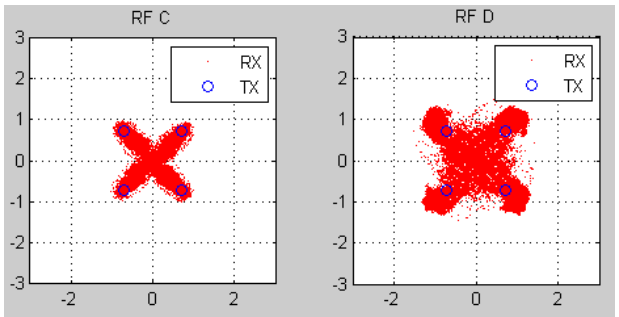

Fig.6.73: Constellation Diagram for QPSK modulation under SVD precoding at TX RF Gain = 10, AGC level = -21

Fig.6.62, Fig.6.63, Fig.6.64, Fig.6.65, Fig.6.66 and Fig.6.67 illustrates the Constellation Diagrams for BPSK and QPSK modulations respectively, at the two receiving antennas, RF C and RF D correspondingly, with the employment of SVD precoding scheme and setting the TX RF Gain to 20 while changing the AGC levels from -17 to -21, through a step of two. Figures 6.68 to 6.73 presents the Constellation Diagrams for BPSK and QPSK modulations respectively, and an alike scenario as above, with only difference being in the TX RF Gain which is set to 10, while adjusting the AGC levels from -17 to -21, through a step of two. It has been witnessed that for both values of TX RF Gain value, when the AGC levels are varied from -17 to -21, the RX constellation points cluster at the respective TX constellations, at AGC level -17 itself and maintains this till AGC level -19. As soon as the AGC level is decreased to -21, the RX constellations tend to drift towards to the center of the constellation diagram, thereby merging or attempting to merge with one another. In case of SVD precoding too, comparatively larger clusters are formed for TX RF Gain value of 20 in comparison to TX RF Gain value of 10, implying that as the TX power increases, the probability of interference among transmitted signals also rises, thereby affecting the reception of the signals. Also, it is interestingly noteworthy that in the context of the provided precoding scheme and respective scenarios, the reception of signals exhibits a superiority at RF C than at RF D. This distinction can primarily be attributed to the diverse characteristics of the antennas, whereby their position, antenna properties, and the prevailing fading environment result in varied perceptions of signals. These observations are applicable for both BPSK and QPSK modulation schemes.

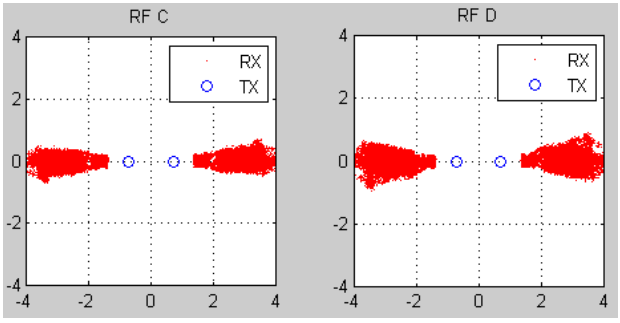

Fig.6.74: Constellation Diagram for BPSK modulation under MODIFIED SVD precoding at TX RF Gain = 20, AGC level = -17

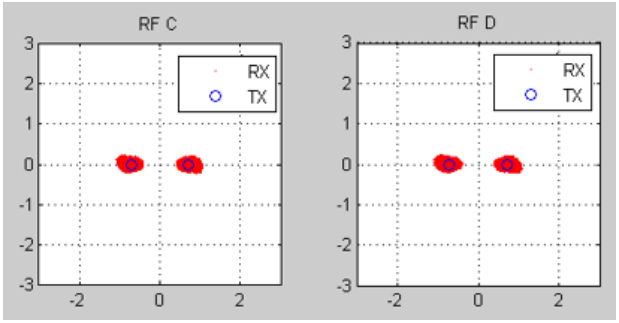

Fig.6.75: Constellation Diagram for BPSK modulation under MODIFIED SVD precoding at TX RF Gain = 20, AGC level = -19

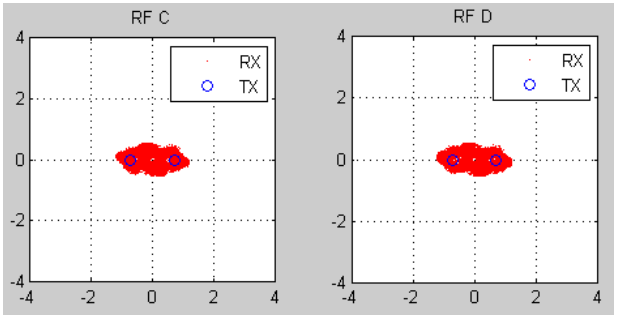

Fig.6.76: Constellation Diagram for BPSK modulation under MODIFIED SVD precoding at TX RF Gain = 20, AGC level = -21

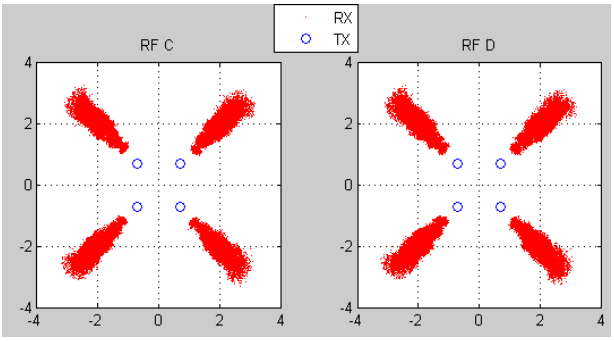

Fig.6.77: Constellation Diagram for QPSK modulation under MODIFIED SVD precoding at TX RF Gain = 20, AGC level = -17

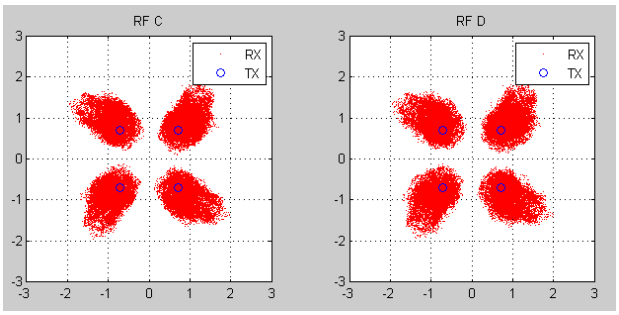

Fig.6.78: Constellation Diagram for QPSK modulation under MODIFIED SVD precoding at TX RF Gain = 20, AGC level = -19

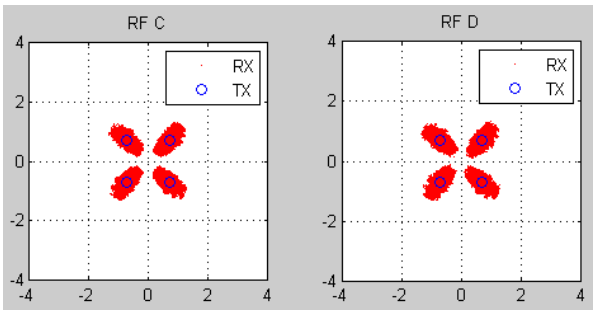

Fig.6.79: Constellation Diagram for QPSK modulation under MODIFIED SVD precoding at TX RF Gain = 20, AGC level = -21

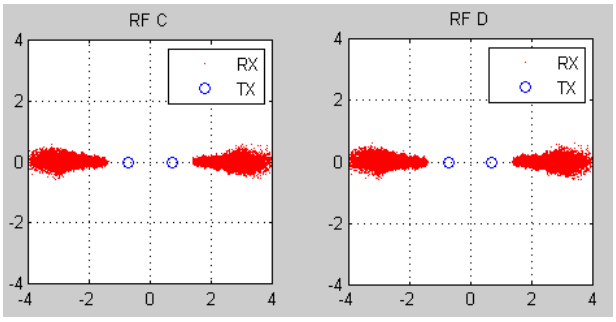

Fig.6.80: Constellation Diagram for BPSK modulation under MODIFIED SVD precoding at TX RF Gain = 10, AGC level = -17

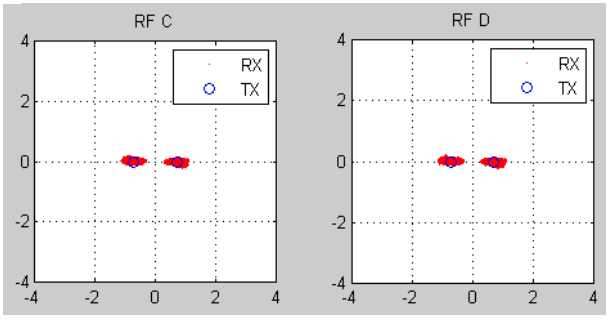

Fig.6.81: Constellation Diagram for BPSK modulation under MODIFIED SVD precoding at TX RF Gain = 10, AGC level = -19

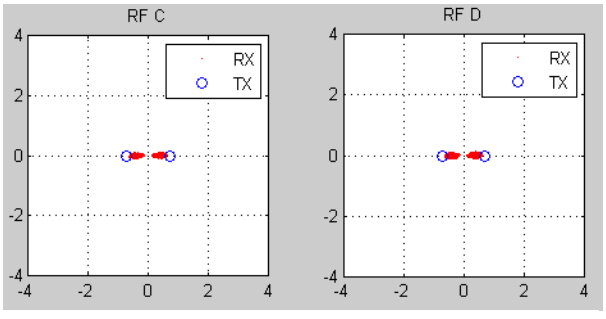

Fig.6.82: Constellation Diagram for BPSK modulation under MODIFIED SVD precoding at TX RF Gain = 10, AGC level = -21

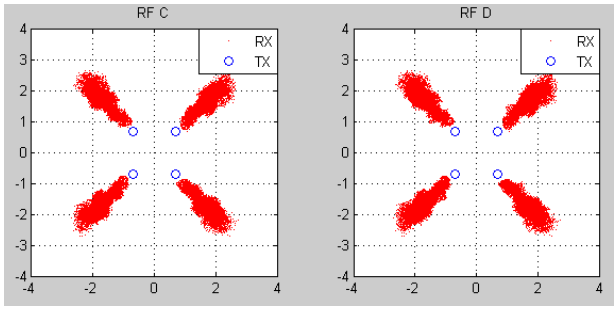

Fig.6.83: Constellation Diagram for QPSK modulation under MODIFIED SVD precoding at TX RF Gain = 10, AGC level = -17

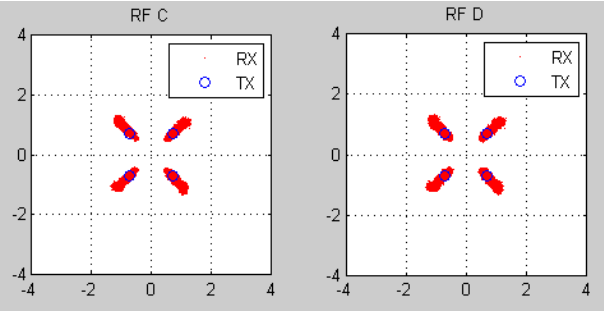

Fig.6.84: Constellation Diagram for QPSK modulation under MODIFIED SVD precoding at TX RF Gain = 10, AGC level = -19

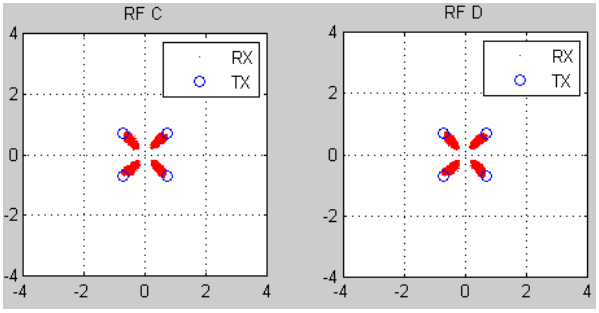

Fig.6.85: Constellation Diagram for QPSK modulation under MODIFIED SVD precoding at TX RF Gain = 10, AGC level = -21

Fig.6.74, Fig.6.75, Fig.6.76, Fig.6.77, Fig.6.78 and Fig.6.79 depicts the Constellation Diagrams for BPSK and QPSK modulations respectively, at the two receiving antennas, RF C and RF D correspondingly, with the application of MODIFIED SVD precoding scheme and setting the TX RF Gain to 20 while changing the AGC levels from -17 to -21, through a step of two. Figures 6.80 to 6.85 presents the Constellation Diagrams for BPSK and QPSK modulations respectively, and an alike scenario as above, with only difference being in the TX RF Gain which is set to 10, while adjusting the AGC levels from -17 to -21, through a step of two. In case of MODIFIED SVD precoding too, observations indicate that when the AGC level is adjusted from -17 to -21, for both TX RF Gain values, the RX constellation points demonstrate a tendency to cluster at a distance and tend to approach towards their corresponding TX constellation points. Notably, this convergence is achieved at an AGC level of -19. However, beyond -19, the RX constellation points begin to exceed their corresponding TX constellation points and strive to drift towards the center of the constellation diagram. Additionally, when comparing the TX RF Gain value of 20 to the TX RF Gain value of 10, it becomes apparent that the RX constellation points are more densely clustered in the former. This suggests that as the TX power increases, the likelihood of interference among transmitted signals also rises, consequently impacting signal reception. Interestingly, for the above stated precoding scheme and respective scenarios, the reception of signals happens to be comparable at both the antennas. This behaviour can be accredited to the dominance of the precoding scheme over antenna diversity, their varying positions and the prevailing fading environment. It is important to note that the aforementioned observations are applicable to both employed modulation schemes.

6.4.2. Comparative Analysis of two-user MIMO-NOMA for different distances using varied precoding techniques and different modulation schemes:

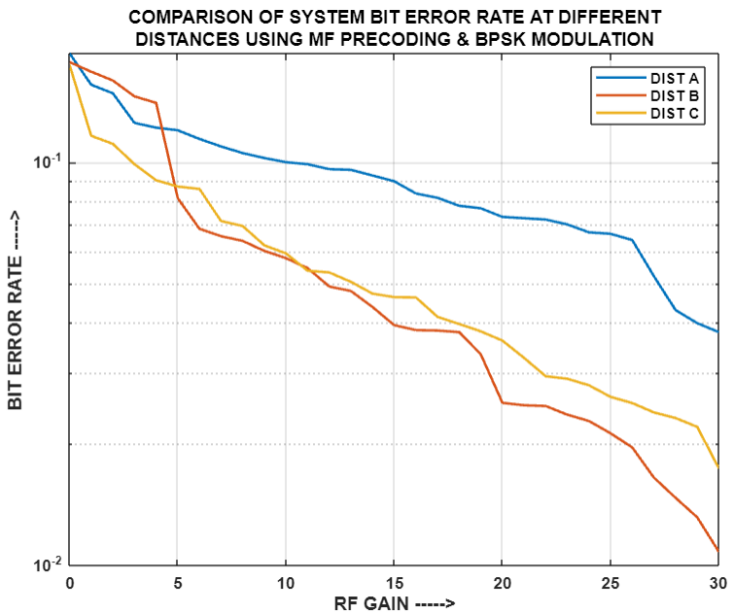

Fig.6.86: Comparison of System BER at different distances using MF and BPSK

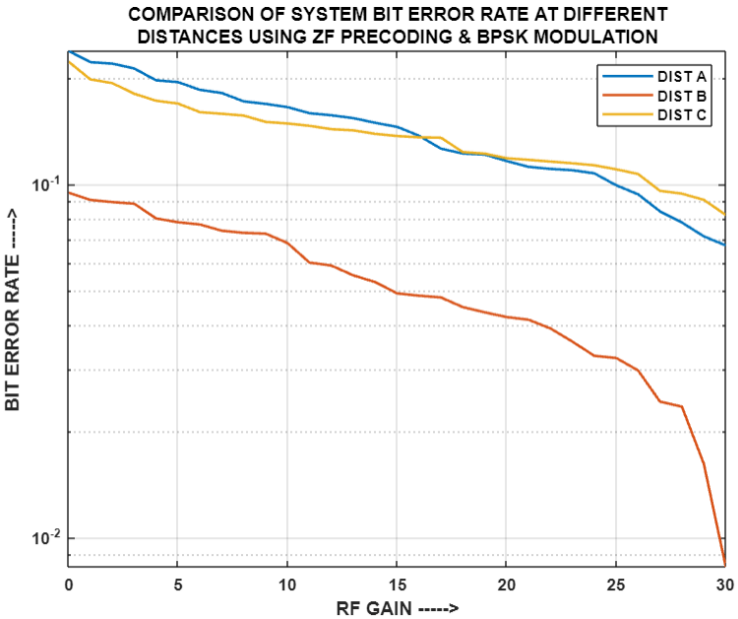

Fig.6.87: Comparison of System BER at different distances using ZF and BPSK

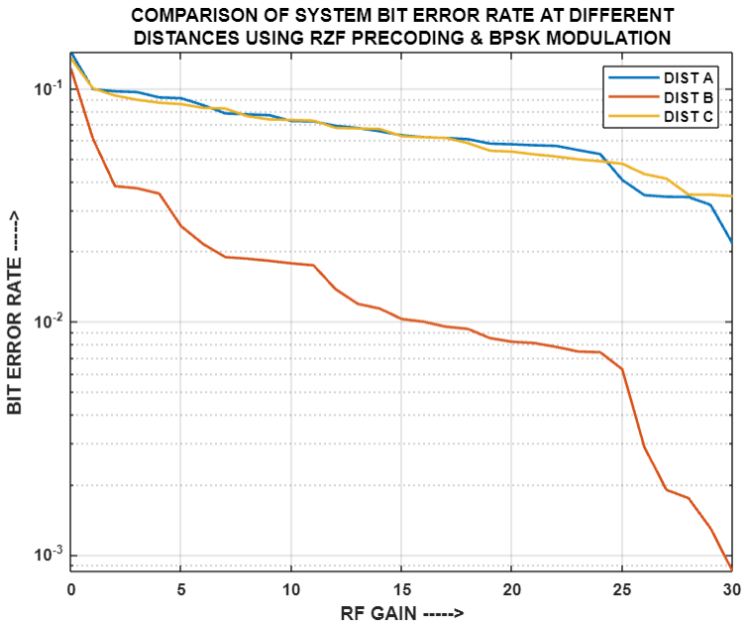

Fig.6.88: Comparison of System BER at different distances using RZF and BPSK

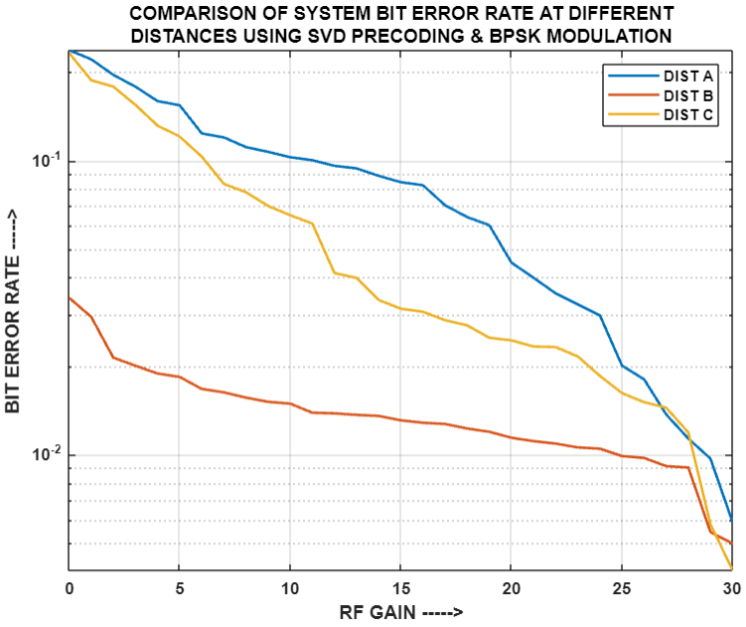

Fig.6.89: Comparison of System BER at different distances using SVD and BPSK

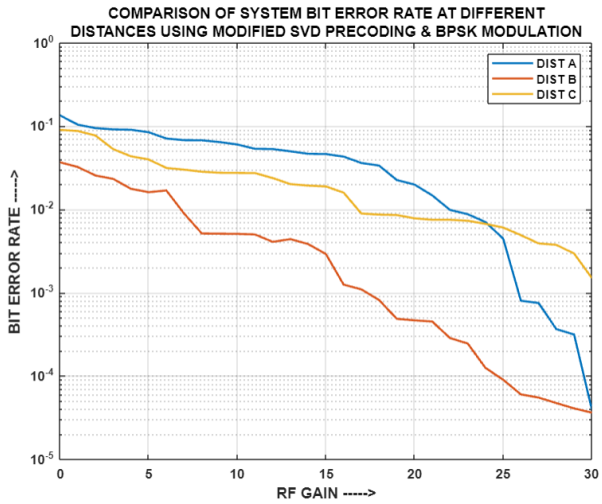

Fig.6.90: Comparison of System BER at different distances using MODIFIED SVD and BPSK

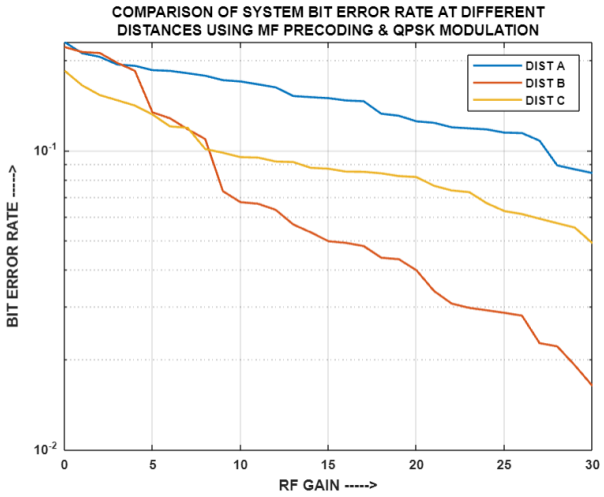

Fig.6.91: Comparison of System BER at different distances using MF and QPSK

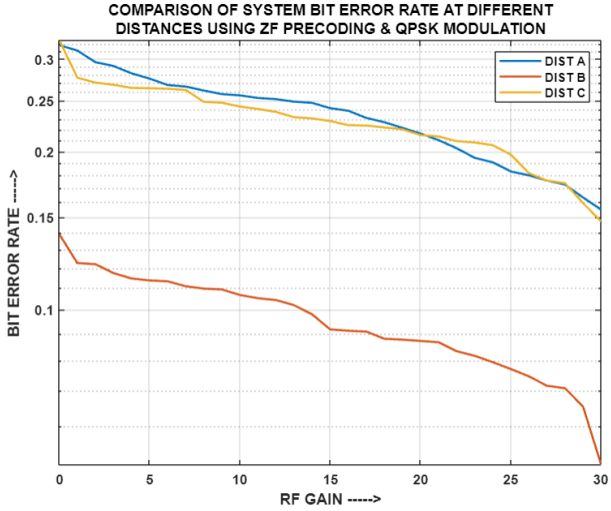

Fig.6.92: Comparison of System BER at different distances using ZF and QPSK

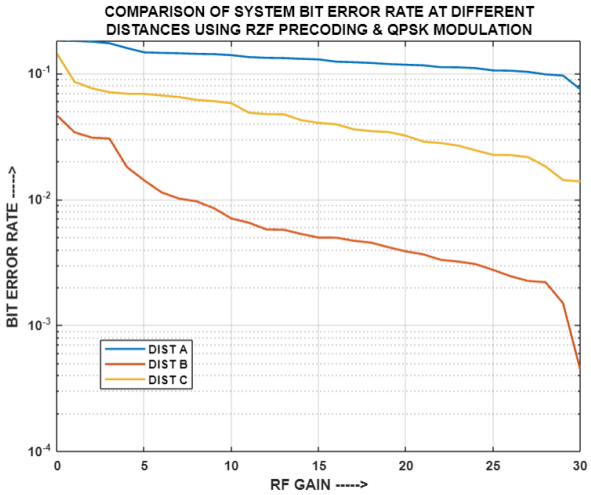

Fig.6.93: Comparison of System BER at different distances using RZF and QPSK

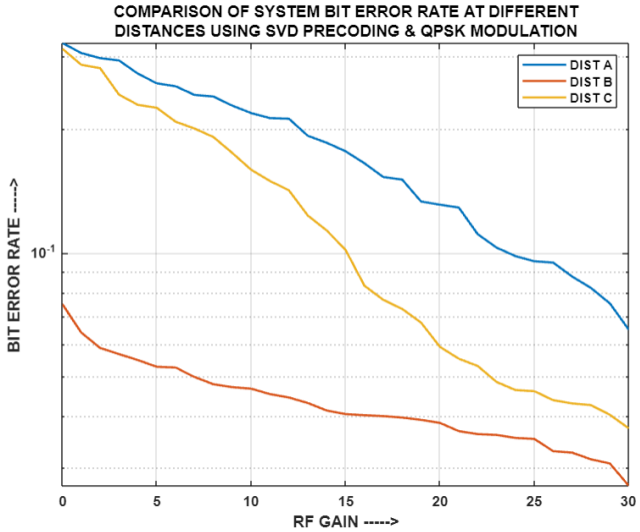

Fig.6.94: Comparison of System BER at different distances using SVD and QPSK

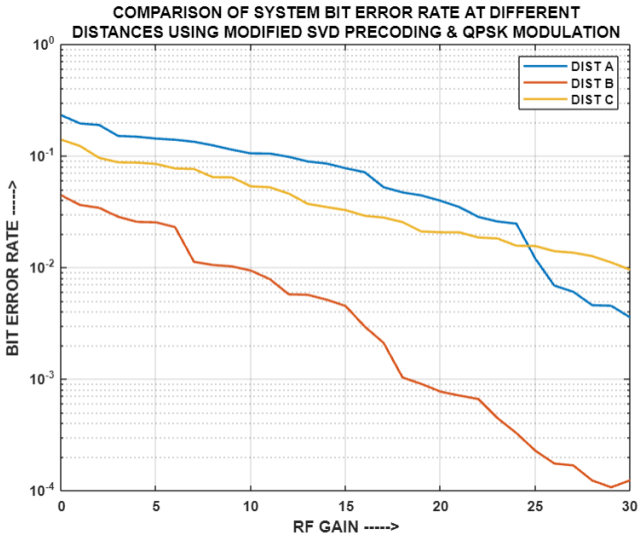

Fig.6.95: Comparison of System BER at different distances using MODIFIED SVD and QPSK

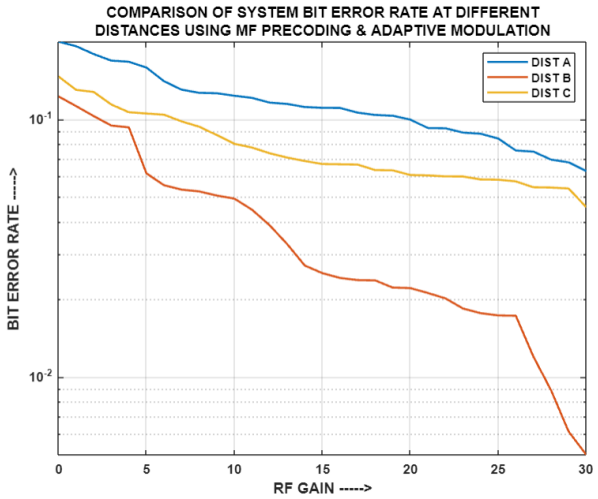

Fig.6.96: Comparison of System BER at different distances using MF and Adaptive Modulation

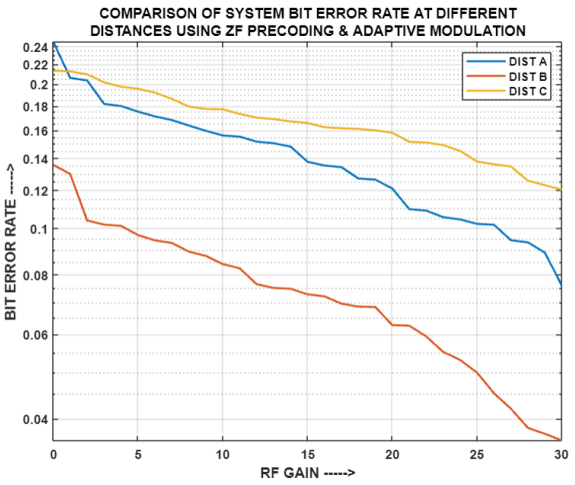

Fig.6.97: Comparison of System BER at different distances using ZF and Adaptive Modulation

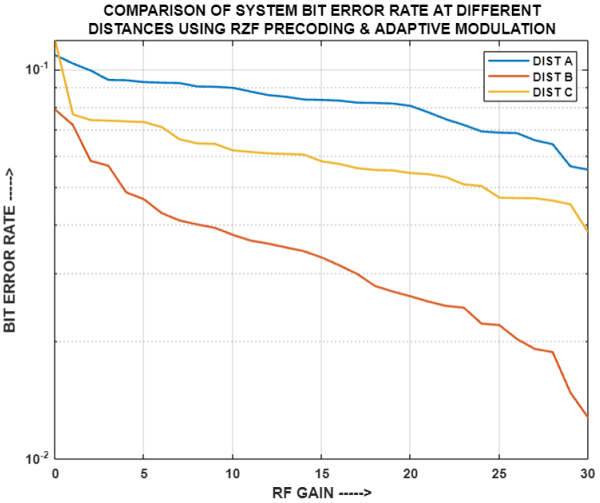

Fig.6.98: Comparison of System BER at different distances using RZF and Adaptive Modulation

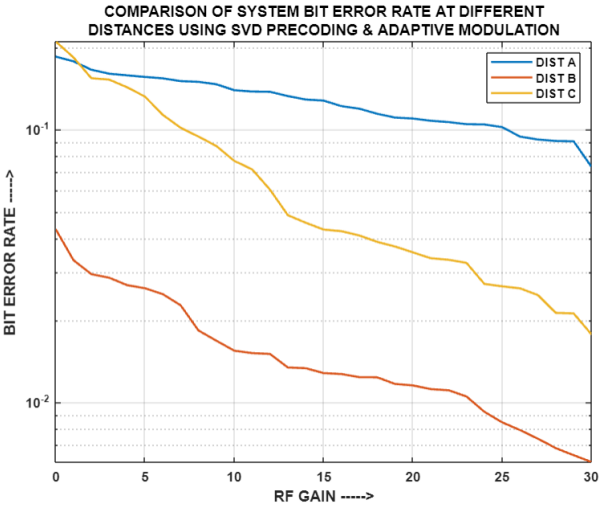

Fig.6.99: Comparison of System BER at different distances using SVD and Adaptive Modulation

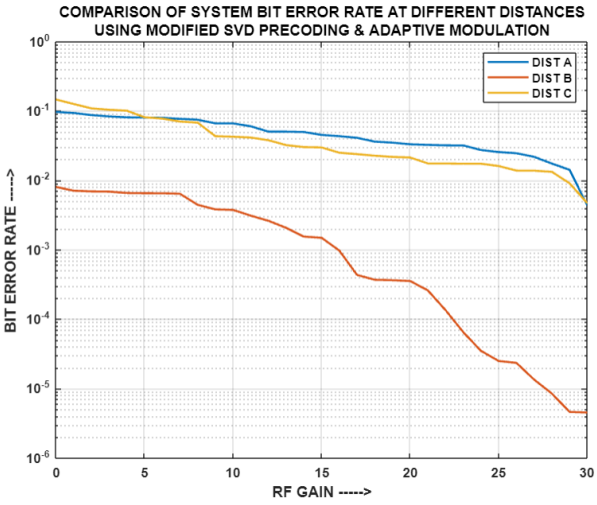

Fig.6.100: Comparison of System BER at different distances using MODIFIED SVD and Adaptive Modulation

Fig.6.86, Fig.6.87, Fig.6.88, Fig.6.89 and Fig.6.90 depicts the comparison of system BER at three different combination of distances, for the two users involved in the NOMA scheme, using diverse precoding techniques, i.e. MF, ZF, RZF, SVD and MODIFIED SVD, respectively, and BPSK modulation. Figures 6.91 to 6.95 showcases the comparison of system BER at the three different user distance combinations, using the above-stated precoding techniques, along with QPSK modulation. Figures 6.96 to 6.100 presents the comparison of system BER at the three distinct user distance combinations, using the aforementioned precoding techniques, in conjunction with Adaptive modulation scheme. It has been observed that for all the above cases, the system BER at distance combination B, is the least compared to those at the other two distance combinations. Although in distance combinations B and C, the near user is placed at a distance greater than the distance at which the near user is located in distance combination A, still the system BER at the former two distance combinations, is better than that obtained at the latter. This behaviour can be attributed to the effects of fading and interference being more significant when the users are placed at distance combination A. Therefore, at distance combination A, the users experience higher level of signal degradation due to presence of other interfering signals and unpredictable sources of interference, along with multipath fading. However, the system BER at distance combination B is better than that at distance combination C, because in the latter, the near user is placed at a distance beyond that at which the near user is positioned in the former, whereby primarily due to the effects of attenuation and path-loss at distance C, in addition to fading and interference, the user's signal quality gets compromised. The channel characteristics, environmental conditions, such as obstacle, reflections and such like, along with noise, also have a role to play in impairing the reception of signals, as they vary at different distances. Thus, considering all the above-stated scenarios and theory, it is seen that when the users are situated at the respective positions of distance combination B, they happen to receive the best quality of signals and hence, distance combination B emerges to be the optimum distance, with respect to system BER, for all the employed precoding and modulation schemes.

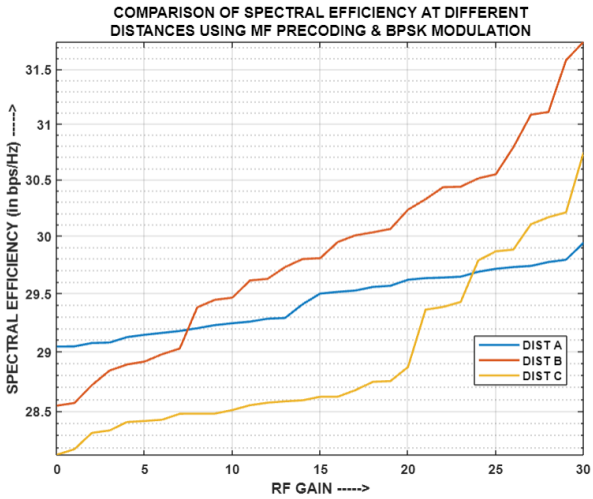

Fig.6.101: Comparison of Spectral Efficiency at different distances using MF and BPSK

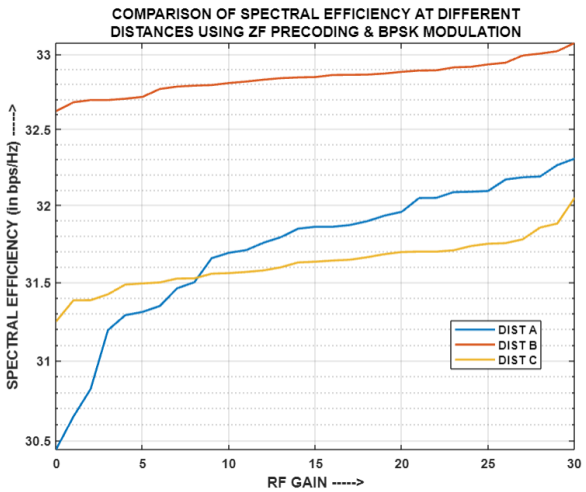

Fig.6.102: Comparison of Spectral Efficiency at different distances using ZF and BPSK

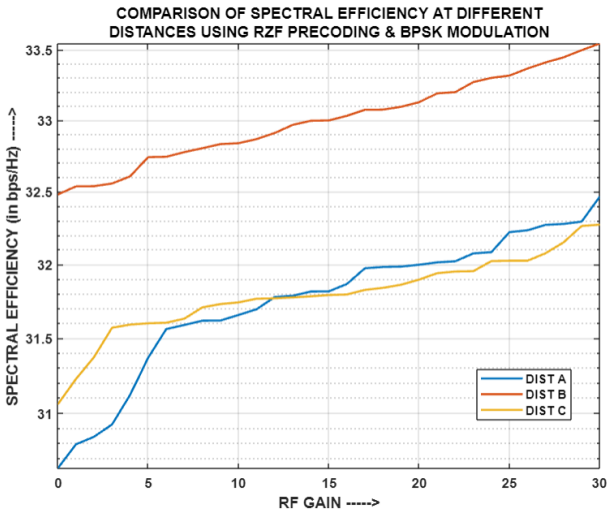

Fig.6.103: Comparison of Spectral Efficiency at different distances using RZF and BPSK

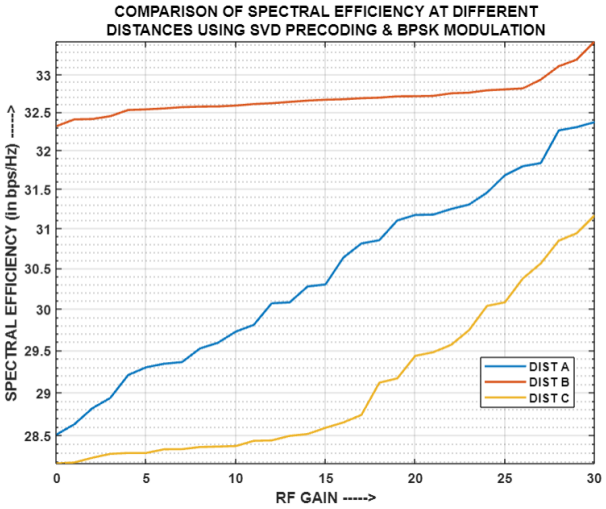

Fig.6.104: Comparison of Spectral Efficiency at different distances using SVD and BPSK

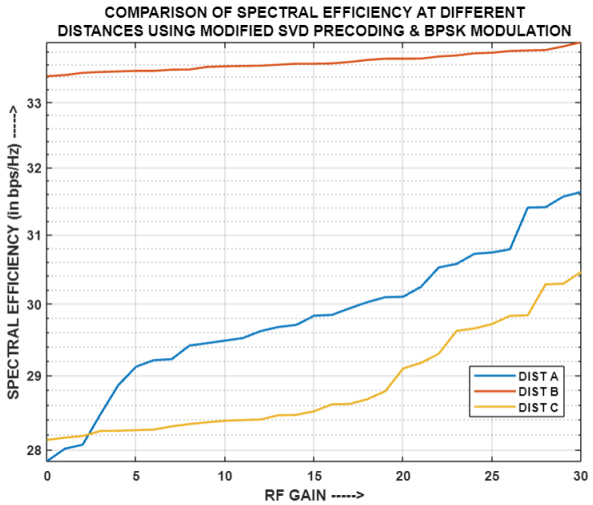

Fig.6.105: Comparison of Spectral Efficiency at different distances using MODIFIED SVD and BPSK

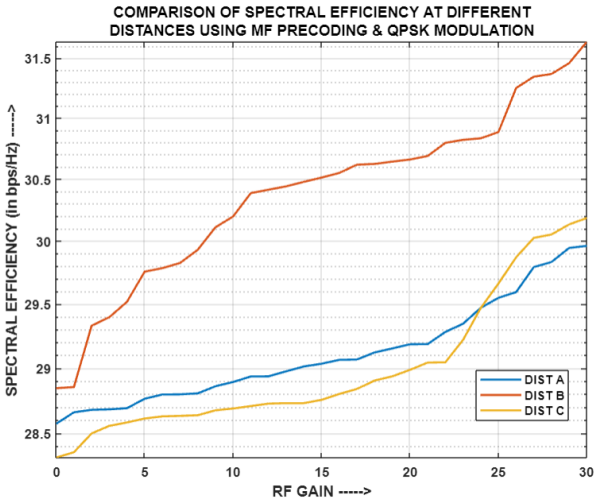

Fig.6.106: Comparison of Spectral Efficiency at different distances using MF and QPSK

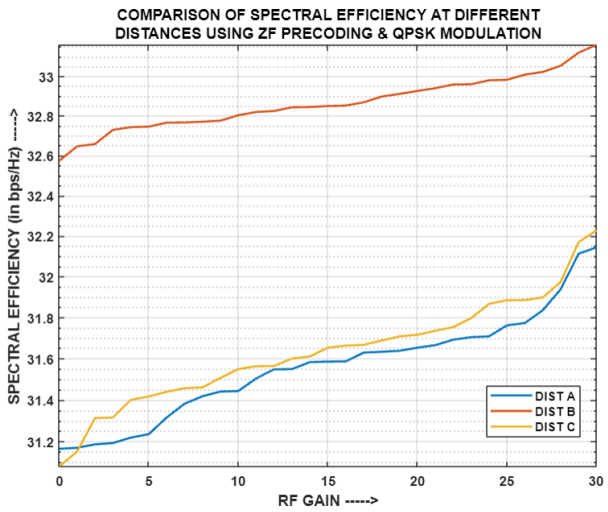

Fig.6.107: Comparison of Spectral Efficiency at different distances using ZF and QPSK

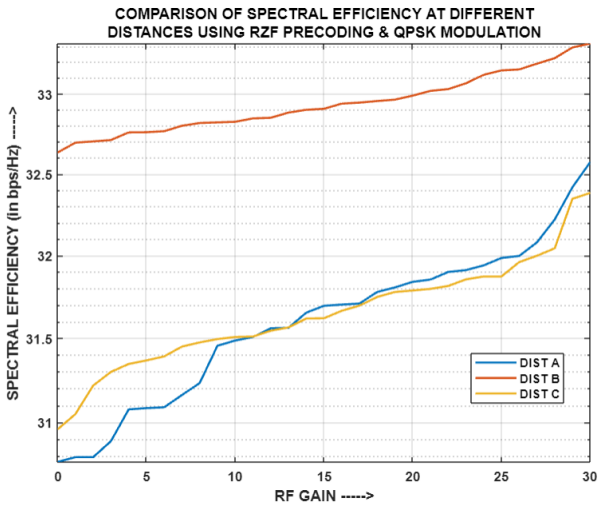

Fig.6.108: Comparison of Spectral Efficiency at different distances using RZF and QPSK

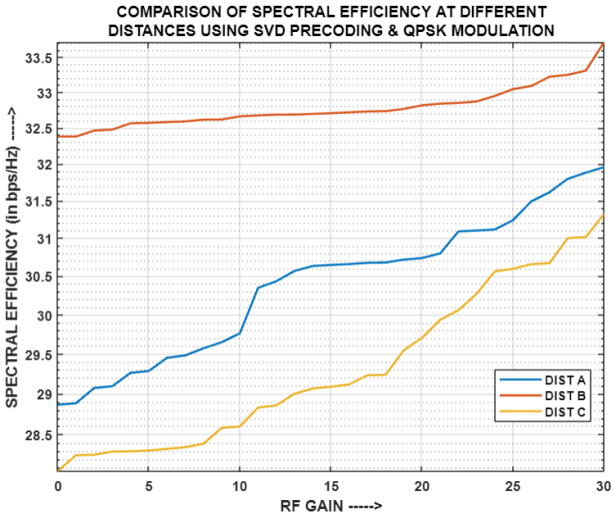

Fig.6.109: Comparison of Spectral Efficiency at different distances using SVD and QPSK

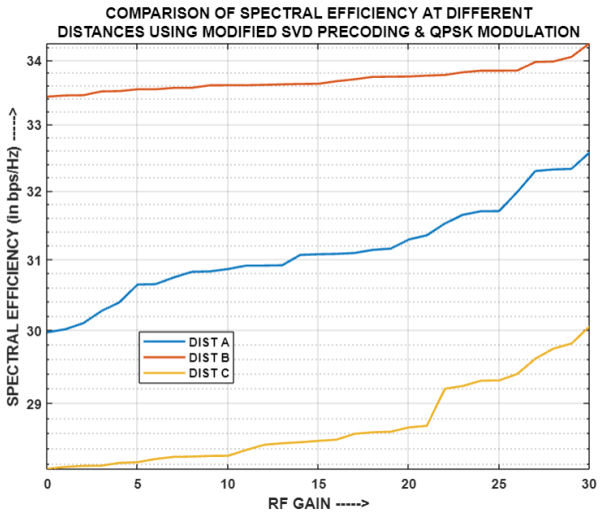

Fig.6.110: Comparison of Spectral Efficiency at different distances using MODIFIED SVD and QPSK

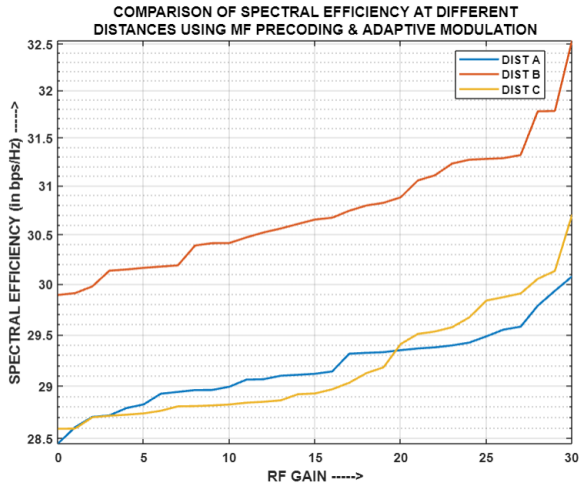

Fig.6.111: Comparison of Spectral Efficiency at different distances using MF and Adaptive Modulation

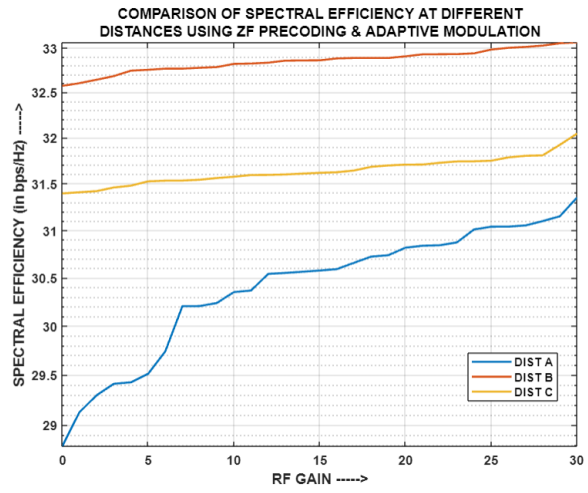

Fig.6.112: Comparison of Spectral Efficiency at different distances using ZF and Adaptive Modulation

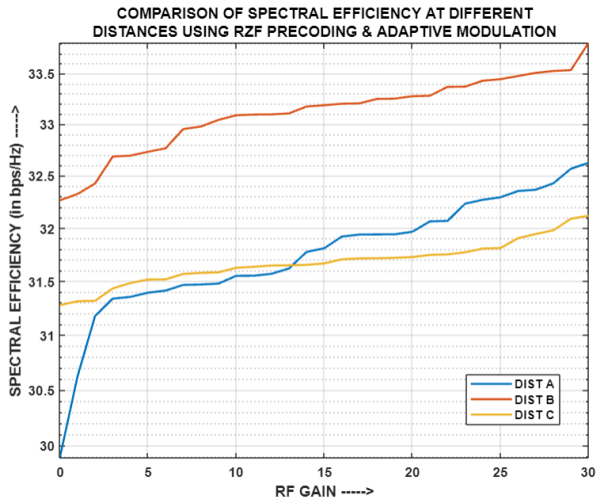

Fig.6.113: Comparison of Spectral Efficiency at different distances using RZF and Adaptive Modulation

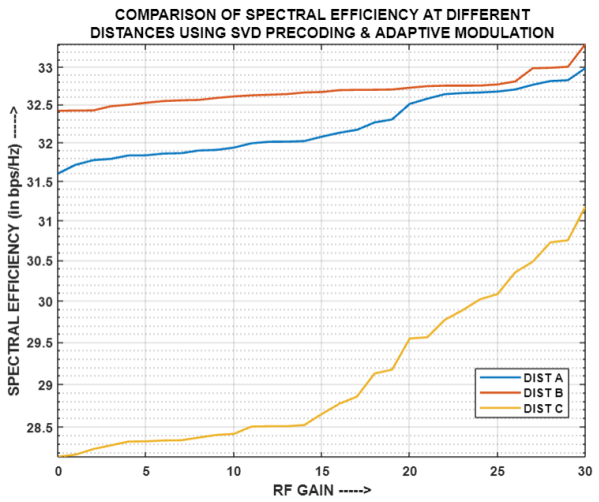

Fig.6.114: Comparison of Spectral Efficiency at different distances using SVD and Adaptive Modulation

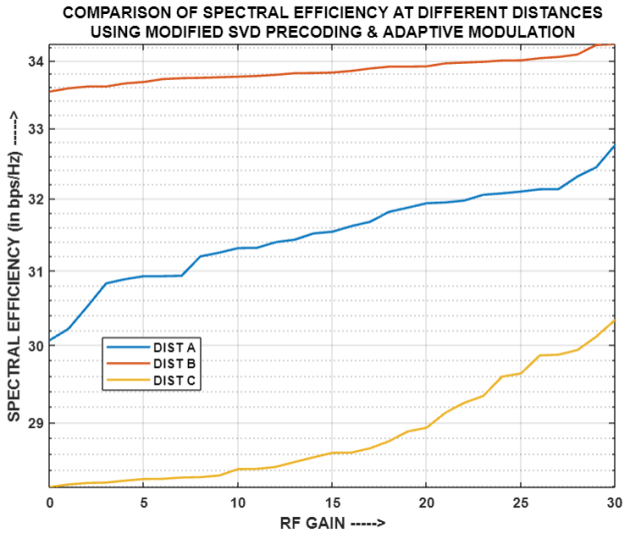

Fig.6.115: Comparison of Spectral Efficiency at different distances using MODIFIED SVD and Adaptive Modulation

Fig.6.101, Fig.6.101, Fig.6.103, Fig.6.104 and Fig.6.105 illustrates the comparison of Spectral Efficiency at three different combinations of distances, for the two users involved in the NOMA scheme, using diverse precoding techniques, i.e. MF, ZF, RZF, SVD and MODIFIED SVD respectively, and BPSK modulation. Figures 6.106 to 6.110 displays the comparison of system BER at the three different user distance combinations, using the aforesaid precoding techniques, along with QPSK modulation. Figures 6.111 to 6.115 portrays the comparison of system BER at the three distinct user distance combinations, using the above-stated precoding techniques, in conjunction with Adaptive modulation scheme. It is observed that at

distance combination B, the spectral efficiency of the system is the highest in comparison to that obtained at the other two distance combinations. This is because the channel gain of the respective users happens to be the highest when they are located as per distance combination B. However, for distance combinations A and C, the users, at times, seem to have comparable effective channel gains, wherein effective channel gain refers to channel gain along with the effect of precoding and post-coding matrices, whereby for some cases, similar spectral efficiency is witnessed for the two distance combinations. On closely scrutinizing the above-stated scenarios, it can be stated that the spectral efficiency at distance combination A is higher than that at distance combination B. The channel gain or the effective channel gain directly influences the throughput of users, and subsequently, the sum capacity of the system. As the spectral efficiency has been computed on basis of the sum capacity, thereby any enhancement in the sum capacity gets projected on the spectral efficiency of the system. Therefore, due to high effective channel gain of users at distance combination B, the sum capacity of the system increases leading to high spectral efficiency. Thus, distance combination B emerges to be the optimum distance, with respect to Spectral Efficiency, for all employed precoding and modulation schemes.

The mathematical proof for distance combination B being the optimum distance in terms of Spectral Efficiency is as follows:

Proof:

As the UE2 is placed at same position for all three distance combinations, therefore

$$\left|z_{2,B}H_{2,B}p_{2,B}\right| = \left|z_{2,A}H_{2,A}p_{2,A}\right| = \left|z_{2,C}H_{2,C}p_{2,C}\right| \tag{6.2}$$

On the contrary, as the position of the UE1 has been varied for the three distance combinations, hence, the following has been observed:

$$\left|z_{1,B}H_{1,B}p_{1,B}\right| > \left|z_{1,A}H_{1,A}p_{1,A}\right| > \left|z_{1,C}H_{1,C}p_{1,C}\right| \tag{6.3}$$

On referring to equations (2.36) and (2.37) in Chapter 2, Section 2.2.7, the following can be implied from equations (6.2) and (6.3), wherein, γ represents the transmit Signal to Noise Ratio (SNR) and W refers to the total bandwidth of the channel:

For UE2:

$$\frac{\alpha_2\gamma\left|z_{2,B}H_{2,B}p_{2,B}\right|^2}{\gamma\left|z_{2,B}H_{2,B}p_{2,B}\right|^2\alpha_2+1} = \frac{\alpha_2\gamma\left|z_{2,A}H_{2,A}p_{2,A}\right|^2}{\gamma\left|z_{2,A}H_{2,A}p_{2,A}\right|^2\alpha_2+1} = \frac{\alpha_2\gamma|z_{2,C}H_{2,C}p_{2,C}|^2}{\gamma|z_{2,C}H_{2,C}p_{2,C}|^2\alpha_2+1} \quad (6.4)$$

$$\Rightarrow SINR_{2,B} = SINR_{2,A} = SINR_{2,C} \quad (6.5)$$

$$\Rightarrow (1+SINR_{2,B}) = \left(1+SINR_{2,A}\right) = (1+SINR_{2,C})$$

$$\Rightarrow \log_2(1+SINR_{2,B}) = \log_2(1+SINR_{2,A}) = \log_2(1+SINR_{2,C})$$

$$\Rightarrow \mathrm{Wlog}_2(1+SINR_{2,B}) = \mathrm{Wlog}_2(1+SINR_{2,A}) = \mathrm{Wlog}_2(1+SINR_{2,C}) \quad (6.6)$$

For UE1:

$$\alpha_1\gamma\left|z_{1,B}H_{1,B}p_{1,B}\right|^2 > \alpha_1\gamma\left|z_{1,A}H_{1,A}p_{1,A}\right|^2 > \alpha_1\gamma|z_{1,C}H_{1,C}p_{1,C}|^2 \quad (6.7)$$

$$\Rightarrow SINR_{1,B} > SINR_{1,A} > SINR_{1,C} \quad (6.8)$$

$$\Rightarrow (1+SINR_{1,B}) > (1+SINR_{1,A}) > (1+SINR_{1,C})$$

$$\Rightarrow \log_2(1+SINR_{1,B}) > \log_2(1+SINR_{1,A}) > \log_2(1+SINR_{1,C})$$

$$\Rightarrow \mathrm{Wlog}_2(1+SINR_{1,B}) > \mathrm{Wlog}_2(1+SINR_{1,A}) > W\log_2(1+SINR_{1,C}) \quad (6.9)$$

Again, from equation (2.38) of Chapter 2, Section 2.2.7, the following relation among throughputs can be inferred from equations (6.6) and (6.9):

$$R_{2,B} = R_{2,A} = R_{2,C} \quad (6.10)$$

$$R_{1,B} > R_{1,A} > R_{1,C} \quad (6.11)$$

In context of equation (2.39) in Chapter 2, Section 2.2.7, the sum capacity at the three distance combinations are as follows:

$$R_{S_A} = R_{2,A} + R_{1,A} \quad (6.12)$$

$$R_{S_B} = R_{2,B} + R_{1,B} \quad (6.13)$$

$$R_{S_C} = R_{2,C} + R_{1,C} \quad (6.14)$$

From equation (6.10), it is evident that since the throughputs for UE2 are same, hence, the sum capacities for the respective distance combinations will also follow the same trend as the throughputs of UE1. Therefore,

$$R_{S_B} > R_{S_A} > R_{S_C} \tag{6.15}$$

$$\Rightarrow \frac{R_{S_B}}{W} > \frac{R_{S_A}}{W} > \frac{R_{S_C}}{W} \tag{6.16}$$

Referring to equation (2.57) in Chapter 2, Section 2.2.7, the above expressions in equation (6.16) are the Spectral Efficiencies at the three distance combinations, whereby:

$$SE_B > SE_A > SE_C \tag{6.17}$$

Thus, the spectral efficiency at distance combination B is the highest, whereby it turns out to be the optimum position for the corresponding users.

6.4.3. Comparative Analysis of two-user MIMO-NOMA for different modulation schemes, at the optimum distance, using varied precoding techniques:

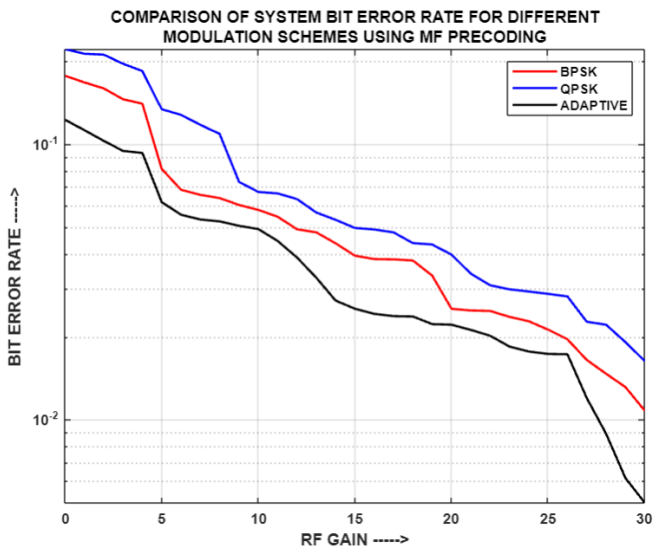

Fig.6.116: Comparison of System BER for different modulation schemes using MF

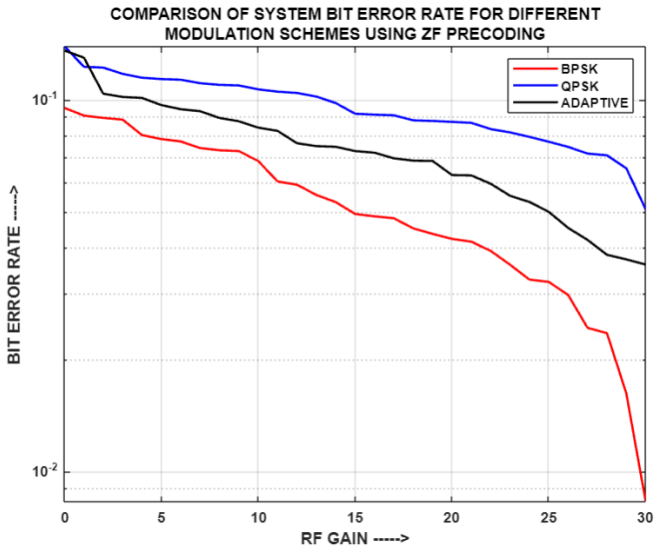

Fig.6.117: Comparison of System BER for different modulation schemes using ZF

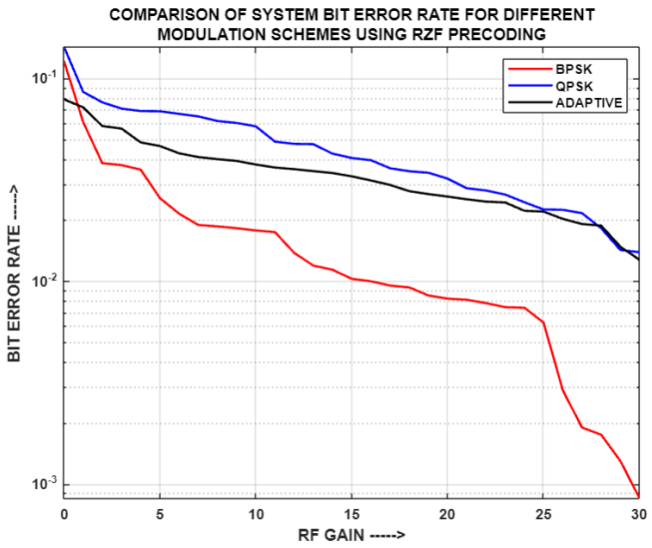

Fig.6.118: Comparison of System BER for different modulation schemes using RZF

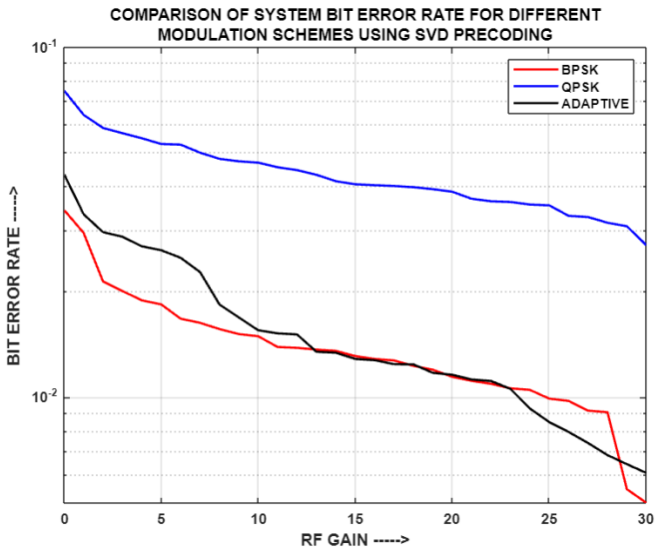

Fig.6.119: Comparison of System BER for different modulation schemes using SVD

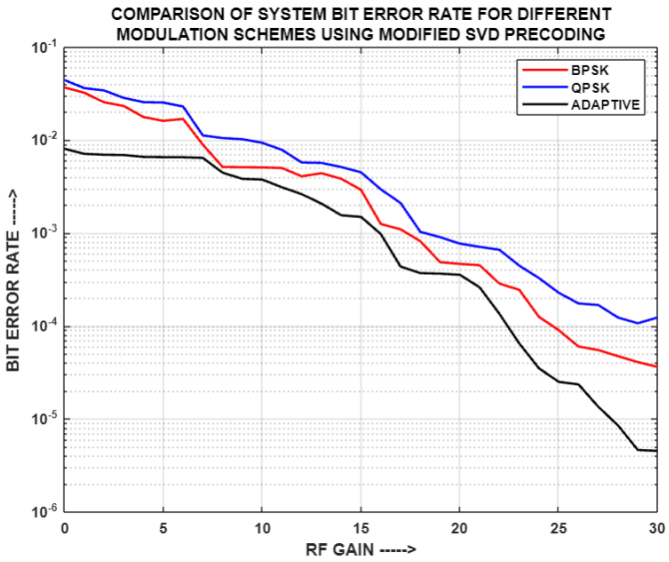

Fig.6.120: Comparison of System BER for different modulation schemes using MODIFIED SVD

Fig.6.116, Fig.6.117, Fig.6.118, Fig.6.119 and Fig.6.120 depicts the comparison of system BER for different modulation schemes, using diverse precoding techniques, i.e. MF, ZF, RZF, SVD and MODIFIED SVD respectively, at the optimum distance declared in the previous sub-section. It is witnessed that for ZF and RZF, it is BPSK that yields the least system BER, followed by Adaptive modulation and QPSK. It is

known that in BPSK, a single bit is transmitted per symbol, whereby the chances of higher bit error probability are less compared to that in QPSK, wherein two bits are transmitted per symbol. Therefore, satisfying this theory, BPSK and QPSK, generate the lowest and the highest system BERs respectively. As Adaptive modulation is a mixture of BPSK and QPSK, therefore its performance, with respect to system BER, lies in the middle of the two. In case of SVD, although QPSK follows its natural trend of producing high system BER, but Adaptive modulation performs comparable to that of BPSK. As long as the TX RF Gain is in the low power range, BPSK performs the best but beyond TX RF Gain value of 10, i.e., once the power is increased, Adaptive modulation performs as good as BPSK and even outperforms it for a particular high TX RF Gain range. The credit for such performance of Adaptive modulation not only goes to high power but also to the effectiveness of SVD precoding technique, which makes it possible to receive the transmitted signals in a good enough form such that they can be effectively demodulated by the respective users. The role of precoding scheme prominently shows its dominance in regard to MF and MODIFIED SVD. In both these schemes, with respect to system BER, Adaptive modulation outperforms BPSK and QPSK. The latter two modulation schemes perform as per their natural characteristics, whereby BPSK produces a lower system BER than QPSK. However, Adaptive modulation superseding BPSK is primarily because of the supremacy of the respective precoding schemes, whereby the transmitted signals successfully combat the channel effects and manages to reach the respective users, in its optimal form and thereby, get credibly demodulated.

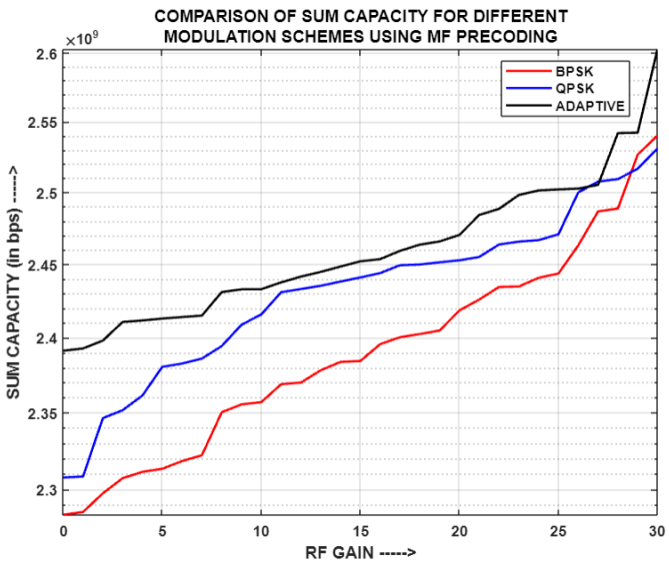

Fig.6.121: Comparison of Sum Capacity for different modulation schemes using MF

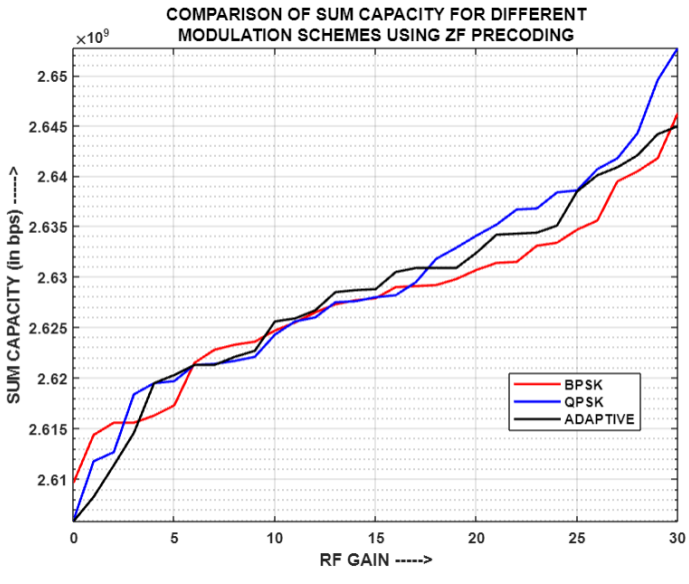

Fig.6.122: Comparison of Sum Capacity for different modulation schemes using ZF

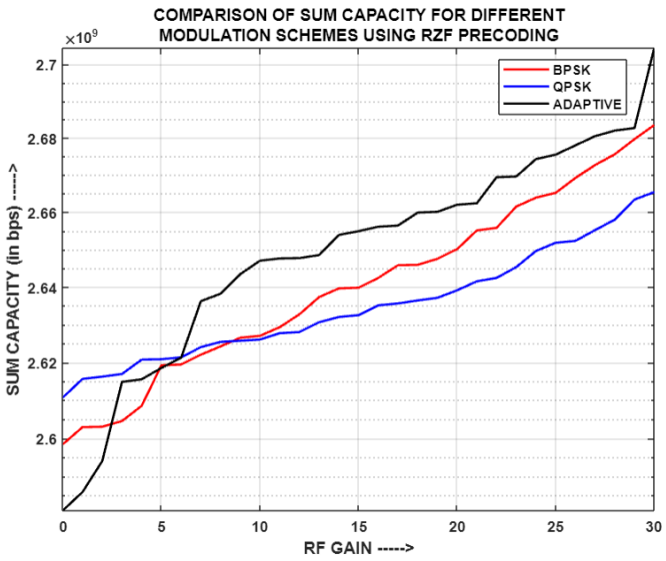

Fig.6.123: Comparison of Sum Capacity for different modulation schemes using RZF

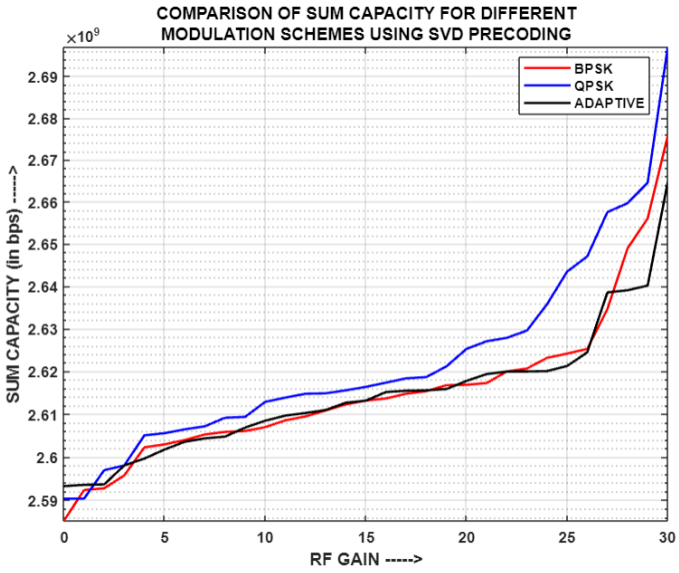

Fig.6.124: Comparison of Sum Capacity for different modulation schemes using SVD

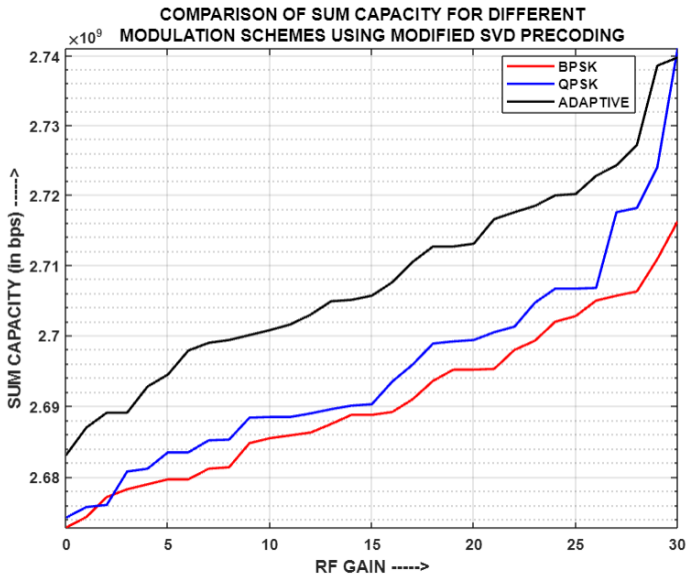

Fig.6.125: Comparison of Sum Capacity for different modulation schemes using MODIFIED SVD

Fig.6.121, Fig.6.122, Fig.6.123, Fig.6.124 and Fig.6.125 portrays the comparison of Sum Capacity for different modulation schemes, using diverse precoding techniques, i.e., MF, ZF, RZF, SVD and MODIFIED SVD respectively, at the optimum distance declared in the previous sub-section. It is seen that for ZF and SVD, comparable sum capacities are obtained across all the modulation schemes.

This is because the users happen to have similar effective channel gain, across all the employed modulation schemes, for both the precoding techniques. Effective channel gain refers to channel gain of respective users along with their corresponding precoding and post-coding vectors. However, in case of SVD, MF and MODIFIED SVD, it is the Adaptive modulation scheme that yields the highest sum capacity; while QPSK and BPSK produces the lowest sum capacity for the former and latter two precoding schemes respectively. This disparity in sum capacities across different modulation schemes attributes to differences in the effective channel gain of users, as the channel gain directly influences the users' throughput and subsequently, the sum capacity of the system.

6.4.4. Comparative Analysis of two-user MIMO-NOMA for different precoding techniques, at the optimum distance, using varied modulation schemes:

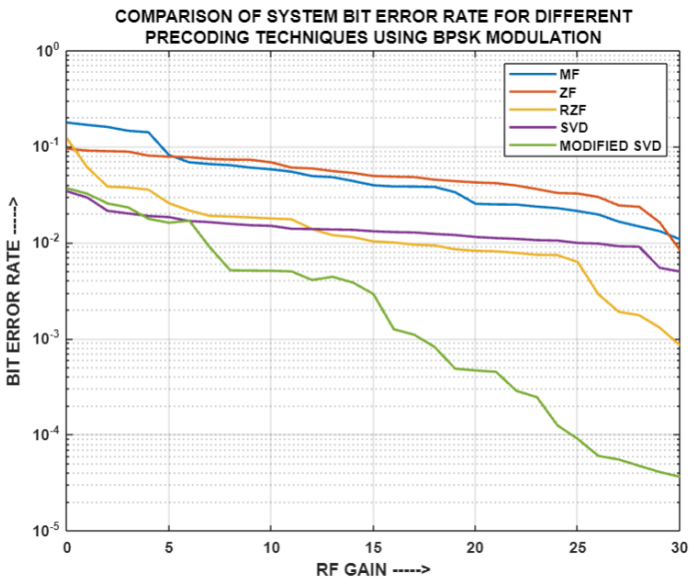

Fig.6.126: Comparison of System BER for different precoding techniques using BPSK

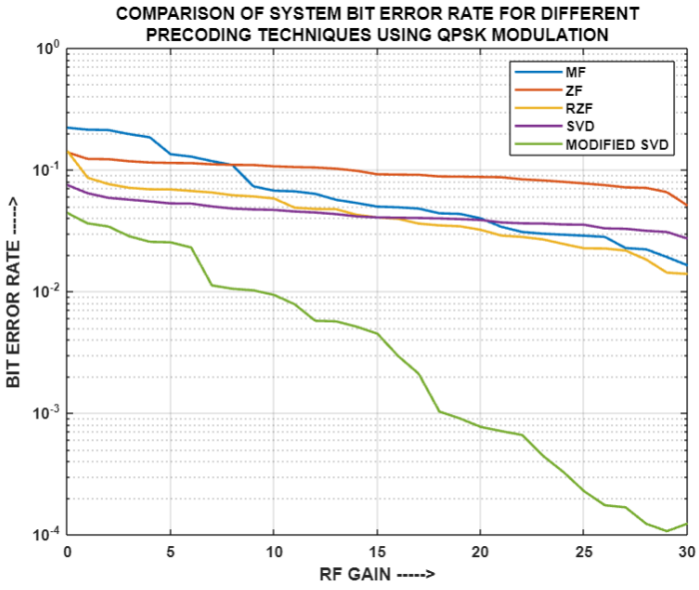

Fig.6.127: Comparison of System BER for different precoding techniques using QPSK

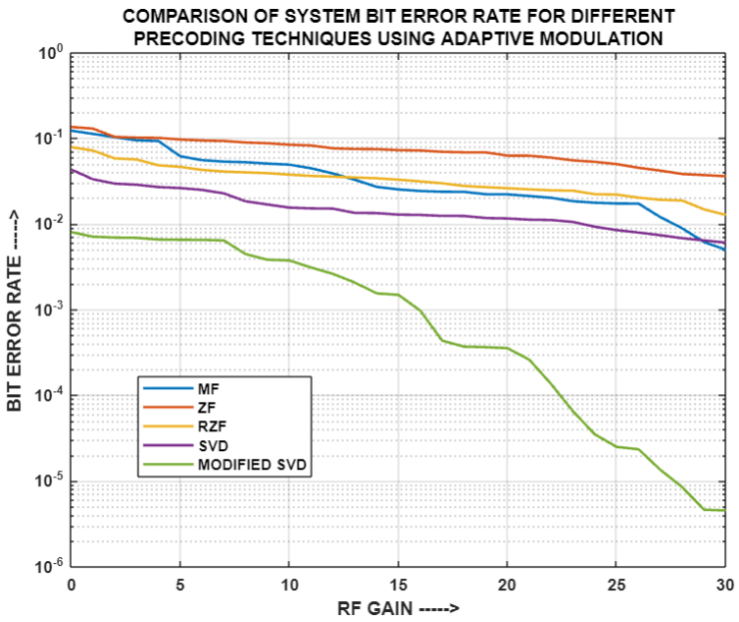

Fig.6.128: Comparison of System BER for different precoding techniques using Adaptive Modulation

Fig.6.126, Fig.6.127 and Fig.6.128 presents the comparison of system BER for different precoding techniques, using diverse modulation schemes, i.e. BPSK, QPSK and Adaptive modulation respectively, at the optimum distance declared in sub-section 6.4.2. It is noted that for all the above-stated cases, MODIFIED SVD yields the least system BER while ZF generates the highest system BER. This is because in MODIFIED SVD, a gain matrix is employed in both the precoding and post-coding process, whereby it strengthens the received signal and leads to efficient demodulation at the respective users. As in ZF precoding, the information signal is just processed with the pseudo inverse of the channel matrix, hence, it doesn't seem to effectively combat the channel effects due to noise enhancement, whereby the system BER gets compromised. However, in case of QPSK and Adaptive modulation schemes, MF and RZF happens to yield comparable system BER performances, indicating that their respective precoding matrices produce similar effect on the information signal, whereby the transmitted signal happens to combat the channel impairments in an alike manner, across the two aforementioned precoding schemes. It is for the same reason that SVD performs comparable to RZF, in terms of system BER, for both BPSK and QPSK. In context of BPSK modulation, RZF performs better than MF, primarily because of superior influence of the former while precoding the information signal. However, in case of Adaptive modulation,

SVD performs better than ZF, RZF and MF, as it efficiently precodes and post-codes the transmitted signals to handle the channel impairments in an efficient way and thereby, produce a good quality signal at the respective receiver output so that it can be credibly demodulated.

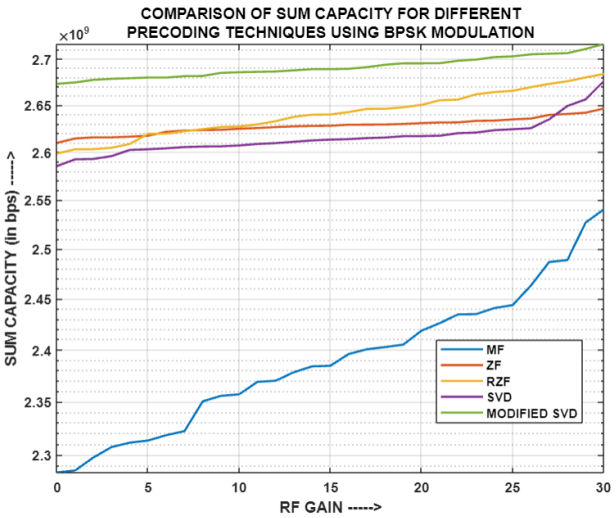

Fig.6.129: Comparison of Sum Capacity for different precoding techniques using BPSK

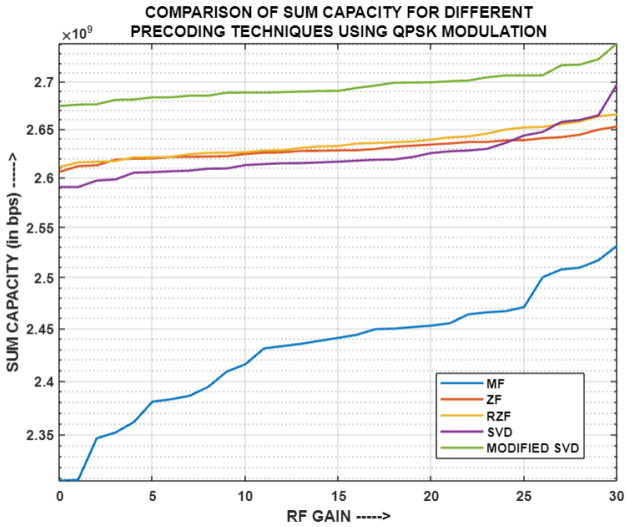

Fig.6.130: Comparison of System BER for different precoding techniques using QPSK

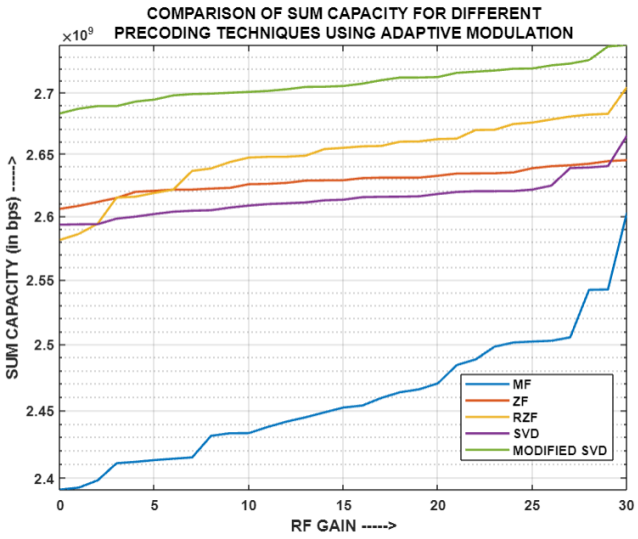

Fig.6.131: Comparison of System BER for different precoding techniques using Adaptive Modulation

Fig.6.129, Fig.6.130 and Fig.6.131 showcases the comparison of Sum Capacity for varied precoding techniques, using different modulation schemes, i.e., BPSK, QPSK

and Adaptive modulation respectively, at the optimum distance declared in sub-section 6.4.2. It is interesting to observe that MODIFIED SVD yields the highest sum capacity for all the above-stated cases. This is because of its usage of a gain matrix at the precoders and post-coders, whereby it enhances the effective users' channel gain and thereby the users' throughput, which generate a positive impact on the sum capacity of the system. On the contrary, MF produces the lowest sum capacity because it just precodes the information signal with the channel's Hermitian conjugate, whereby its effect on the resultant channel gain and thereby sum capacity, happens to be not that significant as compared to the other precoding schemes. However, ZF generates higher sum capacity than SVD, across all three modulation schemes. This behaviour attributes to the fact that the effect of the precoding vector on the effective channel gain of the respective user, in case of former is slightly higher than that of the latter. As channel gain has a direct impact on the user's throughput and subsequently, the sum capacity of the system, hence, ZF yields higher sum capacity than SVD. It is for the same reason that RZF provides slightly comparable sum capacity as of ZF, for QPSK; while the former performs better than the latter in case of BPSK and Adaptive modulation respectively.

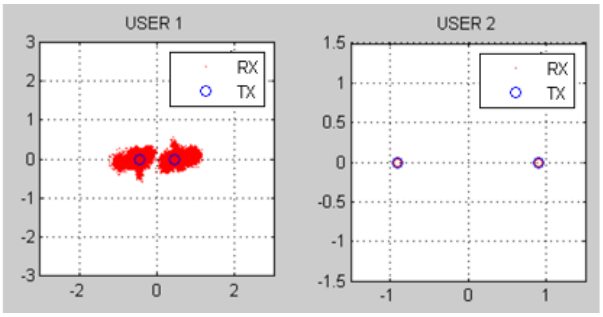

Fig.6.132: Constellation Diagram for BPSK using MF for MIMO-NOMA

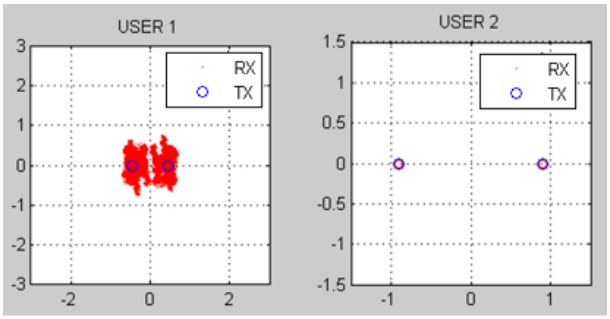

Fig.6.133: Constellation Diagram for BPSK using ZF for MIMO-NOMA

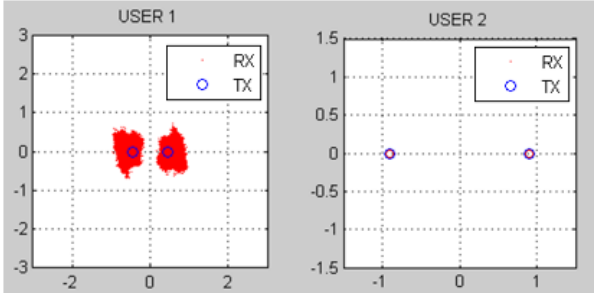

Fig.6.134: Constellation Diagram for BPSK using RZF for MIMO-NOMA

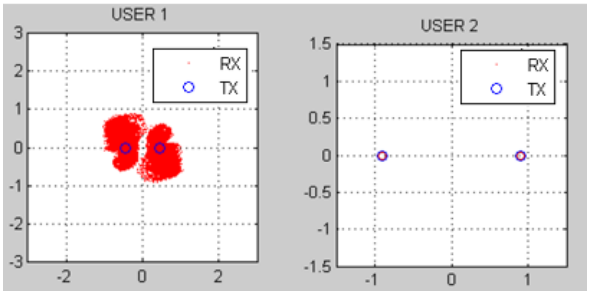

Fig.6.135: Constellation Diagram for BPSK using SVD for MIMO-NOMA

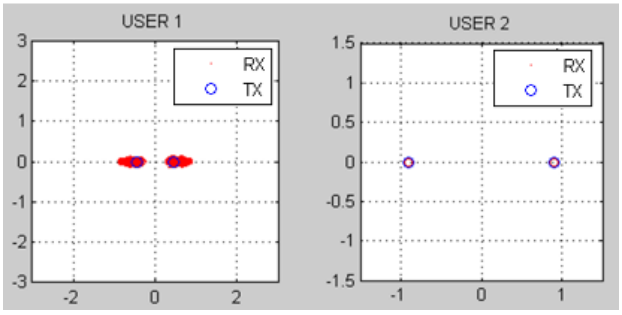

Fig.6.136: Constellation Diagram for BPSK using MODIFIED SVD for MIMO-NOMA

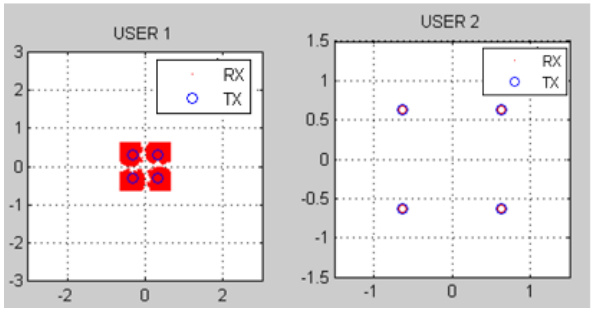

Fig.6.137: Constellation Diagram for QPSK using MF for MIMO-NOMA

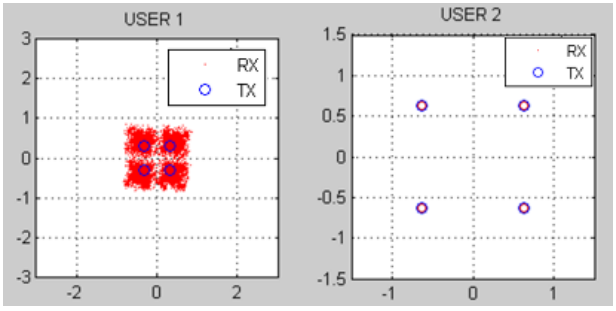

Fig.6.138: Constellation Diagram for QPSK using ZF for MIMO-NOMA

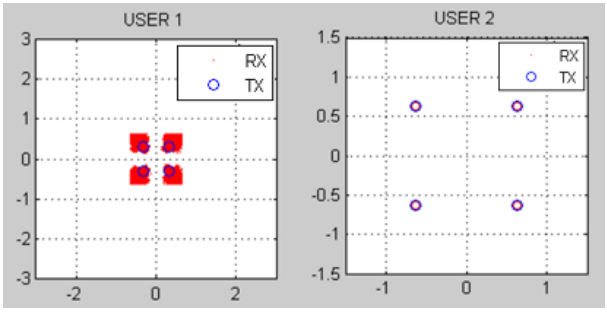

Fig.6.139: Constellation Diagram for QPSK using RZF for MIMO-NOMA

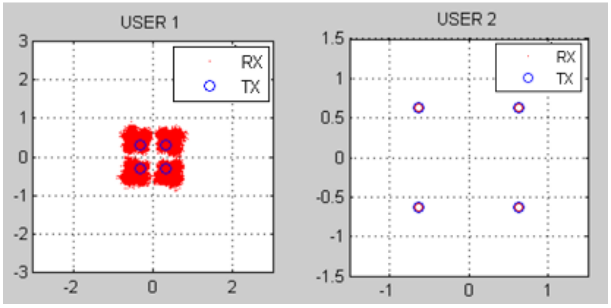

Fig.6.140: Constellation Diagram for QPSK using SVD for MIMO-NOMA

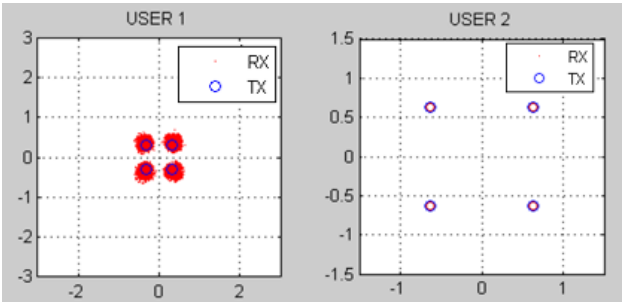

Fig.6.141: Constellation Diagram for QPSK using MODIFIED SVD for MIMO-NOMA

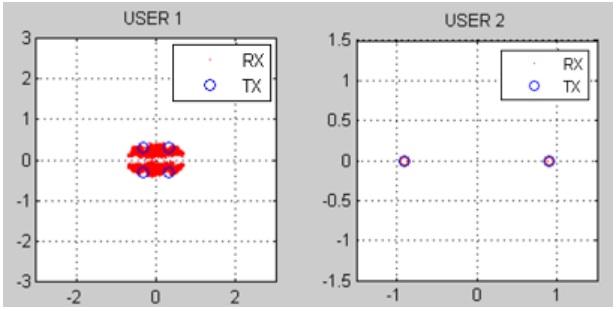

Fig.6.142: Constellation Diagram for Adaptive Modulation using MF for MIMO-NOMA

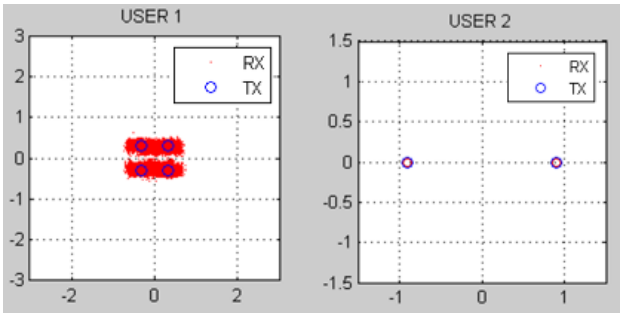

Fig.6.143: Constellation Diagram for Adaptive Modulation using ZF for MIMO-NOMA

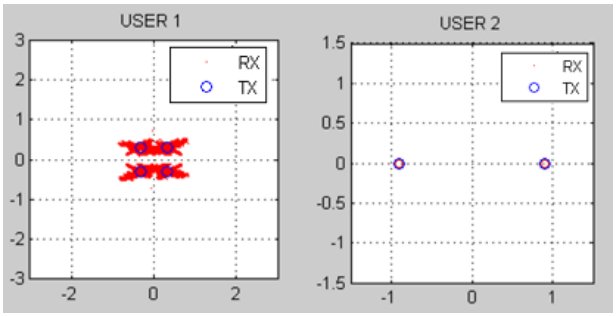

Fig.6.144: Constellation Diagram for Adaptive Modulation using RZF for MIMO-NOMA

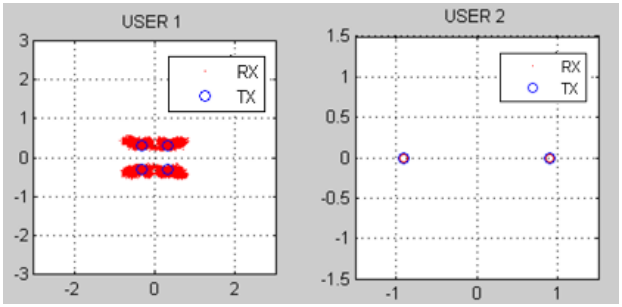

Fig.6.145: Constellation Diagram for Adaptive Modulation using SVD for MIMO-NOMA

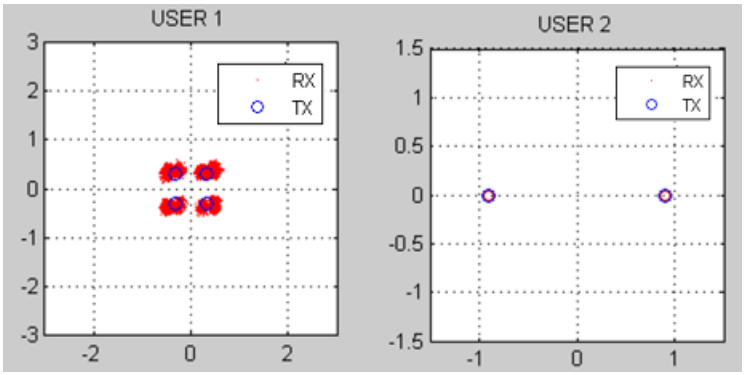

Fig.6.146: Constellation Diagram for Adaptive Modulation using MODIFIED SVD for MIMO-NOMA

Fig.6.132, Fig.6.133, Fig.6.134, Fig.6.135 and Fig.6.136 represents the Constellation Diagrams for varied precoding techniques respectively, using BPSK modulation, at the optimum distance declared in sub-section 6.4.2. Fig.6.137 to Fig.6.141 displays the Constellation Diagrams for the same above-stated scenarios but using QPSK modulation. Figures 6.142 to 6.146 illustrates the Constellation Diagrams for the similar aforesaid situations, using Adaptive modulation. “USER 1” refers to near user while “USER 2” denotes the far user. It has been observed that for all the employed precoding schemes, the RX constellation points of the two users, for both BPSK and QPSK respectively, cluster efficiently at their corresponding TX constellation points. On the contrary, for Adaptive modulation, MODIFIED SVD outperforms the rest of the precoding schemes. This is because in the former, the clusters of RX constellations for User 1 are accurately concentrated at their respective TX constellation points due to the dominant effectiveness of the MODIFIED SVD precoding scheme on the reception of the transmitted signal, whereby User 1 is able to perform SIC efficiently and thereby, extracts out its

intended information signal more precisely. In case of rest of the precoding schemes, although the RX constellations of User 1, for Adaptive modulation, do cluster at the corresponding TX constellation points, but they also tend to mingle with one another, thereby indicating considerable discrepancies in the extracted information signal. Also, for all the above cases, the clustering of RX constellations is more exact for User 2 than for User 1, because the former performs direct decoding on the received signal; while the latter has to perform SIC, whereby it needs to first eliminate User 2's information signal from the received signal and then extract its intended information signal for decoding purpose. As SIC in itself can never be perfect and highly depends on the quality of received signal, therefore, the aforesaid behaviour is witnessed for User 1's RX constellations.

6.4.5. Comparative Analysis of MIMO-NOMA and MIMO-WITHOUT-NOMA:

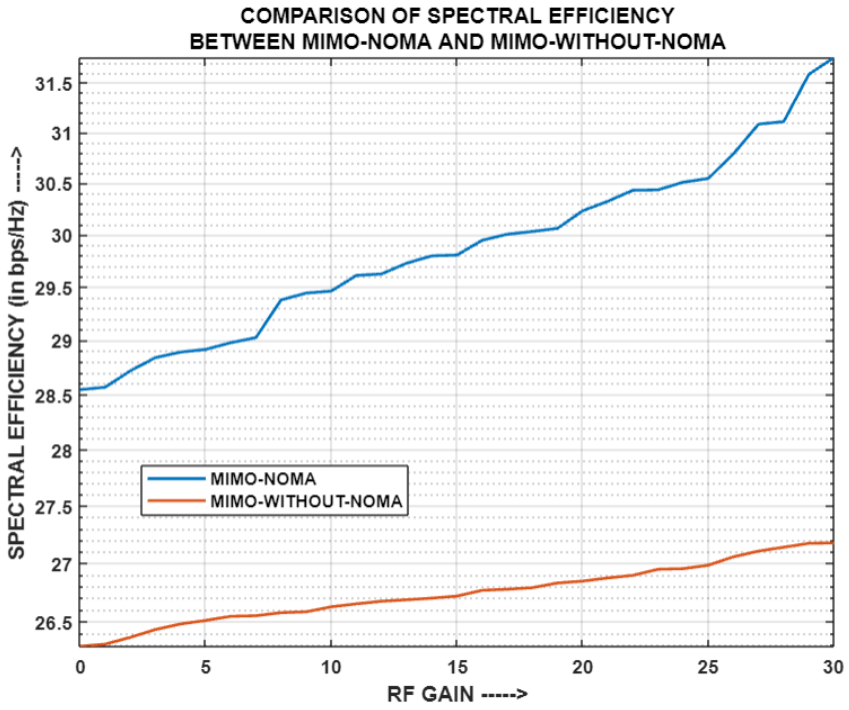

Fig.6.147: Comparison of Spectral Efficiency between MIMO-NOMA and MIMO-WITHOUT-NOMA

Fig.6.147 depicts the comparison of Spectral Efficiency between (2x2)-MIMO-NOMA model and (2x2)-MIMO-WITHOUT-NOMA model, i.e. (2x2)-MIMO-OMA, using MF precoding and BPSK modulation scheme, for a two-user scenario. It is evident that MIMO-NOMA outperforms MIMO-WITHOUT-NOMA, in terms of spectral efficiency, because in the former the entire bandwidth is used by both the users in the system; while in case of latter, each user can transmit information using only half of the total bandwidth of the system. Therefore, MIMO-NOMA experiences a higher spectral efficiency as compared to MIMO-WITHOUT-NOMA.

The mathematical proof for MIMO-NOMA having higher sum capacity than MIMO-OMA is as follows[88]:

Proof:

Let $|z_1 H_1 p_1|^2$ and $|z_2 H_2 p_2|^2$ be the effective channel gains of UE1 and UE2 respectively, where H_i is the channel matrix of the respective user; and p_i and z_i are the precoding and post-coding vectors for the corresponding users.

In MIMO-WITHOUT-NOMA, i.e. MIMO-OMA, the degrees of freedom (time or frequency) are split between the two users, thereby allocating μ of the degrees of freedom to UE2 and (1- μ) to UE1.

Let $\beta_2\gamma/\mu$ be the transmit SNR allocated to UE2, while $\beta_1\gamma/(1-\mu)$ is the transmit SNR allocated to UE1, wherein β_2 and β_1 are the power allocation coefficients, γ is the transmit Signal-to-Noise ratio and W is the total bandwidth of the channel, then the throughput region of the two users are as follows:

$$R_{MIMO-OMA,UE2} \leq W\mu \log_2\left(1 + \frac{\beta_2\gamma|z_2 H_2 p_2|^2}{\mu}\right) \tag{6.18}$$

$$R_{MIMO-OMA,UE1} \leq W\,(1-\mu)\log_2\left(1 + \frac{\beta_1\gamma|z_1 H_1 p_1|^2}{(1-\mu)}\right) \tag{6.19}$$

Therefore, according to Jensen's inequality and the concavity of $\log(.)$, the Sum Capacity of MIMO-OMA system is given by:

$$SC_{MIMO-OMA} = R_{MIMO-OMA,UE2} + R_{MIMO-OMA,UE1} \tag{6.20}$$

$$\Rightarrow SC_{MIMO-OMA} \leq W \log_2\left(1 + (1-\mu)\frac{\beta_1\gamma|z_1 H_1 p_1|^2}{(1-\mu)} + \mu\frac{\beta_2\gamma|z_2 H_2 p_2|^2}{\mu}\right) \tag{6.21}$$

$$\Rightarrow SC_{MIMO-OMA} = \log_2(1 + \beta_1\gamma|z_1 H_1 p_1|^2 + \beta_2\gamma|z_2 H_2 p_2|^2) \tag{6.22}$$

where, the above equality holds true if $\frac{\beta_1\gamma|z_1H_1p_1|^2}{(1-\mu)} = \frac{\beta_2\gamma|z_2H_2p_2|^2}{\mu}$.

In case of MIMO-NOMA, as per equations (2.36) and (2.37) in Chapter 2, Section2.2.7, the throughputs of UE2 and UE1 are as follows:

$$R_{MIMO-NOMA,UE2} = W\log_2\left(1+\frac{\alpha_2\gamma|z_2H_2p_2|^2}{\gamma|z_2H_2p_2|^2\alpha_2+1}\right) \quad (6.23)$$

$$R_{MIMO-NOMA,UE1} = W\log_2(1+\gamma|z_1H_1p_1|^2\alpha_1) \quad (6.24)$$

Therefore, the Sum Capacity of MIMO-NOMA system is given by:

$$SC_{MIMO-NOMA} = R_{MIMO-NOMA,UE2} + R_{MIMO-NOMA,UE1} \quad (6.25)$$

$$\Rightarrow SC_{MIMO-NOMA} = W\log_2\left(1+\frac{\alpha_2\gamma|z_2H_2p_2|^2}{\gamma|z_2H_2p_2|^2\alpha_2+1}\right) + W\log_2(1+\gamma|z_1H_1p_1|^2\alpha_1) \quad (6.26)$$

Since, $|z_1H_1p_1|^2 \geq |z_2H_2p_2|^2$, therefore $\frac{\alpha_1\gamma|z_1H_1p_1|^2+1}{\alpha_2\gamma|z_2H_2p_2|^2\alpha_2+1} \geq 1$, then

$$\Rightarrow SC_{MIMO-NOMA} = \log_2\left(1+\alpha_1\gamma|z_1H_1p_1|^2+\alpha_2\gamma|z_2H_2p_2|^2\times\frac{\alpha_1\gamma|z_1H_1p_1|^2+1}{\alpha_2\gamma|z_2H_2p_2|^2\alpha_2+1}\right) \quad (6.27)$$

$$\Rightarrow SC_{MIMO-NOMA} \geq \log_2(1+\alpha_1\gamma|z_1H_1p_1|^2+\alpha_2\gamma|z_2H_2p_2|^2) \quad (6.28)$$

Let the power allocation coefficients for MIMO-NOMA and MIMO-OMA be equal, i.e. $\alpha_i = \beta_i$, then by inequalities (6.22) and (6.28), the following inequality can be obtained:

$$SC_{MIMO-NOMA} \geq SC_{MIMO-OMA} \quad (6.29)$$

Dividing both sides by the total channel bandwidth (BW), the above inequality stands as:

$$\frac{SC_{MIMO-NOMA}}{BW} \geq \frac{SC_{MIMO-NOMA}}{BW} \tag{6.30}$$

Referring to the equation (2.57) in Chapter 2, Section 2.2.7, it can be inferred that the aforementioned inequality represents the Spectral Efficiency (SE) of the two systems, whereby:

$$SE_{MIMO-NOMA} \geq SE_{MIMO-OMA} \tag{6.31}$$

Thus, MIMO-NOMA has a higher spectral efficiency than MIMO-OMA, i.e. MIMO-WITHOUT-NOMA.

Table 6.5: Compilation of Experimental Results for (2x2)-MIMO-PD-NOMA for different precoding and modulation schemes

Precoding Technique	Modulation Scheme	BER	Sum Capacity	Remarks
MF	BPSK	Moderate	Low	Adaptive modulation yields optimum performance.
	QPSK	Highest	Moderate	
	Adaptive Modulation	Least	High	
ZF	BPSK	Least	High	BPSK is a more favourable choice for modulation.
	QPSK	Highest	High	
	Adaptive Modulation	Moderate	High	
RZF	BPSK	Least	Moderate	Both BPSK and Adaptive modulation can be chosen depending on a trade-off between System BER and Sum Capacity.
	QPSK	Highest	Low	
	Adaptive Modulation	Moderate	High	
SVD	BPSK	Least	Low	BPSK can be a desirable choice with respect to System BER, while if Sum Capacity is the criteria, then QPSK shall be chosen.
	QPSK	Highest	High	
	Adaptive Modulation	Moderate	Low	
MODIFIED SVD	BPSK	Moderate	Low	Adaptive Modulation produces optimal behaviour for both System BER and Sum Capacity.
	QPSK	Highest	Moderate	
	Adaptive Modulation	Least	High	

6.5. DISCUSSION

It is clearly apparent from Table that Adaptive modulation supersedes BPSK and QPSK, for MF and MODIFIED SVD precoding schemes respectively; while for ZF, it is BPSK which yields the best results, in terms of overall system performance. Therefore, it can be stated that the performance of different precoding schemes varies even when the same modulation technique is used. This is because of the respective precoding scheme's own ability to handle a modulation scheme in different environmental conditions. As seen in Chapter 4, for (2x2)-MIMO, in case

of a Rayleigh fading channel in simulation environment, ZF performed the best, while MODIFED SVD performed the worst in terms of System BER. On the contrary, in real-time environment, MODIFIED SVD outperformed the rest of the precoding schemes, with respect to both System BER and Sum Capacity. Therefore, the choice of a suitable precoding scheme primarily depends on the environment of action. Also, it has been observed that for both the simulation and real-time environment, the sum capacity produced by MODIFIED SVD, across all modulation schemes respectively, is the highest in comparison to that yielded by other precoding schemes. This behaviour attributes to the gain matrix utilized in the precoding and post-coding processes entailed in MODIFIED SVD. Thus, MODIFIED SVD employing Adaptive modulation yields optimum system performance in a MIMO-NOMA system.

6.6. CONCLUSION

This chapter experimentally analyses the performance of a (2x2)-MIMO system, with and without precoding, as well as studies the implementation of (2x2)-MIMO system using different precoding schemes along with NOMA, for a two-user scenario. The precoding schemes used involved the proposed precoding technique in Chapter 4, i.e. MODIFIED SVD, along with the existing ones. The exploration was based on System BER, Sum Capacity, Spectral Efficiency and Constellation Diagram. It was practically observed that MIMO system without precoding generated a Gaussian noise cloud due to the effects of channel impairments. MODIFIED SVD emerged to generate optimum system performance, for both with and without NOMA systems. Therefore, the aforementioned precoding scheme can be extended to MIMO systems beyond (2x2). Also, based on System BER and Spectral Efficiency, the optimum distance combination for near and far user, in the respective indoor environment, wherein the experiment was performed, was determined experimentally. Distance combination B turned out to be the best position of users, at which they experience the minimum effects of fading and interference and highest spectral efficiency. Additionally, it has been experimentally verified that MIMO-NOMA has a higher spectral efficiency than MIMO-WITHOUT-NOMA, i.e. MIMO-OMA. Thus, MIMO-NOMA with the suitable choice of precoding can provide robust and efficient communication for all users.

Chapter 7 CONCLUSION AND FUTURE SCOPE

7.1. CONCLUSION

In this thesis, the MIMO-PD-NOMA model has been broadly studied, both on a simulation platform as well as through real-time test-bed implementation on a software defined radio (SDR) kit, named WARP v3, in the 2.4GHz band. The MIMO-NOMA system was examined through simulation, using a Rayleigh fading channel, for different combination of antenna diversity techniques, a proposed and existing precoding schemes, and for a novel and conventional clustering methodologies. The parameters that were thoroughly investigated across varied power allocation mechanisms and modulation schemes, were System BER, Sum Capacity and Spectral Efficiency. In case of experimental analysis, the Constellation Diagrams were also scrutinized for with and without precoding schemes, across diverse modulation techniques and different values of TX RF Gain and AGC levels.

Antenna diversity techniques are indispensable in modern wireless communication systems. It is seen through Chapter 3 that the appropriate choice of transmit-receive antenna diversity pair plays a crucial role in controlling and enhancing the performance of a NOMA system, with respect to both System BER and Sum Capacity. By utilizing multiple antennas, diversity techniques help in mitigating the adverse effects of fading, interference and other channel impairments, thereby improving the received signal quality as well as the overall sum capacity. The better the reliability of the received signal, the higher are the chances of efficient successive interference cancellation (SIC) at the respective users, whereby the system BER is impacted. Furthermore, due to the incorporation of NOMA along with MIMO diversity techniques, the selection of power allocation coefficients through the optimum power allocation mechanism, also contributes in increasing the system sum capacity. Therefore, it is witnessed that MRC technique is indeed the optimum receiver diversity technique and MRT-MRC diversity pair emerged to produce the optimum performance for all the explored scenarios. The continuous

advancements in antenna technology, such as the development of multi-element antennas, smart antennas, and adaptive antenna arrays, offer further opportunities to enhance diversity techniques. Thus, these advancements enable more efficient and adaptive signal processing, thereby allowing dynamic adaptation to varying channel conditions and maximizing the benefits of diversity.

It is explored through Chapter 4 that the employment of precoding schemes to MIMO-NOMA system, using MRC receiver diversity technique, considerably escalates its performance, with respect to both system BER and Sum Capacity. As precoding schemes aim to combat channel effects through necessary processing of the information signal before transmission, therefore it is the perfect way to yield a reliable form of the transmitted signal at the receiver, whereby the SIC can be performed more effectively, depending on which data is demodulated accurately and hence, system BER is dictated. Also, owing to NOMA, power allocation mechanisms also play a pivotal role, whereby the selected power coefficients are also responsible for influencing the user throughput and subsequently, the sum capacity of the system. Further, the number of TX-RX antennas being used in the system impact both signal reception and throughput of users. The proposed precoding scheme, i.e. MODIFIED SVD, happened to yield optimum system performance for beyond (2x2)-MIMO scenarios, for a Rayleigh fading channel. Thus, precoding techniques are powerful tools in wireless communication systems that not only offer significant advantages in terms of signal quality, but also enhances the sum capacity of the system, thereby uplifting the overall system performance.

The primary ability of PD-NOMA is that it can serve multiple users simultaneously on the same time and frequency resources but different allotments of power. Like every other technology, NOMA too undergoes some disadvantages, along with the pros that it offers. The main concern in PD-NOMA is the process of SIC that has a chance of being more imperfect with the increase in the number of users. In order to overcome this matter, the methodology of clustering is applied to MIMO-NOMA system, wherein users are grouped into clusters and NOMA is independently applied on each of the cluster. This behaviour of MIMO-NOMA system is analysed for a proposed, i.e. LCC, and other conventional clustering techniques, through Chapter 5. When a clustering method is employed along with a suitable precoding technique, then the resources, like power coefficients, get optimally allocated among users. This not only improves the sum capacity of the system but also enhances the quality of service and signal reception. Therefore, depending on the clustering of users, the

power allocation mechanism operates accordingly, which thereby influences the performance of the applied modulation scheme. Like in Chapter 5, LCC, along with convex optimization power allocation, and employing MODIFIED SVD precoding, accelerates the performance of all modulation schemes and thereby, leads to Adaptive modulation outperforming BPSK and QPSK, in terms of overall system performance. Furthermore, the number of antennas employed both at the transmitter and receiver end also happen to impact the performance of the system. Thus, clustering methodologies are valuable assets in wireless communication systems and offers numerous benefits in terms of resource allocation, network management and enhancement of overall system performance.

Finally, through Chapter 6 the concept of diversity among antennas as well as the usefulness of precoding is experimentally validated using a (2x2)-MIMO system on WARP v3 board, in the 2.4GHz band. The scenarios without precoding clearly indicate the effects of channel impairments; whereas among the experimental exploration of different precoding schemes, MODIFIED SVD outperforms the rest. This outcome is surprising and contradictory to the one obtained on the simulation platform in Chapter 4. Therefore, for a real-time environment, MODIFIED SVD seems to be a promising precoding scheme to be used in other MIMO systems. Further, a (2x2)-MIMO-PD-NOMA system is also physically implemented on WARP v3, for a downlink two-user scenario. The experiment was conducted at three different combination of user positions, out of which the distance combination B, turned out to be the optimum location in terms of system BER and spectral efficiency. At the optimum position, when all the precoding schemes were experimentally applied and compared using different modulation schemes, MODIFIED SVD superseded the rest, across all modulation schemes and Adaptive modulation yielded the optimum system BER and Sum Capacity for the stated precoding scheme. Therefore, Adaptive modulation, along with MODIFIED SVD, can serve to be a promising choice for modulation and precoding schemes for beyond (2x2)-MIMO-NOMA systems. Further, it is practically proved that MIMO-NOMA has a higher spectral efficiency than MIMO-WITHOUT-NOMA. Thus, the power of MIMO-NOMA and the importance of precoding is experimentally validated.

Thus, MIMO-NOMA does have a scope of employment in beyond 5G and other broadband networks, due to its high spectral efficiency, provided a robust precoding scheme is applied along with it, in order to enhance the signal reception quality.

7.2. FUTURE SCOPE

- **Further Enhancements in Spectral Efficiency:** MIMO-NOMA has shown promising results in improving spectral efficiency by allowing multiple users to share the same time-frequency resources. The future scope involves exploring advanced MIMO-NOMA techniques, such as massive MIMO-NOMA, where a large number of antennas at the base station can serve multiple users simultaneously. This would lead to even higher spectral efficiency and increased system capacity.

- **Integration with beyond-5G (BG5):** MIMO-NOMA can be integrated into beyond 5G and future wireless communication systems. As beyond-5G networks continue to evolve and pave the way for 6G systems, MIMO-NOMA can play a significant role in enhancing the performance, capacity, and reliability of these networks. The future scope involves standardizing MIMO-NOMA as a key feature in these advanced communication systems.

- **Cross-Layer Optimization:** Future research in MIMO-NOMA can focus on cross-layer optimization techniques that jointly consider the physical layer, MAC layer, and network layer aspects. By optimizing the power allocation, modulation schemes, resource allocation, and routing decisions in a coordinated manner, the overall system performance can be further improved.

- **Integration with Other Emerging Technologies:** MIMO-NOMA can be integrated with other emerging technologies to unlock new possibilities in wireless communication. For example, combining MIMO-NOMA with millimeter wave (mmWave) communication or terahertz (THz) communication can enable ultra-high data rates and ultra-dense networks. Additionally, integrating MIMO-NOMA with edge computing or artificial intelligence (AI) techniques can optimize resource allocation and improve network efficiency.

- **Multi-User Massive MIMO-NOMA:** The future scope includes exploring multi-user massive MIMO-NOMA systems where a large number of antennas serve multiple users simultaneously with the aid of advanced precoding and power allocation techniques. This can lead to substantial improvements in system capacity, coverage, and user experience.

- **Security and Privacy Considerations:** As MIMO-NOMA becomes more prevalent, future research should focus on addressing security and privacy challenges associated with this technology. It is crucial to develop robust authentication, encryption, and privacy-preserving mechanisms for the secure operation of MIMO-NOMA networks.

These are some of the potential future directions for MIMO-NOMA in wireless communication systems. Ongoing research and technological advancements will shape the evolution and implementation of MIMO-NOMA to real-time networks, thereby opening up new opportunities for efficient, high-capacity, and reliable wireless communication systems.

REFERENCES

[1] S. Han, X. Xu, S. Fang, Y. Sun, Y. Cao, X. Tao, and P. Zhang, “Energy efficient secure computation offloading in NOMA-based mMTC networks for IoT,” IEEE Internet Things J., vol. 6, no. 3, pp. 5674–5690, Jun. 2019.

[2] W. Hao, Z. Chu, F. Zhou, S. Yang, G. Sun, and K.-K. Wong, “Green communication for NOMA-based CRAN,” IEEE Internet Things J., vol. 6, no. 1, pp. 666–678, Jul. 2018.

[3] A. Ericsson, “Ericsson mobility report,” Recuperado de: https://www. ericsson. com/assets/local/mobility-report/documents/2018/ericssonmobility-report-june-2018. pdf (Accedido el 09/09/2018), pp. 3–13, Jun. 2019.

[4] Mahmoud Aldababsa, Mesut Toka, Selahattin Gökçeli, Güneş Karabulut Kurt, Oğuz Kucur, "A Tutorial on Nonorthogonal Multiple Access for 5G and Beyond", *Wireless Communications and Mobile Computing*, vol. 2018, Article ID 9713450, 24 pages, 2018. https://doi.org/10.1155/2018/9713450

[5] Dai, B. Wang, Y. Yuan, S. Han, I. Chih-Lin, and Z. Wang, “Nonorthogonal multiple access for 5G: solutions, challenges, opportunities, and future research trends,” IEEE Commun. Mag., vol. 53, no. 9, pp. 74–81, Sep. 2015.

[6] Y. Liu, G. Pan, H. Zhang, and M. Song, “On the capacity comparison between mimo-noma and mimo-oma,” IEEE Access, vol. 4, pp. 2123– 2129, 2016.

[7] Z. Ding, R. Schober, and H. V. Poor, “A general mimo framework for noma downlink and uplink transmission based on signal alignment,” IEEE Transactions on Wireless Communications, vol. 15, no. 6, pp. 4438–4454, June 2016.

[8] A. P. Shrestha, T. Han, Z. Bai, J. M. Kim, and K. S. Kwak, “Performance of transmit antenna selection in non-orthogonal multiple access for 5G systems,” in Proc. 8th Int. Conf. Ubiquitous Future Ntw., Jul. 2016, pp. 1031–1034.

[9] N.-L. Nguyen, H.-N. Nguyen, N.-T. Nguyen, D.-T. Do, A.-T. Le, M. Voznak, and J. Zdralek, “On secure cognitive radio networks with NOMA: Design of multiple-antenna and performance analysis,” in Proc. IEEE Microw. Theory Techn. Wireless Commun., vol. 1, Nov. 2020, pp. 1–6.

[10] M. Aldababsa and O. Kucur, “Outage performance of NOMA with majority based TAS/MRC scheme in Rayleigh fading channels,” in Proc. 27th Signal Process. Commun. Appl. Conf. (SIU), Aug. 2019,pp.1-4.

[11] Ding, F. Adachi, and H. V. Poor, “The application of MIMO to nonorthogonal multiple access,” IEEE Trans. Wireless Commun., vol. 15, no. 1, pp. 537–552, Jan. 2016.
[12] B. Wang, L. Dai, Z. Wang, N. Ge, and S. Zhou, “Spectrum and energyefficient beamspace MIMO-NOMA for millimeter-wave communications using lens antenna array,” IEEE J. Sel. Areas Commun., vol. 35, no. 10, pp. 2370–2382, Oct. 2017.
[13] J. Cui, Y. Liu, Z. Ding, P. Fan, and A. Nallanathan, “Optimal user scheduling and power allocation for millimeter wave noma systems,” IEEE Trans. Wireless Commun., vol. 17, no. 3, pp. 1502–1517, Mar. 2018.
[14] Beomju Kim, et.al. “Non-orthogonal Multiple Access in a Downlink Multiuser Beamforming System,” in Proc. IEEE MILCOM, pp. 1278– 1283, 2013.
[15] J. Choi, ‘‘Minimum power multicast beamforming with superposition coding for multiresolution broadcast and application to NOMA systems,’’ IEEE Trans. Commun., vol. 63, no. 3, pp. 791–800, Mar. 2015.
[16] M. F. Hanif, Z. Ding, T. Ratnarajah, and G. K. Karagiannidis, ‘‘A minorization-maximization method for optimizing sum rate in the downlink of non-orthogonal multiple access systems,’’ IEEE Trans. Signal Process., vol. 64, no. 1, pp. 76–88, Jan. 2016.
[17] Z. Ding, F. Adachi, V. Poor, The application of MIMO to non-orthogonal multiple access. IEEE Trans. Wirel. Commun. 15(1), 537–552 (2016).
[18] Abhishek Gupta, Garima Saini, Dr.Sbl Sachan, 2013, An Efficient Linear Precoding Scheme Based on Block Diagonalization for Multiuser MIMO Downlink System, INTERNATIONAL JOURNAL OF ENGINEERING RESEARCH and TECHNOLOGY (IJERT) Volume 02, Issue 10 (October 2013).
[19] W. Shin, M. Vaezi, B. Lee, D. J. Love, J. Lee and H. V. Poor, "Coordinated Beamforming for Multi-Cell MIMO-NOMA," in IEEE Communications Letters, vol. 21, no. 1, pp. 84-87, Jan. 2017, doi: 10.1109/LCOMM.2016.2615097.
[20] R. Alberto and F. A. Monteiro, "Downlink MIMO-NOMA With and Without CSI: A Short Survey and Comparison," 2020 12th International Symposium on Communication Systems, Networks and Digital Signal Processing (CSNDSP), Porto, Portugal, 2020, pp. 1-6, doi: 10.1109/CSNDSP49049.2020.9249527.

[21] Jaime L. Jacob, Cristiano Magalhaes Panazio, Taufik Abrão, Energy and spectral efficiencies trade-off in MIMO-NOMA system under user-rate fairness and variable user per cluster, Physical Communication, Volume 47, 2021, 101348, ISSN 1874-4907, https://doi.org/10.1016/j.phycom.2021.101348.

[22] Rihan, M., Huang, L. and Zhang, P. Joint interference alignment and power allocation for NOMA-based multi-user MIMO systems. J Wireless Com Network 2018, 217 (2018). https://doi.org/10.1186/s13638-018-1226-y

[23] Wei, X., et al. (2019). User Clustering and Power Allocation for MIMO-NOMA Systems with Limited Feedback. IEEE Transactions on Wireless Communications, 18(1), 265-279. doi: 10.1109/TWC.2018.2873331

[24] Zhang, J., et al. (2018). User Clustering and Power Allocation for MIMO-NOMA Systems with Partial Channel State Information. IEEE Transactions on Vehicular Technology, 67(11), 10740-10744. doi: 10.1109/TVT.2018.2864913

[25] Liu, Y., et al. (2018). User Clustering and Precoding for Multi-Antenna Non-Orthogonal Multiple Access Systems. IEEE Journal on Selected Areas in Communications, 36(3), 457-471. doi: 10.1109/JSAC.2018.2815165

[26] Rappaport, T. S. (1996), *Wireless communications - principles and practice.* , Prentice Hall.

[27] Ahamed, Imtiaz and Manoj Vijay. “Comparison of different diversity techniques in MIMO antennas.” *2017 2nd International Conference on Communication and Electronics Systems (ICCES)* (2017): 47-50.

[28] https://en.wikipedia.org/wiki/Antenna_diversity

[29] Panchami S V, Dr. M V Sathyanarayana, 2017, A Review on Mimo Systems with Antenna Selection, INTERNATIONAL JOURNAL OF ENGINEERING RESEARCH and TECHNOLOGY (IJERT) NCICCNDA – 2017 (Volume 5 – Issue 22).

[30] H. A. Suraweera, C. Tellambura, and H. V. Poor, "Transmit Antenna Selection for MIMO Systems with Imperfect CSI," IEEE Transactions on Communications, vol. 54, no. 3, pp. 419-423, March 2006.

[31] A. Goldsmith, "Wireless Communications," Cambridge University Press, 2005.

[32] Y. Li, W. Zhang, K. Zheng, and L. J. Cimini Jr., "Performance analysis of receiver antenna selection for MIMO systems in the presence of interference," IEEE Transactions on Wireless Communications, vol. 7, no. 7, pp. 2534-2543, July 2008.

[33] S. G. Kim, S. Y. Kim, and D. H. Cho, "Performance analysis of maximal ratio combining over correlated Nakagami-m fading channels," IEEE Transactions on Vehicular Technology, vol. 52, no. 4, pp. 962-969, July 2003.

[34] Kshetrimayum, R. (2017). *Fundamentals of MIMO Wireless Communications*. Cambridge: Cambridge University Press. doi:10.1017/9781108234993

[35] R. D. Gitlin, J. H. Salz, and S. Weinstein, "Data transmission principles for digital communication," Wiley, 1998.

[36] N. Fatema, G. Hua, Y. Xiang, D. Peng and I. Natgunanathan, "Massive MIMO Linear Precoding: A Survey," in IEEE Systems Journal, vol. 12, no. 4, pp. 3920-3931, Dec. 2018, doi: 10.1109/JSYST.2017.2776401.

[37] https://en.wikipedia.org/wiki/Zero-forcing_precoding

[38] Y. Huang, C. Xu, and H. Zhang, "Regularized Zero-Forcing Precoding for Multiuser Massive MIMO Systems: Linear Equivalency and Performance Analysis," IEEE Transactions on Vehicular Technology, vol. 68, no. 1, pp. 647-659, January 2019.

[39] L. D. Nguyen, H. D. Tuan, T. Q. Duong and H. V. Poor, "Multi-User Regularized Zero-Forcing Beamforming," in IEEE Transactions on Signal Processing, vol. 67, no. 11, pp. 2839-2853, 1 June1, 2019, doi: 10.1109/TSP.2019.2905833.

[40] https://in.mathworks.com/help/symbolic/singular-value-decomposition.html

[41] Agbo, S., and Sadiku, M. (2017). *Principles of Modern Communication Systems*. Cambridge: Cambridge University Press. doi:10.1017/9781316257364

[42] T. Cover, “Broadcast channels,” IEEE Trans. Inf. Theory, vol. 18, no. 1, pp. 2-14, Jan 1972.

[43] S. Vanka, S. Srinivasa, Z. Gong, P. Vizi, K. Stamatiou, and M. Haenggi, “Superposition coding strategies: Design and experimental evaluation,” IEEE Trans. Wireless Commun., vol. 11, no. 7, pp. 2628–2639, 2012.

[44] D. W. K. Ng, E. S. Lo, and R. Schober, "Robust Power Allocation for Non-Orthogonal Multiple Access," IEEE Transactions on Wireless Communications, vol. 15, no. 7, pp. 4990-5002, July 2016.

[45] X. Ge, H. Zhang, Y. Ji, and V. C. M. Leung, "Power Allocation for NOMA in Downlink HetNets with SWIPT," IEEE Transactions on Vehicular Technology, vol. 66, no. 5, pp. 4050-4061, May 2017.

[46] Y. Saito, A. Benjebbour, Y. Kishiyama, and T. Nakamura, "System-Level Performance Evaluation of Downlink Non-Orthogonal Multiple Access (NOMA)," IEEE Transactions on Wireless Communications, vol. 14, no. 2, pp. 498-513, February 2015.

[47] C. Liu, Y. Li, H. Zhang, M. Hong, and Z. Ding, "Power Allocation for Non-Orthogonal Multiple Access Networks with Simultaneous Wireless Information and Power Transfer," IEEE Transactions on Vehicular Technology, vol. 67, no. 7, pp. 6442-6453, July 2018.

[48] S. Yan, H. Q. Ngo, and M. Matthaiou, "Dynamic Power Allocation for Non-Orthogonal Multiple Access Networks," IEEE Transactions on Communications, vol. 66, no. 3, pp. 1148-1162, March 2018.

[49] J. Xiao, H. Zhang, and V. C. M. Leung, "Dynamic Power Allocation for Non-Orthogonal Multiple Access with Proportional Fairness," IEEE Transactions on Wireless Communications, vol. 16, no. 10, pp. 6722-6735, October 2017.

[50] R. Mondal, S. Jana and I. S. Misra, "Performance Analysis and Experimental Validation of PD-NOMA using Constrained Optimization for Different Modulation Schemes," 2022 IEEE Calcutta Conference (CALCON), Kolkata, India, 2022, pp. 9-13, doi: 10.1109/CALCON56258.2022.10060227.

[51] S. Boyd and L. Vandenberghe, "Convex Optimization," Cambridge University Press, 2004.

[52] Kuhn, H. W., & Tucker, A. W. (1951). Nonlinear programming. In Proceedings of the Second Berkeley Symposium on Mathematical Statistics and Probability (pp. 481-492). University of California Press.

[53] Shankar R. Examination of a non-orthogonal multiple access scheme for next generation wireless networks. The Journal of Defense Modeling and Simulation. 2022;19(3):453-465. doi:10.1177/1548512920951277

[54] Z. Ding, F. Adachi and H. V. Poor, "Performance of MIMO-NOMA Downlink Transmissions," 2015 IEEE Global Communications Conference (GLOBECOM), San Diego, CA, USA, 2015, pp. 1-6, doi: 10.1109/GLOCOM.2015.7417060.

[55] Y. Zhang, M. Xiao, and B. Shou, "Clustering in Wireless Sensor Networks: A Literature Survey," Ad Hoc Networks, vol. 10, no. 8, pp. 1476-1501, November 2012.

[56] H. D. Tuan, S. Yamamoto, Y. Miyamoto, and N. Nakajima, "A Random Clustering Algorithm with a Controlled Cluster Size for Ad Hoc Networks," Proceedings of the 2007 International Symposium on Applications and the Internet, pp. 129-136, January 2007.

[57] H. Zhang, D. -K. Zhang, W. -X. Meng and C. Li, "User pairing algorithm with SIC in non-orthogonal multiple access system," 2016 IEEE International Conference on Communications (ICC), Kuala Lumpur, Malaysia, 2016, pp. 1-6, doi: 10.1109/ICC.2016.7511620.

[58] X. Ge, H. Zhang, and V. C. M. Leung, "User Pairing in Non-Orthogonal Multiple Access Networks: Challenges, Techniques, and Research Trends," IEEE Communications Surveys & Tutorials, vol. 19, no. 4, pp. 2254-2282, Fourth Quarter 2017.

[59] Communications Systems, H. Stern and S. Mahmoud, Pearson Prentice Hall, 2004, p. 283.

[60] M. K. Simon and M.-S. Alouini, "Digital Communication over Fading Channels," John Wiley & Sons, 2005.

[61] https://en.wikipedia.org/wiki/Bit_error_rate

[62] https://en.wikipedia.org/wiki/Channel_capacity

[63] Ali, Z.J.; Noordin, N.K.; Sali, A.; Hashim, F.; Balfaqih, M. Novel Resource Allocation Techniques for Downlink Non-Orthogonal Multiple Access Systems. *Appl. Sci.* **2020**, *10*, 5892. https://doi.org/10.3390/app1017589

[64] P. Sedtheetorn and T. Chulajata, "Spectral efficiency evaluation for non-orthogonal multiple access in Rayleigh fading," 2016 18th International Conference on Advanced Communication Technology (ICACT), PyeongChang, Korea (South), 2016, pp. 747-750, doi: 10.1109/ICACT.2016.7423544.

[65] https://en.wikipedia.org/wiki/Constellation_diagram

[66] Amiri, Karim and Sun, Yang and Murphy, Patrick and Hunter, Christopher and Cavallaro, Joseph and Sabharwal, Ashutosh. (2007*). WARP, a Modular Testbed for Configurable Wireless Network Research at Rice.*

[67] http://www.gnu.org/software/gnuradio

[68] http://www.sundance.com

[69] http://www.lyrtech.com

[70] Rami Akeela, Behnam Dezfouli, *"Software-defined Radios: Architecture, state-of-the-art, and challenges"*, Computer Communications 128 (2018) 106–125, Elsevier

[71] Vigneswara Rao Gannapathy, Ahamed Fayeez Bin Tuani Ibrahim, Zahriladha Bin Zakaria, Abdul Rani Bin Othman , Nur Qalbi Binti Jalaudin, *"A Review on Various Types of Software Defined Radios (SDRS) in Radio Communication",* International Journal of Research in Engineering and Technology, December 2014

[72] Z. Tong, M. S. Arifianto, and C. F. Liau, *"Wireless Transmission using Universal Software Radio Peripheral,"* Int. Conf. Sp. Sci. Commun. 2009, pp. 19– 23, 2009.

[73] N. B. Truong and C. Yu*, "Investigating Latency in GNU Software Radio with USRP Embedded Series SDR Platform,"* 2013 Eighth Int. Conf. Broadband Wireless Comput. Commun. Appl., pp. 9–14, Oct. 2013.

[74] http://warpproject.org/trac/wiki/GettingStarted/WARPv3/Hardware

[75] https://mangocomm.com/products/kits/warp-v3-kit/

[76] https://warpproject.org/trac/wiki/GettingStarted/WARPv3/IntroToTools

[77] https://warpproject.org/trac/wiki/HardwareUsersGuides/FMC-RF-2X245

[78] https://warpproject.org/trac/wiki/repositoryAccess

[79] https://warpproject.org/trac/wiki/WARPLab

[80] https://warpproject.org/trac/wiki/WARPLab/Reference/Interface/X245

[81] https://warpproject.org/trac/wiki/WARPLab/AGC

[82] Titiek Suryani, Suwadi, Hasan, Septriandi Wira Yoga, *"Implementation and Performance Evaluation of Orthogonal Frequency Division Multiplexing (OFDM) using WARP",* 2015 International Seminar on Intelligent Technology and Its Applications.

[83] Mahsa Shafiee, Kyle O'Keefe, Gérard Lachapelle, *"Symbol Timing Acquisition for Collaborative OFDM WLAN-based A-GPS",* Springer International Journal of Wireless Information Networks, June 2013

[84] Suryani, T. and Suwadi,. (2017). Performance evaluation of MIMO-OFDM implementation on Wireless open-Access Research Platform (WARP). ARPN Journal of Engineering and Applied Sciences. 11. 13587-13593.

[85] Speth, Michael, et al. *"Optimum receiver design for wireless broad-band systems using OFDM. I."* Communications, IEEE Transactions on 47.11 (1999).

[86] Schmidl, Timothy M., and Donald C. Cox. *"Robust frequency and timing synchronization for OFDM."* Communications, IEEE Transactions on 45.12 (1997)

[87] https://warpproject.org/trac/wiki/Exercises/FPGABoardIntro/UsingImpact

[88] M. Zeng, A. Yadav, O. A. Dobre, G. I. Tsiropoulos and H. V. Poor, "On the Sum Rate of MIMO-NOMA and MIMO-OMA Systems," in IEEE Wireless Communications Letters, vol. 6, no. 4, pp. 534-537, Aug. 2017, doi: 10.1109/LWC.2017.2712149.